THE CHEMISTRY OF 1,2-DIHYDRO-1,2-AZABORINE AND NITRATED LIPIDS

by

ADAM JOHN VON MARWITZ

A DISSERTATION

Presented to the Department of Chemistry
and the Graduate School of the University of Oregon
in partial fulfillment of the requirements
for the degree of
Doctor of Philosophy

September 2010

University of Oregon Graduate School

Confirmation of Approval and Acceptance of Dissertation prepared by:

Adam Marwitz

Title:

"The Chemistry of 1,2-Dihydro-1,2-azaborine and Nitrated Lipids"

This dissertation has been accepted and approved in partial fulfillment of the requirements for the degree in the Department of Chemistry by:

Michael Haley, Chairperson, Chemistry
Shih-Yuan Liu, Advisor, Chemistry
David Tyler, Member, Chemistry
Raghuveer Parthasarathy, Outside Member, Physics

and Richard Linton, Vice President for Research and Graduate Studies/Dean of the Graduate School for the University of Oregon.

September 4, 2010

Original approval signatures are on file with the Graduate School and the University of Oregon Libraries.

An Abstract of the Dissertation of

Adam John Von Marwitz for the degree of Doctor of Philosophy

in the Department of Chemistry to be taken September 2010

Title: THE CHEMISTRY OF 1,2-DIHYDRO-1,2-AZABORINE AND NITRATED LIPIDS

Approved: _____

Professor Shih-Yuan Liu

1,2-Dihydro-1,2-azaborine is a six-membered aromatic heterocycle that is related to the quintessential aromatic molecule, benzene, via the replacement of a CC fragment in benzene with an isoelectronic BN bond-pair. Like the benzene motif, 1,2-dihydro-1,2-azaborine derivatives could provide opportunities in fields ranging from medicine to materials. Recent breakthroughs in the synthesis of 1,2-dihydro-1,2-azaborine have led to a burgeoning interest in this relatively unexplored heterocycle. This dissertation describes the synthesis, characterization, and potential applications of novel 1,2-dihydro-1,2-azaborines. Chapter I reviews the chemistry of monocyclic and polycyclic BN-heterocycles over the last fifty years. Chapter II introduces the synthesis of numerous boron-substituted 1,2-dihydro-1,2-azaborine derivatives from a versatile precursor. Chapter III discusses the first successful synthesis of the parent 1,2-dihydro-1,2-azaborine, which is isoelectronic with benzene itself. An examination of the chemistry of

1,2-dihydro-1,2-azaborine provides a direct comparison of its properties relative to benzene. Chapter IV discusses the synthesis and characterization of 1,2-dihydro-1,2-azaborines incorporated into phenylacetylenic scaffolds. Chapter V discusses unrelated work on nitrated lipids, which was performed under the guidance of Professor Bruce Branchaud. The chapter introduces the importance of nitrated lipids in a biological context and details the synthetic achievements in this field.

This dissertation includes previously published and unpublished co-authored material.

CURRICULUM VITAE

NAME OF AUTHOR: Adam John Von Marwitz

GRADUATE AND UNDERGRADUATE SCHOOLS ATTENDED:

University of Oregon, Eugene, Oregon
The Colorado School of Mines, Golden, Colorado

DEGREES AWARDED:

Doctor of Philosophy in Chemistry, 2010, University of Oregon
Master of Science in Chemistry, 2005, University of Oregon
Bachelor of Science in Chemical Engineering, 2004, The Colorado School of Mines

AREAS OF SPECIAL INTEREST:

Aromatic boron heterocycles
Nitrated lipids

PROFESSIONAL EXPERIENCE:

Graduate Research Assistant, Department of Chemistry, University of Oregon, Eugene, Oregon, 2005-2010.

Graduate Teaching Assistant, Department of Chemistry, University of Oregon, Eugene, OR, 2004-2005.

GRANTS, AWARDS AND HONORS:

National Science Foundation IGERT Fellowship, 2008-2009

PUBLICATIONS:

Daly, A. M.; Tanjaroon, C.; Marwitz, A. J. V.; Liu, S. –Y.; Kukolich, S. G. "Microwave Spectrum, Structural Parameters, and Quadrupole Coupling for 1,2-Dihydro-1,2-azaborine," *J. Am. Chem. Soc.* **2010**, *132*, 5501-5506.

Marwitz, A. J. V.; McClintock, S. P.; Zakharov, L. N.; Liu, S. –Y. "BN Benzonitrile: An Electron-deficient 1,2-Dihydro-1,2-azaborine Featuring Linkage Isomerism," *Chem. Comm.* **2010**, *46*, 779-781.

Tanjaroon, C.; Daly, A.; Marwitz, A. J. V.; Liu, S. –Y.; Kukolich, S. "Microwave Measurements and Ab Initio Calculations of Structural and Electronic Properties of N-Ethyl-1,2-azaborine," *J. Chem. Phys.* **2009**, *131*, 224312/1-224312/9.

Liu, L.; Marwitz, A. J. V.; Matthews, B. W.; Liu, S. –Y. "Boron Mimetics: 1,2-Dihydro-1,2-azaborine Binds inside a Non-polar Cavity of T4 Lysozyme," *Angew. Chem. Int. Ed.* **2009**, *48*, 6817-6819.

Marwitz, A. J. V.; Matus, M. H.; Zakharov, L. N.; Dixon, D. A.; Liu, S. –Y. "A Hybrid Organic/inorganic Benzene," *Angew. Chem. Int. Ed.* **2009**, *48*, 973-977.

Marwitz, A. J. V.; Abbey, E. R.; Jenkins, J. T.; Zakharov, L. N.; Liu, S. –Y. "Diversity though Isosterism: The Case of Boron-substituted 1,2-Dihydro-1,2-azaborines," *Org. Lett.* **2007**, *9*, 4905-4908.

Woodcock, S. R.; Marwitz, A. J. V.; Bruno, P.; Branchaud, B. P. "Synthesis of Nitro-lipids. All Four Possible Diastereomers of Nitro-oleic Acids: (E)- and (Z)-, 9- and 10-Nitro-octadec-9-enoic Acids," *Org. Lett.* **2006**, *8*, 3931-3934.

ACKNOWLEDGMENTS

I would like to sincerely thank my research advisor, Professor Shih-Yuan Liu, for his continued support and guidance over the last four years. I would also like to thank Professor Bruce Branchaud for the opportunity to work in his group. I would like to extend a special thank you to my committee chair, Professor Michael M. Haley, for his continued support during my graduate career. I would like to acknowledge my other committee members, Professor David R. Tyler, Professor Raghu Parthasarathy, Professor Nathan Tublitz, and Professor Bea Darimont for their advice and scientific input concerning my research. Dr. Lev Zakharov for his crystallographic expertise. Dr. Bartholemew Dahl and Dr. Steven Woodcock for their mentorship during my time in the Branchaud group. Eric Abbey for providing camaraderie and scientific input to a fledgling project in the Liu group. Adam Glass, Pat Campbell, Ashley Lamm, Jesse Jenkins, Jed Volvovic, and Dr. Tshitij Parab for contributing greatly to my research. Dr. Justin Crossland and Dr. Tim Carter for their friendship. My family for their love and support. I would also like to thank every person who has provided assistance throughout my graduate career. There are too many to be named here. Finally, I would like to thank the National Science Foundation IGERT program for over a year of funding.

For my loving wife Katie.

TABLE OF CONTENTS

Chapter Page

Chapter Page

Chapter Page

LIST OF FIGURES

Figure Page

Chapter I

Figure Page

Chapter II

Figure Page

Figure Page

Chapter IV

Figure Page

Chapter V

LIST OF TABLES

Table Page

LIST OF SCHEMES

Scheme Page

Chapter I

Scheme Page

Scheme Page

Scheme Page

Chapter II

Scheme Page

Chapter III

Chapter IV

Scheme Page

CHAPTER I

THE CHEMISTRY OF HYBRID BORON-NITROGEN HETEROCYCLES

1.1. Introduction

Benzene (c-C_6H_6) was first isolated from the distillate of coal tar nearly two centuries ago,[1] yet the study of benzene and its derivatives continues to drive research in the 21st century. The study of benzene's fundamental properties has given rise to the concept of aromaticity and bond delocalization. Beyond its fundamental importance, benzene derivatives are commonly found in fields such as polymer science, biomedical research, and material science.

Borazine (c-$B_3N_3H_6$), the inorganic, isoelectronic counterpart to benzene, was isolated by Alfred Stock in 1926,[2] and has also received significant attention in pure and applied chemistry. The analogy of borazine as an "inorganic" benzene is derived from the donation of a lone pair of electrons from nitrogen into the vacant p-orbital of the sp^2-hybridized boron (Figure 1). The number and geometry of electrons is the same in the B-N and C=C bond units, and therefore borazine and benzene are isoelectronic. On the other hand, borazine tenuously meets the criteria for aromaticity, and its relative instability has limited its utility.

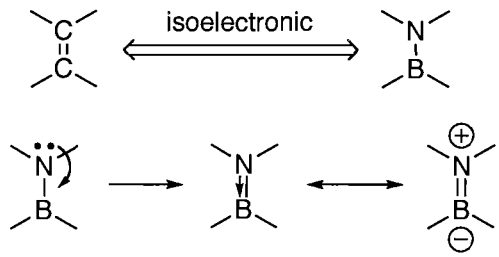

Figure 1. Isoelectronic relationship between CC and BN.

The isoelectronic relationship between B-N and C=C has led to an emergence of aromatic systems *partially* substituted with boron and nitrogen (carbon-boron-nitrogen (CBN) heterocycles). Though somewhat limited in scope, the first major achievements in the synthesis of CBN heterocycles took place in the 1960s. After several decades of diminished activity in the field, modern synthetic protocols have promoted a resurgence in the study of CBN heterocycles.

This chapter will serve to provide a review of the chemistry of 6-membered heterocycles containing one and two B-N bond units. Aromatic CBN heterocycles isoelectronic with benzene will be of primary interest. Non-aromatic six-membered heterocycles will also be discussed, especially as they relate to the aromatic analogs. Isoelectronic analogs of pyridine, such as BODIPY dyes, will not be discussed but have been reviewed extensively.[3-4] Substitution of B-N units in cluster compounds and graphitic materials is beyond the scope of this review.[5] This chapter will be organized by heterocyclic motif and will cover both monocyclic and polycyclic derivatives. It will be organized chronologically to give as much historical context as possible with regard to the general periods of CBN heterocycle research, where relevant. Calculations on CBN heterocycles have contributed greatly to the interest in this field, and thus this work will also be discussed in relation to known or predicted physical properties. However,

an in-depth discussion of calculation methods will not be covered here. Synthetic achievements will be discussed separately from theoretical work as much as possible to avoid confusion.

1.2. C_4BN Heterocycles

1.2.1. Synthesis of Monocyclic 1,2-Azaborine Derivatives

1,2-Dihydro-1,2-azaborine (hereafter 1,2-azaborine unless referring to parent compound **1**) is a 6 π-electron analog of benzene in which a C=C unit has been replaced with a B-N bond pair (Figure 2).

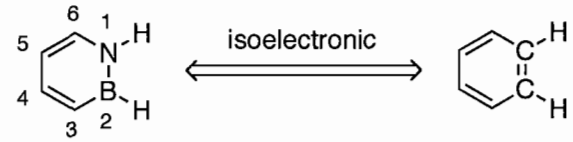

1

Figure 2. 1,2-Dihydro-1,2-azaborine **1** is isoelectronic with benzene.

Dewar and White pioneered the first syntheses of monocyclic 1,2-azaborine derivatives. In 1962, Dewar and co-workers used a desulfurization strategy from BN-benzothiophene **2** to generate highly-substituted 1,2-azaborine **3** (Scheme 1).[6] Compound **3** was resistant to degradation under prolonged exposure to both acid and base in ethanol as monitored by UV-vis spectroscopy (λ_{max} = 306 nm, ε = 15850 $M^{-1}cm^{-1}$). Acid/base stability and the inertness of the 1,2-azaborine double bonds toward Raney Nickel are indications of the aromatic stability of the 1,2-azaborine core. A year later,

White reported the synthesis of 1-H-2-phenyl-1,2-azaborine **5** via Pd-catalyzed dehydrogenation from saturated heterocycle **4** (Scheme 2).[7]

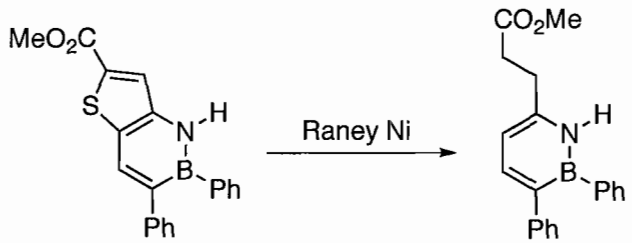

2 **3**

Scheme 1. Synthesis of 1,2-azaborine derivative **3** via desulfurization with Raney Nickel (Dewar, 1962).

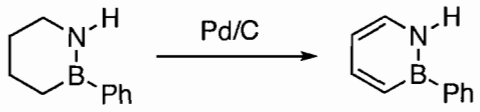

4 **5**

Scheme 2. Dehydrogenation route to 1,2-azaborine **5** (White, 1963).

In 1967, Dewar and co-workers attempted the first synthesis of 1,2-Dihydro-1,2-azaborine **1** via a hydroboration-oxidation protocol but were unsuccessful.[8] They concluded that, "Borazarene [1,2-Dihydro-1,2-azaborine] therefore seems to be a very reactive and chemically unstable system, prone to polymerization and other reactions..." In fact, multiple attempts to isolate the parent 1,2-Dihydro-1,2-azaborine **1** from BN-triphenylene **7** (Scheme 3) were unsuccessful.

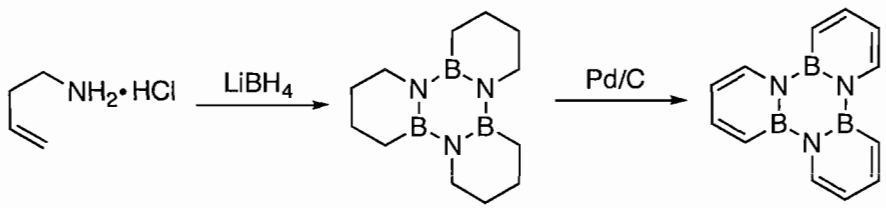

6 **7**

Scheme 3. Hydroboration-oxidation protocol leading to undesired trimerization to BN-triphenylene **7**.

Polivka et al. followed a similar route to generate 1,2-azaboracyclohexane **8** from dimethylaminobut-3-ene (Scheme 4).[9,10] Alkylation of the amine prevents the trimerization of **8**; heterocycle **8** is readily isolated via vacuum distillation. Compound **8** is formally isoelectronic with 1,1-dimethylcyclohexane, and the tetracoordinate boron and nitrogen atoms are unable to participate in π-bonding. Instead the B-N bond pair can be considered a dative σ-bond. The generation of a 1,2-azaborine motif from **8** was not observed. Baboulène and co-workers have recently used N-alkyl amine-boranes such as **8** to form aminoalkylboronic acid salts as surfactant materials.[11]

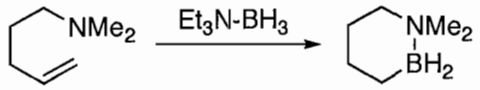

8

Scheme 4. Hydroboration to stable 1,2-azaboracyclohexane **8**.

Goubeau and co-workers used a secondary butenyl amine (as in White's earlier work) to form 1,2-azaborine **9** via hydroboration (Scheme 5).[12] Dehydrogenation with Pd/Al_2O_3 provided the first B-H substituted 1,2-azaborine **10**, which was characterized by mass spectrometry.[13]

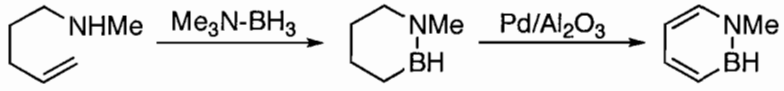

9 **10**

Scheme 5. Hydroboration-oxidation to generate B-H substituted 1,2-azaborine **10**.

Gronowitz and co-workers synthesized a series of BN-benzothiophenes, which upon desulfurization yielded the first examples of monocyclic 1,2-azaborines substituted at C4 and/or C5.[14-17] Desulfurization of BN-benzothiophene **11** generated 1,2-azaborine **12** (Scheme 6) selectively, which reacted further with Raney-Ni to produce the first 1,2-

azaborine substituted at the C5 position with an aliphatic (ethyl) group (**13** in Scheme 6).[16] Reaction of BN-benzodithiophene **14** with Raney-Ni afforded 4,5-diethyl-1,2-azaborine **15**.[14]

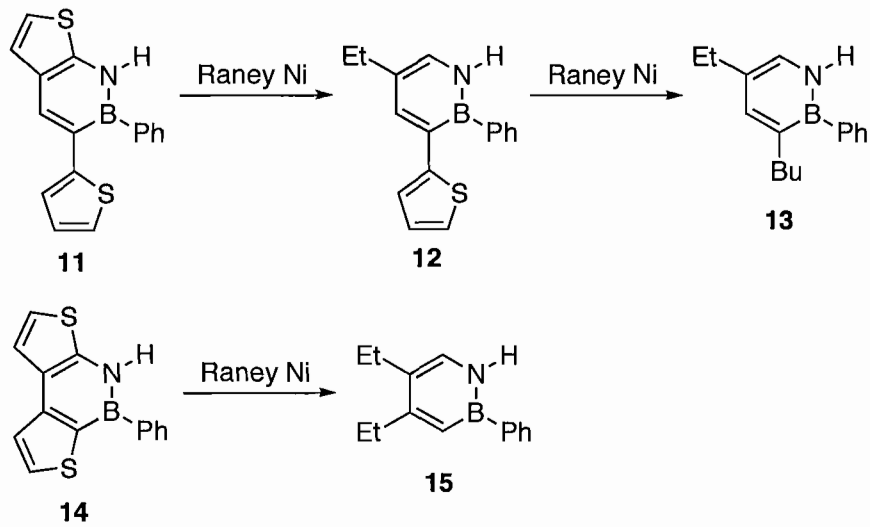

Scheme 6. Desulfurization of BN-benzothiophenes with Raney Nickel to generate 4-, and 5-substituted 1,2-azaborines.

Bürger and co-workers reported another route to monocyclic 1,2-azaborine derivatives in 1990.[18] The reaction of dialkylaminobis(trifluoromethyl)boranes (e. g. **16** in Scheme 7) with a variety of alkyl-substituted 1,3-dienes led to the formation of a CBN heterocycle (e. g. **17**) via a [4+2] cycloaddition. The X-ray crystal structure of **17** revealed a long B-N bond (1.621(3) Å) consistent with a σ-bonded complex for the tetra-coordinate boron and nitrogen atoms. The reaction of aminoborane **16** to generate cyclic amine-boranes was later accomplished via a two-step substitution sequence (Scheme 8).[19] 5-Bromopentanenitrile underwent an ene-type reaction to generate ring-opened **18**. Deprotonation with KOH led to the intramolecular N-alkylation of **18** to generate nitrile-substituted BN heterocycle **19**. Interestingly, in compounds similar to **19**, reduction of

the nitrile using (^{i}Bu)$_2$AlH followed by hydrolysis furnished the corresponding aldehyde, which is a testament to the stability of these compounds.

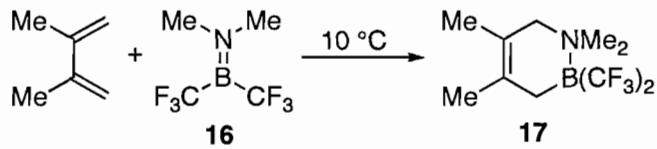

16 **17**

Scheme 7. [4+2] Cycloaddition of aminoborane **16** with a 1,3-diene generates cyclic amine-borane **17**.

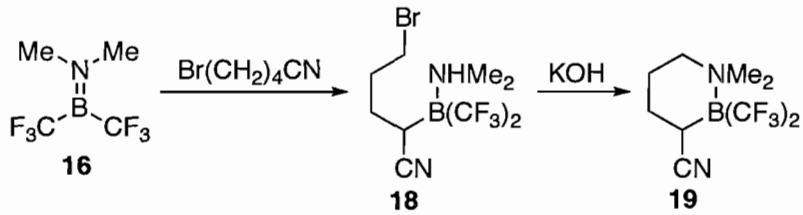

16 **18** **19**

Scheme 8. Ene-type reaction of **16** generates ring-opened **18** which undergoes an intramolecular N-alkylation to give heterocycle **19**.

In a preparation of ω-aminoboronic esters from azides (Scheme 9), Vaultier and co-workers reported ^{11}B NMR chemical shifts for compounds **20a-i** that indicated a substituent and chain-length dependence on intramolecular cyclization (Table 1).[20] The upfield chemical shift in ^{11}B NMR spectroscopy of several of these compounds is consistent with an equilibrium between 3- and 4-coordinate boron for the ring-opened and ring-closed forms, respectively (Scheme 9). Mikhailov and co-workers observed temperature-dependence in the equilibrium of intramolecular cyclization of amine-boranes.[21-22]

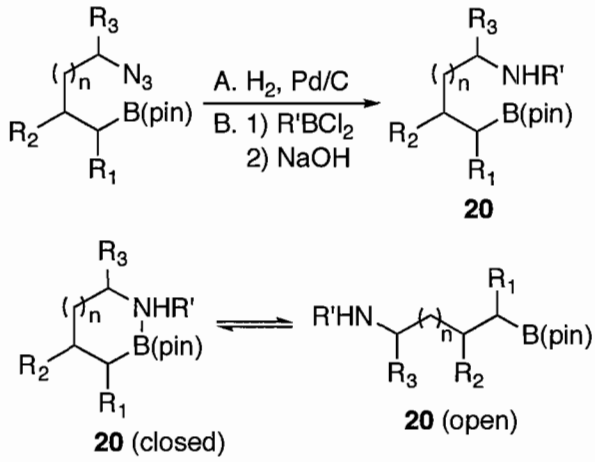

Scheme 9. Intramolecular cyclization of ω-aminoboronic esters.

Table 1. ^{11}B NMR Shifts of ω-Aminoboronic Esters **20a-i**

Compound	*n*	R^1	R^2	R^3	R'	δ ^{11}B (ppm)
20a	0	H	H	H	H	27.5
20b	1	H	H	H	H	19.1
20c	1	^{i}Pr	H	H	H	32.3
20d	1	H	Me	H	H	11.4
20e	1	H	Me	H	Hex	18.4
20f	2	H	H	H	H	33.8
20g	2	H	H	H	Ph	33.8
20h	2	H	H	H	Hex	33.8
20i	3	H	H	H	H	34.0

In subsequent work, Vaultier and co-workers reported that the reaction of aminoborane **21** with benzyl azide and HCl formed reduced 1,2-azaborine **22** which reacted further with HCl, producing dichloroborane **23** (Scheme 10).[23] Unfortunately, characterization of **23** was limited to ^{11}B NMR spectroscopy (δ 7.8 ppm). Paetzold and co-workers used a similar ring-expansion strategy to generate bicyclic aminoborane **24** (Scheme 11), which could be further reacted with Me_3SiN_3 to give azide-substituted amino-borane **25**.[24]

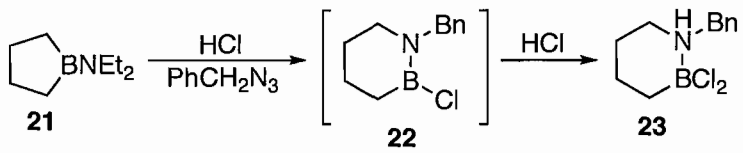

21 22 23

Scheme 10. Reaction of aminoborane **21** with benzyl azide and HCl.

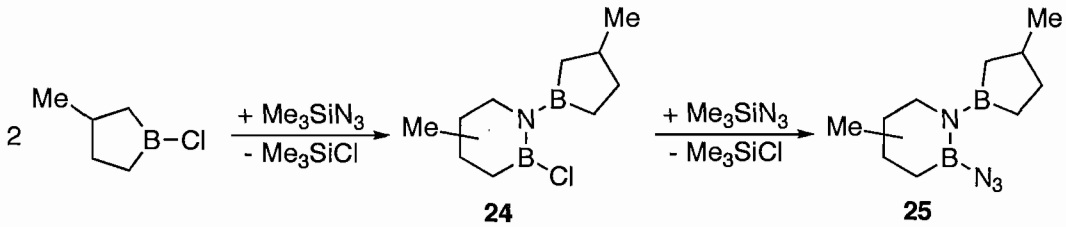

24 25

Scheme 11. Formation of B-Cl aminoborane **24** and azide-substituted aminoborane **25**.

The Ashe group achieved a breakthrough in the mild synthesis of monocyclic 1,2-azaborines in 2000. Whereas previous syntheses relied on desulfurization or dehydrogenation at extreme temperatures as discussed above, Ashe and co-workers used a ring-closing metathesis/oxidation protocol for the efficient formation of 1,2-azaborines (Scheme 12).[25] Transmetallation of allyltributyltin with BCl_3 generated allylboron dichloride **26** in situ. Condensation with allylethylamine produced bisallyl aminoborane **27**. The addition of PhLi led to the displacement of chloride from the labile B-Cl bond to give B-Ph aminoborane **28** in good yield. Ring-closing metathesis with Grubbs' 1st Generation catalyst formed 1,2-azaborine precursor **29** featuring an olefin at the 4-position. The oxidation to 1,2-azaborine **30** was accomplished in good yield using 2,3-dichloro-5,6-dicyano-1,4-benzoquinone (DDQ) at 35 °C.

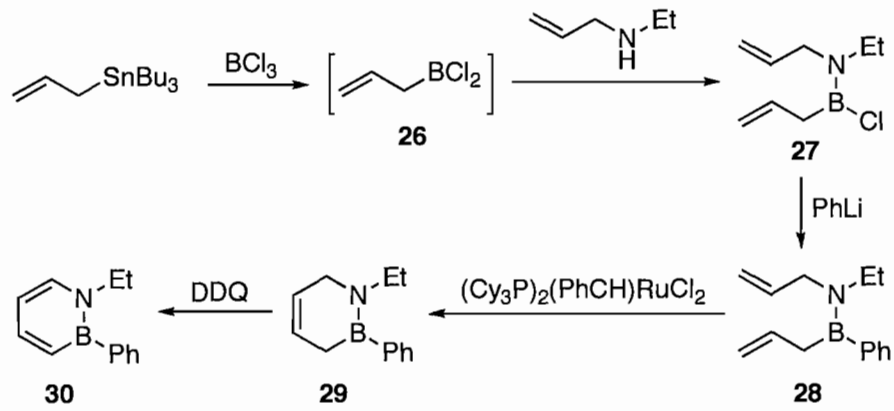

Scheme 12. Synthesis of 1,2-azaborine **30** via ring-closing metathesis.

A year later, Ashe et al. explored a ring-expansion route to 1,2-azaborines from the 1,2-azaborolide heterocycle, which is formally isoelectronic with the ubiquitous cyclopentadienide (Cp) anion. Ring-closing metathesis from B-vinyl aminoboranes **31a-c** provided heterocycles **32a-c** (Scheme 13), which were deprotonated to give 1,2-azaborolides **33a-c**.[26] The reaction of **33a-c** with CH_2Cl_2 and lithium diisopropylamide (LDA) (the Katz reaction) gave 1,2-azaborines **34a-c**. A deuterium labeling study suggested that the initial attack of chlorocarbene occurs at the C3 position of **33c**. Carbene insertion into the B-C bond leads to a 3-deuterio isomer of **34c** via carbene **35**. Deuterium incorporation at this position rules out initial substitution at C5.

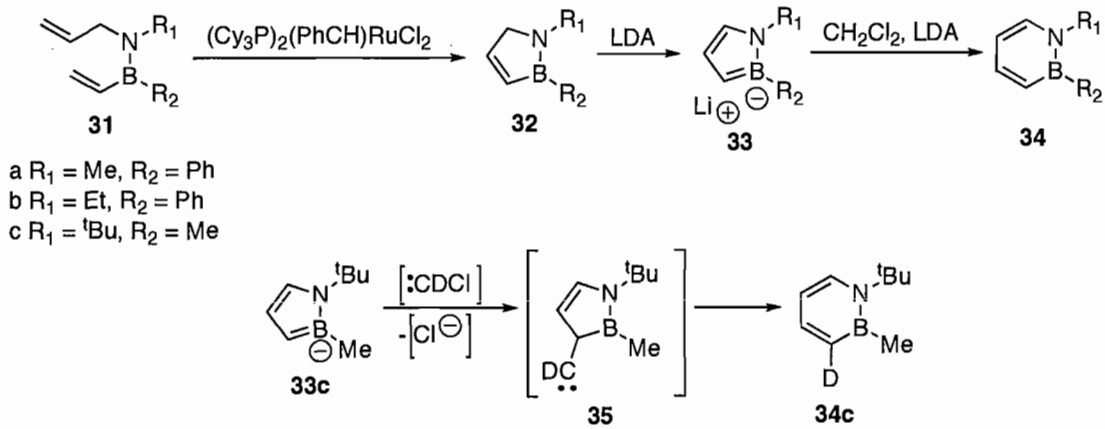

Scheme 13. Ring-expansion route to 1,2-azaborines **34a-c** and deuterium labeling.

The Ashe group has extensively studied the coordination chemistry of 1,2-azaborine with transition metals. The reaction of $(MeCN)_3Cr(CO)_3$ with **34a** leads to the formation of piano-stool structure **36** (Scheme 14).[26] The solid-state structure of **36** revealed that the 1,2-azaborine ligand binds in an η^6 fashion to chromium. The 1,2-azaborine ring is planar, and the phenyl ring is twisted out the 1,2-azaborine plane. The B-N bond length is 1.466(6) Å, which is slightly longer than a typical unconjugated aminoborane B-N bond (1.41 Å),[27] indicating some delocalization of the B-N π-electrons. The structural features of **36** and **37** are typical for other arene piano-stool complexes.[28]

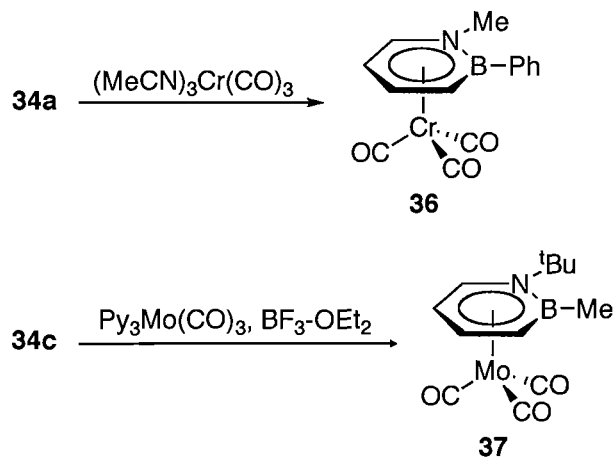

Scheme 14. Formation of η^6 complexes of 1,2-azaborines with group 6 transition metals.

Ashe and co-workers synthesized 1,2-azaborine **38** via the ring-expansion route discussed above.[29] The addition of Bu_4NF to TMS-protected **38** provided an alternate route to N-H 1,2-azaborine **5** (Scheme 15), which could be reversibly deprotonated at the nitrogen position to give **39**. 1,2-Azaborine **39** was found to be a good ligand for ruthenium (**40** in Scheme 15). Protonation of sandwich complex **40** with AcOH gave salt **41**. Whereas the pKa of heterocycle **5** was found to be comparable to

pentamethylcyclopentadiene (~ 26), the pKa of **41** was determined to be 9.2 via potentiometric titration.

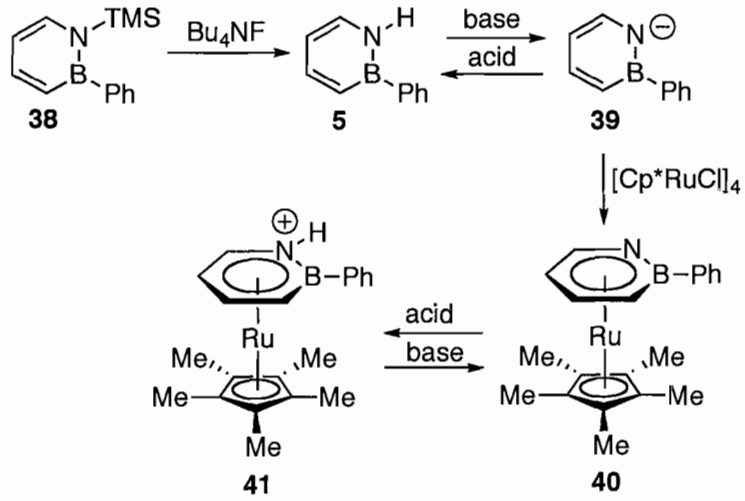

Scheme 15. The reversible deprotonation of **5** and Ru-complex **41**.

The reversible protonation of **5** was also used to probe the haptotropic migration of $Cr(CO)_3$ between 1,2-azaborine and the B-phenyl substituent.[30] Ashe and co-workers determined that piano-stool complex **42** was formed as the sole kinetic product of the reaction of **5** with $(MeCN)_3Cr(CO)_3$ at 50 °C (Scheme 16). Heating at elevated temperature drove the haptotropic migration of the $Cr(CO)_3$ fragment from the 1,2-azaborine ring to the phenyl ring, indicating complex **43** was the thermodynamic product of the reaction. The kinetic-thermodynamic relationship between the 1,2-azaborine and phenyl rings was reversibly switched when complex **43** was deprotonated to give **44**. Complex **44** was cleanly converted to **45** when heated, indicating **45** was the thermodynamic product. The increased electron-richness of the anionic 1,2-azaborine ring makes it a better ligand toward $Cr(CO)_3$. Complex **45** was protonated to give **42**, making the overall sequence of reactions (**42** to **43** to **44** to **45**) thermodynamically

neutral. The acid-base steps were determined to be approximately 19 kcal/mol based on the 13.5 pKa unit difference between **42** and **43**, and these steps energetically balance the thermal migration steps.

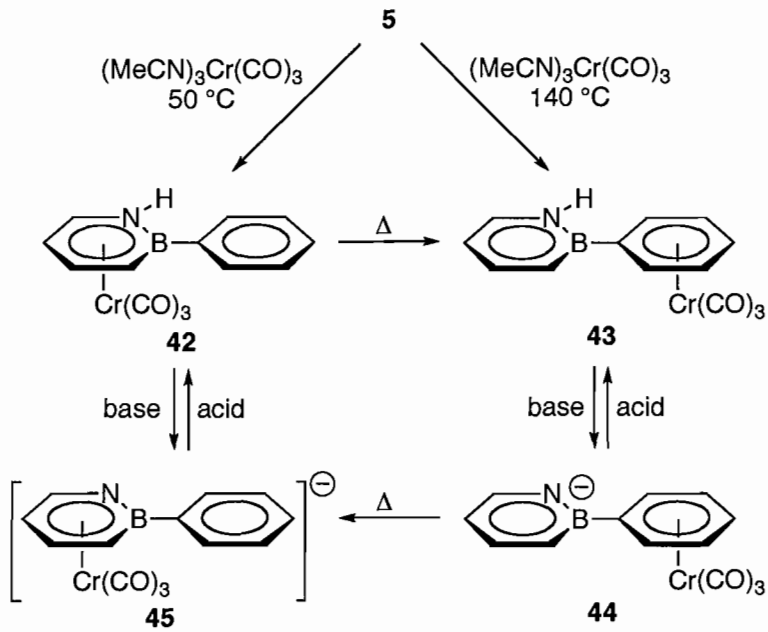

Scheme 16. Switchable haptotropic migrations of the 2-phenyl-1,2-azaborine ligand.

Table 2. Selected Bond Distances (Å) for **42** and **43**.

	42	**43**
B1-N1	1.450(2)	1.430(5)
N1-C1	1.383(2)	1.368(5)
C1-C2	1.389(2)	1.353(6)
C2-C3	1.421(2)	1.413(7)
C3-C4	1.395(2)	1.370(6)
C4-B1	1.524(2)	1.500(5)

The solid-state structure of **43** was determined, which was the first crystallographic characterization of a 1,2-azaborine that was not directly bound to a metal. The 1,2-azaborine bond distances for **43** are presented in Table 2 and are

consistent with bond delocalization throughout the planar 1,2-azaborine ring. The formal single bonds (N1-C1, C2-C3, and B1-C4) are shortened and the formal double bonds (B1-N1, C1-C2, and C3-C4) are lengthened relative to typical B-N and C=C bonds. The crystal structure of **42** was also obtained. The 1,2-azaborine ring distances for **42** (Table 2) are lengthened relative to **43**. This is consistent with the donation of π-electron density from the 1,2-azaborine ring of **42** into chromium as well as backdonation of chromium's d-electrons into the anti-bonding orbitals of the ring system.

The coordination chemistry of 1,2-azaborine is not only tunable via protonation/deprotonation, but is also dependent on the choice of metal. The reaction of anionic 1,2-azaborine **39** with Cp_2ZrCl_2 led to the formation of complex **44** (Scheme 17) in which the 1,2-azaborine ligand was σ-bonded to zirconium.[31]

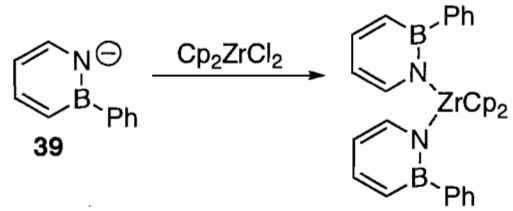

39 **44**

Scheme 17. Formation of η^1-zirconium complex **44** (not balanced).

The Ashe group also explored the ligand properties of deprotonated BN-styrene **45** (Scheme 18),[32] which was synthesized via the ring expansion route discussed above. The reaction of **45** with 1 equivalent of $[Cp^*RuCl]_4$ gave complex **46** in which BN-styrene was bound to ruthenium in an η^6 fashion. However, when 2 equivalents of $[Cp^*RuCl]_4$ were added, diruthenium complex **47** was formed. In complex **47**, η^6

binding occurred between a ruthenium atom and the 1,2-azaborine ring, while the second ruthenium bound η^1 to the 1,2-azaborine nitrogen. An additional η^2 interaction between ruthenium and the B-vinyl group was observed.

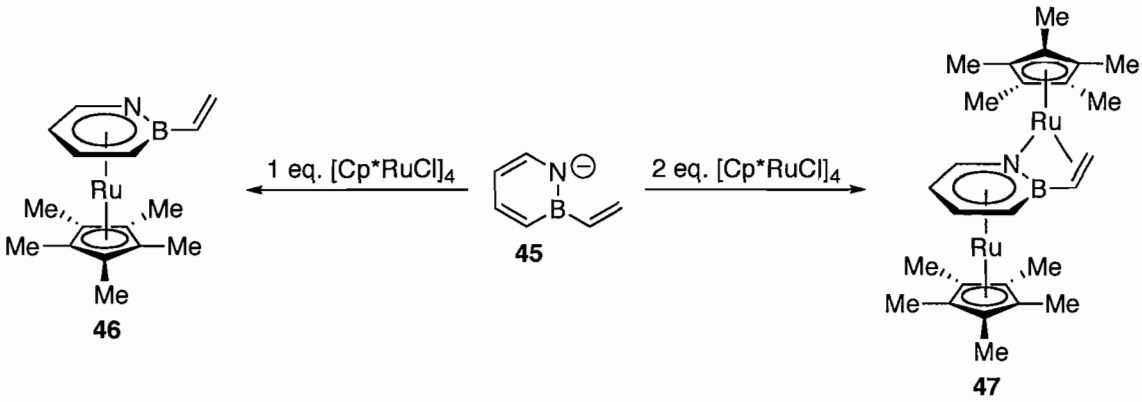

Scheme 18. Synthesis of complexes **46** and **47** from BN-styrene **45**.

Ashe and co-workers recently demonstrated electrophilic aromatic substitution (EAS) reactivity in 1,2-azaborines (Scheme 19).[33] 1,2-Azaborine **30** reacted with a variety of electrophiles to give 3-substituted **48a-d** and 5-substituted **49e-f**. Deuterium exchange with CD_3COOD/CF_3COOD gave **48a** by ^1H NMR, however only degradation products were isolated. A competition experiment showed that **30** was more reactive than furan and thiophene toward deuterium exchange, but not as reactive as 1-methylindole. Bromination to **48b** readily occurred with Br_2. CN-Substituted **48c** was produced via the coupling of CuCN and bromide **48b**. In the case of BN-phenol **48d**, iodination with I-Cl was followed by the addition of Na_2SO_3/H_2O to give –OH substitution. C5-Substituted **49e** was produced in low yield via Friedel-Crafts acylation upon treatment with Ac_2O and $SnCl_4$. The Mannich reaction of **30** with *N,N*-dimethylmethyleneiminium chloride gave C5-substituted **49f** in good yield. The substitution pattern was rationalized by resonance stabilization whereby substitution at

either the 3- or 5-positions leads to resonance forms with the positive charge at the nitrogen (Scheme 20).

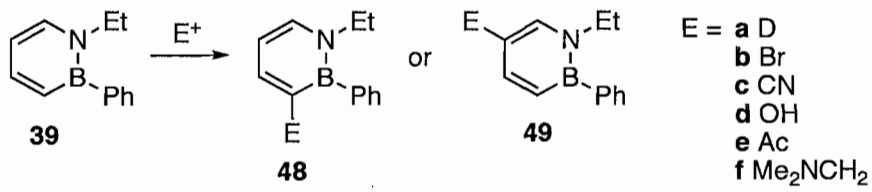

Scheme 19. EAS reactivity of 1,2-azaborine **39**.

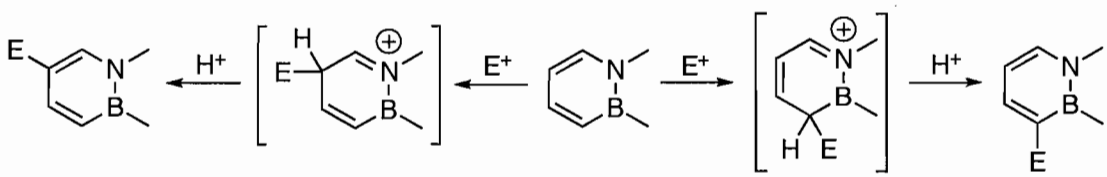

Scheme 20. Resonance stabilization of 3- and 5-substituted 1,2-azaborine.

As discussed above, solid-state structural parameters of 1,2-azaborine provide some evidence of bond delocalization.[30] However, Liu and co-workers obtained conclusive evidence of bond delocalization in 1,2-azaborine via crystallographic analysis.[34] 1,2-Azaborine precursor **50** was a versatile intermediate in the formation of a family of aminoboranes in various oxidation state with respect to the intra-ring carbon atoms (**51-54** in Scheme 21). Transition-metal catalysis was used in all cases to generate the desired heterocycle. The isomerization of **50** to B-vinyl **51** was achieved using $Ru(Cl)_2(PPh_3)_3$ in good yield. Alternatively, ruthenium catalyst $Ru(H)(Cl)(CO)(PPh_3)_3$ catalytically isomerized the olefin in **50** to N-vinyl **52**. Oxidation with Pd black heterogeneously catalyzed the formation of 1,2-azaborine **53**. The same catalyst in the presence of H_2 reduced **50** to **54**. Structural data for compounds **50-54** were obtained via single-crystal X-ray diffraction and are presented in Table 3. An examination of the B-N bond shows that upon oxidation to 1,2-azaborine **53**, the B-N bond lengthens relative to

the other heterocycles. Similarly, the C=C bonds in **51** and **52** are shorter than the corresponding bonds in **53**. The lengthening of these formal double bonds in the structure of **53** is a clear indication of bond delocalization. Conversely, the C4-C5 single bond in **53** is shorter than the corresponding bonds in **51** and **52** by over 0.07 Å. A similar shortening of the B-C3 and C6-N bonds in 1,2-azaborine **53** versus all other derivatives is consistent with bond delocalization.

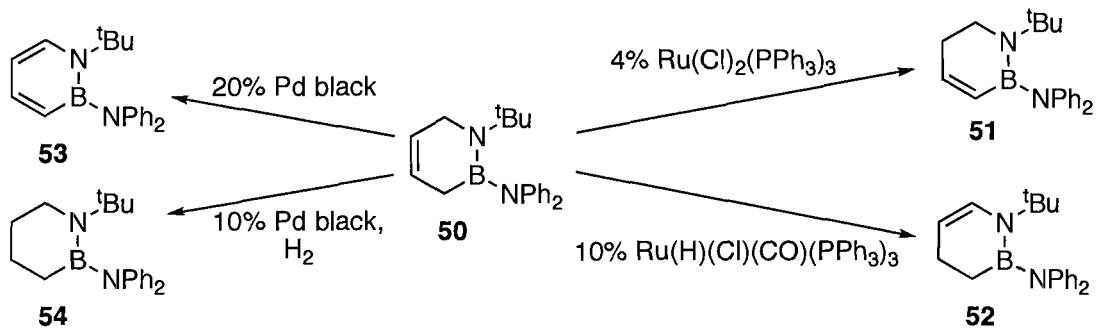

Scheme 21. Catalytic formation of 1,2-azaborine isomers **50-54**.

Table 3. Selected Bond Distances and Deviations from Planarity (Å) for Heterocycles **50-54**

	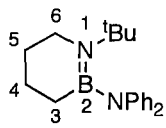 **54**	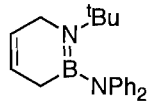 **50**	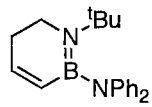 **51**	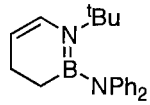 **52**	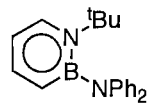 **53**
N_{ring}-B	1.403(2)	1.405(2)	1.407(2)	1.417(3)	1.446(2)
B-C3	1.584(3)	1.590(2)	1.559(2)	1.579(4)	1.518(2)
C3-C4	1.511(3)	1.493(2)	1.338(2)	1.504(4)	1.363(2)
C4-C5	1.511(3)	1.319(2)	1.479(2)	1.494(4)	1.412(2)
C5-C6	1.508(3)	1.493(2)	1.503(2)	1.319(3)	1.356(2)
C6-N1	1.479(2)	1.477(2)	1.479(2)	1.432(3)	1.383(2)
B-N_{exo}	1.488(2)	1.478(2)	1.483(2)	1.480(3)	1.486(2)
planarity[a]	0.226	0.164	0.199	0.183	0.048

[a] Root mean square deviation of intra-ring atoms from the least-squares plane (in Å).

The facile reduction and physical properties of 1,2-azaborine has made it an attractive material for H_2 storage. Liu and co-workers have recently described the formation of a "charged" amine-borane fuel from fully "spent" 1,2-azaborine, in which 3 equivalents of H_2 (formally) have been added to the 1,2-azaborine (Scheme 22).[35]

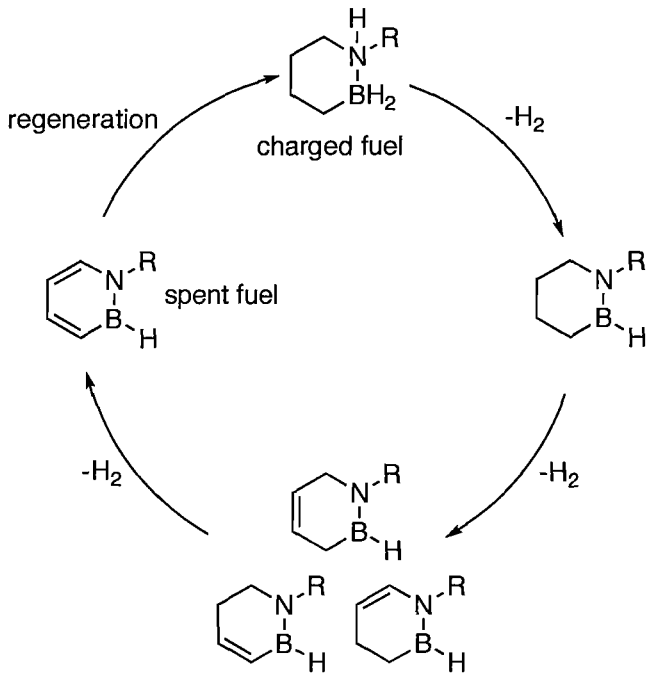

Scheme 22. Hydrogen storage by CBN heterocycles.

The catalytic reduction of **55** with Pd/C adds two equivalents of H_2 across the formal C=C bonds to give heterocycle **56** (Scheme 23). The reduction is relatively mild; in a comparative study, the reduction of benzene under identical conditions was not observed. The third equivalent of "H_2" was added across the B-N bond in a sequential manner (Scheme 24). The reaction of KH with **56** installed H^- at the boron atom to give anionic intermediate **57**. The protonation of the nitrogen of **57** was then accomplished with HCl to give **58** (the fully charged fuel). Vedejs and co-workers recently observed

reactivity consistent with the formation of a fully charged fuel (Scheme 25), yet the monocyclic products of these reactions were not isolated.[36]

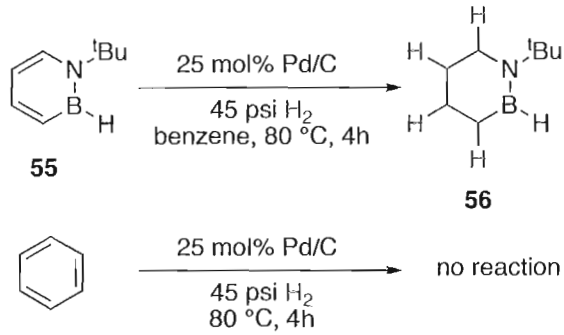

Scheme 23. Partial regeneration of 1,2-azaborine spent fuel.

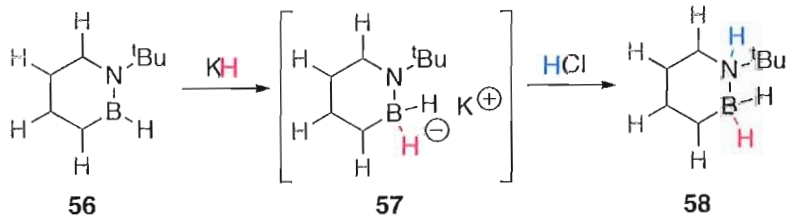

Scheme 24. Sequential addition of H^-/H^+ across the B-N bond.

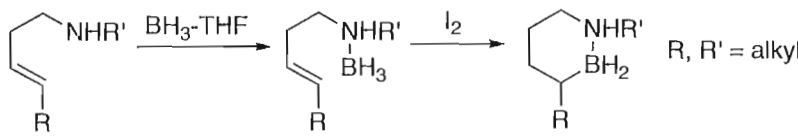

Scheme 25. Mild route to fully-charged cyclic aminoborane fuels.

1.2.2. Computational Studies on 1,2-Azaborine Derivatives

As much attention as the 1,2-azaborine motif has received in organic synthesis, there has been as much or more attention paid by theoreticians interested in predicting or explaining its properties.[37-55] Roald Hoffmann was the first to examine some of the properties of 1,2-Dihydro-1,2-azaborine **1** computationally.[37] In his initial report, Hoffmann calculated the charge distribution in **1** using a linear combination of atomic

orbitals (LCAO-MO) analysis and determined that boron has the greatest positive charge. Correspondingly, nitrogen is the position with the greatest negative charge. Significant negative charge was found at the C3 position. Additional calculations support this prediction[38-39] and are in agreement with the observation nearly 50 years later that EAS reactivity occurs primarily at the C3 position.[33] The calculated total energy of **1** compared to benzene and borazine indicated that **1** was significantly higher in energy than both.

The first rigorous calculations using comparative methods on 1,2-dihydro-1,2-azaborine **1** were performed by Carbó and co-workers in 1969.[40] The methods used included LCAO, self-consistent Hückel molecular orbital (SCHMO), extended Hückel theory (EHT), an iterative EHT (IEHT) method, and a complete neglect of differential overlap (CNDO) extending the Pariser-Parr-Pople (PPP) formalism to all valence electrons. The iterative determination of molecular geometry by SCHMO was later used for calculations by the other methods, the parameters of which are presented in Table 4.

Table 4. Geometric Parameters of **1**[a]

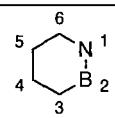

Distances (Å)	
1-2	1.449
2-3	1.555
3-4	1.355
4-5	1.455
5-6	1.358
6-1	1.399
Angles (°)	
1	118.3
2	121.5
3	114.3

4	121.8
5	123.8
6	120.2

[a] N- and B-bonded hydrogen atoms omitted for clarity

Energy levels were calculated using the EHT, IEHT, and CNDO methods and are presented in Table 5. The assignment of the highest occupied molecular orbital (HOMO) to lowest unoccupied molecular orbital (LUMO) was inconsistent between the three methods (EHT/IEHT: $\sigma \rightarrow \pi^*$, CNDO: $\pi \rightarrow \pi^*$) as was the energy of this transition (EHT: 3.24 eV, CNDO: 15.73 eV).

Table 5. σ and π Energy Levels for **1** (in eV)

EHT	IEHT	CNDO
- 4.63 π^*	- 4.80 π^*	6.26 π^*
- 6.99 π^*	- 7.34 π^*	4.77 π^*
- 8.72 π^*	- 8.69 π^*	2.73 π^*
- 11.96 σ	- 11.94 σ	- 13.00 π
- 12.10 π	- 12.06 π	- 13.45 σ
- 12.93 σ	- 12.77 σ	- 14.51 σ
- 13.63 σ	- 13.26 π	- 15.55 π
- 13.68 π	- 13.62 σ	- 17.52 σ
- 14.36 σ	- 14.20 σ	- 19.39 σ
- 14.85 σ	- 14.61 σ	- 20.49 σ
- 15.11 σ	- 14.92 π	- 21.42 σ
- 15.47 π	- 14.99 σ	- 23.12 π

Carbó and co-workers calculated the π-electron distribution in **1**, which predicted the donation of between 0.148 and 0.705 π-electrons from nitrogen to boron, depending on the calculation method. The B-N π-bond was found to be polarized toward nitrogen, whereas the carbon atoms had a π-electron distribution of approximately unity. The calculated σ net charges are negative for nitrogen and positive for boron. Taken together, the calculations confirm the canonical view of the B-N bond; the σ-bond is

polarized toward the electronegative nitrogen, whereas *some* π-electron density is donated by nitrogen into boron's vacant p-orbital.

Michl has used semi-empirical calculations to determine the electronic features of **1**.[41] Excited singlet transitions were found at wavelengths of 171, 184, 217, and 272 nm. The longest wavelength calculated absorption at 272 nm was red-shifted relative to benzene's lowest energy absorption (260 nm), however no experimental data was available for **1**. The ionization potential of **1** was calculated to be 8.40 eV, which was somewhat lower than benzene (9.23 eV). The π-electron densities at boron and nitrogen were calculated to be 0.462 and 1.470 electrons, respectively, indicating a significant degree of π-overlap in **1**. The bond order of the B-N π-bond was calculated to be 0.562 versus a value of 0.667 for the corresponding C-C π-bond in benzene.

Massey and Zoellner used an improved MNDO (modified neglect of diatomic overlap) method to calculate electronic, thermochemical, and structural parameters of **1** (summarized in Table 6).[42] The heat of formation for **1** was calculated to be -8.147 kcal/mol whereas corresponding values for benzene and borazine were +21.20 and -131.10 kcal/mol, respectively. The ionization potential of **1** (9.001 eV) was calculated to be lower than both benzene (9.392 eV) and borazine (10.957 eV). The dipole moment was also calculated for **1** (2.046 D) and indicated **1** is more polarized than benzene and borazine, both of which had negligible dipole moments. Molecular orbitals calculated using MNDO for benzene, borazine, and **1** are presented in Figure 3.

Table 6. Electronic and Structural Parameters of **1** by MNDO

ΔH_f (kcal/mol)	Ionization potential (eV)	Dipole moment (debye)	*d*(C-C) (Å)	*d*(N-B) (Å)	*d*(N-C) (Å)	*d*(B-C) (Å)
-8.147	9.001	2.046	1.3765(5)[a] 1.4404[b]	1.4191	1.3958	1.5033

[a] Average of *d*(C3-C4) and *d*(C5-C6).
[b] Bond *d*(C4-C5).

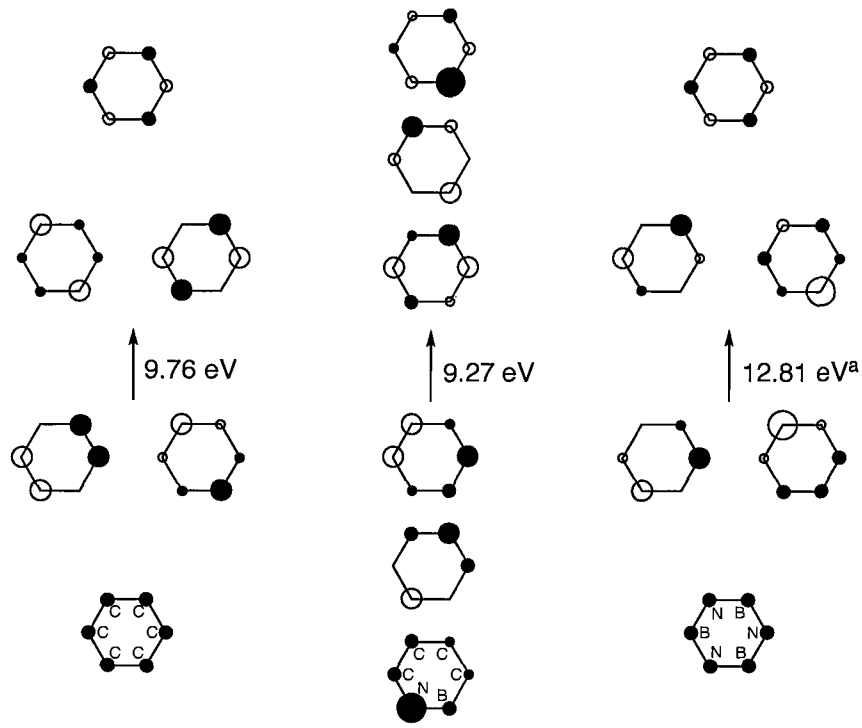

Figure 3. The π-molecular orbitals for benzene (left), borazine (right), and 1,2-Dihydro-1,2-azaborine **1** (middle). HOMO-LUMO energies (in eV) are designated by the arrows. [a]HOMO-LUMO transition for borazine is reported to be $\pi \rightarrow \sigma^*$.

Kranz and Clark performed the first high level ab initio calculations on 1,2-dihydro-1,2-azaborine **1**.[43] The geometric parameters of **1** were optimized using several methods (AM1, 6-31G*, MP2/6-31G*), which correlated well to the MNDO method. The delocalization energy of **1**, benzene, and borazine were calculated using several reaction strategies (Table 7). First, each bond constituting **1**, benzene, and borazine was

broken into its fundamental bond fragment (the C=C bonds into ethylene, the B-N bond into amine-borane, etc.), and the energy of these constituent parts was compared to the parent ring. The apparent delocalization energy was the difference in these energies. In method A, the delocalization energy for **1** was found to be less than benzene by approximately 23 kcal/mol, but significantly greater than borazine, which was actually calculated to have a negative stabilization energy compared to the sum of its parts. Method B corrects for the stabilization energy of the butadiene fragment by keeping this unit intact in the thermochemical reaction. Again, the difference in resonance stabilization energy between benzene and **1** was 23 kcal/mol. The large value obtained by method C reflected the large stabilizing effect the heteroatoms have on each other.

Table 7. Thermochemical Reactions and Energies (in kcal/mol) at RHF/6-31G* (and MP2/6-31G*)

(A)	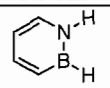 + 4 CH_4 + NH_3 + BH_3 ⟶ 2 CH_2=CH_2 + CH_3-CH_3 + CH_3-NH_2 + CH_3-BH_2 + NH_2-BH_2	+34.8 (+47.9)
	 + 6 CH_4 ⟶ 3 CH_2=CH_2 + 3 CH_3-CH_3	+58.2 (+72.0)
	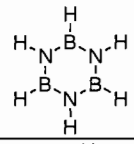 3 NH_3 + 3 BH_3 ⟶ 6 NH_2-BH_2	- 38.0
(B)	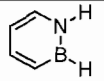 + 2 CH_4 + NH_3 + BH_3 ⟶  + CH_3-NH_2 + CH_3-BH_2 + NH_2-BH_2	+ 27.5
	 + 4 CH_4 ⟶  + CH_2=CH_2 + 2 CH_3-CH_3	+ 50.9
(C)	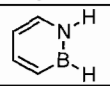 ⟶ 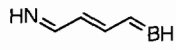	+ 88.1

Kranz and Clark also calculated the expected ^{13}C and ^{11}B chemical shifts for **1** using the IGLO method using DZ and II' basis sets (Figure 4). Though there was no experimental data available for comparison, the calculated and experimental values for other heterocycles were in good agreement.

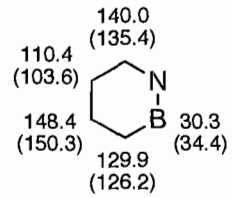

Figure 4. ^{13}C and ^{11}B chemical shifts for **1** calculated via IGLO DZ and IGLO II' ( ). N- and B-bonded hydrogen atoms omitted for clarity.

Del Bene and co-workers used calculated hydrogenation enthalpies as a measure of the resonance energy in 1,2-azaborine.[44] The hydrogenation enthalpy of **1** was calculated to be 23 kcal/mol. The corresponding resonance enthalpy of benzene was calculated as the difference between the hydrogenation of benzene and 3 molecules of cyclohexene. In this way a value of 48 kcal/mol was obtained for benzene. Matus et al. reported detailed computations on the dehydrogenation of cyclic aminoborane **59** to 1,2-dihydro-1,2-azaborine **1** (Figure 5).[45] The energies of intermediates resulting from the stepwise loss of H_2 indicated that dehydrogenation from the B-N bond was the most thermodynamically favorable. The change in hybridization in the B-N σ bond (sp^3-sp^3 to sp^2-sp^2) was favored by 85 kcal/mol while the corresponding hybridization change in the C-C bond was only favored by 15 kcal/mol. This is explained by the fact that the σ(sp^3-sp^3) B-N bond is a dative bond whereas the C-C bond is a normal σ bond.

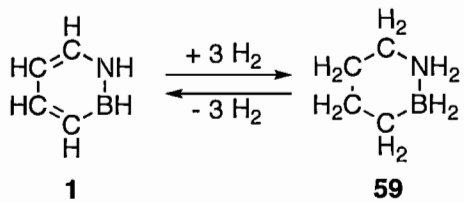

1 **59**

Figure 5. Dehydrogenation/hydrogenation of 1,2-dihydro-1,2-azaborine.

Silva and Ramos have recently reported a computational study on the reactivity of 1,2-azaborine toward various electrophiles.[46] The nitration of 1,2-azaborine via EAS

was calculated to be more energetically favorable than benzene and occurred selectively at the C3 position (via Wheland intermediate **60** in Scheme 26). In the case of B-H 1,2-azaborines, intermediate **61** was lower in energy than **60**. Rearomatization via the loss of H^+ from C3 resulted in the formation of nitrated 1,2-azaborine **62**. Calculations indicated that 1,2-azaborine **63** was 26-28 kcal/mol more stable than **62**, however the formation of nitrite-substituted 1,2-azaborine **63** would require the loss of H^+ from the boron position. It is unclear whether this is likely given the hydridic nature of the B-H hydrogen. The electrophilic chlorination of 1,2-azaborine, which has yet to be explored experimentally, predicted a similar bridged intermediate (**64** in Figure 6), which led to the favored formation of B-Cl 1,2-azaborines over C3 substitution.

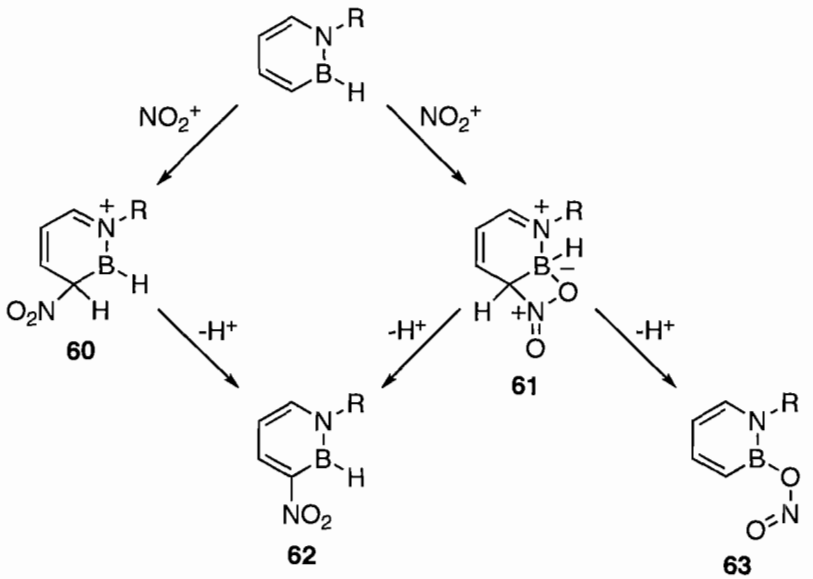

Scheme 26. Proposed reaction pathways in the nitration of 1,2-azaborine at C3.

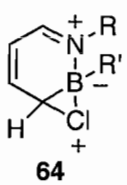

Figure 6. Bridged chloronium **64** as an intermediate in the chlorination of 1,2-azaborine.

Contrary to Ashe's experimental observations, the acylation of 1,2-azaborine was calculated to occur selectively at the C3 position over C5. Also counter to experiment were the calculations that suggested Mannich-type reactivity should occur primarily at the C3 position (favored by ~ 2 kcal/mol over C5 substitution).

Interest in BN-doped materials for H_2 storage has led Sagara and Ganz to examine the theoretical aspects of non-covalent H_2 binding with BN heterocycles including 1,2-azaborine **65** (Figure 7).[47] Dicarboxylate **65** was used as a model for a metal-organic framework (MOF) containing the 1,2-azaborine fragment. The energetic stability of H_2 physisorbed to the face of the 1,2-azaborine ring was calculated to be approximately 1 kcal/mol, and it was concluded that MOFs containing 1,2-azaborine would not be suitable for H_2 storage applications. However, Dunietz and co-workers provided a direct comparison between the H_2 adsorption energies of benzene and **1**.[48] Face- and edge-site adsorption geometries were optimized (Figure 8), and the energies are presented in Table 8. The energies of successive face-site (f) and edge-site (e) adsorption indicated in all cases that adsorption to **1** was more favorable than benzene. 1,2-Azaborine incorporation into MOFs may in fact be a feasible strategy for storing H_2.

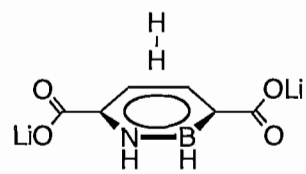

65

Figure 7. Physisorption of H_2 with MOF model compound **65**.

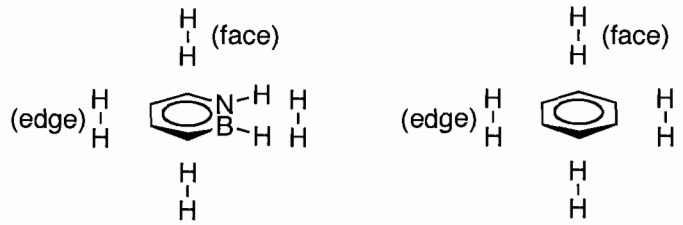

Figure 8. Face- and edge-site adsorption of H_2 with **1** (left) and benzene (right).

Table 8. Adsorption Energies for Successive H_2 Loading in benzene and **1**

	Adsorption energies (kcal/mol)	
Site occupation	C_6H_6	C_4BNH_6
1 (f)	-3.51	-3.60
2 (f, f)	-7.41	-7.44
3 (f, f, e)	-8.67	-9.61
4 (f, f, e, e)	-9.99	-10.81

Fazen and Burke have performed a theoretical study of BN-benzyne **66** (IUPAC: 1,2-azaborine), in which boron and nitrogen are divalent and form a B≡N bond (Figure 9).[49] The optimized geometry of **66** in its ground-state provided a B≡N bond length of 1.311 Å, indicating significant triple-bond character. Nucleus-independent chemical shift (NICS) calculations provided an indication of aromatic character in **66** (NICS(0) = -10.4, NICS(1) = -9.3), however these values are less negative than for benzyne (NICS(0) = -17.8, NICS(1) = -12.5), indicating BN-benzyne **66** is less aromatic than benzyne.

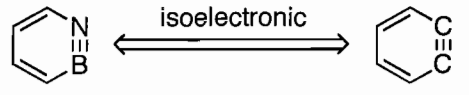

66
BN-benzyne
(1,2-azaborine)

benzyne

Figure 9. BN-Benzyne **66** (1,2-azaborine) is isoelectronic with benzyne.

Gilbert has calculated ring strain energies for several CBN heterocycles, including fully hydrogenated **59**,[50] which is isoelectronic with cyclohexane. It was

determined that the ring strain energy of **59** was actually lower than cyclohexane by 0.9-2.4 kcal/mol, whereas larger or smaller rings have an increased ring strain versus their carbon analogs. It is unclear whether the reaction schemes that were used provided an accurate assessment of the ring strain. The effect of B-N substitution on ring strain was later calculated for cycloiminoborane **67** (Figure 10) and was found to be over 10 kcal/mol less than the corresponding carbon cycloalkyne.[51]

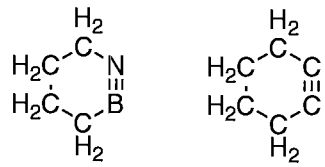

67 31.5 41.2

Figure 10. Ring strain energies, in kcal/mol, for cycloiminoborane **67** and its carbon analog.

Gilbert has also performed high-level calculations on the pericyclic reactions of amino- and imino-boranes.[52-55] In the transition state of the reaction of dimethylaminobis(trifluoromethyl)borane **16** with butadiene, the formation of the B-C bond occurred due to the coordination of the Lewis-acidic boron atom with the carbon π system (**68ts** in Figure 11). The elongation of the N-C bond in the transition state was ascribed to the repulsion between the carbon π system and nitrogen's lone-pair. The elongation of the B-N bond from the transition state to adduct **68** is consistent with the disruption of the B-N π system in **16**, leaving only a dative B-N σ bond in **68**.

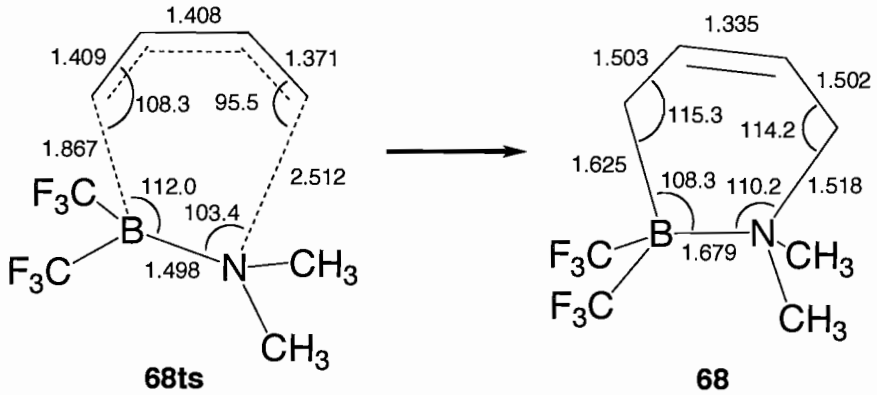

Figure 11. Representation of the optimized structures (B3LYP/6-31G*) of the transition state for the Diels-Alder reaction of **16** and butadiene (**68ts**, left), and product **68** (right).

Gilbert was also interested in the regioselectivity of amine-borane cycloaddition reactions. The original report by Bürger and co-workers[18] described the formation of heterocycle **69** regioselectively from **16** and *cis*-2-methyl-1,3-butadiene (Scheme 27). Regioisomer **70** was not observed in the reaction. The calculated transition state energy for the formation of regioisomer **69** was shown to be about 3 kcal/mol lower in energy than the transition state leading to **70**.[53] The regioselectivity was attributed to the slightly larger negative charge at C1 over C4 in *cis*-2-methyl-1,3-butadiene, which directed the formation of the B-C1 bond in **69**. Bissett and Gilbert described the feasibility of ene-type reactions of imineboranes versus [2+2] dimerization (Scheme 28).[54] They provided strong evidence that the dimerization of cyclic iminoborane **71** to **72** required overcoming very high energy barriers, whereas **71** could readily undergo an ene-type reaction with propyne to generate B-allenyl amine-borane **72a**. However, ene-type reactions of iminoboranes have not been shown experimentally. Diels-Alder cycloaddition reactions of iminoboranes were also predicted to occur readily in a regiospecific manner.[55]

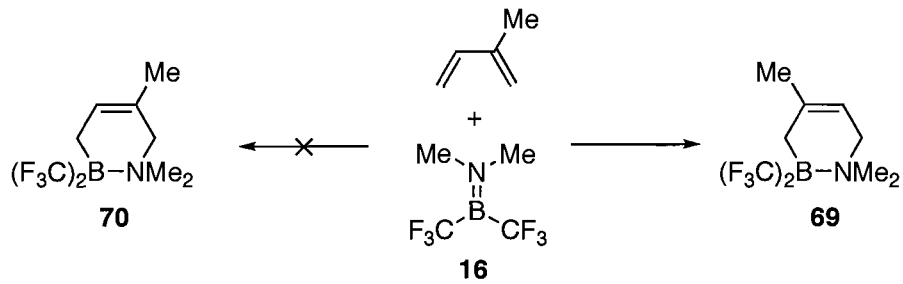

Scheme 27. Regioselectivity in the [4+2] cycloaddition of **16**.

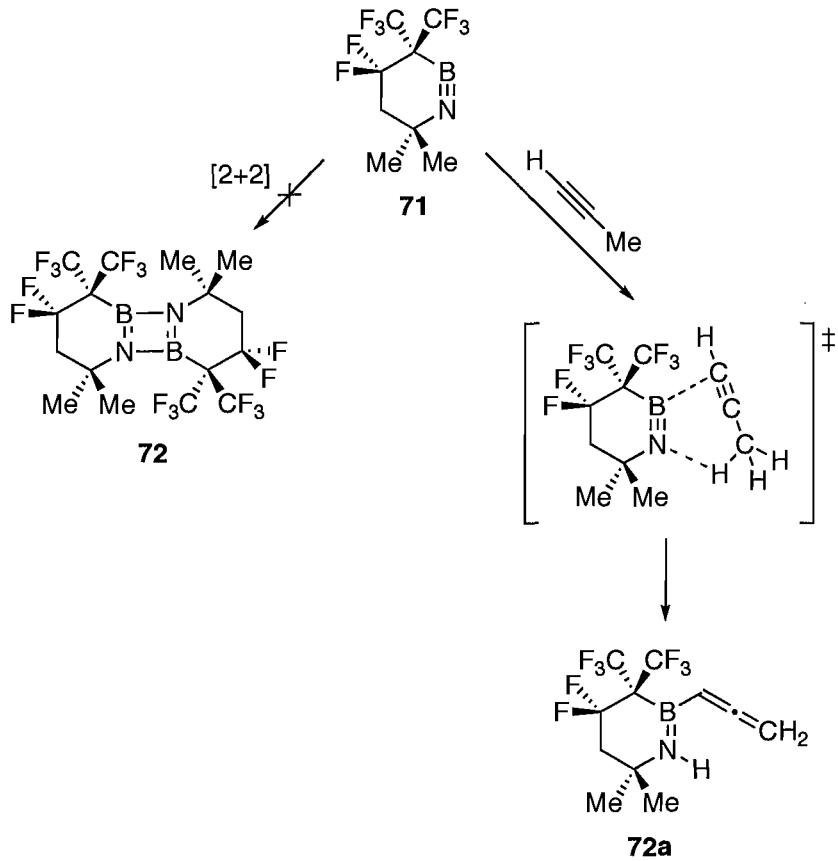

Scheme 28. [2+2] and [4+2] reactivity of **71**.

1.2.3. Bicyclic [4.4.0] C_4BN Derivatives

The study of BN/CC isosterism in aromatic systems has been extended to derivatives of naphthalene. The substitution of a C-C unit in naphthalene for a B-N bond pair leads to several isomers of BN-naphthalene (Figure 12).

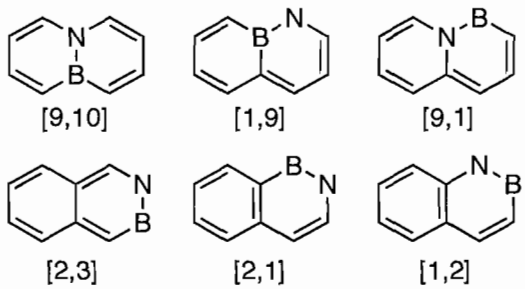

Figure 12. All 6 isomers of BN-naphthalene (N- and B-bonded H atoms omitted, where appropriate) with [N,B] substitution labels.

The first BN-naphthalene (hereafter referred to as azaboronaphthalene) was synthesized by Dewar and co-workers in 1959 (**73** in Scheme 29).[56] The reaction of 2-aminostyrene with phenylboron dichloride led to the direct formation of 2-phenyl-1,2-azabornaphthalene **73**. Alternatively, the reaction of 2-aminostyrene with BCl_3 led to the formation of 2-chloro-1,2-azabornaphthalene **74**. The hydrolysis of **74** occurred readily, from which B-O-B ether **75** was isolated. Reaction of **74** with PhMgBr provided another route to **73**. Addition of MeMgI to **74** gave alkyl-substituted BN-naphthalene **76**. Parent BN-naphthalene **77** was produced in the reaction of **74** with $LiAlH_4$. The UV-Vis absorption spectra of **77** and naphthalene indicated that BN-naphthalene was electronically similar to its carbon analog. The technical difficulties in working with air-sensitive 2-chloro-1,2-azabornaphthalene **74** were overcome when it was determined that Grignard and hydride substitutions were feasible from anhydride **75**.[57] This was a more practical synthetic approach, as B-O-B ether **75** was much easier to handle than the B-Cl precursor.

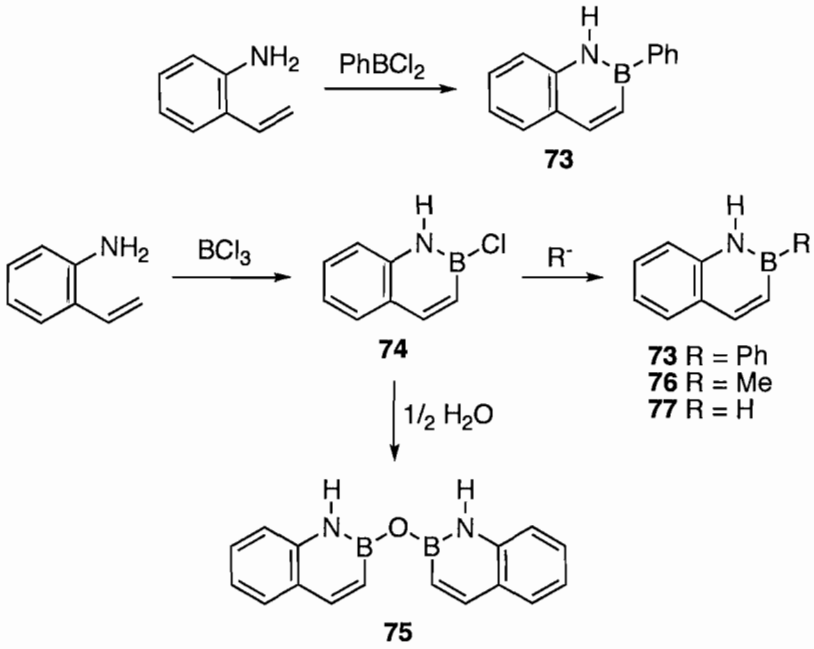

Scheme 29. Synthesis of B-substituted 1,2-azaboronaphthalenes.

BN-Naphthalene **73** was unreactive toward strong base and $KMnO_4$, which signified a high degree of resonance stabilization. Further evidence of resonance stabilization in BN-naphthalene was provided via the comparative reactivity of partially reduced heterocycle **77**, which reacted immediately with acid or base to give ring-opened **78** (Scheme 30).[58] In contrast, BN-naphthalene **79** was completely stable to hydrolysis, even upon heating.

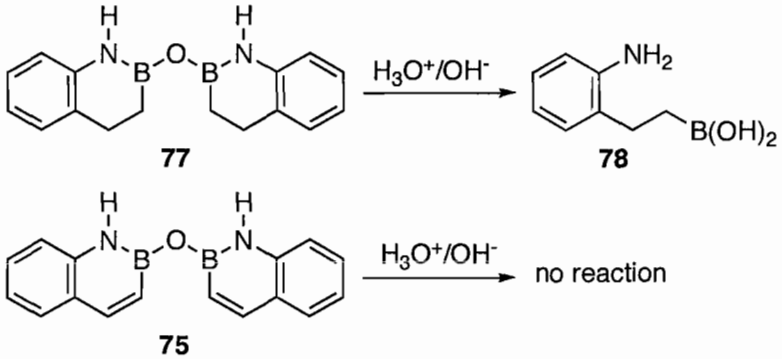

Scheme 30. Comparison of hydrolytic stability of BN-naphthalene **75** versus reduced anhydride **77**.

Dewar and co-workers also reported the first electrophilic aromatic substitution reactions on BN-naphthalene (Scheme 31).[59] The halogenation of 1,2-azabornaphthalene **76** with Cl_2 and Br_2 produced C3-substituted products **80** (X = Cl) and **81** (X = Br), respectively. The structural assignments of **80** and **81** were confirmed by an independent synthesis of these compounds. It is of note that the substitution occurred at the carbon alpha to boron as in the halogenation of monocyclic 1,2-azaborine. Unlike the EAS of the monocycle, however, the halogenated BN-naphthalenes were obtained as mixtures with ring-opened side-products **82** (X = Cl) and **83** (X = Br). The observation of degradation products was likely due to the use of acetic acid as the solvent in these reactions rather than instability of BN-naphthalene toward EAS reactions.

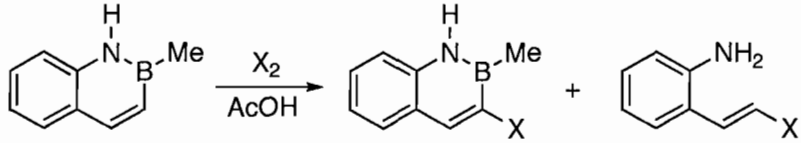

76 **80** X = Cl, **81** X = Br **82** X = Cl, **83** X = Br

Scheme 31. EAS reactivity of BN-naphthalene **76**.

The aqueous stability of 1,2-azabornaphthalenes made them attractive targets for the biological incorporation of boron (e. g. for cancer treatment using boron neutron capture therapy). However, 1,2-azabornaphthalene was found to be water-insoluble, limiting its use in biological systems. Dewar and co-workers were able to improve the solubility of 1,2-azabornaphthalenes via the functionalization of **76** at nitrogen (Scheme 32).[60] Deprotonation of **76** with MeLi gave N-lithio derivative **84**. Nucleophilic substitution with 1-bromo-3-chloropropane readily produced N-alkylated **85**. Water-

soluble amine groups were then installed via substitution at the chlorine position of **85** to give derivatives **86-89**. The reaction of **85** with KCN provided BN-naphthalene **90**. Alternatively, the formation of carbamate **91** was achieved via the addition of **84** to ethyl chloroformate.

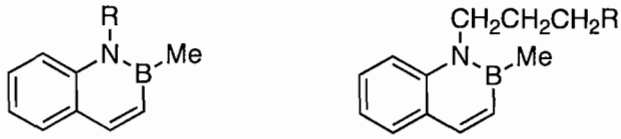

76 R = H
84 R = Li
85 R = $CH_2CH_2CH_2Cl$
91 R = CO_2Et

86 R = NMe_2
87 R = NEt_2
88 R = piperidino
89 R = morpholino
90 R = CN

Scheme 32. Synthesis of water-soluble BN-naphthalenes.

Dewar and co-workers synthesized the [9,10] isomer of BN-naphthalene (**92** in Scheme 33).[61] Treatment of di-3-butenylamine with trimethylamine borane led to the formation of bicycle **93**. Oxidation of **93** with Pd/C at high temperature led to the formation of **92**, which was characterized by ^1H and ^{11}B NMR spectroscopy and mass spectrometry. Interestingly, bridgehead-substituted BN-naphthalene **92** had the same odor as naphthalene, which was a qualitative yet astounding testament to the chemical similarity between B-N heterocycles and their all-carbon analogs.

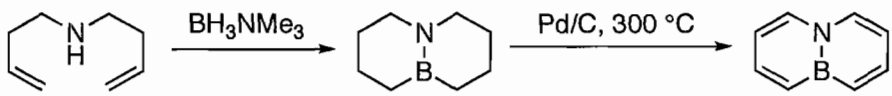

93 **92**

Scheme 33. Synthesis of bridgehead BN-naphthalene **92**.

Improvements in the synthesis of **93** were achieved by replacing BH_3NMe_3 with B_2H_6, which also permitted the characterization of BN-naphthalene precursor **94** by infrared spectroscopy (Scheme 34).[62] Reduced bicycle **94** is formally isoelectronic with

decalin, however unlike decalin, **94** readily releases H_2 to give **93** when warmed. BN-Hydroxydecalin **95** was also synthesized from the addition of H_2O across the B-N bond in **93**, whereas BN-naphthalene **92** was stable in aqueous media. A comparison of the ^{11}B NMR chemical shifts of **92** and **93** were used as further evidence of electron delocalization in BN-naphthalene.[63] The ^{11}B chemical shift of **92** (δ 28 ppm) was upfield relative to **93** (δ 43 ppm), and this shift was attributed in part to the shielding effect of electron delocalization in **92**. The ^{11}B NMR spectrum of bridgehead-substituted **92** also showed a marked upfield shift versus [1,2]-substituted derivatives such as **76** (δ 37.5 ppm), indicating substantial shielding of the boron atom in the bridgehead position.[64] Dewar and co-workers also performed photoelectron spectroscopy on **92**, which revealed the first ionization potential (ionization energy) of 9,10-azabornaphthalene **92** was 8.24 eV,[65] virtually identical to the value predicted in calculations by Michl (8.27 eV).

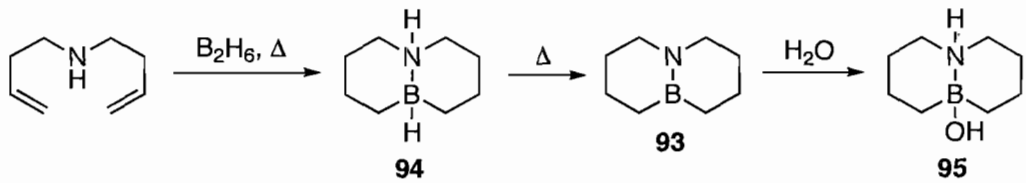

94 **93** **95**

Scheme 34. Synthesis of BN-decalin **94** and hydrate **95**.

The EAS reactivity of **92** was demonstrated via H/D exchange to occur at the carbons alpha to boron.[62] Dewar and co-workers therefore sought to synthesize the 10,11-azaborphenalenium cation **94** via substitution at the alpha carbons of **92**.[66] The reaction of **92** with malonaldehyde bis-diethylacetal and CF_3CO_2H led to the formation of an intense purple solution attributed to the formation of **94** (characterized by ^1H NMR

spectroscopy and mass spectrometry) that was stable at -78 °C but decomposed at higher temperatures (Scheme 35). The ^{1}H NMR spectrum of the BN-phenalenium cation was similar to that of its carbon analog.

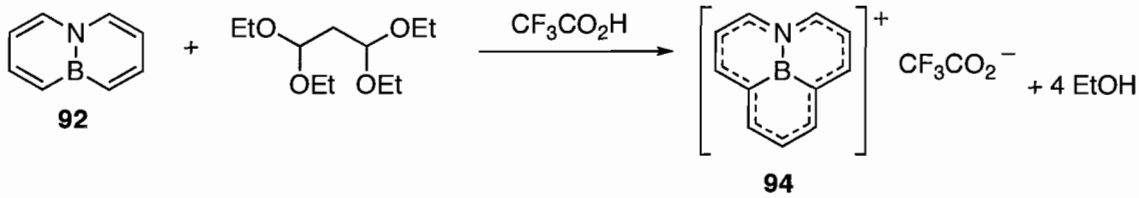

Scheme 35. Formation of BN-phenalenium cation **94** from BN-naphthalene **92**.

Paetzold et al. explored an alternate route to the 1,2-azabornaphthalene motif via the cyclization of an iminoborane and an alkyne (Scheme 36).[67] Highly reactive iminoborane **95** was formed in situ and reacted with phenylacetylene to give 1,2-azabornaphthalene **96** rather than the [2+2] cyclized product **97**. Meller et al. also used this route to install functionality at several positions on the BN-heterocycle.[68] Years later, an alternate mechanism for the formation of **96** was postulated to occur via chloroboration and alkynylation of the ortho-position of the aniline ring.[69] The reaction of chloroborane **98** with phenylacetylene gave BN-naphthalene **99** incorporating the labile B-Cl motif (Scheme 37). Substitution at boron with an alkyl Grignard gave alkylated BN-naphthalene **100**, which readily reacted with $(MeCN)_3Cr(CO)_3$ to form the first piano-stool complex of BN-naphthalene (**101** in Scheme 37). The complexation of chromium occurs at the benzenoid ring rather than the 1,2-azaborine ring, in contrast to boratanaphthalene derivatives which have been shown to preferentially complex chromium at the heteroaromatic ring.[70]

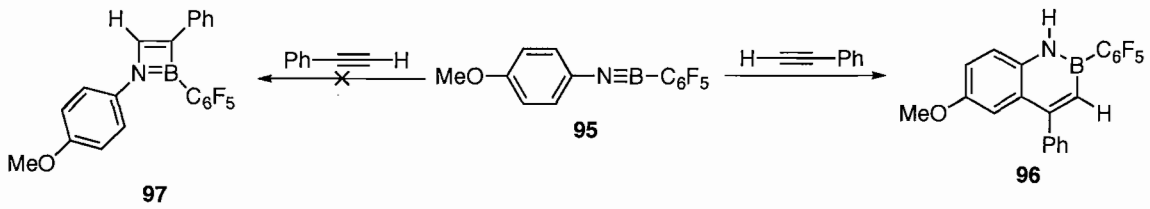

Scheme 36. Cyclization to BN-naphthalene **96** versus [2+2] cyclization.

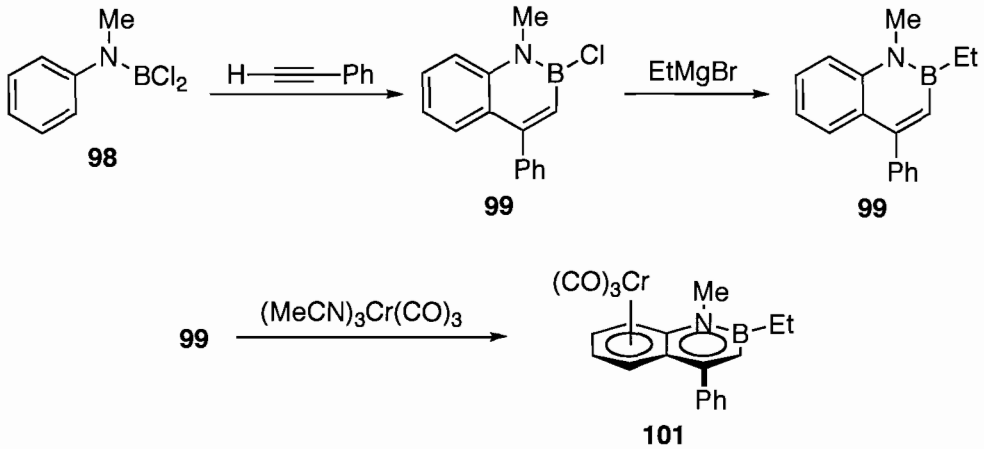

Scheme 37. Formation of BN-naphthalene piano-stool complex **101**.

Ashe and co-workers recently investigated the haptotropic migration of B-phenyl 1,2-azabornaphthalene **102** in $Cr(CO)_3$ piano-stool complexes.[71] The synthesis of **102** (Scheme 38) was achieved via the substitution of PhMgBr at the B-Cl position of previously synthesized BN-naphthalene **74**. The complexation of **102** with $Cr(CO)_3$ was envisioned to occur at the benzenoid, 1,2-azaborine, or even the boron-substituted phenyl ring. In fact, the complexation to the benzenoid ring (**103** in Scheme 38) was observed under mild heating, which was in agreement with the observations made by Paetzold and co-workers discussed above. At higher temperatures, however, a shift of chromium complexation to the boron-substituted phenyl ring (**104** in Scheme 38) occurred with no evidence for the formation of complex **105**. In fact, even when **104** was deprotonated with LiTMP to give complex **106**, no haptotropic migration to **107**

was observed and instead complex **106** was prone to thermal degradation. These data indicate that the heterocyclic ring of BN-naphthalene is a poor ligand for transition metals relative to the monocyclic 1,2-azaborine.

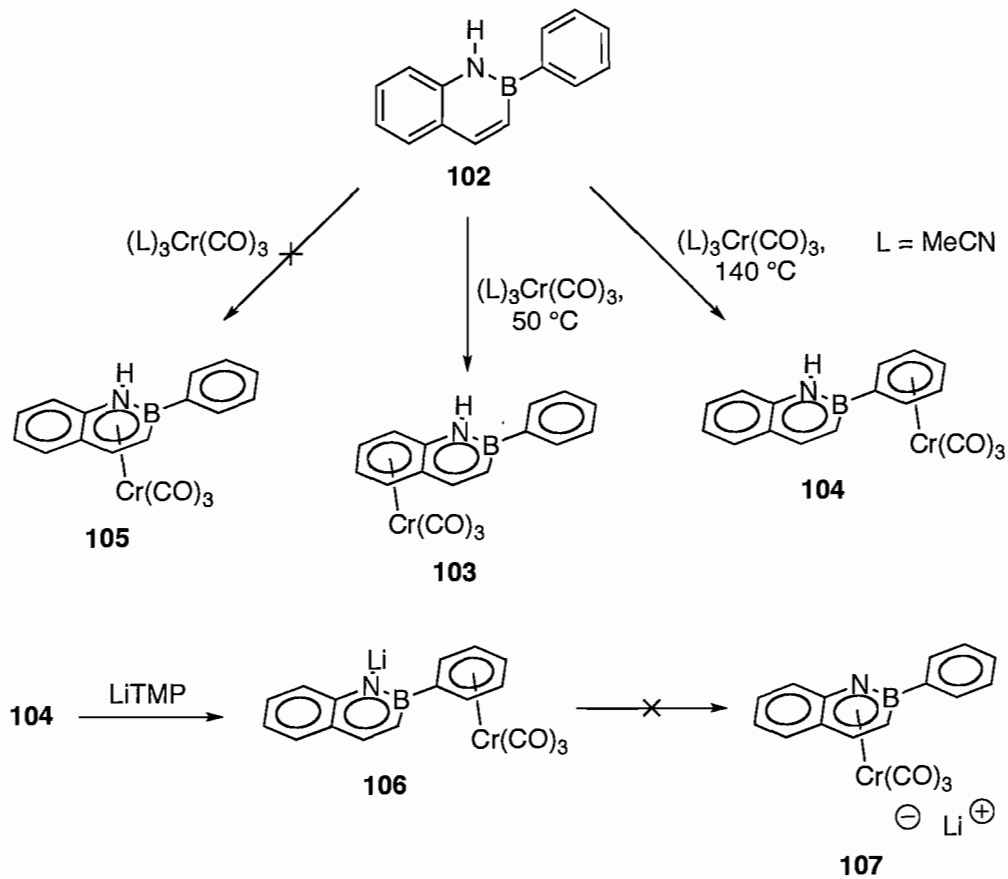

Scheme 38. Haptotropic migration in B-phenyl 1,2-azabornaphthalene **102**.

Ashe and co-workers strategized that removal of the competitive B-phenyl binding site would allow for the binding of transition metals to the heterocyclic fragment of BN-naphthalene. To that end, B-methyl 1,2-azabornaphthalene **76** was reacted with $(MeCN)_3Cr(CO)_3$ to give complex **108** (Scheme 39). Though no complexation to the heterocyclic fragment was observed, deprotonation of **108** with potassium hexamethyldisilazide provided **109**, which increased the electron-richness of the 1,2-

azaborine heterocycle. Upon heating, complex **109** underwent a haptotropic migration to afford the desired complex **110** in which chromium was bound in an η^6-fashion to the heterocyclic ring. Methylation of **110** presumably led to complex **111**, however the coordination of the neutral heterocyclic fragment was so tenuous that decomplexation to free BN-naphthalene **112** occurred at room temperature.

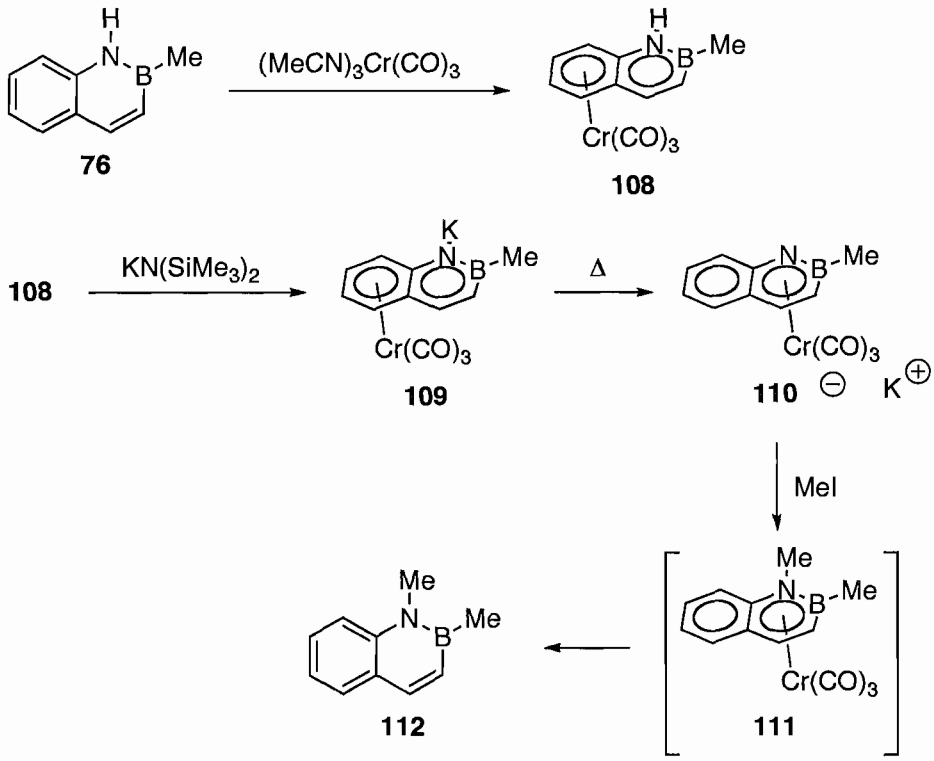

Scheme 39. Haptotropic migration in B-methyl 1,2-azaboronaphthalene.

Alternative syntheses of 1,2- and 9,10-substituted derivatives have recently been reported. In 2006, Ashe and co-workers used a ring-expansion from bridehead-substituted BN-indene **113** to generate 9,10-azabornaphthalene **92** (via **114** in Scheme 40),[72] in analogy to the ring-expansion of 1,2-azaborolides discussed in section 1.2.1. The chemistry of BN-indenes will be discussed below. Murakami and co-workers prepared anilinium borate **115** and found that Pd-catalyzed ring-closure gave bicycle **116**

in good yield (Scheme 41).[73] The B-N bond in **116** is a dative σ-interaction and thus **116** is not formally isoelectronic with naphthalene. In a crossover experiment, Murakami and co-workers determined that aryl migration to the 3-position occurs intramolecularly from the borate.

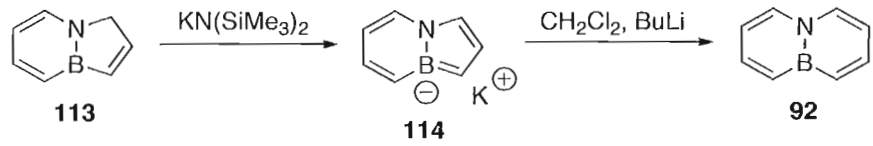

Scheme 40. Ring-expansion of BN-indene to BN-naphthalene **92**.

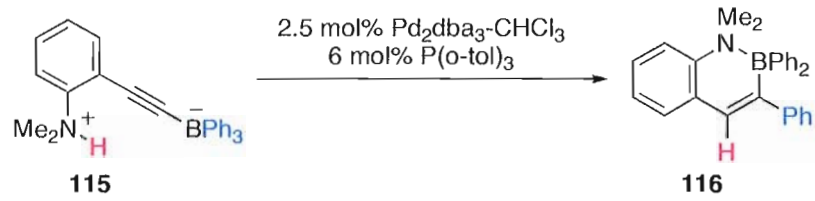

Scheme 41. Pd-catalyzed ring-closure to bicycle **116**.

Additional [4.4.0] bicycles containing the B-N bond pair have been prepared. Butler and co-workers prepared bridgehead-substituted BN-decalin derivatives via Dewar's established route.[74] The first example of 2,1-substitution in [4.4.0] BN-heterocycles was achieved by Catlin and Snyder in 1968 via the hydrolysis of nitrile **117** to bicycle **118** (Scheme 42).[75] Reduction with $LiAlH_4$ produced 2,1-substituted **119**. Alternatively, the direct formation of **119** resulted from the reduction of **117** with $LiAlH_4$.[76] Köster et al. synthesized derivatives of **119** a year later through the arylation of aminoboranes at extreme temperatures.[77]

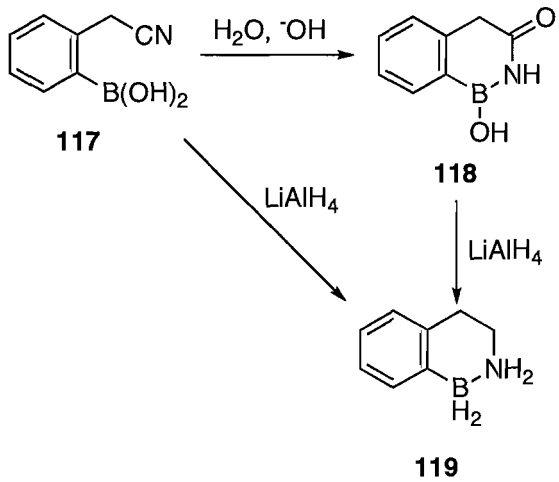

117 **118** **119**

Scheme 42. 2,1-Substituted BN-heterocycles synthesized from ortho-boronic acid **117**.

Vedejs and co-workers described the synthesis of a reduced analog of **119**, parent BN-decalin **120** (Scheme 43).[78] The hydroboration of amine-borane **121** to 2,1-azabordecalin **120** occurred readily when catalytic amounts of I_2 were added. No attempts to oxidize **119** or **120** to the unexplored 2,1-azabornaphthalene were described in either of these reports.

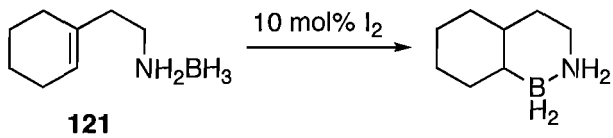

121 **120**

Scheme 43. Hydroboration of **121** to 2,1-azabordecalin **120** catalyzed by I_2.

Midland et al. have explored the use of chiral amine-boranes as enantioselective reducing agents.[79] The formation of terpenic ring-fused heterocycle **123** was accomplished via the condensation-hydroboration of aminoterpene **122** (Scheme 44). The coordination of BH_3 to the amine of enantiopure **123** formed complex **124**, which was found to provide good enantioselectivity in the reduction of acetophenone to the

corresponding alcohol. The stereochemistry of the major enantiomer in these reductions was not reported.

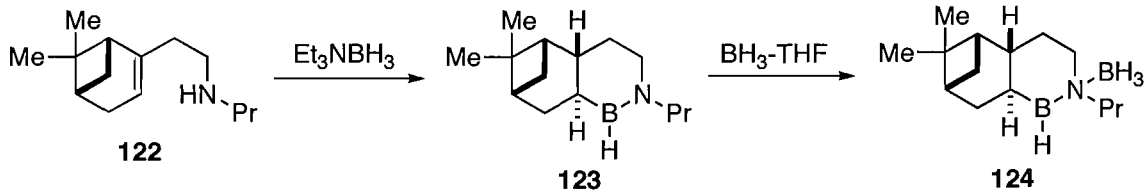

Scheme 44. Synthesis of terpenoid BN-heterocycle **124** for the stereoselective reduction of ketones.

Roberts and co-workers examined the use of chiral amine-boryl radicals for the kinetic resolution of esters via hydrogen-atom abstraction (equations 1 and 2).[80-81] Hydrogen abstraction from electron-deficient C-H bonds, such as the alpha C-H group in carbonyl compounds, occurs slowly using an electrophilic tert-butoxy radical. The addition of amine-borane complexes has been shown to catalyze this transformation through the formation of a nucleophilic boryl radical which readily abstracts the electrophilic hydrogen atom.

$$^{t}BuO^{\bullet} + \text{amine-}BH_2R \rightarrow {}^{t}BuOH + \text{amine-}\dot{B}HR \quad (1)$$

$$\text{amine-}\dot{B}HR + HCR^1R^2CO_2R^3 \rightarrow \text{amine-}BH_2R + R^1R^2\dot{C}CO_2R^3 \quad (2)$$

Bicycle **125** was found to be an effective catalyst for the selective hydrogen abstraction from the (*R*)-enantiomer of racemic lactone **126**, and was relatively unreactive toward the (*S*)-enantiomer (Scheme 45). The enriched (S)-lactone **126** was recollected via column chromatography in high enantiomeric excess.

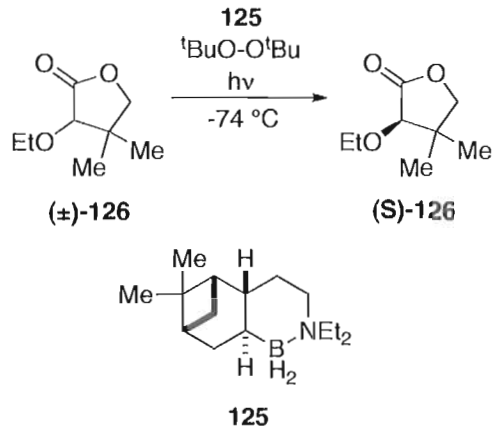

Scheme 45. Kinetic resolution of racemic lactone **126** with amine-borane **125**.

Hancock and co-workers reported the photo-induced cyclization of B-vinyl aminoborane derivatives (Scheme 46).[82] Irradiation of aminoborane **127** led to the formation of a C-C bond in the ortho-position of the aniline ring to give **128**. A mechanistic study of this cyclization revealed that the ortho-hydrogen underwent an intramolecular 1,5-shift.[83]

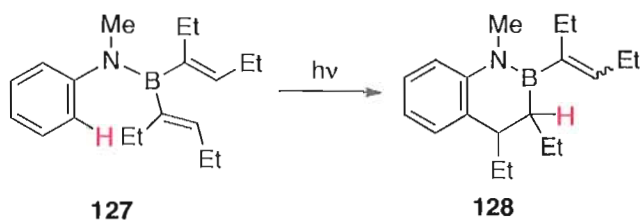

Scheme 46. Photocyclization of vinylborane **127**.

The only synthesis of a 2,3-substituted [4.4.0] BN-heterocycle was reported by Kafka et al.[84] The condensation-hydroboration of benzyl amine **129** with Et_3N-BH_3 led to a mixture of non-aromatic [4.4.0] 2,3-aminoborane **130** and [4.5.0] heterocycle **131** (Scheme 47). Though the synthesis of 2,3-azaboronaphthalene utilizing this route seems feasible, there have been no reports of its attempted synthesis.

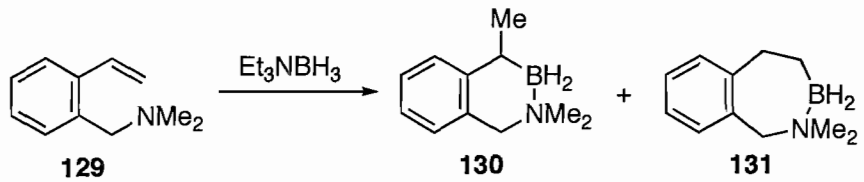

129 **130** **131**

Scheme 47. Synthesis of 2,3-substituted BN-heterocycle **130**.

Several theoretical studies of BN-naphthalene have been reported.[37,38,41,47,85-89] Michl et al. calculated the electronic features of the isomers of BN-naphthalene, which are summarized in Table 9.[41] The predicted UV-Vis absorption energies of BN-naphthalene varied for each isomer, with 9,1-azaboronaphthalene having the largest bathochromic shift at 366 nm. The BN-naphthalene isomers that have been synthesized, i.e. the 1,2- and 9,10-isomers, were calculated to have significantly highest energy absorptions. The experimentally determined absorption of 1,2-azaboronaphthalene **76** at 318 nm was in good agreement with these calculations. Similarly, the calculated absorption maximum for 9,10-azaboronaphthalene **92** was identical to the experimental value (λ_{max} = 301 nm).[85] It is of note that all BN-naphthalene derivatives were calculated to have a red-shifted absorption relative to unsubstituted naphthalene. The isomers with the greatest π-electron density at boron were 1,9- and 9-10-azaboronaphthalene, both of which have the boron atom in a bridgehead position. This may in part explain the hydrolytic stability and upfield ^{11}B NMR chemical shift of 9,10-azabornaphthalene **92**. Conversely, the B-N π-bond order was calculated to be greatest in the 1,2- and 2,1-isomers, indicating more double-bond character in the B-N bond pair for these isomers. The electronic features predicted by Michl et al. corroborated earlier work by Hammond.[86]

Table 9. Electronic Features of BN-Naphthalene Isomers

[N,B] Subst. Position	1st Singlet Transition (nm)	Ioniz. Pot. (eV)	π-electron density at boron (e⁻)	π-electron density at nitrogen (e⁻)	B-N π-bond order
None	299	8.11			
[1,2]	309	8.41	0.425	1.528	0.587
[2,1]	304	7.79	0.412	1.516	0.583
[2,3]	350	7.57	0.498	1.423	0.525
[9,10]	301	8.27	0.558	1.359	0.476
[1,9]	346	7.92	0.554	1.422	0.484
[9,1]	366	7.57	0.484	1.366	0.475

Scheiner and co-workers calculated the relative energies of the isomers of BN-naphthalene (Figure 13).[87] The most stable isomer was 2,1-azabornaphthalene, followed by the 1,9-isomer. The least stable isomer was predicted to be the 9,1-isomer. The only calculations of a synthetically available BN-naphthalene were on 9,10-azabornaphthalene **92**, which was predicted to have an intermediate stability with respect to the other isomers. Unfortunately, calculations on the other accessible isomer, 1,2-azabornaphthalene **76**, were not performed.

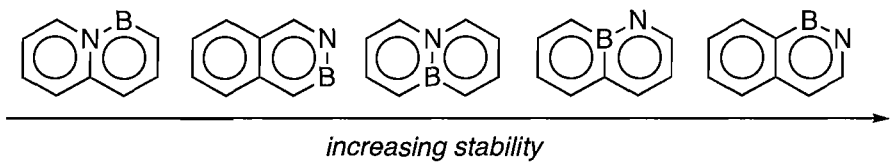

Figure 13. Relative stabilities of BN-naphthalene isomers (N- and B-bonded H atoms omitted where appropriate).

1.2.4. Additional C_4BN-Containing Bicyclic Motifs

Paetzold and co-workers extended their work (see section 1.2.3) on iminoboranes to include cyclizations with cyclopentadiene.[90-91] The reaction of aminoborane **132a** with cyclopentadiene led to the formation of a BN-substituted derivative of norbornadiene (**133a** in Scheme 48).[90] It was unclear whether this occurred via the

formation of an intermediate iminoborane **134a**, however Gilbert has performed calculations that suggest iminoborane **134a** is a precursor in the cyclization.[92] The scope of this reaction was extended to include an amino group to provide BN-norbornadiene **133b** from aminoborane **132b**.[91]

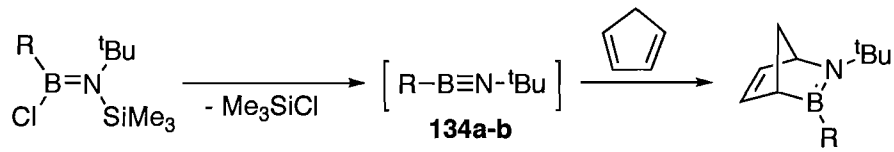

132a-b **134a-b** **133a-b**

a R = C_6F_5
b R = $N(SiMe_3)^tBu$

Scheme 48. Cyclization to BN-norbornadiene **133**.

Ashe and co-workers more recently synthesized an analog of indene substituted at the bridgehead position by the B-N bond pair (Scheme 49).[93] The formation of aminoborane **135** was accomplished in an analogous method to that used for the creation of the monocyclic derivatives discussed above. Substitution of vinyl Grignard provided **136**, which was reacted with Grubbs' 1st generation catalyst to form both the 5- and 6-membered rings of **137**. Oxidation with DDQ provided BN-indene **138**. The use of BN-indenyl as a ligand in transition-metal complexes was next examined. Deprotonation of the 5-membered ring in **138** gave anionic BN-indenyl **139** which was reacted with Cp^*ZrCl_3 to provide complex **140**. The preferred binding site for zirconium was η^5-coordination to the Cp-like ring of BN-indenyl, which was confirmed by X-ray crystallography. The heterocycle was completely planar, but the bridgehead atoms of the 5-membered ring were slightly distorted away from zirconium.

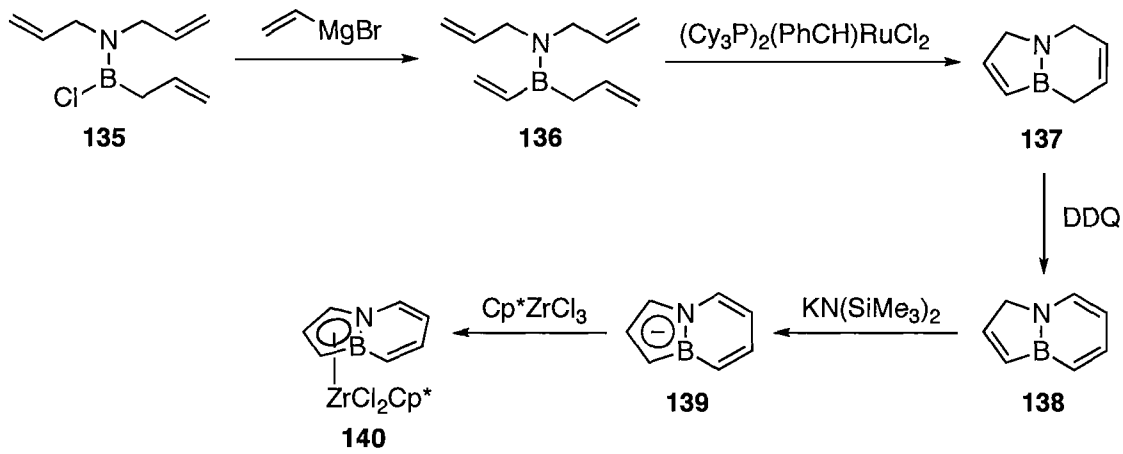

Scheme 49. Synthesis of BN-indene **138** and coordination chemistry of the BN-indenyl ligand.

The haptotropic migration of the indenyl ligand was also explored by Ashe and co-workers.[94] Complexation of neutral BN-indene **138** with chromium led to the preferential formation of η^6-complex **141** (Scheme 50). Deprotonation at low temperature gave complex **142** as evidenced by the disappearance of the allylic signals in the ^{1}H NMR spectrum. Whereas significant heating was required to force the haptotropic shift in B-phenyl 1,2-azaborines, simply warming the solution of **142** to room temperature caused a shift in chromium complexation to the anionic ring (**143** in Scheme 50). Intermediate **143** was trapped with Me_3SnCl as complex **144**, which was analyzed by X-ray crystallography. The crystallographic parameters of η^5-coordinated indenyl complexes **140** and **142** matched the geometric parameters calculated for similar complexes.[95]

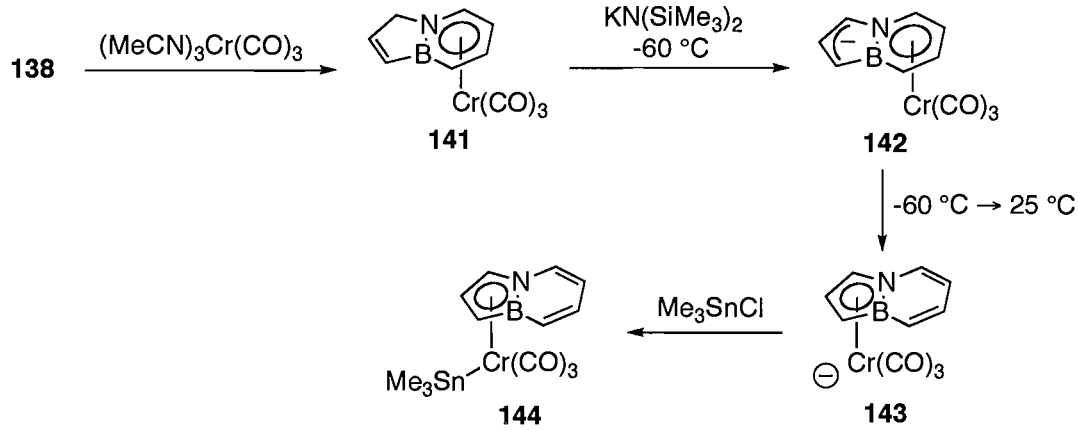

Scheme 50. Haptotropic migration of the BN-indenyl ligand.

Wrackmeyer et al. have published numerous reports on a closely related [4.3.0] bicyclic system containing a B-N bond pair.[96-98] The substitution of boron and nitrogen at the 7- and 8-positions, respectively, was achieved via the coordination of an allyl borane to a pendant N-heteroaromatic pyrrole (Scheme 51).[96] Alkoxy-substituted bicycle **145** was synthesized readily from dilithiate pyrrole **146**. Compound **146** was reacted with $B(OEt)_3$, providing 4-coordinate compound **147**. Heterocycle **147** was reacted with Me_3SiCl, which abstracted an ethoxy group from the 4-coordinate boron to give **145**. Alternatively, alkyl-substituted derivatives were prepared via transmetallation from bicyclic stannane **149**. Wrackmeyer et al. expanded the synthetic scope of the bicyclic ring formation by reacting various hydroborating reagents with 2-allylpyrrole,[97] and the reactivity of these derivatives was explored.[98] Though **145**, **149**, and subsequent derivatives can be considered tautomers of BN-indene (Figure 14), no attempt to tautomerize **150** to 1,2-azaborine-containing **151** was reported. This could be due to the large aromatic stabilization of the pyrrole unit in tautomer **150** relative to the 1,2-azaborine unit of tautomer **151**.

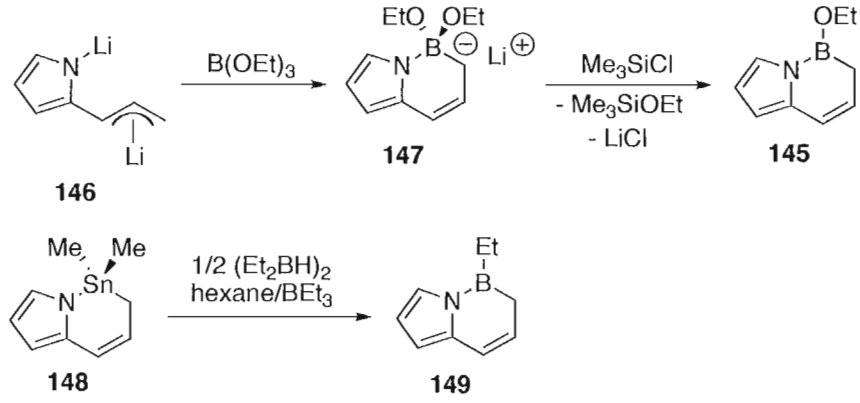

Scheme 51. Formation of 7,8-substituted BN-indene analogs.

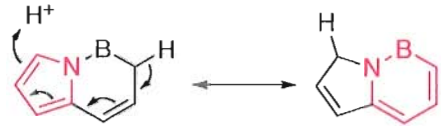

Figure 14. Tautomerism in 7,8-substituted BN-indene.

Matteson et al. achieved the synthesis of the 8,7-azaborquinazoline analog presented in Figure 15. The authors' motivation was directed toward biomedical applications, though compound **152** was determined to be inactive in standard leukemia screening.[99]

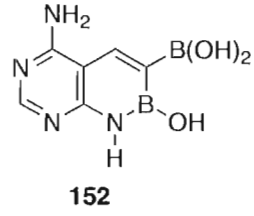

Figure 15. BN-Quinazoline **152**.

1.2.5. Tricyclic C_4BN-Containing Motifs

Tricyclic analogs of phenanthrene were among the first B-N aromatics synthesized. Dewar pioneered the synthesis of 9,10-azaborphenanthrene derivatives

over 50 years ago,[100] from which numerous studies on the properties and reactivity of BN-phenanthrene have since emerged. The early achievements in the study of BN-phenanthrene were due to its relatively simple preparation. The reaction of 2-phenylaniline with BCl_3 and $AlCl_3$ gave 9,10-azaborphenanthrene (**153** in Scheme 52), presumably through the Friedel-Crafts cyclization of intermediate **154**. The substitution of various nucleophiles at the reactive B-Cl unit of **153** allowed for the synthesis of several BN-phenanthrene derivatives. Hydrolysis of **153** gave hydroxy-substituted **154** (Scheme 52), while reaction with alkyl and aryl Grignard reagents produced the corresponding boron-substituted derivatives **155** and **156**, respectively. Addition of $LiAlH_4$ to **153** readily produced the parent BN-phenanthrene **157**. The isoelectronic relationship between BN-phenanthrene **157** and its carbon analog was explored via UV-Vis spectroscopy. The spectrum of **157** resembled very closely that of phenanthrene in the position of the main absorption bands. However, an increase in the intensity of the α-band was observed, an effect that was attributed to removing the molecular orbital degeneracy in the BN-substituted heterocycle.

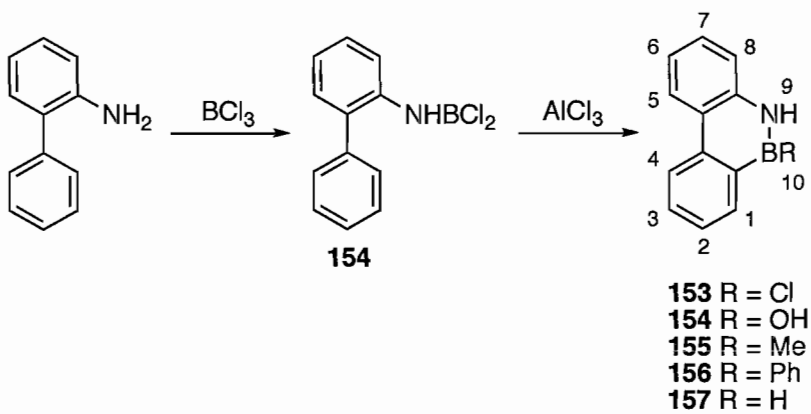

Scheme 52. Preparation of 9,10-azaborphenanthrene **153** and boron-substituted derivatives.

The reactivity of BN-phenanthrene toward EAS was successfully demonstrated, and like 1,2-azabornaphthalene and 1,2-azaborine, was found to be highly regioselective.[101] The chlorination of **155** with Cl_2 provided 8-chloro derivative **156** (Figure 16) as the major product, which was confirmed by an independent synthesis of **156**. A second chlorinated product was also observed in very small quantities and was likely 6-chloro BN-phenanthrene **157** based on a comparison of absorption spectra. The observed substitution pattern was consistent with the predicted products; the ortho- and para-directing nitrogen atom at the 9-position resulted in substitution at the 8- (ortho-) and 6- (para-) positions. Conversely, the deactivating boron substituent at the 10-position was expected to act as a meta-directing group, leading to 2-chloro derivative **158**. However, product **158** was not detected in the chlorination reaction. The nitration of **155** with nitric acid led to the formation of the 8-nitro **159** and 6-nitro **160** products in a 1 to 2 ratio, respectively. Isomer **161** was not observed. It was also determined that chlorination and bromination at both the 6- and 8-positions readily occurred at room temperature if more than 1 equivalent of halogen was added to the reaction.[102] Similarly, mono- and di-acetylated products were obtained from the Friedel-Crafts acylation of **155**, with the first acylation likely taking place at the 6-position.[103]

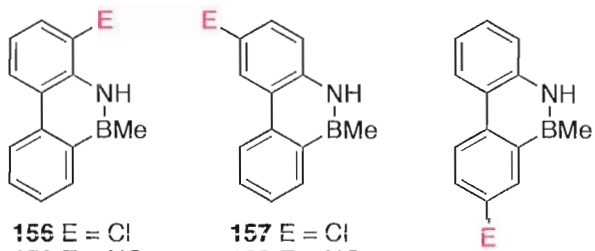

156 E = Cl
159 E = NO_2

157 E = Cl
160 E = NO_2

158 E = Cl
161 E = NO_2

Figure 16. Chlorination and nitration products of BN-phenanthrene.

Dewar et al. determined that the nitrogen position of 9,10-azaborphenanthrene could be deprotonated with butyl lithium to give N-lithio derivatives.[104] These anionic nucleophiles were then reacted with electrophiles to afford additional substitution at nitrogen. It was realized that tuning the electronics of the nitrogen substituent could have an effect on the electronics of the heterocycle as a whole. If the aromatic stability of BN-phenanthrene was in part due to the participation of the nitrogen lone-pair in the aromatic π-system, then the stability would be reduced by functional groups that interrupt the π-donation. This was examined via the installation of an acyl group at nitrogen, which was expected to reduce the ability of nitrogen to act as a π-donor.[105] The reaction of N-lithio BN-phenanthrene **162** with ethyl chloroformate gave carbamate **163** (Scheme 53). While compound **163** was reasonably stable toward hydrolysis, it rapidly oxidized when exposed to air, in sharp contrast to other derivatives that were quite air-stable. The degradation products of this oxidation showed evidence of reactivity at boron and cleavage of the B-N bond. Thus, it is probable that the aromatic stability of **163**, and in particular the B-N π-bond, was significantly disrupted by the N-acyl substituent.

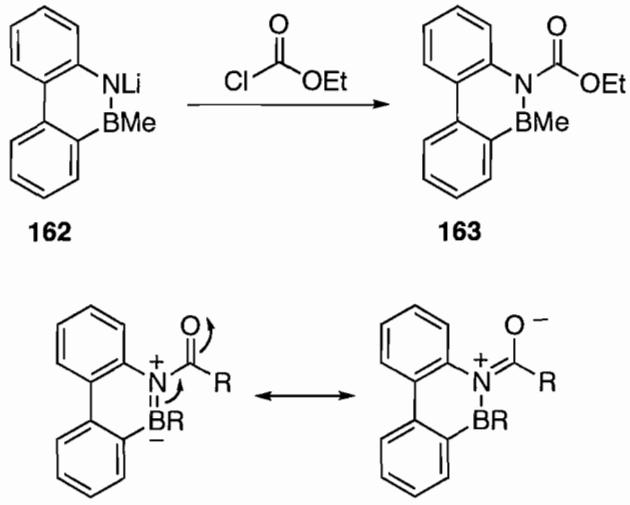

162 **163**

Scheme 53. Installation of a π-accepting group at the nitrogen of BN-phenanthrene **163**.

Subsequent studies have focused on intermolecular interactions of several derivatives of BN-phenanthrene. For example, in an attempted preparation of parent 9,10-dihydro-9,10-azaborphenanthrene **157** from 2-phenyl aniline and triethylamine-borane, Köster et al. observed the evolution of hydrogen and isolated the trimerized product **164** containing a borazine core (Figure 17).[106]

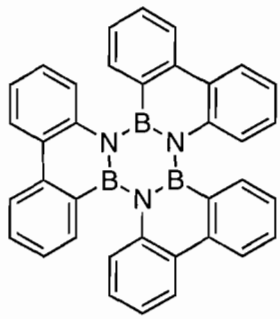

164

Figure 17. Trimerization of BN-phenanthrene with a borazine core.

Philp and co-workers recognized that the adjacent boron and nitrogen atoms in **154** could potentially act as neighboring hydrogen-bond donor and acceptor groups, leading to intermolecular interactions like those seen in dimeric complexes of benzoic

acid. In the solid-state structure of **154**, the oxygen atom bound to boron forms a hydrogen bond with the N-H group of an adjacent heterocycle to form a dimeric structure containing two hydrogen-bonds (Figure 18).[107-108] Philp and co-workers also achieved the efficient dehydration of **154** to its corresponding B-O-B ether.[107]

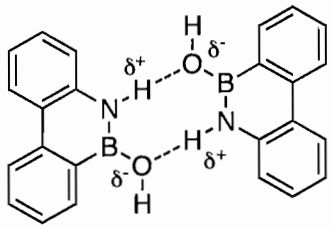

[154]$_2$

Figure 18. Hydrogen-bonding of **154** in the solid-state.

Several additional isomers of BN-phenanthrene have been reported. Dewar and co-workers achieved the ring-closure of 1,2-azabornaphthalene **165** to give bridgehead-substituted tricycle **166** (Scheme 54).[109] Oxidation to BN-phenanthrene **167** was performed with Pd/C at 300 °C. The UV-Vis spectrum of **167** closely resembled that of the 9,10-isomer. Piers and co-workers recently described the synthesis and optoelectronic properties of another BN-phenanthrene isomer, **168** in Scheme 55.[110] The reaction of 2-ethylnylpyridine with 1-chloro-2-trimethylsilyl-boracyclohexa-2,5-diene led to the formation of alkyne-substituted BN-biphenyl **169** via the elimination of Me_3SiCl. Heterocycle **169** spontaneously ring-closed to afford 4a-aza-4b-boraphenanthrene **168** containing the internalized B-N bond pair.

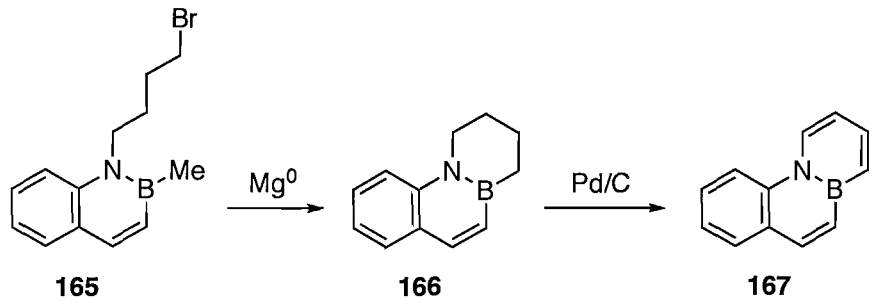

165 **166** **167**

Scheme 54. Cyclization to bridgehead-substituted BN-phenanthrene **167**.

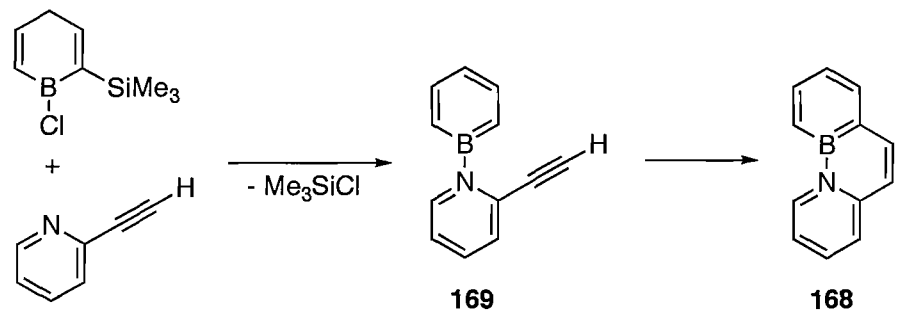

169 **168**

Scheme 55. Formation of BN-phenanthrene **168** with an internalized BN bond pair.

Piers and co-workers explored the electronic properties of internally substituted **169** in relation to the previously known isomer **157** with the B-N bond pair at the periphery. It was determined that the position of B-N substitution played a major role in the photophysical properties of BN-phenanthrene isomers, which are summarized in Table 10. The absorption and emission spectra of **157** indicated that the B-N bond pair acted mainly as a bridging group for a fluorogenic biphenyl moiety. On the other hand, the internalized B-N bond pair of **169** was found to be intimately involved in absorption-emission, leading to a drastic change in the observed spectra. Fluorescence in **169** was found to be more efficient than phenanthrene and the λ_{max} was red-shifted into the visible spectrum. The observation of blue fluorescence in **169** was an exciting result and opens the way to BN-substituted aromatics with improved properties for materials

applications. Piers and co-workers found that **169** was exceptionally stable to moisture and they demonstrated through NICS calculations that all three rings of BN-phenanthrene **169** have significant aromatic character.

Table 10. Absorption-Emission Properties of BN-Phenanthrene

	UV-Vis	Fluorescence	
Compound	λ_{max} (nm)	λ_{em} (nm)	Φ_F
157	326	327	0.61
169	446	450	0.58
phenanthrene	293	347	0.09

The same synthetic strategy was employed to create larger scaffolds containing internally-substituted BN-phenanthrenes (Scheme 56).[111] Boracycles **170** and **171** were reacted with 2 equivalents each of terminally-substituted 2-ethynylpyridines to generate the corresponding dimeric BN-phenanthrene structures **172-175**. The fluorescence in these compounds ranged from yellow to orange to green (see Scheme 56). In the case of dimer **175**, excimer formation was observed at high concentration, indicating the presence of intermolecular π-interactions in this compound.

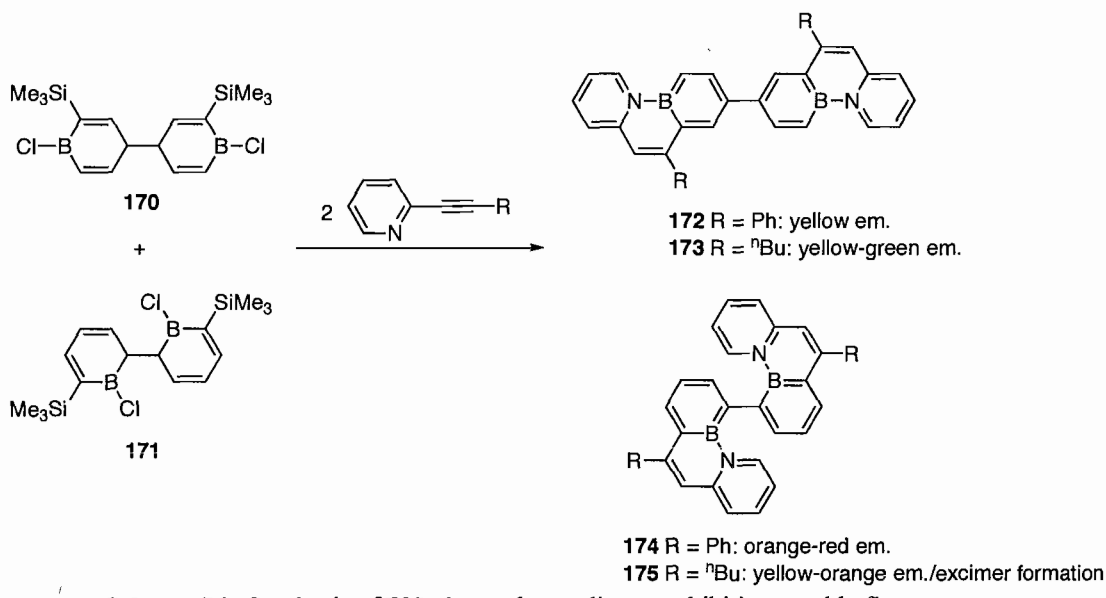

Scheme 56. Synthesis of BN-phenanthrene dimers exhibiting tunable fluorescence.

The photochemical generation of BN-phenanthrenes has been extensively studied.[112-116] Whereas in previous routes, 9,10-azaborphenanthrene was generated from a biphenylene precursor, Grisdale and co-workers determined that the intramolecular formation of a aryl-aryl bond from a diaryl aminoborane gave the same BN-phenanthrene structure (Scheme 57). The authors found that when ortho-iodoanilinoborane **176** was irradiated, the previously known BN-phenanthrene **156** was produced.[112] Grisdale et al. later demonstrated that the simple irradiation of a mixture of **177** and I_2 provided a direct route to **156**.[113] Interestingly, when the aniline group of **177** was functionalized with ortho-methyl groups, the cyclization led to the elimination of CH_4.[114] Iodine was postulated to act as an electron-acceptor which facilitated the formation of a radical-cation at the aminoborane, which then underwent the intramolecular cyclization.[115] Perfluorinated derivatives of BN-phenanthrene were prepared in an analogous manner by Bochmann and co-workers several years later.[116] Furthmore, Niedenzu and co-workers used this photocyclization protocol to generate pyridyl-substituted analogs of BN-phenanthrene.[117]

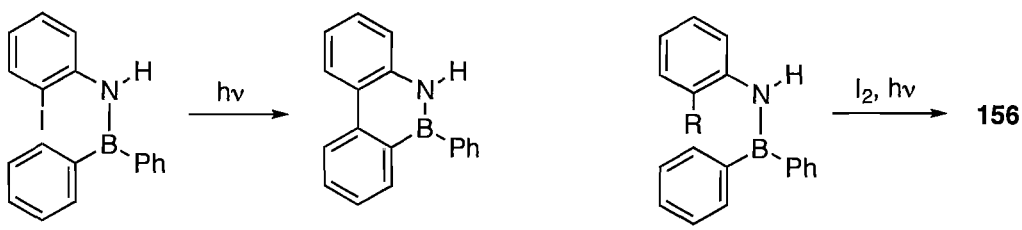

176 **156** **177a** R = H **177b** R = CH_3

Scheme 57. Photochemical cyclization of aminoboranes to BN-phenanthrene **156**.

Several additional tricyclic derivatives have been reported. Dewar and co-workers synthesized the first BN-anthracene via the reaction of symmetric dianiline **178** and $PhBCl_2$ to give **179** (Scheme 58, top).[118] BN-Anthracene **179** contains two flanking 1,2-azaborine rings fused to benzene and was formed by the elimination of four molecules of HCl. Zanirato and co-workers have described the formation of BN-benzodithiophene **181** from the reaction of azide **180** and $PhBCl_2$ (Scheme 58, middle).[119-120] Barton et al. reported the reaction of anilinothiophene **182** with BCl_3 to form **183** after hydrolysis of the presumed B-Cl intermediate (Scheme 58, bottom).[121] In work similar to that discussed above regarding BN-indene, Wrackmeyer et al. synthesized a tricyclic heterocycle (**184** in Figure 19) that is a reduced form of BN-acenaphthalene.[122] Unfortunately, no attempts were made to oxidize **184** to the fully aromatic acenaphthalene analog.

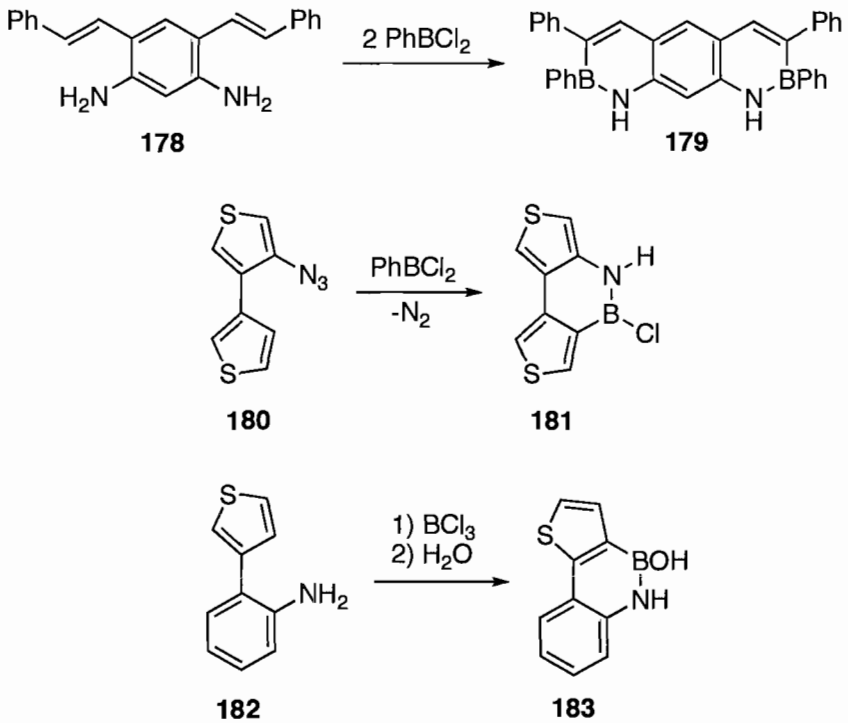

Scheme 58. Condensation route to tricyclic aromatic BN-heterocycles.

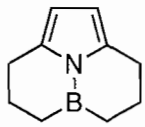

184

Figure 19. BN-Acenaphthalene derivative with bridgehead B-N substitution.

1.2.6. Tetracyclic Analogs

Dewar and co-workers extended the synthetic methods discussed above to prepare numerous BN-substituted polycyclic aromatic hydrocarbons (Figure 20).[39,123-126] Aminonaphthalene precursors were condensed with chloroboranes to generate BN-benz[a]anthracene isomers **185** and **186**, which displayed similar, yet not identical, absorption spectra. Interestingly, the condensation reaction that formed **186** was entirely selective; the alternate chrysene derivative was not produced in the reaction. BN-Triphenylene **187** was synthesized from an N-bromobutyl BN-phenanthrene.[124] Tetracycle **187** was the second analog of triphenylene synthesized, the first being inadvertently produced in the failed synthesis of 1,2-dihydro-1,2-azaborine (see section 1.2.1). The UV-Vis spectrum of **187** displayed a strong absorption at 330 nm, which was slightly red-shifted relative to heterocycle **7** containing a borazine core (λ_{max} = 316 nm). Derivatives of pyrene incorporating one and two BN bond-pairs (**188** and **189**, respectively) were synthesized in a similar way to BN-phenanthrene.[118,125] The UV-Vis spectrum of **188** showed a strong absorption at 365 nm, in marked contrast to the di-substituted analog **189**, which showed a broad absorption at 335 nm. Decades later, Philp and co-workers reproduced the synthesis of **189** and explored the chemistry and solid-state parameters of B-O-B ethers derived from **189**.[126] Dewar and co-workers also

synthesized BN-chrysene derivatives such as **190** via the condensation of 1-aminonapthalenes with chloroboranes.[125,127]

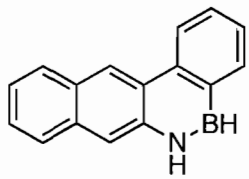

185
6,5-azaborbenz[a]anthracene

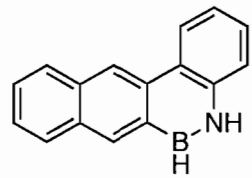

186
5,6-azaborbenz[a]anthracene

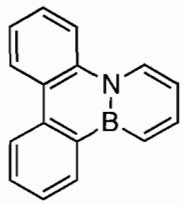

187
13,14-azabortriphenylene

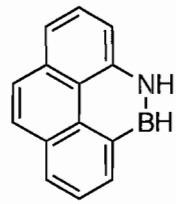

188
4,5-azaborpyrene

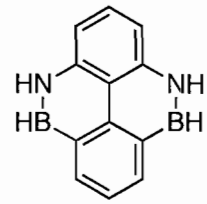

189
4,10-diaza-5,9-borpyrene

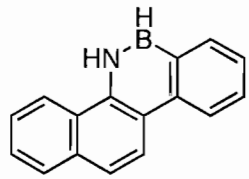

190
6,5-azaborchrysene

Figure 20. Tetracyclic analogs of aromatic hydrocarbons containing the B-N bond unit.

Piers and co-workers developed the first synthesis of BN-pyrene **191** containing an internalized B-N moiety (Scheme 59).[128] In analogy to the previous synthesis of BN-phenanthrene, the cyclization of bis-(ortho-alkynyl) pyridine with a boracyclohexadiene generated BN-phenanthrene **192**. The addition of $PtCl_2$ led to the cyclization to BN-pyrene **191**.

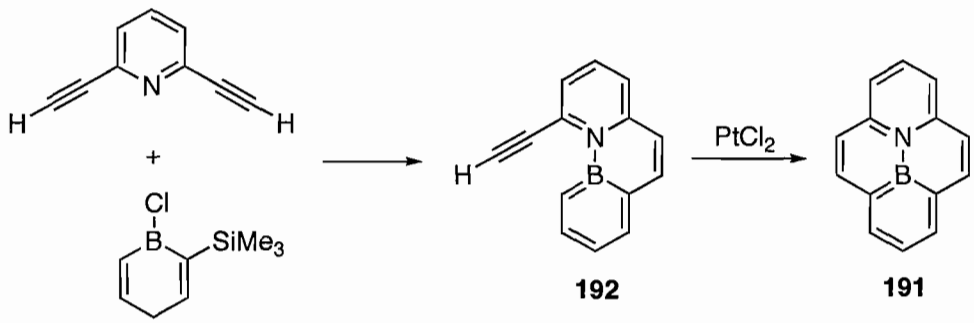

Scheme 59. Sythesis of BN-pyrene **191** featuring an internalized BN bond-pair.

The X-ray crystal structure of **191** revealed an interesting π-stacking head-to-tail arrangement wherein BN dipoles of adjacent molecules were opposed (Figure 21). In comparison to the derivatives prepared by Dewar, the internally-substituted **191** displayed a similar absorption spectrum (λ_{max} = 321 nm, ε = 5.8 x 10^4 $M^{-1}cm^{-1}$), though an additional weak absorption was observed at longer wavelengths (λ_{max} = 443 nm, ε = 0.29 x 10^4 $M^{-1}cm^{-1}$). BN-Pyrene **191** displayed several fluorescence bands between 480 and 514 nm. Piers and co-workers also synthesized larger scaffolds containing the internalized BN-pyrene in analogy to the BN-phenanthrene dimers discussed above.[111]

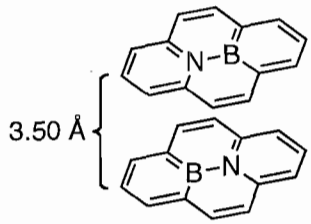

Figure 21. Crystal packing in BN-pyrene **191**.

A few other examples of polycyclic scaffolds incorporating a non-aromatic C_4BN heterocycle have been reported, notably the quinoline-containing derivative **193** (Figure 22) reported by Enders and co-workers[129] and BN-fluoranthrene **194** (Figure 23) reported by Nöth and co-workers.[130] It is notable that the crystallographic analysis of

194 indicated little bond delocalization in the C_4BN ring; alternating long and short single and double bonds were observed, respectively.

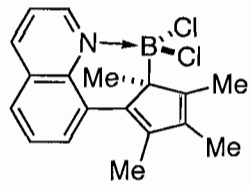

193

Figure 22. Quinoline-substituted BN-heterocycle **193**.

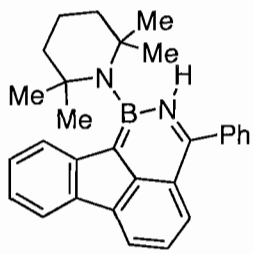

194

Figure 23. BN-Fluoranthrene **194**.

1.2.7. 1,3- and 1,4-Substituted C_4BN Heterocycles

The substitution of boron and nitrogen at non-adjacent positions on the benzene ring gives rise to two additional isoelectronic analogs of benzene, 1,3- and 1,4-azaborine (Figure 24). Massey and Zoellner calculated the relative thermodynamic stabilities of all three isomers and determined that the 1,2 isomer was the most stable, followed by the 1,4 isomer.[42] The 1,3 isomer, for which no classical charge-neutral form can be written, was predicted to be significantly less stable. Kranz and Clark performed additional DFT calculations, which corroborated the relative stabilities of the three isomers.[43] Interestingly, the π-system of the 1,3 isomer was predicted to be highly delocalized, and

the optimized geometry of the 1,3 isomer displayed significant bond-length contraction of the carbon-carbon and carbon-heteroatom bonds relative to the other isomers.[131]

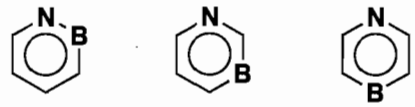

1,2 **1,3** **1,4**

Figure 24. Azaborine isomers (N- and B-bonded H atoms omitted).

The preparation of all three azaborine isomers would provide the opportunity to examine fundamental properties relating to aromaticity and bond delocalization. Unfortunately, derivatives of 1,3- and 1,4-azaborine are rare, and in fact there are no known examples of aromatic 1,3-azaborines in the literature. The only known example of a saturated 1,3-substituted BN-heterocycle was prepared by Toyota and co-workers (**195** in Scheme 60), but no route to an aromatic structure was explored.[132]

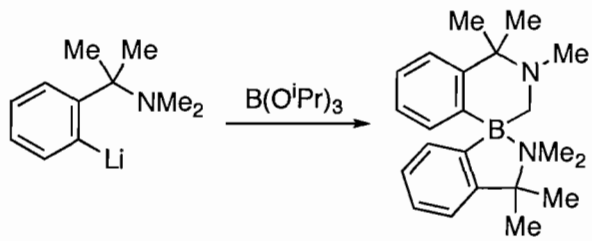

195

Scheme 60. Preparation of non-aromatic 1,3-substituted heterocycle **195**.

While monocyclic derivatives of 1,4-azaborine are unknown, several polycyclic analogs have been reported. Almost 50 years ago, Maitlis prepared BN-anthracene **196** featuring a central 1,4-azaborine ring (Scheme 61).[133] The reaction of dilithiate **197** with $PhB(OBu)_2$ produced **196** in good yield. 9,10-Azaboranthracene **196** was reported to be air- and moisture-stable, indicating some degree of aromatic stabilization in the heterocycle. The UV-Vis spectrum of **196** showed a broad, strong absorption band just

beyond 400 nm, whereas the longest wavelength absorption band of anthracene is much weaker and cuts off at about 380 nm. The first crystallographic analysis of a 9,10-substituted BN-anthracene was undertaken by Reikhsfel'd and co-workers and revealed the BN-anthracene system to be planar.[134] There was also evidence of bond delocalization in the 1,4-azaborine ring which was confirmed by Clark and co-workers in a derivative prepared several years later.[135]

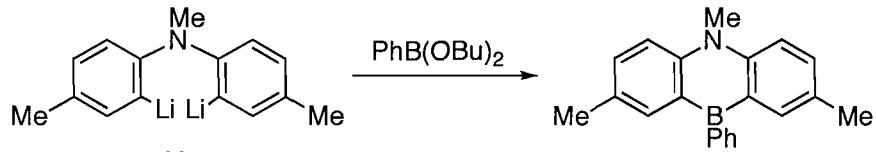

197 **196**

Scheme 61. Synthesis of 9,10-substituted BN-anthracene **196** featuring a 1,4-azaborine core.

Kawashima and co-workers have expanded the synthesis of BN-acenes featuring the 1,4-azaborine moiety to include pentacene and heptacene derivatives.[136-137] The synthesis of BN-pentacene derivative **199** was achieved from para-diamino arene **198** (Scheme 62). A similar transformation from meta-diamino arene **200** afforded BN-pentancene **201**. Both **199** and **201** were air- and moisture-stable, which was ascribed in part to the sterically-demanding mesityl groups at boron. This protocol was also expanded to include BN-heptacene **203** from triaminoarene **202**.

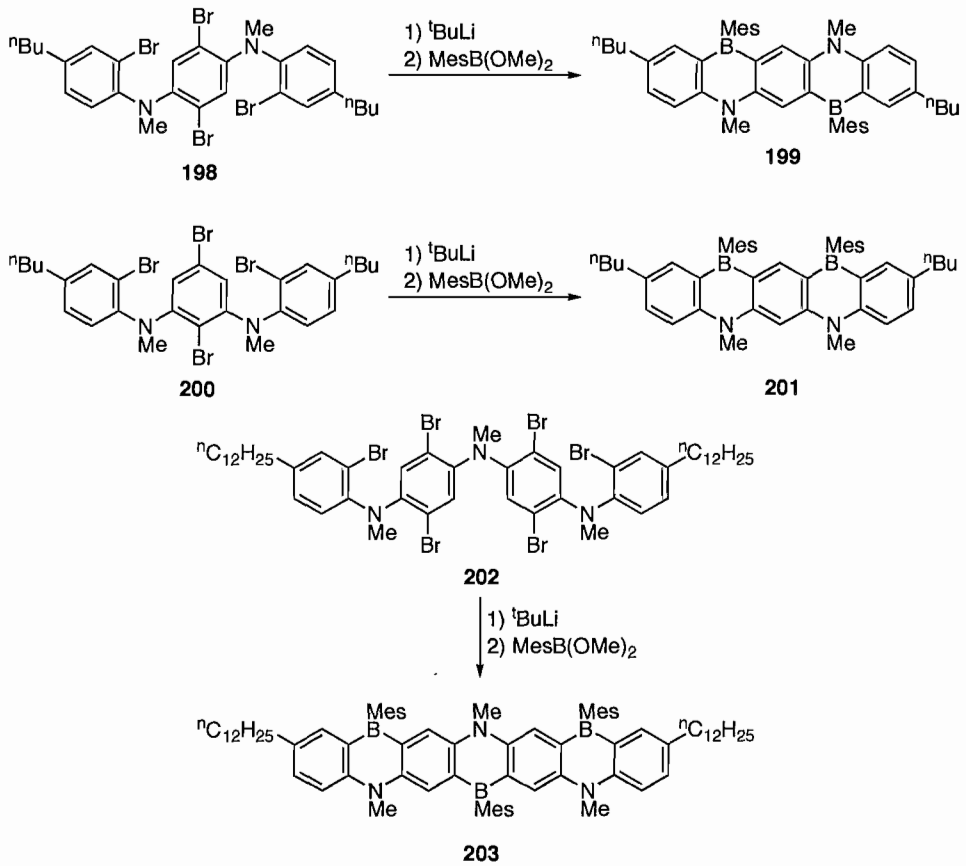

Scheme 62. Synthesis of BN-pentacene isomers **199** and **201** and BN-heptacene **203**.

The X-ray crystal structure of **199** revealed that the BN-pentacene framework was virtually co-planar, indicating an extended π-conjugated system. Surprisingly, no evidence of intermolecular π-stacking was observed. The absorption-emission properties of BN-pentacene **199** and **201** were examined along with BN-heptacene **203**, the results of which are summarized in Table 11. The red-shifted absorption and emission maxima observed in **199** and **203** is consistent with an extended conjugation relative to BN-anthracene. BN-Pentacene **201**, in which the 1,4-azaborine rings are oriented parallel to each other, displayed optoelectronic properties which were very similar to BN-anthracene. The anti-parallel orientation of the 1,4-azaborine sub-units in

199 and **203** was clearly an important feature for the future design of BN-acenes in optoelectronic materials. In fact, Kawashima and co-workers have recently described the use of functionalized BN-acenes as fluorescent sensors for biologically relevant anions such as fluoride and cyanide.[138-139] They have also constructed conjugated dendrimeric structures featuring pendant BN-acene groups.[140]

Table 11. Photophysical Properties of BN-Acenes

compound	λ_{max} (nm) / log (ε)	λ_{em} (nm)	Φ
199	523 / 4.23	534	0.69
201	415 / 3.94	428	0.21
203	608 / 4.28	625	0.55

1.3. The Diazadiborine Motif as a Benzene Analog

1.3.1. Isomers of Diazadiborine

The diazadiborine heterocycle is an analog of benzene in which two CC units have been replaced with isoelectronic BN groups ($C_2B_2N_2$). There are several isomers of the diazadiborine heterocycle, as seen in Figure 26. Several of these isomers have only been examined from a theoretical perspective; the focus of this section will be on the synthetically available derivatives, which are highlighted in red in Figure 25. With the exception of 1,3-diaza-2,5-diborine, all of the synthetically available isomers of diazadiborine contain the B-N bond pair, that is each boron is directly bound to at least one nitrogen atom. This correlates with the relative stabilities seen in the three isomers of the azaborine heterocycle. It is probable that the stability of the accessible diazadiborine isomers follows a similar trend. In fact, Massey and Zoellner calculated the thermodynamic stabilities of all eleven isomers and found that four of the five

synthetically unknown isomers are significantly less stable than the known isomers.[141] Interestingly, the synthetically unexplored 1,4-diaza-2,6-diborine isomer was calculated to one of the most thermodynamically stable forms of diazadiborine.

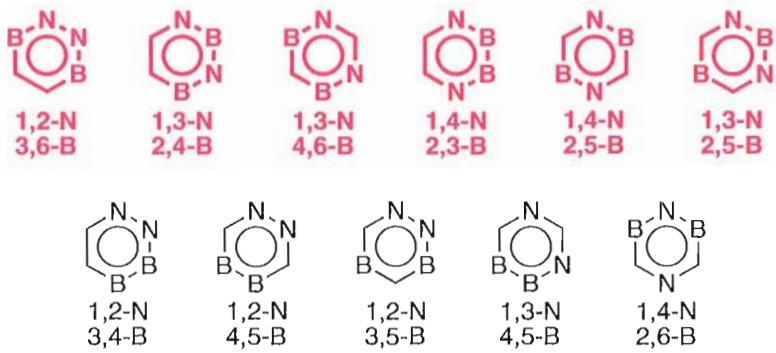

Figure 25. All possible isomers of diazadiborine. Isomers which have been prepared are in red. N- and B-bonded H atoms have been omitted for clarity.

1.3.2. 1,3-Diaza-2,4-diborines

Polycyclic 1,3-diaza-2,4-diborines were the first synthesized examples of diazadiborine, however the monocyclic structure has received significantly less attention. Paetzold and co-workers were able to produce 1,3-diaza-2,4-diborine **205** via the cycloaddition of diazadiboretidine **204** with dimethylacetylenedicarboxylate (Scheme 63).[142] The X-ray crystal structure of **205** revealed the diazadiborine ring to be slightly out of plane with alternating long and short intra-ring bond lengths. The bulky tert-butyl groups were likely responsible for the observed twisting in the structure.

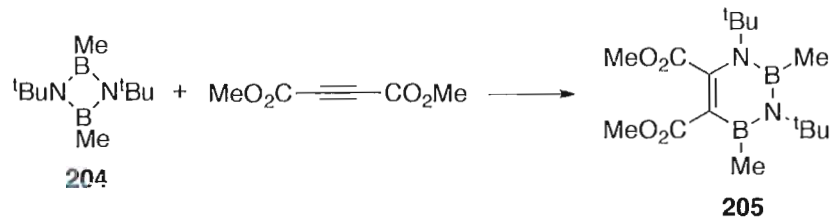

Scheme 63. Synthesis of 1,3-diaza-2,4-diborine **205**.

Köster et al. prepared the benzo-fused 1,3-diaza-2,4-diborine **206** from the high temperature, high pressure reaction of a mixture of amine-boranes (Scheme 64).[143]

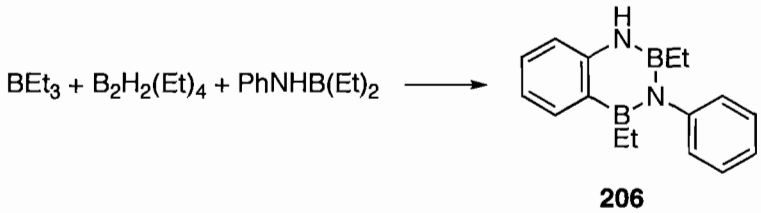

206

Scheme 64. Formation of benzo-fused 1,3-diaza-2,4-diborine **206**.

Turner et al. formed a similar naphthalene derivative **207** from the more controlled reaction of ortho-toluidine with boron trichloride (Scheme 65).[144] The competitive formation of trimeric borazine derivatives over dimeric structures like **207** was found when the aryl substituents were varied.[145] However, improved selectivities in the formation of 1,3-diaza-2,4-diborine over borazine were obtained when BCl_3 was replaced with BI_3[146] or BBr_3.[147]

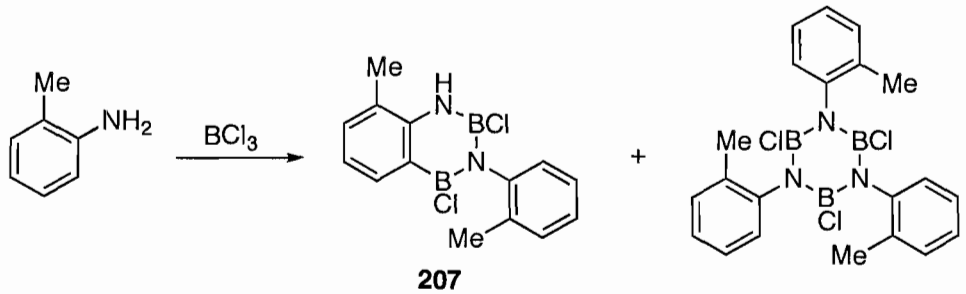

207

Scheme 65. Condensation to benzo-fused 1,3-diaza-2,4-diborine naphthalene analog **207**.

Frange and co-workers have prepared phenanthrene derivatives containing the 1,3-diazo-2,4-diborine ring via a similar route from naphthyl amine and BCl_3.[148] Nucleophilic substitution at boron furnished several derivatives of the B-Cl compound **208**, including methylated **209** and B-H substituted **210** (Figure 26).[149] The electronic features and optimized geometries were predicted for these derivatives.[150] In particular,

the π-electron densities were calculated, which indicated that the boron at the 2-position had slightly more π-electron density than at the 4-position. This is reasonable given that the boron at the 2-position is bound to both π-electron donating nitrogen atoms, whereas the boron at position 4 is bound to a single nitrogen. Conversely, the nitrogen flanked by two boron atoms (3-position) was found to be less electron-rich than the nitrogen at position 1.

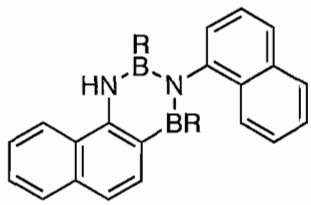

208 R = Cl
209 R = Me
210 R = H

Figure 26. Phenanthrene derivatives containing the 1,3-diaza-2,4-diborine unit.

Frange and co-workers described the coordination chemistry of benzo-fused 1,3-diaza-2,4-diborines with Group 6 transition-metals. The reaction of BN-naphthalene **211** with $Cr(CO)_6$ and $W(CO)_6$ led to the formation of piano-stool complexes **212** and **213**, respectively (Scheme 66).[151-152] The coordination of the metal to the fused benzene ring was seen in both cases, and no evidence of coordination to the 1,2-diaza-2,4-diborine or pendant tolyl rings was observed. Upfield chemical shifts were observed in the ^{1}H and ^{13}C NMR signals for the benzo substituent, consistent with π-coordination of the metal at this ring. The sterically crowded environment around the biaryl bond results in restricted rotation of the pendant tolyl ring. As a result, a one-to-one ratio of diastereomers is formed by coordination of the metal to either face of the benzo ring.

The identities of the diastereomers were determined by 2D NMR and X-ray crystallography.[153]

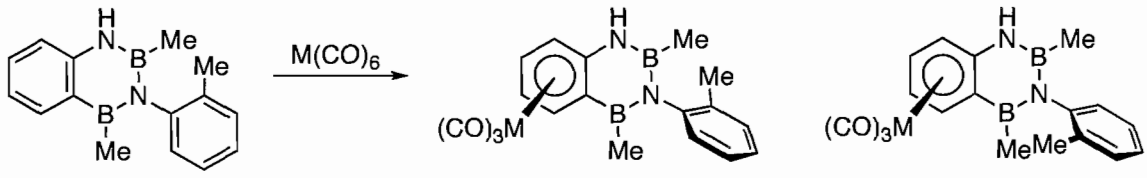

211

212 M = Cr
213 M = W

Scheme 66. Atropisomerism in piano-stool complexes of BN-naphthalene **211**.

1.3.3. 1,4-Diaza-2,3-diborines

Though the number of 1,4-diaza-2,3-diborine derivatives is limited, there have been significant efforts toward the synthesis of this interesting benzene analog which features a B-B bond. To date there has been no report on the synthesis of a monocyclic, aromatic 1,4-diaza-2,3-diborine. Nöth has reported the preparation of naphthalene, phenanthrene, and anthracene derivatives **214-216**, respectively (Figure 27), via the reaction of an ortho-diaminoarene and a diboradiamide.[154] The complexation of a B-butyl analog of **214** with $Cr(CO)_3$ took place at the benzo ring as evidenced by the substantial upfield shifts in the ^1H NMR signals of the homoaromatic ring protons.[155] Cowley, Marder, Norman and co-workers prepared an oxo-bridged dimer of 1,4-diaza-2,3-diborine (**217** in Figure 28) and obtained an X-ray crystal structure.[156] The structure is completely co-planar and the bond lengths are consistent with a delocalized π-system. In fact, the B-B bond is quite short (1.683(3) Å) compared to that of another boron oxide discussed in the report (1.732(3) Å). It was the first solid-state structure containing a B-B bond as part of an aromatic ring.

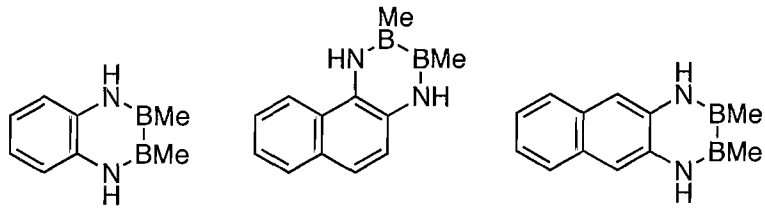

214 **215** **216**

Figure 27. 1,4-Diaza-2,3-diborine analogs of polycyclic aromatic hydrocarbons.

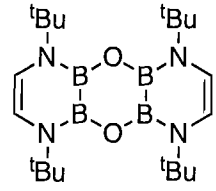

217

Figure 28. 1,4-Diaza-2,3-diborine **217** containing the first structurally characterized "aromatic" B-B bond.

The inherent difficulty in the synthesis of 1,4-diaza-2,3-diborine is in part due to the preferred formation of a bicyclic structure over the ring-fused isomer (Figure 29). Shore and co-workers found that when nitrogen was replaced with oxygen or sulfur, the ring-fused structure was preferred.[157] In contrast, the reaction of ethylenediamines with diboranes leads to the bicyclic structure almost exclusively. Norman, Russell and co-workers determined that the bicyclic isomer was the thermodynamic product of the reaction of $B_2(NMe_2)_4$ and ortho-diaminobenzene.[158] However, the intermediate formation of a ring-fused BN-tetracene was demonstrated and both compounds were isolated and analyzed by X-ray crystallography. The B-B bond in the ring-fused isomer was shortened relative to the bicyclic B-B bond, consistent with the data for **217**.

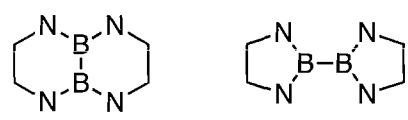

ring-fused **bicyclic**

Figure 29. Ring-fused and bicyclic isomers of tetraaminodiborane (N-bonded H atoms omitted).

The conversion of the ring-fused structure to the bicyclic motif was demonstrated in the presence of additional ortho-diaminobenzene. Marder, Norman, Orpen and co-workers have also had some success in generating the 1,4-diaza-2,3-diborine motif from 2,2'-dipyridine and 1,10-phenanthroline.[159]

1.3.4. 2,3-Diaza-1,4-diborines

Siebert and co-workers published the first example of a monocyclic diazadiborine in 1976,[160] the preparation of which was detailed a few years later.[161] The reaction of thiaborole **218** with hydrazines provided 2,3-diaza-1,4-diborine **219** and **220** with the loss of H_2S (Scheme 67). Crystallization of **219** at low temperature permitted the collection of single-crystal X-ray diffraction data, which indicated a planar ring structure. Complexation of 2,3-diaza-1,4-diborines **219** and **220** to $Cr(CO)_3$ gave piano-stool complexes **221** and **222**, respectively, which were purified by sublimation. The η^6-binding of **221** to chromium was confirmed by X-ray crystallography and NMR spectroscopy. A similar route to benzannulated analogs (isoelectronic with naphthalene) was estabilished,[162-163] and in this case it was found that metal coordination with chromium, molybdenum, and tungsten occurred selectively at the benzo-fused carbocycle, similar to the 1,3-diaza-2,4-diborine isomer discussed in section 1.3.2.

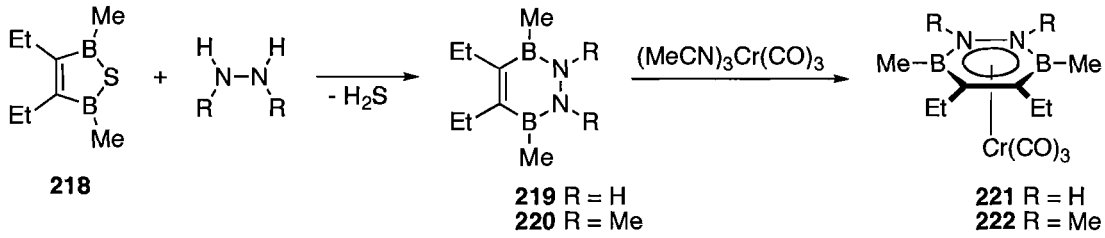

Scheme 67. Synthesis of 2,3-diaza-1,4-diborines **219-220** and respective $Cr(CO)_3$ complexes **221-222**.

An alternate route to the 2,3-diaza-1,4-diborine motif was explored by Paetzold and co-workers.[164] The highly reactive head-to-head dimer **223** was reported to undergo a cycloaddition reaction with 3-hexyne to furnish the highly-substituted 2,3-diaza-1,4-diborine **224** (Scheme 68). The same heterocyclic motif was obtained when 2 equivalents of *tert*-butylisocyanide were added to **223**, providing imine-substituted **225**.

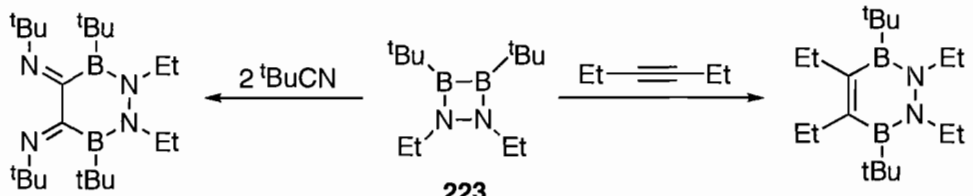

Scheme 68. Cycloaddition of **223** to 2,3-diaza-1,4-borine derivatives **224** and **225**.

Analogs of polycyclic aromatic hydrocarbons containing a 2,3-diaza-1,4-diborine core have recently been explored. 2,2'-Bisborabenzene, the Lewis acidic counterpart to 2,2'-bipyridine, was synthesized via the reaction of precursor **226** with neutral Lewis bases (Scheme 69).[165] When pyridazine and benzo[c]cinnoline were used as the base, the formation of BN-triphenylene **227** and dibenzo[g,p]chrysene **228** occurred. Both of these BN-aromatics contained the 2,3-diaza-1,4-diborine core and displayed absorption spectra consistent with a highly conjugated π-system. While the structure of BN-triphenylene **227** was presumably planar, the steric repulsion of the 3,3'-hydrogen atoms in **228** forced the molecule to twist out of planarity. Electrochemical measurements showed that **228** was more easily reduced than **227**, indicating a lesser degree of aromatic stabilization in the non-planar **228**. These data were confirmed via X-ray crystallography where it was shown that BN-triphenylene **227** was completely planar whereas **228** was twisted out of plane.[166] The fluorescence of **227** was in sharp contrast

to the non-fluorescent nature of **228**, which was again ascribed to the structure of **228** in which molecular twisting disrupts conjugation in the scaffold. The absorption and emission maxima of **227** were both red-shifted by over 100 nm relative to triphenylene, suggesting as in previously described BN-heterocycles that substitution of the B-N bond pair has the potential to impart unique optoelectronic properties.

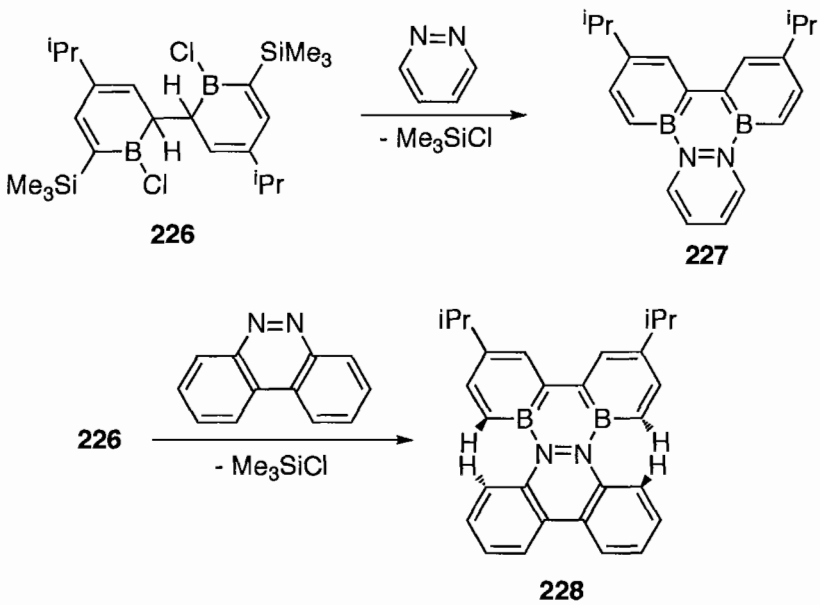

Scheme 69. Polycyclic aromatic hydrocarbons substituted with a 2,3-diaza-1,4-diborine core.

1.3.5. 1,3-Diaza-4,6-diborines

There have only been two reports to date on the preparation of an aromatic 1,3-diaza-4,6-diborine heterocycle, both by Roesler and co-workers.[167-168] The reaction of an aryl-substituted trimethylsilyl formamidinate with a bis(chloroboryl)ethane formed the corresponding zwitterionic heterocycles **229-231** (Scheme 70). Deprotonation at the 5-position provided the 1,3-diaza-4,6-diborines **232-234**, all of which were structurally characterized by X-ray crystallography. The heterocycles were planar in all cases and

the intra-ring bond lengths indicated significant delocalization of the π-electron density over the B-C-B and N-C-N fragments. However, the long intra-ring B-N distances (~ 1.50 Å) suggested that the bonding in the 1,3-diaza-4,6-diborine heterocycle was more accurately described by two allyl fragments which formed the zwitterionic structure illustrated in Scheme 70 rather than a fully delocalized aromatic system. This bonding depiction was supported by calculations on a related BN-heterocycle.[169] Heterocycle **232** was deprotonated at the 2-position with a lithium base to generate a metal-coordinated phenylide-like structure.[167] Alternatively, deprotonation of **233** or **234** with a potassium base in the presence of 18-crown-6 provided the corresponding free carbanions, which were characterized by X-ray crystallography.[168]

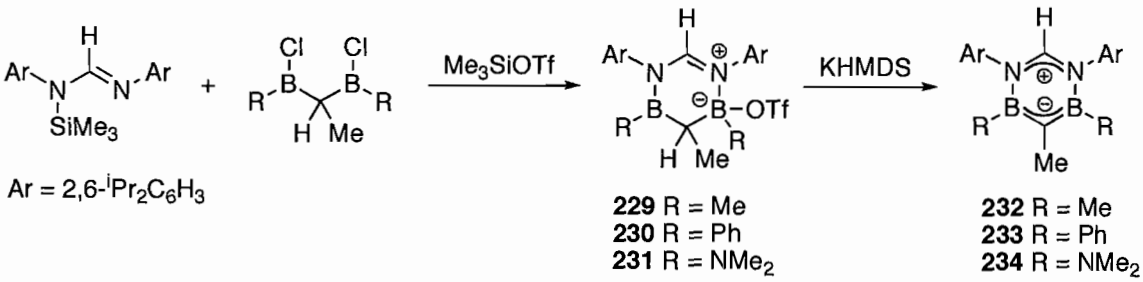

Scheme 70. Synthesis of 1,3-diaza-4,6-diborines **232-234**.

1.3.6. Non-aromatic Analogs of 1,3-Diaza-2,5-diborine and 1,4-Diaza-2,5-diborine

The 1,3- and 1,4-diaza-2,5-diborine isomers were predicted to be thermodynamically stable,[141] yet no route to these aromatic motifs has been reported. There have been numerous reports on the preparation of related compounds featuring 4-coordinate boron and carbon atoms.

The first example of a fully saturated 1,4-diaza-2,5-diborine was described by Miller and co-workers in 1964.[170] The reaction of $H_2B(N(CH_3)_3)_2Cl$ with sodium

hydride resulted in the formation **235**, which was an isoelectronic analog of 1,1,4,4-tetramethylcyclohexane (Figure 30). Over the next three decades, several studies emerged from Miller[171-179] and others[180-181] regarding the reactivity and intrinsic characteristics of this cyclohexane mimic. Structurally, the saturated 1,4-diaza-2,5-diborine was determined to be quite similar to cyclohexane; the chair conformation observed in the X-ray crystal structure of **235**[180] and the stereochemistry of substituted derivatives[177] resembled cyclohexane. However, the highly reactive nature of the BN-heterocycle was in marked contrast to the hydrocarbon analog; derivatives of **235** were often hydrolytically unstable.

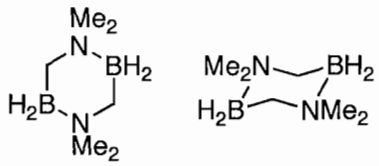

235

Figure 30. Saturated 1,4-diaza-2,5-diborocyclohexane **235** is isolectronic with tetramethyl cyclohexane.

The generation of partially oxidized 1,4-diaza-2,5-diborine heterocycles has been readily achieved via the dimerization of various CN-containing moieties that are tethered by two borane groups (Figure 31). Examples include dimerized isocyanide, imidazole, and pyridyl groups to give the corresponding heterocycles **236**, **237**, and **238**, respectively. Hesse and co-workers prepared the first dimer of type **236** (R = Ph, R' = Et) via reaction of phenylisocyanide with triethylborane.[182] The condensation reaction was accompanied by the migration of an ethyl group from boron to carbon. This initial work and subsequent studies showed that the migration of an second R' group from boron to carbon occurred upon heating.[183-185] Variation in the R' group was achieved by

Carter and co-workers,[186] and later Bresadola et al.,[187] via the reaction of B_2H_6 with isocyanides to furnish **236** in which R' = H. Hesse and co-workers determined that HCN reacted with BEt_3 to afford **236** where R = H,[188] though there has been no reported synthesis of **236** where both R and R' are hydrogen. Recent examples by Casanova and Hahn have examined the rearrangement chemistry of derivatives of **236**.[189-190]

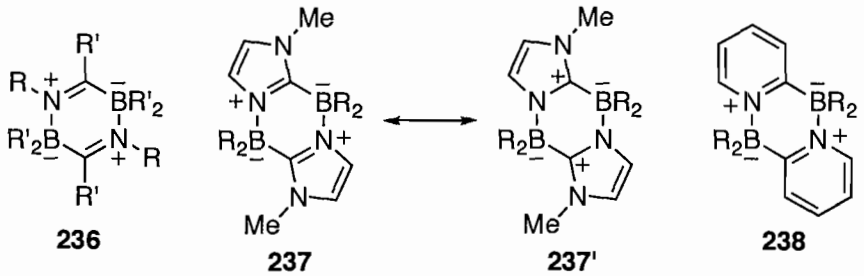

Figure 31. Head-to-tail dimerization of CN groups to generate 1,4-diaza-2,5-diborine derivatives.

Contreras, Wrackmeyer and co-workers formed borane-bridged head-to-tail imidazole dimer **237a** via the high-temperature reaction of imidazole-borane adduct **239** in the presence of MeI/Al (Scheme 71).[191] Diaza-2,5-diborine **237a** was formed as a separable mixture with the head-to-head isomer, 1,3-diaza-2,5-diborine **237b**. The X-ray crystal structure of **237a** revealed the 1,4-diaza-2,5-diborine core to be close to planar, which was attributed to packing effects. The B-N bond length of 1.55 Å was shorter than expected for a dative σ-bond and was closer in length to a typical $N(sp^2)$-$B(sp^3)$ bond. This structural data, coupled with NMR spectroscopic data, indicated a significant contribution from the carbenoid resonance form **237'**.[192]

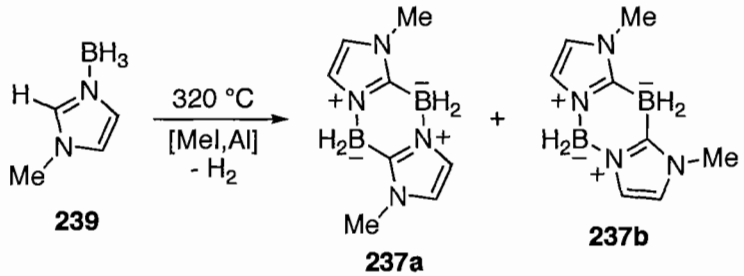

Scheme 71. Formation of **237a** and **237b** from imidazole-borane **239**.

Okada, Oda, and co-workers selectively formed a derivative of **237** substituted with mesityl groups at boron (R = 2,4,6-trimethylphenyl), and they determined via X-ray crystallography that the bulky mesityl groups force the 1,4-diaza-2,5-diborine core into a boat-like conformation with an elongated B-N bond (~1.64 Å).[193] Siebert and co-workers,[194] and later Hill and co-workers[195] reported the synthesis of derivatives of **237** via unexpected dimerization of imidazoles, suggesting the formation of **237** is thermodynamically favorable.

A related dimerization was observed in dialkyl(2-pyridyl) boranes to form the 1,4-diaza-2,5-diborine scaffold **238** (Figure 32). In the characterization of diethyl(2-pyridyl)borane, Terashima and co-workers noted that the compound displayed a high melting point (205-206 °C) and mass spectrometry showed a prominent peak at m/z 294, consistent with dimer **238** (R = Et, molecular formula $C_{18}H_{28}B_2N_2$).[196] Hodgkins and Powell determined that the dimerized product was present in two isomeric forms, the head-to-tail 1,4-diaza-2,5-diborine **238** and head-to-head 1,3-diaza-2,5-diborine **238'** (R = Me, Figure 32).[197-198] In fact, isomer **238'** (R = Me) was found to be the major product of the reaction of 2-lithiopyridine and bromodimethylborane at low temperature. Wright and co-workers determined via ^1H and ^{11}B NMR that isomer **238'** (R = Me) is

quantitatively converted to **238** in 30 minutes when refluxed in toluene-d_8, suggesting **238** was the thermodynamic product while **238'** was kinetically favored.[199]

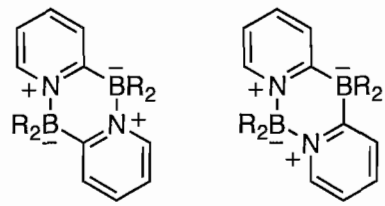

238 **238'**

R = Me

Figure 32. Isomerism in the dimerization of 2-pyridyl boranes.

The X-ray crystal structure obtained by Murafuji, Sugihara, and co-workers unambiguously established the identity of dimerized diethyl-2-(3-methyl)pyridyl borane and demonstrated that the 1,4-diaza-2,5-diborine core was planar and possessed long intra-ring B-N and B-C bonds (1.61 and 1.62 Å, respectively).[200]

Another route to 1,4-diaza-2,5-diborines has been detailed by Paetzold and co-workers.[201-202] The reaction of 3-membered heterocycle **240** (Scheme 72) with 2,6-dimethylphenyl isocyanide was shown to form monomeric 4-membered ring **241**. However, when a less bulky isocyanide was added to **240**, the formation of dimeric 1,4-diaza-2,5-diborine **242** was observed. The compound was found to be relatively stable and was structurally characterized by X-ray crystallography. Due to the strained structure incorporating bulky substituents at several positions, all three rings were found to be slightly out of plane with long intra-ring bond distances.

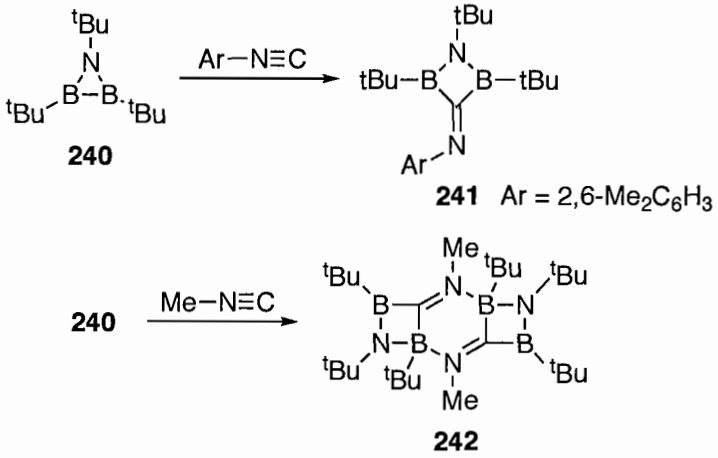

Scheme 72. Ring-opening of **240** with isocyanides.

1.4. Summary

Over the last half-century, interest in the fundamental consequences of B-N incorporation in heterocyclic compounds has led to a wide array of synthetically available motifs based on the azaborine and diazadiborine cores. Azaborine and diazadiborine can be considered to lie on the continuum between organic benzene and its "inorganic" counterpart, borazine. The physical properties, chemical reactivity, and computational analysis of azaborine and diazadiborine suggest that most of these hybrid organometalloidal heterocycles display significant aromatic character. The last decade has been a renaissance in the synthesis of monocyclic azaborines, which was fueled by the replacement of older methods with mild, efficient protocols. Currently there are several routes to the monocyclic azaborine motif, yet the incorporation of additional functionality has been relatively unexplored. Various polycyclic motifs have become more readily available since the 1960s, and their chemistry is well understood. The preparation of non-aromatic azaborine derivatives has been demonstrated, and in some

cases these have been developed as precursors to the corresponding aromatic heterocycle. Several isomers of azaborine and diazadiborine have been prepared, yet many of these are constrained to non-aromatic derivatives. The application of aromatic BN heterocycles to areas such as material science and medicine will rely on efficient, general synthetic methods that have yet to be fully realized.

1.5. Bridge to Chapter II

This chapter reviewed the literature on azaborine and diazadiborine heterocycles as benzene analogs. Chapter II will describe the synthesis, characterization, and reactivity of 1,2-azaborine derivatives containing unprecedented functionality at the boron position. Chapter II contains previously published and unpublished co-authored material. The synthetic efforts discussed in Chapter II will be expanded to include the synthesis of the parent compound, 1,2-dihydro-1,2-azaborine, and will include biochemical and spectroscopic studies on 1,2-dihydro-1,2-azaborine as it relates to benzene. Chapter III contains previously published co-authored material. Chapter IV will discuss the synthesis, characterization, and photophysical properties of 1,2-azaborines that have been incorporated into conjugated organic scaffolds. Chapter IV contains previously published co-authored material. Chapter V will provide a short introduction into the chemistry of nitrated lipids and then discuss the work accomplished in this field as a member of the Branchaud group. Chapter V contains previously published and unpublished co-authored material. Chapter VI will summarize the work

discussed in earlier chapters. Appendices A-D discuss experimental details related to chapters II-V, and contain previously published and unpublished co-authored material.

CHAPTER II

EXPANDING THE SCOPE OF 1,2-AZABORINE SYNTHESIS VIA NUCLEOPHILIC SUBSTITUTION AT BORON

2.1. General Overview

This chapter discusses the generation of a family of boron-substituted 1,2-dihydro-1,2-azaborines which are derived from a versatile 2-chloro-1,2-azaborine intermediate. This excerpt includes material published as Marwitz, A. J. V.; Abbey, E. R.; Jenkins, J. T.; Zakharov, L. N.; Liu, S. –Y. "Diversity though isosterism: the case of boron-substituted 1,2-dihydro-1,2-azaborines," *Org. Lett.* **2007**, *9*, 4905-4908. The X-ray crystallographic data was collected and analyzed by Dr. Lev Zakharov. Jesse Jenkins prepared some of the chemical compounds and Eric Abbey established some of the early protocols. Otherwise all experimental work was performed by me. This excerpt was written entirely by me.

The discussed work also includes material published as Marwitz, A. J. V.; McClintock, S. P.; Zakharov, L. N.; Liu, S. –Y. "BN benzonitrile: an electron-deficient 1,2-dihydro-1,2-azaborine featuring linkage isomerism," *Chem. Comm.* **2010**, *46*, 779-781. The experimental work was conducted by me with the exception of the X-ray crystallographic data, which was collected and analyzed by Dr. Lev Zakharov.

Computational studies were performed by Dr. Sean McClintock. This excerpt was written entirely by me.

This chapter includes the synthesis and characterization of cationic 1,2-azaborines. The excerpt includes unpublished co-authored material with Dr. Lev Zakharov and Jesse Jenkins. X-ray crystallographic data was collected and analyzed by Dr. Lev Zakharov. Some of the presented chemical compounds were first prepared and characterized by Jesse Jenkins. Otherwise I performed all the experimental work. The co-authored excerpt was written entirely by me.

This chapter discusses spectroscopic studies of 1,2-azaborine published as Tanjaroon, C.; Daly, A.; Marwitz, A. J. V.; Liu, S. –Y.; Kukolich, S. "Microwave measurements and ab initio calculations of structural and electronic properties of N-Et-1,2-azaborine," *J. Chem. Phys.* **2009**, *131*, 224312/1-224312/9. Compounds were prepared by me and spectroscopic characterization was performed by Tanjaroon, Daly, and Kukolich. The co-authored excerpt as presented here was written by me.

Professor Shih-Yuan Liu has provided editorial assistance and scientific guidance for all material (published and un-published) covered in this chapter.

2.2. Introduction

1,2-Dihydro-1,2-azaborine is a six-membered aromatic heterocycle that is related to benzene via replacement of a C=C unit in benzene with an isoelectronic B-N bond pair. The exploration of the chemistry of 1,2-dihydro-1,2-azaborine (hereafter referred

to as 1,2-azaborine) could offer opportunities in a broad range of applications from drug design to conjugated organic materials.

Whereas polycyclic derivatives of 1,2-azaborine have been explored extensively,[1-4] monocyclic 1,2-azaborines have received significantly less attention, presumably due to limited synthetic access. Dewar and White pioneered the first syntheses of 1,2-azaborines in the early 1960s and demonstrated that these compounds have substantial aromatic character.[5-6] More recently, Ashe and co-workers have developed two complementary synthetic strategies for monocyclic 1,2-azaborines: (1) a ring expansion of lithium azaborolides[7] and (2) a ring-closing metathesis (RCM)-oxidation sequence (Scheme 1).[8] These protocols have provided novel 1,2-azaborine structures that have been studied primarily as tunable ligands in organometallic complexes.[9-12]

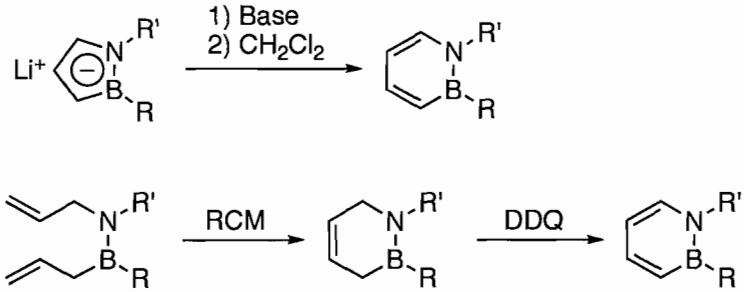

Scheme 1. RCM-oxidation (top) and ring-expansion (bottom) routes to 1,2-azaborines.

Despite the recent advances in the synthesis of monocyclic 1,2-azaborines, significant synthetic challenges remained when we began our work. Specifically, the scope with respect to the exocyclic boron substituent was limited to carbon- and oxygen-based groups. In contrast, the ubiquity of the phenyl motif in chemistry is due in part to the availability of countless substituted derivatives. If the unique features of 1,2-

azaborine as a benzene mimic are to be fully realized, access to a wide array of 1,2-azaborine derivatives must be achieved.

2.3. Generation of a Versatile 2-Chloro-1,2-azaborine

We envisioned that an advanced 1,2-azaborine intermediate bearing an electrophilic boron atom would serve to provide a wide array of boron-substituted 1,2-azaborine structures via nucleophilic displacement of an appropriate leaving group. The RCM-oxidation protocol developed by Ashe avoids the use of nucleophilic reagents and thus would not likely interfere with an electrophilic B-Cl bond. Therefore we prepared the bisallyl aminoborane **1** by Ashe's established method and subjected it to Grubbs' first-generation catalyst ($(Cy_3P)_2(PhCH)RuCl_2$). Gratifyingly, ring-closed heterocycle **2** was readily produced in the reaction and was isolated in 66% yield by vacuum distillation (Scheme 2).

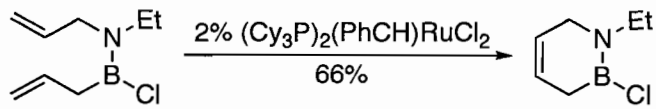

1 **2**

Scheme 2. Ring-closing of aminoborane **1** to generate BN-heterocycle **2**.

The aromatization of **2** to 1,2-azaborine **3** proved to be more challenging (Table 1). Our initial attempts using stoichiometric oxidant 2,3-dichloro-5,6-dicyano-1,4-benzoquinone (DDQ) produced the desired B-Cl 1,2-azaborine **3**, albeit in low yield (Table 1, entry 1). However, screening a series of heterogeneous catalysts showed that palladium can serve as a catalyst for this transformation (entry 2). The catalytic oxidation of **2** to **3** proceeds readily without the addition of a stoichiometric oxidant.

Therefore it seems likely that the elimination of H_2 occurs to regenerate the Pd. With this in mind, the addition of a hydrogen acceptor (i.e., cyclohexene) as solvent was explored, leading to improvements in the yield (entry 3). A survey of transition metals reveals that Pd black catalyzes the aromatization of **3** most efficiently (entries 3-6). Finally, we determined that a homogeneous Pd source is ineffective in mediating this transformation (entry 7).

Table 1. Survey of Aromatization Conditions for Heterocycle **2**

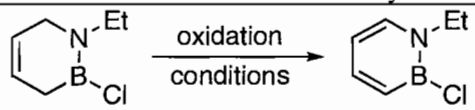

2 **3**

Entry	Conditions	Yield[a] (%)
1	1 equiv. DDQ, pentane, 35 °C, 24 h	14
2	Pd/C (20 mol%), pentane, 80 °C, 16 h	31
3	Pd/C (20 mol%), cyclohexene, 80 °C, 16 h	43
4	Ru/C (20 mol%), cyclohexene, 80 °C, 16 h	1
5	Rh/Al_2O_3 (20 mol%), cyclohexene, 80 °C, 16 h	23
6	**Pd black (20 mol%), cyclohexene, 80 °C, 16 h**	**75**
7	$Pd(PPh_3)_4$ (10 mol%), benzene, 80 °C, 16 h	0

[a] Determined by ^{11}B NMR analysis versus a calibrated internal standard (see Appendix A).

Somewhat unfortunately, a small amount of reduced compound **4** was present in all explored oxidation conditions (Scheme 3). Also disappointing was the observation that side-product **4** was not effectively separated from **3** by vacuum distillation, nor were these compounds found to be particularly stable to silica gel chromatography. In a testament to the increased chemical stability of fully aromatic heterocycle **3** relative to non-aromatic **4**, it was determined that the reaction of an alkynyl Grignard at low temperature occurred almost entirely at the B-Cl bond of **4** in the presence of **3**. This provided a means of purifying 1,2-azaborine **3**, wherein the mixture of **3** and **4** was reacted with phenylethynylmagnesium bromide to selectively generate **5** (Scheme 3).

Purified 1,2-azaborine **3** was obtained via distillation, whereas **5** was left behind as a viscous oil.

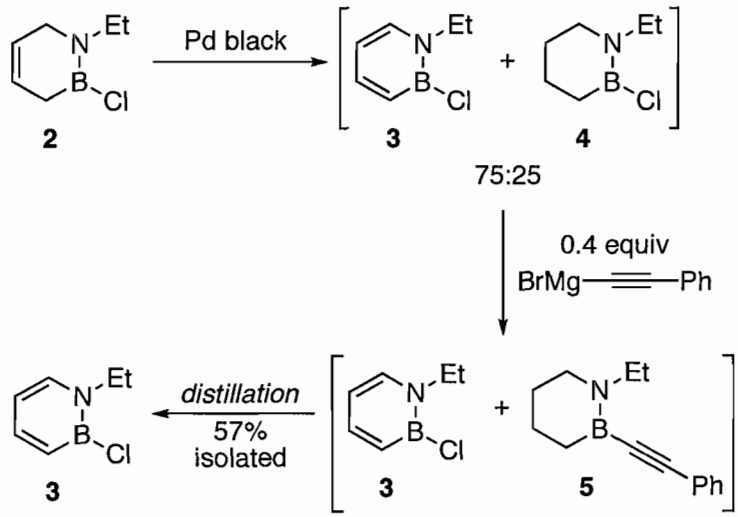

Scheme 3. Purification strategy for 1,2-azaborine **3**.

Heterocycle **3** serves as a general precursor to *B*-substituted 1,2-azaborines (Table 2). Displacement of the chloride in **3** occurs readily in the presence of alkyl- (entry 1), vinyl- (entry 2), aryl- (entry 3), and alkynyl-based (entry 4) nucleophiles.[13] Furthermore, heteroatom substitution also proceeded smoothly, resulting in the isolation of nitrogen-, oxygen-, phosphorus-, and sulfur-substituted 1,2-azaborines (entries 5-8). Treatment of **3** with Superhydride furnished the first monocyclic 1,2-azaborine containing the unique B-H bond (**6i**, entry 8). Compound **6i** is stable to silica gel chromatography. A number of the compounds in Table 2 resemble aromatic structures of significance in chemistry. For instance, the vinyl-substituted 1,2-azaborine **6b** is a heteroaromatic derivative of styrene. The alkynyl-substituted derivative **6d** is an isoelectronic analog of diphenylacetylene (tolan). Intriguingly, phosphorus-substituted **6h** is an isoelectronic analog of triphenylphosphine. Hence, this synthetic protocol can

provide structures of potential value to polymer science, organic materials, and catalysis.

Table 2. Synthesis of B-Substituted 1,2-Azaborines from **3**

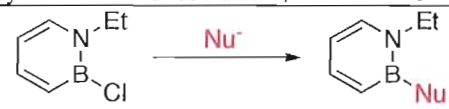

3 **6**

Entry	Nucleophile (Nu)	Product	Yield[a] (%)
1	Li—Bu	**6a**	79
2	Li—vinyl	**6b**	50
3	BrMg—Ph	**6c**	76
4	BrMg—≡—Ph	**6d**	83
5	Li—NMe_2	**6e**	66
6	K—O^{t}Bu	**6f**	71
7	K—SBn	**6g**	80
8	K—PPh_2	**6h**	66
9	$LiBEt_3$—H	**6i**	92

[a] Isolated yield.

To demonstrate the utility of our synthetic method toward drug design, we have prepared **7**, which is isoelectronic with methyl 2-ethylphenoxyacetate **8** (Scheme 4). Compound **8** and its derivatives have demonstrated potent hypolipidemic activity in animal studies.[14] Treatment of 1,2-azaborine precursor **3** with methyl glycolate **9** in the presence of triethylamine furnishes **7** in good yield. Experimental details regarding the synthesis and characterization of compounds **2**-**8** can be found in Appendix A.

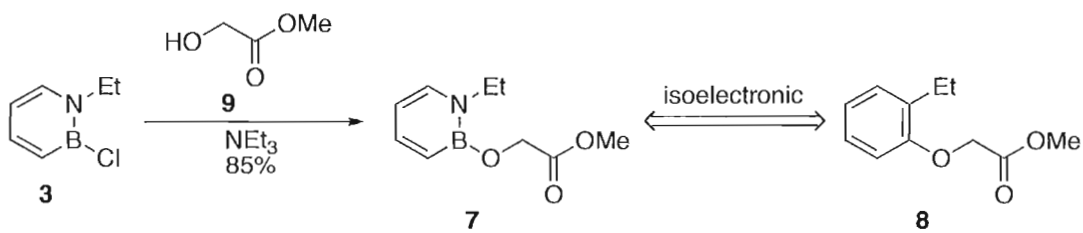

Scheme 4. Synthesis of 1,2-azaborine **7**, isoelectronic analog of hypolipidemic agent **8**.

2.4. The Synthesis and Coordination Chemistry of BN-benzonitrile

In our continued efforts to create diversity of important aromatic structures through BN/CC isosterism, we recognized that 1,2-azaborines bearing electron-withdrawing boron substituents are still elusive. In particular, benzonitrile structures have attracted our attention because of their wide utility as biologically active agents[15] and as ligands in transition metal complexes.[16] We were therefore interested in generating and exploring the chemistry of a 1,2-azaborine analog of benzonitrile (Figure 1).

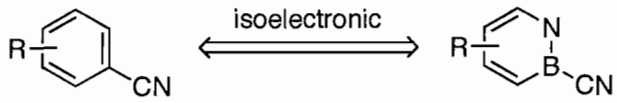

benzonitrile BN-benzonitrile

Figure 1. Benzonitrile and isoelectronic 1,2-azaborine analog.

Benzonitriles are commonly synthesized from aryl halides via the Rosenmund von Braun reaction using stoichiometric amounts of copper(I) cyanide.[17] More recently, transition metal-catalyzed methods for cyanation of aryl halides have been developed.[15] We envisioned that nucleophilic displacement of chloride from B-Cl 1,2-azaborine **3** using cyanide would efficiently generate BN-benzonitrile **10** (Scheme 5). We believed NaCN could serve as a suitable nucleophile to yield the desired BN-benzonitrile **10**. However, treatment of **3** with NaCN resulted in no reaction, even upon heating. After screening a variety of conditions, we determined that the addition of AgCN to a solution of **3** led to the immediate precipitation of AgCl and quantitative formation of **10** as an air- and moisture-sensitive clear and colorless liquid.[18]

The cyanide anion is an ambident nucleophile,[19] and as such, it was unclear whether the product formed was BN-benzonitrile **10** or BN-benzoisonitrile **10'** (Scheme 5). To determine the connectivity of **10**, we treated precursor **3** with labeled $Ag^{13}C^{15}N$. Isotopic enrichment permitted the observation of the nitrile carbon as a broad quartet (δ 126 ppm, q, $^{1}J_{BC}$ = 85 Hz) in the ^{13}C NMR spectrum due to coupling with the ^{11}B atom (S = 3/2). The ^{15}N NMR spectrum shows a sharp doublet ($^{1}J_{CN}$ = 15 Hz), consistent with coupling to the ^{13}C nucleus. IR spectra of **10** and **10'** were calculated at the DFT B3LYP/ DZVPZ level (see Appendix A). Whereas the calculated spectrum of **10** shows a strong vibration for the C≡N bond at 2190 cm^{-1}, the corresponding calculated vibration in **10** is extremely weak at 2300 cm^{-1}, providing another distinction between **10** and **10'**. The experimentally observed IR spectrum of **10** does not exhibit a peak in the expected stretching frequency of cyanides around 2200 cm^{-1}. Thus, the experimental NMR and IR data are consistent with the formation of **10**, not **10'**. The calculated relative zero-point energies (ZPE) of **10** and **10'** indicate that BN benzonitrile **10** is thermodynamically more stable than its isomer **10'** by 3.7 kcal mol^{-1}. Nucleus Independent Chemical Shift (NICS)[20] calculations suggest nitrile **10** (NICS(1) = -7.55) is slightly more aromatic than isonitrile **10'** (NICS(1) = -6.96).

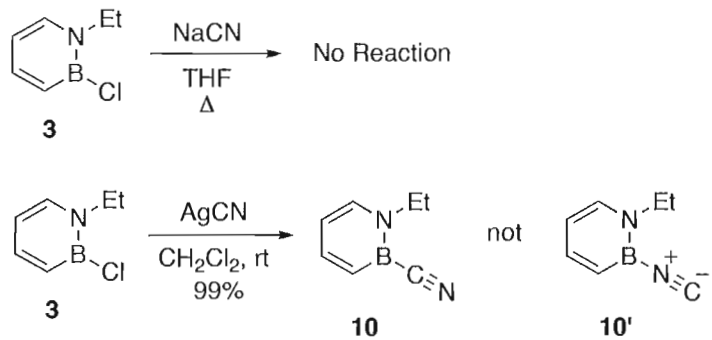

Scheme 5. Synthesis of BN-benzonitrile **10**.

To gain additional insight into the electronic structure of **10**, we calculated the electrostatic potential surface (ESP) of **10** and contrasted it with the ESP for the BH-substituted 1,2-azaborine **6i**. Figure 2 illustrates that in BN-benzonitrile **10**, most of the negative charge (highlighted by the red color) is localized at the electron-withdrawing CN substituent. In contrast, the ESP map of **6i** indicates a greater localization of negative charge on the 1,2-azaborine ring.

Figure 2. Electrostatic potential maps at the 0.002 electron/a.u.^{3} density iso-contour level with an electrostatic potential range from -13.6 to 54.4 kcal mol^{-1} for 1,2-azaborines **10** and **6i**. Blue is positive potential (repulsive for the positive charge), red is negative potential (attractive for the positive charge) and green represents near zero potential.

Analysis of substituent effects on the π-electron density of aromatic molecules has been achieved using NMR spectroscopy.[21] In particular, studies by Herberich et al.[22]

and Fu et al.[23] have shown that electron donation by boron-bound substituents in boratabenzenes, a family of boron-containing heterocycles similar to 1,2-azaborines, leads to upfield shifts of the ortho and para resonances in the ^{1}H and ^{13}C NMR spectra. The ^{1}H and ^{13}C NMR chemical shifts observed for BN benzonitrile **10** (Table 3) suggest that **10** is an electron-deficient 1,2-azaborine. The calculated HOMO and LUMO of BN benzonitrile **10** are presented in Figure 3. The HOMO orbital coefficients are largest at the ortho (3) and para (5) positions of the heterocycle with additional π-electron density predominantly localized at the nitrogen atom of the cyano group. The LUMO of **10** shows a relatively large coefficient at boron, which is consistent with the electrophilic character of boron. Also of note is the fact that the LUMO is antibonding with respect to the CN π bond whereas the HOMO of **10** has bonding character.

Table 3. ^{1}H and ^{13}C NMR Shifts of B-Substituted 1,2-Azaborines

Boron substituent	H_{ortho}	H_{para}	C_{ortho}	C_{para}
NMe_2	6.21	5.72	124	105.5
H	6.84	6.40	131	112.3
CN	6.99	6.64	131	115.1

Experimental chemical shifts [ppm] in CD_2Cl_2.

We next explored the coordination behavior of BN benzonitrile **10**. When **10** was treated with $(MeCN)_3Cr(CO)_3$ in THF at 60 °C, we observed evidence for the formation of the piano-stool complex **11** by ^{1}H and ^{11}B NMR as a minor component of a complex mixture (Scheme 6). The upfield chemical shifts in the ^{1}H and ^{11}B NMR spectra of the reaction are consistent with η^6 coordination of the 1,2-azaborine ring.[10] However, upon work-up we were only able to isolate complex **12** as yellow crystals in low yield.

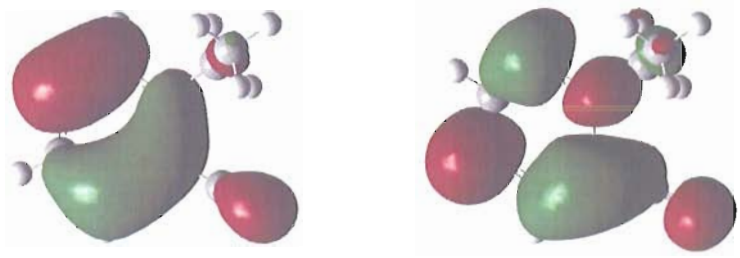

Figure 3. HOMO and LUMO of **10** calculated at the B3LYP/DGDVP2 level.

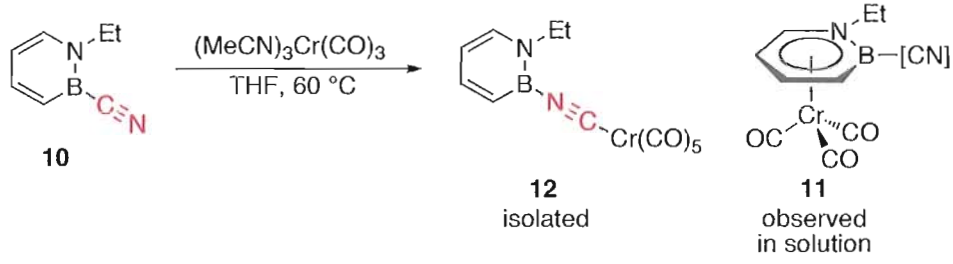

Scheme 6. Complexation of **10** with chromium(0).

Crystals of **12** suitable for single-crystal X-ray analysis were grown from a saturated pentane solution. The X-ray structure of **12** revealed that the original BCN linkage in **10** underwent linkage isomerization under the reaction conditions (Figure 4).[24-26] The structure is nearly co-linear through the B-N-C-Cr group (∠B(1)-N(1)-C(6) = 172.4(3)°, ∠N(1)-C(6)-Cr(1) = 179.3(3)°), indicating sp hybridization for both C(6) and N(1). The slight bend in the B(1)-N(1)-C(6) angle (7.6°) is consistent with a weak M(dπ)→CNR back-bonding interaction, similar to that observed in arylisocyanidechromium pentacarbonyl complexes ($Cr(CO)_5(CNAr)$).[27-29] The B(1)-

N(1) bond (B(1)-N(1) = 1.489(4) Å) is comparable to the boron-isonitrile bond in $Cr(CO)_5(CNB(CH(SiMe_3)_2)_2)$ (B-N = 1.475(6) Å),[30] which to the best of our knowledge is the only other reported crystal structure of a trigonal planar boron atom bound to an isocyanide. The N(1)-C(6) bond distance in **12** (1.153(4) Å) is similar to the NC bond length observed in $Cr(CO)_5(CNB(CH(SiMe_3)_2)_2)$ (N-C = 1.159(5) Å),[30] as well as other reported $Cr(CO)_5(CNAr)$ structures (N-C = 1.151(3) Å).[27-29] The C(6)-Cr(1) bond distance (1.981(3) Å) in **12** is also very similar to the ones exhibited by $(CO)_5Cr(CNB(CH(SiMe_3)_2)_2)$[30] (C–Cr = 1.971(4) Å) and $(CO)_5Cr(CNAr)$[27-29] complexes (C–Cr = 1.968(3) Å. Electron-rich pentacarbonyl(isocyanide)-chromium(0) complexes show long NC–Cr distances (e.g., 2.000(3) Å in $(CO)_5Cr(CNNH_2)$)[31] whereas electron-withdrawing groups on the cyano moiety shorten the C–Cr distance (e.g., 1.883(3) Å in $CO)_5Cr((CNCN)$).[32] The observed structural parameters are consistent with a strong contribution of the resonance form A relative to B in complex **12** (Figure 4). We are interested in the effects of the electron-withdrawing $NCCr(CO)_5$ substituent on the intra-ring bond distances of the six-membered BN heterocycle. We determined that the intra-ring bond distances to boron in **12** are the shortest reported for a 1,2-azaborine (N(2)–B(1) = 1.412(4) Å and B(1)–C(7) = 1.486(5) Å), consistent with substantial positive charge at boron. Complete structural data for **12** are presented in Appendix A.

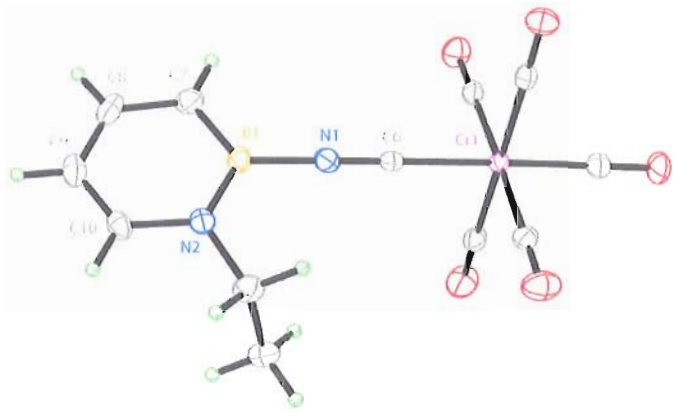

A B

Figure 4. ORTEP illustration of **12**, with ellipsoids drawn at the 35% probability level.

The low-yielding synthesis of **12** outlined in Scheme 7 prevented us from fully characterizing complex **12**. Thus, we sought to independently synthesize **12** via alternative routes. Gratifyingly, we discovered that treatment of 1,2-azaborine precursor **3** with sodium pentacarbonylcyanochromate[33] furnished the desired adduct **12** in quantitative yield (Scheme 7).

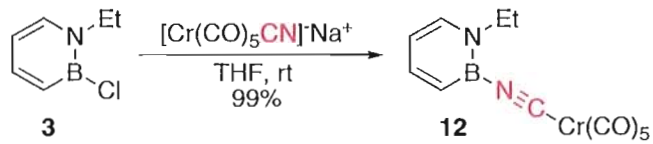

3 **12**

Scheme 7. Alternate route to **12**.

^{1}H and ^{11}B NMR spectra of the material obtained by Scheme 7 were consistent with the previously prepared material via Scheme 6. The ^{13}C NMR spectrum showed the isonitrile carbon as a sharp singlet at 189.2 ppm as well as two unique carbonyl groups, consistent with the cis (215.4 ppm) and trans (217.6 ppm) CO ligands. Finally, in the IR spectrum of **12**, the observed C≡N stretching frequency at 2130 cm^{-1} is

comparable to those observed in related $(CO)_5Cr(CNAr)$ complexes (2121 cm^{-1}),[29] but is at a higher wavenumber than $(CO)_5Cr(CNB(CH(SiMe_3)_2)_2)$ (2113 cm^{-1}).[30] The C≡O vibrations for **12** are at 2051, 1990, and 1954 cm^{-1}. These values are in good agreement with known $(CO)_5Cr(CNAr)$ complexes.[27-29] The experimentally determined IR spectrum of **12** is also in accord with its calculated spectrum (DFT B3LYP/ DZVPZ level, see Appendix A).

The mechanism for the formation of **12** in Scheme 6 remains unclear. We hypothesize that reaction of **10** with $Cr(CO)_5(L)$ or $Cr(CO)_6$ present or generated in the reaction mixture could lead to **12**. To test this hypothesis, we reacted BN benzonitrile **10** with $Cr(CO)_6$ in THF at 60 °C and determined that **12** is generated in 23% yield.

2.5. Cationic B-substituted 1,2-Azaborines

The previous sections discussed the substitution of anionic nucleophiles at the reactive B-Cl bond of 1,2-azaborine **3**. We hypothesized that activation to an even more electrophilic intermediate might make the boron atom susceptible to nucleophilic attack by neutral nucleophiles (Scheme 8). The resulting 1,2-azaborine adducts would be positively charged, opening the way to the study of a novel class of cationic boron heterocycles.

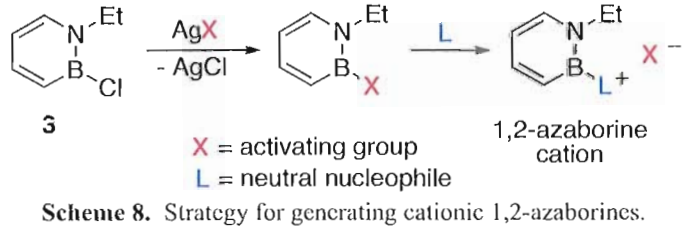

Scheme 8. Strategy for generating cationic 1,2-azaborines.

The reaction of B-Cl 1,2-azaborine **3** with AgOTf gratifyingly produced B-OTf 1,2-azaborine **13**, which was distilled under vacuum in 59% yield as an extremely air- and moisture-sensitive liquid (Scheme 9). In fact, we noticed that the residue of compound **13** on the distillation apparatus fumed instantly when exposed to air. Furthermore, solvents such as THF were incompatible with 1,2-azaborine **13**. The solidification of the entire solution of **13** in THF over the course of a few hours led us to conclude that Lewis acid-catalyzed polymerization of the solvent was taking place.[34] The enhanced Lewis acidity of **13** is likely due to the triflate substituent at boron which is generally an excellent leaving group. 1,2-Azaborine **13** was characterized by ^{1}H, ^{11}B, and ^{13}C NMR spectroscopy as well as IR spectroscopy.

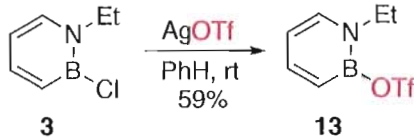

3 **13**

Scheme 9. Synthesis of **13**.

The reaction of **13** with neutral nucleophiles was then examined, the results of which are summarized in Table 4. Pyridine-substituted 1,2-azaborines **14a** (entry 1) was formed quantitatively when 4-phenylpyridine was added to **13**. Phosphine-substituted 1,2-azaborine cation **14b** (entry 2) readily formed upon reaction of PMe_3 with **13**. The reaction of phosphine oxides and pyridine N-oxides with **13** readily provided the cationic adducts **14c** and **14d**, respectively (entries 3 and 4). The intriguing formation of DMSO adduct **14e** (entry 5) was achieved readily.

Table 4. Synthesis of 1,2-Azaborine Cations **14a-e**

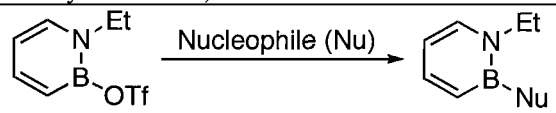

13 **14**

Entry	Nucleophile (Nu)	Product	Yield[a] (%)
1	4-phenylpyridine	**14a**	97
2	PMe_3	**14b**	99
3	Ph_3PO	**14c**	89
4	Pyridine N-oxide	**14d**	99
5	Me_2SO	**14e**	95

[a] Isolated yield.

We have fully characterized compounds **14a-e** by ^{1}H, ^{11}B, and ^{13}C NMR spectroscopy. Phosphorus-containing compounds **14b** and **14c** were further characterized by ^{31}P NMR spectroscopy. The NMR spectroscopic data were consistent with the assigned structures of **14a-e**. Furthermore, X-ray crystallography confirmed the structures of **14a-d**.

The solid-state structure of **14a** is presented in Figure 5 and reveals that the pyridyl nitrogen is bonded to the boron atom with the displacement of the triflate group as a non-coordinating anion. The exocyclic B-N bond length (B(1)-N(2) = 1.531(2) Å) in **14a** is significantly longer than the exocyclic *B*-*N*Ph_2 bond in a 1,2-azaborine recently reported by Liu and co-workers (B-N = 1.486(2) Å,[35] which indicates weaker coordination of the pyridyl nitrogen relative to an amino substituent. The exocyclic B-N bond in cationic **14a** is slightly shorter than the B-N bond in the charge-neutral borabenzene-4-phenylpyridine adduct (B-N = 1.551(3) Å) reported by Fu and co-workers.[36] In the latter example, the B-N bond is dative and is therefore elongated relative to **14a**. The 1,2-azaborine ring in **14a** is completely planar and is twisted by

approximately 50° relative to the pyridine ring. In contrast, the phenyl ring of **14a** is only slightly twisted relative to the pyridine ring (18°). There is a minor degree of bond length heterogeneity within the pyridine ring, as the C(7)-C(8) bond (1.368(2) Å) is slightly shorter than the C(8)-C(9) bond (1.401(2) Å). We were also interested in examining the structural features of the 1,2-azaborine ring in cationic **14a**. The intra-ring B-N bond is short (B(1)-N(1) = 1.413(2) Å), as is the intra-ring B-C bond (B(1)-C(4) = 1.496(2) Å), consistent with an electron-deficient 1,2-azaborine. Additional crystallographic information for **14a** can be found in Appendix A.

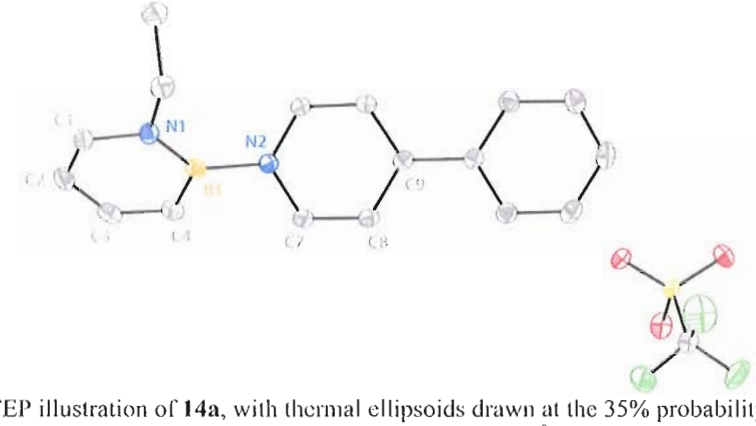

Figure 5. ORTEP illustration of **14a**, with thermal ellipsoids drawn at the 35% probability level (hydrogen atoms have been omitted for clarity). Bond distances (in Å): B(1)-N(1) 1.413(2); B(1)-N(2) 1.531(2); B(1)-C(4) 1.496(2); C(4)-C(3) 1.369(2); C(3)-C(2) 1.408(3); C(2)-C(1) 1.358(2); C(1)-N(1) 1.3736(19); C(7)-C(8) 1.368(2); C(8)-C(9) 1.401(2); Torsion angles: 1,2-azaborine-pyridine 50.5°; pyridine-phenyl 18.0°.

The solid-state structure of phosphine-substituted **14b** is illustrated in Figure 6. The structural parameters of **14b** are similar to the observed structure of the trimethylphenylphosphonium cation,[37] with which **14b** is isoelectronic. The B-P bond in **14b** is long (B(1)-P(1) = 1.947(3) Å) relative to the C_{aryl}-P bond in trimethylphosphonium iodide (C_{aryl}-P = 1.797(6) Å) which is likely due to the increased van der Waals radius of boron (1.92 Å) relative to carbon (1.70 Å).[38] The 1,2-azaborine

ring is planar and the intra-ring bond distances are virtually identical to those of pyridyl-substituted **14a**. The phosphorus atom in **14b** is pyramidal, with the sum of the three Me-P-Me angles equal to 320°. The sum of Me-P-Me angles in the corresponding $PhPMe_3^+I^-$ was 327°.[37] Additional crystallographic information for **14b** can be found in Appendix A.

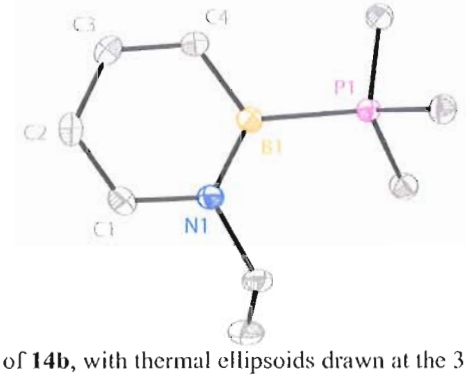

Figure 6. ORTEP illustration of **14b**, with thermal ellipsoids drawn at the 35% probability level (hydrogen atoms and triflate counterion have been omitted for clarity). Bond distances (in Å): B(1)-N(1) 1.419(3); B(1)-P(1) 1.947(3); B(1)-C(4) 1.492(3); C(4)-C(3) 1.368(3); C(3)-C(2) 1.402(3); C(2)-C(1) 1.358(3); C(1)-N(1) 1.365(3).

The crystal structures of **14c** and **14d** are presented in Figures 7 and 8, respectively. In **14c**, the phosphine oxide is bound to boron through oxygen. The B(1)-O(1) bond is long (1.433(2) Å) relative to typical $B(sp^2)$-OR bonds (1.35-1.38 Å),[39] consistent with the difference between dative versus covalent bonding. Despite this observation, the C(4)-B(1)-O(1)-P(1) dihedral angle of 18° indicates a somewhat favorable π-overlap between oxygen's lone-pair and boron's p-orbital. Furthermore, the long P(1)-O(1) bond in **14c** (1.5563(13) Å) relative to typical phosphine oxides (1.48-1.50 Å)[39] indicates a significant reduction of the double-bond character in the P-O bond upon coordination to boron. The structural parameters of **14d** are virtually identical to **14c** with regard to the 1,2-azaborine ring. An examination of the relevant bond lengths

in the exocyclic pyridine N-oxide substituent again indicates very little π-overlap between oxygen and boron. However, the C(4)-B(1)-O(1)-P(1) dihedral angle in **14d** of approximately 3° is ideal for π-overlap between boron and oxygen. Interestingly, the pyridine ring is twisted completely perpendicular to the 1,2-azaborine ring.

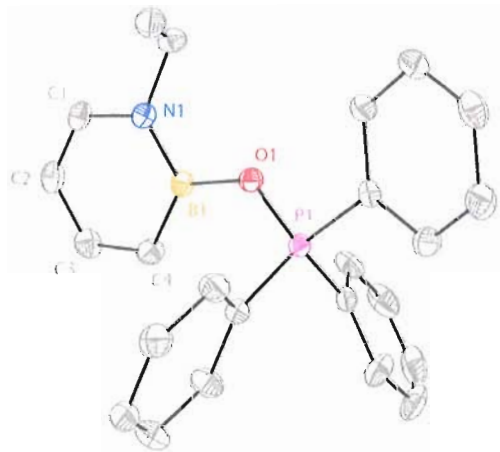

Figure 7. ORTEP illustration of **14c**, with thermal ellipsoids drawn at the 35% probability level (hydrogen atoms and triflate counterion have been omitted for clarity). Bond distances (in Å): B(1)-N(1) 1.420(3); B(1)-O(1) 1.433(2); B(1)-C(4) 1.496(3); C(4)-C(3) 1.369(3); C(3)-C(2) 1.403(3); C(2)-C(1) 1.357(3); C(1)-N(1) 1.368(2); P(1)-O(1) 1.5563(13); Torsion angles: C(4)-B(1)-O(1)-P(1) 18.0°.

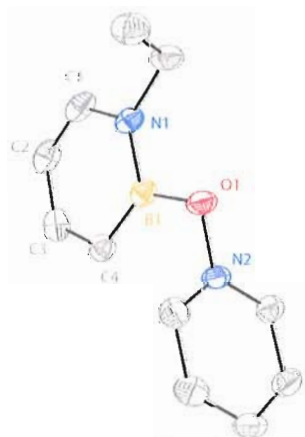

Figure 8. ORTEP illustration of **14d**, with thermal ellipsoids drawn at the 35% probability level (hydrogen atoms and triflate counterion have been omitted for clarity). Bond distances (in Å): B(1)-N(1) 1.414(3); B(1)-O(1) 1.429(3); B(1)-C(4) 1.492(3); C(4)-C(3) 1.363(3); C(3)-C(2) 1.408(4); C(2)-C(1) 1.349(4); C(1)-N(1) 1.371(3); N(2)-O(1) 1.383(2); Torsion angles: C(4)-B(1)-O(1)-N(2) 2.7°; 1,2-azaborine-pyridine 85.5°

Though we were unable to structurally characterize the DMSO adduct **14e** via X-ray crystallography, a comparison of the ^{11}B NMR spectra of **14e** with compounds **14c** and **14d** led us to conclude that boron is likely bound to oxygen in **14e**.

In a continued effort to understand the effects that the exocyclic boron substituent has on the structure and electronics of the 1,2-azaborine system, we have prepared a series of B-pyridyl 1,2-azaborine cations with various groups at the para position of the pyridine ring (Table 5).[40] The phenyl-substituted derivative **14a** (entry 1) was prepared in good yield as discussed above. We observed that the crystals of phenyl-substituted **14a** were light-green in color and solutions of **14a** appeared highly fluorescent. The absorption spectrum of **14a** in CH_2Cl_2 showed a broad, featureless peak at 292 nm (ε = 21869 $M^{-1}cm^{-1}$) as well as less intense bands at higher energy. In MeCN the major absorption was at 251 nm (ε = 17202 $M^{-1}cm^{-1}$) with the lower energy absorption at 290 nm appearing as a shoulder peak. The fluorescence spectrum of **14a** in CH_2Cl_2 showed an emission peak at 360 nm (Φ_{PL} = 0.06) while this emission peak was red-shifted to 382 nm (Φ_{PL} = 0.17) in MeCN. The large Stokes shift of 68 nm for **14a** (in CH_2Cl_2) is indicative of a large degree of structural change in the excited state. Furthermore, at higher sample concentration a prominent emission peak at 500 nm was observed. The concentration dependence of this peak is consistent with excimer formation. It is noteworthy that solid samples of **14a** are highly blue-fluorescent. It was qualitatively determined that the visible fluorescence of **14a** was quenched by the addition of tetrabutylammonium fluoride, presumably through the nucleophilic attack of fluoride at boron.

Pyridine adduct **14f** was prepared in good yield from the reaction of B-OTf 1,2-azaborine **13** with pyridine (Table 5). The absorption spectrum of **14f** in CH_2Cl_2 showed a broad peak at 286 nm ($\varepsilon = 8624\ M^{-1}cm^{-1}$), which was 6 nm blue-shifted relative to **14a**. Though solid samples of **14f** appeared to fluoresce in the blue region of the visible spectrum, dilute solutions of **14f** were non-fluorescent. This suggests that the phenyl ring in **14a** plays a significant role in the solution phase fluorescence of this compound.

The reaction of **13** with 4-(trifluoromethyl)pyridine provided **14g** in good yield. The X-ray crystal structure of **14g** was obtained and selected parameters are presented in Table 5. It is interesting that the selected bond distances and angles for the electron-deficient **14g** are virtually identical to **14a**. The characteristic broad absorption maximum for **14g** was observed at 285 nm ($\varepsilon = 8126\ M^{-1}cm^{-1}$). In contrast to other derivatives, the most prominent absorption band in **14g** was the band at 269 nm ($\varepsilon = 8810\ M^{-1}cm^{-1}$). No emission was observed for solutions of **14g**, though solid samples of **14g** appeared quite fluorescent.

The incorporation of a para-methyl group in the pyridine nucleophile readily provided **14h** in 95% yield (Table 5). The crystal structure of **14h** was obtained and important structural features are summarized in Table 5. Somewhat unfortunately, there appears to be no effect of the inductively donating methyl group on the structure of **14h** relative to the inductively withdrawing CF_3 group in **14g**. Electronically, the absorption maximum at 287 nm ($\varepsilon = 12713\ M^{-1}cm^{-1}$) for **14h** is unchanged from **14g**. Again, no solution phase fluorescence was observed; solid-state fluorescence was qualitatively observed for **14h**.

The substitution of **13** with para-dimethylaminopyridine (DMAP) provided **14i** in 98% yield. The structure of **14i** was confirmed by X-ray crystallography. The structural parameters for **14i** are virtually identical to the derivatives mentioned above. It is of note that the DMAP ring is almost completely perpendicular to the 1,2-azaborine ring (Table 5), which is in contrast to the other derivatives. The absorption spectrum of **14i** showed a broad peak at 283 nm (ε = 21303 $M^{-1}cm^{-1}$), which was relatively unchanged relative to the other pyridinium-substituted derivatives. However, the intensity of this peak was similar to phenyl-substituted **14a**. The emission of **14i** in solution was negligible, in contrast to the observation of fluorescence in the solid-state.

Normalized absorption spectra for **14a** and **14f-i** in CH_2Cl_2 can be found in Figure 9. The absorption and emission spectra of **14a** in CH_2Cl_2 and MeCN are presented in Figure 10. Crystallographic data for compounds **14a**, **14g**, **14h**, and **14i** can be found in Appendix A.

Table 5. Structural and Electronic Properties for Pyridine-substituted 1,2-Azaborines

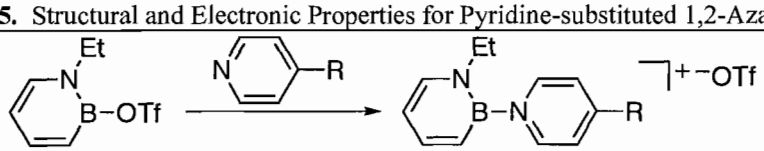

13 **14**

Product	**14a**	**14f**	**14g**	**14h**	**14i**
R	Ph	H	CF_3	CH_3	NMe_2
Yield[a] (%)	97	95	90	95	98
B(1)-N(1) (Å)	1.413(2)	n/a	1.418(5)	1.416(4)	1.423(5)
B(1)-C(4) (Å)	1.496(2)	n/a	1.481(5)	1.489(4)	1.489(6)
B(1)-N(2) (Å)	1.531(2)	n/a	1.528(5)	1.526(4)	1.527(5)
Ring torsion[b]	50.5°	n/a	57.1°	58.0°	77.8°
λ_{max} (nm)	292	286	287[c]	287	283
ε ($M^{-1}cm^{-1}$)	21869	8624	8126	12713	21303

[a] Isolated yield.
[b] Torsion angle between the 1,2-azaborine and pyridine rings.
[c] **14g** has a more prominent absorption at 269 nm.

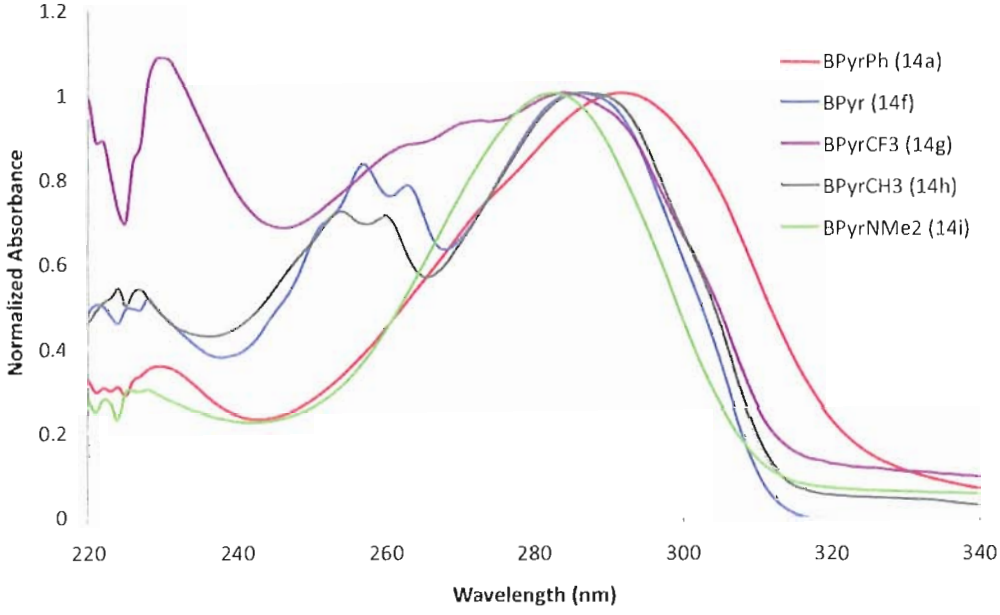

Figure 9. Normalized absorption spectra for pyridine-substituted 1,2-azaborine cations.

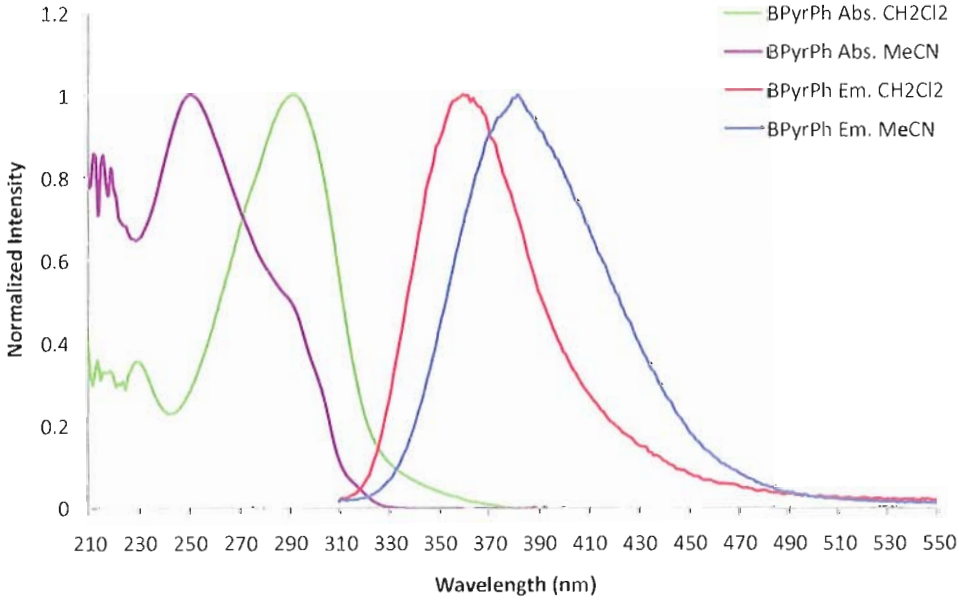

Figure 10. Absorption and emission spectra of **14a** in CH_2Cl_2 and MeCN.

2.6. Substituent Effects in Neutral 1,2-Azaborines

The substitution of carbon- and heteroatom-based nucleophiles at the boron position of 1,2-azaborine has been described in the previous sections. Having expanded the pool of available 1,2-azaborines, we were interested in determining the consequences that various substituents have on bond delocalization within the 1,2-azaborine ring. We rationalized that the substitution of π-donors (e. g. oxygen- and nitrogen-based groups) could disrupt the intra-ring B-N π-bond in 1,2-azaborine (Scheme 10). In analogy, Dewar and co-workers have found that the installation of π-acceptors at the nitrogen position of BN-naphthalenes lowers the chemical stability of these aromatic BN-heterocycles.[41] This was ascribed to the partial removal of nitrogen's lone-pair from the B-N π-bond, leaving boron more susceptible to nucleophilic attack.

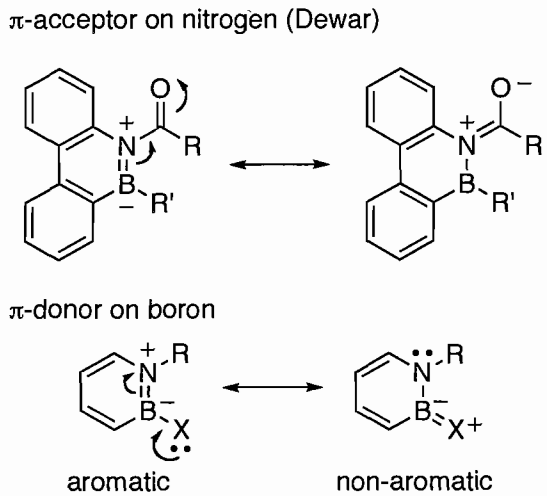

Scheme 10. Disruption of aromaticity in substituted BN-heterocycles.

We have characterized 1,2-azaborine **7** by single-crystal X-ray crystallography, which features an exocyclic oxygen substituent (Figure 11). The exocyclic oxygen atom O(1) of **7** is trigonal (i.e., sp^2-hybridized), with ∠B(1)-O(1)-C(7) = 118.6(1)°. The C(7)-

O(1)-B(1)-N(1) torsion angle of -172.9(1)° and the B(1)-O(1) bond distance of 1.389(2) Å suggest significant π-bonding between oxygen and boron (sum of covalent radii = 1.55 Å),[42] and is significantly shorter than the phosphine oxide (**14c**) pyridine N-oxide (**14d**) structures discussed above. The 1,2-azaborine ring is completely planar within 0.003 Å. The bond distances in the 1,2-azaborine ring (in Å), B(1)-N(1) = 1.436(2), N(1)-C(1) = 1.370(2), C(1)-C(2) = 1.355(2), C(2)-C(3) = 1.413(2), C(3)-C(4) = 1.363(2), and C(4)-B(1) = 1.518(2), are similar to the reported ones with *B*-Ph substitution.[10] Thus, the oxygen heteroatom does not appear to significantly affect the aromatic delocalization of the 1,2-azaborine heterocycle.

We obtained the X-ray crystal structure of phosphorus-substituted **6h** (Figure 12). The structure of **6h** closely resembles triphenylphosphine in that the phosphorus atom is pyramidal with ∠B(1)–P(1)–C(13) = 106.1(1)°, ∠B(1)–P(1)–C(7) = 101.9(1)°, and ∠C(7)–P(1)–C(13) = 103.0(1)° (∑ = 311°). The C(13)–P(1)–B(1)–N(1) torsion angle of 70.3(1)° and the long P(1)–B(1) bond distance (1.948(2) Å) suggest little to no π-bonding between the phosphorus lone-pair and boron. The 1,2-azaborine ring is completely planar within 0.003 Å. The bond distances within the 1,2-azaborine ring (in Å), B(1)–N(1) = 1.439(2), N(1)–C(4) = 1.367(2), C(4)–C(3) = 1.357(2), C(2)–C(3) = 1.403(3), C(2)–C(1) = 1.369(2), and C(1)–B(1) = 1.506(2), are virtually identical to those seen in oxygen-substituted **7**.

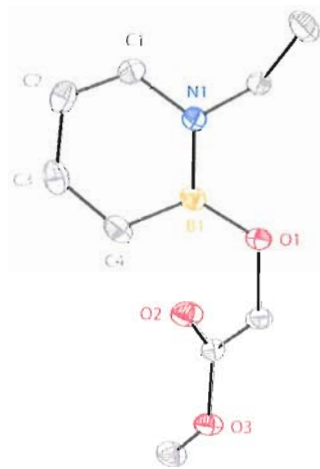

Figure 11. ORTEP illustration of **7**, with thermal ellipsoids drawn at the 35% probability level (hydrogen atoms have been omitted for clarity).

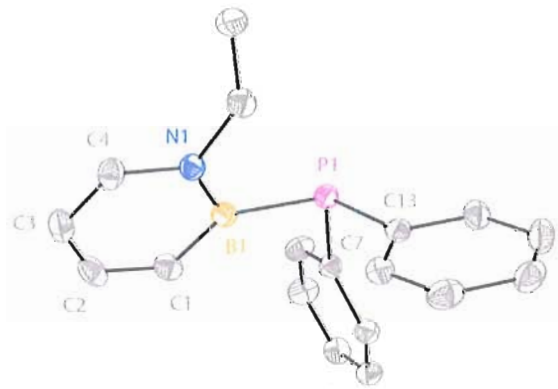

Figure 12. ORTEP illustration of **6h**, with thermal ellipsoids drawn at the 35% probability level (hydrogen atoms have been omitted for clarity).

Thiol-substituted **6g** was isolated as a white crystalline solid which was characterized by single-crystal X-ray crystallography (Figure 13). The exocyclic sulfur atom was found to be in a favorable geometry to participate in π-bonding with boron (C(7)-S(1)-B(1)-C(4) torsion angle = 0.6(3)°). However, the B(1)-S(1) bond (1.838(3) Å) is only marginally shorter than the sum of covalent radii for boron and sulfur (1.89 Å),[42] indicating little π-bonding between sulfur and boron. Furthermore, ∠B(1)-S(1)-C(7) = 103.00(13)°, indicating a tetrahedral sulfur atom. The 1,2-azaborine ring was

planar and intra-ring bond lengths were virtually identical to the 1,2-azaborines discussed above (see Appendix A for full crystallographic data).

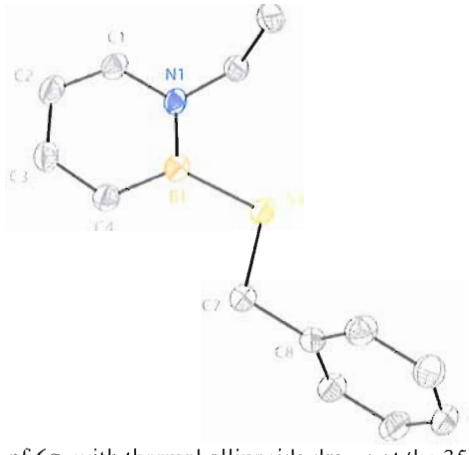

Figure 13. ORTEP illustration of **6g**, with thermal ellipsoids drawn at the 35% probability level (hydrogen atoms have been omitted for clarity).

With the exception of the structures discussed above, N-ethyl 1,2-azaborines were found to be liquids or oils and failed to produce X-ray quality crystals. To complete the survey of crystallographically characterized 1,2-azaborines, we prepared N-benzyl 1,2-azaborine **15** in a similar synthetic sequence to N-ethyl 1,2-azaborine **3**. The reaction of allylbenzylamine with allylboron dichloride (generated in situ from the transmetallation of BCl_3 with allyltriphenyltin) produced bisallyl aminoborane **16** in 46% yield (Scheme 11). The use of allyltriphenyltin in the transmetallation was preferred due to the simple removal of the precipitated triphenyltin chloride prior to distillation. The use of allyltri-n-butyltin resulted in a chlorostannane that was inseparable from the desired product **16**. However, we determined that cold reaction temperatures were required throughout the reaction when using allyltriphenyltin as to avoid undesired transmetallation of the phenyl groups. Ring-closing metathesis with

Grubbs 1st generation catalyst produced **17**, which was isolated in 91% yield by vacuum distillation. Oxidation with Pd/C produced B-Cl 1,2-azaborine **15** in 47% yield as an extremely air-sensitive liquid.

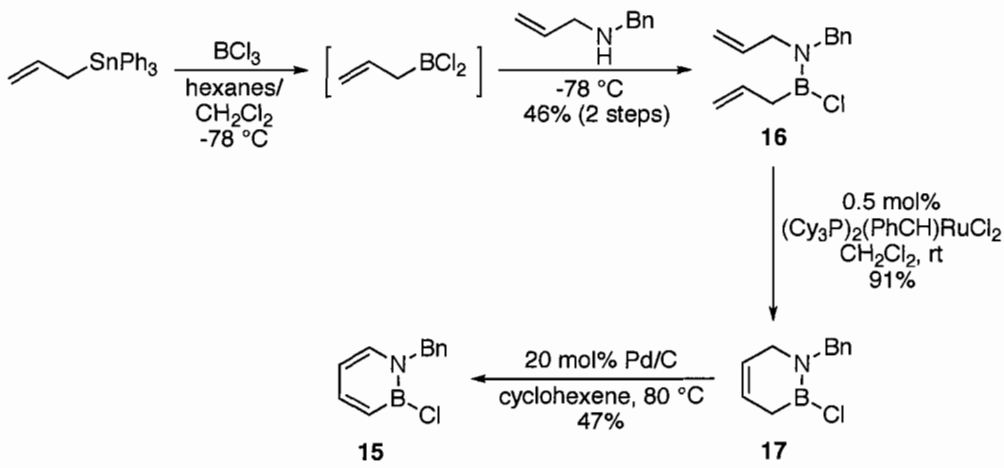

Scheme 11. Synthesis of 1,2-azaborine **15**.

We observed that compound **15** solidified when stored at –20 °C. After Herculean efforts to isolate and mount X-ray quality crystals on the diffractometer, the X-ray crystal structure of **15** was obtained, which is shown in Figure 14. The structure of **15** confirms unambiguously that the B-Cl substituent in **15** has been maintained throughout the synthesis. The B(1)-Cl(1) bond length of 1.7962(15) Å is comparable to B-Cl derivatives of borazine,[44] but is slightly longer than the B-Cl bonds in acyclic $(Me_3Si)_2NBCl_2$ (B-Cl = 1.779(2) Å).[44] The 1,2-azaborine ring is completely planar, in contrast to the known B-Cl borazine derivatives, which show a significant distortion toward a chair-like structure.[44] The intra-ring bond distances in **15** are similar to the previously described structures, however there is a slight contraction in the B-N bond in **15** (1.4220(19) Å).

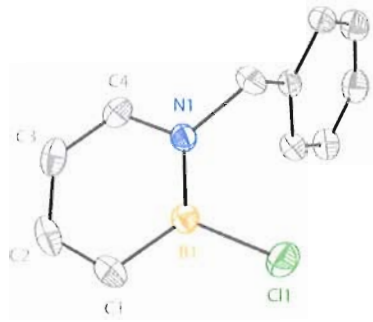

Figure 14. ORTEP illustration of **15**, with thermal ellipsoids drawn at the 35% probability level (hydrogen atoms have been omitted for clarity).

The ^{11}B NMR chemical shift of **15** at 33 ppm was similar to B-Cl 1,2-azaborine **3**, however the ^{11}B NMR spectrum of **15** showed an additional minor peak at 29 ppm, which was ascribed to the hydrolysis of **15** to a B-OH or B-O-B moiety. This is consistent with reports by Dewar,[45] Paetzold,[46] and Philp[47] for polycyclic derivatives. When **15** was distilled to dryness under vacuum, we noticed that a crystalline white solid was left in the distillation flask. Single-crystal X-ray crystallography revealed this material to be the B-O-B ether **18** (Figure 15). It is unclear whether the B-O-B ether was present prior to distillation or was formed via the dehydration of a B-OH 1,2-azaborine during the distillation. Philp and co-workers described the formation of B-O-B ethers by heating a B-OH azaborophenanthrene species under vacuum.[47] We believe the formation of **18** via an analogous process is reasonable.

The unit cell of **18** contains two molecules, however for clarity only one of these is shown in Figure 15. The bridging oxygen atom in **18** is distorted from the sp^2-hybridized geometry observed in **7** with the B-O-B angle closer to linear (∠B(1)-O(1)-B(2) = 132.08(1)°). The B-O bonds in **18** (B(1)-O(1) = 1.382(2) Å, B(2)-O(1) = 1.369(2) Å) are similar in length to the B-O bond in **7**, indicating that both B-O bonds in

18 have significant π-character. The intra-ring bond distances in **18** were quite similar to previously discussed derivatives, and we could not draw any additional conclusions with regard to substituent effects on the 1,2-azaborine system.

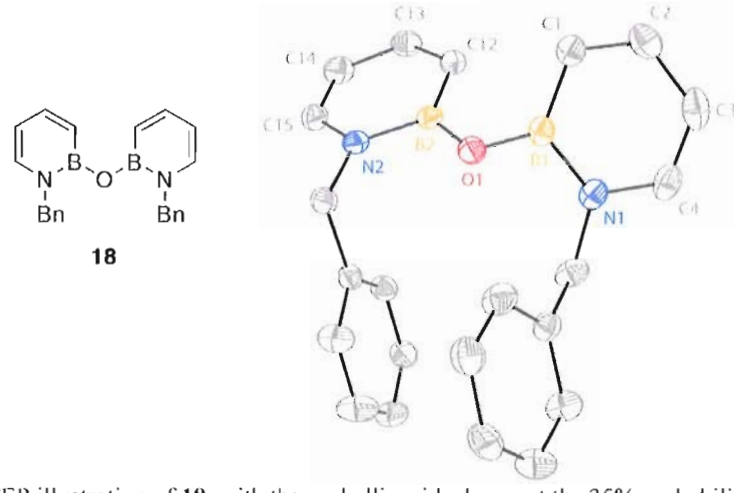

Figure 15. ORTEP illustration of **18**, with thermal ellipsoids drawn at the 35% probability level (hydrogen atoms have been omitted for clarity).

Two additional carbon-based 1,2-azaborines were examined crystallographically. We were interested in determining the contributions made by conjugated materials on the 1,2-azaborine system. Thus, phenyl- and alkynyl-substituted derivatives **19** and **20**, respectively, were synthesized from B-Cl 1,2-azaborine **15** in good yield (Scheme 12).

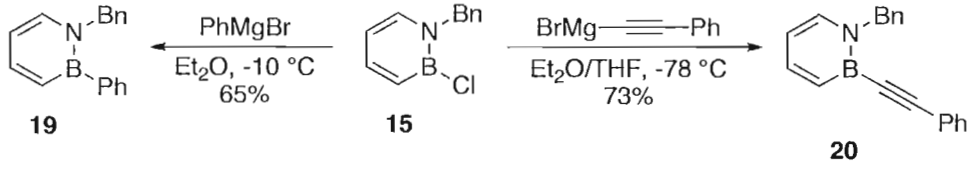

Scheme 12. Synthesis of BN-biphenyl **19** and BN-tolan **20**.

The X-ray crystal structures of **19** and **20** are presented in Figures 16 and 17, respectively. The intra-ring bond distances in **19** and **20** are similar to those discussed

above, which indicates that bond delocalization in the 1,2-azaborine ring is unaffected by π-conjugated substituents. The phenyl ring in BN-biphenyl **19** was twisted relative to the 1,2-azaborine ring with a dihedral angle of –49.0(2)°. This is similar to the 43° dihedral angle reported for borabenzene-pyridine adducts,[36] another heteroatomic analog of biphenyl. With respect to the BN-tolan **20**, the structure is close to planar through the tolan unit, though the phenyl ring is twisted out of plane by 14° relative to the 1,2-azaborine ring. The alkyne bridge is only slightly deviated from linearity (∠B(1)-C(5)-C(6) = 177.4(3)°; ∠C(5)-C(6)-C(7) = 177.1(3)°) and the C≡C bond distance in **20** (1.208(3) Å) is on par with diphenylacetylene (1.198(3) Å).[48] Crystallographic data for the 1,2-azaborines discussed above can be found in Appendix A.

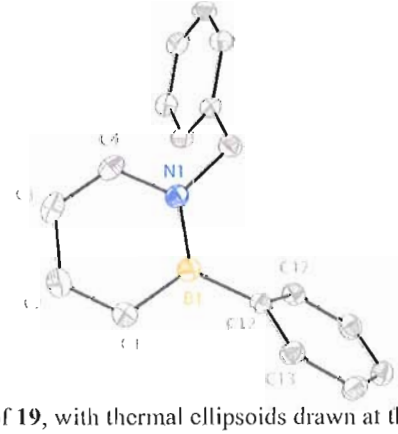

Figure 16. ORTEP illustration of **19**, with thermal ellipsoids drawn at the 35% probability level (hydrogen atoms have been omitted for clarity).

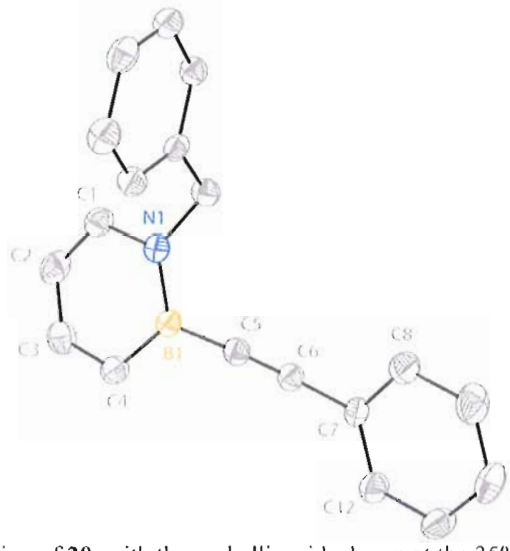

Figure 17. ORTEP illustration of **20**, with thermal ellipsoids drawn at the 35% probability level (hydrogen atoms have been omitted for clarity).

While this study has been focused on the effects that boron substituents have on the structural features of 1,2-azaborines, some additional general observations can be made regarding the preferred geometry of these derivatives. Specifically, the geometries at the nitrogen position in N-alkylated 1,2-azaborines display an interesting trend. In the eleven N-ethyl derivatives presented, the ethyl substituent is consistently bent in a perpendicular fashion to the 1,2-azaborine ring. The *N*-*C*H_2-*C*H_3 angle (θ) ranges from 111.4(3)° to 113.2(2)° (Figure 18, left), but more interestingly the dihedral angle between the 1,2-azaborine ring and the N-ethyl substituent deviates from 90° by no more than 24° with an average value of $\varphi = 13°$ (Figure 18, right). The preference for this perpendicular conformation has been studied in ethylbenzene,[49] for which it was found that both electronic and steric effects play a role in the observed conformational preference. The perpendicular conformation of the ethyl group in 1,2-azaborine is consistent with the donation of nitrogen's lone-pair into the σ^* orbital of the ethyl C-C

bond. Alternatively, the perpendicular conformation may be a consequence of steric repulsion that is minimized when the methylene hydrogens are in a pseudo-gauche conformation with the 1,2-azaborine ring (Figure 18, right). The *N*-CH_2-*Ph* angle (θ) ranged between 113.04(11)° and 114.7(3)° for the four structures containing an N-benzyl groups. The dihedral angle (φ) between the N-benzyl substituent and the 1,2-azaborine ring is generally similar to the values observed in the N-ethyl derivatives. However, in the case of B-phenyl N-benzyl 1,2-azaborine **19**, there is a substantial twist of the N-benzyl substituent away from the phenyl ring on boron (B(1)-N(1)-C(5)-C(6) = 125.26(15)°), which is likely due to steric repulsion between these two groups.

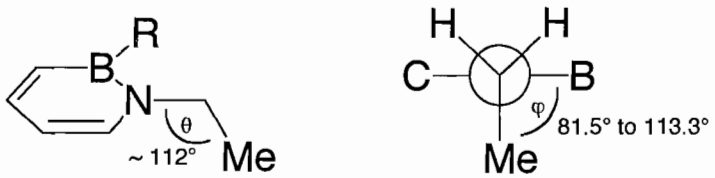

Figure 18. Geometric orientation of the N-ethyl substituent in 1,2-azaborines.

In collaboration with the Kukolich group, we have recently shown via microwave spectroscopy and DFT calculations that the energy-minimized structure of B-H N-Et 1,2-azaborine **6i** places the ethyl substituent at a perpendicular position relative to the 1,2-azaborine ring.[50] Furthermore, the Kukolich group calculated the change in energy (torsional barrier) as a function of the dihedral angle, which suggested that the torsional barrier of **6i** was approximately 3.2 kcal/mol (*B*-*N*-CH_2-CH_3 = 0°). The torsional barrier at *B*-*N*-CH_2-CH_3 = 180° was found to be slightly higher (3.9 kcal/mol), indicating rotation of the ethyl group past the boron position is slightly more favorable. In contrast, the symmetric torsional barrier in ethylbenzene was calculated to be approximately half that of **6i**.

We expected to observe structural changes in the 1,2-azaborine ring as the exocyclic boron substituent was varied. However, the crystallographic parameters in 1,2-azaborine appear relatively immune to the effects of carbon- and heteroatom-based substituents at this position. The significantly contracted bond lengths in cationic and other electron-deficient structures are the only examples for which structural variation was observed. The consistency of 1,2-azaborine structural parameters suggests significant aromatic character in the 1,2-azaborine system.

Though 1,2-azaborines are structurally unaffected by exocyclic substituents, we envisioned that subtle electronic differences could result in measurable differences in reactivity. Electrophilic aromatic substitution (EAS) of 1,2-azaborines has been demonstrated by Ashe and co-workers[51] and more recently by Liu and co-workers.[52] The bromination of 1,2-azaborine is facile and selective for substitution at the C3 position. We believed that this reaction could provide a metric to determine the electronic contribution of boron-substituted groups. A survey of the bromination of several 1,2-azaborines revealed that chloro-, alkyl-, aryl-, and alkoxy-substituted 1,2-azaborines cleanly react with Br_2 to generate C3-brominated products. Unfortunately, amino- and H-substituted derivatives provided a mixture of products and appeared somewhat prone to degradation upon the addition of Br_2. Thus these were not suitable substrates for a competition experiment. Nevertheless, in a competition experiment between chloro-, phenyl-, n-butyl-, and methoxy-substituted 1,2-azaborines **15**, **19**, **21**, and **22** respectively (Figure 19), it was found that the order of reactivity toward Br_2 was **19** > **22** > **21** > **15**. Phenyl-substituted **19** was 5.4 times more reactive than **15**, while

methoxy-substituted **22** was 2.0 times as reactive as **15**. B-Butyl **21** was 1.9 times more reactive than **15**. These data indicate that the electron-deficient B-Cl derivative **15** is deactivated relative to the other derivatives, while more electron-rich groups facilitate EAS reactivity. Furthermore, the highly reactive nature of phenyl-substituted **19** relative to butyl-substituted **21** suggests that both inductive and resonance contributions affect EAS reactivity. Experimental details for the competition reactions and for the preparation of **21**, **22**, and **23** can be found in Appendix A.

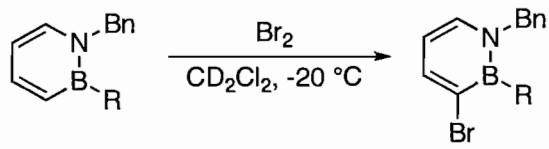

Compound	Relative Rate
15 R = Cl	1
19 R = Ph	5.4
21 R = Bu	1.9
22 R = OMe	2.0

Figure 19. Relative rates of bromination for B-substituted 1,2-azaborines.

2.7. Conclusion

In summary, we have developed a general method for the synthesis of a wide range of *B*-substituted 1,2-azaborines, including the first examples containing *B*-heteroatoms. The synthesis and coordination chemistry of an especially electron-deficient 1,2-azaborine, BN-benzonitrile, has been explored. We have also provided an efficient route to a novel class of cationic 1,2-azaborines. A systematic examination of the structural features of the 1,2-azaborine system has revealed that bond delocalization in the heterocycle is relatively unperturbed by exocyclic substituents. The use of 1,2-

azaborines as isoelectronic analogs of the ubiquitous benzene motif may provide new opportunities in the areas of drug discovery and material science.

2.8. Bridge to Chapter III

Chapter III discusses the work toward the synthesis of the parent 1,2-dihydro-1,2-azaborine, which is isoelectronic with benzene itself. The preparative methods discovered in Chapter II are coupled with the installation of a cleavable protecting group at nitrogen, leading to the first successful synthesis of 1,2-dihydro-1,2-azaborine. The comprehensive characterization of 1,2-dihydro-1,2-azaborine is explored, including rotational spectroscopy in collaboration with the Kukolich group at the University of Arizona. Experimental results are compared to high-level calculations performed by the Dixon group at the University of Alabama in order to elucidate the structural and electronic features of this fundamentally important molecule. The last section of Chapter III discusses a proof of principle protein binding study of 1,2-dihydro-1,2-azaborine in relation to benzene.

CHAPTER III

SYNTHESIS AND CHARACTERIZATION OF 1,2-DIHYDRO-1,2-AZABORINE

3.1. General Overview

This chapter discusses the synthesis, isolation, and characterization of 1,2-dihydro-1,2-azaborine. This excerpt includes unpublished material as well as material published as Marwitz, A. J. V.; Matus, M. H.; Zakharov, L. N.; Dixon, D. A.; Liu, S. –Y. "A hybrid organic/inorganic benzene," *Angew. Chem. Int. Ed.* **2009**, *48*, 973-977. The X-ray crystallographic data was collected and analyzed by Dr. Lev Zakharov. DFT calculations were performed by Myrna Matus and Professor David Dixon. Otherwise all experimental work was performed by me. The co-authored excerpt was written entirely by me.

This chapter also includes vibrational spectroscopy performed on 1,2-dihydro-1,2-azaborine. This excerpt includes material published as Daly, A. M.; Tajaroon, C.; Marwitz, A. J. V.; Liu, S. –Y.; Kukolich, S. G. "Microwave spectrum, structural parameters, and quadrupole coupling for 1,2-dihydro-1,2-azaborine," *J. Am. Chem. Soc.* **2010**, *132*, 5501-5506. Vibrational spectroscopy and DFT calcuations were performed by Adam Daly, Chakree Tanjaroon, and Professor Stephen Kukolich. Otherwise all

experimental work was performed by me. The co-authored excerpt as presented here was written entirely by me.

This chapter also includes a protein binding study of 1,2-azaborines. This excerpt includes material published as Liu, L.; Marwitz, A. J. V.; Matthews, B. W.; Liu, S. –Y. "Boron mimetics: 1,2-dihydro-1,2-azaborines bind inside a non-polar cavity of T4 lysozyme," *Angew. Chem. Int. Ed.* **2009**, *48*, 6817-6819. The X-ray crystallographic data was collected and analyzed by Dr. Lijun Liu. Protein purification and crystal growth was performed by Dr. Lijun Liu. Professor Brian Matthews provided editorial input for this section. Otherwise all experimental work was performed by me. The co-authored excerpt as presented here was written entirely by me.

Professor Shih-Yuan Liu has provided editorial assistance and scientific guidance for all material (published and un-published) presented in this chapter.

3.2. Introduction

Benzene (*c*-C_6H_6) is arguably one of the most fundamentally significant small molecules in chemistry. First discovered by Faraday in 1825,[1] the study of benzene introduced the basic concept of aromaticity and delocalization.[2] In addition to its fundamental importance, benzene and its derivatives (arenes) are ubiquitous in chemical research with numerous applications ranging from biomedical research to materials science.[3] Borazine (c-$B_3N_3H_6$), the inorganic, isoelectronic relative of benzene, was first isolated in 1926 by Alfred Stock,[4] and since then has also played a pivotal role in fundamental and applied chemistry. The isoelectronic and isostructural relationship

between B-N versus C=C bonds has stimulated discussion regarding the aromaticity of borazine.[5-7] In more applied fields, borazine serves as a precursor to BN-based ceramic materials.[8,9] In the area of chemical hydrogen storage, borazine has been implicated as an intermediate in the hydrogen release from ammonia borane.[10] While benzene and borazine have been thoroughly studied over the last 80 years, the hybrid "organometalloidal" structure containing carbon, boron, and nitrogen, that is, 1,2-dihydro-1,2-azaborine **1**, has thus far eluded characterization (Figure 1).

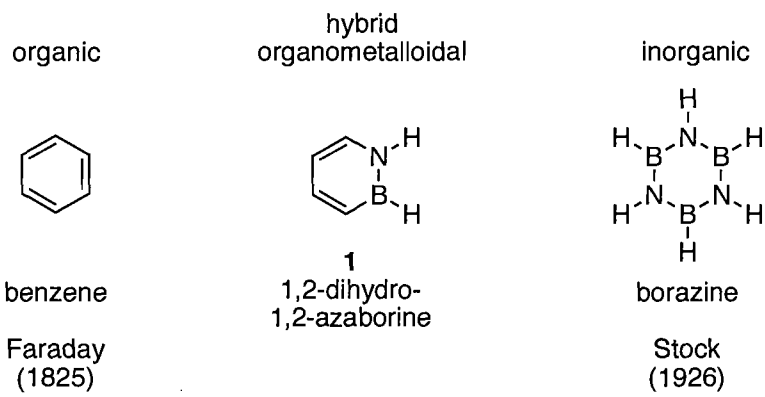

Figure 1. Benzene, borazine, and 1,2-dihydro-1,2-azaborine **1**.

While the chemistry of polycyclic boron-nitrogen heterocycles is well understood,[11-13] monocyclic derivatives have been relatively unexplored. Dewar and White pioneered the chemistry of monocyclic 1,2-dihydro-1,2-azaborines (hereafter referred to as 1,2-azaborine unless referring to the parent compound **1**) in the 1960s.[14-15] Recent contributions by the Ashe and Liu groups have expanded the scope of available 1,2-azaborines.[16-18] Yet the synthesis of the relatively simple heterocycle **1** remained unrealized 50 years after the first report of its attempted synthesis.[19] This chapter discusses the development of the first successful synthesis of 1,2-dihydro-1,2-azaborine

1. The in-depth characterization of **1** follows the synthetic discussion, and provides information regarding its aromaticity in relation to benzene and borazine. Our experimentally determined structural and spectroscopic properties are consistent with values derived from high-level computations. Finally, a protein binding study is discussed which provides a "proof-of-principle" demonstration of the bio-mimetic potential of 1,2-azaborines.

3.3. Synthesis and Characterization of 1,2-Dihydro-1,2-azaborine

We have reported the synthesis of 1,2-azaborines incorporating various heteroatoms at the boron position, including the B-H functionality of 1,2-dihydro-1,2-azaborine **1**.[18] We believed a comparable route to **1** would be possible via the incorporation of a protecting group at the nitrogen position of an advanced 1,2-azaborine. The synthesis of **1** was envisioned to occur from this intermediate in a two-step protocol (Scheme 1): 1) hydride substitution at boron would provide the B-H functionality, and 2) cleavage of the nitrogen protecting group would give **1**.

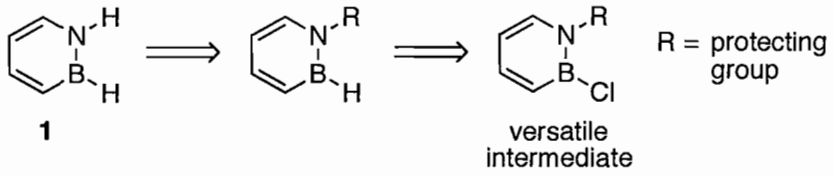

Scheme 1. Retrosynthesis of **1** from a versatile 1,2-azaborine intermediate.

The first nitrogen protecting group we screened was the benzyl group, which is a chemically robust group that can generally be cleaved without the use of strong acid or base.[20] Ashe and co-workers demonstrated that B-phenyl 1,2-azaborines are remarkably

resistance to hydrolysis and can even be treated with aqueous work-up.[21] Therefore, to probe the viability of N-benzyl deprotection, we synthesized B-phenyl 1,2-azaborine **2** (previously described in Chapter II, Scheme 13) and screened a variety of reaction conditions for the cleavage of the N-benzyl group of **2** to N-H 1,2-azaborine **3**[15] (Table 1). The deprotection of N-benzyl groups is commonly achieved using heterogeneous Pd catalysts and H_2.[20] Unfortunately, we failed to observe evidence for the cleavage of the benzyl group using heterogeneous Pd (entries 1-5). Instead, we discovered that the 1,2-azaborine ring is prone to reduction under these conditions (**4** in Table 1). The addition of trimethylsilyliodide (TMSI) was ineffective at cleaving the N-benzyl group in **2** (entry 6).[22] 2,3-Dichloro-5,6-dicyanobenzoquinone (DDQ) has been shown to cleave benzyl groups,[23] yet no reaction was observed with **2** (entry 7). Finally, oxidative debenzylation was attempted with ceric ammonium nitrate,[24] but no product formation was observed (entry 8).

Table 1. Survey of Debenzylation Conditions for Heterocycle **2**

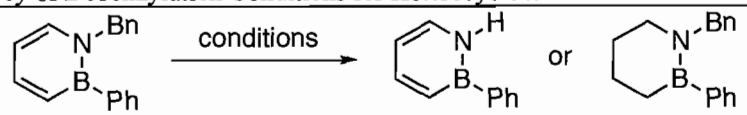

2 **3** **4**

Entry	Conditions	Product
1	20 mol% Pd/C, 80 °C, C_6D_6, 40 psi H_2, 6 h	50% **4**[a]
2	10 mol% Pd/C, 60 °C, C_6D_6, 40 psi H_2, 4 h	40% **4**[a]
3	20 mol% Pd/C, 80 °C, THF-d_8, 1 atm H_2, 14 h	100% **4**[a]
4	10 mol% $Pd(OH)_2$/C, 25 °C, EtOH, 50 psi H_2, 18 h	no reaction
5	12.5 mol% Pd/C, 25 °C, MeOH, excess HCO_2H, 48 h	degradation[b]
6	excess TMSI, 60 °C, CD_2Cl_2 then MeOH, 4 h	no reaction
7	1 equiv. DDQ, 75 °C, pentane, 4 h	no reaction
8	2 equiv. $(NH_4)_2Ce(NO_3)_6$, 25 °C, MeCN/H_2O, 4 h	no reaction

[a] ^{1}H NMR integration versus starting material.
[b] ^{11}B NMR indicated the formation of a 4-coordinate boron-containing compound.

We next explored the synthetic availability of silicon-based protecting groups at the nitrogen position of 1,2-azaborine. The Ashe group has demonstrated the incorporation and facile removal of an N-trimethylsilyl (N-TMS) protecting group from a B-phenyl 1,2-azaborine.[21] We therefore endeavored to produce the analogous B-H N-TMS 1,2-azaborine on the way to the parent 1,2-dihydro-1,2-azaborine **1**. The reaction of TMS-allylamine with allylboron dichloride (generated in situ from the transmetallation of BCl_3 and allyltriphenylstannane) gave a mixture of products, including the desired bisallyl aminoborane **5** (Scheme 2). We were unfortunately unable to purify **5**.

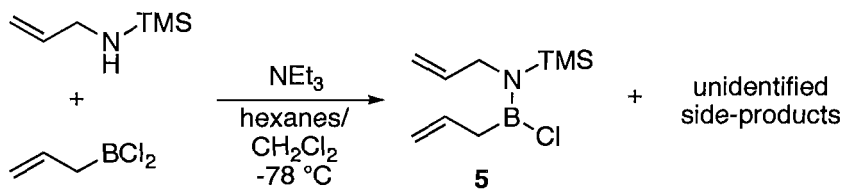

Scheme 2. Observation of TMS-protected aminoborane **5**.

We next turned to the bulky triisopropylsilyl (TIPS) protecting group.[20] The improved stability of the TIPS protecting group permitted the formation of aminoborane **6**, which was purified by vacuum distillation in 24% yield (Scheme 3). However, ring-closing metathesis (RCM) of **6** with the first-generation Grubbs catalyst proved sluggish. We believe that the intramolecular ring closing to form heterocycle **7** is hindered by the steric bulk of the TIPS group.

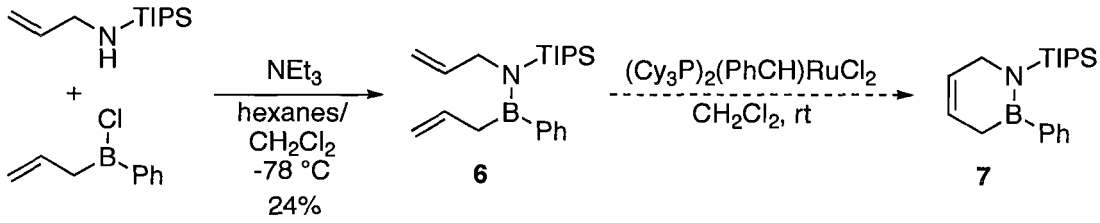

Scheme 3. Formation of TIPS-protected **6** and attempted ring-closing metathesis.

The *tert*-butyldimethylsilyl (TBS) group is generally intermediate between the TMS and TIPS groups with regard to stability and steric bulk.[20] The reaction of allylboron dichloride with TBS-allyl amine furnished aminoborane **8** in 58% yield (Scheme 4).[25] Ring-closing metathesis of **8** with Grubbs 1st generation catalyst readily provided the six-membered heterocycle, albeit as an isomeric mixture of **9** and **9'** (60:40 ratio). Catalytic dehydrogenation of this mixture with Pd/C produced 1,2-azaborine **10** in 35% yield. The reaction of **10** with $LiBHEt_3$ installed the desired B-H functionality to give **11** in quantitative yield. The direct formation of the parent compound **1** from **11** was unsuccessful. The addition of tetrabutylammonium fluoride (TBAF) and other fluoride sources failed to provide **1**, yielding either unreacted starting material or undesired side-products resulting from nucleophilic attack at boron. Alternatively, complexation of 1,2-azaborine **11** with tricarbonylchromium(0) trisacetonitrile produced piano-stool adduct **12** in 71% yield. Subsequent removal of the N-protecting group with a protic fluoride source (HF-pyridine) gave **13** in 76 % yield. Decomplexation of **1** from the $Cr(CO)_3$ group was accomplished using triphenylphosphine. Compound **1** proved difficult to isolate owing to its high volatility. The isolation of **1** in 10% yield (Scheme 4) was realized via the addition of triphenylphosphine to a mixture of isopentane and complex **13**, followed by fractional vacuum transfer. While the isolated yield was low,

the efficient formation of **1** was demonstrated via ^{1}H NMR spectroscopy (84% yield against an internal standard).

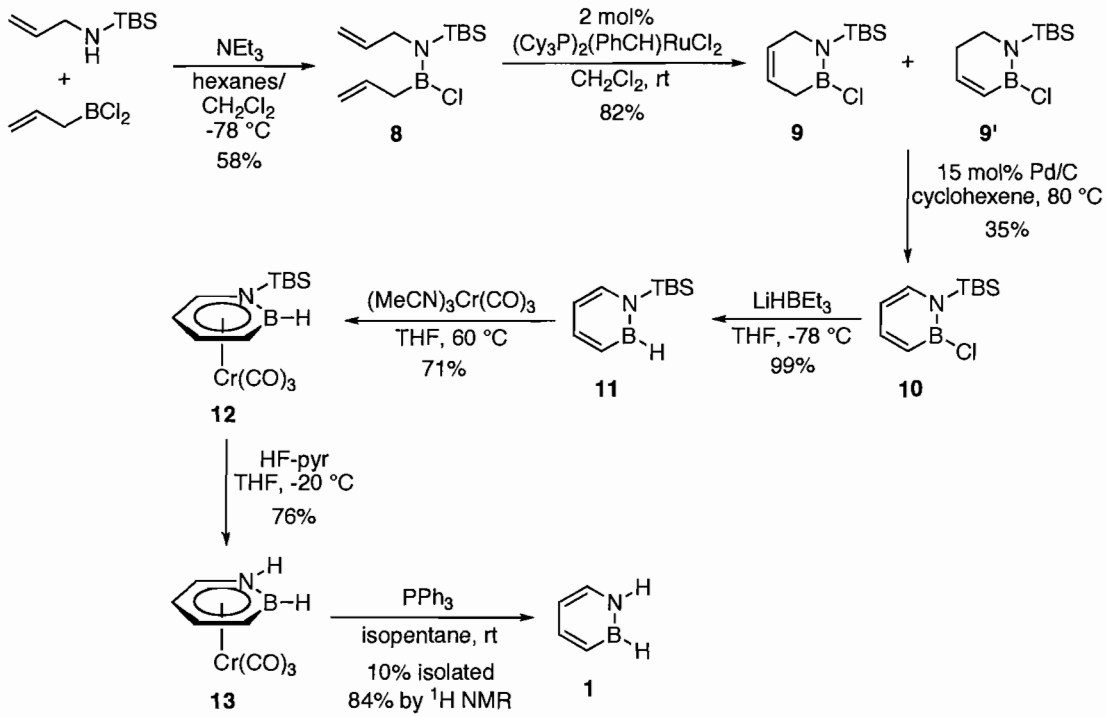

Scheme 4. Synthesis of 1,2-dihydro-1,2-azaborine **1**.

The technical problem of isolating compound **1** was somewhat overcome by the use of the high-boiling 1,6-dicyanooctane as solvent (Scheme 5). Whereas the isolation of **1** from PPh_3 and isopentane required the successive removal of non-volatile solids and the highly volatile isopentane, parent compound **1** was purified in 53% yield via a single vacuum transfer of the product from the reaction mixture.

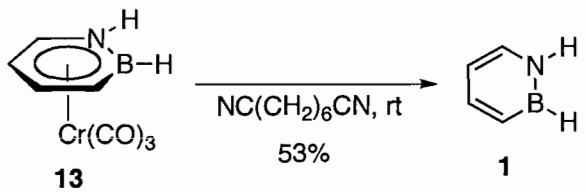

Scheme 5. Improved conditions for the isolation of **1**.

The melting point of **1** is –45 °C. In comparison, the melting points of borazine and benzene are –58 °C and 5 °C, respectively. Compound **1** is stable to silica gel chromatography and is relatively non-polar (Rf = 0.4 with pentane as eluent). Furthermore, 1,2-dihydro-1,2-azaborine **1** is quite thermally stable; a solution of **1** in CD_2Cl_2 showed no appreciable degradation by ^1H NMR when heated to 60 °C for 5 days.

We characterized compound **1** by NMR, UV/Vis, and IR spectroscopy, and high-resolution mass spectrometry. The data are consistent with the proposed structure of **1**. The ^1H NMR spectrum of heterocycle **1** is shown in Figure 2. The C-H resonances all appear in the aromatic region and are characteristic of a 1,2-azaborine. The B-H resonance appears upfield of the other resonances and is split into a broad quartet ($^1J_{BH}$ = 130 Hz) by the ^{11}B atom (S = 3/2). The coupling of the N-H proton with the ^{14}N nucleus (S = 1) results in a triplet ($^1J_{NH}$ = 57 Hz) that is observed for solutions of **1** in CD_3CN, C_6D_6, CD_3OD, and CD_2Cl_2. The proton resonances were unambiguously assigned by a combination of COSY and HETCOR NMR techniques (see Appendix B).

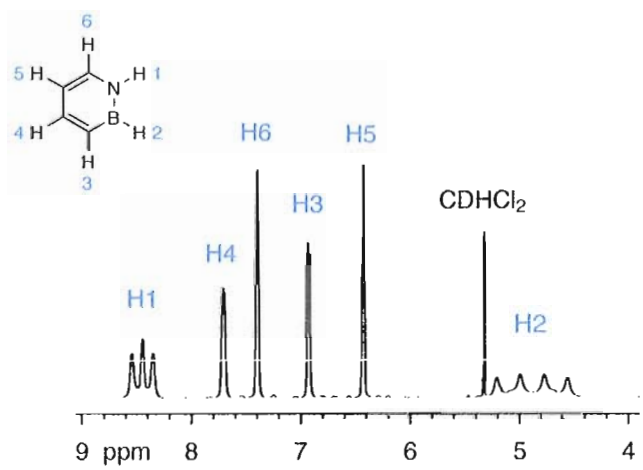

Figure 2. ^1H NMR spectrum of **1** in CD_2Cl_2.

The UV/Vis absorption spectra of benzene, borazine, and 1,2-dihydro-1,2-azaborine **1** are shown in Figure 3. The spectrum for compound **1** displays λ_{max} at 269 nm (ε = 15632 $M^{-1}cm^{-1}$), with two smaller transitions at 219 nm (ε = 8495 $M^{-1}cm^{-1}$) and at 205 nm (ε = 7459 $M^{-1}cm^{-1}$). The absorbance at 269 nm is only slightly red-shifted relative to the α band of benzene (255 nm, ε = 977 $M^{-1}cm^{-1}$), but absorbs much more strongly than benzene. Benzene's strongest absorption band is located at 208 nm (ε = 12380 $M^{-1}cm^{-1}$). In contrast to benzene and 1,2-azaborine **1**, the absorption spectrum of borazine shows only a very weak band at 203 nm (ε = 1299 $M^{-1}cm^{-1}$) and negligible absorbance at higher wavelengths. The electronic features of **1** are consistent with a delocalized aromatic motif, in marked contrast with the behavior exhibited by borazine.

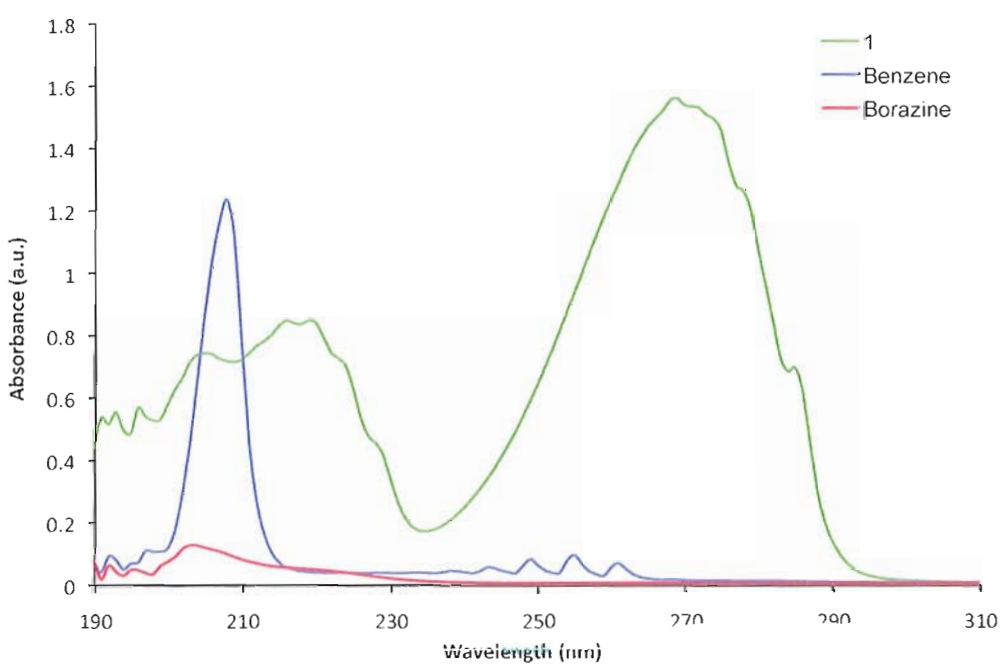

Figure 3. Absorption spectra of **1**, benzene, and borazine. All substrates are 10^{-4} M in pentane.

Our experimentally determined spectroscopic data are supported by electronic structure calculations (see Appendix B for computational details). The chemical shifts in ^{1}H, ^{13}C, ^{11}B, and ^{14}N NMR spectroscopy of benzene, compound **1**, and borazine were calculated at the density functional theory (DFT) B3LYP/Alhrichs-vtzp level. The excitation energies and oscillator strengths for the prediction of the UV/Vis spectra of benzene, 1,2-azaborine **1**, and borazine were calculated with time dependent DFT (TD-DFT) at the B3LYP/aug-cc-pVDZ//MP2/cc-pVTZ and B3LYP/aug-cc- pVTZ//MP2/cc-pVTZ levels, and with equations of motion CCSD (EOM-CCSD/aug-cc-pVDZ//MP2/cc-pVTZ) level (Appendix B). The IR stretching frequencies of benzene, borazine, and **1** were calculated at the MP2/cc-pVTZ level (Appendix B). Our high-level calculations supported the experimentally determined spectroscopic data for 1,2-dihydro-1,2-azaborine **1** (see Appendix B for full characterization of **1**).

While benzene is considered the quintessential aromatic molecule, the aromaticity of borazine has remained a topic of discussion in the 21st century.[5-7] With regard to 1,2-dihydro-1,2-azaborine **1**, Ashe and co-workers showed that 1,2-azaborines readily undergo electrophilic aromatic substitution reactions.[26] Abbey et al. have provided crystallographic evidence of bond delocalization in 1,2-azaborines.[27] To complete the analysis, we have directly compared the magnetic and energetic data for 1,2-dihydro-1,2-azaborine **1** along with the corresponding data for benzene and borazine. Experimentally, the N-H and B-H chemical shifts of **1** are significantly downfield shifted compared to the corresponding signals for borazine (Table 2, entries 1 and 2). The nucleus-independent chemical shift (NICS)[28] values for benzene, 1,2-dihydro-1,2-

azaborine **1**, and borazine indicate a trend of decreasing aromaticity going from benzene to borazine. The experimentally observed and computed chemical shifts are consistent with 1,2-dihydro-1,2-azaborine **1** possessing substantial aromatic character. We have also predicted the resonance stabilization energy (RSE)[29] of 1,2-dihydro-1,2-azaborine **1** to be 21 kcal mol^{-1} (Table 2, entry 5). This value was derived computationally from the reaction schemes illustrated in Schemes 6 (see Appendix B for full computational details). The RSE of **1** appears to be approximately 13 kcal mol^{-1} less than benzene (34 kcal mol^{-1}). Furthermore, the heat of formation has been accurately calculated for benzene and borazine.[30,31] The same methods were used to calculate the heat of formation of **1** (Table 2, entry 6). Thus, 1,2-dihydro-1,2-azaborine **1** appears to meet all four major criteria of aromaticity.

Table 1. Magnetic and Energetic Data for Benzene, **1**, and Borazine.[a]

Entry			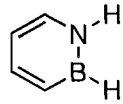 **1**	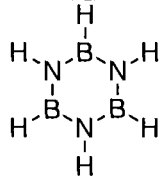
1	δ N-*H*		8.44,[b] [7.8]	5.63,[b] [5.3]
2	δ B-*H*		4.9,[b] [5.4]	4.4,[b] [5.0]
3	NICS (0)	[–8.76]	[–5.62]	[–2.02]
4	NICS (1)	[–10.39]	[–7.27]	[–3.01]
5	RSE (kcal mol^{-1})	[34.1]	[21 (±2)]	[10.0][c]
6	$\Delta H_{f(298)}$ (kcal mol^{-1})	[20.5]	[3.0]	[–119.0]

[a] Numbers in brackets are calculated values.
[b] Experimentally determined ^1H NMR chemical shifts in CD_2Cl_2.
[c] Value taken from reference 5 based on a different reaction scheme.

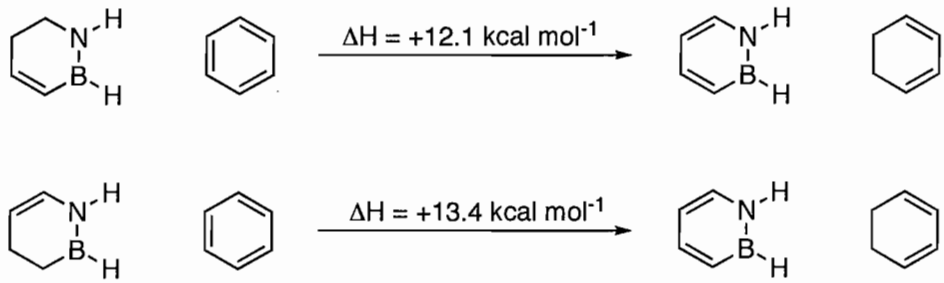

Scheme 6. Reaction schemes for the calculation of RSE in **1** versus benzene.

1,2-Dihydro-1,2-azaborine **1** displays unique molecular features relative to its organic counterpart, benzene. Therefore we explored the reactivity of **1** resulting from substitution by the B-N bond pair. In particular, we were interested in determining whether the N-H proton is protic and the B-H hydrogen is hydridic. The N-H functionality in **1** undergoes a deuterium exchange in CD_3OD (Scheme 7). The disappearance of the N-H resonance in the ^1H NMR spectrum of **1** was monitored over the course of approximately 24 h, from which it was determined that the rate constant for exchange in CD_3OD was $k_{HD} = 7(\pm 2) \times 10^{-7}\ M^{-1}s^{-1}$. The B-H group is commonly hydridic in character. With regard to boron heterocycles, Fu and co-workers demonstrated the reduction of aldehydes to alcohols using 1-*H*-boratabenzene.[32] However, no reaction between **1** and benzaldehyde occurred over the course of several days at 60 °C (Scheme 8). The complete consumption of benzaldehyde with borazine was observed within 24 h, furnishing reduced benzaldehyde derivatives including dibenzylamine and tribenzylamine. The relatively unreactive nature of **1** led us to speculate that the hybrid heterocycle **1** more closely resembles benzene than borazine.

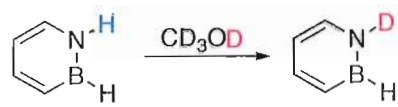

Scheme 7. H/D exchange in 1,2-dihydro-1,2-azaborine.

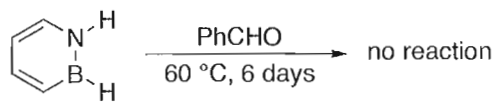

Scheme 8. Exploration of aldehyde reduction using 1,2-dihydro-1,2-azaborine.

Although we were unable to determine the crystal structure of **1**, we were able to obtain the structure of its chromium(0) tricarbonyl adduct **13**. Selected structural parameters for complex **13** are provided in Figure 4 (left). A direct comparison of the features of **13** with the known benzene-$Cr(CO)_3$ piano-stool complex **14**[33] (Figure 4, right) indicates overall that the binding geometry of the 1,2-dihydro-1,2-azaborine ring in **13** is quite similar to that of the benzene ligand in **14**. The planar 1,2-azaborine ring of **13** is coordinated in an η^6-fashion to chromium and closely resembles the binding geometry in **14**. Accordingly, the Cr-CO and C≡O distances are remarkably similar in **13** and **14**, indicating that the coordination behavior of 1,2-dihydro-1,2-azaborine **1** is quite similar to benzene. This is further supported by the nearly identical carbonyl stretching frequencies of **13** (ν(CO) = 1898, 1975 cm^{-1}) and **14** (ν(CO) = 1892, 1972 cm^{-1}) measured by IR spectroscopy. The binding energy of the 1,2-azaborine ring to the $Cr(CO)_3$ fragment in **13** was calculated at the DFT B3LYP/DZVPZ level to be –54.4 kcal mol^{-1} (see Appendix B), which was virtually identical to the benzene derivative (–54.9 kcal mol^{-1}). In contrast, the binding energy of borazine was calculated to be significantly weaker (–42.7 kcal mol^{-1}).

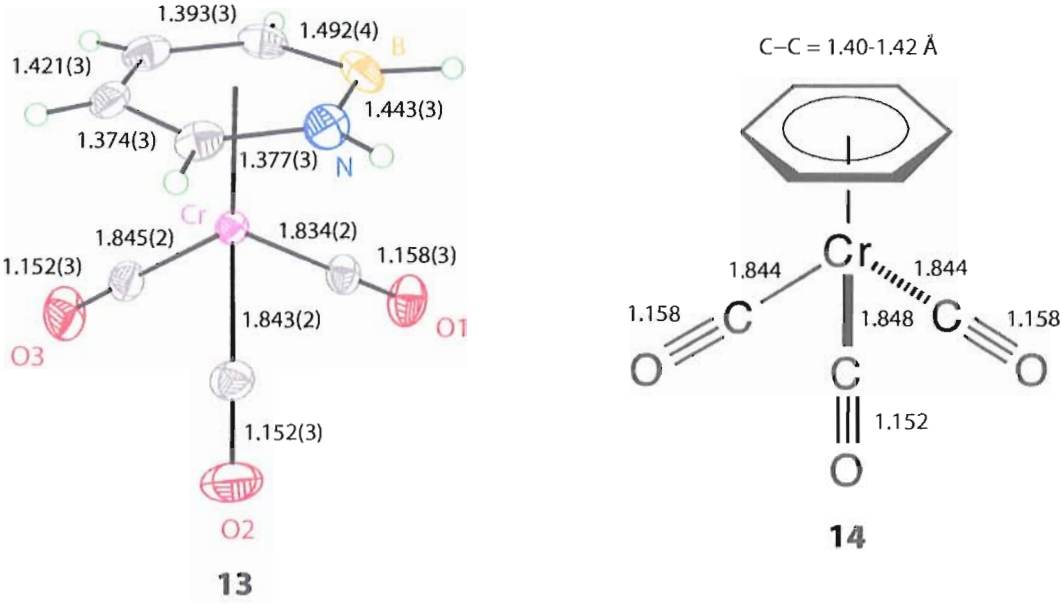

Figure 4. ORTEP illustration (at the 35% probability level) of **13** in direct comparison with the known benzene chromium(0) tricarbonyl complex **14**.

Electronic structure calculations of compound **1** at the B3LYP/DZVP2 level show that, in contrast to benzene and borazine, the HOMO of 1,2-azaborine is not degenerate. The HOMO–LUMO gap in **1** (5.32 eV) is smaller than those for benzene (6.55 eV) and borazine (7.91 eV). This trend is consistent with the electronic spectra (Figure 3) and with previous calculations.[34-35] The orbital diagram of the HOMO of **1** is shown in Figure 5(A). We also determined the charge distribution of **1** in the form of an electrostatic potential (ESP) surface (Figure 5(B)). The calculated electronic structure reveals substantial electron density at the 3 and 5 positions of the 1,2-azaborine ring. This is consistent with the experimental observations made by Ashe, in which electrophilic aromatic substitutions occur exclusively at the 3 and 5 positions of the heterocycle.[26] Furthermore, the ESP diagram shows a positive electrostatic potential

(blue color) at the N-H group, which correlates well with the observed H/D exchange in heterocycle **1**.

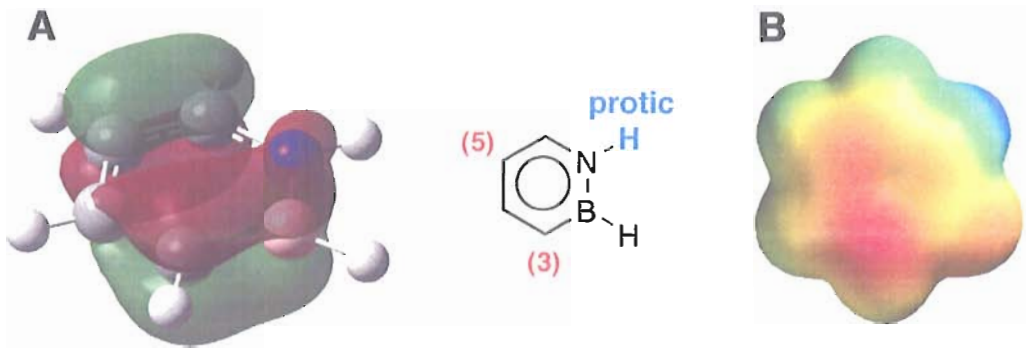

Figure 5. A) HOMO of 1,2-dihydro-1,2-azaborine. B) ESP map of 1,2-dihydro-1,2-azaborine at the 0.002 electron a.u.$^{-3}$ density iso-contour level (-13.6 to 39.9 kcal mol^{-1}).

3.4. Microwave Spectroscopy of 1,2-Dihydro-1,2-azaborine

Microwave spectroscopy has been an accurate method for the determination of molecular structure in the gas phase. As we were unable to determine the X-ray crystal structure of 1,2-dihydro-1,2-azaborine **1**, we were interested in elucidating the structural features of **1** via microwave spectroscopy. The microwave spectra for compounds of boron and nitrogen have been reported.[36-38] While the lack of a permanent molecular dipole in borazine precludes its study by microwave spectroscopy, the asymmetry in the 1,2-azaborine heterocycle presents an opportunity to collect the microwave spectrum of **1**.

In collaboration with the Kukolich group, we have performed microwave spectroscopy on 1,2-dihydro-1,2-azaborine **1**.[39] The complicated microwave spectrum of heterocycle **1** was analyzed using highly accurate modeling techniques (see Appendix B), which yielded valuable information regarding structure and electron distribution.

1,2-Dihydro-1,2-azaborine was determined to be completely planar in the gas phase (see Appendix B), consistent with the X-ray crystal structures of the numerous derivatives discussed in Chapter II. Furthermore, several of the intra-ring bond lengths have been determined and are presented in Figure 6. The B-N bond length of 1.45(3) Å is comparable to the values obtained in the solid-state for related derivatives. Similarly, the B-C and N-C bond lengths of 1.51(1) and 1.37(3) Å, respectively, are close to the bond lengths observed in the X-ray crystal structures of other 1,2-azaborines. The intra-ring bond angles of **1** are presented in Figure 6 and do not deviate greatly (within error limits) from 120°. It is worth noting that the β and γ angles include error limits as these were the only angles completely determined using modeling techniques. The N-H bond length of 1.02 Å is short relative to the B-H bond (1.19-1.21 Å), however more experiments would be required for the highly accurate determination of these bond lengths.

The dipole moment of **1** was calculated to be 2 D (Figure 6), pointing from the C6 position (most positive) toward the C3 position (most negative). The microwave spectrum of **1** also permitted an analysis of the p_z-electron occupancy at boron and nitrogen. It was determined that the valence p_z-electron occupation of boron is 0.3 electrons versus 1.3-1.5 electrons at the nitrogen position, indicating a partial overlap of the π-system with boron's p_z orbital.

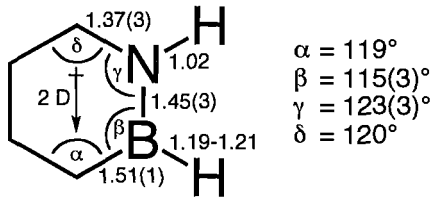

Figure 6. Geometric and electronic features of **1** via gas-phase microwave spectroscopy. Carbon-carbon double bonds have been omitted for clarity.

3.5. 1,2-Azaborine Protein Binding

The element boron has received little attention in biomedical applications compared to its main group neighbors, carbon, nitrogen, and oxygen. The relative insignificance of boron to living systems may be responsible for the scarcity of boron-containing biomolecules.[40,41] Nevertheless, boron has several useful elemental and chemical features that include nuclear spin, large cross section for neutron capture, and Lewis acidity. The incorporation of boron in biologically-relevant molecules could provide opportunities in marker technologies,[42] pharmacological agents,[43] or in cancer therapy.[44] 1,2-Azaborines may serve as biological agents due to their structural and electronic similarity to the biologically prevalent phenyl ring. Therefore, we were interested in probing the ability of the 1,2-azaborine ring to mimic the phenyl system in a biological context.

Benzene and ethylbenzene have recently been shown to selectively bind an engineered hydrophobic pocket of T4 lysozyme.[45] The L99A mutant of T4 lysozyme creates a non-polar, disc-shaped cavity which is well-suited to bind aromatic substrates. Though internalized within the protein scaffold, aromatic groups readily bind to this pocket. Modified T4 lysozyme therefore appeared to be a suitable candidate for a 'proof

of principle' binding study with 1,2-dihydro-1,2-azaborine **1** and other derivatives (i. e. **15**[18] in Figure 7) as a test of the biomimetic capabilities of this heterocyclic motif.

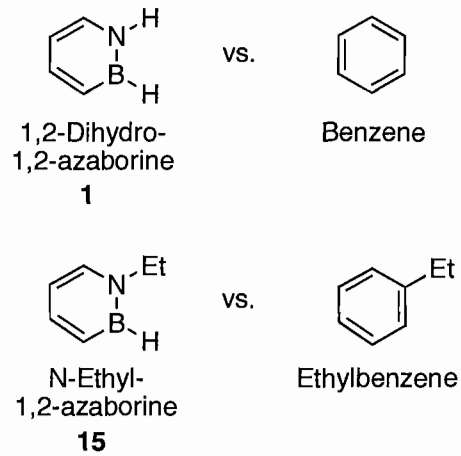

Figure 7. 1,2-Dihydro-1,2-azaborine **1**, N-ethyl-1,2-azaborine **15**, and carbon analogs.

Our collaborators in the Matthews group prepared crystals of L99A T4 lysozyme, which were transferred to an inert atmosphere glovebox. The crystals were soaked in a degassed, buffered solution (2.2 M sodium/potassium phosphate, pH 6.9, 50 mM 2-mercaptoethanol, 50 mM hydroxyethyldisulfide), whereupon a few drops of 1,2-dihydro-1,2-azaborine **1** or N-ethyl 1,2-azaborine **15** were added to the vessel containing the protein crystals. The sample was quickly cooled to 277 K and stored under inert atmosphere for three days. Diffraction data (see Appendix B) for these samples were then collected at 100 K to 1.25 Å resolution.

The diffraction data clearly indicated that the parent heterocycle **1** as well as the N-ethyl derivative **15** bound the hydrophobic pocket of L99A T4 lysozyme.[46] The binding of N-ethyl 1,2-azaborine **15** was found to be quite similar to ethylbenzene (Figure 8). Furthermore, **15** binds to the hydrophobic pocket in essentially 100% occupancy, whereas ethylbenzene binds in approximately 60% occupancy. Compound

15 and its carbon analog both bind in two alternative geometries; the electron density maps indicate that the aromatic rings are present in opposing ring-flipped conformations. No close contacts were observed between **15** and the protein scaffold, indicating 1,2-azaborine is a non-polar surrogate for the phenyl ring.

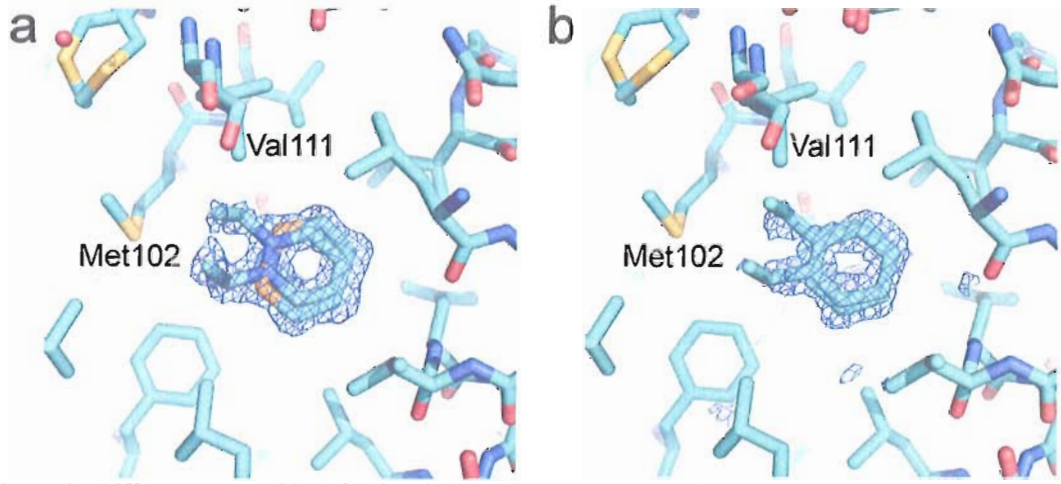

Figure 8. Difference maps (blue) for the binding of a) **15** and b) ethylbenzene in the T4 lysozyme L99A cavity. The maps are contoured at 3 σ and 2 σ for **15** and ethylbenzene, respectively, at a resolution of 1.25 Å. The nitrogen atom on the 1,2-azaborine ring of **15** is colored blue and the boron atom is colored orange. The sites for the boron atoms could not be specified unambiguously (see text).

In contrast to ethyl-substituted **15**, parent 1,2-azaborine **1** contains an exchangeable N-H moiety and is more polar than benzene, and therefore might reasonably be expected to bind in a very different manner to L99A T4 lysozyme. Furthermore, it has been shown that polar ligands such as pyridine, phenol, and aniline do not bind significantly to the L99A cavity. Despite this, heterocycle **1** bound the hydrophobic pocket of L99A T4 lysozyme in virtually 100% occupancy and closely resembled the binding of benzene (Figure 9). The binding of heterocycle **1** was again found to occur in two ring-flipped conformations. The absence of any short contacts with or significant changes to the protein scaffold suggests that 1,2-dihydro-1,2-

azaborine **1** is a reasonable mimic for benzene. It is of note that this represents the first crystallographic characterization of the parent heterocycle **1**.

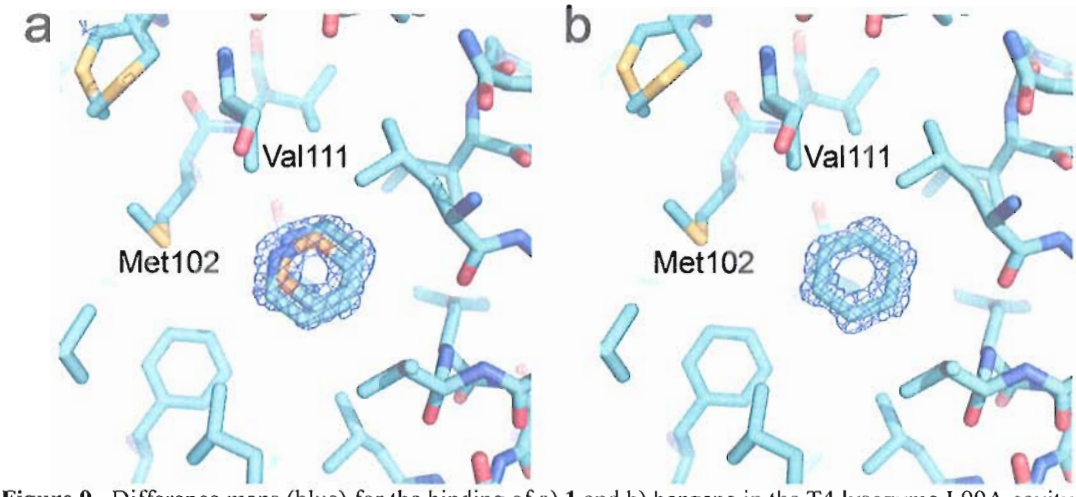

Figure 9. Difference maps (blue) for the binding of a) **1** and b) benzene in the T4 lysozyme L99A cavity. The maps are contoured at the 3 σ level. The nitrogen atom on the 1,2-azaborine ring of **1** is colored blue and the boron atom is colored orange.

3.6. Conclusion

In summary, we prepared 1,2-dihydro-1,2-azaborine **1**, a hybrid organic/inorganic benzene that had been elusive until now. The structural, spectroscopic, and chemical data presented in this work were fully supported by high-level calculations, and indicated that 1,2-dihydro-1,2-azaborine is a stable aromatic molecule with features that are distinct from its "organic" and "inorganic" counterparts. The synthesis and characterization of the parent compound of this family of heterocycles fills an important gap in the study of boron-nitrogen heterocycles and aromaticity. The properties of 1,2-dihydro-1,2-azaborine make it an attractive target for materials applications. Furthermore, while the application of 1,2-azaborines to biomedical

research remains unexplored, we have demonstrated the potential of 1,2-azaborines as mimics of the important phenyl motif.

3.7. Bridge to Chapter IV

Chapter IV discusses the synthesis and characterization of conjugated scaffolds incorporating the 1,2-azaborine motif. In a similar route employed toward the synthesis of 1,2-dihydro-1,2-azaborine, BN analogs of diphenylacetylene are produced from a versatile 1,2-azaborine intermediate. The optoelectronic properties of these compounds are discussed in relation to their carbon analogs. The second section of Chapter IV discusses the synthesis of larger diyne scaffolds containing a central 1,2-azaborine core. These derivatives are generated via the unprecedented cross-coupling reactivity of C3-brominated 1,2-azaborines with phenylacetylenes. The consequences of asymmetrically substituting electron-donating and electron-withdrawing groups are explored with respect to optoelectronic properties.

CHAPTER IV

1,2-DIHYDRO-1,2-AZABORINE IN CONJUGATED PHENYLACETYLENIC SCAFFOLDS

4.1. General Overview

This chapter discusses the synthesis and characterization of phenylacetylene derivatives containing the 1,2-azaborine ring. This chapter includes unpublished co-authored material with Jed Volvolic, Dan Chase, and Dr. Lev Zakharov. Some compound preparation was performed by Jed Volvovic and Dan Chase, and X-ray crystallographic data was collected and analyzed by Dr. Lev Zakharov. Otherwise all experimental work was performed by me. The co-authored excerpt as presented here was written entirely by me. Professor Shih-Yuan Liu has provided editorial assistance and scientific guidance for all material presented in this chapter.

4.2. Introduction

Conjugated organic materials are of great interest in areas such as light-emitting diodes,[1] photovoltaic devices,[2] and non-linear optical materials.[3] The incorporation of sp^2-hybridized boron into small molecule[4] and polymeric[5] structures has become a key strategy in the design of π-conjugated materials. Recent pioneering work in the

synthesis of aromatic boron heterocycles has provided insight into the fundamental consequences of boron substitution.[6-9] Many of these compounds display unique photophysical properties. Recent work has demonstrated that the replacement of C=C units in polycyclic aromatic hydrocarbons with isoelectronic B-N bond pairs imparts favorable photophysical properties while maintaining significant compound stability.[10,11] The photophysics of monocyclic derivatives of 1,2-dihydro-1,2-azaborine, isoelectronic with the ubiquitous phenyl ring, have received much less attention. However, the resurgence in the chemistry of 1,2-dihydro-1,2-azaborine (hereafter referred to as 1,2-azaborine)[12-15] has led us to consider the integration of 1,2-azaborine units in conjugated materials.

We have chosen diphenylacetylene (tolan) as an attractive target for conjugated materials containing the B-N bond pair (Figure 1). The photophysics of diphenylacetylene are well documented.[16] Diphenylacetylene serves as an important building block in material science[17] and is the fundamental sub-unit in the structure of the carbon allotrope graphyne.[18] An extension of the synthetic methods described in Chapters II and III could provide tolan derivatives containing the 1,2-azaborine ring (e. g., **1** and **2** in Figure 1). The photophysical consequences of substituting multiple phenylacetylene groups at various positions on the 1,2-azaborine ring are also of interest.

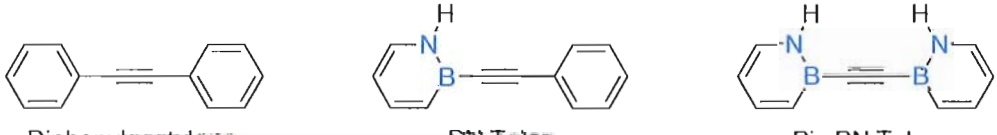

Figure 1. Derivatives of tolan containing the 1,2-azaborine ring.

4.3. Synthesis of BN Tolan Derivatives

The synthesis of BN tolan **1** is described in Scheme 1. Nucleophilic substitution of B-Cl azaborine **3** (see Chapter III, Scheme 4) with phenylethynylmagnesium bromide furnished TBS-protected BN tolan **4** in 76% isolated yield. Attempts to selectively remove the N-silyl group of **4** were unsuccessful. The addition of tetrabutylammonium fluoride (TBAF) to **4** provided **1** in 15% isolated yield, however the competitive nucleophilic attack at the boron position led to the formation of undesired side-products. As in our previous isolation of the parent 1,2-dihydro-1,2-azaborine,[15] complexation with chromium(0) provided an alternate route to BN tolan **1**. The reaction of **4** with $(MeCN)_3Cr(CO)_3$ gave piano-stool complex **5** in 91% yield. Deprotection of the N-TBS group with HF-pyridine afforded the chromium tricarbonyl complex **6** in 85% yield. Simple dissolution of **6** in MeCN, followed by chromatographic purification gave **1** in good yield.

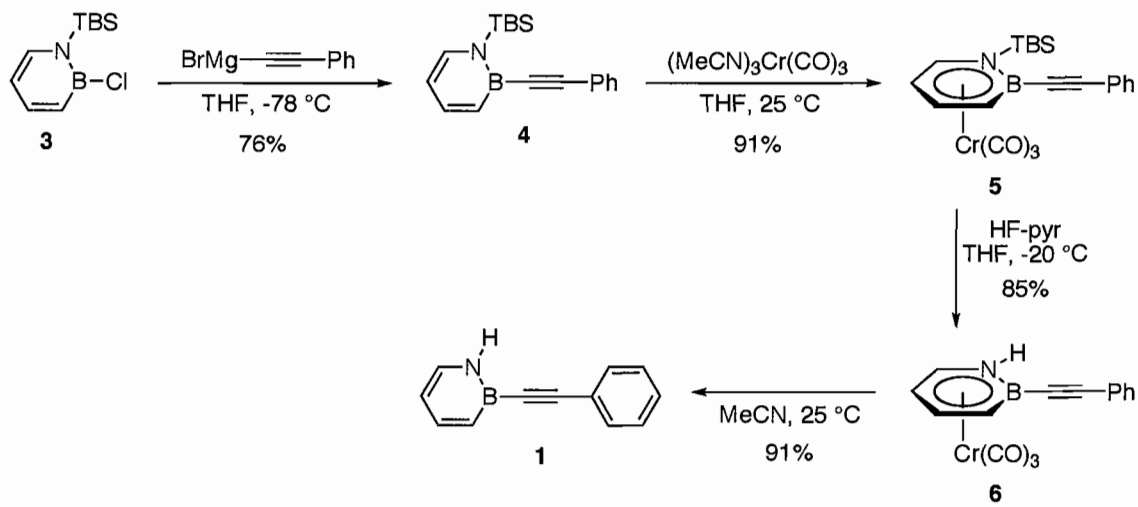

Scheme 1. Synthesis of BN tolan **1**.

Next we turned to the synthesis of **2** (Scheme 2). In situ generation of Grignard **7**[19] and reaction with **3** gave N-TBS protected BN tolan **8** in good yield. The complexation of **8** with Cr(0) proved more challenging, however complex **10** was isolated in 20% yield from the reaction of **8** with $(MeCN)_3Cr(CO)_3$. The major product in the reaction of **8** with $(MeCN)_3Cr(CO)_3$ was piano-stool complex **9**, however complex **9** was recovered and reacted with additional $(MeCN)_3Cr(CO)_3$ to give **10** in 20% isolated yield (84% based on recovered compounds **8** and **9**). Complex **10** was characterized by X-ray crystallography (see Appendix C). N-TBS deprotection with HF-pyridine afforded **11** as a highly insoluble orange solid, which was dissolved directly in MeCN to yield bis BN tolan **2** (47%, two steps).

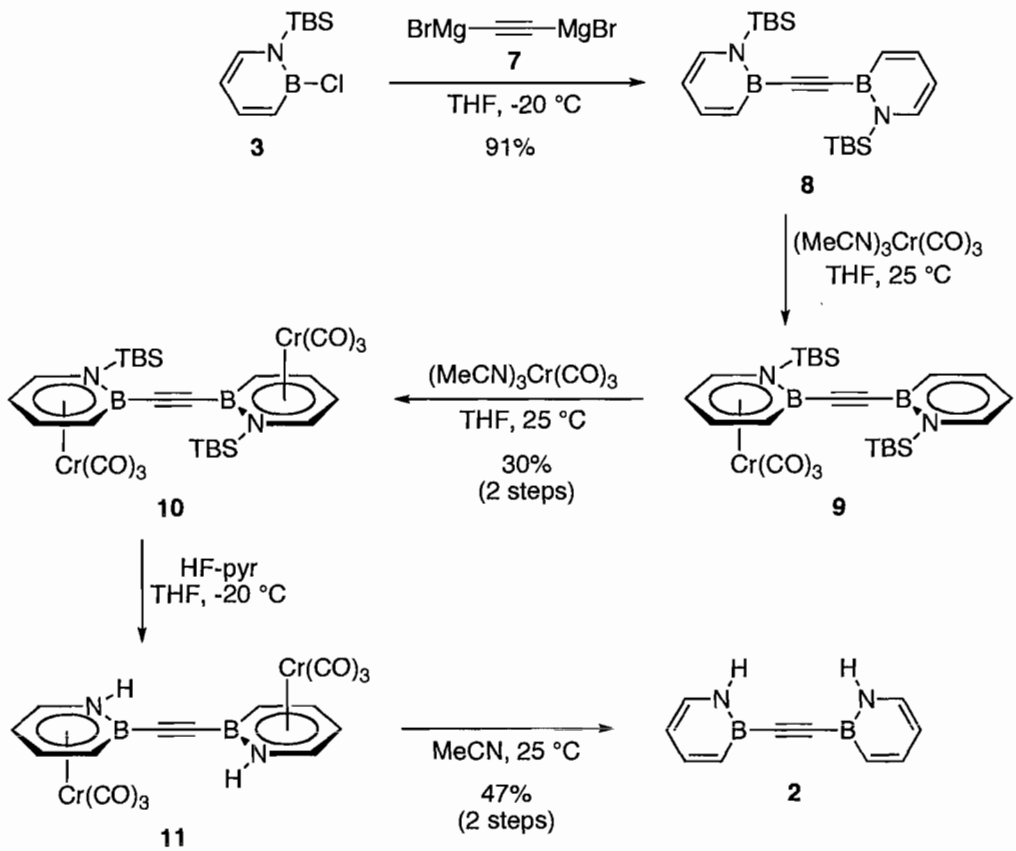

Scheme 2. Synthesis of bis BN tolan **2**.

We obtained the X-ray crystal structures of **1** and **2**. The structure of **1** is illustrated in Figure 2, which confirms the structural assignment of the BN tolan analog. The structure of **1** is nearly co-planar through the alkyne-bridged rings with the 1,2-azaborine and phenyl rings twisted less than 3° relative to each other. The structure is linear through the B-C≡C-C unit and the exocyclic B(1)-C(5) bond is slightly longer (1.545(5) Å) than the corresponding C(7)-C(6) bond (1.436(5) Å) due to the increased size of the boron atom relative to carbon. The intra-ring 1,2-azaborine bond distances in **1** are similar to those observed in the N-benzyl derivative presented in Chapter II, Figure 17. The boron atom appears completely planar, indicating sp^2 geometry. Interestingly, the exocyclic alkyne substituent is bent away from the C(4) atom (∠C(4)-B(1)-C(5) = 128.3(3)°) toward the nitrogen position (∠N(1)-B(1)-C(5) = 116.6(3)°). The intra-ring angles (∠N(1)-B(1)-C(4) = 114.9(3)°, ∠C(1)-N(1)-B(1) = 123.5(3)°) very closely resemble those determined for the parent 1,2-azaborine via microwave spectroscopy (Chapter III, Figure 6).[20] The full crystallographic data for **1** are presented in Appendix C.

Figure 2. ORTEP illustration of **1**, with thermal ellipsoids drawn at the 35% probability level.

The solid-state structure of **2** is presented in Figure 3. The structure is co-planar and the B-C≡C-B axis is linear, indicating π-overlap throughout the bicycle. Surprisingly, the nitrogen atoms of the 1,2-azaborine rings are in a cis conformation

about the B-C≡C-B axis. This is in contrast to compound **8**, which preferred a trans conformation (see Appendix C for crystallographic data of **8**). In the crystal packing of **8** there appears to be a short contact between the N-H proton and alkyne bridge of adjacent molecules (Figure 4, left: H····π = 2.55 Å, ∠N-H-π = 159°). Hydrogen-bonding between an N-H donor and alkyne acceptor is rare.[21-22] The formally isoelectronic relationship between 1,2-azaborine and the phenyl ring lead us to speculate that the short N-H····π interaction could potentially be a mimic of C-H····π, for which there are numerous examples.[21] Solid-state C-H····π interactions are generally longer than N-H····π and deviate more greatly from 180°. The interactions in **2** are intermediary between typical C-H····π and N-H····π hydrogen bonds. Thin-film infra-red spectroscopy also indicates modest weakening of the N-H bond in **2** (3370 cm^{-1}) relative to the parent compound, 1,2-dihydro-1,2-azaborine (3800 cm^{-1})[15] and other reported (N-H)-1,2-azaborines.[23] We also observe π-stacking in the crystal structure of **2** (Figure 4, right). The separation between adjacent molecules of **2** is 3.5 Å and is offset such that the boron atom of one molecule is aligned with C(4) of its dimeric partner. The boron atom of **2** is electrophilic while DFT calculations have shown that the carbon attached to boron has the largest negative potential on the 1,2-azaborine ring.[15,20] Therefore, the offset π-stacking in **2** could result from a minimized dipole in the solid-state.

Figure 3. ORTEP illustration of **2**, with thermal ellipsoids drawn at the 35% probability level.

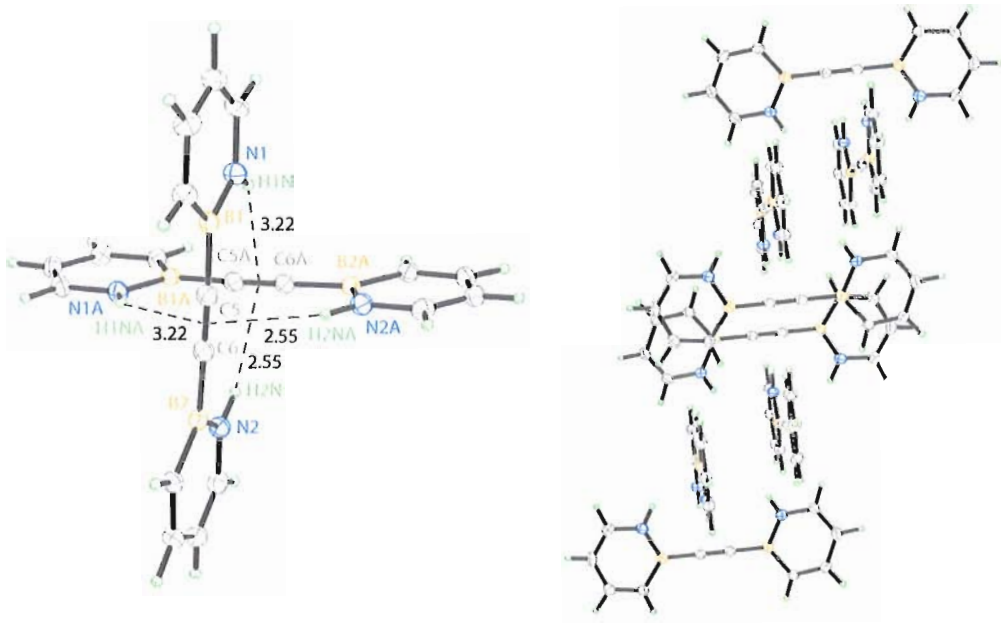

Figure 4. ORTEP illustrations, with thermal ellipsoids drawn at the 30% probability level, of N-H····π (left) and π-stacking (right) interactions in BN tolan **2**. All distances are in Å.

The absorption spectra of **1**, **2**, and tolan in THF are presented in Figure 5. The absorption spectra of **1** and **2** display similar features. Both compounds have a strong absorption at 299 nm. The weaker absorption in **1** at 268 nm is blue-shifted to 256 nm in **2**. The absorption band at 299 nm is broadened significantly for the BN tolan derivatives relative to tolan. As a result, **1** and **2** absorb out to a wavelength of 325 nm. The intensity in the 299 nm band is greater in **2** than **1** (58789 and 35072 $M^{-1}cm^{-1}$ respectively), which correlates with the number of 1,2-azaborine units in each molecule. Though broadened, some fine structure is observed in the absorption spectra of **1** and **2**; both compounds display an absorption "shoulder" band at about 320 nm.

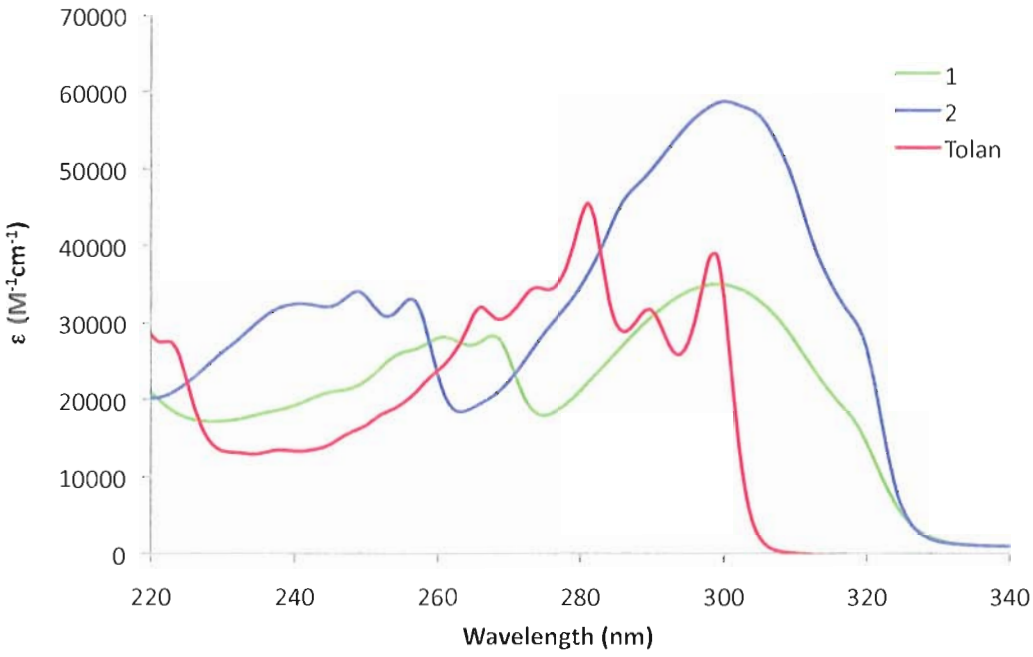

Figure 5. Absorption spectra for **1**, **2**, and diphenylacetylene (tolan). All substrates are 10^{-5} M in THF.

The emission spectra of **1**, **2**, and tolan in THF are shown in Figure 6. The emission of **1** (350 nm, Φ_{PL} = 0.021) is red-shifted relative to tolan (317 nm, Φ_{PL} = 0.00336),[16] while the emission of **2** (388 nm, Φ_{PL} = 0.08) is shifted to an even longer wavelength. The emission intensity in **1** and **2** is greatest when an excitation wavelength near the "shoulder" band at 320 nm is used, indicating that absorption from this band is likely involved in the observed emission. The photoluminescence quantum yields (Φ_{PL}) of both BN tolan derivatives are quite modest, yet relative to tolan these efficiencies are significantly improved.

The emission of **1** and **2** is marginally solvent-dependent. The solvatochromism of **2** is presented in Figure 7. A bathochromic shift occurs upon increasing solvent polarity; positive solvatochromism indicates greater charge stabilization in the excited

state. The emission in **1** was slightly solvent-dependent (see Appendix C). In contrast, very little solvent-dependence was observed in the fluorescence of tolan. Solvent effects were negligible in the absorption spectra of **1** and **2** (see Appendix C).

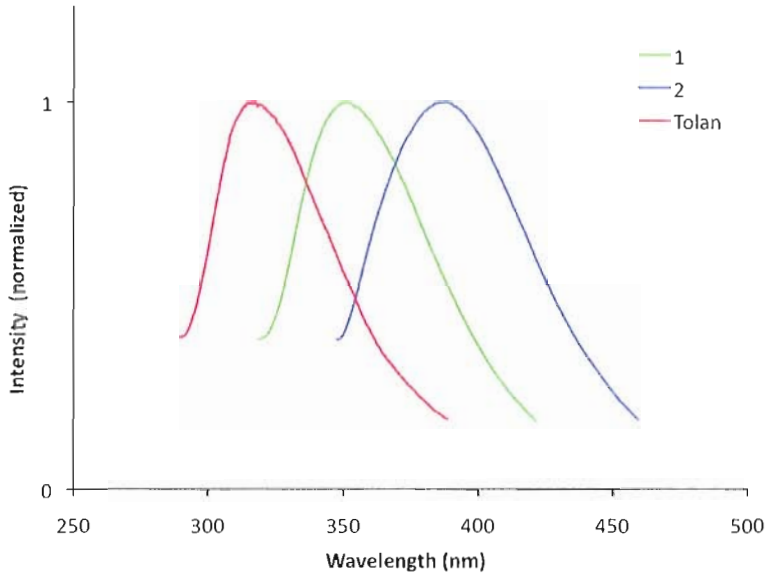

Figure 6. Normalized emission spectra for **1**, **2**, and tolan (all substrates are 10^{-5} M in THF).

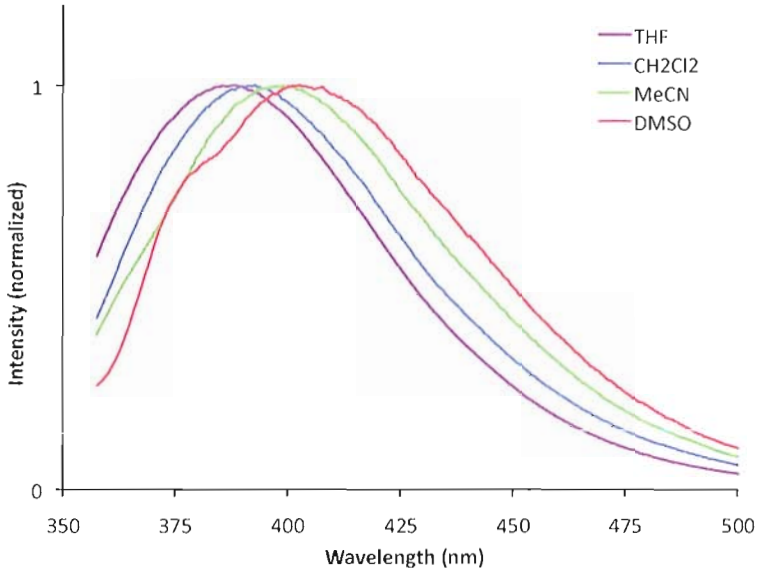

Figure 7. Normalized emission spectra of **2** in various solvents (all samples 10^{-5} M).

4.4. Diyne Scaffolds with a 1,2-Azaborine Core

Conjugated organic scaffolds based on the phenylacetylene sub-unit have been extensively studied, including dehydrobenzoannulenes[24] and poly-(phenylene)ethynylenes.[25,26] With respect to small molecules, ortho-diyne structures such as 1,2-bis(phenylethynyl)benzene[27] (Figure 8) have been examined for their interesting optoelectronic properties[28] and Bergman cyclization reactivity.[29] We have chosen the 1,2-azaborine-containing mimic of 1,2-bis(phenylethynyl)benzene (**12** in Figure 8) as a synthetic target. This is due in part to the availability of C3-brominated 1,2-azaborines,[30] from which we envisioned a cross-coupling methodology would provide alkyne functionality at the C3 position (Scheme 3). Transition metal-catalyzed cross-coupling has been one of the last frontiers of organic synthesis. This also remains one of the areas of classic arene reactivity which has yet to be reported in a 1,2-azaborine. We were hopeful that the orthogonal, stepwise installation of phenylethynyl groups at boron and C3 would be a viable route to **12** (Scheme 3).

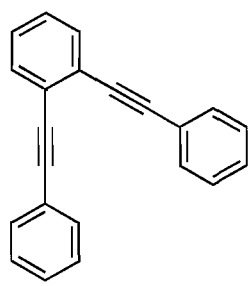

1,2-Bis(phenylethynyl)benzene

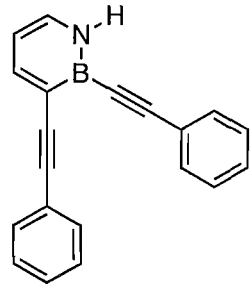

12

2,3-Bis(phenylethynyl)-
1-H-1,2-azaborine

Figure 8. 1,2-Azaborine **12**, an isoelectronic analog of 1,2-bis(phenylethynyl)benzene.

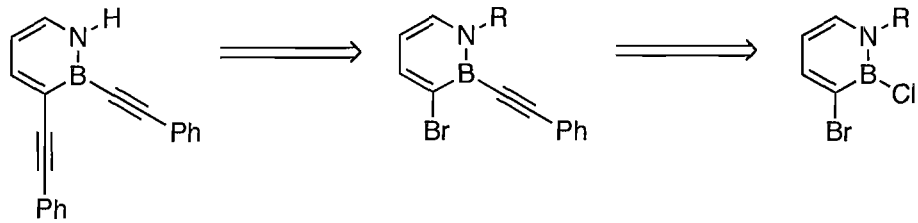

Scheme 3. Retrosynthetic analysis of **12**.

Our synthetic route to **12** is presented in Scheme 4. The bromination of B-Cl 1,2-azaborine **3** proceeded smoothly to provide **13** in good yield after vacuum distillation. Nucleophilic substitution of **13** with phenylethynylmagnesium bromide provided alkyne-substituted **14** in 76% yield. The lynchpin of our synthesis was the cross-coupling of brominated **14** with phenylacetylene, which was sluggish using a standard Sonogashira cross-coupling protocol (method A in Scheme 4).[31] Nevertheless, the observation of diyne **15** by ^{1}H NMR led us to consider the more reactive catalyst system developed specifically for the cross-coupling of aryl bromides.[32] Gratifyingly, the coupling of **14** with phenylacetylene under these conditions (method B in Scheme 4) produced **15** in 85% isolated yield. We were unable to directly cleave the TBS protecting group from diyne **15**. Instead, the complexation of **15** with tricarbonylchromium(0) trisacetonitrile provided piano-stool complex **16** in 43% yield. The N-TBS group of **16** was cleaved with HF-pyridine. The reaction mixture was directly added to MeCN, whereupon diyne **12** was isolated via silica gel chromatography, albeit in low yield.

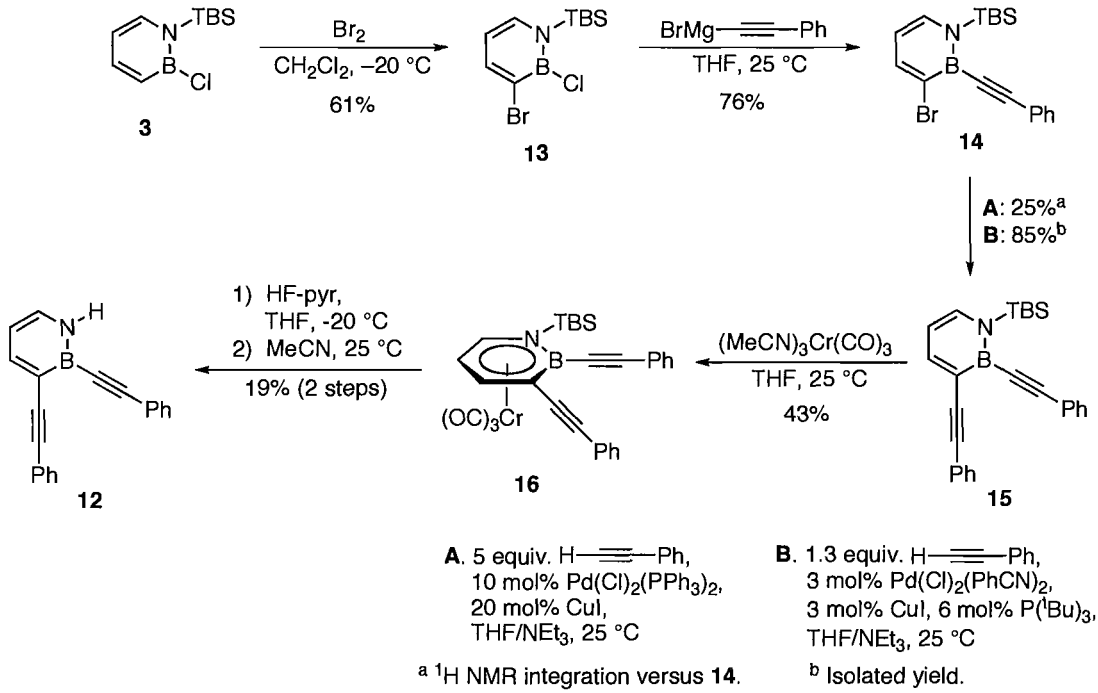

Scheme 4. Synthesis of diyne **12**.

We have characterized **12** by NMR, IR, UV-Vis, and fluorescence spectroscopy, as well as high resolution mass spectrometry (HRMS), all of which are consistent with the assigned structure. The structure of **12** has been unambiguously determined by X-ray crystallography, though disorder in the structure prevents the accurate determination of bond parameters. We have also obtained the X-ray crystal structure of chromium complex **16**; crystallographic data for **16** are given in Appendix C.

The absorption and emission spectra of **12** are shown in Figure 9. The absorption spectrum (blue) of **12** shows a broad absorption maximum at 328 nm ($\varepsilon = 23316\ M^{-1}cm^{-1}$). By comparison, the absorption spectrum of 1,2-bis(phenylethynyl)benzene in benzene shows an absorption at approximately 320 nm. Therefore, the HOMO-LUMO transition appears quite similar in **12** and the carbon-based analog. A second absorption

at higher energy is seen in the absorption spectrum of **12** (259 nm, ε = 23913 $M^{-1}cm^{-1}$). The fluorescence spectrum of heterocycle **12** (Figure 9, red trace) displays a strong peak at 378 nm (Φ_{PL} = 0.08). In contrast, 1,2-bis(phenylethynyl)benzene shows an emission at 346 nm (Φ_{PL} = 0.34) in benzene.[28]

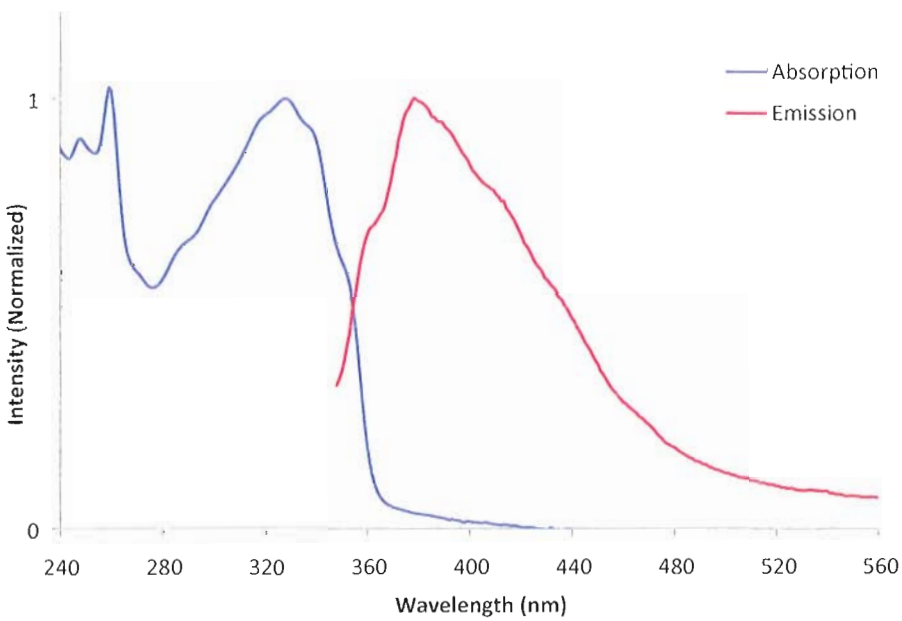

Figure 9. Absorption and emission spectra of **12** (10^{-5} M in THF).

The incorporation of donor and acceptor groups in conjugated organic materials can provide tunable optoelectronic properties.[28,33-35] Furthermore, variation in the substitution pattern of arylethynylbenzenes can significantly alter the photophysics of these materials.[36,37] We were therefore interested in preparing derivatives of **12** substituted at the para positions of the pendant phenyl rings with donor and acceptor groups (Figure 10). We have chosen amino and cyano moieties as the donor and acceptor groups, respectively; these substituents have been shown to greatly alter the photophysical properties of conjugated scaffolds relative to the parent hydrocarbon.[28]

The asymmetry imparted by the 1,2-azaborinc core in ortho-diynes also provides an opportunity to examine the effects of opposing conjugation pathways in the isomers of these structures (**17** and **18** in Figure 10). The phenyl-based diyne (Figure 10) does not offer the same opportunity, as switching the positions of the donor and acceptor groups does not change the identity of the molecule.

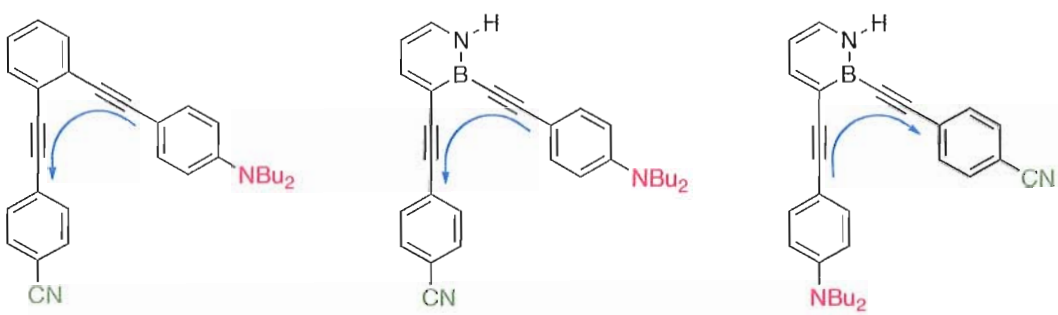

17 **18**

Figure 10. Conjugation pathways in **17**, **18**, and carbon analog **19**.

The synthesis of **17** is shown in Scheme 5. The generation of an appropriate nucleophile from 4-(dibutylamino)phenylacetylene was examined, whereupon it was determinecl that the in situ gcneration of alkynyl Grignard **19** occurred upon addition of ethylmagnesium bromide to the alkyne. Grignard **19** was added to B-Cl 1,2-azaborine **13**, which afforded alkyne **20** in 65% yield. This protocol was preferred over the formation and addition of the corresponding lithiate, for which yields of **20** were typically lower. Sonogashira cross-coupling of **20** with 4-cyanophenylacetylene readily produced **21**, establishing the desired donor-acceptor diyne framework. Initially, the route used to generate **12** (chromium complexation, silyl group cleavage, decomplexation) appeared promising toward the synthesis of **17**. We also re-examined the direct formation of **17** from **21** and TBAF in the hopes that substituent effects might

favor silyl group cleavage over nucleophilic attack at boron. We were delightfully surprised to find that target diyne **17** was isolated in 40% yield from the single-step reaction of **21** with TBAF; the donor and/or acceptor groups apparently alter the electronics of the boron and/or silicon atoms enough to induce a reversal of the selectivity in this reaction.

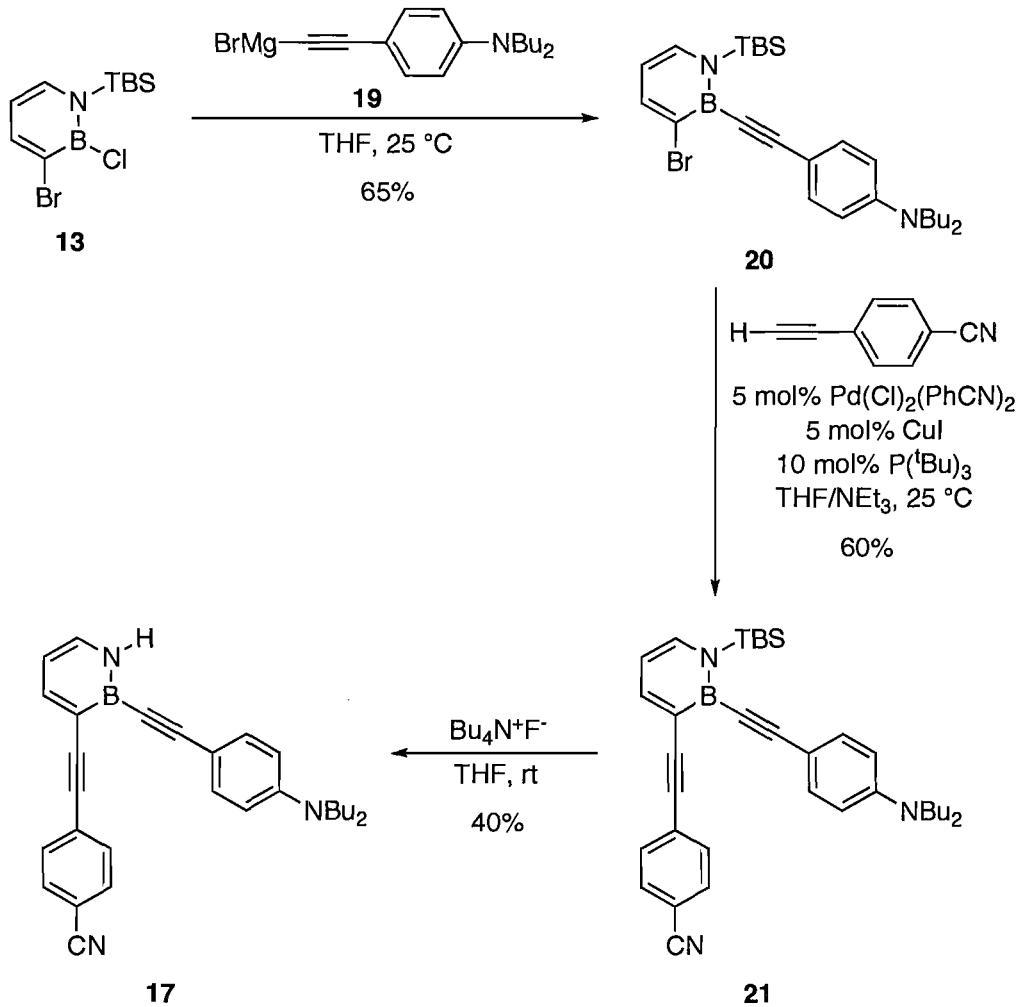

Scheme 5. Synthesis of **17**.

We next explored the synthesis of the alternate donor-acceptor diyne **18** (Scheme 6). Grignard **22** was formed in situ from 4-cyanophenylacetylene and ethylmagnesium

bromide. The addition of **22** to B-Cl 1,2-azaborine **13** gave alkyne **23** in 69% yield. The Sonogashira reaction of **23** with the donor alkyne led to the 40% conversion of **23** to diyne **24** (by ^{1}H NMR integration of **24** versus **23** in the crude reaction mixture), however we were unable to separate unreacted **23** from the desired product. Negishi cross-coupling has been used to synthesize ethynylbenzenes in cases where Sonogashira protocols proved ineffective.[38] Applied to our system, Negishi cross-coupling of C3-brominated **23** with the in situ-generated alkynyl zincate of 4-(di-n-butylamino)phenylacetylene gave diyne **24** in modest yield with the complete consumption of **23**. Unfortunately, yields were hampered by the formation of an unidentified side-product that was difficult to remove from the desired product.

We were puzzled by the uncooperative reactivity of **23** toward cross-coupling; electron-deficient aryl bromides generally undergo cross-coupling more readily than electron-rich substrates. We hypothesized that the cyano group on alkyne **23** was somehow interfering with the cross-coupling. Taking a step back, we instead subjected B-Cl 1,2-azaborine **13** to the Sonogashira protocol (Scheme 7) and found that the reaction cleanly produced alkyne **25** (as evidenced by ^{1}H and ^{11}B NMR spectroscopy), though this compound was not purified further. The addition of Grignard **22** provided diyne **24** in 44% over two steps. Deprotection of **24** directly to N-H 1,2-azaborine **18** was unsuccessful. A three-step, one-pot protocol (chromium complexation, TBS cleavage, decomplexation) gave the desired diyne **18** in 6% from **24**.

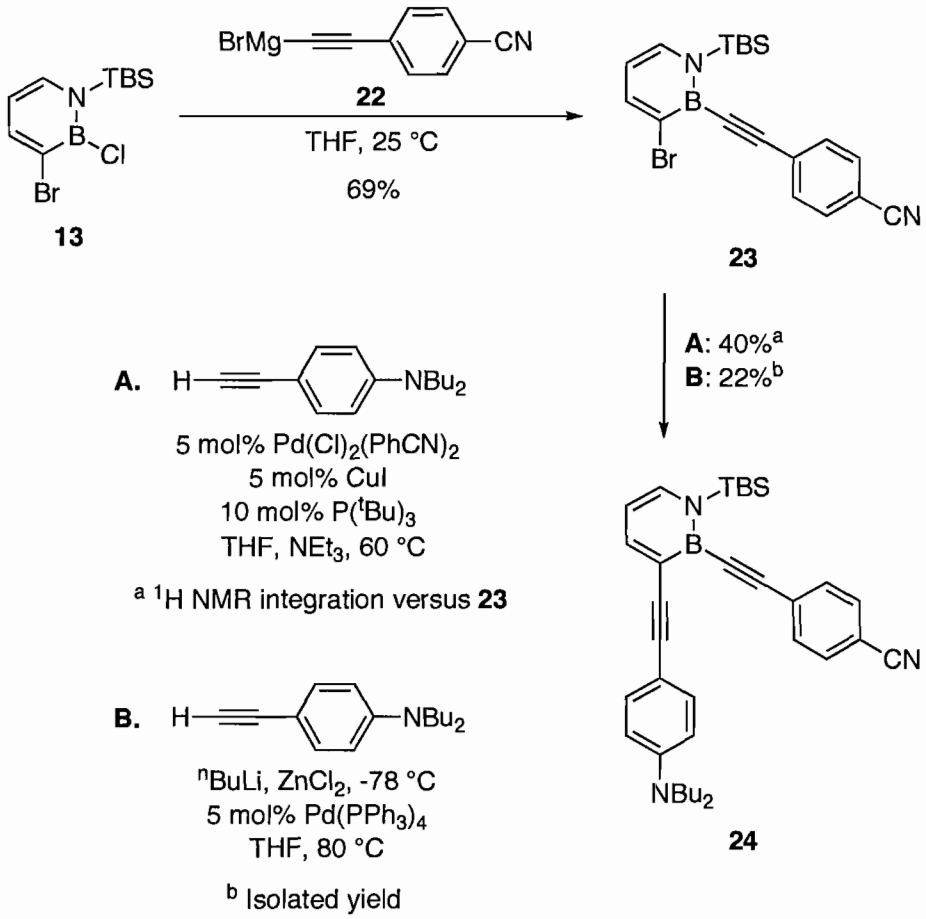

Scheme 6. Exploration of cross-coupling toward the synthesis of **18**.

Normalized absorption spectra of **12**, **17**, and **18** are presented in Figure 11. It is immediately obvious that the substitution of donor and acceptor groups has an effect on the electronic structure of the diyne scaffold. More intriguing is the difference in the absorption spectra between **17** and **18**. The longest wavelength absorption maximum for **18** is at 362 nm (ε = 10386 $M^{-1}cm^{-1}$), which is red-shifted relative to the corresponding peak in **17** (λ_{max} = 335 nm, ε = 18075 $M^{-1}cm^{-1}$); compound **17** exhibits a weaker shoulder absorption at approximately 380 nm.

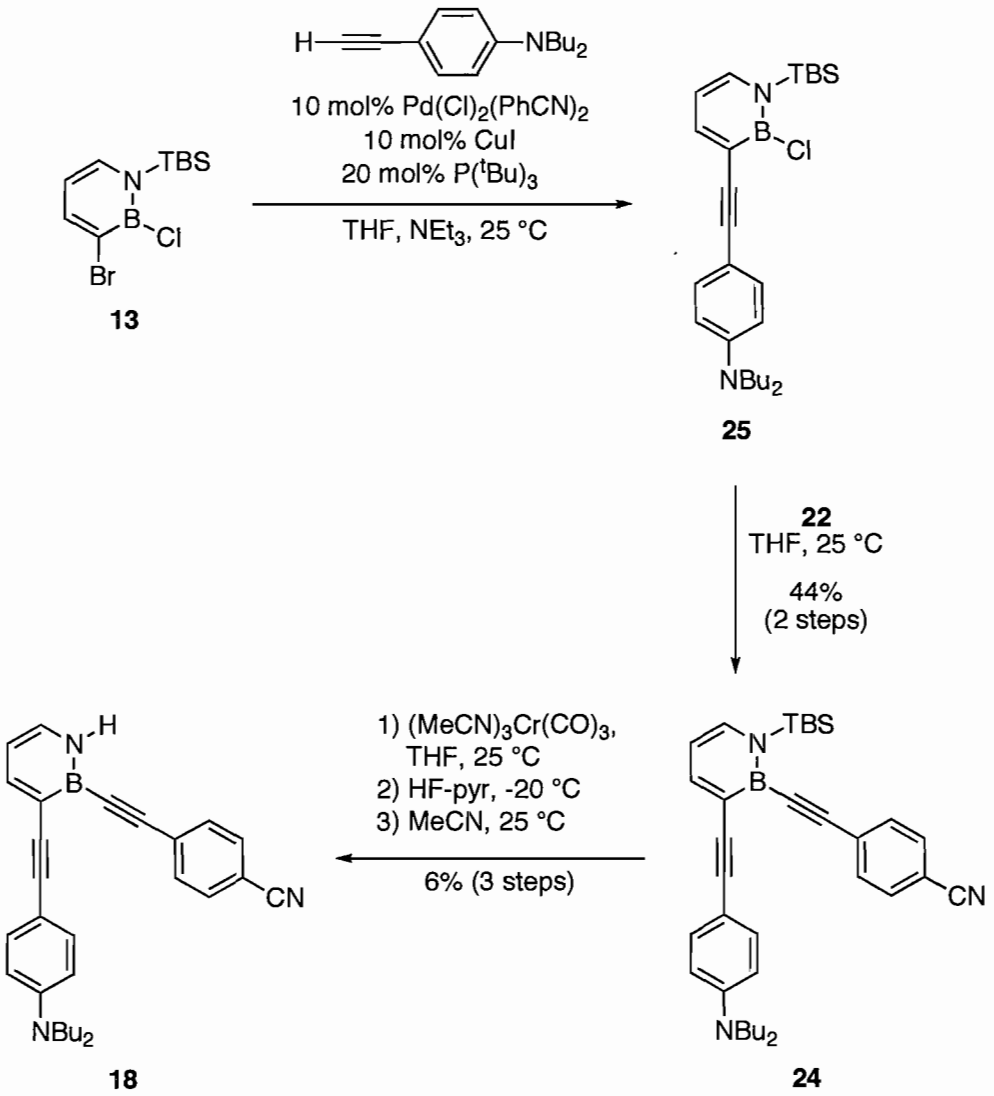

Scheme 7. Synthesis of **18**.

Normalized emission spectra of **12**, **17**, and **18** are shown in Figure 12. In comparison to the parent diyne **12**, the emission peaks of **17** and **18** are significantly red-shifted, indicating intramolecular charge transfer from the donor to the acceptor in the excited state. Compound **17** displays a broad, featureless emission at 503 nm (Φ_{PL} = 0.35), which varies minimally from a related carbon analog with respect to the λ_{PL} and Φ_{PL} values.[28] The emission maximum of **18** is bathochromically shifted to 552 nm, but

is much weaker (Φ_{PL} = 0.04) than the corresponding emission in **17**. A second emission peak is evident in the emission of **18**; this peak becomes more prominent when **18** is excited at 339 nm. As a result of this dual emission, compound **18** emits visible white light in THF.

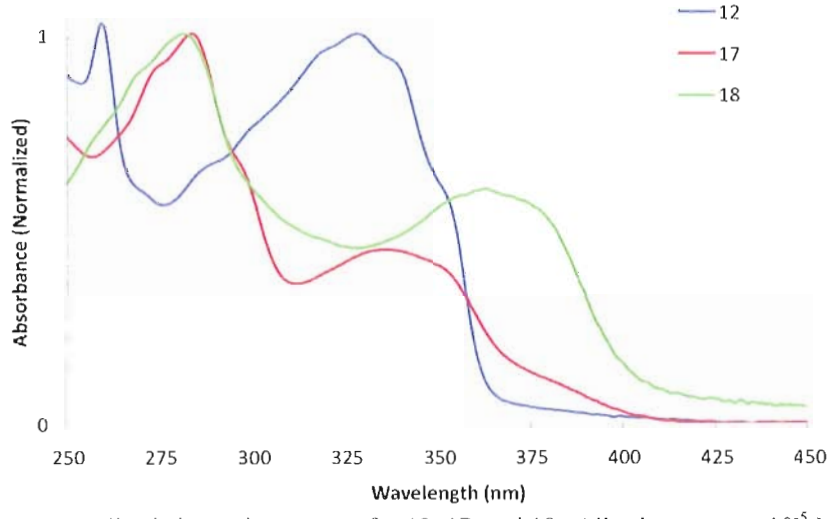

Figure 11. Normalized absorption spectra for **12**, **17**, and **18**. All substrates are 10^{-5} M in THF.

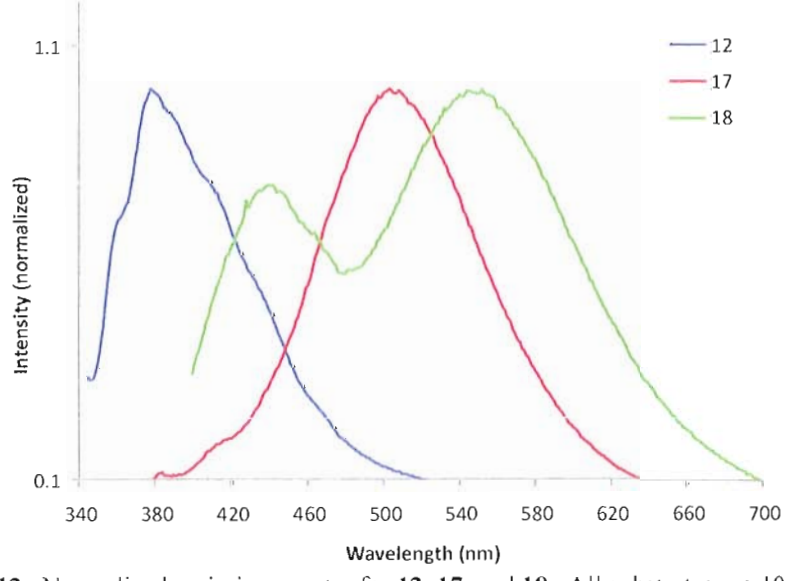

Figure 12. Normalized emission spectra for **12**, **17**, and **18**. All substrates are 10^{-5} M in THF.

To further understand the photophysical properties of donor-acceptor compounds **17** and **18**, we have constructed the phenylethynyl 1,2-azaborines **26** and **27** shown in Figure 13. Boron-substituted **26** is a sub-unit of diyne **17**, while **27** can be considered a sub-unit of **18**. The photophysical examination of **26** and **27** could provide insight into the conjugation pathways in the corresponding diyne structures.

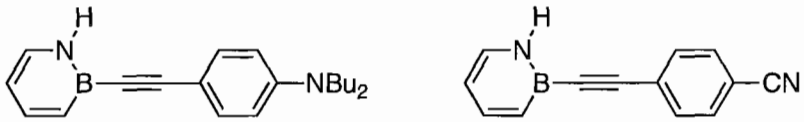

26 **27**

Figure 13. 1,2-Azaborines **26** and **27** are fundamental sub-units of diyne scaffolds **17** and **18**.

The synthesis of boron-substituted alkynes **26** and **27** is shown in Scheme 8. The addition of a donor- or acceptor-functionalized alkynyl Grignard to 1,2-azaborine **3** generates the TBS-protected BN tolans **28** and **29**, respectively. Reaction of **28** and **29** with tricarbonylchromium(0) trisacetonitrile forms the η^6 complexes **30** (R = NBu_2) and **31** (R = CN). Cleavage of the silyl group with HF-pyridine gives the isolable complexes **32** (R = NBu_2) and **33** (R = CN). Decomplexation of the 1,2-azaborine ligands in **32** and **33** gives the desired BN tolans **26** and **27**, respectively.

The absorption and emission properties for **26** and **27** are summarized in Table 1, and diynes **17** and **18** are included for comparison. The data indicate that conjugation extends throughout the diyne scaffold of **17** and **18**. The observed photophysical properties of the donor-acceptor diynes are not a result of one of the arms acting as the sole fluorophore; an intramolecular charge transfer process in likely taking place in both diynes. The emission energies for **17** and its sub-unit **26** are higher than those of **18** and

its sub-unit **27**, respectively, by approximately 50 nm. A trend is also apparent in the quantum yields, in which **17** and **26** have much higher quantum yields than **18** and **27**. It is clear that the phenylethynyl substituent at the boron position plays a significant role in the observed optoelectronic properties of these compounds.

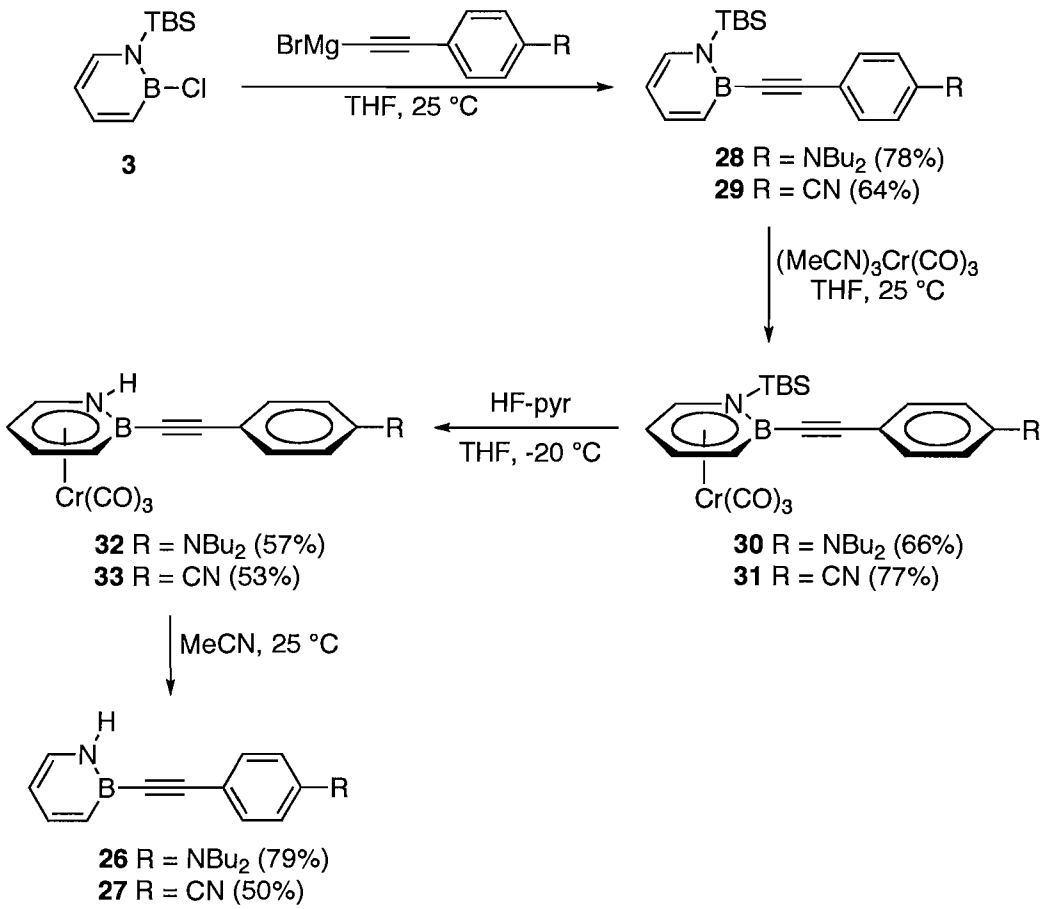

Scheme 8. Synthesis of **26** and **27**.

Table 1. Photophysical Data for Compounds **17**, **18**, **26**, and **27**[a]

Compound	λ_{max} (nm)	ε ($M^{-1}cm^{-1}$)	λ_{PL} (nm)	Φ_{PL}
17	335	18075	503	0.35
18	362	10386	552	0.04
			435	
26	338	5970	369	0.47
27	312	13343	412	0.01

[a] All substrates are 10^{-5} M in THF.

4.5. Conclusion

In summary, we have synthesized BN-doped tolan derivatives that exhibit novel N-H····π hydrogen bonding in the solid state. Furthermore, these derivatives display enhanced photophysical properties relative to their carbonaceous analog. The improvements in recent years in 1,2-azaborine synthesis make it an attractive building block for the construction of larger conjugated scaffolds. The hitherto unreported transition metal-catalyzed cross-coupling of 1,2-azaborines provides an extended conjugated π-system with the heterocycle at its core. Functionalized derivatives of these diynes display non-equivalent photophysical properties and novel white emission. This study opens the way to the use of the 1,2-azaborine motif in materials applications.

4.6. Bridge to Chapter V

Chapter V involves the synthesis of biologically relevant nitrated lipids as a member of Professor Bruce Branchaud's research group. The chapter begins with a discussion of nitrated lipids in a biological context, and moves on to a review of the first-generation synthesis of nitrated lipids. The next section of Chapter V covers the regioselective synthesis of all four possible isomers of nitro-oleic acid. Finally, the syntheses of several derivatives of nitrolipids are presented. Several of these derivatives may offer insight into the biochemical reactivity of nitrated lipids.

CHAPTER V

SYNTHESIS OF NITROLIPIDS

5.1. General Overview

This chapter discusses the synthesis and characterization of nitrated lipids. This chapter includes unpublished co-authored material as well as material published as Woodcock, S. R.; Marwitz, A. J. V.; Bruno, P.; Branchaud, B. P. "Synthesis of nitrolipids. All four possible diastereomers of nitrooleic acids: (E)- and (Z)-, 9- and 10-nitro-octadec-9-enoic acids," *Org. lett.* **2006**, *8*, 3931-4. Experimental work presented in this chapter was performed in part by Dr. Steven Woodcock. Early synthetic protocols were developed by Paulo Bruno. Otherwise, all experimental work was performed by me.

5.2. Introduction

Nitric acid ($^{\bullet}NO$)[1] and oxidative stress generate reactive nitrating species (RNS).[2,3] Nitrated lipids are produced endogenously in the reaction of RNS with unsaturated lipids. Recent work has shown that nitrated derivatives of linoleic and oleic acid (Figure 1) are ubiquitous to cell-signaling pathways.[4,5] Nitrated lipids act as hormone-like signaling molecules specifically activate PPAR-γ,[6] which is a key homeostatic and metabolic control point. The demonstration of $^{\bullet}NO$-independent

signaling in nitrated lipids suggests that these molecules are responsible for facilitating cellular responses.

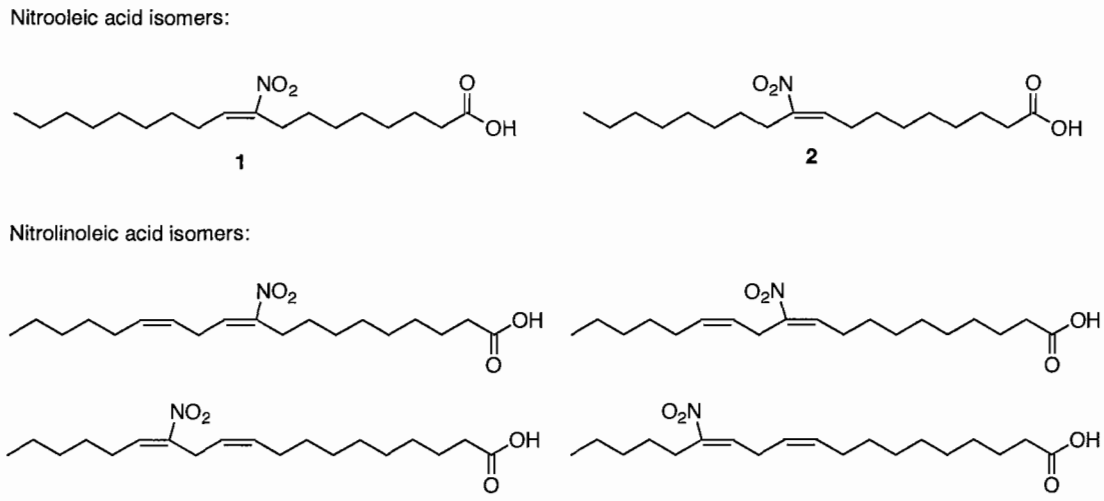

Figure 1. (*E*)-Isomers of nitrooleic acid and nitrolinoleic acids.

Structurally, nitration of unsaturated fatty acids at an olefinic carbon generates the nitroalkene motif. Nitroalkenes are susceptible to nucleophilic attack via Michael addition (Figure 2). In a biological context, Freeman and co-workers demonstrated that the nucleophilic cysteine and histidine residues bind nitrated lipids via a Michael addition to the nitroolefin.[7,8] The electrophilic nature of the nitroalkene group suggests that nitrated lipids may activate biological targets through covalent bond formation with nucleophilic receptors. As part of a comprehensive effort to understand the biochemistry of nitrated lipids, we were interested in developing a concise method for the synthesis of all possible isomers of nitrooleic acid, (*E*)- and (*Z*)-, 9- and 10-nitrooleic acids.

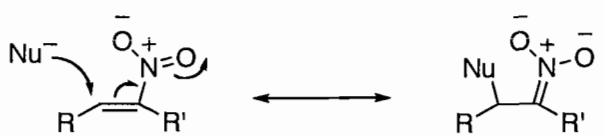

Figure 2. Biologically relevant Michael addition to nitroalkenes. Nu^- = nucleophile.

5.3. Synthesis of All Four Diastereomers of Nitrooleic Acid

The direct reaction of oleic and linoleic acid with $^{\bullet}NO_2$ radical or NO_2^+ generates the corresponding nitrated lipid.[9-12] These methods, although useful, produce a mixture of isomers in low yield along with byproducts such as nitronate esters and allylic nitroalkanes. Freeman and co-workers recently described an improved generation of nitrooleic acids.[6] The nitro group was installed via a phenylselenation/nitration protocol, which was followed by oxidative elimination to produce a statistical distribution of (*E*)-9- and 10-nitrooleic acids (Scheme 1). Our approach was based on a nitroaldol addition (Henry reaction),[13] which fixes the regiochemistry of the nitro group. We envisioned that the resulting beta-hydroxyl group would be positioned to undergo an activation-elimination sequence to provide 9- and 10-nitrooleic acids **1** and **2**, respectively. The King group reported a similar protocol for the synthesis of nitrated lipids in 2006 which parallels the synthesis outlined below.[14]

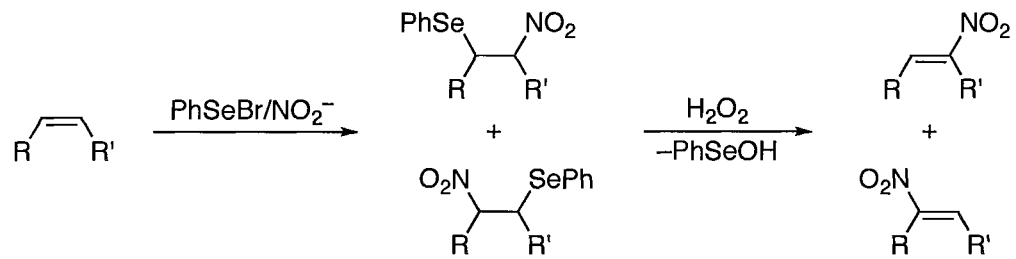

Scheme 1. Synthesis of nitrated lipids in a non-regioselective manner.

The synthesis of (*E*)-9-nitrooleic acid **1** begins with the preparation of the nitroalkane precursor **3** (Scheme 2). 9-Bromononanol was oxidized to carboxylic acid **4**[15] in decent yield using Jones' reagent. The acid was readily esterified with allyl

alcohol and pyridinium para-toluene sulfonate (PPTS). Bromoalkane **4** was converted to nitroalkane **5** via the method developed by Kornblum.[16]

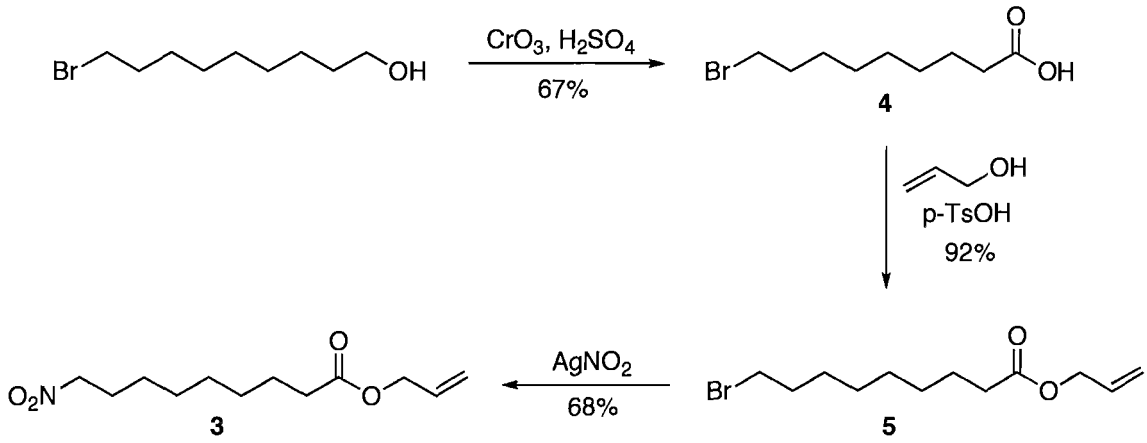

Scheme 2. Synthesis of nitroalkane **3**.

The nitroaldol condensation of **5** and nonyl aldehyde (Scheme 3) was performed neat[17] with a catalytic amount (10 mol%) of DBU added as base, providing β-hydroxynitro **6** as a 1:1 mixture of diastereomers. Compound **6** was acetylated with acetic anhydride and para-toluenesulfonic acid (*p*-TsOH) to **7** in 86% yield. The base-mediated elimination of **7** with sodium carbonate furnished the (*E*)-nitroalkene **8** in 84% yield. The formation of **8** as the sole isomer in the elimination is consistent with an E1cB mechanism; bond rotation about the intermediate carbanion in an E1cB reaction would lead to the formation of the more thermodynamically stable isomer.

The base sensitivity of both nitroalkanes and nitroalkenes led us to use consistently acidic conditions (when possible) throughout the synthesis. However, many of the commonly employed methods for allylester cleavage are base-mediated. We determined that palladium-catalyzed allyl isomerization of **8** in the presence of formic

acid[18] as a hydride donor promoted facile ester cleavage, affording isomerically pure nitroolefin **1** in 95% yield.[19]

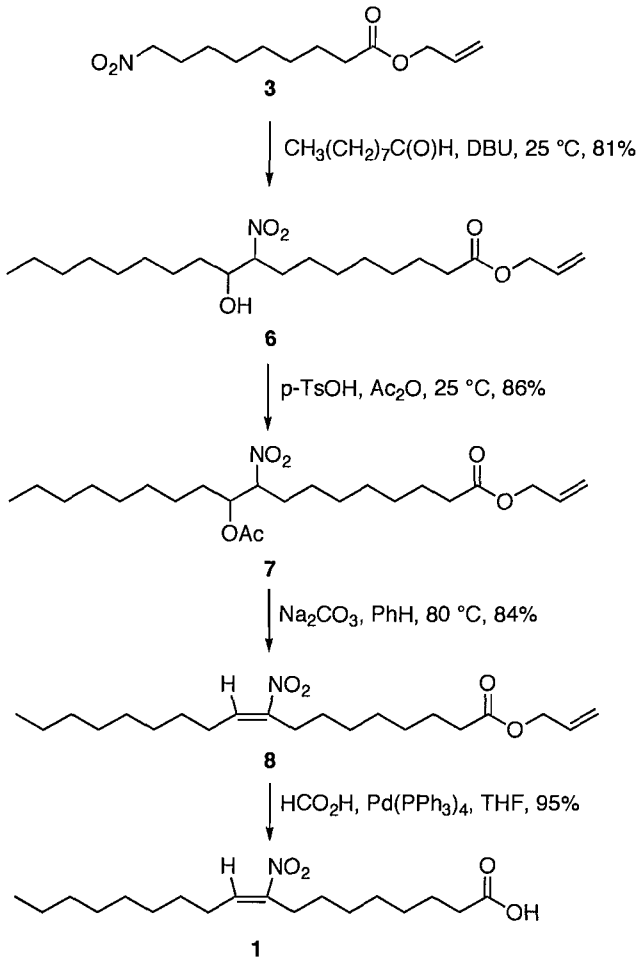

Scheme 3. Synthesis of **1**.

The synthesis of **2** was followed a similar synthetic path (Scheme 4). The conversion of nonyl bromide to nitroalkane **9** was achieved in 60% yield. The corresponding aldehyde fragment was synthesized in two steps; reductive ozonolysis of oleic acid gave aldehyde **10**, which was protected via a DCC/DMAP-promoted esterification to **11** in 59% for the two steps.

A DBU-promoted Henry reaction was performed with nitroalkane **9** and aldehyde **11** (Scheme 5), which provided the β-hydroxynitroalkane **12** in 85% isolated yield. Activation to the acetoxy-substituted compound **13** was readily achieved via the acid-catalyzed reaction of **12** with acetic anhydride. Base-mediated elimination of **13** provided nitroalkene **14**, which was deprotected using the Pd-catalyzed protocol discussed above to give (*E*)-10-nitrooleic acid **2** in 95% yield.

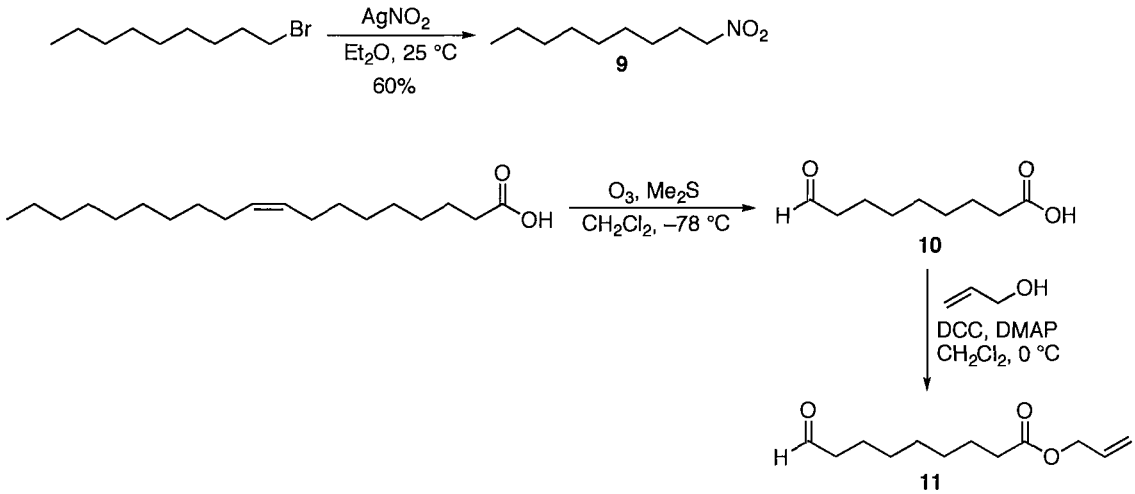

Scheme 4. Synthesis of aldehyde **11** and nitrononane **9**.

We next turned to the synthesis of the (*Z*)-isomers **15** and **16** (9- and 10-nitroelaidic acid, respectively, Scheme 6). These isomers may also be endogenously produced and are of significant interest. The (*E*)-isomer is thermodynamically more stable than the (*Z*)-isomer and therefore the synthesis of **15** and **16** present a challenge. We determined that (*E*)-9-nitrooleic acid **1** reacts cleanly with phenylselenide via a Michael addition to form the anti-β-nitroselenide at low temperatures. The *syn*-elimination of this intermediate led to the selective formation of **15** in 77% yield. 10-

Nitroelaidic acid was synthesized in an identical manner to provide **16** in 75% isolated yield. Experimental details are provided in Appendix D.

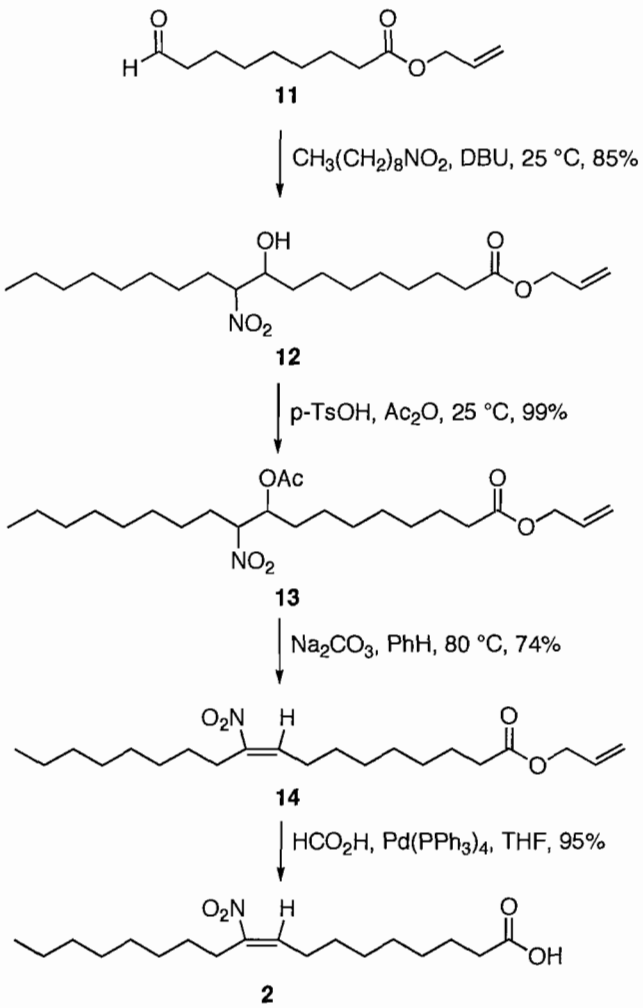

Scheme 5. Synthesis of **2**.

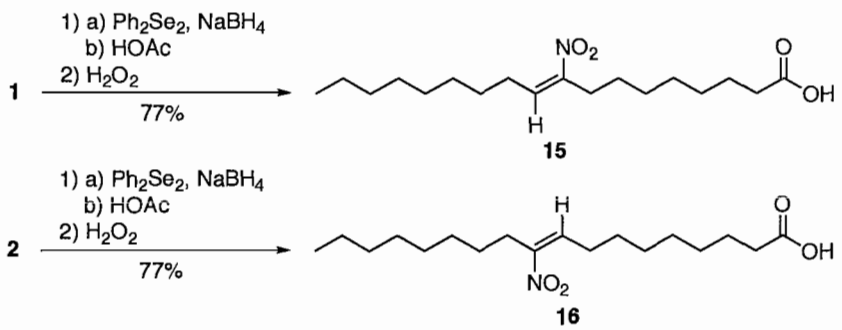

Scheme 6. Isomerization of **1** and **2** to **15** and **16**, respectively.

5.4. Synthesis of Nitrolinoleic Acid Analogs

Nitrated analogs of linoleic acid (e. g. **17** in Figure 3) have also been of considerable interest in recent years and have been implicated in the transduction of $^{\bullet}NO$,[20] in the post-translational modification of proteins,[7,8] and as activators of PPAR-γ.[6]

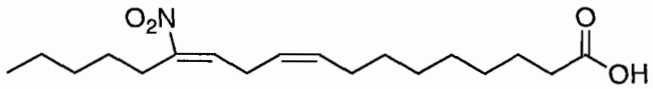

17

Figure 3. 13-Nitrolinoleic acid **17** is one of the 16 possible isomers of nitrolinoleic acid.

The total synthesis of all 16 isomers of nitrolinoleic could provide useful information regarding the biological activity of this class of molecule. The 12- and 13-substituted nitroolefins are of particular interest, as they differ from nitrooleic acids **1** and **2** with respect to the position of the nitro substituent. We were therefore interested in synthesizing nitrolipids **18** and **19** (Figure 4), which are derivatives of 13- and 12-nitrolinoleic acid, respectively. It should be noted that compounds **18** and **19** lack the C=C bond at the 9-position of nitrolinoleic acid, and are therefore model compounds for the study of nitrated linoleic acid.

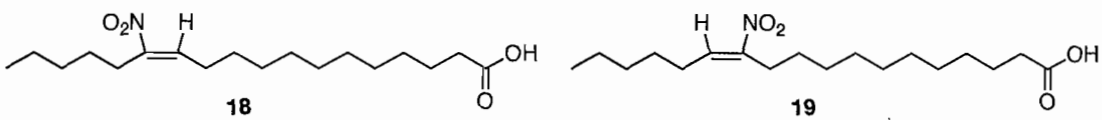

18 **19**

Figure 4. Model compounds **18** and **19**.

The synthesis of **18** is shown in Scheme 7. Baeyer-Villiger oxidation of cyclododecanone[21] gave lactone **20** in good yield. Hydrolytic ring-opening gave acid **21**,[22] which was then esterified to **22** with allylbromide. Swern oxidation of the terminal hydroxyl group of **22** afforded aldehyde **23** in excellent yield. The nitroaldol

condensation of aldehyde **23** with nitrohexane readily provided β-hydroxynitroalkane **24**. Acid-catalyzed acetylation of alcohol **24** gave **25** in 99% yield. The base-mediated elimination of acetoxy-substituted **25** gave nitroalkene **26** in 50% yield. Finally, Pd-catalyzed de-allylation provided **18** in good yield.

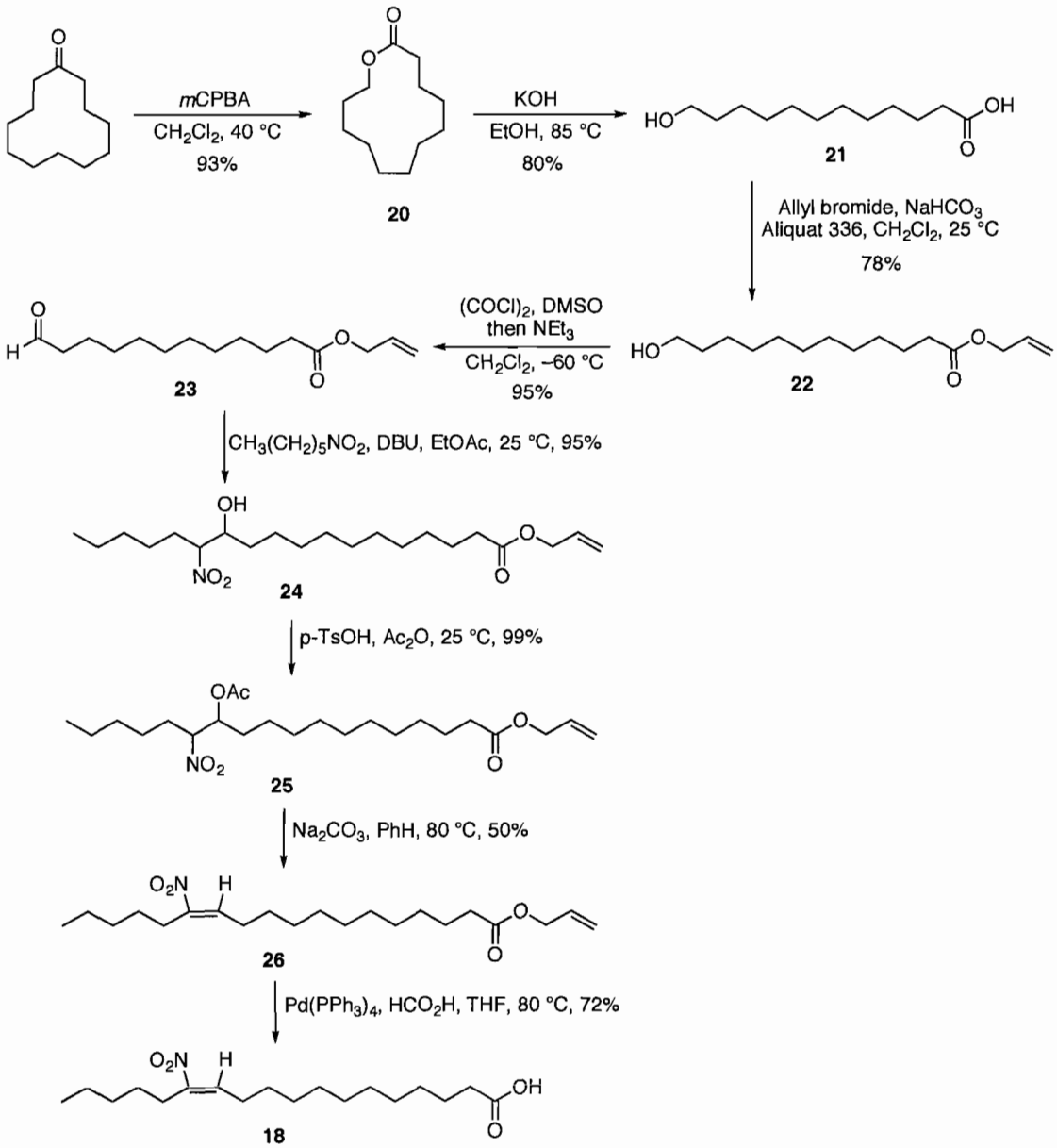

Scheme 7. Synthesis of **18**.

The synthesis of the 12-nitro isomer **19** was accomplished using a similar route from lactone **20**, which serves as a common feedstock for the preparation of **18** and **19**. Ring-opening of lactone **20** with HBr provides ω-bromocarboxylic acid **27**, albeit in low yield (Scheme 8). Ester protection provides **28** in good yield. Nitroalkane **29** was produced in decent yield via the addition of $AgNO_2$ to bromide **28**. Nitroaldol condensation of **29** with capronaldehyde gave β-hydroxynitroalkane **30** in 68% yield. The desired compound **19** was synthesized in an identical manner as described for **18**; activation to acetoxy-substituted **31** was followed by elimination to nitroolefin **32**, which was deprotected to give **19**.

We have previously described the isomerization of (*E*)-nitrooleic acids to the corresponding (*Z*)-nitroelaidic acids. The isomerization of (*E*)-isomers **18** and **19** to the (*Z*)-isomers **33** and **34** was achieved in good yield (Scheme 9). The addition of phenylselenide to **18** and **19** was followed by oxidative elimination, which provided the desired (Z)-isomers **33** and **34**, respectively. The (*E*)-isomer was observed in the ^1H NMR spectra of both **33** and **34**. Nevertheless, the synthesis of both (E)- and (Z)-isomers of these model compounds may provide the opportunity to explore the biochemistry of isomerically-enriched nitroolefins. Experimental details are presented in Appendix D.

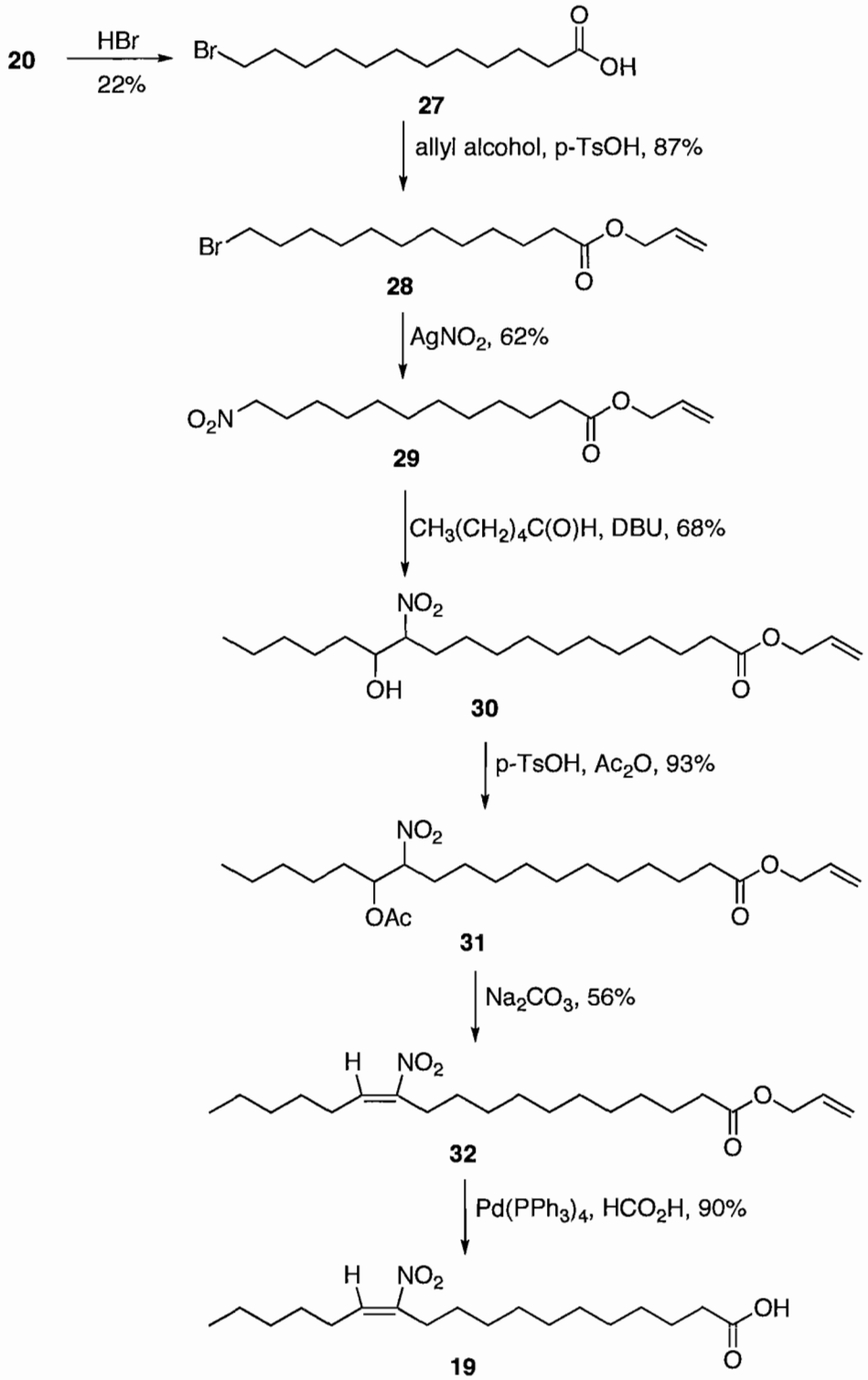

Scheme 8. Synthesis of **19**.

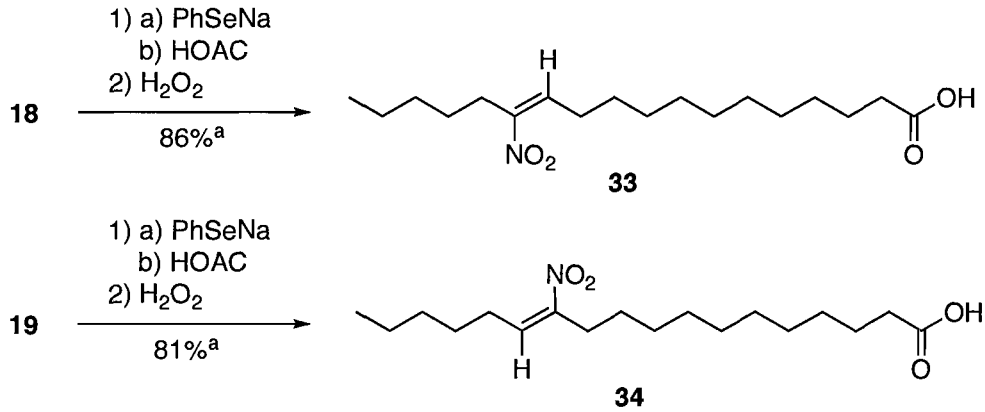

Scheme 9. Synthesis of **33** and **34**. [a] **33**: 70% Z, 30% E, **34**: 72% Z, 28% E.

5.5. Conclusion

In summary, we have developed a mild, scalable synthesis for all desired nitrooleic acids. Regiochemical control was achieved using a Henry reaction to install the nitro group at various positions on the lipid skeleton. Mild ester deprotection afforded isomerically pure (E)-9- and 10-nitrooleic acids. Isomerization to the less stable (Z)-isomers was achieved, which may provide the first opportunity to examine these derivatives in a biological context. Finally, regiochemically pure analogs of nitrolinoleic acid have been synthesized from a common intermediate. The examination of these compounds as models of nitrolinoleic acid may lead to new discoveries in the biology of nitrated lipids.

APPENDIX A

SYNTHESIS AND CHARACTERIZATION OF BORON-SUBSTITUTED 1,2-AZABORINES

A.1 Introduction

The last decade saw significant improvements in the synthesis of 1,2-azaborines; however, there are still only a handful of known 1,2-azaborine derivatives. The scarcity of 1,2-azaborine derivatives limits the utility of this aromatic heterocycle. Thus, the expansion of 1,2-azaborine synthesis to include carbon- and heteroatom-based groups at the boron position is required to realize the potential of this benzene mimic. Prior synthetic achievements used a ring-closing metathesis (RCM)/oxidation protocol to generate the 1,2-azaborine ring.[1] The absence of strongly nucleophilic reagents in the sequence provides an opportunity for generating an advanced 1,2-azaborine that can be substituted by various nucleophiles late in the synthesis.

A.2 Experimental

A.2.1 General

All oxygen- and moisture-sensitive manipulations were carried out under an inert atmosphere using either standard Schlenk techniques or a glove box. THF, Et_2O,

CH_2Cl_2, and pentane were purified by passing through a neutral alumina column under argon. Cyclohexene was dried over CaH_2 and distilled under N_2 prior to use.

Solutions of *n*-BuLi, phenylmagnesium bromide, phenylethynylmagnesium bromide, potassium *t*-butoxide, and Superhydride were purchased from Aldrich and used as received. Potassium hydride (Strem) and sodium hydride (Aldrich) were washed with pentane three times and pumped dry under vacuum prior to use. Benzyl mercaptan and tetravinyltin were purchased from TCI and used as received. Pyridine was purchased from Aldrich and dried over molecular sieves (4 Å) prior to use. Substituted pyridines were purchased from TCI or Aldrich and used as received. Trisacetonitrile(tricarbonyl)chromium(0) was purchased from Acros or Aldrich and used as received. All other chemicals and solvents were purchased (Aldrich or Strem) and used as received.

Silica gel (230-400 mesh) was heated under vacuum in a 200 °C sand bath for 12 hours. Flash chromatography was performed with this silica gel under an inert atmosphere.

^{11}B NMR spectra were recorded on a Varian Unity/Inova 600 spectrometer at ambient temperature. ^{1}H NMR spectra were recorded on a Varian Unity/Inova 300 or Varian Unity/Inova 600 spectrometer. ^{15}N NMR spectra were recorded on a Varian Unity/Inova 500 spectrometer. ^{31}P NMR spectra were recorded on a Varian Unity/Inova 500 spectrometer with complete proton decoupling at ambient temperature. ^{13}C NMR spectra were recorded on a Varian Unity/Inova 300 or Varian Unity/Inova 500

spectrometer. All chemical shifts are externally referenced: ^{31}P NMR to 85% H_3PO_4 (δ 0), ^{11}B NMR to $BF_3 \cdot Et_2O$ (δ 0), and ^{15}N NMR to nitromethane (δ 0).

IR spectra were recorded on a Nicolet Magna 550 FT-IR instrument with OMNIC software. UV-Vis spectra were collected on an Agilent 8453 spectrometer with ChemStation software. Emission spectra were collected on a Jobin Yvon Horiba Fluoromax 4 spectrometer with integrating sphere. Photoluminescence quantum yields are reported as the average of three runs.

High-resolution mass spectroscopy data were obtained at the Mass Spectroscopy Facilities and Services Core of the Environmental Health Sciences Center at Oregon State University. Financial support for this facility has been furnished in part by the National Institute of Environmental Health Sciences, NIH (P30 ES00210).

A.2.2 Electronic Structure Calculations

The electrostatic potential (ESP) was calculated at the B3LYP/6-311+G** level using Spartan.[2] All other computations were calculated using the 03[3] suite of programs at the B3LYP/DGDZVP2 level of theory. All stationary points were confirmed by harmonic frequency analysis ($N_{imag} = 0$). The energies of the stationary points were determined, including zero point energies at the same level of theory. Structure **4** was calculated at 0 K.[4] NICS calculations were carried out using standard GIAO methods with Bq atoms (NICS probes) 1.0 Å above the geometric center of the ring.

A.2.3 Supplemental information for Chapter II, section 2.3

Synthesis of 2. In a glove box, a solution of Grubbs 1st generation catalyst (0.174 g, 0.211 mmol in 50 mL CH_2Cl_2) was added to a stirring solution of aminoborane

1[1] (4.53 g, 26.4 mmol in 150 mL CH_2Cl_2). The solution was stirred at room temperature for 1 h, whereupon additional Grubbs catalyst (0.100 g, 0.122 mmol in 10 mL CH_2Cl_2) was added to the reaction flask. The reaction was stirred at room temperature for 1 h, after which the solvent was removed. The desired product was purified by vacuum distillation (bp 20-21 °C at 1 mm) to furnish **2** as a clear, colorless liquid (2.51 g, 66%).

^{1}H NMR (300 MHz, CD_2Cl_2): δ 5.70 (br, 1H), 5.58 (m, 1H), 3.68 (m, 2H), 3.29 (q, $^3J_{HH}$ = 7.0 Hz, 2H), 1.66 (br, 2H), 1.11 (t, $^3J_{HH}$ = 7.0 Hz, 3H). ^{13}C NMR (125 MHz, CD_2Cl_2): δ 125.2, 124.8, 49.5, 45.4, 18.7 (br), 14.3. ^{11}B NMR (192.5 MHz, CD_2Cl_2): δ 37.3. FTIR (thin film) 3030, 2975, 2934, 2874, 2821, 1667, 1530, 1465, 1444, 1397, 1377, 1358, 1342, 1309, 1281, 1195, 1118, 1079, 1046, 982, 796, 659, 607, 517 cm^{-1}. HRMS (EI) calcd for $C_6H_{11}BClN$ (M^+) 143.06731, found 143.06741.

Aromatization of Heterocycle 2: Optimization Survey. Yields in Table 1 were determined by ^{11}B-NMR analysis using phenylboronic acid pinacol ester as an internal standard. All yields have been corrected for response factors.

General Procedure. A 25 mL Schlenk tube was charged with **2** (0.050 g, 0.35 mmol), the catalyst, and solvent. The reaction was stirred at 80 °C for 16 h. After cooling to room temperature, phenylboronic acid pinacol ester (0.040 g, 0.20 mmol) was added to the reaction mixture. The yield of **3** was then determined by ^{11}B NMR analysis.

Entry 1: A 25 mL Schlenk tube was charged with **2** (0.050 g, 0.35 mmol), 2,3-dichloro-5,6-dicyano-*p*-benzoquinone (0.087 g, 0.38 mmol), and pentane (2.0 mL). The

suspension was stirred at 35 °C for 24 h. After cooling to room temperature, phenylboronic acid pinacol ester (0.041 g, 0.20 mmol) was added to the reaction mixture. ^{11}B NMR analysis indicated the formation of **3** in 13% yield.

Entry 2: The general procedure was followed, using Pd/C (10 wt%; 0.074 g, 0.070 mmol), and pentane (2.0 mL). ^{11}B NMR analysis indicated the formation of **3** in 31% yield.

Entry 3: The general procedure was followed, using Pd/C (10 wt%; 0.074 g, 0.070 mmol), and cyclohexene (2.0 mL). ^{11}B NMR analysis indicated the formation of **3** in 43% yield.

Entry 4: The general procedure was followed, using Ru/C (5 wt%; 0.141 g, 0.070 mmol), and cyclohexene (2.0 mL). ^{11}B NMR analysis indicated the formation of **3** in 1% yield.

Entry 5: The general procedure was followed, using Rh/Al_2O_3 (5 wt%; 0.152 g, 0.070 mmol), and cyclohexene (2.0 mL). ^{11}B NMR analysis indicated the formation of **3** in 23% yield.

Entry 6: The general procedure was followed, using Pd black (7.4 mg, 0.070 mmol), and cyclohexene (2.0 mL). ^{11}B NMR analysis indicated the formation of **3** in 75% yield.

Entry 7: The general procedure was followed, using $Pd(PPh_3)_4$ (0.040 g, 0.035 mmol), and benzene (2.0 mL). ^{11}B NMR analysis indicated no product formation.

Preparatory Scale Synthesis of Compound 3 (Table 1, entry 6). In a glove box, compound **2** (3.50 g, 24.4 mmol in 35 mL cyclohexene) was added to a 100 mL Schlenk tube containing Pd black (0.520 g, 4.88 mmol). The flask was then sealed and heated at 80 °C for 19 h. After cooling to room temperature, the mixture was filtered through an acrodisc and approximately one-half of the solvent was removed under vacuum. Et_2O (100 mL) was added, and the solution was cooled to –78 °C. Phenylethynylmagnesium bromide (1.0 M solution in THF; 9.5 mL, 9.5 mmol) was added, and the solution was then allowed to warm up to room temperature. The reaction mixture was passed through an acrodisc and concentrated under vacuum. The crude material was purified by vacuum distillation (bp 23-25 °C at 50 mtorr) to give **3** as a clear, colorless liquid (1.976 g, 57%). The treatment of the crude reaction mixture with phenylethynylmagnesium bromide is necessary to derivatize undesired boron-containing byproducts into compounds of high molecular weight so that the desired heterocycle **3** can be cleanly isolated via distillation.

^{1}H NMR (600 MHz, CD_2Cl_2): δ 7.33 (br, 1H), 6.86 (d, $^3J_{HH}$ = 11.2 Hz, 1H), 6.47 (d, $^3J_{HH}$ = 6.1 Hz, 1H), 5.96 (t, $^3J_{HH}$ = 6.3 Hz, 1H), 3.38 (q, $^3J_{HH}$ = 7.1 Hz, 2H), 0.87 (t, $^3J_{HH}$ = 7.1 Hz 3H). ^{13}C NMR (75 MHz, CD_2Cl_2): δ 145.1, 139.3, 129 (br), 111.3, 48.9, 17.6. ^{11}B NMR (192.5 MHz, CD_2Cl_2): δ 32.3. FTIR (thin film) 3072, 3044, 2980, 2935, 2900, 1610, 1519, 1474, 1454, 1439, 1399, 1379, 1344, 1248, 1237, 1175, 1118, 1084, 1068, 1030, 1001, 743, 670, 639 cm^{-1}.

Compound 6a. In a glove box, a vial was charged with a solution of **3** (0.150 g, 1.06 mmol in 5.0 mL Et_2O) and cooled to –78 °C. To this stirring solution was added BuLi (2.53 M in hexane; 0.420 mL, 1.06 mmol), and the solution was allowed to warm to room temperature. After stirring for 8 h, approximately 75% of the solvent was removed. The crude material was subjected to silica gel chromatography using pentane as eluent, providing pure **6a** as a clear, colorless liquid (0.136 g, 79%).

^{1}H NMR (600 MHz, CD_2Cl_2): δ 7.52 (dd, $^3J_{HH}$ = 6.3 Hz, 4.4 Hz, 1H), 7.2 (d, $^3J_{HH}$ = 6.8 Hz, 1H), 6.76 (d, $^3J_{HH}$ = 11 Hz, 1H), 6.24 (dt, $^3J_{HH}$ = 5.4 Hz, 1.2 Hz, 1H), 3.80 (q, $^3J_{HH}$ = 7.1 Hz, 2H), 1.62 (m, 2H), 1.47 (m, 2H), 1.33 (t, $^3J_{HH}$ = 7.0 Hz, 3H), 1.27 (q, $^3J_{HH}$ = 8.0 Hz, 2H), 1.01 (t, $^3J_{HH}$ = 7.3 Hz, 3H). ^{13}C NMR (75 MHz, CD_2Cl_2): δ 142.3, 138.9, 130.3(br), 110.4, 48.6, 29.8, 26.6, 18.6, 18.5 (br), 14.6. ^{11}B NMR (192.5 MHz, CD_2Cl_2): δ 37.8. FTIR (thin film) 3069, 2956, 2924, 2871, 2856, 1611, 1516, 1445, 1406, 1377, 1339, 1250, 1123, 740 cm^{-1}. HRMS (EI) calcd for $C_{10}H_{18}BN$ (M^+) 163.15323, found 163.15312.

Compound 6b. In a glovebox, a vial was charged with a solution of **3** (0.200 g, 1.41 mmol in 12.0 mL Et_2O) and cooled to –78 °C. To this stirring solution vinyl lithium[5] (0.060 g, 1.8 mmol in 4.0 mL THF) was added dropwise. Then the reaction was slowly warmed to room temperature and stirred for 1 h. The reaction mixture was then passed through an acrodisc, and solvents were removed under reduced pressure. The crude material was subjected to silica gel chromatography using pentane as eluent, providing **6b** as a clear, colorless liquid (0.095 g, 50%).

^{1}H NMR (500 MHz, CD_2Cl_2): δ 7.54 (dd, $^3J_{HH}$ = 6.1 Hz, 4.4 Hz, 1H), 7.18 (d, $^3J_{HH}$ = 6.7 Hz, 1H), 6.89 (d, $^3J_{HH}$ = 11.2 Hz, 1H), 6.60 (dd, $^3J_{HH}$ = 13.8 Hz, 5.8 Hz, 1H), 6.26 (dt, $^3J_{HH}$ = 5.0 Hz, 1.7 Hz, 1H), 6.08 (dd, $^3J_{HH}$ = 15.5 Hz, 4.1 Hz, 1H), 5.92 (d, $^3J_{HH}$ = 3.1 Hz, 1H), 3.86 (q, $^3J_{HH}$ = 7.0 Hz, 2H), 1.31 (t, $^3J_{HH}$ = 7.3 Hz, 3H). ^{13}C NMR (125 MHz, CD_2Cl_2): δ 142.9, 139.0, 138 (br), 131.1, 128 (br), 111.4, 49.3, 18.7. ^{11}B NMR (160 MHz, CD_2Cl_2): δ 32.9. FTIR (thin film) 3056, 2977, 2954, 2932, 2905, 2872, 1890, 1610, 1516, 1479, 1446, 1415, 1378, 1341, 1249, 1221, 1183, 1132, 1110, 1084, 1051, 1009, 945, 830, 803, 743, 716 cm^{-1}. HRMS (EI) calcd for $C_8H_{12}BN$ (M^+) 133.10628, found 133.10568.

Compound 6c. A vial was charged with a solution of **3** (0.150 g, 1.06 mmol in 5.0 mL Et_2O) and cooled to –78 °C. To this stirring solution phenylmagnesium bromide (2.0 M solution in Et_2O; 0.55 mL, 1.1 mmol) was added dropwise. Then the reaction was allowed to warm to room temperature and stirred for 10 h. Approximately 75% of the solvent was then removed under reduced pressure, and the remaining crude material was subjected to silica gel chromatography using hexane/CH_2Cl_2 as eluent. Pure **6c** was obtained as a clear, colorless oil (0.147 g, 76%).

^{1}H NMR (600 MHz, CD_2Cl_2): δ 7.68 (m, 1H), 7.59 (m, 2H), 7.43-7.35 (m, 4H), 6.85 (dd, $^3J_{HH}$ = 7.6 Hz, 3.2 Hz, 1H), 6.47 (m, 1H), 3.91 (q, $^3J_{HH}$ = 7.3 Hz, 2H), 1.35 (t, $^3J_{HH}$ = 7.3 Hz, 3H). ^{13}C NMR (125 MHz, CD_2Cl_2): δ 143.2, 142 (br), 138.7, 133.3, 132 (br), 128.2, 127.8, 112.0, 48.8, 18.8. ^{11}B NMR (192.5 MHz, CD_2Cl_2): δ 35.5. FTIR (thin film) 3068, 3008, 2975, 2931, 2898, 2871, 1953, 1877, 1824, 1764, 1611, 1514,

1475, 1442, 1430, 1405, 1378, 1333, 1259, 1237, 1210, 1175, 1150, 1115, 1000, 978, 781, 745, 704, 597, 523, 451 cm^{-1}. HRMS (EI) calcd for $C_{12}H_{14}BN$ (M^+) 183.12193, found 183.12236.

Compound 6d. To a stirring solution of **3** (0.150 g, 1.06 mmol in 5.0 mL Et_2O) at –78 °C was added phenylethynylmagnesium bromide (1.0 M solution in THF; 1.1 mL, 1.1 mmol). The solution was allowed to warm to room temperature and stirred for 6 h. Approximately one-half of the solvent was removed, and the remaining mixture was passed through an acrodisc. This material was then subjected to silica gel chromatography using a mixture pentane/CH_2Cl_2 (10:1) as eluent to afford **6d** as a clear, colorless oil (0.183 g, 83%).

^{1}H NMR (600 MHz, CD_2Cl_2): δ 7.63 (dd, $^3J_{HH}$ = 6.8 Hz, 3.7 Hz, 1H), 7.55 (dd, $^3J_{HH}$ = 4.6 Hz, 2.9 Hz, 2H), 7.39-7.32 (m, 4H), 6.90 (d, $^3J_{HH}$ = 11 Hz, 1H), 6.41 (t, $^3J_{HH}$ = 6.6 Hz, 1H), 4.10 (q, $^3J_{HH}$ = 7.2 Hz, 2H), 1.44 (t, $^3J_{HH}$ = 7.1 Hz, 3H). ^{13}C NMR (125 MHz, CD_2Cl_2): δ 143.3, 139.3, 132.3, 132 (br), 128.9, 124.5, 112.2, 107.1, 95 (br), 51.2, 18.6. ^{11}B NMR (192.5 MHz, CD_2Cl_2): δ 26.7. FTIR (thin film) 3067, 3034, 2976, 2932, 2896, 2177, 1875, 1764, 1673, 1604, 1514, 1492, 1472, 1454, 1440, 1409, 1377, 1336, 1264, 1246, 1225, 1177, 1154, 1119, 1104, 1070, 1003, 998, 915, 828, 756, 689, 557, 540 cm^{-1}. HRMS (EI) calcd for $C_{14}H_{14}BN$ (M^+) 207.12193, found 207.12248.

Compound 6e. In a glove box, a flask was charged with a solution of **3** (1.00 g, 7.08 mmol in 15 mL Et_2O) and cooled to –20 °C. To this solution lithium dimethylamide (0.397 g, 7.78 mmol in 45 mL THF) was added dropwise at – 20 °C. The

flask was kept at – 20 °C and shaken every 15 min for 2 h, then allowed to warm to room temperature. After 10 h of stirring, approximately one-half of the solvent was removed under reduced pressure, and 20 mL pentane was added. The resulting mixture was filtered through a glass frit, and the filtrate was concentrated under vacuum. The crude material was purified by vacuum distillation (bp 29-30 °C at 75 mtorr) to give **6e** as a clear, colorless liquid (0.696 g, 66%).

^{1}H NMR (600 MHz, CD_2Cl_2): δ 7.17 (dd, $^3J_{HH}$ = 5.9 Hz, 5.4 Hz, 1H), 6.81 (d, $^3J_{HH}$ = 6.8 Hz, 1H), 6.21 (d, $^3J_{HH}$ = 11.5 Hz, 1H), 5.71 (dt, $^3J_{HH}$ = 5.9 Hz, 1.4 Hz, 1H), 3.66 (q, $^3J_{HH}$ = 7.4 Hz, 2H), 2.81 (s, 6H), 1.31 (t, $^3J_{HH}$ = 7.0 Hz, 3H). ^{13}C NMR (75 MHz, CD_2Cl_2): δ 141.2, 139.5, 124 (br), 105.5, 47.3, 41.1, 17.9. ^{11}B NMR (192.5 MHz, CD_2Cl_2): δ 29.1. FTIR (thin film) 3321, 2977, 2930, 2873, 1613, 1519, 1473, 1457, 1441, 1414, 1350, 1304, 1273, 1143, 1084, 820, 737, 691 cm^{-1}.

Compound 6f. To a stirred solution of **3** (1.00 g, 7.08 mmol in 25 mL THF) was added dropwise a solution of potassium *t*-butoxide (1.0 M in THF; 7.8 mL, 7.8 mmol) at –10 °C. The solution was allowed to warm to room temperature. After 10 h of stirring the mixture was passed through an acrodisc and concentrated under vaccum. The crude material was purified by vacuum distillation (bp 58-60 °C at 200 mtorr) to give **6f** as a clear, colorless liquid (0.904 g, 71%).

^{1}H NMR (600 MHz, CD_2Cl_2): δ 7.40 (dd, $^3J_{HH}$ = 5.8 Hz, 4.7 Hz, 1H), 7.02 (d, $^3J_{HH}$ = 6.3 Hz, 1H), 6.21 (d, $^3J_{HH}$ = 11.4 Hz, 1H), 5.81 (t, $^3J_{HH}$ = 6.4 Hz, 1H), 3.62 (q, $^3J_{HH}$ = 7.1 Hz, 2H), 1.42 (s, 9H), 1.22 (t, $^3J_{HH}$ = 7.0 Hz, 3H). ^{13}C NMR (75 MHz,

CD_2Cl_2): δ 144.4, 139.9, 119 (br), 104.9, 72.8, 45.8, 30.9, 17.7. ^{11}B NMR (192.5 MHz, CD_2Cl_2): δ 27.3. FTIR (thin film) 3073, 3044, 2975, 2931, 2873, 1612, 1519, 1476, 1414, 1390, 1365, 1349, 1281, 1253, 1197, 1156, 1116, 1086, 1056, 1004, 958, 937, 811, 794, 734, 709, 694, 530 cm^{-1}. HRMS (EI) calcd for $C_{10}H_{18}BNO$ (M^+) 179.14815, found 179.14809.

Compound 6g. In a glove box, a vial was charged with **3** (0.150 g, 1.06 mmol) and benzyl mercaptan (0.145 g, 1.17 mmol). Et_2O (5.0 mL) was added, and the mixture was cooled to –20 °C. This solution was then added dropwise to a suspension of KH (0.051 g, 1.3 mmol in 5.0 mL THF) at –20 °C. The reaction was kept at –20 °C and shaken every 15 min for 1 h, then allowed to warm to room temperature. After 12 h of stirring the mixture was passed through an acrodisc and concentrated under vacuum. The desired product was recrystallized from hot pentane as a white solid (0.195 g, 80%).

^1H NMR (600 MHz, CD_2Cl_2): δ 7.47 (dd, $^3J_{HH}$ = 6.6 Hz, 3.9 Hz, 1H), 7.41 (dd, $^3J_{HH}$ = 7.1 Hz, 1.2 Hz, 2H) 7.31 (dd, $^3J_{HH}$ = 5.9 Hz, 1.7 Hz, 2H), 7.22 (t, $^3J_{HH}$ = 7.4 Hz, 1H), 7.15 (d, $^3J_{HH}$ = 6.6 Hz, 1H), 6.70 (d, $^3J_{HH}$ = 11.2 Hz, 1H), 6.17 (dt, = 5.4 Hz, 1.2 Hz, 1H), 4.05 (s, 2H), 3.71 (q, $^3J_{HH}$ = 7.3 Hz, 2H), 1.30 (t, $^3J_{HH}$ = 7.4 Hz, 3H). ^{13}C NMR (75 MHz, CD_2Cl_2): δ 142.5, 141.1, 139.5, 129.1, 128.9, 127.3, 125 (br), 109.4, 49.4, 32.4, 17.4. ^{11}B NMR (192.5 MHz, CD_2Cl_2): δ 36.4. FTIR (thin film) 3063, 3030, 2975, 2931, 2896, 1607, 1512, 1495, 1473, 1452, 1438, 1399, 1377, 1343, 1250, 1227, 1175, 1118, 1082, 1062, 1035, 1003, 955, 919, 798, 777, 739, 706, 676, 664, 639, 563 cm^{-1}. HRMS (EI) calcd for $C_{13}H_{16}BNS$ (M^+) 229.10965, found 229.10939.

Compound 6h. A solution of diphenylphosphine (0.105 g, 0.567 mmol in 8 mL THF) was added dropwise to a vial containing dry KH (0.043 g, 1.06 mmol). The suspension was stirred until there was no visible release of gas (approximately 2 h) and then filtered through an Acrodisc to remove unreacted KH. This solution was cooled to –20 °C and then added dropwise to a stirring solution of azaborine **3** at –20 °C. The reaction was shaken every 15 min for 1 h, at which point it was allowed to warm to rt and stirred an additional 12 h. Approximately one-half of the solvent was removed under reduced pressure and 10 mL pentane added. Solids were removed by filtration through an Acrodisc and solvents were removed under reduced pressure. The crude product was placed under high vac for 1 h whereupon desired product **6h** was recrystallized from hot pentane as a white solid (0.140 g, 85%).

^{1}H NMR (600 MHz, CD_2Cl_2): δ 7.49 (dd, $^{3}J_{HH}$ = 6.8, 4.1, 1H), 7.38-7.27 (m, 11H), 6.45 (m, 2H), 3.93 (ddd, $^{3}J_{HH}$ = 5.8, 1.5, 1.4 Hz, 2H), 1.17 (t, = 7.0 Hz, 3H). ^{13}C NMR (75 MHz, CD_2Cl_2): δ 142.56 (d, J_{CP} = 3.0 Hz), 139.65 (d, J_{CP} = 3.0 Hz), 138.37 (d, J_{CP} = 8.1 Hz), 135.34 (d, J_{CP} = 17.1 Hz), 133 (br), 128.87 (d, J_{CP} = 7.0 Hz), 128.8, 128.0, 113.2, 50.9 (d, J_{CP} = 18.1 Hz), 18.0. ^{11}B NMR (192.5 MHz, CD_2Cl_2): δ 37.9. ^{31}P NMR (202 MHz, CD_2Cl_2): δ –22.8 (minor), -40.1 (minor), -52.9 (br, major). FTIR (thin film) 3066, 2976, 2931, 1954, 1880, 1770, 1601, 1583, 1514, 1476, 1452, 1434, 1399, 1327, 1243, 1216, 1154, 1113, 1025, 1004, 740, 696, 673, 505 cm^{-1}. HRMS (EI) calcd for $C_{18}H_{19}BNP$ (M^+) 291.13482, found 291.13529.

Compound 6i. To a stirred solution of **3** (0.200 g, 1.42 mmol in 8 mL Et_2O) was added dropwise a solution of $LiHBEt_3$ (1.0 M in THF; 1.6 mL, 1.6 mmol) at –20 °C. The reaction mixture was allowed to stand at –20 °C, with occasional stirring, for 1 h, and then it was warmed to room temperature and stirred for 12 h. The mixture was then passed through an acrodisc and concentrated under reduced pressure. The crude material was purified by silica gel chromatography using pentane as eluent to furnish **6i** as a clear, colorless liquid (0.140 g, 92%).

^{1}H NMR (600 MHz, CD_2Cl_2): δ 7.60 (t (br), $^3J_{HH}$ = 7.3 Hz, 1H), 7.31 (d, $^3J_{HH}$ = 6.4 Hz, 1H) 6.84 (d, $^3J_{HH}$ = 10.5 Hz, 1H), 6.40 (t, $^3J_{HH}$ = 6.5 Hz, 1H), 4.9 (q (br), $^1J_{BH}$ = 124 Hz, 1H), 3.87 (q, $^3J_{HH}$ = 7.2 Hz, 2H), 1.37 (t, $^3J_{HH}$ = 7.2 Hz, 3H). ^{13}C NMR (75 MHz, CD_2Cl_2): δ 142.9, 138.7, 131 (br), 112.3, 53.4, 19.3. ^{11}B NMR (192.5 MHz, CD_2Cl_2): δ 32.1 (d, $^1J_{BH}$ = 130 Hz). FTIR (thin film) 3069, 3034, 2977, 2934, 2895, 2520, 1868, 1734, 1605, 1513, 1473, 1452, 1439, 1407, 1378, 1336, 1252, 1179, 1154, 1132, 1082, 1008, 974, 955, 927, 879, 804, 741, 714, 603, 530, 450 cm^{-1}. HRMS (EI) calcd for $C_6H_{10}BN$ (M^+) 107.09063, found 107.09072.

Compound 7. To a solution **3** (0.150 g, 1.06 mmol in 6.0 mL Et_2O) was added dropwise a solution of methyl glycolate (0.096 g, 1.1 mmol) and triethylamine (0.129 g, 1.27 mmol) in THF (6.0 mL) at –20 °C. The reaction mixture was allowed to stand at –20 °C, with occasional stirring, for 1 h, and then it was warmed to room temperature and stirred for 10 h. The mixture was then passed through an acrodisc with washing (2 x 3 mL Et_2O). The combined filtrates were concentrated to one-half of its volume under

vacuum, and the filtration process was repeated. The crude material was concentrated under reduced pressure, and the desired product was recrystallized from hot pentane as pale yellow, sheet-like crystals (0.175 g, 85%).

^{1}H NMR (600 MHz, CD_2Cl_2): δ 7.47 (dd, $^3J_{HH}$ = 6.1 Hz, 4.7 Hz, 1H), 7.03 (d, $^3J_{HH}$ = 6.6 Hz, 1H) 6.05 (d, $^3J_{HH}$ = 11.4 Hz, 1H), 5.93 (t, $^3J_{HH}$ = 5.9 Hz, 1H), 4.57 (s, 2H), 3.72 (s, 3H), 3.69 (q, $^3J_{HH}$ = 7.1 Hz, 2H), 1.27 (t, $^3J_{HH}$ = 7.1 Hz, 3H). ^{13}C NMR (75 MHz, CD_2Cl_2): δ 172.1, 145.8, 139.2, 116 (br), 106.3, 63.4, 52.2, 45.4, 17.7. ^{11}B NMR (192.5 MHz, CD_2Cl_2): δ 29.1. FTIR (thin film) 2977, 2954, 2930, 2875, 1762, 1740, 1612, 1521, 1476, 1457, 1444, 1419, 1378, 1350, 1302, 1259, 1205, 1156, 1124, 1104, 1086, 984, 811, 737, 708, 692 cm^{-1}. HRMS (EI) calcd for $C_9H_{14}BNO_3$ (M^+) 195.10668, found 195.10709.

A.2.4 Supplemental information for Chapter II, section 2.4

Compound 10. In a glovebox, a solution of 2-chloro-1-ethyl-1,2-azaborine **1** (0.150 g, 1.06 mmol in 4 mL CH_2Cl_2) was added dropwise to a stirring suspension of AgCN (0.171 g, 1.28 mmol in 10 mL CH_2Cl_2). The reaction was protected from light and stirred at rt for 8 h, whereupon pentane (10 mL) was added and solids removed by filtration. Removal of solvents under reduced pressure provided **2** as a clear, colorless liquid (0.138 g, 99%). An identical procedure was followed using Ag^{13}C^{15}N (99 atom%) to confirm atom connectivity.

^{1}H NMR (600 MHz, CD_2Cl_2): δ 7.76 (app t, $^3J_{HH}$ = 7.1 Hz, 1H), 7.41 (d, $^3J_{HH}$ = 6.6 Hz, 1H), 7.00 (d, $^3J_{HH}$ = 10.7 Hz, 1H), 6.64 (app t, $^3J_{HH}$ = 6.0 Hz, 1H), 4.06 (q, $^3J_{HH}$ = 7.3

Hz, 2H), 1.43 (t, $^3J_{HH}$ = 7.3 Hz, 1H). ^{13}C NMR (125 MHz, CD_2Cl_2): δ 145.3, 139.8, 131 (br), 125.6 (br q, $^1J_{BC}$ = 85 Hz), 115.1, 52.0, 18.7. ^{15}N NMR (50.7 MHz, CD_2Cl_2): δ -105.0 (d, $^1J_{CN}$ = 15 Hz). ^{11}B NMR (192.5 MHz, CD_2Cl_2): δ 22.5 (d, $^1J_{BC}$ = 85 Hz). FTIR (thin film) 3076, 3047, 2981, 2937, 2904, 2875, 1602, 1524, 1478, 1454, 1443, 1412, 1382, 1355, 1333, 1244, 1178, 1160, 1123, 1110, 1008, 751, 688, 518, 475 cm^{-1}. HRMS (EI) calcd for $C_7H_9BN_2$ (M+) 132.08589, found 132.08628.

Compound 12 from 3. In a glove box, a solution of **3** (0.300 g, 2.12 mmol in 10 mL THF) was added dropwise to a stirred solution of sodium pentacarbonylcyanochromate[15] (0.510 g, 2.12 mmol in 10 mL THF). The reaction was stirred for 1 h at rt, whereupon approximately two-thirds of the solvent was removed under reduced pressure. Pentane (10 mL) was added, and solids were removed by filtration. Removal of solvents under reduced pressure provided **12** as a yellow solid (0.680 g, 99%).

^{1}H NMR (600 MHz, CD_2Cl_2): δ 7.76 (app t, $^3J_{HH}$ = 5.9 Hz, 1H), 7.28 (d, $^3J_{HH}$ = 6.1 Hz, 1H), 6.69 (d, $^3J_{HH}$ = 11.0 Hz, 1H), 6.45 (app t, $^3J_{HH}$ = 6.3 Hz, 1H), 3.95 (q, $^3J_{HH}$ = 6.8 Hz, 2H), 1.43 (t, $^3J_{HH}$ = 7.1 Hz, 3H). ^{13}C NMR (75 MHz, CD_2Cl_2): δ 217.6, 215.4, 189.2, 147.0, 139.0, 126 (br), 112.8, 49.3, 18.0. ^{11}B NMR (192.5 MHz, CD_2Cl_2): δ 22.0. FTIR (CH_2Cl_2) 2130, 2051, 1954, 1605, 1521 cm^{-1}.

Compound 12 from reaction of 10 and $Cr(CO)_3(MeCN)_3$ and observation of 11. In a glove box, a Schlenk tube was charged with $Cr(CO)_3(MeCN)_3$ (0.196, 0.758 mmol) and THF (2 mL). A solution of **10** (0.100 g, 0.758 mmol in 2 mL THF) was then added to the Schlenk tube, which was then sealed. The flask was heated to 60 °C for 3 h, whereupon the solvent was removed. Crystals of **12** suitable for X-ray crystallography

were grown from the resultant dark-brown oil by extraction into hot pentane (10 mL) followed by slow evaporation. Piano-stool complex **11** was identified in the ^{1}H and ^{11}B NMR spectrum of the crude dark-brown oil in 15 mol% abundance relative to **12**.

11: ^{1}H NMR (600 MHz, CD_2Cl_2): δ 6.05 (1H), 5.92 (1H), 5.23 (1H), 4.62 (1H), N-CH_2CH_3 not resolved from **12** and unreacted **10**. ^{11}B NMR (192.5 MHz, CD_2Cl_2): δ 17.2.

NMR yield of 12 from reaction of 10 and $Cr(CO)_6$. In a glovebox, a Schlenk tube was charged with $Cr(CO)_6$ (0.100 g, 0.45 mmol), **10** (0.030 g, 0.23 mmol), and THF (10 mL), which was then sealed. The flask was heated to 60 °C for 3 h, whereupon the solvent was removed under vacuum. The product was extracted into pentane (10 mL) and solids were filtered through an Acrodisc. ^{1}H NMR (CD_2Cl_2) analysis indicated **12** was formed in 23% yield (integrated versus hexamethylbenzene as internal standard).

2D NMR assignment of 6e, 6i, and 10. COSY and HETCOR techniques were used to assign the intra-ring carbon signals and the aromatic C-*H* signals in **6e**, **6i**, and **10**. The ring carbon bound to boron in 1,2-azaborine appears as a broad resonance in the 13C NMR and is readily assigned. From this signal, or lack thereof, we can assign the resonance for the C3-*H* in the HETCOR spectrum. All other ring carbons and C-*H* resonances are easily assigned thereafter.

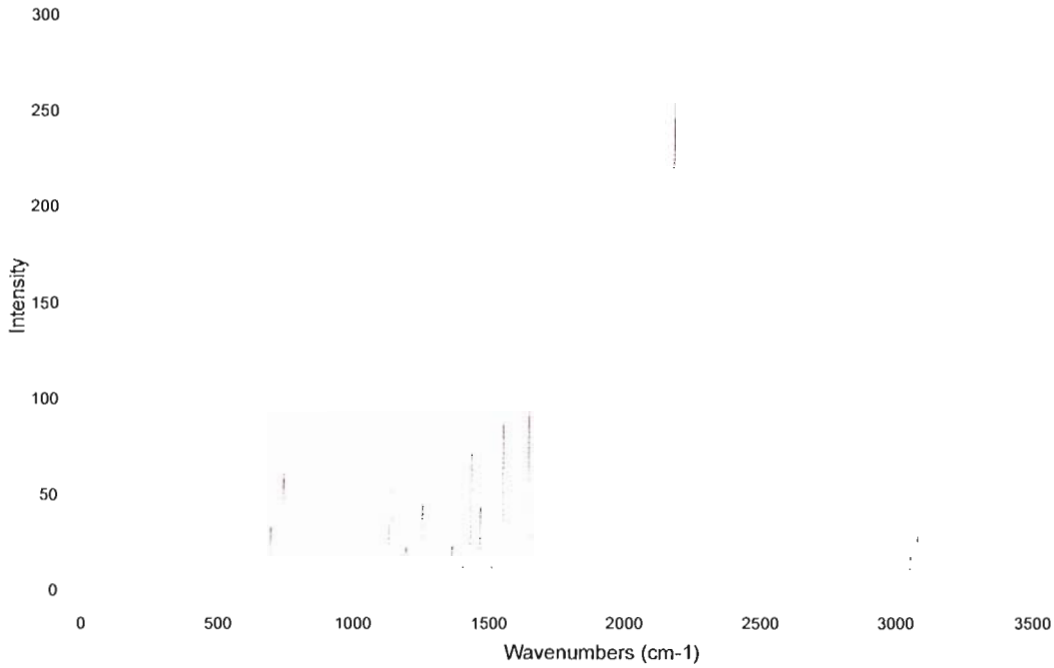

Figure 1. IR spectrum of **10'** at the B3LYP/DGDZVP2 level of calculation.

Table 1. Scaling for C-H, C≡N, and Intra-ring Stretching Vibrational Modes for **2'**. Scaled B3LYP/DGDZVP2 Vibrational Modes and Comparison with Experiment.

Molecule	**Mode type**	**B3LYP/DGDZVP2**	**Expt**	**Scaling**	**Total scaling**
10' (B-NC)					0.9547
	C-H	3170	3076.1	0.9704	
	C-H	3160	3046.7	0.9641	
	C-H	3150	2981.4	0.9465	
	C-H	3140	2937.0	0.9354	
	C-H	3090	2904.2	0.9399	
	C-H	3060	2875.0	0.9395	
	C≡N	2190	Not obsd.	N/A	
		1660	1601.7	0.9649	
		1560	1524.0	0.9769	

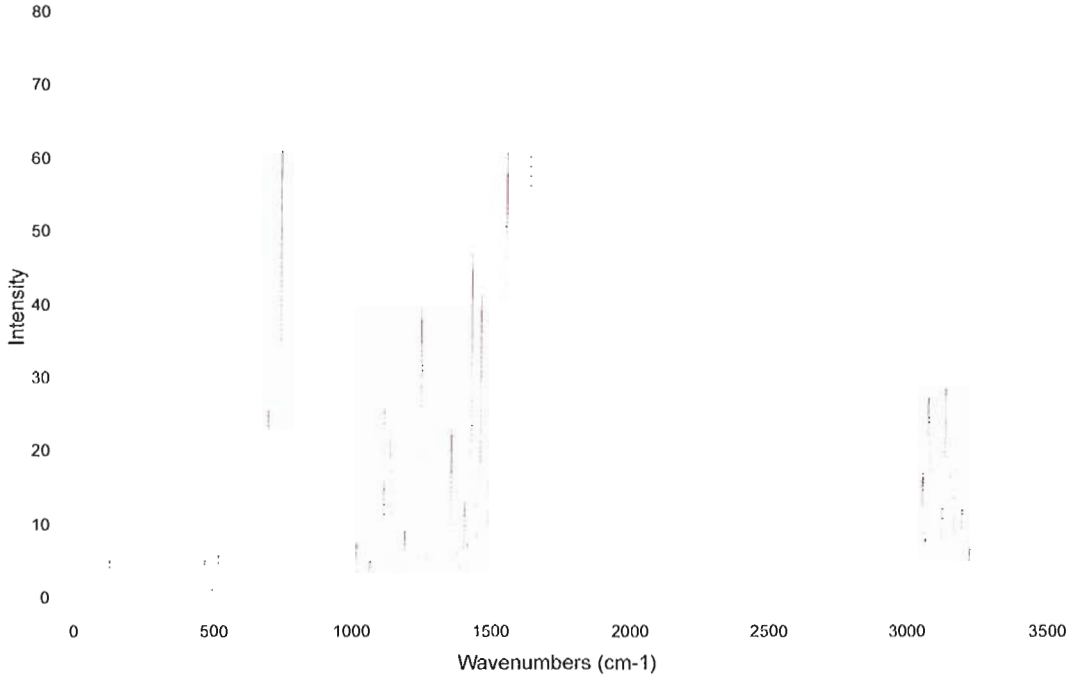

Figure 2. IR spectrum of **10** at the B3LYP/DGDZVP2 level of calculation.

Table 2. Scaling for C-H, C≡N, and Intra-ring Stretching Vibrational Modes for **10** (cm^{-1}). Scaled B3LYP/DGDZVP2 Vibrational Modes and Comparison with Experiment.

Molecule	Mode type	B3LYP/DGDZVP2	Expt	Scaling	Total scaling
10 (B-CN)					0.9554
	C-H	3170	3076.1	0.9704	
	C-H	3160	3046.7	0.9641	
	C-H	3150	2981.4	0.9465	
	C-H	3140	2937.0	0.9354	
	C-H	3090	2904.2	0.9399	
	C-H	3060	2875.0	0.9395	
	C≡N	2300 (very weak)	Not obsd.	N/A	
		1650	1601.7	0.9707	
		1560	1524.0	0.9769	

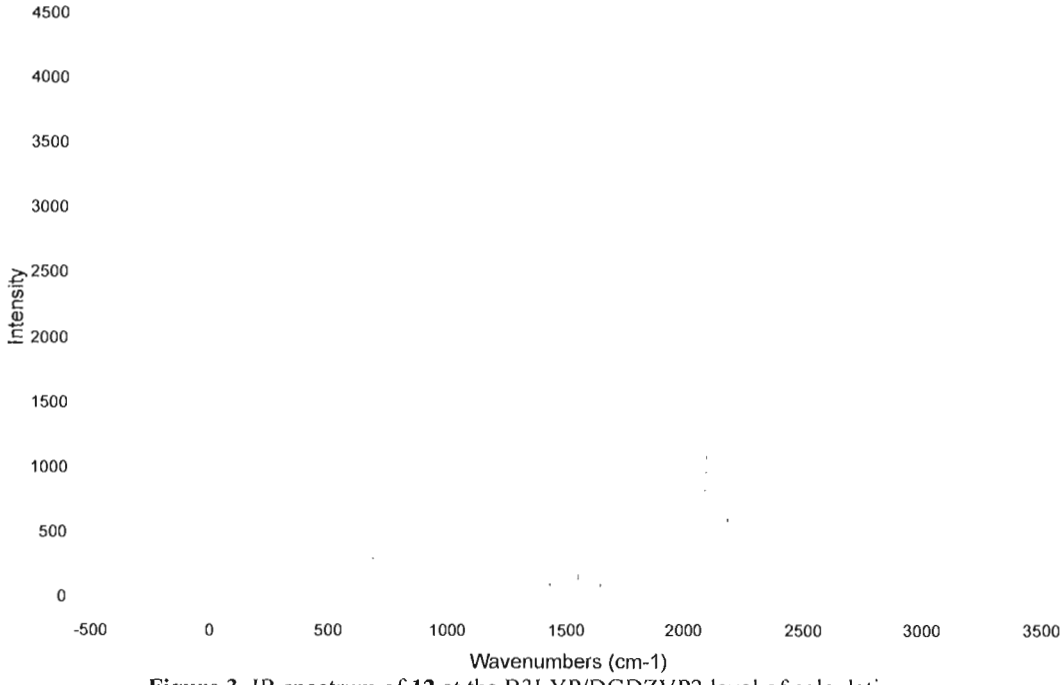

Figure 3. IR spectrum of **12** at the B3LYP/DGDZVP2 level of calculation.

Table 3. Scaling for C≡N, C≡O, and intra-ring stretching vibrational modes for **5**. Scaled B3LYP/DGDZVP2 vibrational modes and comparison with experiment.

Molecule	Mode type	B3LYP/DGDZVP2	Expt	Scaling	Total scaling
12					0.9728
	C-N	2190	2129.7	0.9725	
	C-O	2100	2050.1	0.9762	
	C-O	Not obsd.	1990	N/A	
	C-O	2020	1953.9	0.9673	
		1650	1605.3	0.9729	
		1560	1520.9	0.9749	

Table 4. Zero point energy (ZPE) and relative energy at the B3LYP/DGDZVP2 level of calculation.

Molecule	Zero Point Energy (kcal/mol)	Relative Energy (kcal/mol)
10 (B-CN)	0.00	0.00
10' (B-NC)	3.70	3.97

Table 5. NICS at 0, 1, and 2 Å at the B3LYP/DGDZVP2 level of calculation.

Molecule	NICS(0)	NICS(1)	NICS(2)
10 (B-CN)	-5.8267	-7.5537	-4.1374
10' (B-NC)	-5.7982	-6.9574	-3.7715
12 (gas)	-5.8376	-7.123	-3.864
12 (solid)	-5.0857	-7.2136	-4.0575

Figure 4. Electrostatic potential map is obtained by rolling a positive point charge over a density contour. Electrostatic potential maps at the 0.002 electron/a.u.^{3} density iso-contour level with an electrostatic potential range from -13.6 to 54.4 kcal/mol for compound **10** (left) and **6i** (right). Blue is positive potential (repulsive for the positive charge), red is negative potential (attractive for the positive charge) and green represents near zero potential.

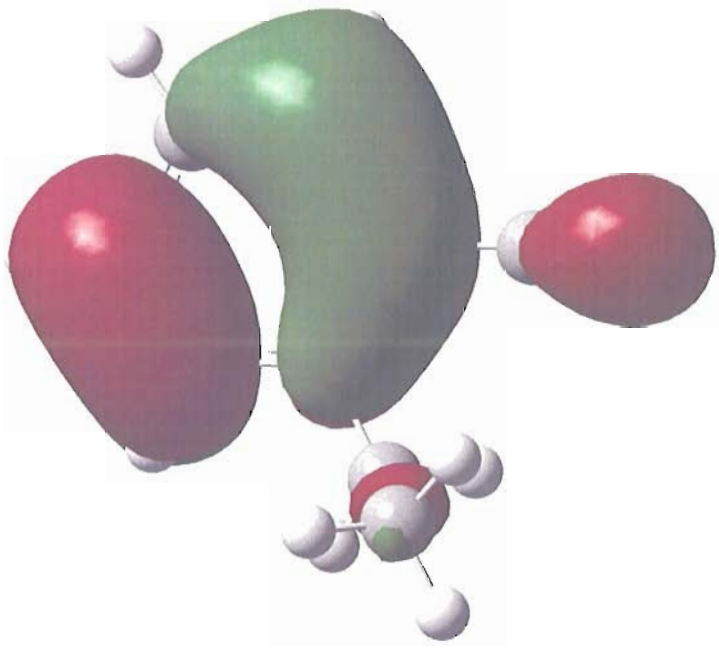

Figure 5. HOMO of **10** (gas phase) at the B3LYP/DGDVP2 level.

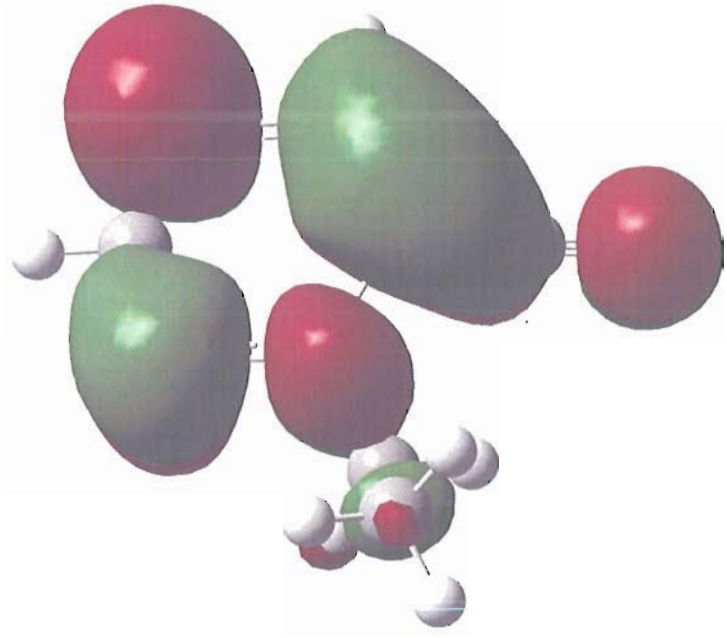

Figure 6. LUMO of **10** (gas phase) at the B3LYP/DGDVP2 level.

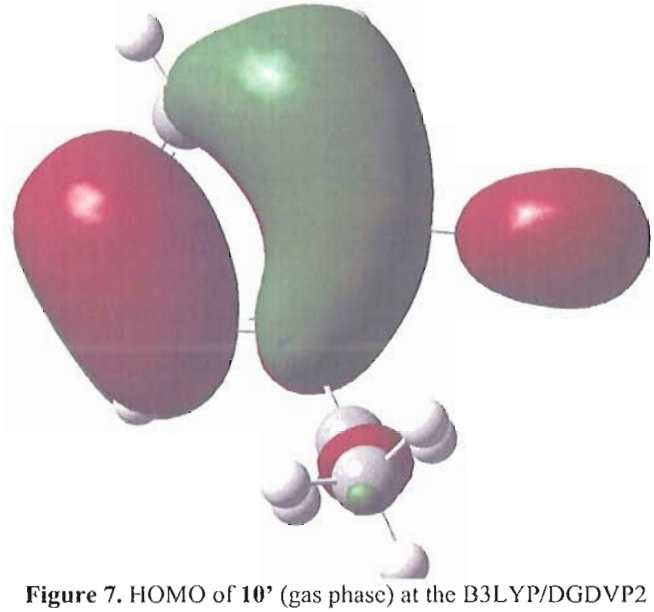

Figure 7. HOMO of **10'** (gas phase) at the B3LYP/DGDVP2 level.

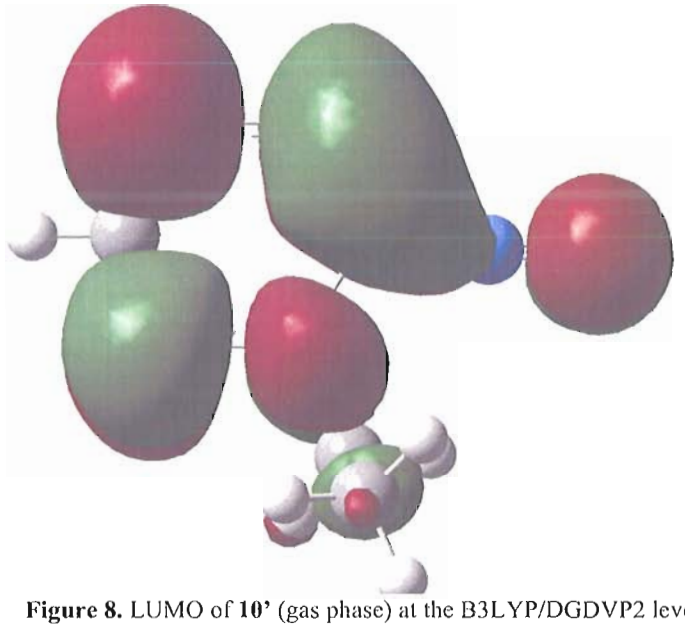

Figure 8. LUMO of **10'** (gas phase) at the B3LYP/DGDVP2 level.

Table 6. Atomic Coordinates for **10**, **10'**, **6i**, and **12** Calculated at the B3LYP/DGDZVP2 Level

Compound: **10** (B-CN)

B3LYP/DGDZVP2 = -406.650745267 au
B3LYP/DGDZVP2 Zero Point Corrected Energy = -406.496849 au
NIMAG = 0

C	-1.36148600	1.48425500	0.23485400
C	-2.47016900	0.65672300	0.23362800
C	-2.34161300	-0.73671500	-0.02690000
C	-1.10639200	-1.28831000	-0.28076000
H	-1.49756500	2.54376500	0.43514200
H	-3.46469600	1.05405800	0.42859600
H	-3.21342600	-1.38151000	-0.03367800
H	-0.99954700	-2.34951600	-0.48492400
N	0.04103400	-0.54460900	-0.30163100
C	1.30913000	-1.26864000	-0.54378600
H	2.01335700	-0.56789500	-0.99442700
H	1.11609900	-2.05936900	-1.27546600
C	1.90311300	-1.85718800	0.74113400
H	1.21138900	-2.56266300	1.21199800
H	2.83173400	-2.38880900	0.51110200
H	2.13159700	-1.06480800	1.45882300
B	-0.01095600	0.87418700	-0.04557900
C	1.31657500	1.68687800	-0.07355200
N	2.30623700	2.30800700	-0.08936500

Compound: **10'** (B-NC)

B3LYP/DGDZVP2 = -406.644419037 au
B3LYP/DGDZVP2 Zero Point Corrected Energy = -406.490948 au
NIMAG = 0

C	-1.47226600	1.36641700	0.22797400
C	-2.49603000	0.43919400	0.23619300
C	-2.23891200	-0.94060900	-0.01596200
C	-0.96003700	-1.37488200	-0.27094200
H	-1.70309700	2.41077500	0.42138700
H	-3.52291200	0.74261700	0.43232000
H	-3.04712900	-1.66334900	-0.01562600
H	-0.75475000	-2.42258900	-0.46943700
N	0.11573300	-0.52775600	-0.30009300
C	1.44399000	-1.12899100	-0.54688900
H	2.06655900	-0.37981100	-1.03745500
H	1.31570600	-1.96064500	-1.24651600
C	2.11955400	-1.61197000	0.74226200
H	1.51065300	-2.36686700	1.24952000

H	3.09252900	-2.05575300	0.50883200
H	2.28059900	-0.77834600	1.43081800
B	-0.07074100	0.88079300	-0.05093300
C	2.02801500	2.49817700	-0.09465200
N	1.10850500	1.75432600	-0.08377600

Compound: **6i** (1-Ethyl-2-H-1,2-azaborine)

B3LYP/DGDZVP2 = -314.370294000 au
B3LYP/DGDZVP2 Zero Point Corrected Energy = -314.216402 au
NIMAG = 0

C	-1.79049100	1.17930800	0.13933800
C	-2.33267000	-0.08894000	0.23352600
C	-1.52238900	-1.24975900	0.05469900
C	-0.17980400	-1.12362600	-0.21406500
H	-2.44990900	2.03316600	0.28098100
H	-3.39190900	-0.23366100	0.44279700
H	-1.95389700	-2.24252300	0.12188200
H	0.44718000	-1.99965700	-0.35726100
N	0.43094400	0.09752700	-0.32632000
C	1.88487600	0.10279200	-0.57437400
H	2.12937100	1.04485500	-1.06888800
H	2.12660100	-0.70689700	-1.27162700
C	2.70766900	-0.04184800	0.71222400
H	2.48201400	-0.98261700	1.22425400
H	3.77763900	-0.02730200	0.47950600
H	2.49204600	0.78090300	1.39982800
B	-0.31227600	1.32577700	-0.16046400
H	0.28249100	2.35459800	-0.27299900

Compound: **12**

B3LYP/DGDZVP2 = -2017.89581592 au
B3LYP/DGDZVP2 Zero Point Corrected Energy = -2017.698074 au
NIMAG = 0

Cr	-1.99984300	-0.07121700	0.00680600
O	-1.66055100	2.82781400	0.96375800
O	-2.12888100	-1.02286700	2.92878400
O	-2.24704100	-2.98440600	-0.94917400
O	-1.82592300	0.87686100	-2.91290800
O	-5.04648000	0.24695300	-0.04706600
N	1.14649200	-0.37873300	0.05912100

N	3.46891900	0.50000400	0.30529300
B	2.59261000	-0.61544700	0.04447900
C	-1.79615000	1.73273700	0.60260400
C	-2.08024500	-0.66488600	1.82694600
C	-2.15484200	-1.88624700	-0.58901700
C	-1.89295800	0.51745500	-1.81210100
C	-3.89145600	0.12587800	-0.02662400
C	-0.03098000	-0.27609300	0.03988100
C	3.21898400	-1.96003100	-0.22896700
H	2.63422000	-2.85398700	-0.42914000
C	4.59782400	-2.04799000	-0.22246500
H	5.09709700	-2.99612100	-0.41359700
C	5.40614700	-0.90305500	0.03797100
H	6.48752200	-0.98035500	0.04751200
C	4.82562400	0.31738300	0.28876600
H	5.43328200	1.19371600	0.49342700
C	2.97264600	1.87153800	0.55010100
H	3.65089400	2.35723300	1.25801800
H	1.99828600	1.79622000	1.03475200
C	2.86016900	2.69671900	-0.73711300
H	2.48621900	3.69860900	-0.50481500
H	2.16741000	2.22847700	-1.44153800
H	3.83279800	2.79849300	-1.22829700

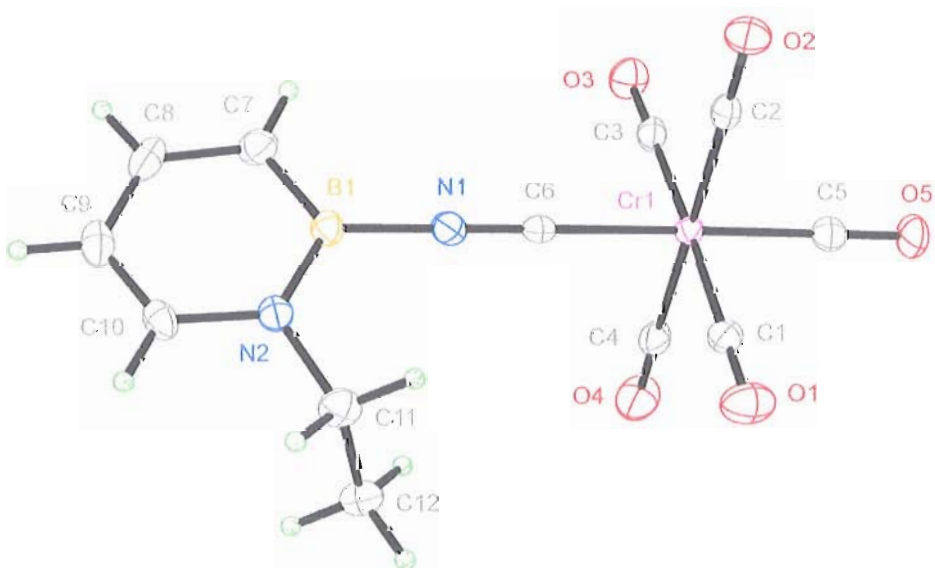

Figure 9. ORTEP illustration of **12**, with ellipsoids drawn at the 35% probability level.

X-ray Crystal Structure Determination. Crystals of **12** suitable for X-ray diffraction were obtained by evaporation of a solution of **12** in pentane.

Diffraction intensity data were collected with a Bruker Smart Apex CCD diffractometer at 173(2) K using MoKα - radiation (0.71073 Å). The structure was solved using direct methods, completed by subsequent difference Fourier syntheses, and refined by full matrix least-squares procedures on F^2. All non-H atoms were refined with anisotropic thermal parameters. H atoms were found on the residual density map and refined with isotropic thermal parameters. The Flack parameter is 0.00(8). All software and sources scattering factors are contained in the SHELXTL (6.10) program package (G.Sheldrick, Bruker XRD, Madison, WI). Crystallographic data and some details of data collection and crystal structure refinement for $C_{13}H_9BCrN_2O_5$ are given in the following tables.

Table 7. Crystal data and structure refinement for **12** (liu12a).

Identification code	liu12a	
Empirical formula	C_{12} H_9 B Cr N_2 O_5	
Formula weight	324.02	
Temperature	173(2) K	
Wavelength	0.71073 Å	
Crystal system	Orthorhombic	
Space group	Pca2(1)	
Unit cell dimensions	a = 12.965(2) Å	α= 90°.
	b = 5.9808(9) Å	β= 90°.
	c = 19.254(3) Å	γ = 90°.
Volume	1493.0(4) $Å^3$	
Z	4	
Density (calculated)	1.441 Mg/m^3	
Absorption coefficient	0.785 mm^{-1}	
F(000)	656	
Crystal size	0.23 x 0.14 x 0.06 mm^3	
Theta range for data collection	2.12 to 27.00°.	

Index ranges	-16<=h<=12, -7<=k<=7, -24<=l<=24
Reflections collected	9061
Independent reflections	3243 [R(int) = 0.0425]
Completeness to theta = 27.00°	99.8 %
Absorption correction	Semi-empirical from equivalents
Max. and min. transmission	0.9544 and 0.8400
Refinement method	Full-matrix least-squares on F^2
Data / restraints / parameters	3243 / 1 / 191
Goodness-of-fit on F^2	1.003
Final R indices [I>2sigma(I)]	R1 = 0.0390, wR2 = 0.0778
R indices (all data)	R1 = 0.0538, wR2 = 0.0864
Absolute structure parameter	0.20(3)
Largest diff. peak and hole	0.301 and -0.206 e.$Å^{-3}$

Table 8. Atomic coordinates (x 10^4) and equivalent isotropic displacement parameters ($Å^2$x 10^3) for liu12a. U(eq) is defined as one third of the trace of the orthogonalized U^{ij} tensor.

	x	y	z	U(eq)
Cr(1)	6657(1)	7430(1)	9776(1)	26(1)
O(1)	7486(2)	3932(4)	8775(1)	55(1)
O(2)	4623(2)	4941(4)	9940(1)	45(1)
O(3)	5789(2)	11017(4)	10726(1)	48(1)
O(4)	8662(2)	10056(4)	9693(2)	63(1)
O(5)	7561(2)	4899(4)	10990(1)	52(1)
N(1)	5758(2)	10066(4)	8506(1)	35(1)
N(2)	5727(2)	11203(4)	7264(1)	30(1)
B(1)	5390(3)	11603(6)	7950(2)	31(1)
C(1)	7175(3)	5237(5)	9153(2)	33(1)
C(2)	5388(2)	5846(5)	9869(2)	30(1)
C(3)	6121(3)	9656(5)	10371(2)	32(1)
C(4)	7910(2)	9078(5)	9713(2)	38(1)
C(5)	7216(3)	5855(6)	10530(2)	34(1)
C(6)	6086(2)	9084(5)	8972(2)	29(1)
C(7)	4700(3)	13536(6)	8088(2)	41(1)
C(8)	4463(3)	14870(6)	7534(2)	47(1)
C(9)	4837(3)	14417(6)	6867(2)	43(1)
C(10)	5449(3)	12648(5)	6749(2)	36(1)
C(11)	6445(3)	9368(6)	7074(2)	40(1)
C(12)	7559(3)	10065(6)	7169(2)	45(1)

Table 9. Bond lengths [Å] and angles [°] for liu12a.

Cr(1)-C(5)	1.875(4)
Cr(1)-C(3)	1.889(4)
Cr(1)-C(1)	1.900(4)
Cr(1)-C(4)	1.904(3)
Cr(1)-C(2)	1.908(3)
Cr(1)-C(6)	1.981(3)
O(1)-C(1)	1.141(4)

O(2)-C(2)	1.138(3)
O(3)-C(3)	1.147(4)
O(4)-C(4)	1.138(3)
O(5)-C(5)	1.146(4)
N(1)-C(6)	1.153(4)
N(1)-B(1)	1.489(4)
N(2)-C(10)	1.365(4)
N(2)-B(1)	1.412(4)
N(2)-C(11)	1.484(4)
B(1)-C(7)	1.486(5)
C(7)-C(8)	1.368(5)
C(7)-H(7A)	0.9500
C(8)-C(9)	1.399(5)
C(8)-H(8A)	0.9500
C(9)-C(10)	1.342(5)
C(9)-H(9A)	0.9500
C(10)-H(10A)	0.9500
C(11)-C(12)	1.514(5)
C(11)-H(11A)	0.9900
C(11)-H(11B)	0.9900
C(12)-H(12A)	0.9800
C(12)-H(12B)	0.9800
C(12)-H(12C)	0.9800
C(5)-Cr(1)-C(3)	91.55(15)
C(5)-Cr(1)-C(1)	90.33(14)
C(3)-Cr(1)-C(1)	178.11(16)
C(5)-Cr(1)-C(4)	88.83(16)
C(3)-Cr(1)-C(4)	89.27(15)
C(1)-Cr(1)-C(4)	90.92(15)
C(5)-Cr(1)-C(2)	90.62(14)
C(3)-Cr(1)-C(2)	88.58(14)
C(1)-Cr(1)-C(2)	91.24(14)
C(4)-Cr(1)-C(2)	177.77(17)
C(5)-Cr(1)-C(6)	179.16(16)
C(3)-Cr(1)-C(6)	89.07(13)
C(1)-Cr(1)-C(6)	89.04(14)
C(4)-Cr(1)-C(6)	90.62(14)
C(2)-Cr(1)-C(6)	89.95(13)
C(6)-N(1)-B(1)	172.4(3)
C(10)-N(2)-B(1)	119.4(3)
C(10)-N(2)-C(11)	117.0(3)
B(1)-N(2)-C(11)	123.3(3)
N(2)-B(1)-N(1)	117.9(3)
N(2)-B(1)-C(7)	119.0(3)
N(1)-B(1)-C(7)	123.0(3)
O(1)-C(1)-Cr(1)	179.5(3)
O(2)-C(2)-Cr(1)	178.1(3)
O(3)-C(3)-Cr(1)	179.2(3)
O(4)-C(4)-Cr(1)	178.3(4)
O(5)-C(5)-Cr(1)	179.7(4)
N(1)-C(6)-Cr(1)	179.3(3)
C(8)-C(7)-B(1)	116.7(3)
C(8)-C(7)-H(7A)	121.6

B(1)-C(7)-H(7A)	121.6
C(7)-C(8)-C(9)	121.7(3)
C(7)-C(8)-H(8A)	119.2
C(9)-C(8)-H(8A)	119.2
C(10)-C(9)-C(8)	120.9(3)
C(10)-C(9)-H(9A)	119.5
C(8)-C(9)-H(9A)	119.5
C(9)-C(10)-N(2)	122.1(3)
C(9)-C(10)-H(10A)	118.9
N(2)-C(10)-H(10A)	118.9
N(2)-C(11)-C(12)	111.4(3)
N(2)-C(11)-H(11A)	109.3
C(12)-C(11)-H(11A)	109.3
N(2)-C(11)-H(11B)	109.3
C(12)-C(11)-H(11B)	109.3
H(11A)-C(11)-H(11B)	108.0
C(11)-C(12)-H(12A)	109.5
C(11)-C(12)-H(12B)	109.5
H(12A)-C(12)-H(12B)	109.5
C(11)-C(12)-H(12C)	109.5
H(12A)-C(12)-H(12C)	109.5
H(12B)-C(12)-H(12C)	109.5

Symmetry transformations used to generate equivalent atoms:

Table 10. Anisotropic displacement parameters ($Å^2 x\ 10^3$)for liu12a. The anisotropic displacement factor exponent takes the form: $-2p^2[\ h^2a^{*2}U^{11} + ... + 2\ h\ k\ a^*\ b^*\ U^{12}\ ]$

	U^{11}	U^{22}	U^{33}	U^{23}	U^{13}	U^{12}
Cr(1)	22(1)	25(1)	29(1)	4(1)	-2(1)	-1(1)
O(1)	49(2)	46(2)	71(2)	-16(1)	15(2)	-4(1)
O(2)	30(1)	48(1)	56(2)	2(1)	0(1)	-11(1)
O(3)	58(2)	38(1)	49(2)	-8(1)	0(1)	6(1)
O(4)	34(1)	51(1)	105(2)	14(2)	-6(2)	-13(1)
O(5)	42(2)	62(2)	52(2)	26(1)	-12(1)	5(1)
N(1)	31(2)	43(2)	31(1)	5(1)	2(1)	0(1)
N(2)	27(2)	32(2)	31(1)	2(1)	-3(1)	-4(1)
B(1)	30(2)	35(2)	29(2)	4(2)	-5(2)	-3(2)
C(1)	26(2)	28(2)	45(2)	4(2)	3(2)	-3(2)
C(2)	33(2)	29(2)	26(2)	2(1)	-5(2)	3(1)
C(3)	30(2)	30(2)	35(2)	7(2)	-6(2)	-2(2)
C(4)	30(2)	30(2)	53(2)	8(2)	-1(2)	-1(1)
C(5)	29(2)	35(2)	39(2)	3(2)	-3(2)	-6(2)
C(6)	22(2)	34(2)	31(2)	2(1)	4(2)	-1(1)
C(7)	36(2)	53(2)	35(2)	-4(2)	-2(2)	7(2)
C(8)	40(2)	40(2)	61(2)	6(2)	-11(2)	10(2)
C(9)	43(2)	42(2)	44(2)	14(2)	-14(2)	-10(2)
C(10)	36(2)	46(2)	27(2)	7(1)	-6(1)	-11(2)
C(11)	44(2)	34(2)	42(2)	-6(2)	5(2)	2(2)
C(12)	33(2)	51(2)	52(2)	2(2)	7(2)	5(2)

Table 11. Hydrogen coordinates (x 10^4) and isotropic displacement parameters ($Å^2$x 10^3) for liu12a.

	x	y	z	U(eq)
H(7A)	4436	13831	8539	49
H(8A)	4033	16137	7603	57
H(9A)	4655	15374	6493	51
H(10A)	5697	12393	6291	44
H(11A)	6328	8938	6584	48
H(11B)	6301	8046	7368	48
H(12A)	8013	8818	7043	68
H(12B)	7678	10477	7655	68
H(12C)	7708	11350	6870	68

Table 12. Hydrogen bonds for liu12a [Å and °].

D-H...A	d(D-H)	d(H...A)	d(D...A)	<(DHA)

A.2.5 Supplemental information for Chapter II, section 2.5

Compound 13. In a glovebox, a solution of **3** (0.600 g, 4.24 mmol in 25 mL benzene) was added dropwise to a stirring suspension of AgOTf (1.31 g, 5.09 mmol in 25 mL benzene). The reaction was stirred at rt for 8 h, whereupon the solvent was removed under reduced pressure. Compound **13** was purified by vacuum distillation (35 °C, 100 mTorr) as a clear, colorless liquid (0.639 g, 59%).

^{1}H NMR (600 MHz, CD_2Cl_2): δ 7.76 (br m, 1H), 7.21 (d, $^3J_{HH}$ = 6.3 Hz, 1H), 6.65 (d, $^3J_{HH}$ = 11.4 Hz, 1H), 6.39 (ddd, $^3J_{HH}$ = 11.4, 6.3, 3.2 Hz, 1H), 3.78 (q, $^3J_{HH}$ = 7.3 Hz, 2H), 1.34 (t, $^3J_{HH}$ = 7.3 Hz, 1H). ^{13}C NMR (75 MHz, CD_2Cl_2): δ 148.6, 138.9, 119 (br), 119 (q, $^1J_{CF}$ = 318 Hz), 111.5, 46.5, 17.7. ^{11}B NMR (192.5 MHz, CD_2Cl_2): δ 28.0. FTIR (thin film) 3139, 3080, 2986, 2939, 2908, 2880, 1870, 1764, 1611, 1528, 1481, 1456, 1444, 1413, 1351, 1209, 1153, 1112, 1060, 1006, 944, 830, 785, 768, 747, 684, 618, 572, 518, 448 cm^{-1}.

Compound 14a. In a glove box, a solution of 4-phenylpyridine (0.073 g, 0.470 mmol in 1 mL CH_2Cl_2) was added to a stirring solution of **13** (0.100 g, 0.392 mmol in 1 mL CH_2Cl_2). The reaction was stirred for 1 h at rt, whereupon the product was crystallized by cooling the reaction to -20 °C for 24 h. The solvent was decanted and the crystallized product was washed with pentane (3 x 5 mL). Residual solvents were removed under reduced pressure to provide **14a** as pale-green crystals (0.155 g, 97%).

^{1}H NMR (600 MHz, CD_2Cl_2): δ 8.82 (d, $^3J_{HH}$ = 6.9 Hz, 2H), 8.44 (d, $^3J_{HH}$ = 6.9 Hz, 2H), 8.02 (dd, $^3J_{HH}$ = 9.8, 6.6 Hz, 1H), 7.97 (dd, $^3J_{HH}$ = 8.1 Hz, $^4J_{HH}$ = 1.7 Hz, 2H), 7.68 (m, 3H), 7.55 (d, $^3J_{HH}$ = 6.6, 1H), 6.85 (app t, $^3J_{HH}$ = 7.5 Hz, 2H), 3.83 (q, $^3J_{HH}$ = 7.3 Hz, 2H), 1.38 (t, $^3J_{HH}$ = 7.3 Hz, 3H). ^{13}C NMR (75 MHz, CD_2Cl_2): δ 158.1, 149.5, 145.8, 139.6, 134.3, 133.2, 130.5, 128.7, 125.7, 124 (br), 123.6, 115.7, 47.7, 18.2. ^{11}B NMR (192.5 MHz, CD_2Cl_2): δ 31.0. FTIR (thin film) 3220, 3138, 3078, 2915, 1638, 1612, 1513, 1488, 1474, 1442, 1412, 1377, 1349, 1292, 1233, 1218, 1174, 1151, 1029, 833, 765, 736, 693 cm^{-1}. HRMS (EI) calcd for $C_7H_9BNO_3SF_3$ (M+) 255.03484, found 255.03528.

Compound 14b. In a glove box, a solution of trimethylphosphine (0.039 g, 0.510 mmol in 1 mL CH_2Cl_2) was added to a stirring solution of **13** (0.100 g, 0.392 mmol in 1 mL CH_2Cl_2). The reaction was stirred for 1 h at rt, whereupon the solvent and residual trimethylphosphine were removed under reduced pressure, providing **14b** as a white solid (0.129 g, 99%).

^{1}H NMR (600 MHz, CD_2Cl_2): δ 7.97 (br, 1H), 7.66 (d, $^3J_{HH}$ = 5.4 Hz, 1H), 7.11 (d, $^3J_{HH}$ = 10.7 Hz, 1H), 6.94 (app t, $^3J_{HH}$ = 6.1 Hz, 2H), 4.06 (q, $^3J_{HH}$ = 7.0 Hz, 2H), 1.99 (d, $^2J_{PH}$ = 12.4 Hz, 9H), 1.51 (t, $^3J_{HH}$ = 7.0 Hz, 3H). ^{13}C NMR (125 MHz, CD_2Cl_2): δ 146.7,

142.0, 130 (br), 121 (q, $^1J_{CF}$ = 321 Hz), 118.0, 52.6, 19.2, 10.1 (d, $^1J_{PC}$ = 45.3 Hz). ^{11}B NMR (192.5 MHz, CD_2Cl_2): δ 28.7. ^{31}P NMR (202 MHz, CD_2Cl_2): δ -25.0 (br). FTIR (thin film) 3054, 3008, 2927, 1598, 1526, 1477, 1428, 1410, 1300, 1259, 1226, 1162, 1032, 964, 872, 758, 673, 639, 573, 517 cm^{-1}.

Compound 14c. In a glove box, a solution of triphenylphosphine oxide (0.060 g, 0.216 mmol in 3 mL CH_2Cl_2) was added to a stirring solution of **13** (0.050 g, 0.196 mmol in 3 mL CH_2Cl_2). The reaction was stirred for 1 h at rt, whereupon the solvent and was removed under reduced pressure. The white solid was washed with pentane (3 x 3 mL), providing **14c** as a white solid (0.093 g, 89%).

^{1}H NMR (600 MHz, CD_2Cl_2): δ 7.94-7.75 (br, 15H), 7.55 (dd, $^3J_{HH}$ = 10.8, 6.8 Hz, 1H), 7.28 (d, $^3J_{HH}$ = 6.4 Hz, 1H), 6.33 (app t, $^3J_{HH}$ = 6.8 Hz, 1H), 5.64 (d, $^3J_{HH}$ = 11.5 Hz), 3.92 (q, $^3J_{HH}$ = 7.3 Hz, 2H), 1.35 (t, $^3J_{HH}$ = 7.3 Hz, 3H). ^{13}C NMR (125 MHz, CD_2Cl_2): δ 145.1, 139.3, 134.2, 133.2, 132.4, 129.1, 111.3, 48.8, 17.6. ^{11}B NMR (192.5 MHz, CD_2Cl_2): δ 28.3. ^{31}P NMR (202 MHz, CD_2Cl_2): δ 57.3.

Compound 14d. In a glove box, a solution of pyridine N-oxide (0.031 g, 0.324 mmol in 3 mL CH_2Cl_2) was added to a stirring solution of **13** (0.075 g, 0.294 mmol in 3 mL CH_2Cl_2). The reaction was stirred for 1 h at rt, whereupon the solvent and was removed under reduced pressure. The solid was washed with pentane (3 x 3 mL), providing **14d** as light green crystals (0.105 g, 99%).

^{1}H NMR (600 MHz, CD_2Cl_2): δ 8.97 (dd, $^3J_{HH}$ = 5.9, 1.0 Hz, 2H), 8.60 (dt, $^3J_{HH}$ = 7.8, 1.2 Hz, 1H), 8.28 (dd, $^3J_{HH}$ = 7.0, 1.7 Hz, 2H), 7.65 (dd, $^3J_{HH}$ = 11.3, 6.6 Hz, 1H), 7.26 (d, $^3J_{HH}$ = 6.6 Hz, 1H), 6.31 (app t, $^3J_{HH}$ = 6.6 Hz, 1H), 5.50 (d, $^3J_{HH}$ = 11.0 Hz, 1H), 3.88

(q, $^3J_{HH}$ = 7.3 Hz, 2H), 1.43 (t, $^3J_{HH}$ = 7.3 Hz, 3H). ^{13}C NMR (125 MHz, CD_2Cl_2): δ 149.6, 145.0, 141.9, 139.7, 130.7, 121 (q, 1JCF = 320 Hz), 112 (br), 110.4, 46.1, 17.5. ^{11}B NMR (192.5 MHz, CD_2Cl_2): δ 31.0. FTIR (thin film) 3117, 3069, 2983, 1610, 1528, 1480, 1444, 1415, 1264, 1224, 1143, 1030, 853, 786, 750, 672, 637 cm^{-1}.

Compound 14e. In a glove box, a solution of dimethylsulfoxide (0.031 g, 0.324 mmol in 3 mL CH_2Cl_2) was added to a stirring solution of **13** (0.075 g, 0.294 mmol in 3 mL CH_2Cl_2). The reaction was stirred for 1 h at rt, whereupon the solvent and was removed under reduced pressure. The solid was washed with pentane (3 x 3 mL), providing **14d** as light green crystals (0.105 g, 99%).

^{1}H NMR (600 MHz, CD_2Cl_2): δ 7.79 (dd, $^3J_{HH}$ = 11.2, 6.6 Hz, 1H), 7.20 (d, $^3J_{HH}$ = 6.3 Hz, 1H), 6.49 (d, $^3J_{HH}$ = 11.5 Hz, 1H), 6.34 (app t, $^3J_{HH}$ = 6.6 Hz, 1H), 3.74 (q, $^3J_{HH}$ = 7.3 Hz, 2H), 3.47 (br, 6H), 1.30 (t, $^3J_{HH}$ = 7.3 Hz, 3H). ^{13}C NMR (125 MHz, CD_2Cl_2): δ 149.5, 139.6, 110.8, 45.9, 37.1, 17.8. ^{11}B NMR (192.5 MHz, CD_2Cl_2): δ 29.1. FTIR (thin film) 3016, 2927, 1683, 1610, 1525, 1475, 1443, 1413, 1255, 1225, 1157, 1029, 988, 899, 780, 744, 686, 638, 573, 517 cm^{-1}. HRMS (EI) calcd for $C_9H_{16}BNO_4S_2F_3$ (M+) 334.0566, found 334.0550.

Compound 14f. In a glove box, a solution of pyridine (0.040 g, 0.506 mmol in 1 mL CH_2Cl_2) was added to a stirring solution of **13** (0.100 g, 0.392 mmol in 1 mL CH_2Cl_2). The reaction was stirred for 1 h at rt, whereupon the solvent and residual pyridine were removed under reduced pressure to provide **14f** as a light-yellow solid (0.125 g, 95%).

^{1}H NMR (600 MHz, CD_2Cl_2): δ 8.85 (dd, $^3J_{HH}$ = 6.1 Hz, $^4J_{HH}$ = 0.9 Hz, 2H), 8.65 (tt, $^3J_{HH}$ = 7.2 Hz, $^4J_{HH}$ = 0.9 Hz, 1H), 8.25 (dd, $^3J_{HH}$ = 7.2, 6.1 Hz, 2H), 7.98 (dd, $^3J_{HH}$ =

11.4, 7.0 Hz, 1H), 7.55 (d, $^3J_{HH}$ = 6.4 Hz, 1H), 6.83 (dt, $^3J_{HH}$ = 7.0, 1.1 Hz, 1H), 6.77 (dd, $^3J_{HH}$ = 11.4, 1.1 Hz, 1H), 3.72 (q, $^3J_{HH}$ = 7.3 Hz, 2H), 1.30 (t, $^3J_{HH}$ = 7.3 Hz, 3H). ^{13}C NMR (75 MHz, CD_2Cl_2): δ 149.4, 147.0, 146.0, 139.5, 129.0, 125 (br), 121 (q, $^1J_{CF}$ = 321 Hz), 115.7, 47.5, 17.9. ^{11}B NMR (192.5 MHz, CD_2Cl_2): δ 30.9. FTIR (thin film) 3116, 3073, 3048, 2985, 1969, 1909, 1799, 1611, 1526, 1463, 1412, 1391, 1360, 1334, 1282, 1226, 1162, 1123, 1081, 1030, 988, 784, 758, 698, 685, 638, 599, 573 cm^{-1}.

Compound 14g. In a glove box, a solution of 4-trifluoromethylpyridine (0.075 g, 0.510 mmol in 1 mL CH_2Cl_2) was added to a stirring solution of **13** (0.100 g, 0.392 mmol in 1 mL CH_2Cl_2). The reaction was stirred for 4 h at rt, whereupon the solvent and residual 4-trifluoromethylpyridine were removed under reduced pressure to give **14g** as a bright-yellow solid (0.142 g, 90%).

^{1}H NMR (600 MHz, CD_2Cl_2): δ 9.10 (d, $^3J_{HH}$ = 5.0 Hz, 2H), 8.27 (br m, 2H), 7.96 (dd, $^3J_{HH}$ = 10.6, 7.4 Hz, 1H), 7.48 (d, $^3J_{HH}$ = 7.1, 1H), 6.80 (d, $^3J_{HH}$ = 10.6 Hz, 1H), 6.75 (br m, 1H), 3.77 (q, $^3J_{HH}$ = 7.3 Hz, 2H), 1.33 (t, $^3J_{HH}$ = 7.3 Hz, 3H). ^{13}C NMR (75 MHz, CD_2Cl_2): δ 149.5, 148.9, 139.5, 124.3, 122 (br), 120.2, 115.1, 47.4, 18.0. ^{11}B NMR (192.5 MHz, CD_2Cl_2): δ 30.0. FTIR (thin film) 3054, 2987, 2361, 2306, 1653, 1609, 1559, 1521, 1473, 1456, 1321, 1264, 1166, 1081, 1031, 896, 740, 639, 574, 518 cm^{-1}.

Compound 14h. In a glove box, a solution of 4-methylpyridine (0.047 g, 0.510 mmol in 1 mL CH_2Cl_2) was added to a stirring solution of **13** (0.100 g, 0.392 mmol in 1 mL CH_2Cl_2). The reaction was stirred for 1 h at rt, whereupon the solvent and residual 4-methylpyridine were removed under reduced pressure to give **14h** as a light-yellow solid (0.130 g, 95%).

^{1}H NMR (600 MHz, CD_2Cl_2): δ 8.64 (d, $^3J_{HH}$ = 6.2 Hz, 2H), 8.01 (d, $^3J_{HH}$ = 6.2 Hz, 2H), 7.96 (dd, $^3J_{HH}$ = 10.5, 7.1 Hz, 1H), 7.54 (d, $^3J_{HH}$ = 7.6, 1H), 6.80 (app t, $^3J_{HH}$ = 6.8 Hz, 1H), 6.75 (d, $^3J_{HH}$ = 10.5 Hz, 1H), 3.72 (q, $^3J_{HH}$ = 7.3 Hz, 2H), 2.72 (s, 3H), 1.30 (t, $^3J_{HH}$ = 7.3 Hz, 3H). ^{13}C NMR (75 MHz, CD_2Cl_2): δ 161.2, 149.2, 144.8, 139.5, 129.4, 124 (br), 121 (q, $^1J_{CF}$ = 320 Hz), 115.5, 47.4, 22.7, 17.9. ^{11}B NMR (192.5 MHz, CD_2Cl_2): δ 30.9. FTIR (thin film) 3112, 3087, 3042, 2976, 2939, 2883, 2309, 1972, 1820, 1707, 1639, 1607, 1528, 1452, 1412, 1388, 1368, 1334, 1267, 1145, 1086, 1028, 989, 858, 832, 806, 767, 754, 738, 720, 700, 661, 636 cm^{-1}.

Compound 14i. In a glove box, a solution of 4-(N,N-dimethyl)pyridine (0.057 g, 0.470 mmol in 1 mL CH_2Cl_2) was added to a stirring solution of **13** (0.100 g, 0.392 mmol in 1 mL CH_2Cl_2). The reaction was stirred for 1 h at rt, whereupon the solvent was removed under reduced pressure. The product was washed with Et_2O (3 x 5 mL) providing **14i** as a tan oil which was crystallized by adding a seed crystal of **14h**. The resultant tan solid was washed with Et_2O (3 x 5 mL) and residual solvent was removed under reduced pressure to provide **14i** as an off-white crystalline solid (0.144 g, 98%).

^{1}H NMR (600 MHz, CD_2Cl_2): δ 7.98 (d, $^3J_{HH}$ = 6.9 Hz, 2H), 7.71 (d, $^3J_{HH}$ = 6.6 Hz, 1H), 7.28 (d, $^3J_{HH}$ = 6.6 Hz, 1H), 6.90 (d, $^3J_{HH}$ = 6.9 Hz, 2H), 6.48 (d, $^3J_{HH}$ = 13.0 Hz), 6.41 (m, 1H), 3.67 (q, $^3J_{HH}$ = 7.3 Hz, 2H), 3.23 (s, 6H), 1.22 (t, $^3J_{HH}$ = 7.3 Hz, 3H). ^{13}C NMR (125 MHz, CD_2Cl_2): δ 156.8, 145.0, 143.7, 138.9, 124 (br), 121 (q, $^1J_{CF}$ = 321 Hz), 110.2, 108.4, 46.7, 40.4, 17.6. ^{11}B NMR (192.5 MHz, CD_2Cl_2): δ 26.7. FTIR (thin film) 3230, 3094, 2976, 2935, 2873, 2822, 2625, 2441, 2296, 1975, 1899, 1796, 1644, 1611, 1564, 1525, 1483, 1445, 1383, 1342, 1266, 1151, 1066, 1031, 948, 917, 822, 754, 735,

656, 637, 573, 517 cm^{-1}.

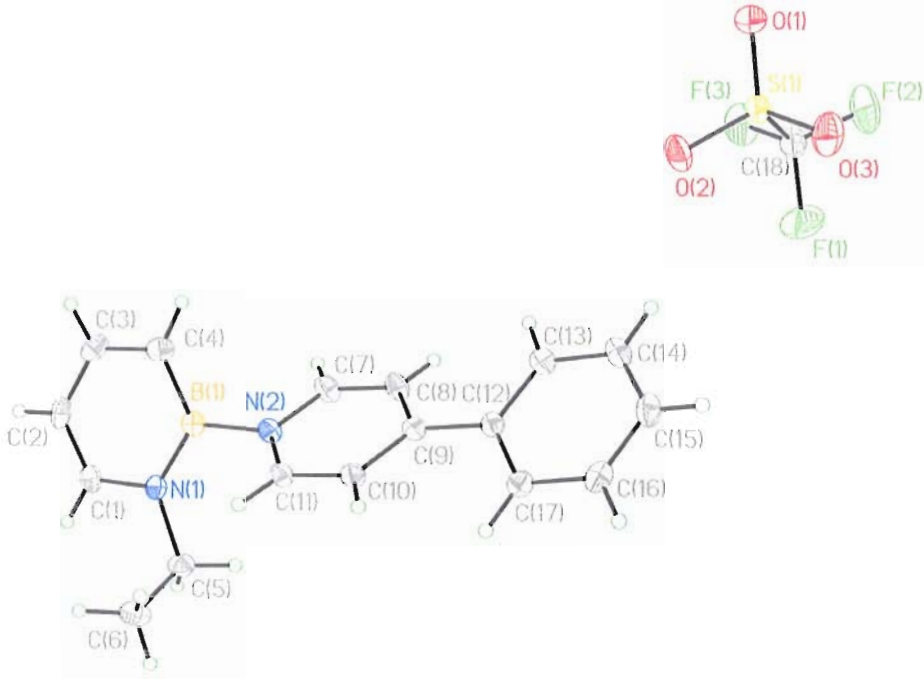

Figure 10. ORTEP illustration of **14a**, with ellipsoids drawn at the 35% probability level.

X-ray Crystal Structure Determination. Crystals of **14a** suitable for X-ray diffraction were obtained by cooling a CH_2Cl_2 solution of **14a** to -20 °C for 24 h.

Diffraction intensity data were collected with a Bruker Smart Apex CCD diffractometer at 173(2) K using MoKα - radiation (0.71073 Å). The structure was solved using direct methods, completed by subsequent difference Fourier syntheses, and refined by full matrix least-squares procedures on F^2. All non-H atoms were refined with anisotropic thermal parameters. H atoms were found on the residual density map and refined with isotropic thermal parameters. The Flack parameter is 0.00(8). All software and sources scattering factors are contained in the SHELXTL (6.10) program package

(G.Sheldrick, Bruker XRD, Madison, WI). Crystallographic data and some details of data collection and crystal structure refinement for $C_{18}H_{18}BF_3N_2O_3S$ are given in the following tables.

Table 13. Crystal data and structure refinement for **14a** (liu9).

Identification code	liu9	
Empirical formula	C_{18} H_{18} B F_3 N_2 O_3 S	
Formula weight	410.21	
Temperature	173(2) K	
Wavelength	0.71073 Å	
Crystal system	Monoclinic	
Space group	P2(1)/n	
Unit cell dimensions	a = 9.3812(9) Å	α= 90°.
	b = 14.3671(13) Å	β= 100.9400(10)°.
	c = 14.2217(13) Å	γ = 90°.
Volume	1882.0(3) $Å^3$	
Z	4	
Density (calculated)	1.448 Mg/m^3	
Absorption coefficient	0.223 mm^{-1}	
F(000)	848	
Crystal size	0.36 x 0.31 x 0.24 mm^3	
Theta range for data collection	2.03 to 27.00°.	
Index ranges	-11<=h<=11, -18<=k<=18, -18<=l<=18	
Reflections collected	17178	
Independent reflections	4101 [R(int) = 0.0255]	
Completeness to theta = 27.00°	100.0 %	
Absorption correction	Semi-empirical from equivalents	
Max. and min. transmission	0.9485 and 0.9241	
Refinement method	Full-matrix least-squares on F^2	
Data / restraints / parameters	4101 / 0 / 325	
Goodness-of-fit on F^2	1.024	
Final R indices [I>2sigma(I)]	R1 = 0.0376, wR2 = 0.1050	
R indices (all data)	R1 = 0.0451, wR2 = 0.1131	
Largest diff. peak and hole	0.380 and -0.287 $e.Å^3$	

Table 14. Atomic coordinates (x 10^4) and equivalent isotropic displacement parameters ($Å^2$x 10^3) for **14a**. U(eq) is defined as one third of the trace of the orthogonalized U^{ij} tensor.

	x	y	z	U(eq)
S(1)	417(1)	2337(1)	10006(1)	27(1)
O(1)	297(1)	1340(1)	9974(1)	42(1)
O(2)	1816(1)	2682(1)	9897(1)	43(1)
O(3)	-221(2)	2781(1)	10730(1)	48(1)
N(1)	10850(1)	5609(1)	6297(1)	25(1)
N(2)	8700(1)	5098(1)	7038(1)	25(1)
B(1)	10005(2)	4880(1)	6572(1)	25(1)
C(1)	12010(2)	5388(1)	5878(1)	30(1)
C(2)	12377(2)	4497(1)	5715(1)	34(1)
C(3)	11570(2)	3745(1)	5975(1)	35(1)
C(4)	10387(2)	3894(1)	6391(1)	33(1)
C(5)	10605(2)	6621(1)	6394(1)	31(1)
C(6)	11710(2)	7055(1)	7189(1)	40(1)
C(7)	7408(2)	4697(1)	6663(1)	32(1)
C(8)	6215(2)	4800(1)	7078(1)	31(1)
C(9)	6291(2)	5314(1)	7923(1)	25(1)
C(10)	7634(2)	5729(1)	8291(1)	26(1)
C(11)	8792(2)	5617(1)	7845(1)	26(1)
C(12)	5042(2)	5390(1)	8411(1)	25(1)
C(13)	3905(2)	4749(1)	8219(1)	30(1)
C(14)	2764(2)	4779(1)	8710(1)	34(1)
C(15)	2727(2)	5461(1)	9392(1)	35(1)
C(16)	3834(2)	6107(1)	9582(1)	35(1)
C(17)	4990(2)	6076(1)	9102(1)	30(1)
C(18)	-769(2)	2684(1)	8901(1)	36(1)
F(1)	-784(2)	3606(1)	8789(1)	71(1)
F(2)	-2129(1)	2423(1)	8882(1)	63(1)
F(3)	-360(1)	2323(1)	8134(1)	55(1)

Table 15. Bond lengths [Å] and angles [°] for **14a**.

S(1)-O(3)	1.4342(13)
S(1)-O(1)	1.4359(13)
S(1)-O(2)	1.4388(12)
S(1)-C(18)	1.8146(19)
N(1)-C(1)	1.3736(19)
N(1)-B(1)	1.413(2)
N(1)-C(5)	1.482(2)
N(2)-C(7)	1.356(2)
N(2)-C(11)	1.357(2)
N(2)-B(1)	1.531(2)
B(1)-C(4)	1.496(2)
C(1)-C(2)	1.358(2)
C(1)-H(1)	0.959(19)
C(2)-C(3)	1.408(3)
C(2)-H(2)	0.91(2)
C(3)-C(4)	1.369(2)

C(3)-H(3)	0.938(19)
C(4)-H(4)	0.98(2)
C(5)-C(6)	1.515(3)
C(5)-H(5A)	0.986(19)
C(5)-H(5B)	0.94(2)
C(6)-H(6A)	1.00(3)
C(6)-H(6B)	0.91(2)
C(6)-H(6C)	0.98(2)
C(7)-C(8)	1.368(2)
C(7)-H(7)	0.94(2)
C(8)-C(9)	1.401(2)
C(8)-H(8)	0.923(19)
C(9)-C(10)	1.402(2)
C(9)-C(12)	1.475(2)
C(10)-C(11)	1.367(2)
C(10)-H(10)	0.912(19)
C(11)-H(11)	0.930(19)
C(12)-C(13)	1.397(2)
C(12)-C(17)	1.399(2)
C(13)-C(14)	1.385(2)
C(13)-H(13)	0.975(19)
C(14)-C(15)	1.385(3)
C(14)-H(14)	0.96(2)
C(15)-C(16)	1.381(3)
C(15)-H(15)	0.90(2)
C(16)-C(17)	1.387(2)
C(16)-H(16)	0.97(2)
C(17)-H(17)	0.97(2)
C(18)-F(2)	1.326(2)
C(18)-F(3)	1.328(2)
C(18)-F(1)	1.333(2)
O(3)-S(1)-O(1)	115.18(9)
O(3)-S(1)-O(2)	115.88(8)
O(1)-S(1)-O(2)	114.10(8)
O(3)-S(1)-C(18)	103.21(8)
O(1)-S(1)-C(18)	102.45(8)
O(2)-S(1)-C(18)	103.50(8)
C(1)-N(1)-B(1)	118.77(14)
C(1)-N(1)-C(5)	114.61(13)
B(1)-N(1)-C(5)	126.61(13)
C(7)-N(2)-C(11)	118.28(13)
C(7)-N(2)-B(1)	118.14(13)
C(11)-N(2)-B(1)	123.40(12)
N(1)-B(1)-C(4)	119.29(14)
N(1)-B(1)-N(2)	120.27(14)
C(4)-B(1)-N(2)	120.44(14)
C(2)-C(1)-N(1)	122.62(15)
C(2)-C(1)-H(1)	120.5(11)
N(1)-C(1)-H(1)	116.9(11)
C(1)-C(2)-C(3)	120.85(15)
C(1)-C(2)-H(2)	118.7(13)
C(3)-C(2)-H(2)	120.5(13)
C(4)-C(3)-C(2)	120.90(16)

C(4)-C(3)-H(3)	121.0(12)
C(2)-C(3)-H(3)	118.1(12)
C(3)-C(4)-B(1)	117.57(16)
C(3)-C(4)-H(4)	118.0(12)
B(1)-C(4)-H(4)	124.3(12)
N(1)-C(5)-C(6)	112.13(14)
N(1)-C(5)-H(5A)	108.4(11)
C(6)-C(5)-H(5A)	111.0(11)
N(1)-C(5)-H(5B)	108.8(12)
C(6)-C(5)-H(5B)	109.3(12)
H(5A)-C(5)-H(5B)	107.1(16)
C(5)-C(6)-H(6A)	109.5(15)
C(5)-C(6)-H(6B)	109.9(16)
H(6A)-C(6)-H(6B)	109(2)
C(5)-C(6)-H(6C)	112.1(13)
H(6A)-C(6)-H(6C)	107.2(19)
H(6B)-C(6)-H(6C)	109(2)
N(2)-C(7)-C(8)	121.87(15)
N(2)-C(7)-H(7)	115.9(11)
C(8)-C(7)-H(7)	122.2(12)
C(7)-C(8)-C(9)	120.96(14)
C(7)-C(8)-H(8)	118.0(11)
C(9)-C(8)-H(8)	121.0(11)
C(8)-C(9)-C(10)	116.08(14)
C(8)-C(9)-C(12)	121.88(13)
C(10)-C(9)-C(12)	122.02(13)
C(11)-C(10)-C(9)	120.88(14)
C(11)-C(10)-H(10)	117.3(11)
C(9)-C(10)-H(10)	121.8(11)
N(2)-C(11)-C(10)	121.91(14)
N(2)-C(11)-H(11)	116.7(11)
C(10)-C(11)-H(11)	121.3(11)
C(13)-C(12)-C(17)	118.32(14)
C(13)-C(12)-C(9)	120.28(14)
C(17)-C(12)-C(9)	121.35(13)
C(14)-C(13)-C(12)	121.03(16)
C(14)-C(13)-H(13)	115.9(11)
C(12)-C(13)-H(13)	123.1(10)
C(15)-C(14)-C(13)	119.99(16)
C(15)-C(14)-H(14)	120.7(12)
C(13)-C(14)-H(14)	119.3(12)
C(16)-C(15)-C(14)	119.70(15)
C(16)-C(15)-H(15)	120.6(13)
C(14)-C(15)-H(15)	119.7(13)
C(15)-C(16)-C(17)	120.70(16)
C(15)-C(16)-H(16)	120.9(11)
C(17)-C(16)-H(16)	118.4(11)
C(16)-C(17)-C(12)	120.25(15)
C(16)-C(17)-H(17)	119.1(11)
C(12)-C(17)-H(17)	120.7(11)
F(2)-C(18)-F(3)	107.47(16)
F(2)-C(18)-F(1)	106.86(15)
F(3)-C(18)-F(1)	106.71(15)

F(2)-C(18)-S(1)	111.65(13)
F(3)-C(18)-S(1)	112.25(12)
F(1)-C(18)-S(1)	111.59(14)

Symmetry transformations used to generate equivalent atoms:

Table 16. Anisotropic displacement parameters ($Å^2 x\ 10^3$)for **14a**. The anisotropic displacement factor exponent takes the form: $-2p^2[\ h^2a^{*2}U^{11} + ... + 2\ h\ k\ a^*\ b^*\ U^{12}\ ]$

	U^{11}	U^{22}	U^{33}	U^{23}	U^{13}	U^{12}
S(1)	23(1)	33(1)	27(1)	-3(1)	7(1)	-1(1)
O(1)	43(1)	33(1)	53(1)	10(1)	15(1)	4(1)
O(2)	27(1)	54(1)	49(1)	-14(1)	11(1)	-12(1)
O(3)	43(1)	67(1)	38(1)	-18(1)	15(1)	2(1)
N(1)	22(1)	29(1)	23(1)	1(1)	4(1)	2(1)
N(2)	25(1)	29(1)	22(1)	-2(1)	6(1)	-4(1)
B(1)	26(1)	31(1)	19(1)	0(1)	3(1)	1(1)
C(1)	24(1)	43(1)	24(1)	1(1)	5(1)	-1(1)
C(2)	26(1)	51(1)	24(1)	-4(1)	4(1)	9(1)
C(3)	41(1)	34(1)	27(1)	-5(1)	1(1)	12(1)
C(4)	40(1)	30(1)	29(1)	-1(1)	6(1)	-1(1)
C(5)	36(1)	26(1)	33(1)	5(1)	9(1)	1(1)
C(6)	47(1)	31(1)	43(1)	-4(1)	13(1)	-9(1)
C(7)	31(1)	40(1)	24(1)	-7(1)	6(1)	-9(1)
C(8)	26(1)	42(1)	26(1)	-6(1)	4(1)	-8(1)
C(9)	24(1)	26(1)	23(1)	3(1)	3(1)	-1(1)
C(10)	27(1)	27(1)	25(1)	-4(1)	4(1)	-2(1)
C(11)	24(1)	28(1)	26(1)	-3(1)	4(1)	-4(1)
C(12)	23(1)	27(1)	24(1)	4(1)	3(1)	2(1)
C(13)	29(1)	33(1)	27(1)	1(1)	4(1)	-3(1)
C(14)	26(1)	42(1)	34(1)	8(1)	5(1)	-4(1)
C(15)	28(1)	46(1)	33(1)	11(1)	11(1)	8(1)
C(16)	34(1)	37(1)	33(1)	1(1)	9(1)	9(1)
C(17)	28(1)	29(1)	32(1)	1(1)	6(1)	2(1)
C(18)	32(1)	41(1)	38(1)	4(1)	10(1)	3(1)
F(1)	86(1)	46(1)	83(1)	27(1)	18(1)	20(1)
F(2)	26(1)	105(1)	57(1)	4(1)	1(1)	-2(1)
F(3)	56(1)	81(1)	29(1)	-2(1)	10(1)	3(1)

Table 17. Hydrogen coordinates ($x\ 10^4$) and isotropic displacement parameters ($Å^2 x\ 10^3$) for **14a**.

	x	y	z	U(eq)
H(1)	12570(20)	5897(13)	5707(13)	37(5)
H(2)	13160(20)	4393(14)	5443(15)	45(5)
H(3)	11890(20)	3140(14)	5882(14)	38(5)
H(4)	9880(20)	3352(14)	6583(14)	42(5)

H(5A)	9610(20)	6713(13)	6507(13)	35(5)
H(5B)	10660(20)	6913(14)	5811(15)	37(5)
H(6A)	12710(30)	6924(18)	7076(18)	70(7)
H(6B)	11570(30)	7680(17)	7197(18)	59(7)
H(6C)	11650(20)	6798(15)	7817(16)	50(6)
H(7)	7370(20)	4366(13)	6086(14)	37(5)
H(8)	5350(20)	4545(13)	6768(13)	35(5)
H(10)	7781(19)	6069(12)	8842(14)	29(4)
H(11)	9690(20)	5879(13)	8092(13)	33(5)
H(13)	3841(19)	4270(13)	7727(13)	31(5)
H(14)	2020(20)	4316(14)	8582(14)	39(5)
H(15)	1980(20)	5479(14)	9708(15)	43(5)
H(16)	3830(20)	6587(14)	10059(14)	36(5)
H(17)	5760(20)	6531(13)	9257(14)	36(5)

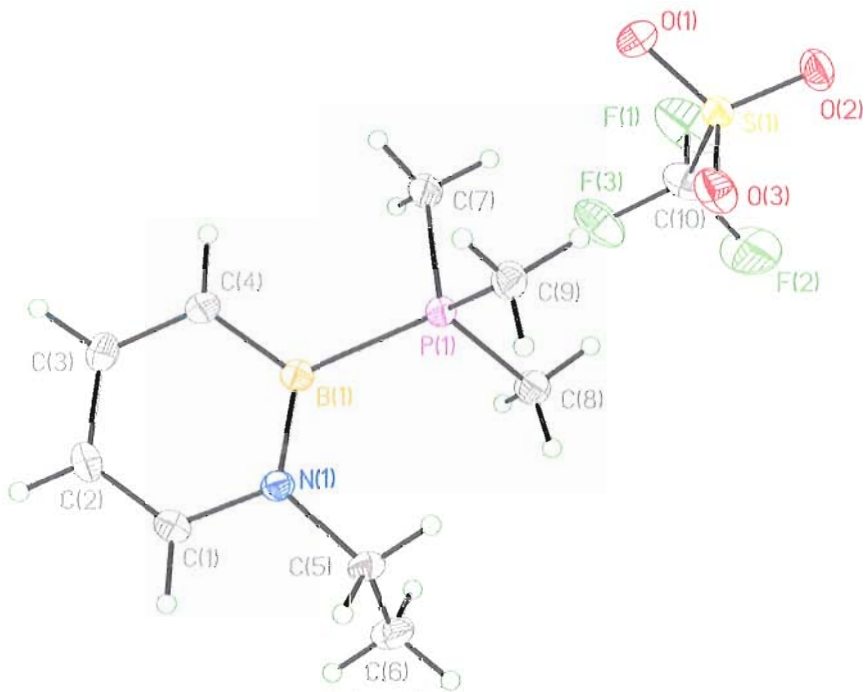

Figure 11. ORTEP illustration of **14b**, with ellipsoids drawn at the 35% probability level.

X-ray Crystal Structure Determination. Crystals of **14b** suitable for X-ray diffraction were obtained by evaporation of a solution of **14b** in CH_2Cl_2.

Diffraction intensity data were collected with a Bruker Smart Apex CCD diffractometer at 173(2) K using MoKα - radiation (0.71073 Å). The structure was

solved using direct methods, completed by subsequent difference Fourier syntheses, and refined by full matrix least-squares procedures on F^2. All non-H atoms were refined with anisotropic thermal parameters. H atoms were found on the residual density map and refined with isotropic thermal parameters. The Flack parameter is 0.00(8). All software and sources scattering factors are contained in the SHELXTL (6.10) program package (G.Sheldrick, Bruker XRD, Madison, WI). Crystallographic data and some details of data collection and crystal structure refinement for $C_{10}H_{18}BF_3NO_3PS$ are given in the following tables.

Table 18. Crystal data and structure refinement for **14b** (liu29).

Identification code	liu29	
Empirical formula	C_{10} H_{18} B F_3 N O_3 P S	
Formula weight	331.09	
Temperature	173(2) K	
Wavelength	0.71073 Å	
Crystal system	Triclinic	
Space group	P-1	
Unit cell dimensions	a = 8.3208(13) Å	α = 108.031(2)°.
	b = 8.7590(13) Å	β = 106.341(2)°.
	c = 11.6164(17) Å	γ = 90.357(2)°.
Volume	768.5(2) $Å^3$	
Z	2	
Density (calculated)	1.431 Mg/m^3	
Absorption coefficient	0.350 mm^{-1}	
F(000)	344	
Crystal size	0.38 x 0.16 x 0.14 mm^3	
Theta range for data collection	1.93 to 27.00°.	
Index ranges	-10<=h<=10, -11<=k<=11, -14<=l<=14	
Reflections collected	7185	
Independent reflections	3253 [R(int) = 0.0249]	
Completeness to theta = 27.00°	96.7 %	
Absorption correction	Semi-empirical from equivalents	
Max. and min. transmission	0.9526 and 0.8784	
Refinement method	Full-matrix least-squares on F^2	
Data / restraints / parameters	3253 / 0 / 253	

Goodness-of-fit on F^2	1.020
Final R indices [I>2sigma(I)]	R1 = 0.0430, wR2 = 0.0949
R indices (all data)	R1 = 0.0598, wR2 = 0.1066
Largest diff. peak and hole	0.394 and -0.318 e.$Å^{-3}$

Table 19. Atomic coordinates (x 10^4) and equivalent isotropic displacement parameters ($Å^2$x 10^3) for **14b**. U(eq) is defined as one third of the trace of the orthogonalized U^{ij} tensor.

	x	y	z	U(eq)
P(1)	5606(1)	8361(1)	7055(1)	23(1)
S(1)	1339(1)	6979(1)	3056(1)	27(1)
O(1)	1688(3)	8684(2)	3361(2)	52(1)
O(2)	430(2)	6148(2)	1759(2)	43(1)
O(3)	2727(2)	6212(2)	3613(2)	45(1)
N(1)	7758(2)	8666(2)	9647(2)	23(1)
B(1)	6856(3)	9477(3)	8821(2)	24(1)
F(1)	-1564(2)	7452(3)	3468(2)	86(1)
F(2)	-588(3)	5287(3)	3715(2)	91(1)
F(3)	446(2)	7573(2)	5130(2)	61(1)
C(1)	8637(3)	9518(3)	10870(2)	29(1)
C(2)	8690(3)	11150(3)	11334(2)	31(1)
C(3)	7848(3)	12036(3)	10569(2)	31(1)
C(4)	6926(3)	11270(3)	9335(2)	29(1)
C(5)	7842(3)	6892(3)	9283(2)	28(1)
C(6)	6634(4)	6071(4)	9718(3)	38(1)
C(7)	4350(4)	9787(3)	6492(3)	34(1)
C(8)	4207(3)	6639(3)	6787(3)	33(1)
C(9)	6905(3)	7656(3)	6034(2)	31(1)
C(10)	-165(3)	6837(4)	3889(3)	45(1)

Table 20. Bond lengths [Å] and angles [°] for **14b**.

P(1)-C(8)	1.792(3)
P(1)-C(7)	1.794(2)
P(1)-C(9)	1.798(2)
P(1)-B(1)	1.947(3)
S(1)-O(2)	1.4299(17)
S(1)-O(1)	1.432(2)
S(1)-O(3)	1.4361(17)
S(1)-C(10)	1.809(3)
N(1)-C(1)	1.365(3)
N(1)-B(1)	1.419(3)
N(1)-C(5)	1.486(3)
B(1)-C(4)	1.492(3)
F(1)-C(10)	1.317(3)
F(2)-C(10)	1.339(4)
F(3)-C(10)	1.327(3)
C(1)-C(2)	1.358(3)
C(1)-H(1)	0.95(3)
C(2)-C(3)	1.402(3)

C(2)-H(2)	0.89(3)
C(3)-C(4)	1.368(3)
C(3)-H(3)	0.99(3)
C(4)-H(4)	0.96(3)
C(5)-C(6)	1.511(4)
C(5)-H(5A)	0.97(2)
C(5)-H(5B)	0.94(2)
C(6)-H(6A)	0.96(3)
C(6)-H(6B)	0.96(3)
C(6)-H(6C)	0.95(3)
C(7)-H(7A)	0.95(3)
C(7)-H(7B)	0.93(3)
C(7)-H(7C)	1.01(3)
C(8)-H(8A)	0.96(3)
C(8)-H(8B)	0.92(3)
C(8)-H(8C)	0.94(3)
C(9)-H(9A)	0.91(3)
C(9)-H(9B)	0.91(3)
C(9)-H(9C)	1.00(3)
C(8)-P(1)-C(7)	107.27(13)
C(8)-P(1)-C(9)	105.49(13)
C(7)-P(1)-C(9)	107.20(13)
C(8)-P(1)-B(1)	115.28(12)
C(7)-P(1)-B(1)	106.81(12)
C(9)-P(1)-B(1)	114.34(12)
O(2)-S(1)-O(1)	114.75(11)
O(2)-S(1)-O(3)	115.94(11)
O(1)-S(1)-O(3)	114.16(13)
O(2)-S(1)-C(10)	103.25(13)
O(1)-S(1)-C(10)	102.95(14)
O(3)-S(1)-C(10)	103.37(12)
C(1)-N(1)-B(1)	120.2(2)
C(1)-N(1)-C(5)	115.20(18)
B(1)-N(1)-C(5)	124.60(19)
N(1)-B(1)-C(4)	117.7(2)
N(1)-B(1)-P(1)	122.91(18)
C(4)-B(1)-P(1)	119.37(17)
C(2)-C(1)-N(1)	121.8(2)
C(2)-C(1)-H(1)	124.2(15)
N(1)-C(1)-H(1)	114.0(15)
C(1)-C(2)-C(3)	121.2(2)
C(1)-C(2)-H(2)	118.3(16)
C(3)-C(2)-H(2)	120.5(16)
C(4)-C(3)-C(2)	120.6(2)
C(4)-C(3)-H(3)	120.5(15)
C(2)-C(3)-H(3)	118.8(15)
C(3)-C(4)-B(1)	118.5(2)
C(3)-C(4)-H(4)	117.4(15)
B(1)-C(4)-H(4)	124.0(15)
N(1)-C(5)-C(6)	112.1(2)
N(1)-C(5)-H(5A)	106.7(13)
C(6)-C(5)-H(5A)	112.1(14)
N(1)-C(5)-H(5B)	108.6(14)

C(6)-C(5)-H(5B)	110.6(14)
H(5A)-C(5)-H(5B)	106.6(19)
C(5)-C(6)-H(6A)	112.7(18)
C(5)-C(6)-H(6B)	112.9(16)
H(6A)-C(6)-H(6B)	105(2)
C(5)-C(6)-H(6C)	108.2(18)
H(6A)-C(6)-H(6C)	110(2)
H(6B)-C(6)-H(6C)	108(2)
P(1)-C(7)-H(7A)	109.7(17)
P(1)-C(7)-H(7B)	110.8(18)
H(7A)-C(7)-H(7B)	109(2)
P(1)-C(7)-H(7C)	110.6(15)
H(7A)-C(7)-H(7C)	109(2)
H(7B)-C(7)-H(7C)	108(2)
P(1)-C(8)-H(8A)	110.5(17)
P(1)-C(8)-H(8B)	110.2(18)
H(8A)-C(8)-H(8B)	110(2)
P(1)-C(8)-H(8C)	108.3(17)
H(8A)-C(8)-H(8C)	106(2)
H(8B)-C(8)-H(8C)	111(2)
P(1)-C(9)-H(9A)	109.8(17)
P(1)-C(9)-H(9B)	109.4(18)
H(9A)-C(9)-H(9B)	106(2)
P(1)-C(9)-H(9C)	107.4(15)
H(9A)-C(9)-H(9C)	112(2)
H(9B)-C(9)-H(9C)	113(2)
F(1)-C(10)-F(3)	108.2(3)
F(1)-C(10)-F(2)	107.1(2)
F(3)-C(10)-F(2)	107.1(2)
F(1)-C(10)-S(1)	111.80(19)
F(3)-C(10)-S(1)	112.46(19)
F(2)-C(10)-S(1)	109.9(2)

Symmetry transformations used to generate equivalent atoms:

Table 21. Anisotropic displacement parameters ($Å^2 x\ 10^3$)for **14b**. The anisotropic displacement factor exponent takes the form: $-2p^2[\ h^2a^{*2}U^{11} + ... + 2\ h\ k\ a^*\ b^*\ U^{12}\ ]$

	U^{11}	U^{22}	U^{33}	U^{23}	U^{13}	U^{12}
P(1)	25(1)	22(1)	23(1)	7(1)	5(1)	3(1)
S(1)	29(1)	26(1)	25(1)	8(1)	5(1)	4(1)
O(1)	74(1)	34(1)	49(1)	16(1)	14(1)	-10(1)
O(2)	51(1)	42(1)	26(1)	5(1)	0(1)	12(1)
O(3)	38(1)	59(1)	35(1)	14(1)	5(1)	22(1)
N(1)	25(1)	22(1)	24(1)	9(1)	7(1)	4(1)
B(1)	23(1)	26(1)	24(1)	9(1)	8(1)	2(1)
F(1)	41(1)	163(2)	74(1)	58(2)	23(1)	45(1)
F(2)	86(2)	96(2)	95(2)	52(1)	10(1)	-45(1)
F(3)	52(1)	100(2)	40(1)	26(1)	23(1)	15(1)
C(1)	28(1)	34(1)	26(1)	13(1)	6(1)	6(1)
C(2)	31(1)	34(1)	22(1)	3(1)	4(1)	-1(1)
C(3)	35(1)	23(1)	33(1)	3(1)	11(1)	3(1)
C(4)	34(1)	23(1)	30(1)	10(1)	8(1)	5(1)

C(5)	30(1)	23(1)	32(1)	12(1)	6(1)	8(1)
C(6)	41(2)	31(2)	46(2)	21(1)	13(1)	2(1)
C(7)	36(1)	30(2)	30(1)	10(1)	1(1)	5(1)
C(8)	32(1)	33(2)	33(1)	13(1)	7(1)	-3(1)
C(9)	36(1)	29(1)	29(1)	7(1)	13(1)	2(1)
C(10)	30(1)	67(2)	44(2)	28(2)	6(1)	3(1)

Table 22. Hydrogen coordinates (x 10^4) and isotropic displacement parameters ($Å^2$x 10^3) for **14b**.

	x	y	z	U(eq)
H(1)	9180(30)	8870(30)	11350(20)	34(7)
H(2)	9300(30)	11650(30)	12130(20)	31(7)
H(3)	7980(30)	13230(30)	10920(20)	43(8)
H(4)	6410(30)	11940(30)	8840(20)	35(7)
H(5A)	7610(30)	6500(30)	8370(20)	23(6)
H(5B)	8950(30)	6700(30)	9630(20)	22(6)
H(6A)	6870(40)	6440(30)	10620(30)	49(8)
H(6B)	5490(40)	6270(30)	9400(20)	40(7)
H(6C)	6710(40)	4940(40)	9420(30)	51(8)
H(7A)	3610(40)	10150(30)	6990(30)	50(8)
H(7B)	3720(40)	9320(40)	5650(30)	52(9)
H(7C)	5090(40)	10740(40)	6550(30)	48(8)
H(8A)	3470(40)	6920(30)	7310(30)	46(8)
H(8B)	4810(30)	5820(30)	6950(30)	43(8)
H(8C)	3520(40)	6320(30)	5950(30)	45(8)
H(9A)	7670(40)	8470(40)	6140(20)	41(8)
H(9B)	7510(40)	6890(40)	6270(30)	45(8)
H(9C)	6140(30)	7250(30)	5140(30)	45(8)

Table 23. Torsion angles [°] for **14b**.

C(1)-N(1)-B(1)-C(4)	0.7(3)
C(5)-N(1)-B(1)-C(4)	-179.1(2)
C(1)-N(1)-B(1)-P(1)	178.76(17)
C(5)-N(1)-B(1)-P(1)	-1.0(3)
C(8)-P(1)-B(1)-N(1)	49.6(2)
C(7)-P(1)-B(1)-N(1)	168.7(2)
C(9)-P(1)-B(1)-N(1)	-72.9(2)
C(8)-P(1)-B(1)-C(4)	-132.4(2)
C(7)-P(1)-B(1)-C(4)	-13.3(2)
C(9)-P(1)-B(1)-C(4)	105.1(2)
B(1)-N(1)-C(1)-C(2)	-0.5(3)
C(5)-N(1)-C(1)-C(2)	179.3(2)
N(1)-C(1)-C(2)-C(3)	-0.4(4)
C(1)-C(2)-C(3)-C(4)	1.0(4)
C(2)-C(3)-C(4)-B(1)	-0.7(4)
N(1)-B(1)-C(4)-C(3)	-0.1(3)
P(1)-B(1)-C(4)-C(3)	-178.25(18)
C(1)-N(1)-C(5)-C(6)	80.7(3)
B(1)-N(1)-C(5)-C(6)	-99.5(3)
O(2)-S(1)-C(10)-F(1)	-57.0(3)

O(1)-S(1)-C(10)-F(1)	62.7(2)
O(3)-S(1)-C(10)-F(1)	-178.2(2)
O(2)-S(1)-C(10)-F(3)	-179.1(2)
O(1)-S(1)-C(10)-F(3)	-59.3(2)
O(3)-S(1)-C(10)-F(3)	59.8(2)
O(2)-S(1)-C(10)-F(2)	61.7(2)
O(1)-S(1)-C(10)-F(2)	-178.57(18)
O(3)-S(1)-C(10)-F(2)	-59.5(2)

Symmetry transformations used to generate equivalent atoms:

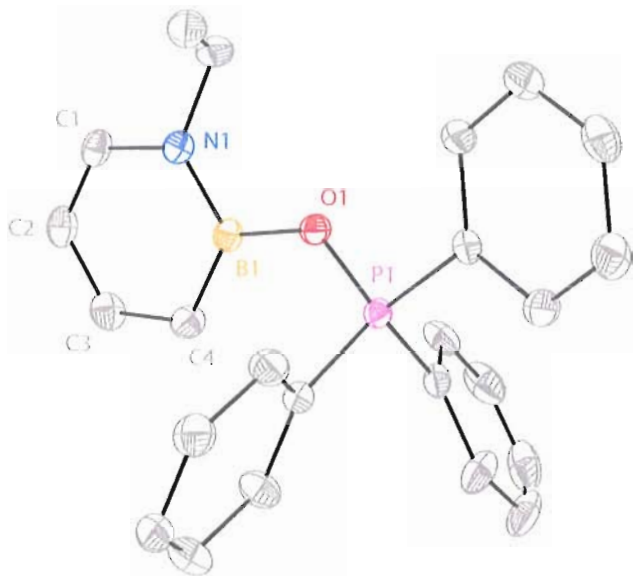

Figure 12. ORTEP illustration of **14c**, with ellipsoids drawn at the 35% probability level.

X-ray Crystal Structure Determination. Crystals of **14c** suitable for X-ray diffraction were obtained by evaporation of a solution of **14c** in CH_2Cl_2.

Diffraction intensity data were collected with a Bruker Smart Apex CCD diffractometer at 173(2) K using MoKα - radiation (0.71073 Å). The structure was solved using direct methods, completed by subsequent difference Fourier syntheses, and refined by full matrix least-squares procedures on F^2. All non-H atoms were refined with anisotropic thermal parameters. H atoms were found on the residual density map and refined with isotropic thermal parameters. The Flack parameter is 0.00(8). All software

and sources scattering factors are contained in the SHELXTL (6.10) program package (G.Sheldrick, Bruker XRD, Madison, WI). Crystallographic data and some details of data collection and crystal structure refinement for $C_{25}H_{24}BF_3NO_4PS$ are given in the following tables.

Table 24. Crystal data and structure refinement for **14c**.

Identification code	liu25	
Empirical formula	C_{25} H_{24} B F_3 N O_4 P S	
Formula weight	533.29	
Temperature	173(2) K	
Wavelength	0.71073 Å	
Crystal system	Orthorhombic	
Space group	Pbca	
Unit cell dimensions	a = 9.1044(4) Å	α = 90°.
	b = 19.8146(8) Å	β = 90°.
	c = 28.1910(11) Å	γ = 90°.
Volume	5085.7(4) $Å^3$	
Z	8	
Density (calculated)	1.393 Mg/m^3	
Absorption coefficient	0.245 mm^{-1}	
F(000)	2208	
Crystal size	0.26 x 0.20 x 0.12 mm^3	
Theta range for data collection	1.44 to 27.00°.	
Index ranges	-11<=h<=10, -25<=k<=25, -36<=l<=36	
Reflections collected	48806	
Independent reflections	5550 [R(int) = 0.0393]	
Completeness to theta = 27.00°	100.0 %	
Absorption correction	Semi-empirical from equivalents	
Max. and min. transmission	0.9712 and 0.9391	
Refinement method	Full-matrix least-squares on F^2	
Data / restraints / parameters	5550 / 0 / 421	
Goodness-of-fit on F^2	1.057	
Final R indices [I>2sigma(I)]	R1 = 0.0450, wR2 = 0.1094	
R indices (all data)	R1 = 0.0550, wR2 = 0.1169	
Largest diff. peak and hole	0.450 and -0.272 $e.Å^{-3}$	

Table 25. Atomic coordinates (x 10^4) and equivalent isotropic displacement parameters ($Å^2$x 10^3) for **14c**. U(eq) is defined as one third of the trace of the orthogonalized U^{ij} tensor.

	x	y	z	U(eq)
P(1)	9768(1)	595(1)	6290(1)	23(1)
S(1)	6965(1)	1870(1)	3602(1)	32(1)
N(1)	7259(2)	2118(1)	5950(1)	28(1)
O(1)	8967(2)	1285(1)	6241(1)	28(1)
O(2)	6775(2)	1168(1)	3496(1)	53(1)
O(3)	5761(2)	2166(1)	3856(1)	49(1)
O(4)	8385(2)	2063(1)	3770(1)	64(1)
B(1)	8277(2)	1598(1)	5840(1)	26(1)
C(1)	6478(2)	2421(1)	5595(1)	33(1)
C(2)	6659(2)	2255(1)	5131(1)	37(1)
C(3)	7686(3)	1763(1)	4999(1)	39(1)
C(4)	8500(2)	1421(1)	5329(1)	35(1)
C(5)	6995(3)	2348(1)	6445(1)	36(1)
C(6)	5949(3)	1890(1)	6701(1)	41(1)
C(7)	8706(2)	-77(1)	6045(1)	26(1)
C(8)	7589(2)	-354(1)	6319(1)	35(1)
C(9)	6699(2)	-857(1)	6136(1)	39(1)
C(10)	6925(2)	-1086(1)	5679(1)	38(1)
C(11)	8036(3)	-817(1)	5405(1)	42(1)
C(12)	8932(3)	-315(1)	5585(1)	36(1)
C(13)	11516(2)	648(1)	6009(1)	29(1)
C(14)	12314(3)	69(1)	5902(1)	43(1)
C(15)	13704(3)	141(2)	5701(1)	58(1)
C(16)	14264(3)	774(2)	5606(1)	59(1)
C(17)	13464(3)	1341(2)	5709(1)	53(1)
C(18)	12089(2)	1287(1)	5912(1)	39(1)
C(19)	9865(2)	440(1)	6913(1)	25(1)
C(20)	10490(2)	-161(1)	7067(1)	34(1)
C(21)	10369(3)	-343(1)	7540(1)	40(1)
C(22)	9630(3)	68(1)	7854(1)	38(1)
C(23)	9043(3)	672(1)	7704(1)	37(1)
C(24)	9159(2)	865(1)	7231(1)	31(1)
C(25)	6839(3)	2259(1)	3023(1)	41(1)
F(1)	7865(2)	2048(1)	2731(1)	80(1)
F(2)	5549(2)	2133(1)	2822(1)	72(1)
F(3)	6969(2)	2927(1)	3045(1)	72(1)

Table 26. Bond lengths [Å] and angles [°] for **14c.**

P(1)-O(1)	1.5563(13)
P(1)-C(13)	1.781(2)
P(1)-C(7)	1.7845(19)
P(1)-C(19)	1.7846(18)
S(1)-O(4)	1.4285(18)
S(1)-O(2)	1.4336(17)
S(1)-O(3)	1.4349(17)
S(1)-C(25)	1.810(2)
N(1)-C(1)	1.368(2)
N(1)-B(1)	1.420(3)
N(1)-C(5)	1.487(3)
O(1)-B(1)	1.433(2)
B(1)-C(4)	1.496(3)
C(1)-C(2)	1.357(3)
C(1)-H(1)	0.95(2)
C(2)-C(3)	1.403(3)
C(2)-H(2)	0.94(3)
C(3)-C(4)	1.369(3)
C(3)-H(3)	0.93(3)
C(4)-H(4)	1.00(3)
C(5)-C(6)	1.501(3)
C(5)-H(5A)	0.99(2)
C(5)-H(5B)	0.99(2)
C(6)-H(6A)	1.03(3)
C(6)-H(6B)	1.00(3)
C(6)-H(6C)	1.00(2)
C(7)-C(8)	1.390(3)
C(7)-C(12)	1.394(3)
C(8)-C(9)	1.384(3)
C(8)-H(8)	0.95(2)
C(9)-C(10)	1.380(3)
C(9)-H(9)	0.93(3)
C(10)-C(11)	1.379(3)
C(10)-H(10)	0.93(2)
C(11)-C(12)	1.382(3)
C(11)-H(11)	0.96(3)
C(12)-H(12)	0.94(3)
C(13)-C(14)	1.391(3)
C(13)-C(18)	1.397(3)
C(14)-C(15)	1.395(4)
C(14)-H(14)	0.92(3)
C(15)-C(16)	1.381(5)
C(15)-H(15)	0.85(3)
C(16)-C(17)	1.370(4)
C(16)-H(16)	0.97(3)
C(17)-C(18)	1.381(3)
C(17)-H(17)	1.00(3)
C(18)-H(18)	0.98(2)
C(19)-C(24)	1.387(3)
C(19)-C(20)	1.391(3)
C(20)-C(21)	1.385(3)
C(20)-H(20)	0.93(3)

C(21)-C(22)	1.378(3)
C(21)-H(21)	0.94(3)
C(22)-C(23)	1.378(3)
C(22)-H(22)	0.92(3)
C(23)-C(24)	1.391(3)
C(23)-H(23)	0.96(3)
C(24)-H(24)	0.96(2)
C(25)-F(1)	1.312(3)
C(25)-F(2)	1.328(3)
C(25)-F(3)	1.332(3)
O(1)-P(1)-C(13)	109.08(9)
O(1)-P(1)-C(7)	111.54(8)
C(13)-P(1)-C(7)	110.83(9)
O(1)-P(1)-C(19)	105.20(8)
C(13)-P(1)-C(19)	113.81(9)
C(7)-P(1)-C(19)	106.26(9)
O(4)-S(1)-O(2)	115.95(13)
O(4)-S(1)-O(3)	114.61(12)
O(2)-S(1)-O(3)	114.13(10)
O(4)-S(1)-C(25)	103.99(11)
O(2)-S(1)-C(25)	102.57(11)
O(3)-S(1)-C(25)	103.23(11)
C(1)-N(1)-B(1)	119.82(17)
C(1)-N(1)-C(5)	117.97(17)
B(1)-N(1)-C(5)	122.21(16)
B(1)-O(1)-P(1)	131.01(12)
N(1)-B(1)-O(1)	115.30(16)
N(1)-B(1)-C(4)	118.01(17)
O(1)-B(1)-C(4)	126.68(18)
C(2)-C(1)-N(1)	122.4(2)
C(2)-C(1)-H(1)	121.0(14)
N(1)-C(1)-H(1)	116.6(14)
C(1)-C(2)-C(3)	120.37(19)
C(1)-C(2)-H(2)	117.0(15)
C(3)-C(2)-H(2)	122.7(15)
C(4)-C(3)-C(2)	121.6(2)
C(4)-C(3)-H(3)	119.8(16)
C(2)-C(3)-H(3)	118.5(15)
C(3)-C(4)-B(1)	117.7(2)
C(3)-C(4)-H(4)	117.4(14)
B(1)-C(4)-H(4)	124.9(14)
N(1)-C(5)-C(6)	111.65(18)
N(1)-C(5)-H(5A)	113.7(13)
C(6)-C(5)-H(5A)	109.1(14)
N(1)-C(5)-H(5B)	108.1(13)
C(6)-C(5)-H(5B)	112.1(13)
H(5A)-C(5)-H(5B)	101.9(19)
C(5)-C(6)-H(6A)	110.7(17)
C(5)-C(6)-H(6B)	108.1(14)
H(6A)-C(6)-H(6B)	110(2)
C(5)-C(6)-H(6C)	110.0(14)
H(6A)-C(6)-H(6C)	109(2)
H(6B)-C(6)-H(6C)	109(2)

C(8)-C(7)-C(12)	119.35(18)
C(8)-C(7)-P(1)	118.40(14)
C(12)-C(7)-P(1)	122.21(15)
C(9)-C(8)-C(7)	120.35(19)
C(9)-C(8)-H(8)	118.8(15)
C(7)-C(8)-H(8)	120.8(15)
C(10)-C(9)-C(8)	119.8(2)
C(10)-C(9)-H(9)	118.9(15)
C(8)-C(9)-H(9)	121.3(15)
C(11)-C(10)-C(9)	120.3(2)
C(11)-C(10)-H(10)	119.3(15)
C(9)-C(10)-H(10)	120.4(15)
C(10)-C(11)-C(12)	120.3(2)
C(10)-C(11)-H(11)	121.6(16)
C(12)-C(11)-H(11)	118.1(16)
C(11)-C(12)-C(7)	119.9(2)
C(11)-C(12)-H(12)	120.5(15)
C(7)-C(12)-H(12)	119.6(15)
C(14)-C(13)-C(18)	120.7(2)
C(14)-C(13)-P(1)	120.95(17)
C(18)-C(13)-P(1)	118.32(16)
C(13)-C(14)-C(15)	118.6(3)
C(13)-C(14)-H(14)	119.4(15)
C(15)-C(14)-H(14)	122.0(15)
C(16)-C(15)-C(14)	120.4(3)
C(16)-C(15)-H(15)	126.8(18)
C(14)-C(15)-H(15)	112.7(18)
C(17)-C(16)-C(15)	120.5(2)
C(17)-C(16)-H(16)	122.2(18)
C(15)-C(16)-H(16)	117.2(18)
C(16)-C(17)-C(18)	120.5(3)
C(16)-C(17)-H(17)	118.3(19)
C(18)-C(17)-H(17)	121.2(19)
C(17)-C(18)-C(13)	119.3(2)
C(17)-C(18)-H(18)	119.9(14)
C(13)-C(18)-H(18)	120.8(14)
C(24)-C(19)-C(20)	120.44(18)
C(24)-C(19)-P(1)	120.64(14)
C(20)-C(19)-P(1)	118.35(15)
C(21)-C(20)-C(19)	119.4(2)
C(21)-C(20)-H(20)	119.0(15)
C(19)-C(20)-H(20)	121.6(15)
C(22)-C(21)-C(20)	120.2(2)
C(22)-C(21)-H(21)	120.2(15)
C(20)-C(21)-H(21)	119.6(15)
C(23)-C(22)-C(21)	120.41(19)
C(23)-C(22)-H(22)	119.1(16)
C(21)-C(22)-H(22)	120.4(16)
C(22)-C(23)-C(24)	120.1(2)
C(22)-C(23)-H(23)	123.0(15)
C(24)-C(23)-H(23)	116.8(15)
C(19)-C(24)-C(23)	119.32(19)
C(19)-C(24)-H(24)	122.0(13)

C(23)-C(24)-H(24)	118.6(13)
F(1)-C(25)-F(2)	107.7(2)
F(1)-C(25)-F(3)	106.5(2)
F(2)-C(25)-F(3)	106.6(2)
F(1)-C(25)-S(1)	112.63(17)
F(2)-C(25)-S(1)	111.10(16)
F(3)-C(25)-S(1)	112.03(16)

Symmetry transformations used to generate equivalent atoms:

Table 27. Anisotropic displacement parameters ($Å^2 x\ 10^3$)for **14c**. The anisotropic displacement factor exponent takes the form: $-2p^2[\ h^2a^{*2}U^{11} + ... + 2\ h\ k\ a^*\ b^*\ U^{12}\ ]$

	U^{11}	U^{22}	U^{33}	U^{23}	U^{13}	U^{12}
P(1)	23(1)	25(1)	20(1)	1(1)	-1(1)	2(1)
S(1)	30(1)	34(1)	32(1)	8(1)	-2(1)	-5(1)
N(1)	27(1)	26(1)	30(1)	4(1)	0(1)	0(1)
O(1)	32(1)	28(1)	24(1)	2(1)	-1(1)	6(1)
O(2)	56(1)	30(1)	74(1)	9(1)	9(1)	3(1)
O(3)	53(1)	46(1)	47(1)	-7(1)	15(1)	-7(1)
O(4)	42(1)	98(2)	51(1)	23(1)	-18(1)	-23(1)
B(1)	25(1)	28(1)	26(1)	5(1)	-1(1)	0(1)
C(1)	28(1)	27(1)	44(1)	10(1)	-4(1)	1(1)
C(2)	35(1)	39(1)	37(1)	16(1)	-8(1)	-2(1)
C(3)	45(1)	48(1)	24(1)	8(1)	0(1)	-2(1)
C(4)	38(1)	41(1)	26(1)	4(1)	4(1)	7(1)
C(5)	40(1)	30(1)	38(1)	-6(1)	0(1)	6(1)
C(6)	37(1)	52(1)	33(1)	-1(1)	3(1)	3(1)
C(7)	25(1)	26(1)	27(1)	0(1)	-2(1)	2(1)
C(8)	27(1)	43(1)	34(1)	-7(1)	5(1)	-2(1)
C(9)	28(1)	40(1)	48(1)	-4(1)	4(1)	-5(1)
C(10)	33(1)	30(1)	50(1)	-8(1)	-10(1)	1(1)
C(11)	53(2)	42(1)	31(1)	-9(1)	-2(1)	-4(1)
C(12)	45(1)	38(1)	26(1)	-2(1)	4(1)	-8(1)
C(13)	23(1)	42(1)	22(1)	2(1)	-2(1)	1(1)
C(14)	37(1)	53(1)	40(1)	16(1)	6(1)	17(1)
C(15)	38(1)	90(2)	46(1)	9(1)	4(1)	33(2)
C(16)	25(1)	114(3)	39(1)	4(1)	0(1)	-11(1)
C(17)	38(1)	79(2)	43(1)	-13(1)	6(1)	-28(1)
C(18)	37(1)	49(1)	31(1)	-11(1)	1(1)	-15(1)
C(19)	24(1)	29(1)	23(1)	2(1)	-4(1)	-1(1)
C(20)	41(1)	32(1)	29(1)	2(1)	-3(1)	7(1)
C(21)	51(1)	36(1)	33(1)	10(1)	-7(1)	4(1)
C(22)	42(1)	48(1)	24(1)	7(1)	-4(1)	-6(1)
C(23)	40(1)	47(1)	25(1)	-4(1)	0(1)	3(1)
C(24)	36(1)	33(1)	25(1)	-1(1)	-2(1)	5(1)
C(25)	42(1)	46(1)	35(1)	7(1)	-3(1)	-8(1)
F(1)	85(1)	109(2)	46(1)	5(1)	28(1)	2(1)
F(2)	63(1)	96(1)	55(1)	18(1)	-31(1)	-19(1)
F(3)	98(1)	45(1)	72(1)	29(1)	-11(1)	-17(1)

Table 28. Hydrogen coordinates (x 10^4) and isotropic displacement parameters (Å^{2}x 10^3) for **14c**.

	x	y	z	U(eq)
H(1)	5800(30)	2760(12)	5687(8)	38(6)
H(2)	6070(30)	2484(12)	4910(9)	45(6)
H(3)	7840(30)	1684(12)	4678(9)	45(7)
H(4)	9210(30)	1076(12)	5210(9)	48(7)
H(5A)	6630(30)	2816(12)	6468(8)	35(6)
H(5B)	7960(30)	2379(12)	6608(8)	37(6)
H(6A)	5830(30)	2039(14)	7050(11)	69(9)
H(6B)	4980(30)	1910(12)	6536(9)	47(7)
H(6C)	6320(30)	1416(12)	6694(8)	40(6)
H(8)	7430(30)	-209(12)	6637(9)	44(6)
H(9)	5950(30)	-1048(12)	6315(9)	46(7)
H(10)	6350(30)	-1430(12)	5555(8)	44(7)
H(11)	8200(30)	-964(13)	5085(10)	56(7)
H(12)	9710(30)	-140(13)	5402(9)	49(7)
H(14)	11910(30)	-350(13)	5963(9)	43(7)
H(15)	14100(30)	-237(13)	5632(9)	45(7)
H(16)	15220(40)	796(15)	5454(11)	70(9)
H(17)	13910(40)	1792(17)	5639(11)	80(10)
H(18)	11530(30)	1695(12)	5988(8)	40(6)
H(20)	11000(30)	-442(12)	6862(9)	45(7)
H(21)	10780(30)	-752(13)	7643(9)	49(7)
H(22)	9510(30)	-61(12)	8166(9)	50(7)
H(23)	8540(30)	979(13)	7914(9)	49(7)
H(24)	8700(30)	1278(11)	7132(8)	36(6)

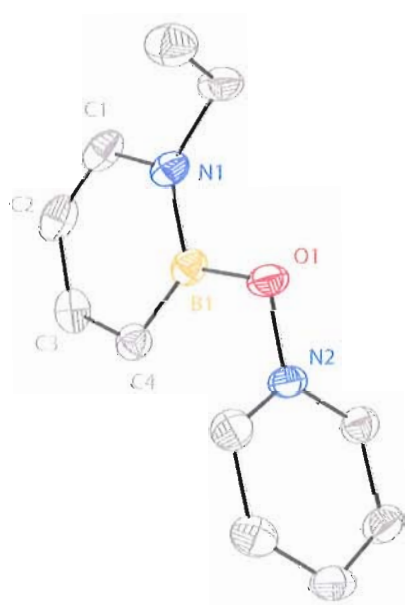

Figure 13. ORTEP illustration of **14d**, with ellipsoids drawn at the 35% probability level.

X-ray Crystal Structure Determination. Crystals of **14d** suitable for X-ray diffraction were obtained by evaporation of a solution of **14d** in CH_2Cl_2.

Diffraction intensity data were collected with a Bruker Smart Apex CCD diffractometer at 173(2) K using MoKα - radiation (0.71073 Å). The structure was solved using direct methods, completed by subsequent difference Fourier syntheses, and refined by full matrix least-squares procedures on F^2. All non-H atoms were refined with anisotropic thermal parameters. H atoms were found on the residual density map and refined with isotropic thermal parameters. The Flack parameter is 0.00(8). All software and sources scattering factors are contained in the SHELXTL (6.10) program package (G.Sheldrick, Bruker XRD, Madison, WI). Crystallographic data and some details of data collection and crystal structure refinement for $C_{12}H_{14}BF_3N_2O_4S$ are given in the following tables.

Table 29. Crystal data and structure refinement for **14d**.

Identification code	liu27	
Empirical formula	C_{12} H_{14} B F_3 N_2 O_4 S	
Formula weight	350.12	
Temperature	173(2) K	
Wavelength	0.71073 Å	
Crystal system	Monoclinic	
Space group	P2(1)/c	
Unit cell dimensions	a = 9.6415(13) Å	$\alpha = 90°$.
	b = 9.9617(14) Å	$\beta = 96.612(2)°$.
	c = 16.668(2) Å	$\gamma = 90°$.
Volume	1590.3(4) $Å^3$	
Z	4	
Density (calculated)	1.462 Mg/m^3	
Absorption coefficient	0.254 mm^{-1}	
F(000)	720	
Crystal size	0.32 x 0.26 x 0.18 mm^3	

Theta range for data collection	2.13 to 27.00°.
Index ranges	-12<=h<=12, -12<=k<=12, -20<=l<=21
Reflections collected	14940
Independent reflections	3448 [R(int) = 0.0393]
Completeness to theta = 27.00°	98.9 %
Absorption correction	Semi-empirical from equivalents
Max. and min. transmission	0.9557 and 0.9232
Refinement method	Full-matrix least-squares on F^2
Data / restraints / parameters	3448 / 0 / 264
Goodness-of-fit on F^2	1.015
Final R indices [I>2sigma(I)]	R1 = 0.0433, wR2 = 0.0976
R indices (all data)	R1 = 0.0688, wR2 = 0.1137
Largest diff. peak and hole	0.280 and -0.269 e.$Å^{-3}$

Table 30. Atomic coordinates (x 10^4) and equivalent isotropic displacement parameters ($Å^2$x 10^3) for **14d**. U(eq) is defined as one third of the trace of the orthogonalized U^{ij} tensor.

	x	y	z	U(eq)
S(1)	6805(1)	1980(1)	1154(1)	43(1)
O(1)	9909(2)	10054(2)	2287(1)	42(1)
O(2)	8172(2)	2574(2)	1232(1)	68(1)
O(3)	6684(2)	693(2)	774(1)	66(1)
O(4)	6093(2)	2107(2)	1859(1)	51(1)
N(1)	7845(2)	9045(2)	2649(1)	37(1)
N(2)	11006(2)	9997(2)	1821(1)	35(1)
F(1)	5815(2)	4335(1)	721(1)	76(1)
F(2)	4490(1)	2722(2)	294(1)	75(1)
F(3)	6316(2)	3131(2)	-267(1)	74(1)
B(1)	8915(2)	8994(2)	2135(2)	36(1)
C(1)	6810(2)	8096(3)	2560(2)	48(1)
C(2)	6779(2)	7119(3)	1998(2)	51(1)
C(3)	7829(2)	7017(2)	1480(2)	48(1)
C(4)	8913(2)	7903(2)	1523(1)	40(1)
C(5)	7808(3)	10061(3)	3289(2)	46(1)
C(6)	8656(3)	9661(3)	4067(2)	57(1)
C(7)	10931(2)	10756(2)	1156(1)	40(1)
C(8)	12044(2)	10742(2)	717(2)	45(1)
C(9)	13203(2)	9978(2)	972(2)	44(1)
C(10)	13221(2)	9215(2)	1658(1)	45(1)
C(11)	12099(2)	9236(2)	2086(1)	41(1)
C(12)	5807(2)	3084(2)	439(2)	45(1)

Table 31. Bond lengths [Å] and angles [°] for **14d**.

S(1)-O(3)	1.4288(18)
S(1)-O(4)	1.4331(16)
S(1)-O(2)	1.4368(18)
S(1)-C(12)	1.815(2)

O(1)-N(2)	1.383(2)
O(1)-B(1)	1.429(3)
N(1)-C(1)	1.371(3)
N(1)-B(1)	1.414(3)
N(1)-C(5)	1.474(3)
N(2)-C(11)	1.332(3)
N(2)-C(7)	1.337(3)
F(1)-C(12)	1.331(3)
F(2)-C(12)	1.316(3)
F(3)-C(12)	1.326(3)
B(1)-C(4)	1.492(3)
C(1)-C(2)	1.349(4)
C(1)-H(1)	0.91(3)
C(2)-C(3)	1.408(4)
C(2)-H(2)	0.91(2)
C(3)-C(4)	1.363(3)
C(3)-H(3)	0.94(2)
C(4)-H(4)	0.90(2)
C(5)-C(6)	1.505(4)
C(5)-H(5A)	0.94(2)
C(5)-H(5B)	0.96(2)
C(6)-H(6A)	0.99(3)
C(6)-H(6B)	0.93(3)
C(6)-H(6C)	0.98(3)
C(7)-C(8)	1.367(3)
C(7)-H(7)	0.92(2)
C(8)-C(9)	1.378(3)
C(8)-H(8)	0.93(2)
C(9)-C(10)	1.372(3)
C(9)-H(9)	0.90(2)
C(10)-C(11)	1.364(3)
C(10)-H(10)	0.95(2)
C(11)-H(11)	0.92(2)
O(3)-S(1)-O(4)	114.91(11)
O(3)-S(1)-O(2)	115.92(12)
O(4)-S(1)-O(2)	114.22(11)
O(3)-S(1)-C(12)	103.98(11)
O(4)-S(1)-C(12)	102.57(10)
O(2)-S(1)-C(12)	102.76(11)
N(2)-O(1)-B(1)	114.28(15)
C(1)-N(1)-B(1)	118.8(2)
C(1)-N(1)-C(5)	118.3(2)
B(1)-N(1)-C(5)	122.86(19)
C(11)-N(2)-C(7)	124.28(19)
C(11)-N(2)-O(1)	117.64(17)
C(7)-N(2)-O(1)	118.00(17)
N(1)-B(1)-O(1)	112.82(19)
N(1)-B(1)-C(4)	119.8(2)
O(1)-B(1)-C(4)	127.4(2)
C(2)-C(1)-N(1)	122.1(2)
C(2)-C(1)-H(1)	122.6(17)
N(1)-C(1)-H(1)	115.3(17)
C(1)-C(2)-C(3)	121.2(2)

C(1)-C(2)-H(2)	116.3(16)
C(3)-C(2)-H(2)	122.5(16)
C(4)-C(3)-C(2)	121.5(2)
C(4)-C(3)-H(3)	118.3(14)
C(2)-C(3)-H(3)	120.1(14)
C(3)-C(4)-B(1)	116.6(2)
C(3)-C(4)-H(4)	118.4(14)
B(1)-C(4)-H(4)	125.0(14)
N(1)-C(5)-C(6)	112.7(2)
N(1)-C(5)-H(5A)	109.0(14)
C(6)-C(5)-H(5A)	113.6(14)
N(1)-C(5)-H(5B)	108.2(15)
C(6)-C(5)-H(5B)	110.7(15)
H(5A)-C(5)-H(5B)	102.0(19)
C(5)-C(6)-H(6A)	109.8(16)
C(5)-C(6)-H(6B)	111.0(18)
H(6A)-C(6)-H(6B)	106(2)
C(5)-C(6)-H(6C)	108.6(15)
H(6A)-C(6)-H(6C)	112(2)
H(6B)-C(6)-H(6C)	109(2)
N(2)-C(7)-C(8)	117.8(2)
N(2)-C(7)-H(7)	115.2(14)
C(8)-C(7)-H(7)	127.0(14)
C(7)-C(8)-C(9)	120.0(2)
C(7)-C(8)-H(8)	118.0(15)
C(9)-C(8)-H(8)	122.0(15)
C(10)-C(9)-C(8)	119.7(2)
C(10)-C(9)-H(9)	121.2(15)
C(8)-C(9)-H(9)	119.1(15)
C(11)-C(10)-C(9)	119.6(2)
C(11)-C(10)-H(10)	117.0(14)
C(9)-C(10)-H(10)	123.4(14)
N(2)-C(11)-C(10)	118.7(2)
N(2)-C(11)-H(11)	114.8(14)
C(10)-C(11)-H(11)	126.5(15)
F(2)-C(12)-F(3)	107.1(2)
F(2)-C(12)-F(1)	106.70(19)
F(3)-C(12)-F(1)	107.02(19)
F(2)-C(12)-S(1)	112.45(16)
F(3)-C(12)-S(1)	112.44(16)
F(1)-C(12)-S(1)	110.76(16)

Symmetry transformations used to generate equivalent atoms:

Table 32. Anisotropic displacement parameters ($Å^2 x\ 10^3$)for **14d**. The anisotropic displacement factor exponent takes the form: $-2p^2[\ h^2a^{*2}U^{11} + ... + 2\ h\ k\ a^*\ b^*\ U^{12}\ ]$

	U^{11}	U^{22}	U^{33}	U^{23}	U^{13}	U^{12}
S(1)	38(1)	54(1)	38(1)	-7(1)	3(1)	14(1)
O(1)	41(1)	45(1)	44(1)	-8(1)	21(1)	-9(1)
O(2)	29(1)	107(2)	69(1)	-11(1)	4(1)	8(1)
O(3)	102(2)	50(1)	47(1)	-6(1)	10(1)	23(1)
O(4)	47(1)	70(1)	37(1)	-5(1)	9(1)	13(1)

N(1)	30(1)	47(1)	35(1)	8(1)	6(1)	1(1)
N(2)	35(1)	39(1)	34(1)	-5(1)	12(1)	-4(1)
F(1)	89(1)	43(1)	93(1)	-7(1)	-4(1)	9(1)
F(2)	47(1)	86(1)	85(1)	30(1)	-22(1)	-13(1)
F(3)	95(1)	78(1)	52(1)	15(1)	20(1)	2(1)
B(1)	33(1)	40(1)	36(1)	7(1)	3(1)	1(1)
C(1)	31(1)	64(2)	48(2)	20(1)	3(1)	-1(1)
C(2)	37(1)	56(2)	58(2)	13(1)	-4(1)	-13(1)
C(3)	49(1)	42(1)	49(2)	2(1)	-9(1)	-3(1)
C(4)	39(1)	41(1)	40(1)	4(1)	4(1)	1(1)
C(5)	42(1)	58(2)	42(1)	3(1)	14(1)	10(1)
C(6)	60(2)	68(2)	43(2)	-3(1)	6(1)	7(1)
C(7)	37(1)	41(1)	43(1)	4(1)	8(1)	2(1)
C(8)	48(1)	49(1)	39(1)	5(1)	13(1)	-3(1)
C(9)	36(1)	51(1)	46(1)	-12(1)	14(1)	-4(1)
C(10)	38(1)	50(1)	45(1)	-6(1)	4(1)	5(1)
C(11)	43(1)	43(1)	36(1)	0(1)	4(1)	0(1)
C(12)	43(1)	45(1)	47(1)	-1(1)	4(1)	-4(1)

Table 33. Hydrogen coordinates (x 10^4) and isotropic displacement parameters (Å^{2}x 10^3) for **14d**.

	x	y	z	U(eq)
H(1)	6150(30)	8180(20)	2899(17)	62(8)
H(2)	6060(30)	6530(20)	1983(14)	53(7)
H(3)	7820(20)	6300(20)	1111(14)	46(7)
H(4)	9580(20)	7780(20)	1189(14)	40(6)
H(5A)	6880(30)	10260(20)	3348(13)	47(6)
H(5B)	8140(20)	10890(20)	3095(15)	52(7)
H(6A)	8290(30)	8820(30)	4268(17)	72(9)
H(6B)	9580(30)	9490(30)	3987(17)	79(9)
H(6C)	8630(30)	10400(30)	4456(16)	61(8)
H(7)	10120(20)	11250(20)	1048(13)	42(6)
H(8)	11990(20)	11260(20)	250(15)	56(7)
H(9)	13930(20)	9980(20)	676(14)	47(7)
H(10)	13970(20)	8640(20)	1847(14)	52(7)
H(11)	12000(20)	8750(20)	2546(15)	49(7)

Table 34. Torsion angles [°] for **14d**.

B(1)-O(1)-N(2)-C(11)	-85.5(2)
B(1)-O(1)-N(2)-C(7)	97.7(2)
C(1)-N(1)-B(1)-O(1)	179.08(18)
C(5)-N(1)-B(1)-O(1)	-2.2(3)
C(1)-N(1)-B(1)-C(4)	-1.2(3)
C(5)-N(1)-B(1)-C(4)	177.53(19)
N(2)-O(1)-B(1)-N(1)	177.08(16)
N(2)-O(1)-B(1)-C(4)	-2.6(3)
B(1)-N(1)-C(1)-C(2)	-0.1(3)
C(5)-N(1)-C(1)-C(2)	-178.9(2)
N(1)-C(1)-C(2)-C(3)	0.9(4)
C(1)-C(2)-C(3)-C(4)	-0.3(4)

C(2)-C(3)-C(4)-B(1)	-0.9(3)
N(1)-B(1)-C(4)-C(3)	1.7(3)
O(1)-B(1)-C(4)-C(3)	-178.6(2)
C(1)-N(1)-C(5)-C(6)	93.1(3)
B(1)-N(1)-C(5)-C(6)	-85.6(3)
C(11)-N(2)-C(7)-C(8)	0.5(3)
O(1)-N(2)-C(7)-C(8)	177.14(18)
N(2)-C(7)-C(8)-C(9)	-1.0(3)
C(7)-C(8)-C(9)-C(10)	1.2(3)
C(8)-C(9)-C(10)-C(11)	-0.9(3)
C(7)-N(2)-C(11)-C(10)	-0.2(3)
O(1)-N(2)-C(11)-C(10)	-176.87(18)
C(9)-C(10)-C(11)-N(2)	0.4(3)
O(3)-S(1)-C(12)-F(2)	60.0(2)
O(4)-S(1)-C(12)-F(2)	-59.97(19)
O(2)-S(1)-C(12)-F(2)	-178.74(17)
O(3)-S(1)-C(12)-F(3)	-60.99(19)
O(4)-S(1)-C(12)-F(3)	178.99(16)
O(2)-S(1)-C(12)-F(3)	60.22(18)
O(3)-S(1)-C(12)-F(1)	179.33(17)
O(4)-S(1)-C(12)-F(1)	59.31(19)
O(2)-S(1)-C(12)-F(1)	-59.46(19)

Symmetry transformations used to generate equivalent atoms:

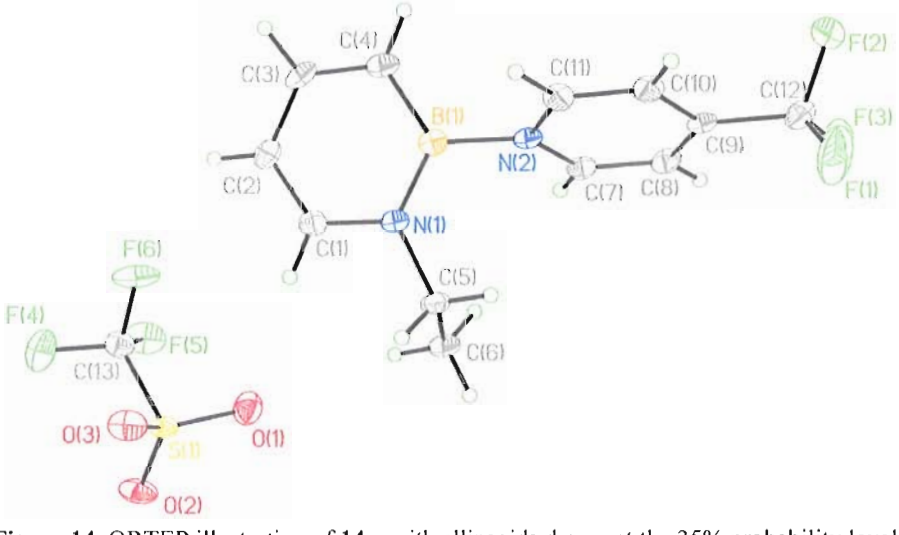

Figure 14. ORTEP illustration of **14g**, with ellipsoids drawn at the 35% probability level.

X-ray Crystal Structure Determination. Crystals of **14g** suitable for X-ray diffraction were obtained by seeding an oil of **14g** oil with **14a**.

Diffraction intensity data were collected with a Bruker Smart Apex CCD diffractometer at 173(2) K using MoKα - radiation (0.71073 Å). The structure was solved using direct methods, completed by subsequent difference Fourier syntheses, and refined by full matrix least-squares procedures on F^2. All non-H atoms were refined with anisotropic thermal parameters. H atoms were found on the residual density map and refined with isotropic thermal parameters. The Flack parameter is 0.00(8). All software and sources scattering factors are contained in the SHELXTL (6.10) program package (G.Sheldrick, Bruker XRD, Madison, WI). Crystallographic data and some details of data collection and crystal structure refinement for $C_{13}H_{13}BF_6N_2O_3S$ are given in the following tables.

Table 35. Crystal data and structure refinement for **14g** (liu56).

Identification code	liu56	
Empirical formula	C_{13} H_{13} B F_6 N_2 O_3 S	
Formula weight	402.12	
Temperature	173(2) K	
Wavelength	0.71073 Å	
Crystal system	Monoclinic	
Space group	P2(1)/c	
Unit cell dimensions	a = 7.206(2) Å	α = 90°.
	b = 16.671(5) Å	β = 96.233(5) °.
	c = 13.755(4) Å	γ = 90°.
Volume	1642.6(9) Å ^{3}	
Z	4	
Density (calculated)	1.626 Mg/m^3	
Absorption coefficient	0.278 mm^{-1}	
F(000)	816	
Crystal size	0.39 x 0.09 x 0.03 mm^3	
Theta range for data collection	1.93 to 25.00°.	
Index ranges	-8<=h<=8, -19<=k<=19, -16<=l<=16	
Reflections collected	14523	
Independent reflections	2902 [R(int) = 0.0790]	
Completeness to theta = 25.00°	100.0 %	
Absorption correction	Semi-empirical from equivalents	

Max. and min. transmission	0.9917 and 0.8993
Refinement method	Full-matrix least-squares on F^2
Data / restraints / parameters	2902 / 0 / 287
Goodness-of-fit on F^2	1.006
Final R indices [I>2sigma(I)]	R1 = 0.0558, wR2 = 0.1251
R indices (all data)	R1 = 0.0894, wR2 = 0.1415
Largest diff. peak and hole	0.342 and -0.361 e. Å $^{-3}$

Table 36. Atomic coordinates (x 10^4) and equivalent isotropic displacement parameters (Å^{2}x 10^3) for **14g**. U(eq) is defined as one third of the trace of the orthogonalized U^{ij} tensor.

	x	y	z	U(eq)
S(1)	1906(1)	7273(1)	2371(1)	27(1)
O(1)	2701(4)	6493(2)	2297(2)	43(1)
O(2)	2268(4)	7827(2)	1615(2)	44(1)
O(3)	33(3)	7288(2)	2643(2)	41(1)
N(1)	2125(4)	4381(2)	4147(2)	24(1)
N(2)	2408(4)	2926(2)	4689(2)	24(1)
B(1)	2431(5)	3822(2)	4925(3)	24(1)
F(1)	765(4)	187(2)	3705(2)	82(1)
F(2)	2550(5)	1(1)	4981(2)	71(1)
F(3)	3679(4)	179(2)	3652(2)	72(1)
F(4)	2723(4)	8426(2)	3635(2)	66(1)
F(5)	5074(3)	7714(2)	3339(2)	51(1)
F(6)	3078(3)	7246(2)	4239(2)	54(1)
C(1)	2179(5)	5181(2)	4362(3)	29(1)
C(2)	2473(5)	5451(2)	5297(3)	32(1)
C(3)	2736(5)	4921(2)	6092(3)	33(1)
C(4)	2714(5)	4112(2)	5949(3)	32(1)
C(5)	1597(5)	4171(2)	3106(3)	29(1)
C(6)	3116(6)	4371(3)	2468(3)	36(1)
C(7)	3653(5)	2593(2)	4144(2)	27(1)
C(8)	3695(5)	1787(2)	3968(3)	28(1)
C(9)	2399(5)	1308(2)	4352(2)	25(1)
C(10)	1137(5)	1642(2)	4913(3)	29(1)
C(11)	1165(5)	2453(2)	5080(3)	28(1)
C(12)	2368(5)	423(2)	4166(3)	34(1)
C(13)	3248(5)	7684(2)	3435(3)	35(1)

Table 37. Bond lengths [Å] and angles [°] for **14g**.

S(1)-O(1)	1.429(3)
S(1)-O(2)	1.436(3)
S(1)-O(3)	1.439(3)
S(1)-C(13)	1.800(4)
N(1)-C(1)	1.367(5)
N(1)-B(1)	1.418(5)
N(1)-C(5)	1.483(4)
N(2)-C(11)	1.348(4)

N(2)-C(7)	1.349(4)
N(2)-B(1)	1.528(5)
B(1)-C(4)	1.481(5)
F(1)-C(12)	1.316(4)
F(2)-C(12)	1.319(4)
F(3)-C(12)	1.305(4)
F(4)-C(13)	1.331(4)
F(5)-C(13)	1.338(4)
F(6)-C(13)	1.342(4)
C(1)-C(2)	1.356(5)
C(1)-H(1)	0.97(3)
C(2)-C(3)	1.403(6)
C(2)-H(2)	0.90(4)
C(3)-C(4)	1.363(5)
C(3)-H(3)	0.97(4)
C(4)-H(4)	0.93(4)
C(5)-C(6)	1.513(5)
C(5)-H(5A)	0.96(3)
C(5)-H(5B)	0.97(3)
C(6)-H(6A)	0.93(4)
C(6)-H(6B)	0.97(4)
C(6)-H(6C)	0.98(4)
C(7)-C(8)	1.367(5)
C(7)-H(7)	0.86(3)
C(8)-C(9)	1.378(5)
C(8)-H(8)	0.91(4)
C(9)-C(10)	1.373(5)
C(9)-C(12)	1.497(5)
C(10)-C(11)	1.370(5)
C(10)-H(10)	0.88(3)
C(11)-H(11)	0.93(3)
O(1)-S(1)-O(2)	115.30(16)
O(1)-S(1)-O(3)	115.44(17)
O(2)-S(1)-O(3)	115.24(16)
O(1)-S(1)-C(13)	102.74(18)
O(2)-S(1)-C(13)	102.67(17)
O(3)-S(1)-C(13)	102.61(17)
C(1)-N(1)-B(1)	118.7(3)
C(1)-N(1)-C(5)	115.9(3)
B(1)-N(1)-C(5)	125.2(3)
C(11)-N(2)-C(7)	119.4(3)
C(11)-N(2)-B(1)	118.7(3)
C(7)-N(2)-B(1)	121.9(3)
N(1)-B(1)-C(4)	119.8(3)
N(1)-B(1)-N(2)	119.0(3)
C(4)-B(1)-N(2)	121.2(3)
C(2)-C(1)-N(1)	121.8(3)
C(2)-C(1)-H(1)	122(2)
N(1)-C(1)-H(1)	116(2)
C(1)-C(2)-C(3)	121.6(4)
C(1)-C(2)-H(2)	119(2)
C(3)-C(2)-H(2)	120(2)
C(4)-C(3)-C(2)	120.9(3)

C(4)-C(3)-H(3)	122(3)
C(2)-C(3)-H(3)	117(3)
C(3)-C(4)-B(1)	117.3(4)
C(3)-C(4)-H(4)	118(2)
B(1)-C(4)-H(4)	124(2)
N(1)-C(5)-C(6)	112.5(3)
N(1)-C(5)-H(5A)	108(2)
C(6)-C(5)-H(5A)	109(2)
N(1)-C(5)-H(5B)	108.5(19)
C(6)-C(5)-H(5B)	110.1(19)
H(5A)-C(5)-H(5B)	108(3)
C(5)-C(6)-H(6A)	109(2)
C(5)-C(6)-H(6B)	109(2)
H(6A)-C(6)-H(6B)	112(3)
C(5)-C(6)-H(6C)	115(2)
H(6A)-C(6)-H(6C)	108(3)
H(6B)-C(6)-H(6C)	105(3)
N(2)-C(7)-C(8)	122.2(3)
N(2)-C(7)-H(7)	117(2)
C(8)-C(7)-H(7)	121(2)
C(7)-C(8)-C(9)	118.2(3)
C(7)-C(8)-H(8)	122(3)
C(9)-C(8)-H(8)	120(3)
C(10)-C(9)-C(8)	119.9(3)
C(10)-C(9)-C(12)	119.9(3)
C(8)-C(9)-C(12)	120.2(3)
C(11)-C(10)-C(9)	119.7(3)
C(11)-C(10)-H(10)	119(2)
C(9)-C(10)-H(10)	121(2)
N(2)-C(11)-C(10)	120.6(3)
N(2)-C(11)-H(11)	115(2)
C(10)-C(11)-H(11)	124(2)
F(3)-C(12)-F(1)	107.2(3)
F(3)-C(12)-F(2)	106.5(3)
F(1)-C(12)-F(2)	104.5(3)
F(3)-C(12)-C(9)	113.7(3)
F(1)-C(12)-C(9)	111.9(3)
F(2)-C(12)-C(9)	112.4(3)
F(4)-C(13)-F(5)	106.9(3)
F(4)-C(13)-F(6)	106.4(3)
F(5)-C(13)-F(6)	106.3(3)
F(4)-C(13)-S(1)	112.5(3)
F(5)-C(13)-S(1)	112.4(3)
F(6)-C(13)-S(1)	111.9(3)

Table 38. Anisotropic displacement parameters ($Å^2 x\ 10^3$)for **14g**. The anisotropic displacement factor exponent takes the form: $-2p^2[\ h^2a^{*2}U^{11} + ... + 2\ h\ k\ a^*\ b^*\ U^{12}\ ]$

	U^{11}	U^{22}	U^{33}	U^{23}	U^{13}	U^{12}
S(1)	26(1)	36(1)	20(1)	5(1)	8(1)	2(1)
O(1)	49(2)	39(2)	44(2)	-5(1)	15(1)	3(1)
O(2)	42(2)	63(2)	29(2)	21(1)	11(1)	3(1)

O(3)	23(1)	65(2)	38(2)	8(1)	9(1)	0(1)
N(1)	21(2)	31(2)	20(2)	1(1)	2(1)	-1(1)
N(2)	21(2)	33(2)	16(1)	1(1)	3(1)	1(1)
B(1)	16(2)	32(2)	26(2)	0(2)	8(2)	-2(2)
F(1)	67(2)	53(2)	117(3)	-34(2)	-32(2)	-6(1)
F(2)	141(3)	37(1)	37(1)	5(1)	17(2)	3(2)
F(3)	89(2)	41(2)	98(2)	-18(2)	62(2)	-3(1)
F(4)	78(2)	48(2)	70(2)	-22(1)	9(2)	-2(1)
F(5)	29(1)	69(2)	53(2)	11(1)	3(1)	-13(1)
F(6)	50(2)	89(2)	24(1)	16(1)	1(1)	-15(1)
C(1)	30(2)	31(2)	28(2)	3(2)	10(2)	-1(2)
C(2)	30(2)	35(2)	32(2)	-8(2)	11(2)	-3(2)
C(3)	28(2)	48(3)	22(2)	-11(2)	7(2)	-1(2)
C(4)	29(2)	45(2)	22(2)	2(2)	6(2)	0(2)
C(5)	35(2)	34(2)	18(2)	1(2)	-1(2)	-2(2)
C(6)	48(3)	43(3)	19(2)	3(2)	9(2)	0(2)
C(7)	25(2)	35(2)	21(2)	2(2)	7(2)	-3(2)
C(8)	25(2)	39(2)	22(2)	-2(2)	9(2)	4(2)
C(9)	25(2)	35(2)	14(2)	-1(1)	4(1)	1(2)
C(10)	31(2)	34(2)	25(2)	3(2)	13(2)	-6(2)
C(11)	25(2)	34(2)	27(2)	4(2)	15(2)	1(2)
C(12)	38(2)	37(2)	27(2)	-7(2)	8(2)	-7(2)
C(13)	33(2)	39(2)	34(2)	5(2)	6(2)	-1(2)

Table 39. Hydrogen coordinates (x 10^4) and isotropic displacement parameters ($Å^2$x 10^3) for **14g**.

	x	y	z	U(eq)
H(1)	1950(40)	5540(20)	3810(30)	22(9)
H(2)	2510(50)	5980(20)	5410(30)	29(10)
H(3)	2950(50)	5160(20)	6740(30)	54(13)
H(4)	2930(50)	3780(20)	6490(30)	38(11)
H(5A)	480(50)	4460(20)	2880(20)	25(9)
H(5B)	1310(40)	3600(20)	3060(20)	18(9)
H(6A)	2720(50)	4230(20)	1820(30)	44(12)
H(6B)	4240(50)	4090(20)	2720(30)	30(10)
H(6C)	3480(50)	4940(20)	2470(30)	39(11)
H(7)	4430(50)	2910(20)	3920(20)	24(10)
H(8)	4550(60)	1560(30)	3610(30)	60(13)
H(10)	300(50)	1350(20)	5170(20)	24(9)
H(11)	400(50)	2710(20)	5480(20)	27(9)

Table 40. Torsion angles [°] for **14g**.

C(1)-N(1)-B(1)-C(4)	2.8(5)
C(5)-N(1)-B(1)-C(4)	-172.2(3)
C(1)-N(1)-B(1)-N(2)	-178.9(3)
C(5)-N(1)-B(1)-N(2)	6.2(5)
C(11)-N(2)-B(1)-N(1)	-121.2(3)
C(7)-N(2)-B(1)-N(1)	62.3(4)
C(11)-N(2)-B(1)-C(4)	57.1(4)
C(7)-N(2)-B(1)-C(4)	-119.4(4)

B(1)-N(1)-C(1)-C(2)	-1.6(5)
C(5)-N(1)-C(1)-C(2)	173.8(3)
N(1)-C(1)-C(2)-C(3)	0.0(6)
C(1)-C(2)-C(3)-C(4)	0.3(6)
C(2)-C(3)-C(4)-B(1)	0.9(5)
N(1)-B(1)-C(4)-C(3)	-2.4(5)
N(2)-B(1)-C(4)-C(3)	179.3(3)
C(1)-N(1)-C(5)-C(6)	71.6(4)
B(1)-N(1)-C(5)-C(6)	-113.4(4)
C(11)-N(2)-C(7)-C(8)	0.3(5)
B(1)-N(2)-C(7)-C(8)	176.9(3)
N(2)-C(7)-C(8)-C(9)	0.9(5)
C(7)-C(8)-C(9)-C(10)	-1.4(5)
C(7)-C(8)-C(9)-C(12)	179.0(3)
C(8)-C(9)-C(10)-C(11)	0.6(5)
C(12)-C(9)-C(10)-C(11)	-179.8(3)
C(7)-N(2)-C(11)-C(10)	-1.2(5)
B(1)-N(2)-C(11)-C(10)	-177.8(3)
C(9)-C(10)-C(11)-N(2)	0.7(6)
C(10)-C(9)-C(12)-F(3)	-177.7(3)
C(8)-C(9)-C(12)-F(3)	1.9(5)
C(10)-C(9)-C(12)-F(1)	60.7(5)
C(8)-C(9)-C(12)-F(1)	-119.7(4)
C(10)-C(9)-C(12)-F(2)	-56.6(5)
C(8)-C(9)-C(12)-F(2)	123.0(4)
O(1)-S(1)-C(13)-F(4)	179.7(3)
O(2)-S(1)-C(13)-F(4)	59.7(3)
O(3)-S(1)-C(13)-F(4)	-60.1(3)
O(1)-S(1)-C(13)-F(5)	59.0(3)
O(2)-S(1)-C(13)-F(5)	-61.0(3)
O(3)-S(1)-C(13)-F(5)	179.2(3)
O(1)-S(1)-C(13)-F(6)	-60.5(3)
O(2)-S(1)-C(13)-F(6)	179.5(3)
O(3)-S(1)-C(13)-F(6)	59.6(3)

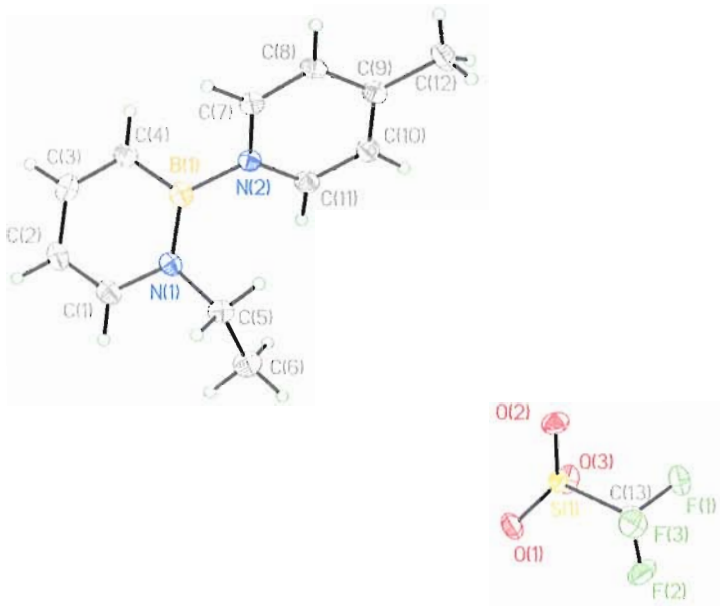

Figure 15. ORTEP illustration of **14h**, with ellipsoids drawn at the 35% probability level.

X-ray Crystal Structure Determination. Crystals of **14h** suitable for X-ray diffraction were obtained by seeding the oil of **14h** with crystals of **14a**.

Diffraction intensity data were collected with a Bruker Smart Apex CCD diffractometer at 173(2) K using MoKα - radiation (0.71073 Å). The structure was solved using direct methods, completed by subsequent difference Fourier syntheses, and refined by full matrix least-squares procedures on F^2. All non-H atoms were refined with anisotropic thermal parameters. H atoms were found on the residual density map and refined with isotropic thermal parameters. The Flack parameter is 0.00(8). All software and sources scattering factors are contained in the SHELXTL (6.10) program package (G.Sheldrick, Bruker XRD, Madison, WI). Crystallographic data and some details of data collection and crystal structure refinement for $C_{13}H_{16}BF_3N_2O_3S$ are given in the following tables.

Table 41. Crystal data and structure refinement for **14h** (liu42a).

Identification code	liu42a	
Empirical formula	C_{13} H_{16} B F_3 N_2 O_3 S	
Formula weight	348.15	
Temperature	173(2) K	
Wavelength	0.71073 Å	
Crystal system	Orthorhombic	
Space group	Pbca	
Unit cell dimensions	a = 13.9209(8) Å	α = 90°.
	b = 13.1486(8) Å	β = 90°.
	c = 17.8275(11) Å	γ = 90°.
Volume	3263.2(3) $Å^3$	
Z	8	
Density (calculated)	1.417 Mg/m^3	
Absorption coefficient	0.243 mm^{-1}	
F(000)	1440	
Crystal size	0.22 x 0.12 x 0.09 mm^3	
Theta range for data collection	2.28 to 25.00°.	
Index ranges	-16<=h<=16, -15<=k<=15, -21<=l<=21	
Reflections collected	24679	
Independent reflections	2874 [R(int) = 0.0819]	
Completeness to theta = 25.00°	100.0 %	
Absorption correction	Semi-empirical from equivalents	
Max. and min. transmission	0.9785 and 0.9486	
Refinement method	Full-matrix least-squares on F^2	
Data / restraints / parameters	2874 / 0 / 272	
Goodness-of-fit on F^2	1.004	
Final R indices [I>2sigma(I)]	R1 = 0.0400, wR2 = 0.0805	
R indices (all data)	R1 = 0.0703, wR2 = 0.0952	
Largest diff. peak and hole	0.213 and -0.273 $e.Å^{-3}$	

Table 42. Atomic coordinates (x 10^4) and equivalent isotropic displacement parameters ($Å^2$x 10^3) for **14h**. U(eq) is defined as one third of the trace of the orthogonalized U^{ij} tensor.

	x	y	z	U(eq)
S(1)	2421(1)	7612(1)	1820(1)	29(1)
O(1)	2516(1)	7660(2)	2621(1)	46(1)
O(2)	1899(1)	6762(1)	1539(1)	44(1)
O(3)	3284(1)	7869(1)	1419(1)	44(1)
F(1)	1456(1)	8748(1)	873(1)	51(1)
F(2)	1986(1)	9562(1)	1831(1)	59(1)

F(3)	772(1)	8566(1)	1939(1)	47(1)
N(1)	744(1)	939(2)	4339(1)	28(1)
N(2)	124(1)	468(2)	3043(1)	27(1)
B(1)	679(2)	211(2)	3756(2)	30(1)
C(1)	1229(2)	690(2)	4983(2)	34(1)
C(2)	1639(2)	-235(2)	5091(2)	37(1)
C(3)	1598(2)	-986(2)	4527(2)	36(1)
C(4)	1137(2)	-803(2)	3864(2)	33(1)
C(5)	291(2)	1962(2)	4338(2)	32(1)
C(6)	1009(2)	2817(2)	4298(2)	42(1)
C(7)	-635(2)	-115(2)	2842(2)	30(1)
C(8)	-1130(2)	56(2)	2191(2)	30(1)
C(9)	-868(2)	849(2)	1719(1)	31(1)
C(10)	-74(2)	1432(2)	1927(2)	34(1)
C(11)	401(2)	1230(2)	2582(2)	33(1)
C(12)	-1414(3)	1076(3)	1016(2)	50(1)
C(13)	1625(2)	8672(2)	1609(2)	34(1)

Table 43. Bond lengths [Å] and angles [°] for **14h**.

S(1)-O(2)	1.4242(18)
S(1)-O(1)	1.4350(18)
S(1)-O(3)	1.4379(18)
S(1)-C(13)	1.820(3)
F(1)-C(13)	1.336(3)
F(2)-C(13)	1.333(3)
F(3)-C(13)	1.334(3)
N(1)-C(1)	1.371(3)
N(1)-B(1)	1.416(4)
N(1)-C(5)	1.486(3)
N(2)-C(11)	1.352(3)
N(2)-C(7)	1.353(3)
N(2)-B(1)	1.526(4)
B(1)-C(4)	1.489(4)
C(1)-C(2)	1.358(4)
C(1)-H(1)	0.93(2)
C(2)-C(3)	1.410(4)
C(2)-H(5)	0.95(3)
C(3)-C(4)	1.367(4)
C(3)-H(3)	0.98(2)
C(4)-H(4)	0.93(3)
C(5)-C(6)	1.505(4)
C(5)-H(5A)	0.98(3)
C(5)-H(5B)	0.97(2)
C(6)-H(6A)	1.02(3)
C(6)-H(6B)	0.98(3)
C(6)-H(6C)	1.00(3)
C(7)-C(8)	1.370(4)
C(7)-H(7)	0.97(3)
C(8)-C(9)	1.388(4)
C(8)-H(8)	0.95(3)
C(9)-C(10)	1.395(4)
C(9)-C(12)	1.495(4)

C(10)-C(11)	1.368(4)
C(10)-H(10)	0.95(3)
C(11)-H(11)	0.96(3)
C(12)-H(12A)	0.97(4)
C(12)-H(12B)	0.96(4)
C(12)-H(12C)	0.82(4)
O(2)-S(1)-O(1)	115.58(12)
O(2)-S(1)-O(3)	115.77(12)
O(1)-S(1)-O(3)	114.03(12)
O(2)-S(1)-C(13)	102.59(12)
O(1)-S(1)-C(13)	103.23(12)
O(3)-S(1)-C(13)	103.06(12)
C(1)-N(1)-B(1)	119.0(2)
C(1)-N(1)-C(5)	115.3(2)
B(1)-N(1)-C(5)	125.7(2)
C(11)-N(2)-C(7)	118.8(2)
C(11)-N(2)-B(1)	121.8(2)
C(7)-N(2)-B(1)	119.3(2)
N(1)-B(1)-C(4)	118.9(2)
N(1)-B(1)-N(2)	119.6(2)
C(4)-B(1)-N(2)	121.5(2)
C(2)-C(1)-N(1)	122.7(3)
C(2)-C(1)-H(1)	121.0(15)
N(1)-C(1)-H(1)	116.4(15)
C(1)-C(2)-C(3)	120.6(3)
C(1)-C(2)-H(5)	119.2(16)
C(3)-C(2)-H(5)	120.2(16)
C(4)-C(3)-C(2)	120.8(3)
C(4)-C(3)-H(3)	120.1(14)
C(2)-C(3)-H(3)	119.0(14)
C(3)-C(4)-B(1)	118.0(3)
C(3)-C(4)-H(4)	119.8(16)
B(1)-C(4)-H(4)	122.1(16)
N(1)-C(5)-C(6)	113.2(2)
N(1)-C(5)-H(5A)	106.8(15)
C(6)-C(5)-H(5A)	110.7(15)
N(1)-C(5)-H(5B)	108.0(14)
C(6)-C(5)-H(5B)	111.5(14)
H(5A)-C(5)-H(5B)	106(2)
C(5)-C(6)-H(6A)	110.9(17)
C(5)-C(6)-H(6B)	112.3(16)
H(6A)-C(6)-H(6B)	109(2)
C(5)-C(6)-H(6C)	111.0(16)
H(6A)-C(6)-H(6C)	108(2)
H(6B)-C(6)-H(6C)	105(2)
N(2)-C(7)-C(8)	121.6(3)
N(2)-C(7)-H(7)	116.8(15)
C(8)-C(7)-H(7)	121.6(15)
C(7)-C(8)-C(9)	120.3(3)
C(7)-C(8)-H(8)	120.3(15)
C(9)-C(8)-H(8)	119.3(15)
C(8)-C(9)-C(10)	117.4(2)
C(8)-C(9)-C(12)	121.6(3)

C(10)-C(9)-C(12)	121.0(3)
C(11)-C(10)-C(9)	120.2(3)
C(11)-C(10)-H(10)	116.0(16)
C(9)-C(10)-H(10)	123.7(16)
N(2)-C(11)-C(10)	121.6(3)
N(2)-C(11)-H(11)	115.9(15)
C(10)-C(11)-H(11)	122.5(15)
C(9)-C(12)-H(12A)	111(2)
C(9)-C(12)-H(12B)	109(2)
H(12A)-C(12)-H(12B)	107(3)
C(9)-C(12)-H(12C)	111(3)
H(12A)-C(12)-H(12C)	106(3)
H(12B)-C(12)-H(12C)	112(4)
F(2)-C(13)-F(3)	107.3(2)
F(2)-C(13)-F(1)	107.0(2)
F(3)-C(13)-F(1)	106.5(2)
F(2)-C(13)-S(1)	112.39(18)
F(3)-C(13)-S(1)	111.73(18)
F(1)-C(13)-S(1)	111.56(18)

Table 44. Anisotropic displacement parameters ($Å^2$x 10^3)for **14h**. The anisotropic displacement factor exponent takes the form: $-2p^2[h^2a^{*2}U^{11} + ... + 2 h k a^* b^* U^{12}]$

	U^{11}	U^{22}	U^{33}	U^{23}	U^{13}	U^{12}
S(1)	28(1)	29(1)	30(1)	0(1)	-2(1)	0(1)
O(1)	51(1)	59(1)	29(1)	0(1)	-8(1)	13(1)
O(2)	40(1)	33(1)	59(1)	-8(1)	-6(1)	-6(1)
O(3)	29(1)	48(1)	54(1)	13(1)	10(1)	2(1)
F(1)	51(1)	62(1)	40(1)	11(1)	-9(1)	8(1)
F(2)	55(1)	30(1)	92(1)	-8(1)	-21(1)	3(1)
F(3)	32(1)	59(1)	52(1)	-7(1)	3(1)	10(1)
N(1)	22(1)	35(1)	27(1)	1(1)	-1(1)	-2(1)
N(2)	24(1)	28(1)	29(1)	0(1)	1(1)	-3(1)
B(1)	20(2)	39(2)	30(2)	4(1)	2(1)	-5(1)
C(1)	30(2)	44(2)	29(2)	-1(1)	0(1)	-7(1)
C(2)	29(2)	51(2)	31(2)	10(1)	-2(1)	-3(1)
C(3)	27(2)	36(2)	45(2)	8(1)	4(1)	4(1)
C(4)	32(2)	37(2)	31(2)	-3(1)	1(1)	0(1)
C(5)	25(2)	34(2)	37(2)	-4(1)	0(1)	0(1)
C(6)	35(2)	41(2)	50(2)	-1(2)	2(2)	-6(1)
C(7)	26(2)	30(2)	33(2)	-2(1)	4(1)	-2(1)
C(8)	23(1)	36(2)	32(2)	-9(1)	-1(1)	-3(1)
C(9)	29(2)	35(2)	30(2)	-4(1)	0(1)	0(1)
C(10)	35(2)	35(2)	32(2)	4(1)	-1(1)	-5(1)
C(11)	30(2)	35(2)	33(2)	-1(1)	-2(1)	-9(1)
C(12)	54(2)	59(2)	37(2)	4(2)	-17(2)	-4(2)
C(13)	30(2)	35(2)	36(2)	-4(1)	-4(1)	-2(1)

Table 45. Hydrogen coordinates (x 10^4) and isotropic displacement parameters (Å^{2}x 10^3) for **14h**.

	x	y	z	U(eq)
H(1)	1266(17)	1195(18)	5350(14)	29(7)
H(3)	1891(17)	-1652(18)	4622(13)	30(7)
H(4)	1101(18)	-1310(19)	3504(14)	38(8)
H(5)	1955(18)	-372(19)	5552(15)	37(8)
H(5A)	-93(18)	2011(18)	4796(14)	32(7)
H(5B)	-161(18)	1989(17)	3922(14)	29(7)
H(6A)	670(20)	3500(20)	4291(15)	58(9)
H(6B)	1420(20)	2770(20)	3859(16)	49(9)
H(6C)	1450(20)	2800(20)	4739(16)	49(9)
H(7)	-791(18)	-680(20)	3169(14)	37(7)
H(8)	-1663(19)	-362(19)	2059(14)	36(8)
H(10)	175(18)	1972(19)	1634(14)	38(8)
H(11)	957(18)	1610(18)	2740(13)	33(7)
H(12A)	-990(30)	1330(30)	620(20)	89(13)
H(12B)	-1880(30)	1600(30)	1120(20)	109(16)
H(12C)	-1660(30)	560(30)	850(20)	95(16)

Table 46. Torsion angles [°] for **14h**.

C(1)-N(1)-B(1)-C(4)	0.1(4)
C(5)-N(1)-B(1)-C(4)	-176.9(2)
C(1)-N(1)-B(1)-N(2)	178.8(2)
C(5)-N(1)-B(1)-N(2)	1.7(4)
C(11)-N(2)-B(1)-N(1)	63.1(3)
C(7)-N(2)-B(1)-N(1)	-120.6(3)
C(11)-N(2)-B(1)-C(4)	-118.3(3)
C(7)-N(2)-B(1)-C(4)	58.0(3)
B(1)-N(1)-C(1)-C(2)	-1.1(4)
C(5)-N(1)-C(1)-C(2)	176.3(2)
N(1)-C(1)-C(2)-C(3)	1.4(4)
C(1)-C(2)-C(3)-C(4)	-0.7(4)
C(2)-C(3)-C(4)-B(1)	-0.1(4)
N(1)-B(1)-C(4)-C(3)	0.4(4)
N(2)-B(1)-C(4)-C(3)	-178.2(2)
C(1)-N(1)-C(5)-C(6)	70.5(3)
B(1)-N(1)-C(5)-C(6)	-112.4(3)
C(11)-N(2)-C(7)-C(8)	-0.7(4)
B(1)-N(2)-C(7)-C(8)	-177.1(2)
N(2)-C(7)-C(8)-C(9)	-0.6(4)
C(7)-C(8)-C(9)-C(10)	1.6(4)
C(7)-C(8)-C(9)-C(12)	-178.0(3)
C(8)-C(9)-C(10)-C(11)	-1.4(4)
C(12)-C(9)-C(10)-C(11)	178.2(3)
C(7)-N(2)-C(11)-C(10)	0.9(4)
B(1)-N(2)-C(11)-C(10)	177.3(3)
C(9)-C(10)-C(11)-N(2)	0.2(4)
O(2)-S(1)-C(13)-F(2)	-179.96(19)
O(1)-S(1)-C(13)-F(2)	59.6(2)
O(3)-S(1)-C(13)-F(2)	-59.4(2)

O(2)-S(1)-C(13)-F(3)	59.4(2)
O(1)-S(1)-C(13)-F(3)	-61.1(2)
O(3)-S(1)-C(13)-F(3)	179.97(18)
O(2)-S(1)-C(13)-F(1)	-59.7(2)
O(1)-S(1)-C(13)-F(1)	179.81(18)
O(3)-S(1)-C(13)-F(1)	60.9(2)

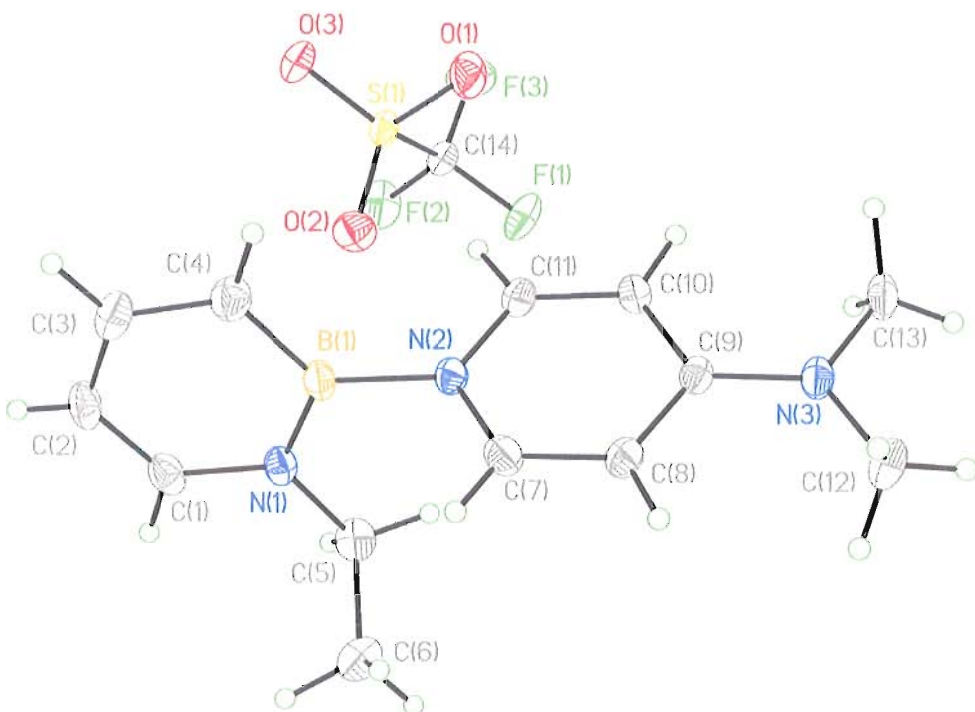

Figure 16. ORTEP illustration of **14i**, with ellipsoids drawn at the 35% probability level.

X-ray Crystal Structure Determination. Crystals of **14i** suitable for X-ray diffraction were obtained by seeding the oil of **14i** with crystals of **14a**.

Diffraction intensity data were collected with a Bruker Smart Apex CCD diffractometer at 173(2) K using MoKα - radiation (0.71073 Å). The structure was solved using direct methods, completed by subsequent difference Fourier syntheses, and refined by full matrix least-squares procedures on F^2. All non-H atoms were refined with

anisotropic thermal parameters. H atoms were found on the residual density map and refined with isotropic thermal parameters. The Flack parameter is 0.00(8). All software and sources scattering factors are contained in the SHELXTL (6.10) program package (G.Sheldrick, Bruker XRD, Madison, WI). Crystallographic data and some details of data collection and crystal structure refinement for $C_{14}H_{19}BF_3N_3O_3S$ are given in the following tables.

Table 47. Crystal data and structure refinement for **14i** (liu54).

Identification code	liu54	
Empirical formula	C_{14} H_{19} B F_3 N_3 O_3 S	
Formula weight	377.19	
Temperature	173(2) K	
Wavelength	0.71073 Å	
Crystal system	Triclinic	
Space group	P-1	
Unit cell dimensions	a = 8.9833(17) Å	α = 69.556(3)°.
	b = 9.9383(19) Å	β = 73.803(3)°.
	c = 10.988(2) Å	γ = 73.958(3)°.
Volume	865.1(3) $Å^3$	
Z	2	
Density (calculated)	1.448 Mg/m^3	
Absorption coefficient	0.236 mm^{-1}	
F(000)	392	
Crystal size	0.18 x 0.12 x 0.08 mm^3	
Theta range for data collection	2.02 to 25.00°.	
Index ranges	-10<=h<=10, -11<=k<=11, -13<=l<=13	
Reflections collected	8158	
Independent reflections	3025 [R(int) = 0.0309]	
Completeness to theta = 25.00°	99.5 %	
Absorption correction	Semi-empirical from equivalents	
Max. and min. transmission	0.9813 and 0.9587	
Refinement method	Full-matrix least-squares on F^2	
Data / restraints / parameters	3025 / 0 / 302	
Goodness-of-fit on F^2	1.047	
Final R indices [I>2sigma(I)]	R1 = 0.0539, wR2 = 0.1311	
R indices (all data)	R1 = 0.0694, wR2 = 0.1395	
Largest diff. peak and hole	0.334 and -0.253 $e.Å^{-3}$	

Table 48. Atomic coordinates (x 10^4) and equivalent isotropic displacement parameters ($Å^2$x 10^3) for **14i**. U(eq) is defined as one third of the trace of the orthogonalized U^{ij} tensor.

	x	y	z	U(eq)
S(1)	7566(1)	6446(1)	2182(1)	27(1)
O(1)	8599(3)	5620(3)	3098(3)	45(1)
O(2)	6914(3)	5580(3)	1738(3)	40(1)
O(3)	6481(3)	7694(3)	2509(3)	36(1)
F(1)	10029(3)	6290(3)	235(3)	52(1)
F(2)	8135(3)	8087(3)	-286(2)	50(1)
F(3)	9622(3)	8168(3)	885(3)	58(1)
B(1)	5541(5)	2471(5)	2895(4)	28(1)
N(1)	5143(3)	2870(3)	1632(3)	28(1)
N(2)	7182(3)	1555(3)	3066(3)	26(1)
N(3)	11666(4)	-971(3)	3380(3)	29(1)
C(1)	3649(5)	3621(4)	1477(5)	35(1)
C(2)	2535(5)	3998(4)	2493(5)	38(1)
C(3)	2867(5)	3664(4)	3739(5)	37(1)
C(4)	4323(5)	2902(5)	4000(4)	36(1)
C(5)	6270(5)	2574(5)	442(4)	35(1)
C(6)	6032(6)	1294(5)	132(5)	42(1)
C(7)	7497(5)	94(4)	3227(4)	32(1)
C(8)	8934(5)	-781(4)	3371(4)	31(1)
C(9)	10201(4)	-170(4)	3324(3)	25(1)
C(10)	9833(4)	1342(4)	3205(4)	28(1)
C(11)	8358(4)	2150(4)	3079(4)	28(1)
C(12)	12005(6)	-2552(5)	3577(6)	41(1)
C(13)	12946(5)	-297(5)	3309(5)	36(1)
C(14)	8902(5)	7286(4)	687(4)	35(1)

Table 49. Bond lengths [Å] and angles [°] for **14i**.

S(1)-O(2)	1.433(3)
S(1)-O(3)	1.437(3)
S(1)-O(1)	1.439(3)
S(1)-C(14)	1.826(4)
F(1)-C(14)	1.327(4)
F(2)-C(14)	1.328(5)
F(3)-C(14)	1.327(5)
B(1)-N(1)	1.423(5)
B(1)-C(4)	1.489(6)
B(1)-N(2)	1.527(5)
N(1)-C(1)	1.368(5)
N(1)-C(5)	1.478(5)
N(2)-C(11)	1.352(5)
N(2)-C(7)	1.357(5)
N(3)-C(9)	1.342(4)
N(3)-C(13)	1.455(5)
N(3)-C(12)	1.464(5)
C(1)-C(2)	1.360(6)
C(1)-H(1)	0.96(5)
C(2)-C(3)	1.389(6)

C(2)-H(2)	0.82(5)
C(3)-C(4)	1.370(6)
C(3)-H(3)	0.97(4)
C(4)-H(4)	0.95(4)
C(5)-C(6)	1.508(6)
C(5)-H(5A)	0.95(5)
C(5)-H(5B)	0.88(4)
C(6)-H(6A)	0.91(5)
C(6)-H(6B)	1.01(5)
C(6)-H(6C)	1.01(5)
C(7)-C(8)	1.358(5)
C(7)-H(7)	0.88(4)
C(8)-C(9)	1.412(5)
C(8)-H(8)	0.92(4)
C(9)-C(10)	1.413(5)
C(10)-C(11)	1.362(5)
C(10)-H(10)	0.95(4)
C(11)-H(11)	1.07(3)
C(12)-H(12A)	0.91(5)
C(12)-H(12B)	0.97(5)
C(12)-H(12C)	0.90(5)
C(13)-H(13A)	0.85(5)
C(13)-H(13B)	0.97(5)
C(13)-H(13C)	1.03(5)
O(2)-S(1)-O(3)	115.53(17)
O(2)-S(1)-O(1)	114.92(18)
O(3)-S(1)-O(1)	114.84(18)
O(2)-S(1)-C(14)	102.90(18)
O(3)-S(1)-C(14)	102.73(17)
O(1)-S(1)-C(14)	103.36(18)
N(1)-B(1)-C(4)	118.9(3)
N(1)-B(1)-N(2)	118.0(3)
C(4)-B(1)-N(2)	123.0(4)
C(1)-N(1)-B(1)	118.9(3)
C(1)-N(1)-C(5)	117.0(3)
B(1)-N(1)-C(5)	124.0(3)
C(11)-N(2)-C(7)	117.7(3)
C(11)-N(2)-B(1)	122.0(3)
C(7)-N(2)-B(1)	120.3(3)
C(9)-N(3)-C(13)	120.5(3)
C(9)-N(3)-C(12)	121.2(3)
C(13)-N(3)-C(12)	118.2(3)
C(2)-C(1)-N(1)	122.0(4)
C(2)-C(1)-H(1)	123(3)
N(1)-C(1)-H(1)	115(3)
C(1)-C(2)-C(3)	121.5(4)
C(1)-C(2)-H(2)	121(3)
C(3)-C(2)-H(2)	118(3)
C(4)-C(3)-C(2)	121.0(4)
C(4)-C(3)-H(3)	117(3)
C(2)-C(3)-H(3)	122(3)
C(3)-C(4)-B(1)	117.6(4)
C(3)-C(4)-H(4)	120(3)

B(1)-C(4)-H(4)	122(3)
N(1)-C(5)-C(6)	112.8(4)
N(1)-C(5)-H(5A)	111(3)
C(6)-C(5)-H(5A)	106(3)
N(1)-C(5)-H(5B)	108(3)
C(6)-C(5)-H(5B)	107(3)
H(5A)-C(5)-H(5B)	111(4)
C(5)-C(6)-H(6A)	115(3)
C(5)-C(6)-H(6B)	113(3)
H(6A)-C(6)-H(6B)	106(4)
C(5)-C(6)-H(6C)	111(3)
H(6A)-C(6)-H(6C)	108(4)
H(6B)-C(6)-H(6C)	102(4)
N(2)-C(7)-C(8)	123.3(4)
N(2)-C(7)-H(7)	116(3)
C(8)-C(7)-H(7)	120(3)
C(7)-C(8)-C(9)	120.0(4)
C(7)-C(8)-H(8)	119(2)
C(9)-C(8)-H(8)	121(2)
N(3)-C(9)-C(8)	122.2(3)
N(3)-C(9)-C(10)	122.0(3)
C(8)-C(9)-C(10)	115.8(3)
C(11)-C(10)-C(9)	121.0(4)
C(11)-C(10)-H(10)	119(2)
C(9)-C(10)-H(10)	120(2)
N(2)-C(11)-C(10)	122.1(3)
N(2)-C(11)-H(11)	115.5(18)
C(10)-C(11)-H(11)	121.7(18)
N(3)-C(12)-H(12A)	110(3)
N(3)-C(12)-H(12B)	114(3)
H(12A)-C(12)-H(12B)	102(4)
N(3)-C(12)-H(12C)	111(3)
H(12A)-C(12)-H(12C)	117(4)
H(12B)-C(12)-H(12C)	102(4)
N(3)-C(13)-H(13A)	107(3)
N(3)-C(13)-H(13B)	108(3)
H(13A)-C(13)-H(13B)	101(4)
N(3)-C(13)-H(13C)	116(3)
H(13A)-C(13)-H(13C)	117(4)
H(13B)-C(13)-H(13C)	106(4)
F(3)-C(14)-F(1)	106.8(3)
F(3)-C(14)-F(2)	106.7(3)
F(1)-C(14)-F(2)	107.1(3)
F(3)-C(14)-S(1)	112.5(3)
F(1)-C(14)-S(1)	111.9(3)
F(2)-C(14)-S(1)	111.5(3)

Symmetry transformations used to generate equivalent atoms:

Table 50. Anisotropic displacement parameters ($Å^2 x\ 10^3$)for **14i**. The anisotropic displacement factor exponent takes the form: $-2p^2[\ h^2a^{*2}U^{11} + ... + 2\ h\ k\ a^*\ b^*\ U^{12}\ ]$

	U^{11}	U^{22}	U^{33}	U^{23}	U^{13}	U^{12}
S(1)	24(1)	24(1)	30(1)	-8(1)	-6(1)	2(1)
O(1)	40(2)	52(2)	36(2)	-9(1)	-16(1)	10(1)
O(2)	44(2)	32(2)	47(2)	-10(1)	-11(1)	-11(1)
O(3)	30(2)	30(2)	41(2)	-14(1)	1(1)	1(1)
F(1)	38(1)	55(2)	53(2)	-27(1)	8(1)	5(1)
F(2)	48(2)	51(2)	36(1)	1(1)	-7(1)	-5(1)
F(3)	53(2)	74(2)	62(2)	-36(2)	9(1)	-36(2)
B(1)	20(2)	25(2)	37(3)	-8(2)	-8(2)	-2(2)
N(1)	23(2)	25(2)	32(2)	-5(1)	-6(1)	-6(1)
N(2)	25(2)	22(2)	30(2)	-7(1)	-9(1)	-1(1)
N(3)	24(2)	29(2)	31(2)	-8(1)	-8(1)	2(1)
C(1)	32(2)	26(2)	47(3)	-5(2)	-20(2)	-3(2)
C(2)	24(2)	26(2)	60(3)	-8(2)	-15(2)	1(2)
C(3)	29(2)	28(2)	45(3)	-11(2)	1(2)	-2(2)
C(4)	34(2)	38(2)	34(2)	-10(2)	-8(2)	-2(2)
C(5)	35(2)	36(2)	28(2)	-4(2)	-4(2)	-9(2)
C(6)	46(3)	36(3)	39(3)	-13(2)	-6(2)	-2(2)
C(7)	29(2)	30(2)	39(2)	-10(2)	-12(2)	-6(2)
C(8)	31(2)	23(2)	40(2)	-11(2)	-10(2)	0(2)
C(9)	25(2)	26(2)	21(2)	-6(2)	-5(2)	0(2)
C(10)	23(2)	29(2)	31(2)	-7(2)	-7(2)	-4(2)
C(11)	27(2)	24(2)	31(2)	-7(2)	-5(2)	-2(2)
C(12)	38(3)	28(2)	52(3)	-13(2)	-12(2)	8(2)
C(13)	21(2)	40(3)	43(3)	-13(2)	-9(2)	4(2)
C(14)	29(2)	37(2)	39(2)	-19(2)	-6(2)	2(2)

Table 51. Hydrogen coordinates ($x\ 10^4$) and isotropic displacement parameters ($Å^2 x\ 10^3$) for **14i**.

	x	y	z	U(eq)
H(1)	3440(50)	3820(50)	610(50)	48(13)
H(2)	1660(60)	4490(50)	2370(40)	48(14)
H(3)	2060(50)	3890(50)	4480(40)	43(12)
H(4)	4530(50)	2690(50)	4850(40)	42(12)
H(5A)	7320(60)	2340(50)	560(40)	49(13)
H(5B)	6120(50)	3350(50)	-240(40)	29(11)
H(6A)	6040(60)	440(60)	810(50)	61(15)
H(6B)	6840(50)	1050(50)	-640(50)	48(13)
H(6C)	5010(60)	1540(60)	-190(50)	69(16)
H(7)	6720(50)	-270(40)	3200(40)	37(12)
H(8)	9070(40)	-1750(40)	3450(40)	28(10)
H(10)	10600(40)	1790(40)	3280(40)	25(10)
H(11)	8110(40)	3320(40)	2830(30)	16(8)
H(12A)	11480(60)	-3010(60)	4380(50)	60(16)
H(12B)	11610(50)	-2830(50)	2980(50)	51(14)
H(12C)	13050(60)	-2890(50)	3380(50)	54(14)
H(13A)	13810(60)	-890(50)	3140(40)	44(13)
H(13B)	13030(50)	520(60)	2500(50)	57(14)

H(13C)	12820(50)	140(50)	4070(50)	57(14)

Table 52. Torsion angles [°] for **14i**.

C(4)-B(1)-N(1)-C(1)	-0.9(5)
N(2)-B(1)-N(1)-C(1)	176.4(3)
C(4)-B(1)-N(1)-C(5)	176.7(4)
N(2)-B(1)-N(1)-C(5)	-6.0(5)
N(1)-B(1)-N(2)-C(11)	102.9(4)
C(4)-B(1)-N(2)-C(11)	-79.9(5)
N(1)-B(1)-N(2)-C(7)	-77.8(5)
C(4)-B(1)-N(2)-C(7)	99.4(5)
B(1)-N(1)-C(1)-C(2)	0.1(6)
C(5)-N(1)-C(1)-C(2)	-177.7(4)
N(1)-C(1)-C(2)-C(3)	1.3(6)
C(1)-C(2)-C(3)-C(4)	-1.9(6)
C(2)-C(3)-C(4)-B(1)	1.0(6)
N(1)-B(1)-C(4)-C(3)	0.3(6)
N(2)-B(1)-C(4)-C(3)	-176.8(4)
C(1)-N(1)-C(5)-C(6)	-79.5(5)
B(1)-N(1)-C(5)-C(6)	102.9(5)
C(11)-N(2)-C(7)-C(8)	-1.3(6)
B(1)-N(2)-C(7)-C(8)	179.3(4)
N(2)-C(7)-C(8)-C(9)	-1.7(6)
C(13)-N(3)-C(9)-C(8)	179.1(4)
C(12)-N(3)-C(9)-C(8)	-3.9(6)
C(13)-N(3)-C(9)-C(10)	-0.4(5)
C(12)-N(3)-C(9)-C(10)	176.6(4)
C(7)-C(8)-C(9)-N(3)	-175.8(4)
C(7)-C(8)-C(9)-C(10)	3.8(6)
N(3)-C(9)-C(10)-C(11)	176.4(4)
C(8)-C(9)-C(10)-C(11)	-3.1(5)
C(7)-N(2)-C(11)-C(10)	2.1(6)
B(1)-N(2)-C(11)-C(10)	-178.6(4)
C(9)-C(10)-C(11)-N(2)	0.2(6)
O(2)-S(1)-C(14)-F(3)	179.1(3)
O(3)-S(1)-C(14)-F(3)	58.7(3)
O(1)-S(1)-C(14)-F(3)	-61.0(3)
O(2)-S(1)-C(14)-F(1)	-60.7(3)
O(3)-S(1)-C(14)-F(1)	179.0(3)
O(1)-S(1)-C(14)-F(1)	59.2(3)
O(2)-S(1)-C(14)-F(2)	59.2(3)
O(3)-S(1)-C(14)-F(2)	-61.1(3)
O(1)-S(1)-C(14)-F(2)	179.1(3)

Symmetry transformations used to generate equivalent atoms:

A.2.6 Supplemental information for Chapter II, section 2.6

Compound 16. A solution of allyltriphenyltin (24.45 g, 62.5 mmol in 110 mL CH_2Cl_2) was cooled to -78 °C, to which was added dropwise a solution of BCl_3 (1M in

hexanes; 62.5 mL, 62.5 mmol). The reaction was stirred at -78 °C for 4 h, whereupon allylbenzylamine (9.19 g, 62.5 mmol) was added dropwise to the reaction flask. After 20 minutes, NEt_3 was added dropwise and the reaction was allowed to warm to rt. After 12 h of stirring, approximately one-half of the solvent was removed under vacuum, and 150 mL pentane was added to the reaction flask. The reaction mixture was passed through a medium-porosity frit, and the filtrate was concentrated under reduced pressure. Vacuum distillation (91 °C, 100 mT) provided **16** as a clear, colorless liquid (6.73g, 46%).

^{1}H NMR (600 MHz, CD_2Cl_2): δ 7.35-7.45 (m, 5H), 6.15 (m, 1H), 5.93 (m, 1H), 5.1-5.4 (m, 4H), 4.5-4.6 (app br d, 2H), 3.8-3.95 (m, 2H), 2.28 (m, 2H). ^{11}B NMR (192.5 MHz, CD_2Cl_2): δ 38.6.

Compound 17. In a glove box, a solution of Grubbs 1st generation catalyst (0.169 g, 0.21 mmol in 20 mL CH_2Cl_2) was added to a stirring solution of aminoborane **16** (9.6 g, 41.1 mmol in 280 mL CH_2Cl_2). The reaction was stirred at room temperature for 2 h, after which the solvent was removed under vacuum. The desired product was purified by vacuum distillation (bp 82 °C at 100 mT) to furnish **17** as a clear, colorless liquid (7.66 g, 91%).

^{1}H NMR (600 MHz, CD_2Cl_2): δ 7.2-7.4 (m, 5H), 5.75 (br, 1H), 5.55 (m, 1H), 4.45 (s, 2H), 3.58 (br m, 2H), 1.79 (br m, 2H). ^{11}B NMR (192.5 MHz, CD_2Cl_2): δ 38.0.

Compound 15. In a glovebox, a Schlenk flask was charged with **17** (7.66 g, 37.3 mmol), Pd/C (10 wt%; 7.93 g, 7.46 mmol), and cyclohexene (120 mL). The flask was sealed, then heated to 80 °C for 24 h. The solvent was removed under reduced pressure, after which vacuum distillation provided **15** as a clear, colorless liquid (3.60 g, 47% yield).

^{1}H NMR (600 MHz, CD_2Cl_2): δ 7.60 (br, 1H), 7.2-7.35 (m, 6H), 6.72 (d, $^{3}J_{HH}$ = 11.2 Hz, 1H), 6.35 (app t, $^{3}J_{HH}$ = 6.3 Hz, 1H), 5.10 (s, 2H). ^{13}C NMR (75 MHz, CD_2Cl_2): δ 145.3, 139.5, 139.0, 129.2, 129 (br), 128.1, 127.8, 111.7, 56.4. ^{11}B NMR (192.5 MHz, CD_2Cl_2): δ 32.7.

Compound **18** was observed in the ^{11}B NMR (δ 29 ppm) of **15** as a minor peak.

Compound 18: ^{1}H NMR (600 MHz, CD_2Cl_2): δ 7.58 (dd, $^{3}J_{HH}$ = 6.1 Hz, 4.7 Hz, 1H), 7.05-7.25 (m, 6H) 6.45 (d, $^{3}J_{HH}$ = 11.4 Hz, 1H), 6.02 (app t, $^{3}J_{HH}$ = 6.1 Hz, 1H), 4.82 (s, 2H).

Compound 19. A vial was charged with a solution of **15** (0.100 g, 0.491 mmol in 3 mL THF) and cooled to –20 °C. To this stirring solution phenylmagnesium bromide (1.8 M solution in Bu_2O; 0.3 mL, 0.54 mmol) was added dropwise. Then the reaction was allowed to warm to room temperature and stirred for 10 h. The solvent was then removed under reduced pressure, and the remaining crude material was subjected to silica gel chromatography using hexane/CH_2Cl_2 as eluent. Pure **19** was obtained as a white, crystalline solid (0.085 g, 71%).

^{1}H NMR (600 MHz, CD_2Cl_2): δ 7.66 (dd, $^{3}J_{HH}$ = 10.9, 6.5 Hz, 1H), 7.48 (d, $^{3}J_{HH}$ = 4.7 Hz, 2H), 7.2-7.4 (m, 7H), 7.05 (d, $^{3}J_{HH}$ = 6.8 Hz, 2H), 6.87 (d, $^{3}J_{HH}$ = 10.6 Hz, 1H), 6.40 (app t, $^{3}J_{HH}$ = 6.5 Hz, 1H), 5.08 (s, 2H). ^{13}C NMR (125 MHz, CD_2Cl_2): δ 143, 142 (br), 139, 138, 133, 132 (br), 129, 128, 127.5, 127, 126, 112, 57. ^{11}B NMR (192.5 MHz, CD_2Cl_2): δ 35.9.

Compound 20. To a stirring solution of **15** (0.150 g, 0.737 mmol in 4 mL THF) at –20 °C was added phenylethynylmagnesium bromide (0.8 M solution in THF; 0.97 mL, 0.774 mmol). The solution was allowed to warm to room temperature and stirred for 6 h. Approximately one-half of the solvent was removed, and the remaining mixture was passed through an acrodisc. This material was then subjected to silica gel chromatography using a mixture pentane/CH_2Cl_2 (10:1) as eluent to afford **20** as a white, crystalline solid (0.145 g, 73%).

^{1}H NMR (300 MHz, CD_2Cl_2): δ 7.69 (dd, $^3J_{HH}$ = 10.8, 6.8 Hz, 1H), 7.56 (dd, $^3J_{HH}$ = 5.6, 4.2 Hz, 2H), 7.4-7.3 (m, 9H), 7.02 (d, $^3J_{HH}$ = 10.9 Hz, 1H), 6.43 (app t, $^3J_{HH}$ = 6.8 Hz, 1H), 5.31 (s, 2H). ^{13}C NMR (125 MHz, CD_2Cl_2): δ 143.6, 140.0, 139.4, 132.3, 132 (br), 129.2, 129.0, 128.9, 128.11, 128.05, 124.2, 112.5, 107.5, 59.0. ^{11}B NMR (192.5 MHz, CD_2Cl_2): δ 27.0.

Compound 21. In a glove box, a vial was charged with a solution of **15** (0.150 g, 0.737 mmol in 3 mL THF) and cooled to –20 °C. To this solution was added BuLi (1.6 M in hexane; 0.51 mL, 0.81 mmol), and the solution was allowed to warm to room temperature. After stirring for 8 h, approximately 75% of the solvent was removed. The crude material was subjected to silica gel chromatography using pentane as eluent, providing pure **21** as a clear, colorless liquid (0.064 g, 42%).

^{1}H NMR (600 MHz, CD_2Cl_2): δ 7.55 (dd, $^3J_{HH}$ = 11.7, 6.3 Hz, 1H), 7.1-7.4 (m, 6H), 6.78 (d, $^3J_{HH}$ = 10.9 Hz, 1H), 6.23 (app t, $^3J_{HH}$ = 6.3 Hz, 1H), 1.55 (m, 2H), 1.48

(m, 2H), 1.16 (m, 2H), 0.88 (t, $^{3}J_{HH}$ = 7.0 Hz, 3H). ^{11}B NMR (96.3 MHz, CD_2Cl_2): δ 39.1.

Compound 22. To a solution of **15** (0.030 g, 0.147 mmol in 1 mL CD_2Cl_2) at -20 °C was added solid NaOMe (0.008 g, 0.15 mmol). The solution was kept at -20 °C, with occasional stirring, for 6h, whereupon it was warmed to rt. The mixture was then passed through an acrodisc. ^{1}H NMR indicated greater than 90% conversion to **22**, and this solution was used directly for the competition bromination experiment with substrate **15**.

Compound 23. To a stirred solution of **15** (0.150 g, 0.737 mmol in 3 mL THF) was added dropwise a solution of $LiHBEt_3$ (1.0 M in THF; 0.81 mL, 0.81 mmol) at –20 °C. The reaction mixture was allowed to stand at –20 °C, with occasional stirring, for 1 h, and then it was warmed to room temperature and stirred for 12 h. Approximately half the solvent was removed, and 5 mL pentane was added. The mixture was then passed through an acrodisc and concentrated under reduced pressure. The crude material was purified by silica gel chromatography using pentane as eluent to furnish **22** as a clear, colorless liquid (0.110 g, 88%).

^{1}H NMR (600 MHz, CD_2Cl_2): δ 7.62 (dd, $^{3}J_{HH}$ = 10.2, 6.7 Hz, 1H), 7.2-7.4 (m, 6H) 6.91 (d, $^{3}J_{HH}$ = 11.2 Hz, 1H), 6.43 (app t, $^{3}J_{HH}$ = 6.8 Hz, 1H), 5.02 (s, 2H), 5 (br). ^{13}C NMR (75 MHz, CD_2Cl_2): δ 143.1, 138.9, 129.2, 128.1, 127.8, 112.8, 61.9, C3 not observed. ^{11}B NMR (192.5 MHz, CD_2Cl_2): δ 33.6 (d, $^{1}J_{BH}$ = 122 Hz).

Competition experiment. Compound 15 and a second 1,2-azaborine substrate

(**19**, **21**, **22**, or **23**) were added to an NMR tube in equimolar amounts. Solvent (1 mL CD_2Cl_2) was added to the tube, followed by hexamethylbenzene (approximately 2 mg). An initial ^1H NMR established the relative ratios of substrates to hexamethylbenzene. The tube was then cooled to -20 °C, whereupon 15 μL of a 10 vol% Br_2 solution in CD_2Cl_2 was added to the tube. The tube was kept at -20 °C for 1 h with periodic shaking. The tube was then warmed to rt and a ^1H NMR spectrum was taken. Integration versus hexamethylbenzene was used to determine the extent of reaction for each substrate, which was compared to the initial spectrum.

15 versus **19**: ^1H NMR indicated 38% of **19** had reacted, while 7% of **15** had reacted; the relative reactivity of **19** to **15** was calculated from these values to be 5.4 to 1.

15 versus **21**: ^1H NMR indicated 28% of **21** had been reacted, while 15% of **15** had reacted; the relative reactivity of **21** to **15** was calculated from these values to be 1.9 to 1.

15 versus **22**: ^1H NMR indicated 35% of **22** had reacted, while 17% of **15** had reacted; the relative reactivity of **22** to **15** was calculated from these values to be 2.1 to 1.

15 versus **23**: ^1H NMR indicated 21% of **23** had reacted, while 19% of **15** had reacted; the relative reactivity of **23** to **15** was calculated from these values to be 1.1 to 1.

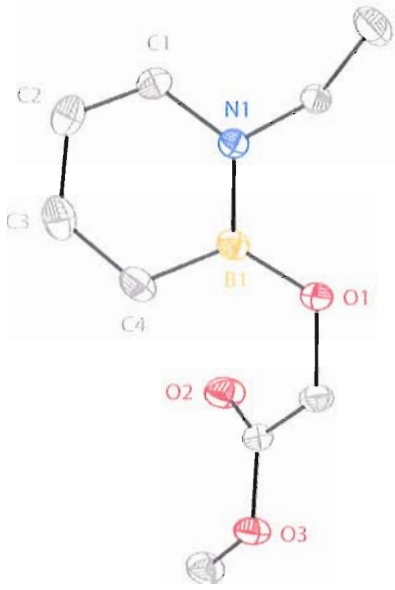

Figure 17. ORTEP illustration of **7**, with ellipsoids drawn at the 35% probability level.

X-ray Crystal Structure Determination. Crystals of **7** suitable for X-ray diffraction were obtained by slow evaporation of an Et_2O solution of **7**.

Diffraction intensity data were collected with a Bruker Smart Apex CCD diffractometer at 173(2) K using MoKα - radiation (0.71073 Å). The structure was solved using direct methods, completed by subsequent difference Fourier syntheses, and refined by full matrix least-squares procedures on F^2. All non-H atoms were refined with anisotropic thermal parameters. H atoms were found on the residual density map and refined with isotropic thermal parameters. The Flack parameter is 0.00(8). All software and sources scattering factors are contained in the SHELXTL (6.10) program package (G.Sheldrick, Bruker XRD, Madison, WI). Crystallographic data and some details of data collection and crystal structure refinement for $C_9H_{14}BNO_3$ are given in the following tables.

Table 53. Crystal data and structure refinement for **7** (liu11).

Identification code	liu11	
Empirical formula	$C_9 H_{14} B N O_3$	
Formula weight	195.02	
Temperature	173(2) K	
Wavelength	0.71073 Å	
Crystal system	Monoclinic	
Space group	P2(1)/c	
Unit cell dimensions	a = 8.0468(12) Å	α = 90°.
	b = 8.2968(13) Å	β = 93.584(2)°.
	c = 15.361(2) Å	γ = 90°.
Volume	1023.5(3) $Å^3$	
Z	4	
Density (calculated)	1.266 Mg/m^3	
Absorption coefficient	0.092 mm^{-1}	
F(000)	416	
Crystal size	0.39 x 0.32 x 0.26 mm^3	
Theta range for data collection	2.54 to 27.00°.	
Index ranges	-10<=h<=10, -10<=k<=10, -19<=l<=19	
Reflections collected	9259	
Independent reflections	2216 [R(int) = 0.0276]	
Completeness to theta = 27.00°	98.9 %	
Absorption correction	Semi-empirical from equivalents	
Max. and min. transmission	0.9764 and 0.9649	
Refinement method	Full-matrix least-squares on F^2	
Data / restraints / parameters	2216 / 0 / 183	
Goodness-of-fit on F^2	1.001	
Final R indices [I>2sigma(I)]	R1 = 0.0376, wR2 = 0.1046	
R indices (all data)	R1 = 0.0445, wR2 = 0.1125	
Largest diff. peak and hole	0.245 and -0.160 $e.Å^{-3}$	

Table 54. Atomic coordinates (x 10^4) and equivalent isotropic displacement parameters ($Å^2$x 10^3) for **7**. U(eq) is defined as one third of the trace of the orthogonalized U^{ij} tensor.

	x	y	z	U(eq)
O(1)	6063(1)	1999(1)	5561(1)	31(1)
O(2)	6803(1)	-947(1)	6266(1)	43(1)
O(3)	8327(1)	-1599(1)	5148(1)	33(1)
N(1)	5792(1)	3738(1)	6793(1)	24(1)
B(1)	6848(2)	2805(2)	6265(1)	26(1)
C(1)	6445(2)	4598(2)	7494(1)	30(1)
C(2)	8099(2)	4626(2)	7723(1)	36(1)
C(3)	9225(2)	3747(2)	7237(1)	38(1)
C(4)	8698(2)	2850(2)	6529(1)	34(1)

C(5)	3972(2)	3846(2)	6610(1)	29(1)
C(6)	3446(2)	5473(2)	6258(1)	49(1)
C(7)	7005(2)	925(2)	5082(1)	31(1)
C(8)	7342(1)	-623(1)	5582(1)	28(1)
C(9)	8660(2)	-3143(2)	5560(1)	42(1)

Table 55. Bond lengths [Å] and angles [°] for **7**.

O(1)-B(1)	1.3894(15)
O(1)-C(7)	1.4076(14)
O(2)-C(8)	1.1933(15)
O(3)-C(8)	1.3392(14)
O(3)-C(9)	1.4468(16)
N(1)-C(1)	1.3696(15)
N(1)-B(1)	1.4359(17)
N(1)-C(5)	1.4764(15)
B(1)-C(4)	1.5183(19)
C(1)-C(2)	1.3552(18)
C(1)-H(1)	0.973(16)
C(2)-C(3)	1.413(2)
C(2)-H(2)	0.971(16)
C(3)-C(4)	1.363(2)
C(3)-H(3)	0.963(16)
C(4)-H(4)	0.952(16)
C(5)-C(6)	1.5051(19)
C(5)-H(5A)	0.933(16)
C(5)-H(5B)	0.983(14)
C(6)-H(6A)	0.99(2)
C(6)-H(6B)	0.959(19)
C(6)-H(6C)	0.923(19)
C(7)-C(8)	1.5111(17)
C(7)-H(7A)	0.970(15)
C(7)-H(7B)	0.985(14)
C(9)-H(9A)	0.94(2)
C(9)-H(9B)	0.973(18)
C(9)-H(9C)	1.006(19)
B(1)-O(1)-C(7)	118.57(9)
C(8)-O(3)-C(9)	114.69(10)
C(1)-N(1)-B(1)	120.87(10)
C(1)-N(1)-C(5)	116.40(10)
B(1)-N(1)-C(5)	122.72(10)
O(1)-B(1)-N(1)	116.23(10)
O(1)-B(1)-C(4)	127.60(11)
N(1)-B(1)-C(4)	116.15(11)
C(2)-C(1)-N(1)	122.37(12)
C(2)-C(1)-H(1)	121.8(8)
N(1)-C(1)-H(1)	115.8(8)
C(1)-C(2)-C(3)	120.37(12)
C(1)-C(2)-H(2)	119.6(9)
C(3)-C(2)-H(2)	119.9(9)
C(4)-C(3)-C(2)	121.70(12)
C(4)-C(3)-H(3)	118.8(9)
C(2)-C(3)-H(3)	119.5(9)

C(3)-C(4)-B(1)	118.54(12)
C(3)-C(4)-H(4)	117.7(9)
B(1)-C(4)-H(4)	123.7(9)
N(1)-C(5)-C(6)	112.10(11)
N(1)-C(5)-H(5A)	108.1(9)
C(6)-C(5)-H(5A)	111.1(9)
N(1)-C(5)-H(5B)	107.8(8)
C(6)-C(5)-H(5B)	111.9(8)
H(5A)-C(5)-H(5B)	105.6(12)
C(5)-C(6)-H(6A)	112.9(12)
C(5)-C(6)-H(6B)	111.3(11)
H(6A)-C(6)-H(6B)	109.1(16)
C(5)-C(6)-H(6C)	109.5(11)
H(6A)-C(6)-H(6C)	105.7(16)
H(6B)-C(6)-H(6C)	107.9(15)
O(1)-C(7)-C(8)	110.97(10)
O(1)-C(7)-H(7A)	109.0(9)
C(8)-C(7)-H(7A)	108.2(9)
O(1)-C(7)-H(7B)	111.8(8)
C(8)-C(7)-H(7B)	109.2(8)
H(7A)-C(7)-H(7B)	107.6(12)
O(2)-C(8)-O(3)	124.09(11)
O(2)-C(8)-C(7)	125.15(11)
O(3)-C(8)-C(7)	110.76(10)
O(3)-C(9)-H(9A)	109.2(11)
O(3)-C(9)-H(9B)	110.6(10)
H(9A)-C(9)-H(9B)	110.8(16)
O(3)-C(9)-H(9C)	102.5(10)
H(9A)-C(9)-H(9C)	111.1(15)
H(9B)-C(9)-H(9C)	112.4(15)

Symmetry transformations used to generate equivalent atoms:

Table 56. Anisotropic displacement parameters ($Å^2 x\ 10^3$)for **7**. The anisotropic displacement factor exponent takes the form: $-2p^2[\ h^2a^{*2}U^{11} + ... + 2\ h\ k\ a^*\ b^*\ U^{12}\ ]$

	U^{11}	U^{22}	U^{33}	U^{23}	U^{13}	U^{12}
O(1)	33(1)	31(1)	28(1)	-4(1)	2(1)	10(1)
O(2)	54(1)	43(1)	33(1)	7(1)	17(1)	13(1)
O(3)	36(1)	28(1)	35(1)	-1(1)	9(1)	7(1)
N(1)	24(1)	24(1)	25(1)	1(1)	3(1)	0(1)
B(1)	30(1)	24(1)	26(1)	5(1)	4(1)	5(1)
C(1)	34(1)	28(1)	28(1)	-1(1)	5(1)	-2(1)
C(2)	36(1)	40(1)	31(1)	-1(1)	0(1)	-10(1)
C(3)	26(1)	48(1)	38(1)	9(1)	-1(1)	-4(1)
C(4)	28(1)	39(1)	35(1)	7(1)	6(1)	9(1)
C(5)	24(1)	34(1)	28(1)	-2(1)	4(1)	3(1)
C(6)	43(1)	40(1)	63(1)	1(1)	-11(1)	14(1)
C(7)	35(1)	32(1)	25(1)	-2(1)	7(1)	8(1)
C(8)	28(1)	30(1)	26(1)	-4(1)	3(1)	3(1)
C(9)	48(1)	30(1)	47(1)	2(1)	5(1)	11(1)

Table 57. Hydrogen coordinates (x 10^4) and isotropic displacement parameters ($Å^2$x 10^3) for **7**.

	x	y	z	U(eq)
H(1)	5644(18)	5172(18)	7827(9)	37(4)
H(2)	8514(19)	5293(19)	8208(10)	42(4)
H(3)	10400(20)	3775(18)	7408(10)	43(4)
H(4)	9520(20)	2291(18)	6226(10)	38(4)
H(5A)	3462(18)	3616(17)	7125(10)	34(4)
H(5B)	3637(17)	2971(16)	6204(9)	30(3)
H(6A)	3790(20)	6360(20)	6653(13)	70(6)
H(6B)	2260(20)	5520(20)	6133(11)	62(5)
H(6C)	3950(20)	5670(20)	5746(12)	51(5)
H(7A)	6383(18)	663(17)	4539(10)	37(4)
H(7B)	8072(18)	1403(16)	4934(9)	29(3)
H(9A)	7640(30)	-3680(20)	5626(13)	69(6)
H(9B)	9270(20)	-3000(20)	6122(12)	51(5)
H(9C)	9340(20)	-3710(20)	5125(12)	58(5)

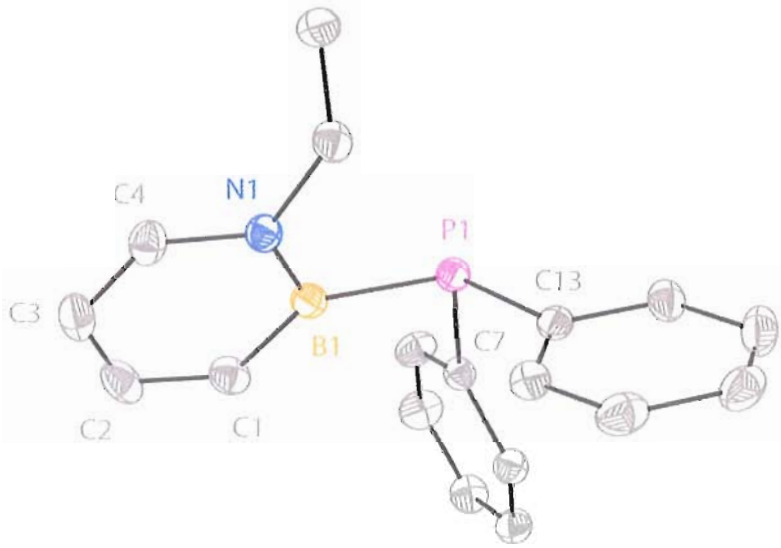

Figure 18. ORTEP illustration of **6h**, with ellipsoids drawn at the 35% probability level.

X-ray Crystal Structure Determination. Crystals of **6h** suitable for X-ray diffraction were obtained by slow evaporation of an Et_2O solution of **6h**.

Diffraction intensity data were collected with a Bruker Smart Apex CCD diffractometer at 173(2) K using MoKα - radiation (0.71073 Å). The structure was solved using direct methods, completed by subsequent difference Fourier syntheses, and

refined by full matrix least-squares procedures on F^2. All non-H atoms were refined with anisotropic thermal parameters. H atoms were found on the residual density map and refined with isotropic thermal parameters. The Flack parameter is 0.00(8). All software and sources scattering factors are contained in the SHELXTL (6.10) program package (G.Sheldrick, Bruker XRD, Madison, WI). Crystallographic data and some details of data collection and crystal structure refinement for $C_{18}H_{19}BNP$ are given in the following tables.

Table 57. Crystal data and structure refinement for **6h** (liu8).

Identification code	liu8	
Empirical formula	C_{18} H_{19} B N P	
Formula weight	291.12	
Temperature	173(2) K	
Wavelength	0.71073 Å	
Crystal system	Orthorhombic	
Space group	P2(1)2(1)2(1)	
Unit cell dimensions	a = 8.9841(6) Å	α = 90°.
	b = 10.1554(7) Å	β = 90°.
	c = 17.6058(12) Å	γ = 90°.
Volume	1606.30(19) $Å^3$	
Z	4	
Density (calculated)	1.204 Mg/m^3	
Absorption coefficient	0.163 mm^{-1}	
F(000)	616	
Crystal size	0.32 x 0.28 x 0.18 mm^3	
Theta range for data collection	2.31 to 27.00°.	
Index ranges	-11<=h<=10, -12<=k<=12, -21<=l<=22	
Reflections collected	14708	
Independent reflections	3511 [R(int) = 0.0203]	
Completeness to theta = 27.00°	99.8 %	
Absorption correction	Semi-empirical from equivalents	
Max. and min. transmission	0.9712 and 0.9497	
Refinement method	Full-matrix least-squares on F^2	
Data / restraints / parameters	3511 / 0 / 266	
Goodness-of-fit on F^2	1.042	
Final R indices [I>2sigma(I)]	R1 = 0.0301, wR2 = 0.0749	
R indices (all data)	R1 = 0.0318, wR2 = 0.0763	

Absolute structure parameter	0.00(8)
Largest diff. peak and hole	0.241 and -0.116 e.Å^{-3}

Table 58. Atomic coordinates (x 10^4) and equivalent isotropic displacement parameters (Å^{2}x 10^3) for **6h**. U(eq) is defined as one third of the trace of the orthogonalized U^{ij} tensor.

	x	y	z	U(eq)
P(1)	2509(1)	4049(1)	8332(1)	27(1)
B(1)	1221(2)	5533(2)	8577(1)	28(1)
N(1)	-47(1)	5818(1)	8106(1)	27(1)
C(1)	1342(2)	6349(2)	9289(1)	35(1)
C(2)	290(2)	7288(2)	9439(1)	41(1)
C(3)	-905(2)	7505(2)	8941(1)	38(1)
C(4)	-1043(2)	6780(1)	8298(1)	33(1)
C(5)	-400(2)	5083(2)	7400(1)	32(1)
C(6)	-1432(2)	3943(2)	7548(1)	48(1)
C(7)	3945(2)	4178(1)	9069(1)	27(1)
C(8)	3629(2)	3622(2)	9774(1)	40(1)
C(9)	4663(2)	3630(2)	10353(1)	44(1)
C(10)	6058(2)	4171(2)	10240(1)	40(1)
C(11)	6394(2)	4729(2)	9546(1)	36(1)
C(12)	5341(2)	4742(2)	8965(1)	31(1)
C(13)	3513(2)	4514(1)	7464(1)	28(1)
C(14)	4388(2)	3554(2)	7111(1)	36(1)
C(15)	5113(2)	3814(2)	6433(1)	46(1)
C(16)	4966(2)	5030(2)	6087(1)	46(1)
C(17)	4109(2)	5995(2)	6428(1)	42(1)
C(18)	3405(2)	5742(2)	7116(1)	34(1)

Table 59. Bond lengths [Å] and angles [°] for **6h**.

P(1)-C(7)	1.8342(14)
P(1)-C(13)	1.8360(15)
P(1)-B(1)	1.9481(17)
B(1)-N(1)	1.439(2)
B(1)-C(1)	1.506(2)
N(1)-C(4)	1.3670(19)
N(1)-C(5)	1.4834(18)
C(1)-C(2)	1.369(2)
C(1)-H(1)	0.911(18)
C(2)-C(3)	1.403(3)
C(2)-H(2)	0.93(2)
C(3)-C(4)	1.357(2)
C(3)-H(3)	0.964(18)
C(4)-H(4)	1.002(18)
C(5)-C(6)	1.506(2)
C(5)-H(5A)	0.965(19)
C(5)-H(5B)	0.943(18)
C(6)-H(6A)	1.09(3)
C(6)-H(6B)	0.99(2)

C(6)-H(6C)	0.85(2)
C(7)-C(12)	1.391(2)
C(7)-C(8)	1.392(2)
C(8)-C(9)	1.380(2)
C(8)-H(8)	0.924(19)
C(9)-C(10)	1.383(3)
C(9)-H(9)	0.97(2)
C(10)-C(11)	1.380(2)
C(10)-H(10)	0.954(19)
C(11)-C(12)	1.394(2)
C(11)-H(11)	0.97(2)
C(12)-H(12)	0.952(16)
C(13)-C(18)	1.393(2)
C(13)-C(14)	1.398(2)
C(14)-C(15)	1.385(2)
C(14)-H(14)	0.973(18)
C(15)-C(16)	1.384(3)
C(15)-H(15)	0.94(2)
C(16)-C(17)	1.384(3)
C(16)-H(16)	0.95(2)
C(17)-C(18)	1.390(2)
C(17)-H(17)	0.93(2)
C(18)-H(18)	0.940(17)
C(7)-P(1)-C(13)	103.02(6)
C(7)-P(1)-B(1)	101.88(7)
C(13)-P(1)-B(1)	106.10(7)
N(1)-B(1)-C(1)	115.20(14)
N(1)-B(1)-P(1)	119.90(11)
C(1)-B(1)-P(1)	124.53(12)
C(4)-N(1)-B(1)	121.30(12)
C(4)-N(1)-C(5)	115.28(13)
B(1)-N(1)-C(5)	123.40(12)
C(2)-C(1)-B(1)	119.67(15)
C(2)-C(1)-H(1)	119.1(11)
B(1)-C(1)-H(1)	121.2(11)
C(1)-C(2)-C(3)	121.09(14)
C(1)-C(2)-H(2)	119.8(12)
C(3)-C(2)-H(2)	119.1(12)
C(4)-C(3)-C(2)	120.39(15)
C(4)-C(3)-H(3)	117.5(10)
C(2)-C(3)-H(3)	122.1(10)
C(3)-C(4)-N(1)	122.34(16)
C(3)-C(4)-H(4)	122.6(10)
N(1)-C(4)-H(4)	115.1(11)
N(1)-C(5)-C(6)	111.91(13)
N(1)-C(5)-H(5A)	109.1(11)
C(6)-C(5)-H(5A)	108.7(11)
N(1)-C(5)-H(5B)	109.3(11)
C(6)-C(5)-H(5B)	111.8(11)
H(5A)-C(5)-H(5B)	105.8(15)
C(5)-C(6)-H(6A)	107.4(14)
C(5)-C(6)-H(6B)	108.8(12)
H(6A)-C(6)-H(6B)	109.5(19)

C(5)-C(6)-H(6C)	111.6(16)
H(6A)-C(6)-H(6C)	114(2)
H(6B)-C(6)-H(6C)	105.4(19)
C(12)-C(7)-C(8)	117.91(14)
C(12)-C(7)-P(1)	124.76(11)
C(8)-C(7)-P(1)	117.28(11)
C(9)-C(8)-C(7)	121.29(15)
C(9)-C(8)-H(8)	119.0(11)
C(7)-C(8)-H(8)	119.7(11)
C(8)-C(9)-C(10)	120.37(15)
C(8)-C(9)-H(9)	119.2(12)
C(10)-C(9)-H(9)	120.4(12)
C(11)-C(10)-C(9)	119.30(15)
C(11)-C(10)-H(10)	121.9(11)
C(9)-C(10)-H(10)	118.8(11)
C(10)-C(11)-C(12)	120.36(15)
C(10)-C(11)-H(11)	121.2(11)
C(12)-C(11)-H(11)	118.4(11)
C(7)-C(12)-C(11)	120.75(14)
C(7)-C(12)-H(12)	116.3(10)
C(11)-C(12)-H(12)	122.9(10)
C(18)-C(13)-C(14)	117.89(14)
C(18)-C(13)-P(1)	124.20(11)
C(14)-C(13)-P(1)	117.84(11)
C(15)-C(14)-C(13)	120.97(16)
C(15)-C(14)-H(14)	118.9(10)
C(13)-C(14)-H(14)	120.1(10)
C(14)-C(15)-C(16)	120.35(16)
C(14)-C(15)-H(15)	117.0(14)
C(16)-C(15)-H(15)	122.6(14)
C(15)-C(16)-C(17)	119.57(16)
C(15)-C(16)-H(16)	119.8(12)
C(17)-C(16)-H(16)	120.6(12)
C(16)-C(17)-C(18)	120.05(17)
C(16)-C(17)-H(17)	120.1(12)
C(18)-C(17)-H(17)	119.8(12)
C(17)-C(18)-C(13)	121.15(15)
C(17)-C(18)-H(18)	117.2(10)
C(13)-C(18)-H(18)	121.7(10)

Symmetry transformations used to generate equivalent atoms:

Table 60. Anisotropic displacement parameters ($Å^2 x\ 10^3$)for **6h**. The anisotropic displacement factor exponent takes the form: $-2p^2[\ h^2a^{*2}U^{11} + ... + 2\ h\ k\ a^*\ b^*\ U^{12}\ ]$

	U^{11}	U^{22}	U^{33}	U^{23}	U^{13}	U^{12}
P(1)	27(1)	30(1)	25(1)	-1(1)	-1(1)	0(1)
B(1)	30(1)	28(1)	25(1)	0(1)	3(1)	-3(1)
N(1)	29(1)	28(1)	25(1)	0(1)	4(1)	-1(1)
C(1)	42(1)	37(1)	27(1)	-3(1)	-2(1)	-3(1)
C(2)	60(1)	34(1)	29(1)	-8(1)	11(1)	-4(1)
C(3)	46(1)	29(1)	39(1)	1(1)	15(1)	5(1)
C(4)	33(1)	32(1)	35(1)	6(1)	8(1)	3(1)

C(5)	33(1)	38(1)	26(1)	-3(1)	-2(1)	3(1)
C(6)	35(1)	60(1)	49(1)	-20(1)	8(1)	-12(1)
C(7)	28(1)	26(1)	28(1)	-1(1)	-2(1)	3(1)
C(8)	35(1)	49(1)	35(1)	7(1)	-1(1)	-9(1)
C(9)	50(1)	56(1)	28(1)	10(1)	-4(1)	-6(1)
C(10)	39(1)	48(1)	33(1)	-2(1)	-10(1)	4(1)
C(11)	31(1)	41(1)	37(1)	-3(1)	-2(1)	-2(1)
C(12)	33(1)	32(1)	29(1)	0(1)	1(1)	-1(1)
C(13)	24(1)	36(1)	24(1)	-4(1)	-2(1)	-2(1)
C(14)	32(1)	44(1)	32(1)	-8(1)	-5(1)	5(1)
C(15)	33(1)	71(1)	35(1)	-17(1)	2(1)	6(1)
C(16)	35(1)	75(1)	29(1)	-8(1)	5(1)	-15(1)
C(17)	42(1)	49(1)	36(1)	5(1)	0(1)	-14(1)
C(18)	33(1)	34(1)	35(1)	-3(1)	3(1)	-4(1)

Table 61. Hydrogen coordinates (x 10^4) and isotropic displacement parameters (Å^{2}x 10^3) for **6h**.

	x	y	z	U(eq)
H(1)	2130(20)	6261(18)	9609(10)	40(5)
H(2)	380(20)	7815(19)	9872(11)	45(5)
H(3)	-1647(19)	8172(17)	9035(9)	32(4)
H(4)	-1870(20)	6915(18)	7926(10)	42(5)
H(5A)	510(20)	4748(19)	7183(10)	42(5)
H(5B)	-794(19)	5670(18)	7037(10)	40(5)
H(6A)	-850(30)	3260(20)	7927(14)	84(8)
H(6B)	-1650(20)	3500(20)	7059(12)	55(6)
H(6C)	-2270(20)	4200(20)	7714(12)	61(6)
H(8)	2720(20)	3221(18)	9854(10)	45(5)
H(9)	4400(20)	3240(20)	10841(11)	51(6)
H(10)	6740(20)	4185(19)	10653(10)	42(5)
H(11)	7350(20)	5148(18)	9456(10)	40(4)
H(12)	5519(18)	5138(16)	8484(9)	29(4)
H(14)	4493(19)	2687(18)	7340(9)	35(4)
H(15)	5700(30)	3130(20)	6227(13)	65(7)
H(16)	5490(20)	5210(20)	5628(11)	50(5)
H(17)	4050(20)	6830(20)	6215(11)	50(5)
H(18)	2881(18)	6441(17)	7342(9)	32(4)

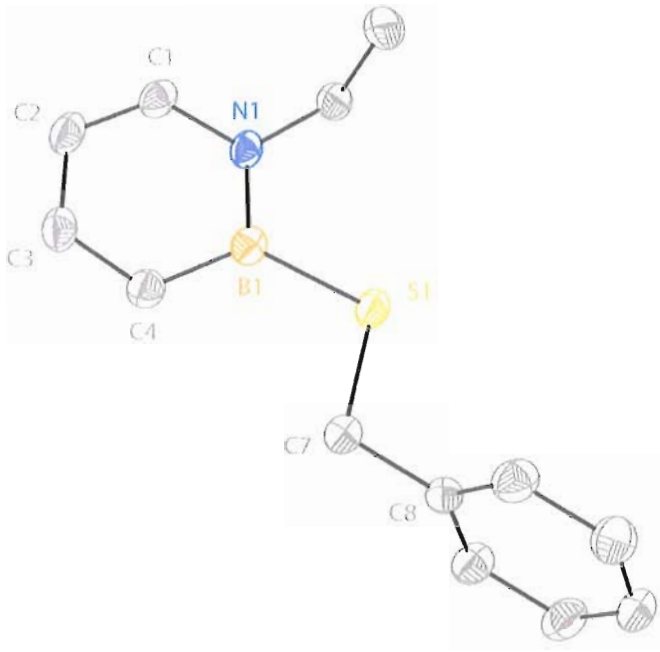

Figure 19. ORTEP illustration of **6g**, with ellipsoids drawn at the 35% probability level.

X-ray Crystal Structure Determination. Crystals of **6g** suitable for X-ray diffraction were obtained by slow evaporation of an Et_2O solution of **6g**.

Diffraction intensity data were collected with a Bruker Smart Apex CCD diffractometer at 173(2) K using MoKα - radiation (0.71073 Å). The structure was solved using direct methods, completed by subsequent difference Fourier syntheses, and refined by full matrix least-squares procedures on F^2. All non-H atoms were refined with anisotropic thermal parameters. H atoms were found on the residual density map and refined with isotropic thermal parameters. The Flack parameter is 0.00(8). All software and sources scattering factors are contained in the SHELXTL (6.10) program package (G.Sheldrick, Bruker XRD, Madison, WI). Crystallographic data and some details of data collection and crystal structure refinement for $C_{13}H_{16}BNS$ are given in the

following tables.

Table 62. Crystal data and structure refinement for **6g** (liu37).

Identification code	liu37	
Empirical formula	C_{13} H_{16} B N S	
Formula weight	229.14	
Temperature	173(2) K	
Wavelength	0.71073 Å	
Crystal system	Monoclinic	
Space group	P2(1)/c	
Unit cell dimensions	a = 4.6680(10) Å	α = 90°.
	b = 13.476(3) Å	β = 91.043(5)°.
	c = 19.953(4) Å	γ = 90°.
Volume	1254.9(5) $Å^3$	
Z	4	
Density (calculated)	1.213 Mg/m^3	
Absorption coefficient	0.229 mm^{-1}	
F(000)	488	
Crystal size	0.40 x 0.05 x 0.04 mm^3	
Theta range for data collection	1.82 to 27.00°.	
Index ranges	-5<=h<=5, -17<=k<=17, -25<=l<=25	
Reflections collected	13796	
Independent reflections	2723 [R(int) = 0.0845]	
Completeness to theta = 27.00°	100.0 %	
Absorption correction	Semi-empirical from equivalents	
Max. and min. transmission	0.9909 and 0.9141	
Refinement method	Full-matrix least-squares on F^2	
Data / restraints / parameters	2723 / 0 / 209	
Goodness-of-fit on F^2	1.021	
Final R indices [I>2sigma(I)]	R1 = 0.0518, wR2 = 0.1035	
R indices (all data)	R1 = 0.0995, wR2 = 0.1276	
Largest diff. peak and hole	0.250 and -0.263 $e.Å^{-3}$	

Table 63. Atomic coordinates (x 10^4) and equivalent isotropic displacement parameters ($Å^2$x 10^3) for **6g**. U(eq) is defined as one third of the trace of the orthogonalized U^{ij} tensor.

	x	y	z	U(eq)
S(1)	903(1)	4422(1)	3511(1)	41(1)
N(1)	488(4)	6028(1)	2618(1)	34(1)
B(1)	1862(6)	5669(2)	3216(2)	34(1)
C(1)	1177(6)	6942(2)	2360(2)	40(1)
C(2)	3188(6)	7530(2)	2648(2)	44(1)
C(3)	4609(6)	7237(2)	3244(2)	44(1)

C(4)	4042(6)	6352(2)	3544(1)	39(1)
C(5)	-1649(6)	5442(2)	2233(1)	40(1)
C(6)	-292(8)	4836(2)	1688(2)	51(1)
C(7)	3157(6)	4270(2)	4263(1)	40(1)
C(8)	2806(5)	3238(2)	4534(1)	35(1)
C(9)	991(6)	3043(2)	5055(1)	45(1)
C(10)	662(7)	2094(2)	5305(2)	54(1)
C(11)	2163(7)	1322(2)	5029(2)	55(1)
C(12)	3968(8)	1505(2)	4507(2)	55(1)
C(13)	4282(7)	2451(2)	4259(2)	47(1)

Table 64. Bond lengths [Å] and angles [°] for **6g**.

S(1)-C(7)	1.828(3)
S(1)-B(1)	1.838(3)
N(1)-C(1)	1.376(3)
N(1)-B(1)	1.429(3)
N(1)-C(5)	1.477(3)
B(1)-C(4)	1.512(4)
C(1)-C(2)	1.348(4)
C(1)-H(1)	0.97(2)
C(2)-C(3)	1.408(4)
C(2)-H(2)	0.96(3)
C(3)-C(4)	1.362(4)
C(3)-H(3)	0.95(3)
C(4)-H(4)	0.96(3)
C(5)-C(6)	1.507(4)
C(5)-H(5A)	0.99(2)
C(5)-H(5B)	0.99(2)
C(6)-H(6A)	1.04(3)
C(6)-H(6B)	0.96(3)
C(6)-H(6C)	0.94(3)
C(7)-C(8)	1.503(3)
C(7)-H(7A)	0.97(3)
C(7)-H(7B)	1.01(2)
C(8)-C(9)	1.379(4)
C(8)-C(13)	1.384(4)
C(9)-C(10)	1.382(4)
C(9)-H(9)	0.95(2)
C(10)-C(11)	1.375(4)
C(10)-H(10)	1.00(3)
C(11)-C(12)	1.374(4)
C(11)-H(11)	0.91(3)
C(12)-C(13)	1.375(4)
C(12)-H(12)	0.90(3)
C(13)-H(13)	0.89(3)
C(7)-S(1)-B(1)	103.00(13)
C(1)-N(1)-B(1)	120.7(2)
C(1)-N(1)-C(5)	116.4(2)
B(1)-N(1)-C(5)	122.9(2)
N(1)-B(1)-C(4)	116.3(2)
N(1)-B(1)-S(1)	118.0(2)
C(4)-B(1)-S(1)	125.8(2)

C(2)-C(1)-N(1)	122.2(3)
C(2)-C(1)-H(1)	123.5(14)
N(1)-C(1)-H(1)	114.1(14)
C(1)-C(2)-C(3)	120.5(3)
C(1)-C(2)-H(2)	117.2(16)
C(3)-C(2)-H(2)	122.2(16)
C(4)-C(3)-C(2)	121.6(3)
C(4)-C(3)-H(3)	116.6(16)
C(2)-C(3)-H(3)	121.7(16)
C(3)-C(4)-B(1)	118.6(3)
C(3)-C(4)-H(4)	120.2(16)
B(1)-C(4)-H(4)	121.3(15)
N(1)-C(5)-C(6)	112.1(3)
N(1)-C(5)-H(5A)	108.9(14)
C(6)-C(5)-H(5A)	109.6(14)
N(1)-C(5)-H(5B)	108.5(13)
C(6)-C(5)-H(5B)	111.5(14)
H(5A)-C(5)-H(5B)	106(2)
C(5)-C(6)-H(6A)	108.5(17)
C(5)-C(6)-H(6B)	110.8(17)
H(6A)-C(6)-H(6B)	105(2)
C(5)-C(6)-H(6C)	109.7(17)
H(6A)-C(6)-H(6C)	117(2)
H(6B)-C(6)-H(6C)	106(2)
C(8)-C(7)-S(1)	109.49(18)
C(8)-C(7)-H(7A)	109.8(15)
S(1)-C(7)-H(7A)	109.4(16)
C(8)-C(7)-H(7B)	109.7(14)
S(1)-C(7)-H(7B)	109.1(13)
H(7A)-C(7)-H(7B)	109(2)
C(9)-C(8)-C(13)	118.1(3)
C(9)-C(8)-C(7)	121.3(2)
C(13)-C(8)-C(7)	120.6(3)
C(8)-C(9)-C(10)	121.5(3)
C(8)-C(9)-H(9)	121.0(15)
C(10)-C(9)-H(9)	117.6(15)
C(11)-C(10)-C(9)	119.7(3)
C(11)-C(10)-H(10)	121.2(17)
C(9)-C(10)-H(10)	119.1(17)
C(10)-C(11)-C(12)	119.5(3)
C(10)-C(11)-H(11)	121(2)
C(12)-C(11)-H(11)	119(2)
C(13)-C(12)-C(11)	120.7(3)
C(13)-C(12)-H(12)	117(2)
C(11)-C(12)-H(12)	121.9(19)
C(12)-C(13)-C(8)	120.7(3)
C(12)-C(13)-H(13)	119.8(18)
C(8)-C(13)-H(13)	119.3(18)

Symmetry transformations used to generate equivalent atoms:

Table 65. Anisotropic displacement parameters ($Å^2 x\ 10^3$)for **6g**. The anisotropic displacement factor exponent takes the form: $-2p^2[\ h^2a^{*2}U^{11} + ... + 2\ h\ k\ a^*\ b^*\ U^{12}\ ]$

	U^{11}	U^{22}	U^{33}	U^{23}	U^{13}	U^{12}
S(1)	47(1)	31(1)	45(1)	7(1)	-8(1)	-5(1)
N(1)	40(1)	22(1)	39(1)	1(1)	3(1)	3(1)
B(1)	36(2)	28(1)	39(2)	-1(1)	9(1)	6(1)
C(1)	50(2)	28(1)	43(2)	5(1)	6(1)	7(1)
C(2)	57(2)	26(1)	48(2)	4(1)	11(2)	-1(1)
C(3)	50(2)	31(2)	50(2)	-6(1)	9(1)	-6(1)
C(4)	45(2)	35(2)	38(2)	0(1)	4(1)	-1(1)
C(5)	47(2)	32(2)	42(2)	2(1)	-3(1)	2(1)
C(6)	68(2)	39(2)	48(2)	-6(2)	2(2)	4(2)
C(7)	45(2)	35(2)	39(2)	4(1)	-2(1)	-3(1)
C(8)	37(2)	33(1)	35(1)	1(1)	-5(1)	0(1)
C(9)	50(2)	40(2)	44(2)	4(1)	7(1)	5(1)
C(10)	61(2)	51(2)	49(2)	14(2)	5(2)	-4(2)
C(11)	72(2)	35(2)	56(2)	11(2)	-15(2)	-7(2)
C(12)	71(2)	38(2)	55(2)	-3(2)	-6(2)	16(2)
C(13)	54(2)	45(2)	42(2)	3(1)	7(2)	5(2)

Table 66. Hydrogen coordinates ($x\ 10^4$) and isotropic displacement parameters ($Å^2 x\ 10^3$) for **6g**.

	x	y	z	U(eq)
H(1)	200(50)	7100(16)	1944(12)	32(7)
H(2)	3610(50)	8140(20)	2426(13)	53(8)
H(3)	6000(50)	7640(20)	3456(13)	49(8)
H(4)	5040(50)	6168(18)	3948(14)	49(8)
H(5A)	-3080(50)	5898(19)	2032(12)	42(7)
H(5B)	-2710(50)	5015(18)	2550(12)	35(7)
H(6A)	-1910(70)	4480(20)	1414(16)	71(10)
H(6B)	620(60)	5260(20)	1371(15)	60(9)
H(6C)	1150(60)	4430(20)	1876(14)	54(9)
H(7A)	5140(60)	4382(18)	4152(13)	51(8)
H(7B)	2560(50)	4769(17)	4611(12)	35(7)
H(9)	-100(50)	3558(19)	5252(12)	42(7)
H(10)	-680(70)	1980(20)	5684(15)	72(10)
H(11)	1950(60)	690(20)	5180(16)	72(10)
H(12)	5030(60)	1020(20)	4324(15)	62(9)
H(13)	5560(60)	2568(19)	3947(14)	49(9)

Table 67. Torsion angles [°] for **6g**.

C(1)-N(1)-B(1)-C(4)	0.8(3)
C(5)-N(1)-B(1)-C(4)	178.8(2)
C(1)-N(1)-B(1)-S(1)	-178.03(18)
C(5)-N(1)-B(1)-S(1)	0.1(3)
C(7)-S(1)-B(1)-N(1)	179.2(2)
C(7)-S(1)-B(1)-C(4)	0.6(3)
B(1)-N(1)-C(1)-C(2)	1.2(4)
C(5)-N(1)-C(1)-C(2)	-177.0(2)
N(1)-C(1)-C(2)-C(3)	-2.1(4)
C(1)-C(2)-C(3)-C(4)	0.9(4)
C(2)-C(3)-C(4)-B(1)	1.0(4)
N(1)-B(1)-C(4)-C(3)	-1.8(4)
S(1)-B(1)-C(4)-C(3)	176.8(2)
C(1)-N(1)-C(5)-C(6)	86.2(3)
B(1)-N(1)-C(5)-C(6)	-92.0(3)
B(1)-S(1)-C(7)-C(8)	-175.1(2)
S(1)-C(7)-C(8)-C(9)	-98.2(3)
S(1)-C(7)-C(8)-C(13)	81.0(3)
C(13)-C(8)-C(9)-C(10)	0.7(4)
C(7)-C(8)-C(9)-C(10)	180.0(3)
C(8)-C(9)-C(10)-C(11)	-0.3(5)
C(9)-C(10)-C(11)-C(12)	-0.1(5)
C(10)-C(11)-C(12)-C(13)	-0.1(5)
C(11)-C(12)-C(13)-C(8)	0.6(5)
C(9)-C(8)-C(13)-C(12)	-0.9(4)
C(7)-C(8)-C(13)-C(12)	179.9(3)

Symmetry transformations used to generate equivalent atoms:

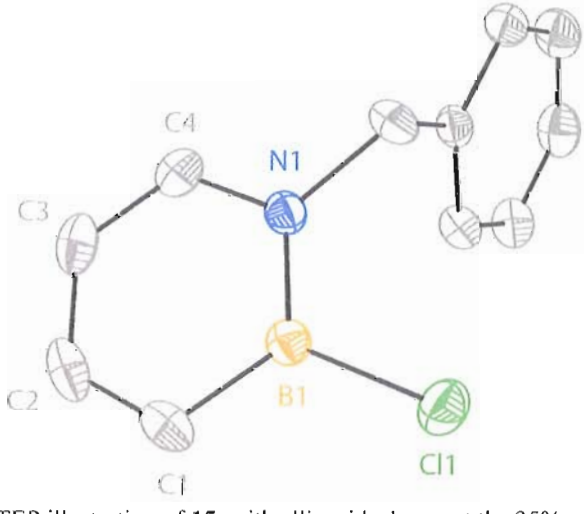

Figure 20. ORTEP illustration of **15**, with ellipsoids drawn at the 35% probability level.

X-ray Crystal Structure Determination. Crystals of **15** suitable for X-ray diffraction were obtained by placing a vial containing **15** in a glove box freezer at -20 °C. Frozen crystals of **15** were quickly transferred to the diffractometer while attempting to keep the crystals air-free.

Diffraction intensity data were collected with a Bruker Smart Apex CCD diffractometer at 173(2) K using MoKα - radiation (0.71073 Å). The structure was solved using direct methods, completed by subsequent difference Fourier syntheses, and refined by full matrix least-squares procedures on F^2. All non-H atoms were refined with anisotropic thermal parameters. H atoms were found on the residual density map and refined with isotropic thermal parameters. The Flack parameter is 0.00(8). All software and sources scattering factors are contained in the SHELXTL (6.10) program package (G.Sheldrick, Bruker XRD, Madison, WI). Crystallographic data and some details of data collection and crystal structure refinement for $C_{11}H_{11}BClN$ are given in the following tables.

Table 68. Crystal data and structure refinement for **15** (liu13).

Identification code	liu13	
Empirical formula	C_{11} H_{11} B Cl N	
Formula weight	203.47	
Temperature	173(2) K	
Wavelength	0.71073 Å	
Crystal system	Monoclinic	
Space group	P2(1)/n	
Unit cell dimensions	a = 6.6633(11) Å	α= 90°.
	b = 7.6484(13) Å	β= 97.092(2)°.
	c = 20.966(3) Å	γ = 90°.
Volume	1060.3(3) $Å^3$	
Z	4	
Density (calculated)	1.275 Mg/m^3	

Absorption coefficient	0.316 mm^{-1}
F(000)	424
Crystal size	0.48 x 0.45 x 0.24 mm^3
Theta range for data collection	1.96 to 26.99°.
Index ranges	-8<=h<=8, -9<=k<=9, -26<=l<=26
Reflections collected	9247
Independent reflections	2295 [R(int) = 0.0187]
Completeness to theta = 26.99°	99.1 %
Absorption correction	Semi-empirical from equivalents
Max. and min. transmission	1.000 and 0.642
Refinement method	Full-matrix least-squares on F^2
Data / restraints / parameters	2295 / 0 / 171
Goodness-of-fit on F^2	1.011
Final R indices [I>2sigma(I)]	R1 = 0.0340, wR2 = 0.0942
R indices (all data)	R1 = 0.0371, wR2 = 0.0971
Largest diff. peak and hole	0.336 and -0.287 $e.Å^{-3}$

Table 69. Atomic coordinates (x 10^4) and equivalent isotropic displacement parameters ($Å^2$x 10^3) for **15**. U(eq) is defined as one third of the trace of the orthogonalized U^{ij} tensor.

	x	y	z	U(eq)
Cl(1)	8132(1)	1678(1)	246(1)	44(1)
N(1)	5257(2)	3613(1)	800(1)	30(1)
B(1)	7191(2)	3633(2)	580(1)	31(1)
C(1)	8378(2)	5303(2)	649(1)	40(1)
C(2)	7538(3)	6709(2)	911(1)	46(1)
C(3)	5608(3)	6607(2)	1118(1)	47(1)
C(4)	4543(2)	5099(2)	1062(1)	39(1)
C(5)	3937(2)	2060(2)	789(1)	37(1)
C(6)	4063(2)	1142(2)	1432(1)	32(1)
C(7)	5840(2)	1093(2)	1855(1)	37(1)
C(8)	5940(3)	167(2)	2428(1)	45(1)
C(9)	4260(3)	-721(2)	2582(1)	50(1)
C(10)	2490(3)	-675(2)	2170(1)	52(1)
C(11)	2381(2)	254(2)	1597(1)	41(1)

Table 70. Bond lengths [Å] and angles [°] for **15**.

Cl(1)-B(1)	1.7962(15)
N(1)-C(4)	1.3723(18)
N(1)-B(1)	1.4220(19)
N(1)-C(5)	1.4762(17)
B(1)-C(1)	1.500(2)
C(1)-C(2)	1.359(2)
C(1)-H(1)	0.968(18)
C(2)-C(3)	1.409(3)
C(2)-H(2)	0.95(2)
C(3)-C(4)	1.352(2)
C(3)-H(3)	0.93(2)
C(4)-H(4)	0.952(19)
C(5)-C(6)	1.5144(19)
C(5)-H(5A)	0.988(18)
C(5)-H(5B)	0.983(18)
C(6)-C(7)	1.3892(19)
C(6)-C(11)	1.3900(19)
C(7)-C(8)	1.389(2)
C(7)-H(7)	0.971(19)
C(8)-C(9)	1.381(2)
C(8)-H(8)	0.962(18)
C(9)-C(10)	1.374(3)
C(9)-H(9)	0.99(2)
C(10)-C(11)	1.390(2)
C(10)-H(10)	0.93(2)
C(11)-H(11)	0.950(17)
C(4)-N(1)-B(1)	119.57(12)
C(4)-N(1)-C(5)	115.96(12)
B(1)-N(1)-C(5)	124.44(12)
N(1)-B(1)-C(1)	117.78(13)
N(1)-B(1)-Cl(1)	119.43(10)
C(1)-B(1)-Cl(1)	122.78(11)
C(2)-C(1)-B(1)	118.32(14)
C(2)-C(1)-H(1)	119.1(11)
B(1)-C(1)-H(1)	122.6(11)
C(1)-C(2)-C(3)	121.18(14)
C(1)-C(2)-H(2)	122.0(12)
C(3)-C(2)-H(2)	116.8(12)
C(4)-C(3)-C(2)	120.62(14)
C(4)-C(3)-H(3)	116.7(13)
C(2)-C(3)-H(3)	122.6(13)
C(3)-C(4)-N(1)	122.52(14)
C(3)-C(4)-H(4)	122.0(11)
N(1)-C(4)-H(4)	115.5(12)
N(1)-C(5)-C(6)	113.04(11)
N(1)-C(5)-H(5A)	107.4(10)
C(6)-C(5)-H(5A)	109.4(10)
N(1)-C(5)-H(5B)	108.3(11)
C(6)-C(5)-H(5B)	111.9(10)
H(5A)-C(5)-H(5B)	106.4(14)
C(7)-C(6)-C(11)	118.58(13)
C(7)-C(6)-C(5)	122.02(12)

C(11)-C(6)-C(5)	119.34(12)
C(6)-C(7)-C(8)	120.77(14)
C(6)-C(7)-H(7)	119.9(10)
C(8)-C(7)-H(7)	119.3(11)
C(9)-C(8)-C(7)	119.97(15)
C(9)-C(8)-H(8)	119.2(11)
C(7)-C(8)-H(8)	120.8(11)
C(10)-C(9)-C(8)	119.88(15)
C(10)-C(9)-H(9)	123.4(12)
C(8)-C(9)-H(9)	116.7(12)
C(9)-C(10)-C(11)	120.37(15)
C(9)-C(10)-H(10)	123.2(13)
C(11)-C(10)-H(10)	116.5(13)
C(6)-C(11)-C(10)	120.43(15)
C(6)-C(11)-H(11)	117.0(10)
C(10)-C(11)-H(11)	122.6(10)

Symmetry transformations used to generate equivalent atoms:

Table 71. Anisotropic displacement parameters ($Å^2 x\ 10^3$)for **15**. The anisotropic displacement factor exponent takes the form: $-2\pi^2[\ h^2 a^{*2} U^{11} + ... + 2\ h\ k\ a^*\ b^*\ U^{12}\ ]$

	U^{11}	U^{22}	U^{33}	U^{23}	U^{13}	U^{12}
Cl(1)	43(1)	39(1)	51(1)	-8(1)	8(1)	7(1)
N(1)	31(1)	28(1)	31(1)	2(1)	2(1)	-2(1)
B(1)	32(1)	30(1)	29(1)	1(1)	2(1)	0(1)
C(1)	41(1)	42(1)	35(1)	3(1)	5(1)	-12(1)
C(2)	67(1)	30(1)	39(1)	2(1)	-2(1)	-15(1)
C(3)	66(1)	30(1)	43(1)	-4(1)	3(1)	9(1)
C(4)	40(1)	40(1)	39(1)	0(1)	7(1)	9(1)
C(5)	33(1)	39(1)	38(1)	1(1)	1(1)	-11(1)
C(6)	35(1)	26(1)	36(1)	-3(1)	8(1)	-2(1)
C(7)	40(1)	35(1)	37(1)	-1(1)	4(1)	-6(1)
C(8)	57(1)	40(1)	38(1)	0(1)	1(1)	0(1)
C(9)	70(1)	41(1)	42(1)	7(1)	16(1)	1(1)
C(10)	54(1)	44(1)	62(1)	7(1)	26(1)	-7(1)
C(11)	36(1)	37(1)	51(1)	1(1)	12(1)	-3(1)

Table 72. Hydrogen coordinates (x 10^4) and isotropic displacement parameters ($Å^2 x\ 10^3$) for **15**.

	x	y	z	U(eq)
H(1)	9720(30)	5410(20)	519(8)	50(5)
H(2)	8200(30)	7820(30)	950(9)	57(5)
H(3)	5000(30)	7550(30)	1294(10)	61(5)
H(4)	3260(30)	4990(20)	1212(9)	54(5)
H(5A)	4360(30)	1250(20)	464(8)	47(5)
H(5B)	2550(30)	2420(20)	632(8)	45(4)
H(7)	7030(30)	1700(20)	1750(8)	50(5)
H(8)	7170(30)	140(20)	2723(8)	49(5)
H(9)	4410(30)	-1350(30)	2996(9)	57(5)
H(10)	1320(30)	-1240(30)	2253(10)	71(6)

H(11)	1190(30)	300(20)	1299(8)	44(4)

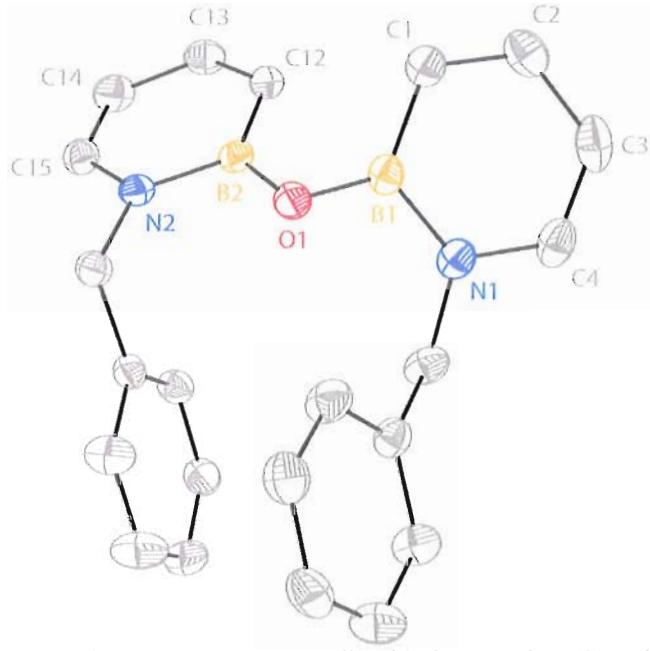

Figure 21. ORTEP illustration of **18**, with ellipsoids drawn at the 35% probability level.

X-ray Crystal Structure Determination. Crystals of **18** suitable for X-ray diffraction were obtained by collecting the crystals that had formed when 15 was distilled to dryness after having inadvertently been exposed to air.

Diffraction intensity data were collected with a Bruker Smart Apex CCD diffractometer at 173(2) K using MoKα - radiation (0.71073 Å). The structure was solved using direct methods, completed by subsequent difference Fourier syntheses, and refined by full matrix least-squares procedures on F^2. All non-H atoms were refined with anisotropic thermal parameters. H atoms were found on the residual density map and refined with isotropic thermal parameters. The Flack parameter is 0.00(8). All software and sources scattering factors are contained in the SHELXTL (6.10) program package

(G.Sheldrick, Bruker XRD, Madison, WI). Crystallographic data and some details of data collection and crystal structure refinement for $C_{22}H_{22}B_2N_2O$ are given in the following tables.

Table 73. Crystal data and structure refinement for **18** (Liu3).

Identification code	liu3	
Empirical formula	C_{22} H_{22} B_2 N_2 O	
Formula weight	352.04	
Temperature	173(2) K	
Wavelength	0.71073 Å	
Crystal system	Monoclinic	
Space group	C2/c	
Unit cell dimensions	a = 19.339(2) Å	α = 90°.
	b = 10.9026(12) Å	β = 106.372(2)°.
	c = 28.379(3) Å	γ = 90°.
Volume	5741.1(11) $Å^3$	
Z	12	
Density (calculated)	1.222 Mg/m^3	
Absorption coefficient	0.074 mm^{-1}	
F(000)	2232	
Crystal size	0.23 x 0.19 x 0.12 mm^3	
Theta range for data collection	1.50 to 27.00°.	
Index ranges	-24<=h<=24, -13<=k<=13, -36<=l<=36	
Reflections collected	31623	
Independent reflections	6263 [R(int) = 0.0469]	
Completeness to theta = 27.00°	99.9 %	
Absorption correction	Semi-empirical from equivalents	
Max. and min. transmission	0.9912 and 0.9833	
Refinement method	Full-matrix least-squares on F^2	
Data / restraints / parameters	6263 / 0 / 498	
Goodness-of-fit on F^2	1.040	
Final R indices [I>2sigma(I)]	R1 = 0.0485, wR2 = 0.0972	
R indices (all data)	R1 = 0.0774, wR2 = 0.1109	
Largest diff. peak and hole	0.168 and -0.133 $e.Å^{-3}$	

Table 74. Atomic coordinates (x 10^4) and equivalent isotropic displacement parameters ($Å^2$x 10^3) for **18**. U(eq) is defined as one third of the trace of the orthogonalized U^{ij} tensor.

	x	y	z	U(eq)
O(1)	2026(1)	7562(1)	913(1)	40(1)

O(2)	0	4830(1)	2500	33(1)
N(1)	1660(1)	8000(1)	53(1)	36(1)
N(2)	2598(1)	7593(1)	1775(1)	33(1)
N(3)	902(1)	4954(1)	2066(1)	36(1)
B(1)	1655(1)	7176(2)	446(1)	34(1)
B(2)	2443(1)	6945(2)	1313(1)	33(1)
B(3)	341(1)	4271(2)	2190(1)	31(1)
C(1)	1226(1)	6005(2)	306(1)	39(1)
C(2)	868(1)	5815(2)	-175(1)	45(1)
C(3)	901(1)	6679(2)	-540(1)	49(1)
C(4)	1285(1)	7726(2)	-422(1)	44(1)
C(5)	2059(1)	9169(2)	138(1)	42(1)
C(6)	1598(1)	10277(2)	147(1)	35(1)
C(7)	1030(1)	10238(2)	355(1)	47(1)
C(8)	644(1)	11293(2)	385(1)	49(1)
C(9)	822(1)	12391(2)	218(1)	48(1)
C(10)	1381(1)	12435(2)	4(1)	53(1)
C(11)	1759(1)	11385(2)	-33(1)	46(1)
C(12)	2782(1)	5689(2)	1331(1)	38(1)
C(13)	3214(1)	5271(2)	1767(1)	44(1)
C(14)	3342(1)	5976(2)	2201(1)	48(1)
C(15)	3041(1)	7096(2)	2194(1)	42(1)
C(16)	2310(1)	8832(2)	1800(1)	37(1)
C(17)	2715(1)	9835(1)	1620(1)	32(1)
C(18)	2405(1)	10985(2)	1534(1)	47(1)
C(19)	2757(1)	11939(2)	1377(1)	58(1)
C(20)	3423(1)	11756(2)	1303(1)	48(1)
C(21)	3737(1)	10616(2)	1389(1)	42(1)
C(22)	3384(1)	9659(2)	1546(1)	37(1)
C(23)	172(1)	3023(2)	1951(1)	36(1)
C(24)	538(1)	2641(2)	1633(1)	44(1)
C(25)	1081(1)	3368(2)	1532(1)	51(1)
C(26)	1253(1)	4471(2)	1748(1)	47(1)
C(27)	1103(1)	6198(2)	2251(1)	41(1)
C(28)	701(1)	7201(2)	1917(1)	36(1)
C(29)	498(1)	7100(2)	1407(1)	42(1)
C(30)	145(1)	8054(2)	1115(1)	51(1)
C(31)	-15(1)	9117(2)	1323(1)	56(1)
C(32)	186(1)	9230(2)	1828(1)	56(1)
C(33)	544(1)	8280(2)	2121(1)	46(1)

Table 75. Bond lengths [Å] and angles [°] for **18**.

O(1)-B(2)	1.369(2)
O(1)-B(1)	1.382(2)
O(2)-B(3)#1	1.3797(18)
O(2)-B(3)	1.3797(18)
N(1)-C(4)	1.371(2)
N(1)-B(1)	1.434(2)
N(1)-C(5)	1.474(2)
N(2)-C(15)	1.367(2)
N(2)-B(2)	1.445(2)
N(2)-C(16)	1.471(2)

N(3)-C(26)	1.378(2)
N(3)-B(3)	1.440(2)
N(3)-C(27)	1.467(2)
B(1)-C(1)	1.514(3)
B(2)-C(12)	1.514(2)
B(3)-C(23)	1.515(2)
C(1)-C(2)	1.362(2)
C(1)-H(1)	0.944(17)
C(2)-C(3)	1.415(3)
C(2)-H(2)	0.971(18)
C(3)-C(4)	1.350(3)
C(3)-H(3)	0.936(19)
C(4)-H(4)	0.959(18)
C(5)-C(6)	1.506(2)
C(5)-H(5A)	0.999(18)
C(5)-H(5B)	1.03(2)
C(6)-C(11)	1.381(2)
C(6)-C(7)	1.386(2)
C(7)-C(8)	1.387(2)
C(7)-H(7)	0.974(19)
C(8)-C(9)	1.368(3)
C(8)-H(8)	0.99(2)
C(9)-C(10)	1.382(3)
C(9)-H(9)	0.995(18)
C(10)-C(11)	1.379(3)
C(10)-H(10)	0.98(2)
C(11)-H(11)	0.966(18)
C(12)-C(13)	1.363(2)
C(12)-H(12)	0.964(16)
C(13)-C(14)	1.413(3)
C(13)-H(13)	0.996(18)
C(14)-C(15)	1.351(3)
C(14)-H(14)	0.98(2)
C(15)-H(15)	0.993(17)
C(16)-C(17)	1.516(2)
C(16)-H(16A)	0.980(16)
C(16)-H(16B)	1.010(18)
C(17)-C(18)	1.381(2)
C(17)-C(22)	1.383(2)
C(18)-C(19)	1.384(3)
C(18)-H(18)	0.994(18)
C(19)-C(20)	1.378(3)
C(19)-H(19)	0.97(2)
C(20)-C(21)	1.374(3)
C(20)-H(20)	0.948(19)
C(21)-C(22)	1.387(2)
C(21)-H(21)	0.987(18)
C(22)-H(22)	0.982(16)
C(23)-C(24)	1.359(2)
C(23)-H(23)	0.959(16)
C(24)-C(25)	1.408(3)
C(24)-H(24)	1.003(18)
C(25)-C(26)	1.349(3)

C(25)-H(25)	0.974(18)
C(26)-H(26)	0.988(18)
C(27)-C(28)	1.512(2)
C(27)-H(27A)	1.006(18)
C(27)-H(27B)	0.997(17)
C(28)-C(33)	1.382(2)
C(28)-C(29)	1.392(2)
C(29)-C(30)	1.384(3)
C(29)-H(29)	0.956(18)
C(30)-C(31)	1.374(3)
C(30)-H(30)	0.977(19)
C(31)-C(32)	1.379(3)
C(31)-H(31)	0.98(2)
C(32)-C(33)	1.385(3)
C(32)-H(32)	1.00(2)
C(33)-H(33)	0.965(18)
B(2)-O(1)-B(1)	132.08(14)
B(3)#1-O(2)-B(3)	127.59(18)
C(4)-N(1)-B(1)	120.72(15)
C(4)-N(1)-C(5)	117.14(15)
B(1)-N(1)-C(5)	122.14(14)
C(15)-N(2)-B(2)	121.00(14)
C(15)-N(2)-C(16)	118.37(14)
B(2)-N(2)-C(16)	120.58(14)
C(26)-N(3)-B(3)	120.53(15)
C(26)-N(3)-C(27)	117.22(15)
B(3)-N(3)-C(27)	122.20(14)
O(1)-B(1)-N(1)	116.11(15)
O(1)-B(1)-C(1)	127.32(15)
N(1)-B(1)-C(1)	116.53(15)
O(1)-B(2)-N(2)	115.81(15)
O(1)-B(2)-C(12)	128.35(16)
N(2)-B(2)-C(12)	115.80(15)
O(2)-B(3)-N(3)	117.13(15)
O(2)-B(3)-C(23)	126.99(15)
N(3)-B(3)-C(23)	115.84(14)
C(2)-C(1)-B(1)	118.52(17)
C(2)-C(1)-H(1)	119.2(11)
B(1)-C(1)-H(1)	122.2(11)
C(1)-C(2)-C(3)	121.21(19)
C(1)-C(2)-H(2)	119.9(11)
C(3)-C(2)-H(2)	118.9(10)
C(4)-C(3)-C(2)	120.99(18)
C(4)-C(3)-H(3)	120.3(12)
C(2)-C(3)-H(3)	118.7(12)
C(3)-C(4)-N(1)	122.02(17)
C(3)-C(4)-H(4)	123.3(11)
N(1)-C(4)-H(4)	114.7(11)
N(1)-C(5)-C(6)	114.32(14)
N(1)-C(5)-H(5A)	109.4(10)
C(6)-C(5)-H(5A)	108.8(10)
N(1)-C(5)-H(5B)	106.7(10)
C(6)-C(5)-H(5B)	109.0(10)

H(5A)-C(5)-H(5B)	108.4(14)
C(11)-C(6)-C(7)	118.22(16)
C(11)-C(6)-C(5)	119.93(15)
C(7)-C(6)-C(5)	121.77(15)
C(6)-C(7)-C(8)	120.44(18)
C(6)-C(7)-H(7)	118.1(11)
C(8)-C(7)-H(7)	121.4(11)
C(9)-C(8)-C(7)	120.72(18)
C(9)-C(8)-H(8)	121.4(11)
C(7)-C(8)-H(8)	117.9(11)
C(8)-C(9)-C(10)	119.23(17)
C(8)-C(9)-H(9)	120.2(10)
C(10)-C(9)-H(9)	120.5(10)
C(11)-C(10)-C(9)	120.14(19)
C(11)-C(10)-H(10)	122.3(12)
C(9)-C(10)-H(10)	117.6(12)
C(10)-C(11)-C(6)	121.21(17)
C(10)-C(11)-H(11)	119.7(11)
C(6)-C(11)-H(11)	119.1(11)
C(13)-C(12)-B(2)	118.77(16)
C(13)-C(12)-H(12)	118.0(10)
B(2)-C(12)-H(12)	123.3(10)
C(12)-C(13)-C(14)	121.53(17)
C(12)-C(13)-H(13)	120.3(10)
C(14)-C(13)-H(13)	118.1(10)
C(15)-C(14)-C(13)	120.65(17)
C(15)-C(14)-H(14)	118.6(11)
C(13)-C(14)-H(14)	120.7(11)
C(14)-C(15)-N(2)	122.23(17)
C(14)-C(15)-H(15)	122.1(10)
N(2)-C(15)-H(15)	115.6(10)
N(2)-C(16)-C(17)	114.01(13)
N(2)-C(16)-H(16A)	108.8(9)
C(17)-C(16)-H(16A)	108.2(9)
N(2)-C(16)-H(16B)	109.1(10)
C(17)-C(16)-H(16B)	107.8(10)
H(16A)-C(16)-H(16B)	108.8(13)
C(18)-C(17)-C(22)	118.55(15)
C(18)-C(17)-C(16)	118.34(14)
C(22)-C(17)-C(16)	123.10(15)
C(17)-C(18)-C(19)	120.72(17)
C(17)-C(18)-H(18)	117.9(10)
C(19)-C(18)-H(18)	121.4(10)
C(20)-C(19)-C(18)	120.43(18)
C(20)-C(19)-H(19)	119.4(13)
C(18)-C(19)-H(19)	120.2(13)
C(21)-C(20)-C(19)	119.25(18)
C(21)-C(20)-H(20)	119.7(11)
C(19)-C(20)-H(20)	121.0(11)
C(20)-C(21)-C(22)	120.36(17)
C(20)-C(21)-H(21)	119.8(10)
C(22)-C(21)-H(21)	119.9(10)
C(17)-C(22)-C(21)	120.69(16)

C(17)-C(22)-H(22)	118.7(9)
C(21)-C(22)-H(22)	120.6(9)
C(24)-C(23)-B(3)	119.17(17)
C(24)-C(23)-H(23)	117.4(9)
B(3)-C(23)-H(23)	123.4(9)
C(23)-C(24)-C(25)	121.30(18)
C(23)-C(24)-H(24)	120.7(10)
C(25)-C(24)-H(24)	118.0(10)
C(26)-C(25)-C(24)	120.86(17)
C(26)-C(25)-H(25)	118.8(11)
C(24)-C(25)-H(25)	120.3(11)
C(25)-C(26)-N(3)	122.27(18)
C(25)-C(26)-H(26)	123.8(10)
N(3)-C(26)-H(26)	113.9(10)
N(3)-C(27)-C(28)	114.00(14)
N(3)-C(27)-H(27A)	109.1(10)
C(28)-C(27)-H(27A)	110.0(10)
N(3)-C(27)-H(27B)	107.9(9)
C(28)-C(27)-H(27B)	109.6(9)
H(27A)-C(27)-H(27B)	105.9(14)
C(33)-C(28)-C(29)	118.13(17)
C(33)-C(28)-C(27)	119.22(16)
C(29)-C(28)-C(27)	122.62(16)
C(30)-C(29)-C(28)	120.63(19)
C(30)-C(29)-H(29)	119.5(11)
C(28)-C(29)-H(29)	119.7(11)
C(31)-C(30)-C(29)	120.64(19)
C(31)-C(30)-H(30)	121.3(11)
C(29)-C(30)-H(30)	118.1(11)
C(30)-C(31)-C(32)	119.2(2)
C(30)-C(31)-H(31)	119.0(12)
C(32)-C(31)-H(31)	121.8(12)
C(31)-C(32)-C(33)	120.2(2)
C(31)-C(32)-H(32)	120.4(12)
C(33)-C(32)-H(32)	119.3(12)
C(28)-C(33)-C(32)	121.10(19)
C(28)-C(33)-H(33)	117.8(11)
C(32)-C(33)-H(33)	121.1(11)

Symmetry transformations used to generate equivalent atoms:
#1 -x,y,-z+1/2

Table 76. Anisotropic displacement parameters ($Å^2 x\ 10^3$)for **18**. The anisotropic displacement factor exponent takes the form: $-2p^2[\ h^2a^{*2}U^{11} + ... + 2\ h\ k\ a^*\ b^*\ U^{12}\ ]$

	U^{11}	U^{22}	U^{33}	U^{23}	U^{13}	U^{12}
O(1)	49(1)	34(1)	35(1)	2(1)	8(1)	2(1)
O(2)	37(1)	32(1)	34(1)	0	16(1)	0
N(1)	37(1)	37(1)	37(1)	4(1)	17(1)	10(1)
N(2)	34(1)	30(1)	36(1)	1(1)	12(1)	-3(1)
N(3)	34(1)	40(1)	35(1)	4(1)	14(1)	2(1)
B(1)	34(1)	36(1)	33(1)	1(1)	13(1)	9(1)
B(2)	33(1)	34(1)	34(1)	2(1)	13(1)	-5(1)

B(3)	30(1)	35(1)	28(1)	5(1)	9(1)	6(1)
C(1)	41(1)	39(1)	40(1)	2(1)	14(1)	7(1)
C(2)	41(1)	41(1)	51(1)	-10(1)	9(1)	9(1)
C(3)	52(1)	59(1)	32(1)	-7(1)	4(1)	23(1)
C(4)	51(1)	51(1)	35(1)	7(1)	19(1)	21(1)
C(5)	39(1)	41(1)	53(1)	11(1)	23(1)	7(1)
C(6)	35(1)	39(1)	33(1)	3(1)	13(1)	4(1)
C(7)	51(1)	44(1)	55(1)	7(1)	31(1)	6(1)
C(8)	49(1)	54(1)	54(1)	-5(1)	28(1)	8(1)
C(9)	47(1)	43(1)	52(1)	-10(1)	12(1)	10(1)
C(10)	51(1)	37(1)	71(1)	6(1)	19(1)	5(1)
C(11)	41(1)	42(1)	58(1)	8(1)	21(1)	6(1)
C(12)	44(1)	34(1)	39(1)	-1(1)	16(1)	-3(1)
C(13)	42(1)	37(1)	52(1)	6(1)	11(1)	4(1)
C(14)	48(1)	46(1)	42(1)	9(1)	0(1)	-1(1)
C(15)	44(1)	45(1)	33(1)	0(1)	7(1)	-7(1)
C(16)	39(1)	36(1)	42(1)	-4(1)	18(1)	-2(1)
C(17)	31(1)	34(1)	30(1)	-5(1)	9(1)	-3(1)
C(18)	35(1)	39(1)	70(1)	3(1)	19(1)	2(1)
C(19)	49(1)	37(1)	89(2)	12(1)	22(1)	5(1)
C(20)	50(1)	41(1)	56(1)	7(1)	20(1)	-9(1)
C(21)	39(1)	43(1)	48(1)	-7(1)	19(1)	-7(1)
C(22)	37(1)	34(1)	44(1)	-3(1)	15(1)	0(1)
C(23)	39(1)	34(1)	35(1)	2(1)	9(1)	4(1)
C(24)	57(1)	39(1)	33(1)	0(1)	9(1)	17(1)
C(25)	61(1)	57(1)	43(1)	7(1)	28(1)	23(1)
C(26)	42(1)	60(1)	47(1)	14(1)	26(1)	10(1)
C(27)	40(1)	47(1)	37(1)	4(1)	11(1)	-12(1)
C(28)	33(1)	40(1)	39(1)	3(1)	15(1)	-11(1)
C(29)	47(1)	43(1)	38(1)	1(1)	16(1)	-10(1)
C(30)	51(1)	59(1)	40(1)	12(1)	8(1)	-13(1)
C(31)	43(1)	50(1)	70(2)	19(1)	10(1)	-5(1)
C(32)	50(1)	45(1)	74(2)	-3(1)	21(1)	-2(1)
C(33)	46(1)	50(1)	45(1)	-5(1)	15(1)	-8(1)

Table 77. Hydrogen coordinates (x 10^4) and isotropic displacement parameters ($Å^2$x 10^3) for **18**.

	x	y	z	U(eq)
H(1)	1208(9)	5398(16)	539(6)	50(5)
H(2)	591(9)	5070(17)	-273(6)	52(5)
H(3)	649(10)	6516(17)	-867(7)	63(6)
H(4)	1328(10)	8323(17)	-660(7)	56(6)
H(5A)	2310(9)	9287(16)	-122(6)	53(5)
H(5B)	2441(11)	9092(17)	471(7)	61(6)
H(7)	909(10)	9452(18)	474(7)	60(6)
H(8)	233(11)	11221(17)	525(7)	67(6)
H(9)	537(9)	13140(16)	237(6)	51(5)
H(10)	1487(10)	13225(19)	-122(7)	69(6)
H(11)	2147(10)	11421(16)	-185(6)	55(5)
H(12)	2704(9)	5160(15)	1048(6)	41(5)
H(13)	3451(10)	4453(17)	1788(6)	56(5)
H(14)	3656(10)	5665(17)	2513(7)	65(6)

H(15)	3127(9)	7612(15)	2493(6)	47(5)
H(16A)	2329(8)	9011(14)	2142(6)	37(4)
H(16B)	1791(10)	8859(15)	1594(6)	49(5)
H(18)	1927(10)	11104(16)	1593(6)	57(5)
H(19)	2531(11)	12740(20)	1311(7)	79(7)
H(20)	3668(10)	12404(17)	1195(6)	58(6)
H(21)	4214(10)	10477(16)	1336(6)	53(5)
H(22)	3606(9)	8843(15)	1607(6)	41(5)
H(23)	-194(8)	2490(14)	2002(6)	38(4)
H(24)	439(9)	1815(17)	1472(6)	54(5)
H(25)	1332(9)	3088(16)	1299(7)	56(5)
H(26)	1633(10)	5010(16)	1692(6)	53(5)
H(27A)	1638(10)	6308(15)	2311(6)	51(5)
H(27B)	1013(9)	6269(14)	2579(6)	43(5)
H(29)	578(9)	6348(17)	1258(6)	51(5)
H(30)	4(10)	7941(17)	759(7)	63(6)
H(31)	-275(10)	9773(18)	1107(7)	66(6)
H(32)	59(11)	9980(20)	1986(8)	78(7)
H(33)	678(10)	8339(16)	2474(7)	57(6)

Table 78. Torsion angles [°] for **18**.

B(2)-O(1)-B(1)-N(1)	-142.21(16)
B(2)-O(1)-B(1)-C(1)	40.0(3)
C(4)-N(1)-B(1)-O(1)	-177.43(14)
C(5)-N(1)-B(1)-O(1)	2.3(2)
C(4)-N(1)-B(1)-C(1)	0.6(2)
C(5)-N(1)-B(1)-C(1)	-179.74(14)
B(1)-O(1)-B(2)-N(2)	-165.22(15)
B(1)-O(1)-B(2)-C(12)	17.1(3)
C(15)-N(2)-B(2)-O(1)	-176.41(14)
C(16)-N(2)-B(2)-O(1)	0.8(2)
C(15)-N(2)-B(2)-C(12)	1.6(2)
C(16)-N(2)-B(2)-C(12)	178.71(14)
B(3)#1-O(2)-B(3)-N(3)	-154.12(15)
B(3)#1-O(2)-B(3)-C(23)	28.07(13)
C(26)-N(3)-B(3)-O(2)	-178.17(13)
C(27)-N(3)-B(3)-O(2)	-0.9(2)
C(26)-N(3)-B(3)-C(23)	-0.1(2)
C(27)-N(3)-B(3)-C(23)	177.16(14)
O(1)-B(1)-C(1)-C(2)	176.92(16)
N(1)-B(1)-C(1)-C(2)	-0.8(2)
B(1)-C(1)-C(2)-C(3)	0.8(2)
C(1)-C(2)-C(3)-C(4)	-0.5(3)
C(2)-C(3)-C(4)-N(1)	0.2(3)
B(1)-N(1)-C(4)-C(3)	-0.3(2)
C(5)-N(1)-C(4)-C(3)	180.00(15)
C(4)-N(1)-C(5)-C(6)	79.51(19)
B(1)-N(1)-C(5)-C(6)	-100.18(18)
N(1)-C(5)-C(6)-C(11)	-145.76(16)
N(1)-C(5)-C(6)-C(7)	37.5(2)
C(11)-C(6)-C(7)-C(8)	-0.9(3)
C(5)-C(6)-C(7)-C(8)	175.96(18)

C(6)-C(7)-C(8)-C(9)	-0.9(3)
C(7)-C(8)-C(9)-C(10)	1.8(3)
C(8)-C(9)-C(10)-C(11)	-0.9(3)
C(9)-C(10)-C(11)-C(6)	-0.9(3)
C(7)-C(6)-C(11)-C(10)	1.8(3)
C(5)-C(6)-C(11)-C(10)	-175.13(18)
O(1)-B(2)-C(12)-C(13)	176.32(16)
N(2)-B(2)-C(12)-C(13)	-1.3(2)
B(2)-C(12)-C(13)-C(14)	0.8(3)
C(12)-C(13)-C(14)-C(15)	-0.4(3)
C(13)-C(14)-C(15)-N(2)	0.6(3)
B(2)-N(2)-C(15)-C(14)	-1.2(2)
C(16)-N(2)-C(15)-C(14)	-178.45(16)
C(15)-N(2)-C(16)-C(17)	99.37(17)
B(2)-N(2)-C(16)-C(17)	-77.86(19)
N(2)-C(16)-C(17)-C(18)	167.06(15)
N(2)-C(16)-C(17)-C(22)	-14.2(2)
C(22)-C(17)-C(18)-C(19)	0.1(3)
C(16)-C(17)-C(18)-C(19)	178.89(18)
C(17)-C(18)-C(19)-C(20)	0.1(3)
C(18)-C(19)-C(20)-C(21)	-0.3(3)
C(19)-C(20)-C(21)-C(22)	0.4(3)
C(18)-C(17)-C(22)-C(21)	0.0(2)
C(16)-C(17)-C(22)-C(21)	-178.72(16)
C(20)-C(21)-C(22)-C(17)	-0.3(3)
O(2)-B(3)-C(23)-C(24)	176.43(15)
N(3)-B(3)-C(23)-C(24)	-1.4(2)
B(3)-C(23)-C(24)-C(25)	1.5(2)
C(23)-C(24)-C(25)-C(26)	-0.1(3)
C(24)-C(25)-C(26)-N(3)	-1.6(3)
B(3)-N(3)-C(26)-C(25)	1.6(3)
C(27)-N(3)-C(26)-C(25)	-175.81(17)
C(26)-N(3)-C(27)-C(28)	85.82(19)
B(3)-N(3)-C(27)-C(28)	-91.55(18)
N(3)-C(27)-C(28)-C(33)	147.24(15)
N(3)-C(27)-C(28)-C(29)	-34.6(2)
C(33)-C(28)-C(29)-C(30)	-0.4(2)
C(27)-C(28)-C(29)-C(30)	-178.51(16)
C(28)-C(29)-C(30)-C(31)	-0.3(3)
C(29)-C(30)-C(31)-C(32)	0.5(3)
C(30)-C(31)-C(32)-C(33)	0.0(3)
C(29)-C(28)-C(33)-C(32)	0.8(3)
C(27)-C(28)-C(33)-C(32)	179.03(16)
C(31)-C(32)-C(33)-C(28)	-0.6(3)

Symmetry transformations used to generate equivalent atoms:
#1 -x,y,-z+1/2

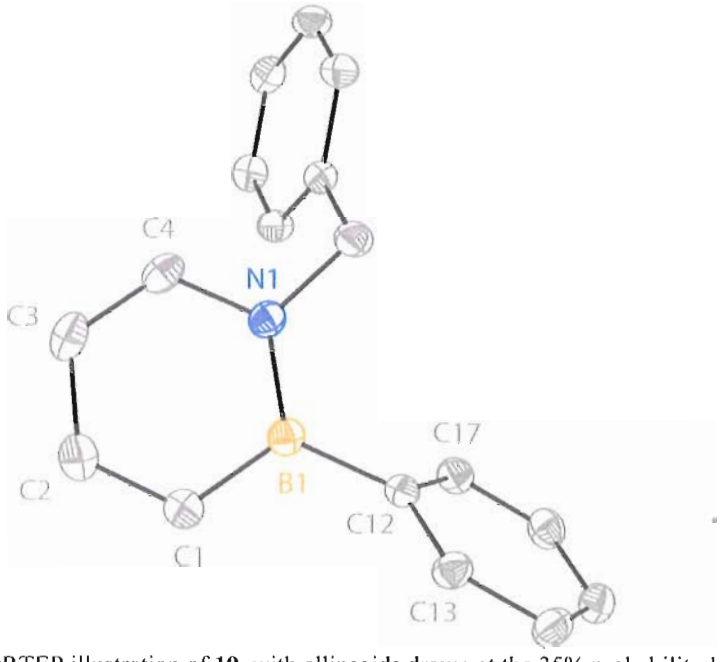

Figure 22. ORTEP illustration of **19**, with ellipsoids drawn at the 35% probability level.

X-ray Crystal Structure Determination. Crystals of **19** suitable for X-ray diffraction were obtained by slow evaporation of an Et_2O solution of **19**.

Diffraction intensity data were collected with a Bruker Smart Apex CCD diffractometer at 173(2) K using MoKα - radiation (0.71073 Å). The structure was solved using direct methods, completed by subsequent difference Fourier syntheses, and refined by full matrix least-squares procedures on F^2. All non-H atoms were refined with anisotropic thermal parameters. H atoms were found on the residual density map and refined with isotropic thermal parameters. The Flack parameter is 0.00(8). All software and sources scattering factors are contained in the SHELXTL (6.10) program package (G.Sheldrick, Bruker XRD, Madison, WI). Crystallographic data and some details of data collection and crystal structure refinement for $C_{17}H_{16}BN$ are given in the following tables.

Table 79. Crystal data and structure refinement for **19** (liu5).

Identification code	liu5	
Empirical formula	$C_{17}H_{16}BN$	
Formula weight	245.12	
Temperature	173(2) K	
Wavelength	0.71073 Å	
Crystal system	Triclinic	
Space group	P-1	
Unit cell dimensions	a = 8.0839(8) Å	α = 103.079(2)°.
	b = 9.9545(10) Å	β = 102.604(2)°.
	c = 10.0860(10) Å	γ = 113.009(2)°.
Volume	683.79(12) $Å^3$	
Z	2	
Density (calculated)	1.191 Mg/m^3	
Absorption coefficient	0.068 mm^{-1}	
F(000)	260	
Crystal size	0.29 x 0.16 x 0.12 mm^3	
Theta range for data collection	2.21 to 27.50°.	
Index ranges	-10<=h<=10, -12<=k<=12, -12<=l<=12	
Reflections collected	7826	
Independent reflections	3079 [R(int) = 0.0193]	
Completeness to theta = 27.50°	97.9 %	
Absorption correction	Semi-empirical from equivalents	
Max. and min. transmission	0.9919 and 0.9806	
Refinement method	Full-matrix least-squares on F^2	
Data / restraints / parameters	3079 / 0 / 236	
Goodness-of-fit on F^2	1.014	
Final R indices [I>2sigma(I)]	R1 = 0.0476, wR2 = 0.1206	
R indices (all data)	R1 = 0.0602, wR2 = 0.1302	
Largest diff. peak and hole	0.266 and -0.181 $e.Å^{-3}$	

Table 80. Atomic coordinates (x 10^4) and equivalent isotropic displacement parameters ($Å^2$x 10^3) for **19**. U(eq) is defined as one third of the trace of the orthogonalized U^{ij} tensor.

	x	y	z	U(eq)
B(1)	1564(2)	2558(2)	4775(2)	28(1)
N(1)	1968(2)	1904(1)	5858(1)	29(1)
C(1)	162(2)	3208(2)	4880(2)	33(1)
C(2)	-586(2)	3173(2)	5975(2)	37(1)
C(3)	-96(2)	2500(2)	6991(2)	38(1)
C(4)	1116(2)	1884(2)	6901(2)	34(1)
C(5)	3193(2)	1117(2)	5902(2)	33(1)
C(6)	4812(2)	1808(2)	7335(2)	28(1)

C(7)	5236(2)	828(2)	7973(2)	33(1)
C(8)	6707(2)	1433(2)	9288(2)	37(1)
C(9)	7766(2)	3029(2)	9988(2)	36(1)
C(10)	7351(2)	4014(2)	9359(2)	35(1)
C(11)	5889(2)	3408(2)	8039(2)	32(1)
C(12)	2433(2)	2557(2)	3520(2)	27(1)
C(13)	1168(2)	1982(2)	2093(2)	31(1)
C(14)	1809(2)	2011(2)	925(2)	35(1)
C(15)	3742(2)	2632(2)	1150(2)	36(1)
C(16)	5035(2)	3219(2)	2545(2)	36(1)
C(17)	4384(2)	3176(2)	3705(2)	32(1)

Table 81. Bond lengths [Å] and angles [°] for **19**.

B(1)-N(1)	1.434(2)
B(1)-C(1)	1.520(2)
B(1)-C(12)	1.576(2)
N(1)-C(4)	1.377(2)
N(1)-C(5)	1.483(2)
C(1)-C(2)	1.371(2)
C(1)-H(1)	0.994(18)
C(2)-C(3)	1.412(2)
C(2)-H(2)	1.02(2)
C(3)-C(4)	1.353(2)
C(3)-H(3)	0.96(2)
C(4)-H(4)	0.961(19)
C(5)-C(6)	1.515(2)
C(5)-H(5A)	1.00(2)
C(5)-H(5B)	1.001(19)
C(6)-C(7)	1.390(2)
C(6)-C(11)	1.391(2)
C(7)-C(8)	1.388(2)
C(7)-H(7)	0.971(19)
C(8)-C(9)	1.386(2)
C(8)-H(8)	0.948(19)
C(9)-C(10)	1.387(2)
C(9)-H(9)	0.970(18)
C(10)-C(11)	1.387(2)
C(10)-H(10)	0.98(2)
C(11)-H(11)	0.965(18)
C(12)-C(17)	1.400(2)
C(12)-C(13)	1.404(2)
C(13)-C(14)	1.389(2)
C(13)-H(13)	0.972(17)
C(14)-C(15)	1.380(2)
C(14)-H(14)	0.974(19)
C(15)-C(16)	1.386(2)
C(15)-H(15)	1.00(2)
C(16)-C(17)	1.386(2)
C(16)-H(16)	0.97(2)
C(17)-H(17)	0.960(18)
N(1)-B(1)-C(1)	115.24(14)
N(1)-B(1)-C(12)	123.18(14)

C(1)-B(1)-C(12)	121.54(13)
C(4)-N(1)-B(1)	120.87(13)
C(4)-N(1)-C(5)	114.82(13)
B(1)-N(1)-C(5)	124.18(13)
C(2)-C(1)-B(1)	120.01(15)
C(2)-C(1)-H(1)	119.5(11)
B(1)-C(1)-H(1)	120.4(11)
C(1)-C(2)-C(3)	120.40(15)
C(1)-C(2)-H(2)	119.6(11)
C(3)-C(2)-H(2)	120.0(11)
C(4)-C(3)-C(2)	120.64(15)
C(4)-C(3)-H(3)	119.2(12)
C(2)-C(3)-H(3)	120.2(12)
C(3)-C(4)-N(1)	122.80(15)
C(3)-C(4)-H(4)	121.2(11)
N(1)-C(4)-H(4)	116.0(11)
N(1)-C(5)-C(6)	113.06(12)
N(1)-C(5)-H(5A)	109.6(11)
C(6)-C(5)-H(5A)	108.5(10)
N(1)-C(5)-H(5B)	108.4(11)
C(6)-C(5)-H(5B)	110.4(10)
H(5A)-C(5)-H(5B)	106.7(15)
C(7)-C(6)-C(11)	118.79(14)
C(7)-C(6)-C(5)	119.66(14)
C(11)-C(6)-C(5)	121.54(13)
C(8)-C(7)-C(6)	120.73(15)
C(8)-C(7)-H(7)	119.1(10)
C(6)-C(7)-H(7)	120.2(10)
C(9)-C(8)-C(7)	120.16(15)
C(9)-C(8)-H(8)	119.0(12)
C(7)-C(8)-H(8)	120.9(12)
C(8)-C(9)-C(10)	119.45(15)
C(8)-C(9)-H(9)	121.7(11)
C(10)-C(9)-H(9)	118.8(11)
C(9)-C(10)-C(11)	120.32(15)
C(9)-C(10)-H(10)	120.4(12)
C(11)-C(10)-H(10)	119.3(12)
C(10)-C(11)-C(6)	120.55(15)
C(10)-C(11)-H(11)	117.9(11)
C(6)-C(11)-H(11)	121.5(11)
C(17)-C(12)-C(13)	116.43(14)
C(17)-C(12)-B(1)	125.62(13)
C(13)-C(12)-B(1)	117.82(13)
C(14)-C(13)-C(12)	121.96(14)
C(14)-C(13)-H(13)	118.5(10)
C(12)-C(13)-H(13)	119.5(10)
C(15)-C(14)-C(13)	119.98(15)
C(15)-C(14)-H(14)	120.4(11)
C(13)-C(14)-H(14)	119.6(12)
C(14)-C(15)-C(16)	119.63(15)
C(14)-C(15)-H(15)	120.3(11)
C(16)-C(15)-H(15)	119.9(11)
C(15)-C(16)-C(17)	120.08(15)

C(15)-C(16)-H(16)	119.0(11)
C(17)-C(16)-H(16)	120.9(11)
C(16)-C(17)-C(12)	121.91(15)
C(16)-C(17)-H(17)	119.8(11)
C(12)-C(17)-H(17)	118.2(11)

Symmetry transformations used to generate equivalent atoms:

Table 82. Anisotropic displacement parameters ($Å^2 x\ 10^3$)for **19**. The anisotropic displacement factor exponent takes the form: $-2p^2[\ h^2a^{*2}U^{11} + ... + 2\ h\ k\ a^*\ b^*\ U^{12}\ ]$

	U^{11}	U^{22}	U^{33}	U^{23}	U^{13}	U^{12}
B(1)	28(1)	27(1)	25(1)	6(1)	6(1)	11(1)
N(1)	30(1)	31(1)	22(1)	7(1)	6(1)	14(1)
C(1)	33(1)	34(1)	33(1)	12(1)	11(1)	17(1)
C(2)	33(1)	38(1)	37(1)	7(1)	12(1)	17(1)
C(3)	35(1)	48(1)	27(1)	8(1)	14(1)	15(1)
C(4)	35(1)	39(1)	23(1)	11(1)	7(1)	13(1)
C(5)	39(1)	31(1)	26(1)	8(1)	6(1)	19(1)
C(6)	30(1)	31(1)	27(1)	11(1)	11(1)	16(1)
C(7)	33(1)	32(1)	35(1)	15(1)	11(1)	16(1)
C(8)	37(1)	46(1)	40(1)	24(1)	14(1)	25(1)
C(9)	27(1)	50(1)	31(1)	15(1)	9(1)	18(1)
C(10)	29(1)	34(1)	35(1)	9(1)	10(1)	11(1)
C(11)	34(1)	31(1)	31(1)	13(1)	10(1)	15(1)
C(12)	31(1)	27(1)	27(1)	11(1)	10(1)	16(1)
C(13)	29(1)	37(1)	29(1)	14(1)	10(1)	16(1)
C(14)	38(1)	41(1)	27(1)	13(1)	10(1)	19(1)
C(15)	43(1)	39(1)	36(1)	16(1)	21(1)	22(1)
C(16)	31(1)	38(1)	44(1)	14(1)	17(1)	17(1)
C(17)	31(1)	33(1)	30(1)	7(1)	6(1)	16(1)

Table 83. Hydrogen coordinates (x 10^4) and isotropic displacement parameters ($Å^2 x\ 10^3$) for **19**.

	x	y	z	U(eq)
H(1)	-180(30)	3700(20)	4180(20)	39(5)
H(2)	-1500(30)	3630(20)	6050(20)	47(5)
H(3)	-620(30)	2480(20)	7760(20)	45(5)
H(4)	1430(30)	1400(20)	7570(20)	41(5)
H(5A)	2400(30)	-10(20)	5720(20)	42(5)
H(5B)	3710(30)	1170(20)	5090(20)	42(5)
H(7)	4500(30)	-290(20)	7501(19)	37(5)
H(8)	7000(30)	770(20)	9720(20)	42(5)
H(9)	8790(30)	3480(20)	10910(20)	37(5)
H(10)	8110(30)	5150(30)	9830(20)	53(6)
H(11)	5640(20)	4130(20)	7637(19)	37(5)
H(13)	-200(20)	1565(19)	1911(17)	29(4)
H(14)	890(30)	1620(20)	-50(20)	47(5)
H(15)	4220(30)	2720(20)	320(20)	51(5)
H(16)	6390(30)	3650(20)	2690(20)	46(5)
H(17)	5280(30)	3610(20)	4670(20)	37(5)

Table 84. Torsion angles [°] for **19**.

C(1)-B(1)-N(1)-C(4)	0.2(2)
C(12)-B(1)-N(1)-C(4)	-177.59(13)
C(1)-B(1)-N(1)-C(5)	175.90(13)
C(12)-B(1)-N(1)-C(5)	-1.9(2)
N(1)-B(1)-C(1)-C(2)	1.4(2)
C(12)-B(1)-C(1)-C(2)	179.17(14)
B(1)-C(1)-C(2)-C(3)	-1.5(2)
C(1)-C(2)-C(3)-C(4)	0.0(3)
C(2)-C(3)-C(4)-N(1)	1.6(3)
B(1)-N(1)-C(4)-C(3)	-1.7(2)
C(5)-N(1)-C(4)-C(3)	-177.78(15)
C(4)-N(1)-C(5)-C(6)	-58.78(18)
B(1)-N(1)-C(5)-C(6)	125.26(15)
N(1)-C(5)-C(6)-C(7)	136.53(15)
N(1)-C(5)-C(6)-C(11)	-43.2(2)
C(11)-C(6)-C(7)-C(8)	-0.1(2)
C(5)-C(6)-C(7)-C(8)	-179.77(15)
C(6)-C(7)-C(8)-C(9)	0.5(2)
C(7)-C(8)-C(9)-C(10)	-0.4(2)
C(8)-C(9)-C(10)-C(11)	0.0(2)
C(9)-C(10)-C(11)-C(6)	0.4(2)
C(7)-C(6)-C(11)-C(10)	-0.4(2)
C(5)-C(6)-C(11)-C(10)	179.29(15)
N(1)-B(1)-C(12)-C(17)	-55.8(2)
C(1)-B(1)-C(12)-C(17)	126.60(17)
N(1)-B(1)-C(12)-C(13)	128.60(16)
C(1)-B(1)-C(12)-C(13)	-49.0(2)
C(17)-C(12)-C(13)-C(14)	0.5(2)
B(1)-C(12)-C(13)-C(14)	176.50(14)
C(12)-C(13)-C(14)-C(15)	-0.6(2)
C(13)-C(14)-C(15)-C(16)	0.3(2)
C(14)-C(15)-C(16)-C(17)	0.2(2)
C(15)-C(16)-C(17)-C(12)	-0.4(2)
C(13)-C(12)-C(17)-C(16)	0.0(2)
B(1)-C(12)-C(17)-C(16)	-175.65(14)

Symmetry transformations used to generate equivalent atoms:

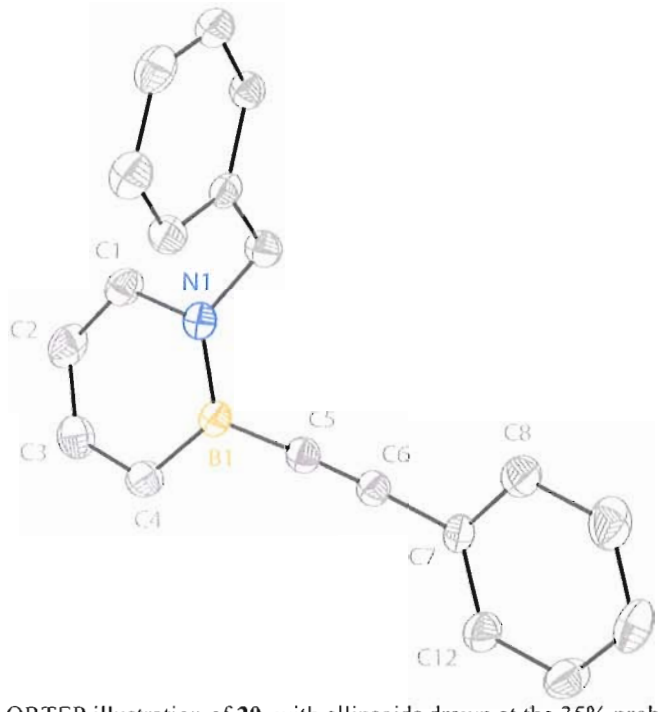

Figure 23. ORTEP illustration of **20**, with ellipsoids drawn at the 35% probability level.

X-ray Crystal Structure Determination. Crystals of **20** suitable for X-ray diffraction were obtained by slow evaporation of an Et_2O solution of **20**.

Diffraction intensity data were collected with a Bruker Smart Apex CCD diffractometer at 173(2) K using MoKα - radiation (0.71073 Å). The structure was solved using direct methods, completed by subsequent difference Fourier syntheses, and refined by full matrix least-squares procedures on F^2. All non-H atoms were refined with anisotropic thermal parameters. H atoms were found on the residual density map and refined with isotropic thermal parameters. The Flack parameter is 0.00(8). All software and sources scattering factors are contained in the SHELXTL (6.10) program package (G.Sheldrick, Bruker XRD, Madison, WI). Crystallographic data and some details of

data collection and crystal structure refinement for $C_{17}H_{16}BN$ are given in the following tables.

Table 85. Crystal data and structure refinement for **20** (liu39a).

Identification code	liu39a	
Empirical formula	$C_{17}H_{16}BN$	
Formula weight	269.14	
Temperature	173(2) K	
Wavelength	0.71073 Å	
Crystal system	Orthorhombic	
Space group	Pna2(1)	
Unit cell dimensions	a = 11.1782(11) Å	α = 90°.
	b = 16.9314(17) Å	β = 90°.
	c = 8.1703(8) Å	γ = 90°.
Volume	1546.3(3) $Å^3$	
Z	4	
Density (calculated)	1.156 Mg/m^3	
Absorption coefficient	0.066 mm^{-1}	
F(000)	568	
Crystal size	0.28 x 0.18 x 0.04 mm^3	
Theta range for data collection	2.18 to 26.00°.	
Index ranges	-11<=h<=13, -20<=k<=20, -10<=l<=7	
Reflections collected	8760	
Independent reflections	2798 [R(int) = 0.0498]	
Completeness to theta = 26.00°	99.9 %	
Absorption correction	Semi-empirical from equivalents	
Max. and min. transmission	0.9974 and 0.9818	
Refinement method	Full-matrix least-squares on F^2	
Data / restraints / parameters	2798 / 1 / 254	
Goodness-of-fit on F^2	1.029	
Final R indices [I>2sigma(I)]	R1 = 0.0547, wR2 = 0.1137	
R indices (all data)	R1 = 0.0887, wR2 = 0.1353	
Absolute structure parameter	0(5)	
Largest diff. peak and hole	0.211 and -0.127 $e.Å^{-3}$	

Table 86. Atomic coordinates (x 10^4) and equivalent isotropic displacement parameters ($Å^2$x 10^3) for **20**. U(eq) is defined as one third of the trace of the orthogonalized U^{ij} tensor.

	x	y	z	U(eq)
N(1)	144(2)	1505(1)	8225(3)	36(1)
B(1)	1125(3)	1917(2)	7485(6)	33(1)
C(1)	126(3)	676(2)	8296(5)	46(1)
C(2)	1036(3)	248(2)	7585(6)	59(1)
C(3)	2028(3)	603(2)	6892(5)	55(1)
C(4)	2142(3)	1420(2)	6837(4)	45(1)
C(5)	1088(2)	2822(2)	7441(4)	37(1)
C(6)	1108(2)	3536(2)	7407(5)	35(1)
C(7)	1189(2)	4391(1)	7411(4)	34(1)
C(8)	425(3)	4833(2)	8412(4)	51(1)
C(9)	537(4)	5649(2)	8439(5)	60(1)
C(10)	1370(3)	6024(2)	7477(5)	54(1)
C(11)	2122(3)	5585(2)	6508(5)	51(1)
C(12)	2037(3)	4780(2)	6467(5)	46(1)
C(13)	-919(3)	1899(2)	8918(4)	41(1)
C(14)	-1007(3)	1865(2)	10742(4)	34(1)
C(15)	9(3)	1937(2)	11729(4)	41(1)
C(16)	-101(3)	1945(2)	13416(5)	47(1)
C(17)	-1195(3)	1885(2)	14130(5)	45(1)
C(18)	-2206(3)	1807(2)	13194(5)	44(1)
C(19)	-2111(3)	1795(2)	11500(4)	37(1)

Table 87. Bond lengths [Å] and angles [°] for **20**.

N(1)-C(1)	1.405(3)
N(1)-B(1)	1.433(4)
N(1)-C(13)	1.477(4)
B(1)-C(4)	1.510(5)
B(1)-C(5)	1.534(4)
C(1)-C(2)	1.377(5)
C(1)-H(1)	0.96(3)
C(2)-C(3)	1.382(5)
C(2)-H(2)	1.00(3)
C(3)-C(4)	1.390(5)
C(3)-H(3)	1.02(3)
C(4)-H(4)	0.82(3)
C(5)-C(6)	1.208(3)
C(6)-C(7)	1.450(3)
C(7)-C(12)	1.389(4)
C(7)-C(8)	1.400(4)
C(8)-C(9)	1.386(5)
C(8)-H(8)	1.05(4)
C(9)-C(10)	1.375(5)
C(9)-H(9)	0.89(3)
C(10)-C(11)	1.373(5)
C(10)-H(10)	0.95(3)
C(11)-C(12)	1.367(4)
C(11)-H(11)	0.99(3)

C(12)-H(12)	0.96(3)
C(13)-C(14)	1.494(5)
C(13)-H(13A)	1.03(3)
C(13)-H(13B)	0.97(3)
C(14)-C(19)	1.386(4)
C(14)-C(15)	1.399(4)
C(15)-C(16)	1.384(5)
C(15)-H(15)	1.00(4)
C(16)-C(17)	1.359(5)
C(16)-H(16)	0.98(4)
C(17)-C(18)	1.370(5)
C(17)-H(17)	0.91(4)
C(18)-C(19)	1.389(5)
C(18)-H(18)	0.97(4)
C(19)-H(19)	0.92(4)
C(1)-N(1)-B(1)	121.0(3)
C(1)-N(1)-C(13)	115.1(3)
B(1)-N(1)-C(13)	123.9(2)
N(1)-B(1)-C(4)	116.9(2)
N(1)-B(1)-C(5)	118.4(3)
C(4)-B(1)-C(5)	124.7(3)
C(2)-C(1)-N(1)	119.8(3)
C(2)-C(1)-H(1)	118(2)
N(1)-C(1)-H(1)	121(2)
C(1)-C(2)-C(3)	122.5(3)
C(1)-C(2)-H(2)	116.8(18)
C(3)-C(2)-H(2)	120.7(18)
C(2)-C(3)-C(4)	121.3(3)
C(2)-C(3)-H(3)	116.8(19)
C(4)-C(3)-H(3)	121.9(19)
C(3)-C(4)-B(1)	118.3(3)
C(3)-C(4)-H(4)	122(2)
B(1)-C(4)-H(4)	120(2)
C(6)-C(5)-B(1)	177.4(3)
C(5)-C(6)-C(7)	177.1(3)
C(12)-C(7)-C(8)	119.1(3)
C(12)-C(7)-C(6)	121.0(3)
C(8)-C(7)-C(6)	119.8(3)
C(9)-C(8)-C(7)	119.2(3)
C(9)-C(8)-H(8)	118.5(18)
C(7)-C(8)-H(8)	122.2(18)
C(10)-C(9)-C(8)	120.8(3)
C(10)-C(9)-H(9)	126(2)
C(8)-C(9)-H(9)	113(2)
C(11)-C(10)-C(9)	119.6(3)
C(11)-C(10)-H(10)	117(2)
C(9)-C(10)-H(10)	124(2)
C(12)-C(11)-C(10)	120.8(4)
C(12)-C(11)-H(11)	116.2(18)
C(10)-C(11)-H(11)	123.0(18)
C(11)-C(12)-C(7)	120.5(3)
C(11)-C(12)-H(12)	122.5(19)
C(7)-C(12)-H(12)	117.0(19)

N(1)-C(13)-C(14)	114.7(3)
N(1)-C(13)-H(13A)	105.3(17)
C(14)-C(13)-H(13A)	108.6(17)
N(1)-C(13)-H(13B)	106.9(17)
C(14)-C(13)-H(13B)	104.5(19)
H(13A)-C(13)-H(13B)	117(2)
C(19)-C(14)-C(15)	118.2(3)
C(19)-C(14)-C(13)	120.5(3)
C(15)-C(14)-C(13)	121.2(3)
C(16)-C(15)-C(14)	120.2(4)
C(16)-C(15)-H(15)	122.6(19)
C(14)-C(15)-H(15)	117.2(18)
C(17)-C(16)-C(15)	120.5(4)
C(17)-C(16)-H(16)	118(2)
C(15)-C(16)-H(16)	121(2)
C(16)-C(17)-C(18)	120.6(4)
C(16)-C(17)-H(17)	116(2)
C(18)-C(17)-H(17)	124(2)
C(17)-C(18)-C(19)	119.7(4)
C(17)-C(18)-H(18)	119(2)
C(19)-C(18)-H(18)	121(2)
C(18)-C(19)-C(14)	120.8(4)
C(18)-C(19)-H(19)	120(2)
C(14)-C(19)-H(19)	119(2)

Symmetry transformations used to generate equivalent atoms:

Table 88. Anisotropic displacement parameters ($Å^2 x\ 10^3$)for **20**. The anisotropic displacement factor exponent takes the form: $-2p^2[\ h^2a^{*2}U^{11} + ... + 2\ h\ k\ a^*\ b^*\ U^{12}\ ]$

	U^{11}	U^{22}	U^{33}	U^{23}	U^{13}	U^{12}
N(1)	40(1)	33(1)	35(1)	-1(1)	-5(1)	1(1)
B(1)	38(2)	33(2)	30(2)	1(2)	-8(2)	-3(1)
C(1)	51(2)	36(2)	51(2)	1(2)	-3(2)	-9(2)
C(2)	76(3)	28(2)	71(2)	-2(2)	4(2)	-2(2)
C(3)	60(2)	44(2)	59(3)	-9(2)	2(2)	12(2)
C(4)	47(2)	41(2)	48(2)	-1(2)	8(2)	3(2)
C(5)	35(1)	38(2)	39(2)	0(2)	-7(2)	-1(1)
C(6)	35(2)	36(2)	33(2)	1(2)	-4(1)	0(1)
C(7)	38(2)	28(1)	37(2)	2(2)	-7(1)	1(1)
C(8)	54(2)	42(2)	57(2)	5(2)	17(2)	7(2)
C(9)	78(3)	42(2)	59(2)	-6(2)	15(2)	14(2)
C(10)	80(3)	28(2)	54(2)	-2(2)	-5(2)	-1(2)
C(11)	56(2)	40(2)	58(2)	-2(2)	11(2)	-9(2)
C(12)	50(2)	35(2)	54(2)	-1(2)	9(2)	2(2)
C(13)	38(2)	49(2)	36(2)	1(2)	-3(2)	0(2)
C(14)	40(2)	26(2)	34(2)	2(1)	3(1)	0(1)
C(15)	36(2)	42(2)	45(2)	2(2)	-3(2)	-2(1)
C(16)	52(2)	45(2)	42(2)	1(2)	-10(2)	-5(2)
C(17)	66(3)	38(2)	32(2)	1(2)	-2(2)	1(2)
C(18)	46(2)	37(2)	49(2)	5(2)	7(2)	1(1)
C(19)	36(2)	39(2)	35(2)	1(2)	-5(2)	0(1)

Table 89. Hydrogen coordinates (x 10^4) and isotropic displacement parameters ($Å^2$x 10^3) for **20**.

	x	y	z	U(eq)
H(1)	-560(30)	390(20)	8700(40)	64(11)
H(2)	970(20)	-339(18)	7640(50)	61(9)
H(3)	2660(30)	237(19)	6400(40)	64(10)
H(4)	2730(30)	1633(18)	6430(50)	56(11)
H(8)	-280(30)	4573(19)	9070(40)	67(11)
H(9)	-60(30)	5880(20)	8970(40)	66(11)
H(10)	1500(30)	6577(19)	7490(50)	64(9)
H(11)	2740(30)	5825(19)	5790(40)	53(9)
H(12)	2520(30)	4460(18)	5760(40)	50(9)
H(13A)	-850(30)	2480(20)	8570(40)	63(10)
H(13B)	-1610(30)	1609(16)	8530(40)	48(9)
H(15)	800(30)	1958(18)	11170(40)	49(9)
H(16)	600(30)	1987(19)	14120(50)	58(11)
H(17)	-1200(30)	1916(19)	15240(50)	52(11)
H(18)	-2980(30)	1789(18)	13730(50)	65(11)
H(19)	-2770(30)	1679(19)	10880(40)	60(11)

Table 90. Torsion angles [°] for **20**.

C(1)-N(1)-B(1)-C(4)	-1.7(5)
C(13)-N(1)-B(1)-C(4)	-180.0(3)
C(1)-N(1)-B(1)-C(5)	179.7(3)
C(13)-N(1)-B(1)-C(5)	1.4(5)
B(1)-N(1)-C(1)-C(2)	-2.8(5)
C(13)-N(1)-C(1)-C(2)	175.6(3)
N(1)-C(1)-C(2)-C(3)	4.7(7)
C(1)-C(2)-C(3)-C(4)	-1.8(7)
C(2)-C(3)-C(4)-B(1)	-2.8(6)
N(1)-B(1)-C(4)-C(3)	4.4(6)
C(5)-B(1)-C(4)-C(3)	-177.1(3)
N(1)-B(1)-C(5)-C(6)	151(8)
C(4)-B(1)-C(5)-C(6)	-27(9)
B(1)-C(5)-C(6)-C(7)	-29(14)
C(5)-C(6)-C(7)-C(12)	70(8)
C(5)-C(6)-C(7)-C(8)	-108(8)
C(12)-C(7)-C(8)-C(9)	-0.2(6)
C(6)-C(7)-C(8)-C(9)	178.1(3)
C(7)-C(8)-C(9)-C(10)	1.2(6)
C(8)-C(9)-C(10)-C(11)	-1.7(6)
C(9)-C(10)-C(11)-C(12)	1.2(6)
C(10)-C(11)-C(12)-C(7)	-0.2(6)
C(8)-C(7)-C(12)-C(11)	-0.3(6)
C(6)-C(7)-C(12)-C(11)	-178.5(3)
C(1)-N(1)-C(13)-C(14)	71.7(4)
B(1)-N(1)-C(13)-C(14)	-109.9(4)
N(1)-C(13)-C(14)-C(19)	-144.6(3)
N(1)-C(13)-C(14)-C(15)	38.2(4)
C(19)-C(14)-C(15)-C(16)	-0.7(5)
C(13)-C(14)-C(15)-C(16)	176.6(3)

C(14)-C(15)-C(16)-C(17)	-0.1(5)
C(15)-C(16)-C(17)-C(18)	0.7(5)
C(16)-C(17)-C(18)-C(19)	-0.5(5)
C(17)-C(18)-C(19)-C(14)	-0.3(5)
C(15)-C(14)-C(19)-C(18)	0.9(5)
C(13)-C(14)-C(19)-C(18)	-176.4(3)

Symmetry transformations used to generate equivalent atoms:

APPENDIX B

SYNTHESIS AND CHARACTERIZATION OF 1,2-DIHYDRO-1,2-AZABORINE

B.1. Introduction

Benzene and borazine are the prototypical organic and inorganic aromatic motifs, respectively. Hybrid aromatic compounds containing both BN and CC units, such as the 1,2-azaborine motif, have been studied since the late 1950s (see Chapter I), yet the synthesis and characterization of the simplest member of this class of heterocycle, 1,2-dihydro-1,2-azaborine **1**, has been elusive. Dewar and co-workers reported an attempted synthesis of **1** in 1967,[1] but ultimately concluded that it "seems to be a very reactive and chemically unstable system, prone to polymerization and other reactions."[1]

Mild, efficient syntheses of 1,2-azaborines have recently been reported.[2,3] These protocols have led us to revisit the synthesis of the parent heterocycle **1**. The isolation of **1** has permitted a direct comparison between benzene, borazine, and 1,2-dihydro-1,2-azaborine **1**.

B.2. Experimental

B.2.1. General

All oxygen- and moisture-sensitive manipulations were carried out under an inert

atmosphere using either standard Schlenk techniques or a glove box.

THF, Et_2O, CH_2Cl_2, and pentane were purified by passing through a neutral alumina column under argon. Cyclohexene was dried over CaH_2 and distilled under N_2 prior to use.

Solutions of Superhydride, *tert*-butyldimethylsilyl chloride, and boron trichloride were purchased from Aldrich and used as received. Trisacetonitrile(tricarbonyl)chromium(0) was purchased from Acros or Aldrich and used as received. Pd/C was purchased from Strem and heated under vacuum in a 100 °C oil bath for 12 hours prior to use. Triphenylphosphine was purchased from TCI and used as received. Borazine was purchased from Gelest and used as received. All other chemicals and solvents were purchased (Aldrich or Strem) and used as received.

Silica gel (230-400 mesh) was heated under vacuum in a 200 °C sand bath for 12 hours. Flash chromatography was performed with this silica gel under an inert atmosphere.

^{11}B NMR spectra were recorded on a Varian Unity/Inova 600 spectrometer at ambient temperature. ^{1}H NMR spectra were recorded on a Varian Unity/Inova 300 or Varian Unity/Inova 600 spectrometer. ^{13}C NMR spectra were recorded on a Varian Unity/Inova 300 or Varian Unity/Inova 500 spectrometer. COSY and HETCOR NMR spectroscopy was performed on a Varian Unity/Inova 300 spectrometer. ^{11}B NMR spectra were externally referenced to $BF_3 \cdot Et_2O$ (δ 0).

IR spectra were recorded on a Nicolet Magna 550 FT-IR instrument with OMNIC software. UV-Vis spectra were recorded on an Agilent 8453 spectrometer with

ChemStation software.

High-resolution mass spectroscopy data were obtained at the Mass Spectroscopy Facilities and Services Core of the Environmental Health Sciences Center at Oregon State University. Financial support for this facility has been furnished in part by the National Institute of Environmental Health Sciences, NIH (P30 ES00210).

B.2.2. Supplemental information for Chapter III, section 3.3

Electronic Structure Calculations. The electronic structure calculations were done at different levels as follows. The heat of formation of c-C_4BNH_6 (**1**) was calculated using a composite approach[4-9] developed for the prediction of the thermodynamic properties of molecules based on molecular orbital theory using coupled cluster methods at the CCSD(T)[10] (coupled cluster with single and double excitations with an approximate triple corrections) level extrapolated to the complete basis set level with the correlation consistent basis sets[11,12] using equation (1) where n = 2 (aug-cc-pVDZ), 3 (aug-cc-pVTZ), and 4 (aug-cc-pVQZ), as proposed by Peterson et al.[13]

$$E(n) = E_{CBS} + A \exp[-(n-1)] + B \exp[-(n-1)^2] \quad (1)$$

Additional corrections were included: (1) core-valence correlation effects at the CCSD(T)/cc-pwCVTZ level;[14,15] (2) scalar relativistic effects at the CCSD(T)/Douglas-Kroll-Hess level with the cc-PVTZ-DK basis set;[16-19] and atomic spin orbit from experimental atomic excitation energies.[20] The vibrational frequencies and geometries were calculated at the MP2/cc-pVTZ level.[21] The B-H, C-H and N-H frequencies were scaled by the ratio A-H_{expt}/A-H_{calc} for the molecules BH_3, CH_4 and NH_3.[22,23] We also calculated heats of formation at the computationally cheaper G3MP2 level for use in the

resonance energy calculations.[24] By combining our computed ΣD_0 values with the known heats of formation[25] at 0 K for the elements $\Delta H_f^0(H) = 51.63$, $\Delta H_f^0(B) = 135.1 \pm 0.2$, $\Delta H_f^0(N) = 112.53$, and $\Delta H_f^0(N) =$ kcal/mol, we can derive ΔH_f^0 values for the molecules under study in the gas phase. The heat of formation of the boron atom was taken from Karton and Martin.[26] We obtain heats of formation at 298K by following the procedures outlined by Curtiss *et al.*[27]

The geometries and vibrational frequencies of the $Cr(CO)_3$ complexes were calculated at the density functional theory (DFT) B3LYP/DZVP2 level.[28-30] The NMR chemical shift calculations were obtained at the DFT B3LYP level with the Alhrichs-vtzp basis set[31] using the GIAO formalism[32] to treat the gauge invariance problem. The nucleus-independent chemical shifts (NICS)[33] were calculated at the approximate center of the rings and at 1 Å and 2 Å above the ring on the axis perpendicular to the ring and passing through the approximate center of the ring. The excitation energies and oscillator strengths for *c*-C_6H_6, *c*-C_4BNH_6 and *c*-$B_3N_3H_6$ were calculated with time dependent DFT (TD-DFT)[34-36] and the B3LYP/aug-cc-pVDZ//MP2/cc-pVTZ and B3LYP/aug-cc-pVTZ//MP2/cc-pVTZ levels, and with equations of motion[37] CCSD (EOM-CCSD/aug-cc-pVDZ//MP2/cc-pVTZ) level.

DFT and MP2 calculations were carried out using Gaussian-03,[38] coupled cluster calculations using MOLPRO-2006,[39] and TD-DFT using NWChem.[40] The electrostatic potential (ESP) is obtained by rolling a positive point charge over a density contour. The ESP was calculated at the B3LYP/6-311+G** level with the program system Spartan.[41]

Survey of N-Benzyl cleavage. Compound **4** was observed in entries 1-3 in Table 1. **4:** ^{1}H NMR (600 MHz, C_6D_6): δ 7.42 (d, $^{3}J_{HH}$ = 7.0 Hz, 2H), 7.0-7.2 (m, 8H), 4.19 (s, 2H), 2.65 (t, $^{3}J_{HH}$ = 5.4 Hz, 2H), 1.5-1.6 (m, 4H), 1.20 (m, 2H). ^{11}B NMR (192.5 MHz, C_6D_6) δ 43.2.

Entry 1: Compound **2** (0.050 g, 0.20 mmol), Pd/C (10 wt% Pd, 0.043 g, 0.041 mmol), and C_6D_6 (1 mL) were combined in a sealed high-pressure reaction vessel. The vessel was charged with H_2 (40 psi) and heated to 80 °C for 6h. ^{1}H NMR indicated that compound **4** was formed in a 1:1 ratio with unreacted **2**.

Entry 2: Compound **2** (0.050 g, 0.20 mmol), Pd/C (10 wt% Pd, 0.022 g, 0.021 mmol), and C_6D_6 (1 mL) were combined in a sealed high-pressure reaction vessel. The vessel was charged with H_2 (40 psi) and heated to 60 °C for 6h. ^{1}H NMR indicated that compound **4** was formed in a 40:60 ratio with unreacted **2**.

Entry 3: Compound **2** (0.050 g, 0.20 mmol), Pd/C (10 wt% Pd, 0.043 g, 0.041 mmol), and THF-d_8 (1 mL) were combined in a sealed high-pressure reaction vessel. The vessel was charged with 1 atm of H_2 (flushed for 1 minute with a steady stream of H_2) and heated to 80 °C for 14h. Compound **4** was the only identifiable species in the ^{1}H NMR spectrum.

Entry 4: Compound **2** (0.050 g, 0.20 mmol), $Pd(OH)_2/C$ (20 wt% Pd, 0.015 g, 0.02 mmol), and EtOH (2 mL) were combined in a sealed high-pressure reaction vessel. The vessel was charged with H_2 (50 psi) and stirred at 25 °C for 4 h. Solvent was removed and the crude reaction mixture was redissolved in C_6D_6. Compound **2** was the only identifiable species in the ^{1}H NMR spectrum.

Entry 5: Compound **2** (0.010 g, 0.041 mmol), Pd/C (10 wt% Pd, 0.005 g, 0.005 mmol), HCO_2H (0.1 mL), and MeOH (2.1 mL) were combined in a flask and stirred at rt for 48 h. ^{11}B NMR indicated the formation of 4-coordinate boron (δ 19 ppm); numerous unassigned peaks were observed in the ^1H NMR spectrum.

Entry 6: Compound **2** (0.010 g, 0.041 mmol), TMSI (0.2 mL), and CD_2Cl_2 (1 mL) were combined in a vial and heated at 60 °C for 2h. MeOH (0.05 mL) was then added and the vial was heated at 60 °C for an additional 2 h. Compound **2** was the only identifiable species in the ^1H NMR spectrum.

Entry 7: Compound **2** (0.045 g, 0.184 mmol), DDQ (0.042 g, 0.184 mmol), and pentane (1 mL) were combined in a vial and heated at 75 °C for 4h. Solvent was removed and the crude mixture was redissolved in CD_2Cl_2. Compound **2** was the only identifiable species in the ^1H NMR spectrum.

Entry 8. Compound **2** (0.010 g, 0.041 mmol), ceric ammonium nitrate (0.047 g, 0.086 mmol), MeCN (1 mL), and H_2O (0.2 mL) were combined in a vial and stirred at rt for 4 h. Compound **2** was the only identifiable species in the ^1H NMR spectrum.

Compound 5. Tributylallyl tin (4.068 g, 12.29 mmol) was added to a solution of BCl_3 (1.0 M in hexanes; 10 mL, 10 mmol) at –78 °C under N_2. The reaction was slowly warmed to rt and stirred for 30 min. The reaction was cooled to –78 °C, whereupon TMS-allylamine (1.29 g, 10 mmol) was added dropwise. The reaction was then warmed to rt and stirred for 4h. The flask was then cooled to –78 °C and NEt_3 (1.66 mL, 12 mmol) was added. The flask was warmed to rt and stirred for 4 h. Solids were then filtered through an Acrodisc and solvents removed under reduced pressure. 1H and 11B NMR were

consistent with the formation of **5**, however vacuum distillation (49-60 °C, 200 mT) provided **5** as a mixture of compounds, including tributyltin chloride.

^{1}H NMR (300 MHz, C_6D_6): δ 5.6-6.2 (br m), 4.9-5.2 (br m), 3.6 (br m), 2.2 (br m), 0.30 (s). ^{11}B NMR (192.5 MHz, C_6D_6): δ 43.1.

Compound 6. Allylphenylboron chloride2 (0.700 g, 4.3 mmol) and CH2Cl2 (4 mL) were combined in a flask and cooled to –78 °C under N_2, whereupon TIPS-allylamine (0.909 g, 4.3 mmol) was added dropwise with stirring. The mixture was stirred for 1 h, at which point Net3 (0.711 mL, 5.1 mmol) was added dropwise. The solution was allowed to warm to rt and was stirred for 48 h. Solids were then filtered and the solvent removed. Vacuum distillation (50-71 °C, 10 mT) provided 6 as a clear, colorless liquid (0.352, 24%).

^{1}H NMR (300 MHz, CD_2Cl_2): δ 7.2-7.4 (br m, 5H), 5.6-5.8 (br m, 2H), 4.8-5.0 (br m, 4H), 3.8 (br m, 2H), 1.8 (br m, 2H), 1.0-1.3 (br, 18H). ^{11}B NMR (192.5 MHz, CD_2Cl_2): δ 46.3.

Compound 8. In a glove box, allyltriphenyl tin (28.6 g, 73.1 mmol) was dissolved in 200 mL CH_2Cl_2 and cooled to –78 °C under nitrogen. A solution of BCl_3 (1.0 M in hexanes; 73.1 mL, 73.1 mmol) was then added dropwise maintaining vigorous stirring at all times. The reaction was stirred at –78 °C for 4 h, whereupon TBS-allyl amine (12.5 g, 73.1 mmol in 20 mL pentane) was then added to the reaction flask. After 20 minutes, NEt_3 was added dropwise and the reaction was allowed to warm to rt and stirred for 12 h. At the conclusion of the reaction, approximately one-half of the solvent was removed under vacuum, and 200 mL pentane was added. The reaction mixture was filtered through a

medium-porosity frit, and the filtrate was concentrated under reduced pressure. Vacuum distillation (60-75 °C, 300 mTorr) afforded **8** as a clear, colorless liquid (10.8 g, 58%).

^{1}H and ^{13}C NMR were consistent with the formation of rotamers in a 1:1 ratio. ^{1}H NMR (600 MHz, CD_2Cl_2): δ 5.85 (br, 2H), 5.0 (br, 4H), 3.92 (br s, 1H), 3.80 (br s, 1H), 2.08 (br s, 1H), 2.00 (br s, 1H), 0.93 (s, 9H), 0.28 (s, 6H). ^{13}C NMR (75.4 MHz, CD_2Cl_2): δ 138.5, 136.3, 136.1, 115.0, 114.5, 51.4, 50.4, 30 (br), 27.5, 27.1, 20.5, 20.1, –1.46, –1.53. ^{11}B NMR (192.5 MHz, CD_2Cl_2): δ 43.0. FTIR (thin film) 3079, 2956, 2931, 2886, 2859, 1634, 1466, 1382, 1340, 1324, 1257, 1210, 1101, 1074, 1043, 1006, 994, 959, 903, 839, 785, 743, 679, 575, 554 cm^{-1}. HRMS (EI) calcd for $C_{12}H_{25}BClNSi$ (M^+) 257.15378, found 257.15316.

Compound 9. In a glove box, a solution of Grubbs 1st generation catalyst (2.08 g, 2.52 mmol in 40 mL CH_2Cl_2) was added to a stirring solution of aminoborane **8** (32.44 g, 126.2 mmol in 400 mL CH_2Cl_2). The solution was stirred at rt for 30 min, after which the solvent was removed. The product was distilled under reduced pressure (50-55 °C, 50 mTorr) to give the desired ring-closed compound **9** and isomer **9'** in a 1:0.9 (**9**:**9'**) ratio as a clear, colorless liquid (23.62 g, 82%).

^{1}H NMR (600 MHz, CD_2Cl_2): δ 6.78 (d, $^{3}J_{HH}$ = 11.7 Hz, 1H (**9'**)), 5.80 (dt, $^{3}J_{HH}$ = 8.5, 1.7 Hz, 1H (**9'**)), 5.76 (br, 1H (**9**)), 5.60 (m, 1H (**9**)), 3.74 (m, 2H (**9**)), 3.16 (t, $^{3}J_{HH}$ = 6.6 Hz, 2H (**9'**)), 2.19 (m, 2H (**9'**)), 1.70 (br, 2H (**9**)), 0.97 (s, 9H), 0.95 (s, 9H), 0.33 (s, 6H), 0.31 (s, 6H). ^{13}C NMR (125 MHz, CD_2Cl_2): δ 148.5, 130 (br), 125.7, 125.3, 48.8., 45.6, 29.8, 27.5, 27.2, 21 (br), 20.6, 20.0, –1.5, –1.9. ^{11}B NMR (192.5 MHz, CD_2Cl_2): δ 42.1 (**9**), 36.7 (**9'**). FTIR (thin film) 3027, 2930, 2858, 1670, 1599, 1463, 1424, 1362,

1306, 1255, 1198, 1177, 1147, 1074, 1008, 959, 886, 824, 780, 730, 707, 685, 671, 641, 588, 531, 462, 417 cm^{-1}.

Compound 10. A 500 mL Schlenk tube was charged with **9(9')** (14.04 g, 61.13 mmol), Pd/C (10 wt%; 9.76 g, 9.17 mmol), and cyclohexene (150 mL). The suspension was stirred at 100 °C for 16 h, cooled to rt and filtered through a medium-porosity frit. The resulting filtrate was cooled to –78 °C, and a solution of phenylethynylmagnesium bromide (1.0 M solution in THF; 6.1 mL, 6.1 mmol) was then added. The mixture was allowed to warm to rt and passed through an Acrodisc. The resulting filtrate was concentrated under reduced pressure. Vacuum distillation (52-55 °C, 50 mTorr) gave 1,2-azaborine **10** as a clear, colorless liquid (4.79 g, 35%).

^{1}H NMR (600 MHz, CH_2Cl_2): δ 7.56 (dd, $^3J_{HH}$ = 6.1, 3.6, 1H), 7.28 (d, $^3J_{HH}$ = 6.3 Hz, 1H), 6.61 (d, $^3J_{HH}$ = 11.2 Hz, 1H), 6.33 (dd, $^3J_{HH}$ = 6.6, 4.9 Hz, 1H), 0.94 (s, 9H), 0.56 (d, 6H). ^{13}C NMR (75 MHz, CD_2Cl_2): δ 145.8, 139.2, 129 (br), 112.0, 26.9, 19.7, –1.4. ^{11}B NMR (192.5 MHz, CD_2Cl_2): δ 35.0. FTIR (thin film) 3072, 3034, 2931, 2885, 2860, 1606, 1508, 1471, 1450, 1388, 1364, 1265, 1237, 1214, 1153, 1111, 1044, 1025, 980, 938, 823, 788, 740, 716, 683, 669, 619, 575 cm^{-1}. HRMS (EI) calcd for $C_{10}H_{19}BNSiCl$ (M^+) 227.10684, found 227.10680.

Compound 11. To a stirred solution of 1,2-azaborine **10** (4.785 g, 21.08 mmol in 100 mL Et_2O) was added dropwise a solution of $LiHBEt_3$ (1.0 M in THF; 22.1 mL, 22.1 mmol) at –78 °C. The solution was warmed to rt and stirred for 6 h. The mixture was then passed through an Acrodisc and concentrated under reduced pressure. The crude material was purified by silicagel chromatography (pentane as eluent) to furnish **11** as a clear,

colorless liquid (4.035 g, 99%).

^{1}H NMR (600 MHz, CD_2Cl_2): δ 7.65 (dd, $^3J_{HH}$ = 5.4, 4.0 Hz, 1H), 7.40 (d, $^3J_{HH}$ = 6.4 Hz, 1H), 6.88 (d, $^3J_{HH}$ = 10.8 Hz, 1H), 6.43 (t, $^3J_{HH}$ = 6.6 Hz, 1H), 5.1 (br q, $^1J_{BH}$ = 141 Hz, 1H), 0.90 (s, 9H), 0.46 (s, 6H). ^{13}C NMR (75 MHz, CD_2Cl_2): δ 144.2, 138.5, 130 (br), 113.2, 26.3, 18.4, -3.9. ^{11}B NMR (192.5 MHz, CD_2Cl_2): δ 33.9 (d, $^1J_{BH}$ = 125 Hz). FTIR (thin film) 3067, 3029, 2956, 2859, 2530, 1603, 1533, 1504, 1471, 1391, 1363, 1270, 1160, 1141, 1021, 939, 927, 885, 840, 784, 736, 697, 655, 603, 574 cm^{-1}. HRMS (EI) calcd for $C_{10}H_{20}BNSi$ (M^+) 193.14581, found 193.14566.

Compound 12. 1,2-Azaborine **11** (0.162 g, 0.839 mmol), trisacetonitrile(tricarbonyl)chromium(0) (0.326 g, 1.26 mmol), and THF (10 mL) were combined in a 25 mL Schlenk tube and heated at 60 °C for 16 h. The mixture was concentrated under reduced pressure, and the resulting crude material was purified by silica gel chromatography (pentane/Et_2O as eluent) to afford complex **12** as an orange-red solid (0.197 g, 71%).

^{1}H NMR (600 MHz, CD_2Cl_2): δ 6.03 (d, $^3J_{HH}$ = 4.6 Hz, 1H), 5.93 (dd, $^3J_{HH}$ = 6.3, 3.0 Hz, 1H), 5.28 (t, $^3J_{HH}$ = 4.9 Hz, 1H), 4.63 (d, $^3J_{HH}$ = 9.3 Hz, 1H), 3.7 (q, br, $^1J_{BH}$ = 164 Hz, 1H), 0.88 (s, 9H), 0.40 (s, 3H), 0.37 (s, 3H). ^{13}C NMR (75 MHz, CD_2Cl_2): δ 230.7, 108.8, 103.9, 86 (br), 84.2, 26.2, 19.0, –3.3, –6.0. ^{11}B NMR (192.5 MHz, CD_2Cl_2): δ 17.2 (d, $^1J_{BH}$ = 102 Hz. FTIR (thin film) 2955, 2937, 2862, 1976, 1912, 1870, 1507, 1464, 1443, 1365, 1261, 1200, 1109, 1012, 932, 882, 846, 788, 697, 669, 634, 604, 536 cm^{-1}. HRMS (EI) calcd for $C_{13}H_{20}BNO_3SiCr$ (M^+) 329.07107, found 329.07120.

1,2-Dihydro-1,2-azaborine tricarbonylchromium(0) (13). To a stirred solution

of complex **12** (4.67 g, 14.2 mmol in 100 mL THF) was added dropwise a solution of HF-pyridine (0.1 M solution in THF of 70 wt% HF; 28.4 mL, 14.2 mmol) at –20 °. The reaction was maintained at –20 °C, with occasional stirring, for 3 h, and then it was warmed to rt and stirred 1 h. The mixture was concentrated under reduced pressure, and the resulting crude material was purified by column chromatography (pentane/Et_2O as eluent) to yield complex **13** as an orange solid (2.31 g, 76%).

^{1}H NMR (600 MHz, CD_2Cl_2): δ 6.19 (t, $^3J_{HH}$ = 5.3 Hz, 1H), 5.85 (dd, $^3J_{HH}$ = 6.4, 2.7 Hz, 1H), 5.38 (br t, $^1J_{NH}$ = 48.2 Hz, 1H), 5.31 (ddd, $^3J_{HH}$ = 5.3, 1.3, 0.9 Hz, 1H), 4.70 (dd, $^3J_{HH}$ = 8.3, 1.2 Hz, 1H), 3.6 (br q, $^1J_{BH}$ = 133 Hz, 1H). ^{13}C NMR (75 MHz, CD_2Cl_2): δ 230.1, 108.5, 99.4, 86 (br), 82.9. ^{11}B NMR (192.5 MHz, CD_2Cl_2): δ 15.4 (d, $^1J_{BH}$ = 144 Hz. FTIR (CH_2Cl_2) 3371, 2583, 1975, 1898 cm^{-1}. UV λ_{max}(pentane) 215 nm. HRMS (EI) calcd for $C_7H_6BNO_3Cr$ (M^+) 214.98459, found 214.98510.

1,2-Dihydro-1,2-azaborine (1). Complex **13** (0.150 g, 0.698 mmol), triphenylphosphine (0.915 g, 3.49 mmol), and isopentane (3.0 mL) were combined under N_2 atmosphere in a Schlenk tube and sonicated at rt for 3 h. Isopentane and **1** were transferred under vacuum to a cold trap at –78 °C. Residual isopentane was removed under vacuum to provide **1** as a clear and colorless liquid upon warming to rt. ^{1}H NMR (CD_3OD) of this liquid in the presence of hexamethylbenzene as an internal standard (1 mL; 1 mM hexamethylbenzene) indicated a yield of 0.006 g (10%).

^{1}H NMR (600 MHz, CD_2Cl_2): δ 8.44 (t, $^1J_{NH}$ = 57.4 Hz, 1H), 7.70 (br t, 1H), 7.40 (t, $^3J_{HH}$ = 6.5 Hz, 1H), 6.92 (d, $^3J_{HH}$ = 10.7 Hz, 1H), 6.43 (t, $^3J_{HH}$ = 6.3 Hz, 1H), 4.9 (br q, $^1J_{BH}$ = 128.2 Hz, 1H). ^{13}C NMR (75 MHz, CD_2Cl_2): δ 144.5, 134.7, 131.6, 112.1. ^{11}B

NMR (192.5 MHz, CD_2Cl_2): δ 31.0 (d, $^1J_{BH}$ = 131 Hz). FTIR (thin film) 3398, 3027, 3008, 2525, 1613, 1533, 1453, 1427, 1350, 1216, 1162, 1109, 894, 820, 715, 579 cm^{-1}. UV λ_{max} (pentane) 269 nm. HRMS (EI) calcd for C_4H_6BN (M^+) 79.059330, found 79.059269. Melting point = –46 to –45 °C.

^{1}H NMR yield of 1. Complex **13** (0.0105 g, 0.0469 mmol) and triphenylphosphine (0.0660 g, 0.252 mmol) were combined in a J. Young NMR tube, to which was added a solution of hexamethylbenzene in CD_2Cl_2 (1.0 mL; 0.65 mM hexamethylbenzene). At t = 1.5 h, ^{1}H NMR indicated the formation of **1** in 84% yield (integration versus hexamethylbenzene).

Isolation of 1 via the addition of 1,6-dicyanooctane to 13. Complex 13 (# g, # mmol) and 1,6-dicyanooctane (# mL) were combined in a flask and stirred for 24 h at rt. Heterocycle **1** was isolated in 53% yield (# g) via vacuum transfer to a cold trap at –78 °C.

Thermal stability of 1. Hexamethylbenzene (0.0030 g, 0.018 mmol) was added to a solution of 1,2-dihydro-1,2-azaborine **1** (0.7 M in CD_2Cl_2; 0.4 mL) in a J. Young NMR tube. The tube was sealed and heated to 60 °C for 72 h. ^{1}H NMR integration of **1** versus hexamethylbenzene indicated no degradation of **1**.

COSY NMR Spectrum of 1,2-Dihydro-1,2-azaborine (1).

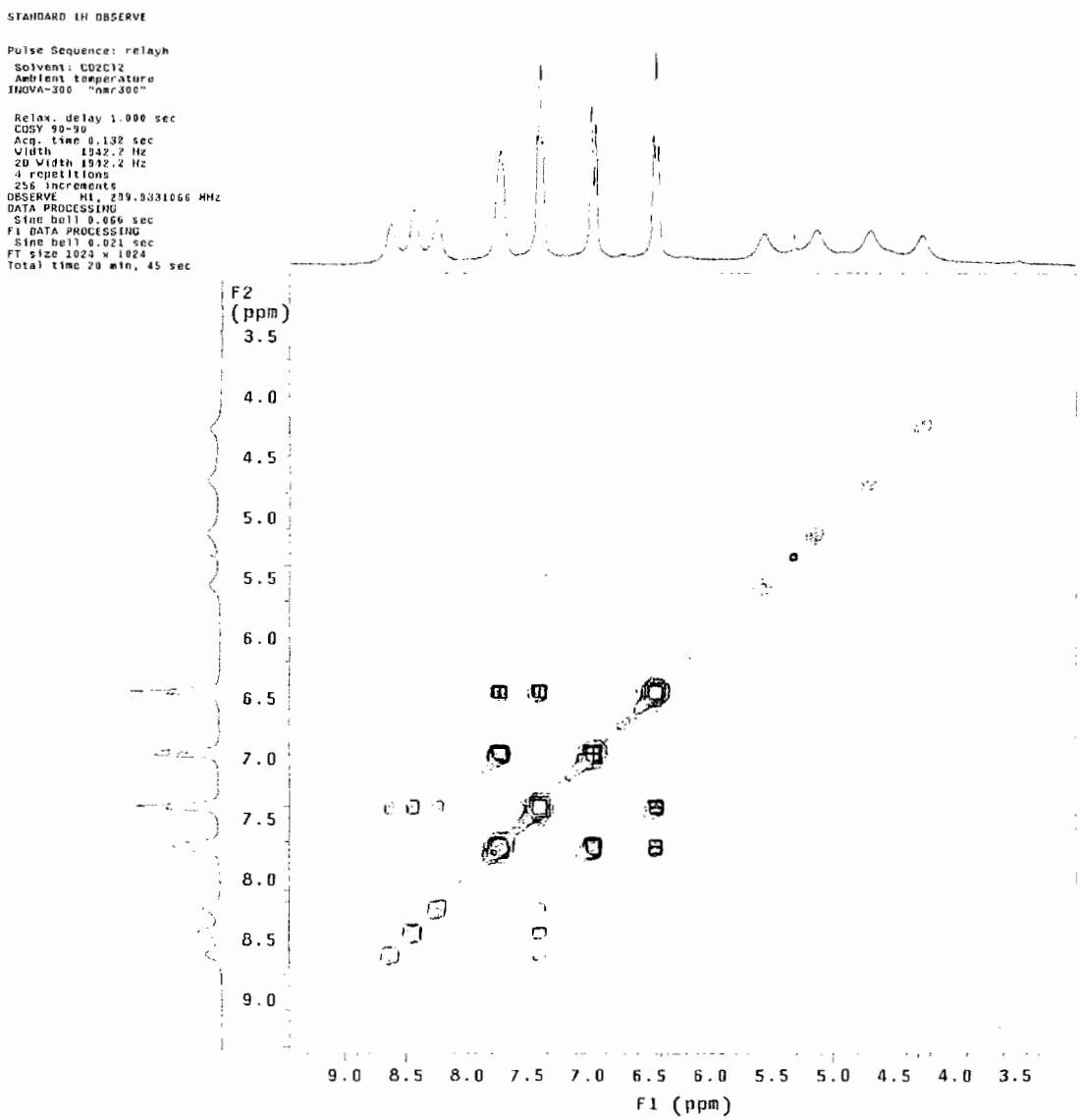

HETCOR NMR Spectrum of 1,2-Dihydro-1,2-azaborine (1).

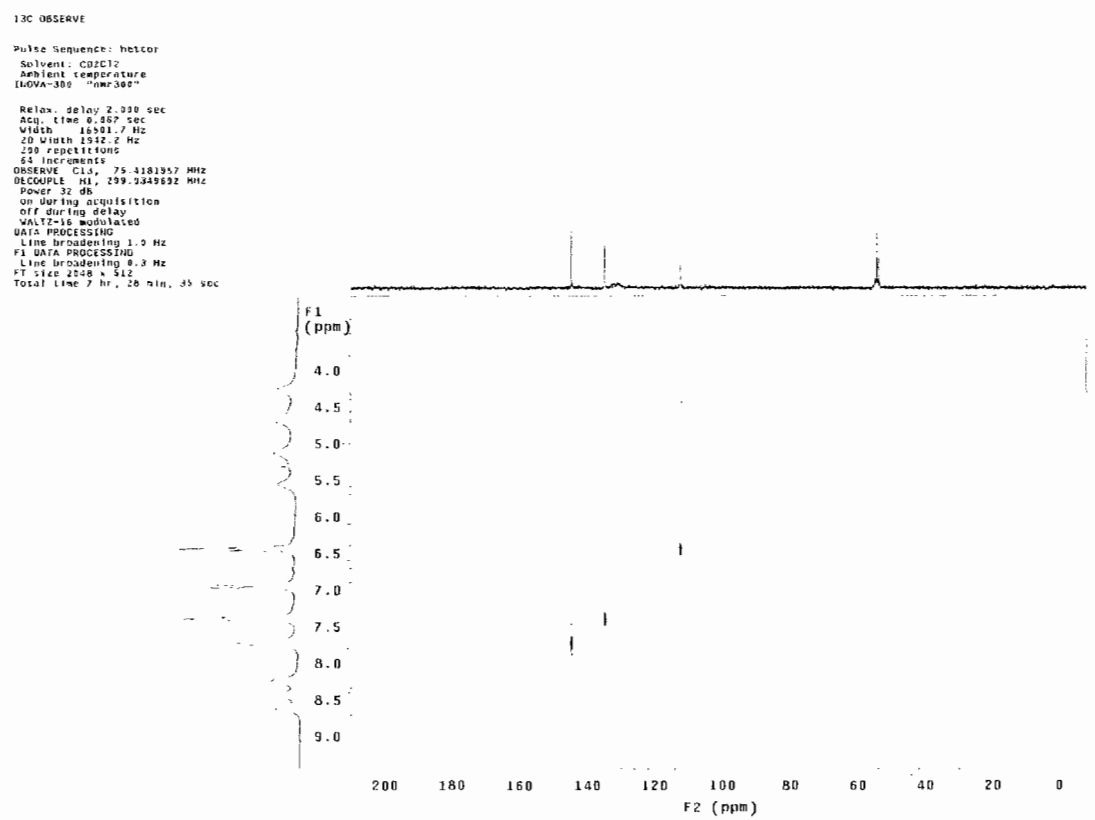

Electronic Structure Calculations Results. The NICS and NMR chemical shift calculations are given in Table 1. The structures and labels are shown in Figures 1 and 2. The calculated electronic spectra are given in Table 2. The calculated spectra with the two different approaches are in reasonable agreement with each other. The calculated spectra show that the first band for c-BNC_4H_6 is predicted to be quite intense and red shifted with respect to the predicted intense bands in c-C_6H_6 and c-$B_3N_3H_6$. The bands in c-$B_3N_3H_6$ are substantially blue-shifted in comparison to c-C_6H_6. The calculated infrared frequencies are in Table 3. The scaled calculated value for c-BNC_4H_6 for the

N–H stretch is within 30 cm^{-1} of the experimental value, the scaled B–H stretch is within 8 cm^{-1} of experiment and the C–H stretches are within 40 cm^{-1} of experiment.

The total CCSD(T) electronic energies in a. u. as a function of basis set extrapolated to the complete basis set limit are given in Table 4 and the components for the atomization energies in kcal/mol are given in Table 5 for *c*-BNC_4H_6 and *c*-$B_3N_3H_6$. The calculated heats of formation are given in Table 6 and should be good to ± 1.5 kcal/mol for *c*-BNC_4H_6 on the basis of our previous calculations on benzene.

The DFT R-$Cr(CO)_3$ bond dissociation energies are given in Table 7. The binding energies for R = *c*-C_6H_6 and R = *c*-BNC_4H_6 are comparable whereas the binding energy for R = *c*-$B_3N_3H_6$ is substantially lower.

There are many ways to define the resonance stabilization energy (RSE) as it represents an energy stabilization with respect to a model system.[42] The "resonance" or "delocalization" energy is totally dependent on the definition of the model. For benzene, one could use the dehydrogenation reaction (1) in Table 8 and compare it to the same reaction for 3 ethylene molecules (Reaction (4) in Table 8). This gives an effective RSE of 48 kcal/mol at the G3MP2 level and 50.4 kcal/mol at the best level.[43-45] This RSE is larger than usually expected because C_2H_4 is not the right structure. The correct model is to dehydrogenate cyclohexane and make 3 C=C bonds and 3 C-C sp^2 sigma bonds. The RSE calculated in this way for *c*-BNC_4H_6 is given by the comparison of reactions (2) and (5) in Table 8 and is 30.9 kcal/mol. For *c*-$B_3N_3H_{12}$, reactions (3) and (6) give RSE's near 0 kcal/mol in this model. Thus the ordering is the same as given in the paper. An improved way to estimate the resonance energies would be to compare the

difference in the energies of reactions (7) and (8). In this case we obtain an RSE of 32.2 kcal/mol for *c*-C_6H_6. The situation for *c*-C_4BNH_6 is more complicated. We start from the diene containing a B=N bond and one of two C=C bonds as shown in reactions (9) and (11). The difference in energies between reactions (9) and (10) gives an RSE of 21 kcal/mol and between reactions (11) and (12) gives an RSE of 18.3. This provides an estimate of RSE (*c*-C_4BNH_6) = 20 ± 2 kcal/mol, which is about 12 kcal/mol below that of benzene. This same approach gives a somewhat higher estimate for the RSE (*c*-$B_3N_3H_6$) = 25.8 kcal/mol from reactions (13) and (14). The exchange reaction (15) is consistent with benzene having a resonance energy about 14 to 15 kcal/mol larger than that of *c*-BNC4H_6. The exchange reactions (16) and (17) have been used to define the RSE of benzene and give comparable values. Use of similar exchange reactions suggests that the RSE of c-C_4BNH_6 is 12 to 13 kcal/mol less than that of benzene consistent with all of the above energies. We note that use of this approach for the definition of RSE (*c*-$B_3N_3H_6$) gives larger values than might be expected due to the different energies of the $\sigma(sp^2\text{-}sp^2)$ bonds being formed. The change in the $\sigma(sp^3\text{-}sp^3)$ bond to the $\sigma(sp^2\text{-}sp^2)$ for a C–C bond is about 15 kcal/mol whereas for a B–N bond it is about 84 kcal/mol.[46] The reactions to form acetylene or HBNH are all very endothermic and the results for reactions (22) and (23) are consistent with benzene having larger RSE than *c*-BNC_4H_6.

The calculated geometry parameters are given in Tables 9 and 10. The calculated electrostatic potential maps are given in Figure 3.

NICS and NMR Chemical Shift Calculations. See the Table 1 for NICS and NMR chemical shift calculations.

Table 1. NICS at 0, 1, and 2 Å and NMR at the B3LYP/Alhrichs-vtzp level of calculation.

Molecule	NICS(0)	NICS(1)	NICS(2)	Atom	δ (ppm)
c-C_6H_6	-8.76	-10.39	-2.57	C	135.2
				H	7.5
c-BNC_4H_6	-5.62	-7.27	-3.89	B1	26.9
				N2	-246.9
				C3	140.2
				C4	118.8
				C5	151.5
				C6	139.0
				H7	5.4
				H8	7.8
				H9	7.3
				H10	6.6
				H11	8.0
				H12	7.4
c-$B_3N_3H_6$	-2.02	-3.01	-1.59	B	26.1
				N	-287.6
				H (from BH)	5.0
				H (from NH)	5.3

Calculated Electronic Spectra: See the following tables for calculated electronic spectra.

Table 2. Excitation energy and oscillator strength for C_6H_6, C_4BNH_6 and $B_3N_3H_6$ cycles calculated with TD-DFT at the B3LYP/aug-cc-pVDZ//MP2/cc-pVTZ and B3LYP/aug-cc-pVTZ//MP2/cc-pVTZ levels, and with EOM-CCSD/aug-cc-pVDZ//MP2/cc-pVTZ level.

	***c*-C_6H_6 : B3LYP/aVDZ[a]**		
State	**ΔE (eV)**	**ΔE (nm)**	**Osc strength**
1-^{1}A	5.40	230	0.00000
2-^{1}A	6.07	205	0.00000
3-^{1}A	6.36	195	0.00000
4-^{1}A	6.36	195	0.00000
5-^{1}A	6.96	178	0.58378
6-^{1}A	6.96	178	0.58378
7-^{1}A	6.98	178	0.06381
8-^{1}A	7.02	177	0.00000
9-^{1}A	7.02	177	0.00000

10-^{1}A	7.09	175	0.00000
1-^{3}A	3.83	324	
2-^{3}A	4.71	263	
3-^{3}A	4.71	263	
4-^{3}A	5.07	245	
5-^{3}A	6.32	196	
6-^{3}A	6.32	196	
7-^{3}A	6.91	180	
8-^{3}A	6.99	177	
9-^{3}A	6.99	177	
10-^{3}A	7.08	175	

c-C_6H_6 : B3LYP/aVTZ[a]

	ΔE (eV)	**ΔE (nm)**	**Osc strength**
1-^{1}A	5.39	230	0.00000
2-^{1}A	6.05	205	0.00000
3-^{1}A	6.30	197	0.00000
4-^{1}A	6.30	197	0.00000
5-^{1}A	6.89	180	0.05878
6-^{1}A	6.92	179	0.00000
7-^{1}A	6.92	179	0.00000
8-^{1}A	6.94	179	0.58183
9-^{1}A	6.94	179	0.58184
10-^{1}A	6.98	178	0.00000
1-^{3}A	3.81	326	
2-^{3}A	4.70	264	
3-^{3}A	4.70	264	
4-^{3}A	5.05	246	
5-^{3}A	6.26	198	
6-^{3}A	6.26	198	
7-^{3}A	6.82	182	
8-^{3}A	6.90	180	
9-^{3}A	6.90	180	
10-^{3}A	6.98	178	

c-C_6H_6 : CCSD/aVDZ[b]

State	**ΔE (eV)**	**ΔE (nm)**	**Osc strength**
1-^{1}A	5.20	238	0.00000
2-^{1}A	6.48	191	0.00000
3-^{1}A	6.48	191	0.00000
4-^{1}A	6.55	190	0.00000
5-^{1}A	7.03	177	0.07141

6-^{1}A	7.10	175	0.00000
7-^{1}A	7.10	175	0.00000
8-^{1}A	7.21	172	0.00000
9-^{1}A	7.74	160	0.00000
10-^{1}A	7.75	160	0.00000

c-BNC_4H_6 : B3LYP/aVDZ[a]

State	ΔE (eV)	ΔE (nm)	Osc strength
1-^{1}A	5.01	248	0.16423
2-^{1}A	5.32	233	0.00000
3-^{1}A	5.89	211	0.07045
4-^{1}A	6.05	205	0.00020
5-^{1}A	6.17	201	0.00151
6-^{1}A	6.31	197	0.03727
7-^{1}A	6.65	187	0.12739
8-^{1}A	6.79	183	0.00434
9-^{1}A	6.90	180	0.00031
10-^{1}A	6.91	179	0.00005
1-^{3}A	3.23	384	
2-^{3}A	4.42	281	
3-^{3}A	4.79	259	
4-^{3}A	5.28	235	
5-^{3}A	5.80	214	
6-^{3}A	6.02	206	
7-^{3}A	6.27	198	
8-^{3}A	6.33	196	
9-^{3}A	6.62	188	
10-^{3}A	6.69	186	

c-BNC_4H_6 : B3LYP/aVTZ[a]

State	ΔE (eV)	ΔE (nm)	Osc strength
1-^{1}A	4.99	248	0.16466
2-^{1}A	5.27	236	0.00000
3-^{1}A	5.87	211	0.07068
4-^{1}A	5.95	208	0.00013
5-^{1}A	6.17	201	0.00430
6-^{1}A	6.21	200	0.02983
7-^{1}A	6.56	189	0.08839
8-^{1}A	6.67	186	0.00318
9-^{1}A	6.79	183	0.00030
10-^{1}A	6.88	180	0.00050
1-^{3}A	3.21	387	
2-^{3}A	4.42	281	

3-^{3}A	4.78	260
4-^{3}A	5.23	237
5-^{3}A	5.79	214
6-^{3}A	5.94	209
7-^{3}A	6.17	201
8-^{3}A	6.32	196
9-^{3}A	6.58	188
10-^{3}A	6.62	187

c-BNC_4H_6 : CCSD/aVDZ[b]

State	ΔE (eV)	ΔE (nm)	Osc strength
1-^{1}A'	5.06	245	0.16373
2-^{1}A'	6.22	199	0.08806
3-^{1}A'	6.63	187	0.05292
4-^{1}A'	7.46	166	0.48962
5-^{1}A'	7.82	159	0.28552
1-^{1}A"	5.52	225	0.00001
2-^{1}A"	6.19	200	0.00001
3-^{1}A"	6.42	193	0.04674
4-^{1}A"	6.88	180	0.00180
5-^{1}A"	6.90	180	0.00220

c-$B_3N_3H_6$: B3LYP/aVDZ[a]

State	ΔE (eV)	ΔE (nm)	Osc strength
1-^{1}A	6.62	187	0.00000
2-^{1}A	7.10	175	0.00000
3-^{1}A	7.10	175	0.00000
4-^{1}A	7.21	172	0.00000
5-^{1}A	7.53	165	0.33435
6-^{1}A	7.53	165	0.33435
7-^{1}A	7.53	165	0.01659
8-^{1}A	7.60	163	0.08702
9-^{1}A	7.68	161	0.00000
10-^{1}A	7.68	161	0.00000
1-^{3}A	5.98	207	
2-^{3}A	6.24	199	
3-^{3}A	6.24	199	
4-^{3}A	6.37	195	
5-^{3}A	6.99	178	
6-^{3}A	6.99	178	
7-^{3}A	7.04	176	
8-^{3}A	7.26	171	
9-^{3}A	7.26	171	

10-^{3}A	7.39	168	
	***c*-$B_3N_3H_6$: B3LYP/aVTZ[a]**		
State	**ΔE (eV)**	**ΔE (nm)**	**Osc strength**
1-^{1}A	6.63	187	0.00000
2-^{1}A	7.10	175	0.00000
3-^{1}A	7.10	175	0.00000
4-^{1}A	7.21	172	0.00000
5-^{1}A	7.52	165	0.33185
6-^{1}A	7.52	165	0.33185
7-^{1}A	7.52	165	0.01514
8-^{1}A	7.60	163	0.08347
9-^{1}A	7.67	162	0.00000
10-^{1}A	7.67	162	0.00000
1-^{3}A	6.01	206	
2-^{3}A	6.25	198	
3-^{3}A	6.25	198	
4-^{3}A	6.37	195	
5-^{3}A	6.99	177	
6-^{3}A	6.99	177	
7-^{3}A	7.02	177	
8-^{3}A	7.25	171	
9-^{3}A	7.25	171	
10-^{3}A	7.38	168	
	***c*-$B_3N_3H_6$: CCSD/aVDZ[b]**		
State	**ΔE (eV)**	**ΔE (nm)**	**Osc strength**
1-^{1}A'	6.74	184	0.00000
2-^{1}A'	7.93	157	0.43339
3-^{1}A'	7.93	157	0.43339
4-^{1}A'	8.05	154	0.00086
5-^{1}A'	8.05	154	0.00085
1-^{1}A"	7.17	173	0.00000
2-^{1}A"	7.17	173	0.00000
3-^{1}A"	7.55	164	0.07268
4-^{1}A"	7.99	155	0.00000
5-^{1}A"	7.99	155	0.00000

[a] Calculations done on C_1 symmetry. [b] Calculations done on C_s symmetry.

Calculated IR Stretching Frequencies: See Table B3 for calculated IR stretching frequencies compared to experimentally determined values.

Table 3. Scaling for C-H, N-H, and B-H stretching vibrational modes for C_6H_6, NH_3, and BH_3. Scaled MP2/cc-pVTZ vibrational modes and comparison with the experiment.

Molecule	Mode type	MP2/cc-pVTZ	Expt	Scaling	Total scaling
C_6H_6					0.9495
	C-H	3239.6	3068.0	0.9470	
	C-H	3229.7	3063.0	0.9484	
	C-H	3229.7	3063.0	0.9484	
	C-H	3213.1	3062.0	0.9530	
	C-H	3213.1	3047.0	0.9483	
	C-H	3201.5	3047.0	0.9517	
NH_3					0.9443
	N-H	3514.2	3337.0	0.9496	
	N-H	3657.3	3444.0	0.9417	
	N-H	3657.3	3444.0	0.9417	
BH_3					0.9478
	B-H	2608.2	2475.0	0.9489	
	B-H	2746.5	2601.6	0.9472	
	B-H	2746.5	2601.6	0.9472	
BNC_4H_6	N-H	3628.9	0.9443	3426.8	
	C-H	3253.9	0.9495	3089.5	
	C-H	3228.8	0.9495	3065.6	
	C-H	3212.4	0.9495	3050.1	
	C-H	3181.8	0.9495	3021.0	
	B-H	2672.2	0.9478	2532.7	
		1659.9			
		1579.7			
		1490.9			
		1467.5			
		1399.9			
		1291.6			
		1239.9			
		1180.9			
		1128.6			
		1028.8			
		1016.9			
		989.5			
		948.6			
		944.2			
		925.6			
		916.4			
		836.5			
		789.6			
		725.6			
		593.5			
		582.7			

		555.7			
		370.8			
		356.6			
$B_3N_3H_6$	N-H	3669.3	0.9443	3465.0	3456
	N-H	3669.3	0.9443	3465.0	
	N-H	3666.2	0.9443	3462.0	
	B-H	2676.2	0.9478	2536.4	2806
	B-H	2667.2	0.9478	2527.9	2517
	B-H	2667.2	0.9478	2527.9	2393
		1495.1			2222
		1495.1			2142
		1402.3			1998
		1402.3			1917
		1315.9			1863
		1255.1			1457
		1087.3			
		1087.3			
		1052.1			
		951.6			
		951.6			
		949.2			
		931.3			
		930.9			
		930.9			
		859.3			
		734.6			
		711.7			
		711.7			
		517.8			
		517.8			
		395.0			
		282.1			
		282.1			

Table 4. Total CCSD(T) electronic energies (in a. u.) as a function of basis set extrapolated to the complete basis set limit.

Molecule	aVDZ	aVTZ	aVQZ	CBS(DTQ)
BNC_4H_6	-235.041382	-235.248760	-235.306936	-235.339076
$B_3N_3H_6$	-242.025660	-242.242606	-242.304885	-242.339469

Table 5. Components for the atomization. Energies in kcal/mol.

Molecule	ΔE_{CBS}	ΔE_{DKH-SR}	ΔE_{CV}	ΔE_{SO}	ΔE_{ZPE}	ΣD_0	TC

BNC_4H_6	1285.3	6.3	-0.99	-0.37	60.8	1229.4	3.53
$B_3N_3H_6$	1218.7	5.9	-1.03	-0.09	58.1	1165.5	3.88

Table 6. Heats of formation in kcal/mol. Entropies in cal/mol-K.

Molecule	$\Delta H_{f,0K}$	$\Delta H_{f,298K}$	$S°$
BNC_4H_6	7.9	3.0	70.10
$B_3N_3H_6$	-112.8	-119.0	68.73

Table 7. B3LYP/DGDZVP2 binding energies at 0 K in kcal/mol for R-$Cr(CO)_3$ complexes.

Structure	$Cr(CO)_3$ Binding energy
C_6H_6-$Cr(CO)_3$	-54.9
BNC_4H_6-$Cr(CO)_3$	-54.4
$B_3N_3H_6$-$Cr(CO)_3$	-42.7

Table 8. High accuracy (High acc.) and G3MP2 reaction enthalpies at 298 K in kcal/mol.

Reaction	Entry	G3MP2	High acc.[a]
H_2-elimination			
c-C_6H_{12} → c-C_6H_6 + 3 H_2	(1)	44.5	0
c-BNC_4H_{12} → c-BNC_4H_6 + 3 H_2	(2)	23.5	
c-$B_3N_3H_{12}$ → c-$B_3N_3H_6$ + 3 H_2	(3)	-22.3	-18.9
3 C_2H_6 → 3 C_2H_4 + 3 H_2	(4)	92.5	100.0[b]
2 C_2H_6 + BH_3NH_3 → 2 C_2H_4 + BH_2NH_2 + 3 H_2	(5)	54.4	61.5[b]
3 BH_3NH_3 → 3 BH_2NH_2 + 3 H_2	(6)	-21.9	-15.3
c-C_6H_{10} → c-C_6H_8 + H_2	(7)	26.5	
c-C_6H_8 → c-C_6H_6 + H_2	(8)	-5.7	
c-C_4BNH_{10} (B=N bond) → c-C_4BNH_8 (B=N, C=C(B)) + H_2	(9)	25.7	
c-C_4BNH_8 (B=N, C=C(B)) → c-C_4BNH_6 + H_2	(10)	4.7	
c-C_4BNH_{10} (B=N bond) → c-C_4BNH_8 (B=N, C=C(N)) + H_2	(11)	24.4	
c-C_4BNH_8 (B=N, C=C(N)) → c-C_4BNH_6 + H_2	(12)	6.1	
c-$B_3N_3H_{10}$ → c-$B_3N_3H_8$ + H_2	(13)		-2.1

$c\text{-}B_3N_3H_8 \rightarrow c\text{-}B_3N_3H_6 + H_2$	(14)		-27.9
Exchange			
$c\text{-}C_6H_6 + BH_2NH_2 \rightarrow c\text{-}C_4BNH_6 + C_2H_4$	(15)	14.7	14.8
$c\text{-}C_6H_6 + 2\ c\text{-}C_{12}H_{12} \rightarrow 3\ c\text{-}C_6H_{10}$	(16)	35.7	35.7
$c\text{-}C_6H_6 + c\text{-}C_{12}H_{12} \rightarrow 3\ c\text{-}C_6H_{10} + c\text{-}C_6H_8$	(17)	34.1	34.0
$c\text{-}C_6H_6 + c\text{-}C_4BNH_8$ (B=N, C=C(B)) $\rightarrow c\text{-}C_4BNH_6 + c\text{-}C_6H_8$	(18)	12.1	
$c\text{-}C_6H_6 + c\text{-}C_4BNH_8$ (B=N, C=C(B)) $\rightarrow c\text{-}C_4BNH_6 + c\text{-}C_6H_8$	(19)	13.4	
$c\text{-}B_3N_3H_6 + 2\ c\text{-}B_3N_3H_{12} \rightarrow 3\ c\text{-}B_3N_3H_{10}$	(20)		52.8
$c\text{-}B_3N_3H_6 + c\text{-}B_3N_3H_{12} \rightarrow c\text{-}B_3N_3H_{10} + c\text{-}B_3N_3H_8$	(21)		39.3
Decomposition			
$c\text{-}C_6H_6 \rightarrow 3\ HC{\equiv}CH$	(22)	144.2	143.6
$c\text{-}BNC_4H_6 \rightarrow HB{\equiv}NH + 2\ HC{\equiv}CH$	(23)	118.0	118.1
$c\text{-}B_3N_3H_6 \rightarrow 3\ HB{\equiv}NH$	(24)	151.9	154.1

[a] From H_2 and C_xH_y experimental values (NIST Tables) and B compounds CCSD(T)/CBS + corrections values.

Table 9. B3LYP/DGDZVP2 and MP2/cc-pVTZ geometrical parameters for C_6H_6, C_4BNH_6, and $B_3N_3H_6$ cycles (bond lengths in angstroms and angles in degrees, see Figure B1 for labeling).

Structure	Bond or angle	B3LYP/DZVP2	MP2/cc-pVTZ
C_6H_6	C-C	1.4018	1.3937
	C-H	1.0863	1.0814
	∠(C-C-C)	120.0	120.0
	∠(C-C-H)	120.0	120.0
BNC_4H_6	B1-N2	1.4419	1.4341
	N2-C3	1.3708	1.3629
	C3-C4	1.3734	1.3683
	C4-C5	1.4304	1.4156
	C5-C6	1.3825	1.3787
	C6-B1	1.5177	1.5115
	B1-H7	1.1920	1.1904
	N2-H8	1.0121	1.0086
	C3-H9	1.0855	1.0805
	C4-H10	1.0843	1.0792
	C5-H11	1.0895	1.0843
	C6-H12	1.0878	1.0826
	∠(B1-N2-C3)	123.7	124.1
	∠(N2-C3-C4)	120.7	120.4
	∠(C3-C4-C5)	120.1	120.4
	∠(C4-C5-C6)	121.7	121.6
	∠(B1-N2-H8)	120.6	120.5
	∠(N2-C3-H9)	117.4	117.3
	∠(C3-C4-H10)	119.3	118.8
	∠(C4-C5-H11)	117.5	117.7
	∠(C5-C6-H12)	118.1	117.6
	∠(C6-B1-H7)	127.1	127.7

$B_3N_3H_6$	B-N	1.4357	1.4307
	B-H	1.1937	1.1910
	N-H	1.0104	1.0059
	∠(B-N-B)	123.0	123.1
	∠(N-B-N)	117.0	116.9
	∠(B-N-H)	118.5	118.5
	∠(N-B-H)	121.5	121.5

Table 10. B3LYP/DGDZVP2 geometrical parameters for C_6H_6-$Cr(CO)_3$, C_4BNH_6-$Cr(CO)_3$, and $B_3N_3H_6$-$Cr(CO)_3$ cycles (bond lengths in angstroms and angles in degrees, see Figure B2 for labeling).

Bond or angle	C_6H_6-$Cr(CO)_3$	Bond or angle	BNC_4H_6-$Cr(CO)_3$	Bond or angle	$B_3N_3H_6$-$Cr(CO)_3$
Cr-C1	1.8564	Cr-C1	1.8646	Cr-C1	1.8495
Cr-C2	1.8564	Cr-C2	1.8508	Cr-C2	1.8495
Cr-C3	1.8564	Cr-C3	1.8547	Cr-C3	1.8494
Cr-C4	2.2438	Cr-B4	2.3676	Cr-B4	2.3387
Cr-C5	2.2438	Cr-N5	2.2274	Cr-N5	2.2674
Cr-C6	2.2444	Cr-C6	2.1691	Cr-B6	2.3384
Cr-C7	2.2443	Cr-C7	2.2341	Cr-N7	2.2664
Cr-C8	2.2443	Cr-C8	2.2508	Cr-B8	2.3371
Cr-C9	2.2444	Cr-C9	2.3008	Cr-N9	2.2674
C1-O10	1.1688	C1-O10	1.1664	C1-O10	1.1697
C2-O11	1.1688	C2-O11	1.1689	C2-O11	1.1696
C3-O12	1.1688	C3-O12	1.1696	C3-O12	1.1696
C4-C5	1.4089	B4-N5	1.4633	B4-N5	1.4515
C5-C6	1.4273	N5-C6	1.3952	N5-B6	1.4516
C6-C7	1.4087	C6-C7	1.4004	B6-N7	1.4514
C7-C8	1.4275	C7-C8	1.4305	N7-B8	1.4515
C8-C9	1.4087	C8-C9	1.4061	B8-N9	1.4516
C9-C4	1.4273	C9-B4	1.5186	N9-B4	1.4517

∠(C1-Cr-C2)	89.0	∠(C1-Cr-C2)	90.1	∠(C1-Cr-C2)	89.2
∠(C2-Cr-C3)	89.0	∠(C2-Cr-C3)	88.1	∠(C2-Cr-C3)	89.4
∠(C3-Cr-C1)	89.0	∠(C3-Cr-C1)	89.0	∠(C3-Cr-C1)	89.1
∠(C1-C2-C3-Cr)	55.5	∠(C1-C2-C3-Cr)	54.9	∠(C1-C2-C3-Cr)	55.4

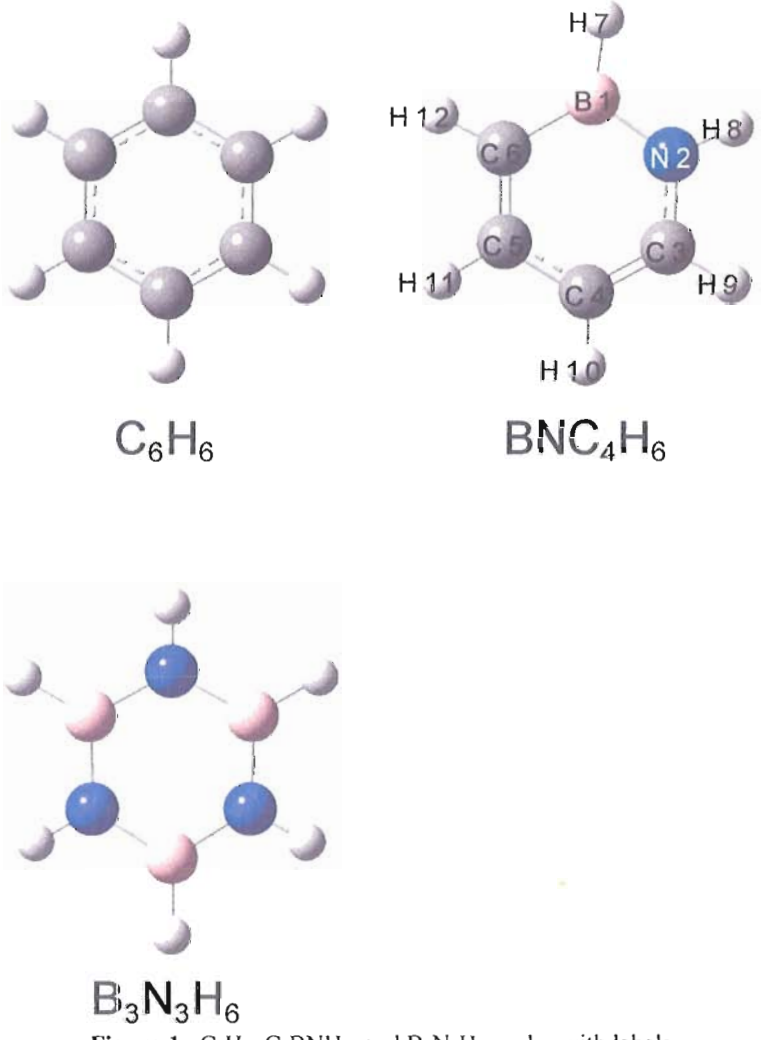

Figure 1. C_6H_6, C_4BNH_6, and $B_3N_3H_6$ cycles with labels.

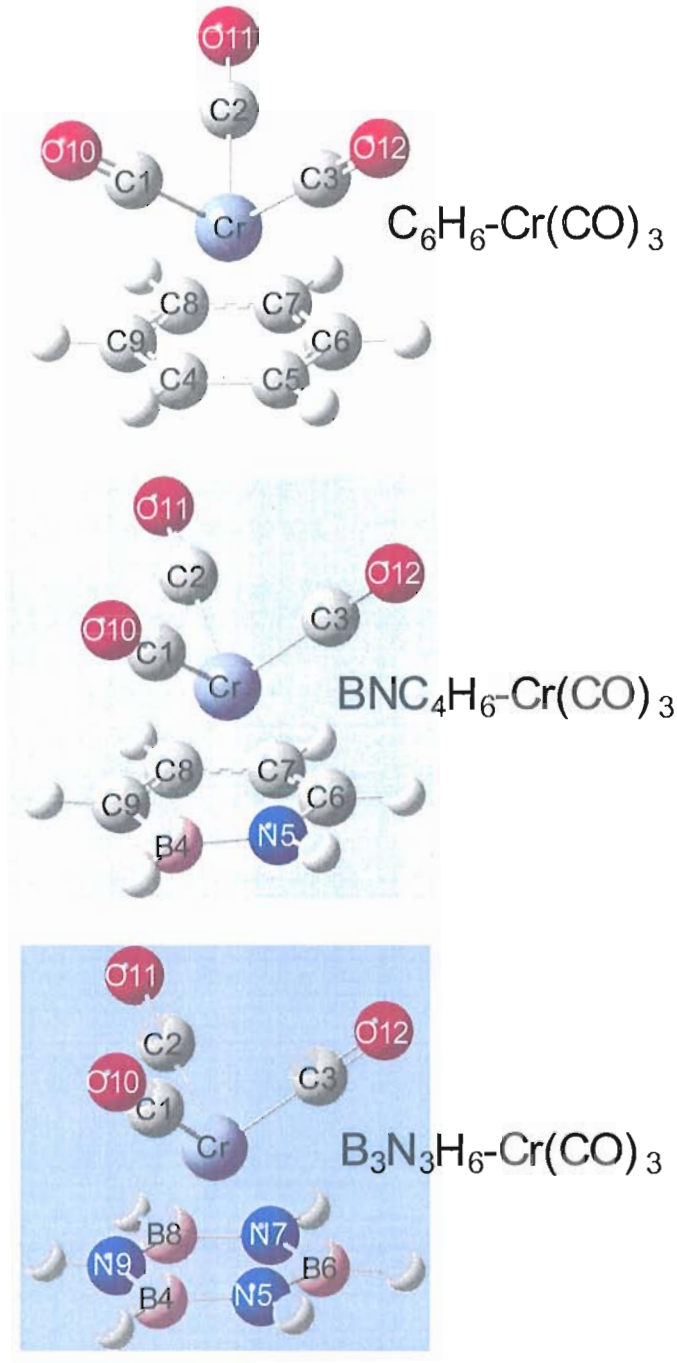

Figure 2. C_6H_6-$Cr(CO)_3$, C_4BNH_6-$Cr(CO)_3$, and $B_3N_3H_6$-$Cr(CO)_3$ structures.

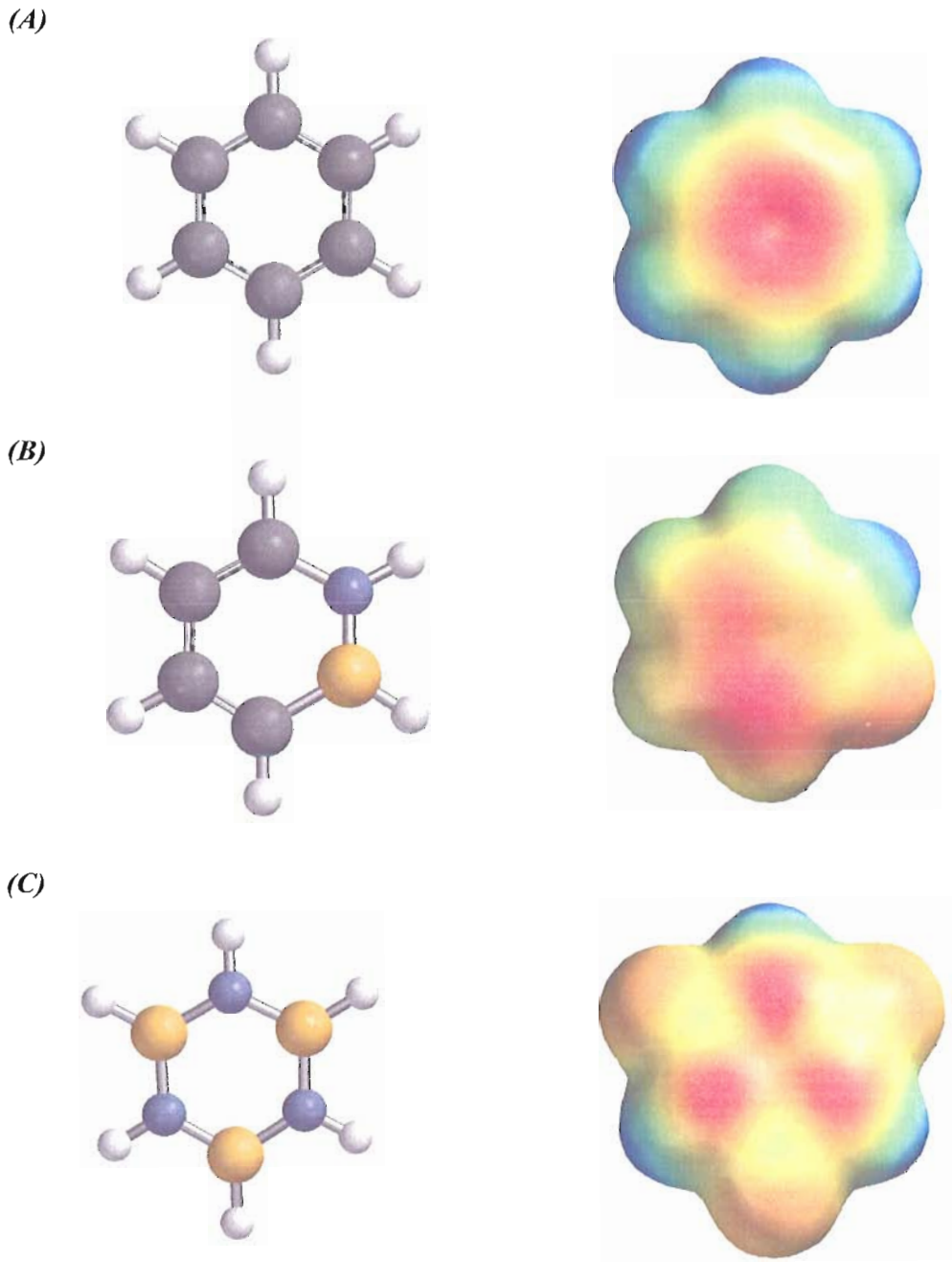

Figure 3. Electrostatic potential maps at the 0.002 electron/a.u.^{3} density iso-contour level (A) c-C_6H_6 (–18.9 to 19.2 kcal.mol), (B) c-BNC_4H_6 (–13.6 to 39.9 kcal/mol), and (C) c-$B_3N_3H_6$ (–20.9 to 54.5 kcal/mol). Blue is positive potential (repulsive for the positive charge), red is negative potential (attractive for the positive charge) and green represents near zero potential.

H/D Exchange: N–H Exchange. A CD_3OD solution containing hexamethylbenzene as internal standard (1 mL; 1 mM hexamethylbenzene) was added to a neat sample of 1,2-dihydro-1,2-azaborine **1** (0.0060 g, 0.070 mmol) under N_2. ^1H NMR indicated a slow exchange of the N–H resonance at 9.8 ppm (integrated versus the 1,2-dihydro-1,2-azaborine C(5)–H resonance at 6.3 ppm). Integration of the 1,2-dihydro-1,2-azaborine C(5)–H resonance versus hexamethylbenzene indicated that no appreciable degradation of **1** took place within the timeframe of the H/D exchange experiment (30 h). We assumed pseudo first-order kinetics and obtained an exchange rate constant $k_{HD} = 7 \pm 2 \times 10^{-7}\ M^{-1}s^{-1}$ (Figure 4).

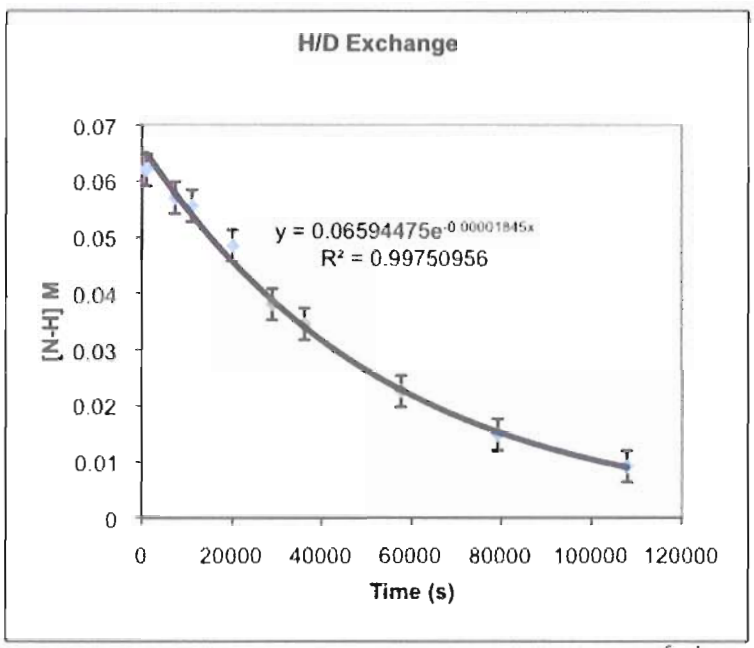

Figure 4. Plot of [N-H] (M) versus time (s). From exponential fit, $k_{obs} = 1.8 \times 10^{-5}\ s^{-1}$ and $k_{HD} = 7.5 \times 10^{-7}\ M^{-1}s^{-1}$ was obtained, where $[CD_3OD] = 24.6$ M.

C(3)–H Exchange. The sample from the N–H exchange experiment was charged with CD_3COOD (4.0 μL, 0.070 mmol) and CF_3COOD (16.3 μL, 0.211 mmol). At t = 24

h, ^{1}H NMR indicated no deuterium exchange at the C(3)–H position of **1**. Minor degradation to unidentified products was noted in the ^{1}H and ^{11}B NMR spectra.

Reactivity with Benzaldehyde: 1,2-Dihydro-1,2-azaborine (1). A J. Young NMR tube was charged with a 0.67 M solution of 1,2-dihydro-1,2-azaborine **1** in CD_2Cl_2 (0.40 mL; 0.27 mmol **1**) and hexamethylbenzene (0.0029 g, 0.018 mmol, internal standard). Benzaldehyde (0.0256 g, 0.241 mmol) was added, the tube was sealed, and the reaction monitored by ^{1}H NMR. ^{1}H NMR showed no evidence of aldehyde reduction after 16 h at rt. Then, the mixture was heated to 60 °C for 60 h and then allowed to cool to rt. ^{1}H NMR again showed no evidence of aldehyde reduction. ^{1}H NMR integration of hexamethylbenzene versus 1,2-dihydro-1,2-azaborine indicated little to no degradation of **1**.

Borazine. A J. Young NMR tube was charged with benzaldehyde (0.050 g, 0.47 mmol), CD_2Cl_2 (1.0 mL), and borazine (0.038 g, 0.47 mmol). The tube was sealed and heated at 60 °C for 24 h. ^{1}H NMR indicated complete consumption of benzaldehyde. Upon workup, reduced benzaldehyde derivatives such as *N*-benzylidenebenzylamine and *N*-tribenzylamine were isolated.

Crystallographic Data for Complex 12 (liu19)

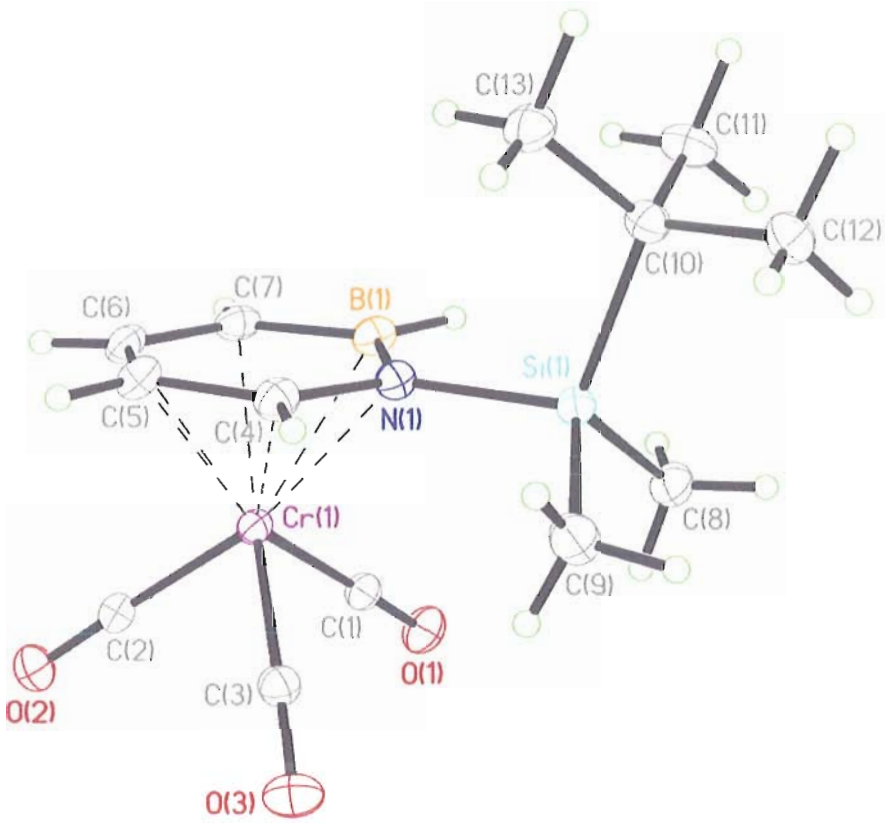

Figure 5. ORTEP illustration of **12**, with ellipsoids drawn at the 35% probability level.

X-ray Crystal Structure Determination. Crystals of **12** suitable for X-ray diffraction were obtained by evaporation of a solution of **12** in Et_2O.

Diffraction intensity data were collected with a Bruker Smart Apex CCD diffractometer at 173(2) K using MoKα - radiation (0.71073 Å). The structure was solved using direct methods, completed by subsequent difference Fourier syntheses, and

refined by full matrix least-squares procedures on F^2. All non-H atoms were refined with anisotropic thermal parameters. H atoms were found on the residual density map and refined with isotropic thermal parameters. The Flack parameter is 0.00(8). All software and sources scattering factors are contained in the SHELXTL (6.10) program package (G.Sheldrick, Bruker XRD, Madison, WI). Crystallographic data and some details of data collection and crystal structure refinement for $C_{13}H_{20}BNO_3SiCr$ are given in the following tables.

Table 11. Crystal data and structure refinement for **12.**

Identification code	liu19	
Empirical formula	C_{13} H_{20} B Cr N O_3 Si	
Formula weight	329.20	
Temperature	173(2) K	
Wavelength	0.71073 Å	
Crystal system	Triclinic	
Space group	P-1	
Unit cell dimensions	a = 6.9391(5) Å	α= 104.0960(10)°.
	b = 10.2736(7) Å	β= 95.5740(10)°.
	c = 12.4331(8) Å	γ = 108.4140(10)°.
Volume	800.92(9) $Å^3$	
Z	2	
Density (calculated)	1.365 Mg/m^3	
Absorption coefficient	0.793 mm^{-1}	
F(000)	344	
Crystal size	0.27 x 0.17 x 0.12 mm^3	
Theta range for data coll.	1.72 to 27.00°.	
Index ranges	-8<=h<=8, -13<=k<=13, -15<=l<=15	
Reflections collected	8584	
Independent reflections	3450 [R(int) = 0.0209]	
Completeness to θ = 27.00°	98.9 %	
Absorption correction	Semi-empirical from equivalents	

Max. and min. transmission	0.9108 and 0.8144
Refinement method	Full-matrix least-squares on F^2
Data / restraints / parameters	3450 / 0 / 261
Goodness-of-fit on F^2	1.076
Final R indices [I>2σ(I)]	R1 = 0.0354, wR2 = 0.0863
R indices (all data)	R1 = 0.0432, wR2 = 0.0925
Largest diff. peak and hole	0.458 and -0.225 e.Å^{-3}

Table 12. Atomic coordinates (x 10^4) and equivalent isotropic displacement parameters (Å^{2}x 10^3) for liu19. U(eq) is defined as one third of the trace of the orthogonalized U^{ij} tensor.

	x	y	z	U(eq)
Cr(1)	9948(1)	9749(1)	2072(1)	23(1)
Si(1)	7156(1)	6555(1)	2816(1)	24(1)
O(1)	6254(2)	9003(2)	266(1)	37(1)
O(2)	11612(3)	12588(2)	1621(2)	46(1)
O(3)	7969(3)	11203(2)	3785(2)	43(1)
N(1)	9429(3)	7702(2)	2451(1)	25(1)
B(1)	9727(4)	7441(3)	1286(2)	29(1)
C(1)	7662(3)	9275(2)	956(2)	27(1)
C(2)	10999(3)	11490(2)	1793(2)	32(1)
C(3)	8714(3)	10618(2)	3117(2)	29(1)
C(4)	10958(4)	8803(2)	3312(2)	30(1)
C(5)	12746(3)	9697(3)	3062(2)	31(1)
C(6)	13021(3)	9547(3)	1936(2)	30(1)
C(7)	11584(4)	8450(3)	1057(2)	30(1)
C(8)	4884(4)	6122(3)	1709(3)	37(1)
C(9)	6758(5)	7573(3)	4182(2)	39(1)
C(10)	7752(3)	4927(2)	2951(2)	29(1)
C(11)	7403(5)	3851(3)	1790(2)	42(1)
C(12)	6282(4)	4202(3)	3652(2)	40(1)
C(13)	9995(4)	5357(3)	3558(2)	38(1)

Table 13. Bond lengths [Å] and angles [°] for liu19.

Cr(1)-C(3)	1.831(2)
Cr(1)-C(2)	1.838(2)
Cr(1)-C(1)	1.854(2)
Cr(1)-C(4)	2.182(2)
Cr(1)-N(1)	2.1927(18)
Cr(1)-C(5)	2.218(2)
Cr(1)-C(6)	2.225(2)
Cr(1)-C(7)	2.253(2)
Cr(1)-B(1)	2.283(3)
Si(1)-N(1)	1.8188(19)
Si(1)-C(8)	1.848(3)
Si(1)-C(9)	1.861(3)
Si(1)-C(10)	1.886(2)
O(1)-C(1)	1.147(3)

O(2)-C(2)	1.154(3)
O(3)-C(3)	1.164(3)
N(1)-C(4)	1.408(3)
N(1)-B(1)	1.455(3)
B(1)-C(7)	1.479(4)
B(1)-H(1B)	1.02(2)
C(4)-C(5)	1.406(3)
C(4)-H(4)	1.03(2)
C(5)-C(6)	1.409(3)
C(5)-H(5)	0.91(3)
C(6)-C(7)	1.391(3)
C(6)-H(6)	0.92(2)
C(7)-H(7)	0.90(2)
C(8)-H(8A)	0.93(3)
C(8)-H(8B)	0.90(3)
C(8)-H(8C)	0.87(3)
C(9)-H(9A)	0.98(3)
C(9)-H(9B)	0.90(3)
C(9)-H(9C)	0.93(3)
C(10)-C(11)	1.533(3)
C(10)-C(13)	1.537(3)
C(10)-C(12)	1.537(3)
C(11)-H(11A)	0.97(3)
C(11)-H(11B)	0.98(3)
C(11)-H(11C)	0.91(3)
C(12)-H(12A)	0.98(3)
C(12)-H(12B)	0.97(3)
C(12)-H(12C)	0.94(3)
C(13)-H(13A)	1.02(3)
C(13)-H(13B)	0.96(3)
C(13)-H(13C)	0.95(3)
C(3)-Cr(1)-C(2)	86.78(10)
C(3)-Cr(1)-C(1)	90.36(9)
C(2)-Cr(1)-C(1)	88.78(10)
C(3)-Cr(1)-C(4)	88.78(9)
C(2)-Cr(1)-C(4)	133.77(10)
C(1)-Cr(1)-C(4)	137.27(9)
C(3)-Cr(1)-N(1)	101.17(8)
C(2)-Cr(1)-N(1)	166.99(9)
C(1)-Cr(1)-N(1)	101.33(8)
C(4)-Cr(1)-N(1)	37.55(8)
C(3)-Cr(1)-C(5)	105.25(9)
C(2)-Cr(1)-C(5)	100.66(10)
C(1)-Cr(1)-C(5)	162.06(9)
C(4)-Cr(1)-C(5)	37.25(9)
N(1)-Cr(1)-C(5)	67.46(8)
C(3)-Cr(1)-C(6)	138.91(9)
C(2)-Cr(1)-C(6)	86.83(9)
C(1)-Cr(1)-C(6)	130.00(9)
C(4)-Cr(1)-C(6)	67.44(9)
N(1)-Cr(1)-C(6)	80.41(8)
C(5)-Cr(1)-C(6)	36.99(8)
C(3)-Cr(1)-C(7)	168.06(9)

C(2)-Cr(1)-C(7) 102.40(9)
C(1)-Cr(1)-C(7) 97.37(9)
C(4)-Cr(1)-C(7) 79.36(9)
N(1)-Cr(1)-C(7) 68.45(8)
C(5)-Cr(1)-C(7) 65.84(9)
C(6)-Cr(1)-C(7) 36.20(9)
C(3)-Cr(1)-B(1) 134.96(10)
C(2)-Cr(1)-B(1) 137.42(10)
C(1)-Cr(1)-B(1) 83.85(9)
C(4)-Cr(1)-B(1) 67.39(9)
N(1)-Cr(1)-B(1) 37.87(8)
C(5)-Cr(1)-B(1) 78.87(9)
C(6)-Cr(1)-B(1) 67.19(9)
C(7)-Cr(1)-B(1) 38.04(9)
N(1)-Si(1)-C(8) 108.92(11)
N(1)-Si(1)-C(9) 107.86(11)
C(8)-Si(1)-C(9) 109.17(14)
N(1)-Si(1)-C(10) 106.18(9)
C(8)-Si(1)-C(10) 113.20(12)
C(9)-Si(1)-C(10) 111.31(12)
C(4)-N(1)-B(1) 119.94(19)
C(4)-N(1)-Si(1) 119.50(15)
B(1)-N(1)-Si(1) 120.47(16)
C(4)-N(1)-Cr(1) 70.83(12)
B(1)-N(1)-Cr(1) 74.45(13)
Si(1)-N(1)-Cr(1) 129.45(9)
N(1)-B(1)-C(7) 117.0(2)
N(1)-B(1)-Cr(1) 67.68(12)
C(7)-B(1)-Cr(1) 69.86(14)
N(1)-B(1)-H(1B) 118.3(14)
C(7)-B(1)-H(1B) 124.7(14)
Cr(1)-B(1)-H(1B) 133.6(14)
O(1)-C(1)-Cr(1) 179.01(19)
O(2)-C(2)-Cr(1) 178.3(2)
O(3)-C(3)-Cr(1) 178.3(2)
C(5)-C(4)-N(1) 121.0(2)
C(5)-C(4)-Cr(1) 72.76(13)
N(1)-C(4)-Cr(1) 71.63(12)
C(5)-C(4)-H(4) 120.7(13)
N(1)-C(4)-H(4) 118.3(13)
Cr(1)-C(4)-H(4) 128.8(13)
C(4)-C(5)-C(6) 120.7(2)
C(4)-C(5)-Cr(1) 69.99(13)
C(6)-C(5)-Cr(1) 71.77(13)
C(4)-C(5)-H(5) 118.3(16)
C(6)-C(5)-H(5) 120.6(16)
Cr(1)-C(5)-H(5) 125.2(16)
C(7)-C(6)-C(5) 120.4(2)
C(7)-C(6)-Cr(1) 72.99(13)
C(5)-C(6)-Cr(1) 71.24(13)
C(7)-C(6)-H(6) 120.6(14)
C(5)-C(6)-H(6) 118.9(15)
Cr(1)-C(6)-H(6) 124.9(15)

C(6)-C(7)-B(1)	120.7(2)
C(6)-C(7)-Cr(1)	70.81(13)
B(1)-C(7)-Cr(1)	72.10(13)
C(6)-C(7)-H(7)	119.1(16)
B(1)-C(7)-H(7)	120.1(16)
Cr(1)-C(7)-H(7)	126.3(15)
Si(1)-C(8)-H(8A)	109.2(19)
Si(1)-C(8)-H(8B)	110(2)
H(8A)-C(8)-H(8B)	110(3)
Si(1)-C(8)-H(8C)	114(2)
H(8A)-C(8)-H(8C)	111(3)
H(8B)-C(8)-H(8C)	103(3)
Si(1)-C(9)-H(9A)	113.4(19)
Si(1)-C(9)-H(9B)	112(2)
H(9A)-C(9)-H(9B)	112(3)
Si(1)-C(9)-H(9C)	106.2(18)
H(9A)-C(9)-H(9C)	108(3)
H(9B)-C(9)-H(9C)	105(3)
C(11)-C(10)-C(13)	109.4(2)
C(11)-C(10)-C(12)	108.6(2)
C(13)-C(10)-C(12)	108.9(2)
C(11)-C(10)-Si(1)	111.12(17)
C(13)-C(10)-Si(1)	110.79(16)
C(12)-C(10)-Si(1)	107.98(16)
C(10)-C(11)-H(11A)	110.9(18)
C(10)-C(11)-H(11B)	109.5(16)
H(11A)-C(11)-H(11B)	109(2)
C(10)-C(11)-H(11C)	110.0(17)
H(11A)-C(11)-H(11C)	109(2)
H(11B)-C(11)-H(11C)	108(2)
C(10)-C(12)-H(12A)	110.7(18)
C(10)-C(12)-H(12B)	110.9(17)
H(12A)-C(12)-H(12B)	106(2)
C(10)-C(12)-H(12C)	111.2(17)
H(12A)-C(12)-H(12C)	110(2)
H(12B)-C(12)-H(12C)	108(2)
C(10)-C(13)-H(13A)	110.6(17)
C(10)-C(13)-H(13B)	111.0(17)
H(13A)-C(13)-H(13B)	107(2)
C(10)-C(13)-H(13C)	112.3(17)
H(13A)-C(13)-H(13C)	109(2)
H(13B)-C(13)-H(13C)	107(2)

Symmetry transformations used to generate equivalent atoms:

Table 14. Anisotropic displacement parameters ($Å^2 x\ 10^3$)for liu19. The anisotropic displacement factor exponent takes the form: $-2\pi^2[\ h^2 a^{*2} U^{11} + ... + 2\ h\ k\ a^*\ b^*\ U^{12}\ ]$

	U^{11}	U^{22}	U^{33}	U^{23}	U^{13}	U^{12}
Cr(1)	20(1)	24(1)	24(1)	6(1)	5(1)	8(1)
Si(1)	24(1)	23(1)	26(1)	6(1)	6(1)	8(1)
O(1)	28(1)	47(1)	33(1)	13(1)	2(1)	11(1)
O(2)	37(1)	28(1)	73(1)	19(1)	12(1)	7(1)

O(3)	48(1)	45(1)	41(1)	6(1)	16(1)	26(1)
N(1)	25(1)	27(1)	24(1)	8(1)	6(1)	10(1)
B(1)	30(1)	37(1)	27(1)	13(1)	9(1)	16(1)
C(1)	27(1)	28(1)	29(1)	10(1)	11(1)	9(1)
C(2)	23(1)	30(1)	41(1)	8(1)	7(1)	8(1)
C(3)	28(1)	29(1)	30(1)	8(1)	4(1)	11(1)
C(4)	30(1)	35(1)	31(1)	13(1)	6(1)	14(1)
C(5)	23(1)	40(1)	32(1)	10(1)	4(1)	13(1)
C(6)	22(1)	36(1)	40(1)	17(1)	11(1)	13(1)
C(7)	33(1)	36(1)	30(1)	14(1)	15(1)	20(1)
C(8)	28(1)	37(1)	46(2)	16(1)	3(1)	12(1)
C(9)	48(2)	33(1)	39(1)	9(1)	24(1)	13(1)
C(10)	32(1)	27(1)	30(1)	10(1)	5(1)	12(1)
C(11)	55(2)	33(1)	41(2)	6(1)	7(1)	23(1)
C(12)	40(2)	35(1)	49(2)	22(1)	11(1)	13(1)
C(13)	33(1)	44(2)	43(2)	20(1)	4(1)	17(1)

Table 15. Hydrogen coordinates (x 10^4) and isotropic displacement parameters ($Å^2$x 10^3) for liu19.

	x	y	z	U(eq)
H(1B)	8650(40)	6590(30)	690(20)	35(7)
H(4)	10740(30)	8930(20)	4131(19)	26(6)
H(5)	13650(40)	10440(30)	3640(20)	33(7)
H(6)	14120(40)	10220(30)	1789(19)	26(6)
H(7)	11750(40)	8400(30)	340(20)	29(6)
H(8A)	3760(50)	5430(30)	1840(30)	58(9)
H(8B)	4590(50)	6920(40)	1720(30)	60(9)
H(8C)	5090(50)	5840(30)	1020(30)	58(10)
H(9A)	7770(50)	7680(30)	4830(30)	66(10)
H(9B)	6670(50)	8420(40)	4160(30)	63(10)
H(9C)	5450(50)	7050(30)	4280(20)	57(9)
H(11A)	5990(50)	3560(30)	1390(30)	57(9)
H(11B)	7680(40)	3000(30)	1880(20)	53(8)
H(11C)	8300(40)	4250(30)	1370(20)	39(8)
H(12A)	6480(50)	3310(30)	3700(20)	55(9)
H(12B)	6570(40)	4810(30)	4420(20)	42(7)
H(12C)	4900(50)	4010(30)	3340(20)	47(8)
H(13A)	10270(50)	4490(30)	3700(20)	53(8)
H(13B)	10260(40)	6050(30)	4280(20)	46(8)
H(13C)	10970(40)	5770(30)	3140(20)	45(8)

Crystallographic Data for 13 (liu22)

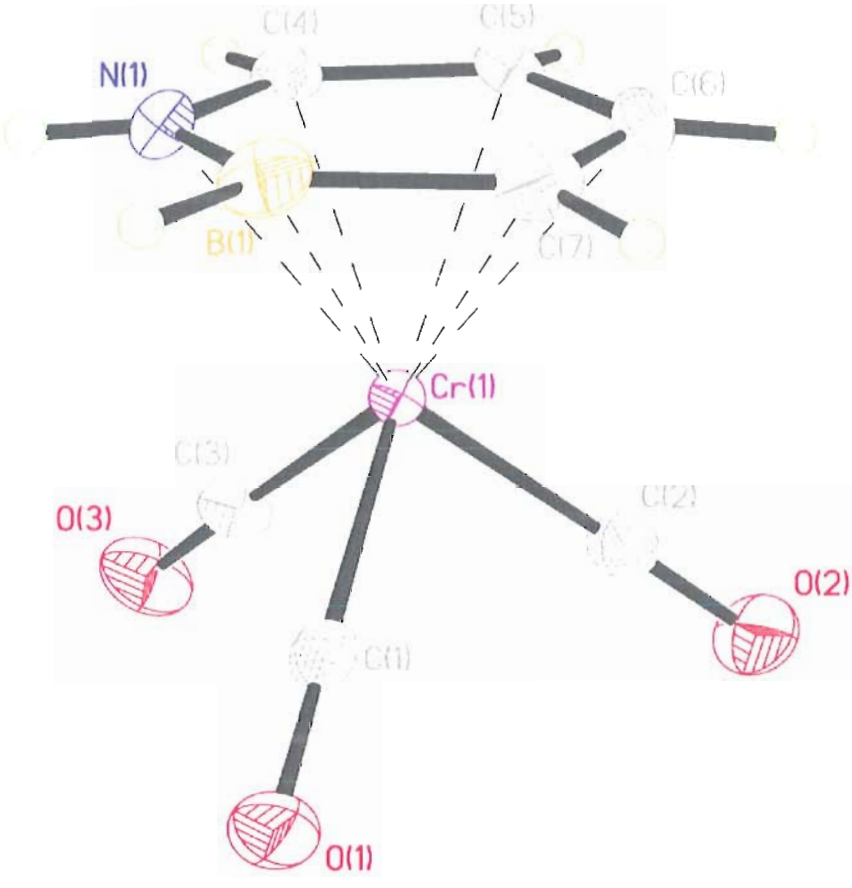

Figure 6. ORTEP illustration of **13**, with ellipsoids drawn at the 35% probability level.

X-ray Crystal Structure Determination. Crystals of **13** suitable for X-ray diffraction were obtained by evaporation of a solution of **13** in Et_2O.

Diffraction intensity data were collected with a Bruker Smart Apex CCD diffractometer at 173(2) K using MoKα - radiation (0.71073 Å). The structure was

solved using direct methods, completed by subsequent difference Fourier syntheses, and refined by full matrix least-squares procedures on F^2. All non-H atoms were refined with anisotropic thermal parameters. H atoms were found on the residual density map and refined with isotropic thermal parameters. The Flack parameter is 0.00(8). All software and sources scattering factors are contained in the SHELXTL (6.10) program package (G.Sheldrick, Bruker XRD, Madison, WI). Crystallographic data and some details of data collection and crystal structure refinement for $C_7H_6BCrNO_3$ are given in the following tables.

Table 16. Crystal data and structure refinement for **13**.

Identification code	liu22	
Empirical formula	$C_7 H_6 B Cr N O_3$	
Formula weight	214.94	
Temperature	173(2) K	
Wavelength	0.71073 Å	
Crystal system	Monoclinic	
Space group	P2(1)/c	
Unit cell dimensions	a = 11.5311(8) Å	α= 90°.
	b = 6.9443(5) Å	β= 115.9460(10)°.
	c = 12.2196(8) Å	γ = 90°.
Volume	879.86(11) $Å^3$	
Z	4	
Density (calculated)	1.623 Mg/m^3	
Absorption coefficient	1.267 mm^{-1}	
F(000)	432	
Crystal size	0.20 x 0.14 x 0.09 mm^3	
Theta range for data coll.	1.96 to 26.99°.	
Index ranges	-14<=h<=14, -8<=k<=8, -15<=l<=15	
Reflections collected	9413	
Independent reflections	1915 [R(int) = 0.0262]	

Completeness to $\theta = 26.99°$	100.0 %
Absorption correction	Semi-empirical from equivalents
Max. and min. transmission	0.8945 and 0.7856
Refinement method	Full-matrix least-squares on F^2
Data / restraints / parameters	1915 / 0 / 142
Goodness-of-fit on F^2	1.027
Final R indices [$I>2\sigma(I)$]	R1 = 0.0293, wR2 = 0.0728
R indices (all data)	R1 = 0.0345, wR2 = 0.0765
Largest diff. peak and hole	0.439 and -0.201 e.Å^3

Table 17. Atomic coordinates (x 10^4) and equivalent isotropic displacement parameters (Å^{2}x 10^3) for liu22. U(eq) is defined as one third of the trace of the orthogonalized U^{ij} tensor.

	x	y	z	U(eq)
Cr(1)	2370(1)	9733(1)	2264(1)	21(1)
O(1)	1041(2)	12842(2)	445(2)	44(1)
O(2)	3615(2)	12715(3)	4195(2)	53(1)
O(3)	186(2)	9828(3)	2967(2)	52(1)
N(1)	1888(2)	7035(3)	1254(2)	32(1)
B(1)	2437(3)	8204(4)	622(2)	36(1)
C(1)	1550(2)	11645(3)	1144(2)	30(1)
C(2)	3144(2)	11566(3)	3442(2)	34(1)
C(3)	1022(2)	9763(3)	2693(2)	33(1)
C(4)	2508(2)	6636(3)	2480(2)	29(1)
C(5)	3719(2)	7363(3)	3174(2)	29(1)
C(6)	4323(2)	8609(3)	2657(2)	35(1)
C(7)	3717(2)	9059(3)	1422(2)	35(1)

Table 18. Bond lengths [Å] and angles [°] for liu22.

Cr(1)-C(2)	1.834(2)
Cr(1)-C(1)	1.843(2)
Cr(1)-C(3)	1.845(2)
Cr(1)-C(4)	2.164(2)
Cr(1)-N(1)	2.1781(18)
Cr(1)-C(5)	2.203(2)
Cr(1)-C(6)	2.228(2)
Cr(1)-C(7)	2.256(2)
Cr(1)-B(1)	2.301(2)
O(1)-C(1)	1.152(3)
O(2)-C(2)	1.158(3)
O(3)-C(3)	1.152(3)
N(1)-C(4)	1.377(3)
N(1)-B(1)	1.443(3)
N(1)-H(1N)	0.80(3)
B(1)-C(7)	1.492(4)
B(1)-H(1B)	1.03(2)

C(4)-C(5)	1.374(3)
C(4)-H(4)	0.88(3)
C(5)-C(6)	1.421(3)
C(5)-H(5)	0.80(2)
C(6)-C(7)	1.393(3)
C(6)-H(6)	0.90(3)
C(7)-H(7)	0.90(3)
C(2)-Cr(1)-C(1)	89.93(9)
C(2)-Cr(1)-C(3)	87.17(10)
C(1)-Cr(1)-C(3)	88.86(9)
C(2)-Cr(1)-C(4)	127.54(9)
C(1)-Cr(1)-C(4)	142.42(9)
C(3)-Cr(1)-C(4)	90.16(9)
C(2)-Cr(1)-N(1)	163.27(9)
C(1)-Cr(1)-N(1)	106.12(8)
C(3)-Cr(1)-N(1)	97.62(9)
C(4)-Cr(1)-N(1)	36.97(7)
C(2)-Cr(1)-C(5)	97.39(9)
C(1)-Cr(1)-C(5)	158.88(9)
C(3)-Cr(1)-C(5)	111.19(9)
C(4)-Cr(1)-C(5)	36.66(8)
N(1)-Cr(1)-C(5)	65.93(8)
C(2)-Cr(1)-C(6)	88.58(9)
C(1)-Cr(1)-C(6)	123.67(9)
C(3)-Cr(1)-C(6)	147.19(9)
C(4)-Cr(1)-C(6)	67.17(8)
N(1)-Cr(1)-C(6)	78.69(8)
C(5)-Cr(1)-C(6)	37.42(8)
C(2)-Cr(1)-C(7)	107.83(9)
C(1)-Cr(1)-C(7)	92.47(9)
C(3)-Cr(1)-C(7)	164.93(9)
C(4)-Cr(1)-C(7)	79.67(8)
N(1)-Cr(1)-C(7)	67.60(8)
C(5)-Cr(1)-C(7)	66.44(8)
C(6)-Cr(1)-C(7)	36.18(9)
C(2)-Cr(1)-B(1)	144.52(10)
C(1)-Cr(1)-B(1)	83.51(9)
C(3)-Cr(1)-B(1)	127.32(10)
C(4)-Cr(1)-B(1)	67.58(9)
N(1)-Cr(1)-B(1)	37.45(8)
C(5)-Cr(1)-B(1)	79.04(9)
C(6)-Cr(1)-B(1)	67.04(10)
C(7)-Cr(1)-B(1)	38.21(9)
C(4)-N(1)-B(1)	123.7(2)
C(4)-N(1)-Cr(1)	70.97(11)
B(1)-N(1)-Cr(1)	75.92(12)
C(4)-N(1)-H(1N)	116.9(19)
B(1)-N(1)-H(1N)	119.4(19)
Cr(1)-N(1)-H(1N)	124.4(19)
N(1)-B(1)-C(7)	114.4(2)
N(1)-B(1)-Cr(1)	66.64(11)
C(7)-B(1)-Cr(1)	69.25(12)
N(1)-B(1)-H(1B)	117.4(13)

C(7)-B(1)-H(1B)	128.1(13)
Cr(1)-B(1)-H(1B)	129.7(14)
O(1)-C(1)-Cr(1)	179.7(2)
O(2)-C(2)-Cr(1)	178.6(2)
O(3)-C(3)-Cr(1)	178.4(2)
C(5)-C(4)-N(1)	120.1(2)
C(5)-C(4)-Cr(1)	73.20(13)
N(1)-C(4)-Cr(1)	72.07(11)
C(5)-C(4)-H(4)	120.2(17)
N(1)-C(4)-H(4)	119.6(17)
Cr(1)-C(4)-H(4)	124.7(17)
C(4)-C(5)-C(6)	120.8(2)
C(4)-C(5)-Cr(1)	70.14(12)
C(6)-C(5)-Cr(1)	72.25(12)
C(4)-C(5)-H(5)	118.0(17)
C(6)-C(5)-H(5)	120.7(17)
Cr(1)-C(5)-H(5)	123.0(17)
C(7)-C(6)-C(5)	120.5(2)
C(7)-C(6)-Cr(1)	73.01(13)
C(5)-C(6)-Cr(1)	70.34(12)
C(7)-C(6)-H(6)	122.7(17)
C(5)-C(6)-H(6)	116.5(17)
Cr(1)-C(6)-H(6)	124.2(17)
C(6)-C(7)-B(1)	120.2(2)
C(6)-C(7)-Cr(1)	70.81(12)
B(1)-C(7)-Cr(1)	72.54(12)
C(6)-C(7)-H(7)	116.1(19)
B(1)-C(7)-H(7)	123.4(19)
Cr(1)-C(7)-H(7)	124.2(18)

Symmetry transformations used to generate equivalent atoms:

Table 19. Anisotropic displacement parameters ($Å^2 x\ 10^3$)for liu22. The anisotropic displacement factor exponent takes the form: $-2\pi^2[\ h^2 a^{*2} U^{11} + ... + 2\ h\ k\ a^*\ b^*\ U^{12}\ ]$

	U^{11}	U^{22}	U^{33}	U^{23}	U^{13}	U^{12}
Cr(1)	20(1)	20(1)	21(1)	0(1)	8(1)	0(1)
O(1)	48(1)	34(1)	37(1)	10(1)	7(1)	5(1)
O(2)	59(1)	44(1)	38(1)	-17(1)	5(1)	1(1)
O(3)	44(1)	61(1)	64(1)	10(1)	37(1)	14(1)
N(1)	30(1)	25(1)	37(1)	-7(1)	12(1)	-5(1)
B(1)	51(2)	34(1)	29(1)	-5(1)	22(1)	3(1)
C(1)	31(1)	26(1)	27(1)	-4(1)	8(1)	-3(1)
C(2)	33(1)	33(1)	28(1)	1(1)	8(1)	6(1)
C(3)	34(1)	31(1)	35(1)	5(1)	16(1)	7(1)
C(4)	30(1)	22(1)	41(1)	5(1)	19(1)	3(1)
C(5)	26(1)	30(1)	31(1)	7(1)	12(1)	9(1)
C(6)	23(1)	34(1)	50(1)	-4(1)	18(1)	-1(1)
C(7)	42(1)	32(1)	45(1)	0(1)	32(1)	-1(1)

Table B20. Hydrogen coordinates ($x\ 10^4$) and isotropic displacement parameters ($Å^2 x\ 10^3$) for liu22.

	x	y	z	U(eq)
H(1N)	1170(30)	6630(40)	890(20)	43(8)
H(1B)	1880(20)	8430(30)	-300(20)	43(7)
H(4)	2110(20)	5950(40)	2820(20)	41(7)
H(5)	4030(20)	7190(30)	3890(20)	35(7)
H(6)	5070(30)	9170(40)	3180(20)	45(7)
H(7)	4110(30)	9960(40)	1170(30)	51(8)

B.2.3. Supplemental information for Chapter III, section 3.4

Table 21. Azaborine line list of measured frequencies (obs) for the normal isotopomer, H_6B^{11}-$N^{14}C_4$. The frequencies are given in MHz. The column (o-c) lists the deviations of the "best fit" calculated frequencies (c) from the measured frequencies (o).

J"	K_a"	K_c"	F1"	F"	J'	K_a'	K_c'	F1'	F '	obs	o-c
1	0	1	2	2	0	0	0	2	2	8097.956	-0.004
1	0	1	2	2	0	0	0	2	3	8097.956	-0.004
1	0	1	2	3	0	0	0	2	2	8098.072	-0.005
1	0	1	2	3	0	0	0	2	3	8098.072	-0.005
1	0	1	2	1	0	0	0	2	1	8098.168	0.012
1	0	1	2	1	0	0	0	2	2	8098.168	0.012
1	0	1	3	4	0	0	0	2	3	8098.458	-0.013
1	0	1	3	3	0	0	0	2	2	8098.580	0.003
1	0	1	3	3	0	0	0	2	3	8098.580	0.003
1	0	1	1	2	0	0	0	2	1	8098.869	0.000
1	0	1	1	2	0	0	0	2	2	8098.869	0.000
1	0	1	1	2	0	0	0	2	3	8098.869	0.000
1	1	1	2	2	0	0	0	2	1	8405.945	-0.018
1	1	1	2	2	0	0	0	2	2	8405.945	-0.018
1	1	1	2	2	0	0	0	2	3	8405.945	-0.018
1	1	1	2	3	0	0	0	2	2	8406.217	0.013
1	1	1	2	3	0	0	0	2	3	8406.217	0.013
1	1	1	2	1	0	0	0	2	1	8406.346	0.008
1	1	1	2	1	0	0	0	2	2	8406.346	0.008
1	1	1	3	2	0	0	0	2	1	8406.439	0.005
1	1	1	3	2	0	0	0	2	3	8406.439	0.005
1	1	1	3	4	0	0	0	2	3	8406.493	0.003
1	1	1	1	1	0	0	0	2	1	8406.816	0.004
1	1	1	1	1	0	0	0	2	2	8406.816	0.004
1	1	1	1	2	0	0	0	2	1	8406.883	-0.005
1	1	1	1	2	0	0	0	2	2	8406.883	-0.005
1	1	1	1	2	0	0	0	2	3	8406.883	-0.005
2	1	1	3	3	2	1	2	3	2	7801.448	0.002
2	1	1	3	2	2	1	2	3	3	7801.369	0.003
2	1	1	2	2	2	1	2	3	2	7801.141	-0.007

2	1	1	2	3	2	1	2	3	3	7801.068	-0.005
2	1	1	4	5	2	1	2	3	4	7801.015	0.003
2	1	1	4	5	2	1	2	3	4	7801.003	-0.009
2	1	1	2	2	2	1	2	3	3	7800.952	-0.008
2	1	1	3	2	2	1	2	2	1	7800.936	-0.003
2	1	1	1	2	2	1	2	3	2	7800.809	-0.008
2	1	1	4	4	2	1	2	3	3	7800.737	0.010
2	1	1	3	3	2	1	2	2	2	7800.658	-0.003
2	1	1	3	4	2	1	2	4	5	7800.617	0.014
2	1	1	3	4	2	1	2	4	3	7800.518	0.011
2	1	1	4	3	2	1	2	2	3	7800.415	-0.003
2	1	1	2	2	2	1	2	2	2	7800.374	0.012
2	1	1	3	4	2	1	2	4	4	7800.246	0.007
2	1	1	4	3	2	1	2	2	2	7800.246	-0.016
2	1	1	1	2	2	1	2	2	3	7800.177	-0.010
2	1	1	1	2	2	1	2	4	3	7799.879	0.013
2	1	1	3	3	2	0	2	3	2	7827.221	-0.003
2	1	1	2	1	2	0	2	3	2	7827.056	0.000
2	1	1	4	3	2	0	2	3	4	7826.695	0.001
2	1	1	3	2	2	0	2	2	3	7826.695	-0.008
2	1	1	3	4	2	0	2	2	3	7826.611	0.005
2	1	1	4	4	2	0	2	3	3	7826.511	0.003
2	1	1	3	3	2	0	2	2	2	7826.437	-0.007
2	1	1	3	4	2	0	2	4	5	7826.381	-0.001
2	1	1	3	4	2	0	2	4	3	7826.301	0.010
2	1	1	2	2	2	0	2	2	1	7826.301	-0.009
2	1	1	4	3	2	0	2	2	3	7826.198	0.002
2	1	1	2	3	2	0	2	4	3	7826.106	0.011
2	1	1	4	3	2	0	2	2	2	7826.026	-0.020
2	1	1	3	3	2	0	2	4	4	7826.026	0.011
2	1	1	4	3	2	0	2	4	3	7825.893	0.011
2	1	1	3	2	2	0	2	1	2	7825.793	-0.017
2	1	1	1	2	2	0	2	2	2	7825.793	-0.021
2	1	1	1	2	2	0	2	4	3	7825.660	0.010
2	1	1	2	2	2	0	2	1	2	7825.403	-0.001
2	1	1	4	3	2	0	2	1	2	7825.294	-0.010
3	2	1	4	3	3	2	2	4	3	7355.761	0.006
3	2	1	4	3	3	2	2	2	2	7355.761	0.006
3	2	1	4	3	3	2	2	3	2	7355.761	0.006
3	2	1	4	3	3	2	2	3	3	7355.761	0.006
3	2	1	4	3	3	2	2	4	3	7355.761	0.006
3	2	1	4	5	3	2	2	3	4	7355.629	-0.012
3	2	1	4	5	3	2	2	4	5	7355.629	-0.013
3	2	1	4	5	3	2	2	5	4	7355.629	-0.013

3	2	1	4	5	3	2	2	5	6	7355.629	-0.013
3	2	1	4	4	3	2	2	2	3	7355.523	0.005
3	2	1	4	4	3	2	2	3	4	7355.523	0.005
3	2	1	4	4	3	2	2	4	4	7355.523	0.005
3	2	1	4	4	3	2	2	5	4	7355.523	0.005
3	2	1	4	4	3	2	2	5	5	7355.523	0.005
3	2	1	3	2	3	2	2	2	1	7355.492	0.002
3	2	1	3	2	3	2	2	2	2	7355.492	0.002
3	2	1	3	2	3	2	2	3	2	7355.492	0.002
3	2	1	3	2	3	2	2	3	3	7355.492	0.002
3	2	1	2	1	3	2	2	2	1	7355.038	0.016
3	2	1	2	1	3	2	2	2	2	7355.038	0.016
3	2	1	5	6	3	2	2	4	5	7355.141	0.002
3	2	1	5	6	3	2	2	5	5	7355.141	0.002
3	2	1	5	6	3	2	2	5	6	7355.141	0.002
3	2	1	5	4	3	2	2	4	4	7355.084	-0.014
3	2	1	5	4	3	2	2	3	3	7355.084	-0.014
3	2	1	5	4	3	2	2	4	5	7355.084	-0.014
3	2	1	5	4	3	2	2	5	4	7355.084	-0.014
2	1	2	3	3	1	1	1	3	2	13596.162	0.008
2	1	2	3	2	1	1	1	2	2	13596.443	0.006
2	1	2	2	3	1	1	1	3	4	13596.544	0.004
2	1	2	3	3	1	1	1	2	2	13596.632	0.006
2	1	2	2	2	1	1	1	2	3	13596.997	0.014
2	1	2	1	2	1	1	1	1	2	13597.040	0.004
2	1	2	2	1	1	1	1	2	2	13597.040	-0.012
2	1	2	2	3	1	1	1	2	2	13597.067	0.000
2	1	2	1	2	1	1	1	1	1	13597.113	-0.001
2	1	2	4	3	1	1	1	2	3	13597.153	0.005
2	0	2	2	2	1	1	1	3	3	13570.718	-0.004
2	0	2	2	3	1	1	1	3	4	13570.764	0.002
2	0	2	3	3	1	1	1	2	2	13570.848	0.004
2	0	2	2	2	1	1	1	2	3	13571.203	0.004
2	0	2	2	1	1	1	1	2	2	13571.264	-0.011
2	0	2	2	3	1	1	1	2	2	13571.293	0.004
2	0	2	1	1	1	1	1	1	2	13571.325	-0.001
2	0	2	1	2	1	1	1	1	1	13571.325	-0.007
2	0	2	1	1	1	1	1	1	1	13571.401	-0.003
2	0	2	2	2	1	1	1	2	2	13571.434	-0.006
2	0	2	1	2	1	1	1	3	3	13571.475	0.012
2	0	2	3	3	1	0	1	3	3	13878.223	-0.008
2	0	2	3	3	1	0	1	3	4	13878.325	-0.011
2	0	2	3	3	1	0	1	3	2	13878.389	0.010
2	0	2	2	3	1	0	1	1	2	13878.389	0.006

2	0	2	3	3	1	0	1	2	3	13878.744	0.013
2	0	2	2	3	1	0	1	3	2	13878.822	-0.001
2	0	2	2	2	1	0	1	3	3	13878.822	-0.004
2	0	2	2	1	1	0	1	2	1	13879.080	-0.002
2	0	2	2	3	1	0	1	2	3	13879.171	-0.004
2	1	2	3	4	1	0	1	3	3	13903.952	-0.007
2	1	2	3	3	1	0	1	3	3	13904.002	-0.010
2	1	2	2	1	1	0	1	1	1	13904.175	-0.001
2	1	2	4	3	1	0	1	1	2	13904.476	-0.006
2	1	2	2	1	1	0	1	3	2	13904.580	-0.007
2	2	1	2	2	2	1	2	1	2	8723.804	-0.002
2	2	1	4	5	2	1	2	4	4	8724.054	0.013
2	2	1	1	1	2	1	2	2	2	8724.108	0.001
2	2	1	2	3	2	1	2	4	4	8724.157	0.003
2	2	1	3	2	2	1	2	1	2	8724.180	-0.009
2	2	1	2	2	2	1	2	4	3	8724.379	-0.001

Table 22. Azaborine line list for H_6B^{10}-$N^{14}C_4$. Frequencies are given in MHz.

J'	K_a'	K_c'	F1	F	J"	K_a"	K_c"	F_1"	F"	Frequency	o-c
1	0	1	3	3	0	0	0	3	2	8133.594	0.0259
1	0	1	3	3	0	0	0	3	3	8133.594	0.0259
1	0	1	3	3	0	0	0	3	4	8133.594	0.0259
1	0	1	3	4	0	0	0	3	4	8133.693	0.0077
1	0	1	3	4	0	0	0	3	3	8133.693	0.0077
1	0	1	4	5	0	0	0	3	4	8134.331	0.0043
1	0	1	4	4	0	0	0	3	3	8134.403	-0.0098
1	0	1	4	4	0	0	0	3	4	8134.403	-0.0098
1	0	1	2	2	0	0	0	3	2	8134.608	-0.0055
1	0	1	2	2	0	0	0	3	3	8134.608	-0.0055
1	1	1	4	5	0	0	0	3	4	8575.871	-0.0216
1	1	1	4	4	0	0	0	3	3	8576.067	-0.0033
1	1	1	4	4	0	0	0	3	4	8576.067	-0.0033
1	1	1	3	4	0	0	0	3	4	8575.561	-0.025
1	1	1	3	4	0	0	0	3	3	8575.561	-0.025
1	1	1	3	2	0	0	0	3	2	8575.678	0.0218
1	1	1	3	2	0	0	0	3	3	8575.678	0.0217
2	0	2	3	4	1	0	1	4	3	14086.77	-0.0034
2	0	2	3	2	1	0	1	4	3	14086.77	-0.0057
2	0	2	2	2	1	0	1	2	3	14086.86	-0.0146
2	0	2	2	2	1	0	1	2	1	14086.96	0.0211
2	0	2	2	1	1	0	1	2	1	14087.2	-0.0168
2	0	2	3	3	1	0	1	3	3	14087.46	0.0104
2	0	2	5	5	1	0	1	4	5	14087.74	0.0047

2	0	2	1	1	1	0	1	2	2	14087.86	0.0255
2	0	2	4	5	1	0	1	3	4	14087.15	-0.0018
2	0	2	5	6	1	0	1	4	5	14087.42	0.0167
2	0	2	5	4	1	0	1	4	3	14087.5	0.0072
2	0	2	3	3	1	0	1	3	2	14087.26	-0.0335
2	0	2	4	5	1	0	1	4	5	14086.52	0.0071
2	0	2	3	4	1	0	1	2	3	14086.41	-0.0061
2	0	2	3	3	1	0	1	2	2	14086.36	-0.0402
2	1	2	3	2	1	1	1	2	1	13697.22	0.0209
2	1	2	3	2	1	1	1	3	2	13697.56	-0.0041
2	1	2	4	4	1	1	1	3	3	13697.64	-0.0071
2	1	2	5	4	1	1	1	2	3	13697.71	-0.0177
2	1	2	2	3	1	1	1	2	3	13697.73	-0.0093
2	1	2	2	3	1	1	1	2	2	13697.82	0.0016
2	1	2	2	1	1	1	1	2	2	13697.82	-0.0001
2	1	2	2	1	1	1	1	2	1	13697.92	-0.0071
2	1	2	5	6	1	1	1	4	5	13697.99	-0.0054
2	1	2	5	4	1	1	1	4	3	13698.13	-0.017
2	1	2	2	3	1	1	1	3	2	13698.3	0.0107
2	1	2	2	1	1	1	1	3	2	13698.3	0.0089
2	1	2	1	0	1	1	1	2	1	13698.37	-0.0248
2	1	2	2	3	1	1	1	3	4	13698.37	0.0128
2	1	2	1	1	1	1	1	2	2	13698.47	-0.0058
2	1	2	2	2	1	0	1	2	2	14139.07	0.0203
2	1	2	2	2	1	0	1	2	1	14139.07	-0.0268
2	1	2	3	3	1	0	1	3	2	14139.46	-0.0088
2	1	2	5	5	1	0	1	4	4	14139.84	0.0211
2	1	2	1	0	1	0	1	2	1	14139.86	0.0105
2	1	2	5	4	1	0	1	4	3	14139.67	0.0091
2	1	2	5	4	1	0	1	4	5	14139.61	0.0036
2	1	2	3	3	1	0	1	3	3	14139.61	-0.0146
2	1	1	5	5	2	1	2	4	4	7712.085	-0.0142
2	1	1	3	3	2	1	2	2	2	7711.826	-0.0318
2	1	2	3	2	1	0	1	3	2	14139.5	0.0096
2	1	2	2	1	1	0	1	2	1	14139.37	-0.0136
2	1	1	1	1	2	0	2	1	2	7762.598	0.0282
2	1	1	2	1	2	0	2	1	1	7762.794	-0.0088
2	1	1	2	3	2	0	2	1	2	7762.794	-0.0026
2	1	1	5	5	2	0	2	5	5	7763.01	-0.0086
2	1	1	3	3	2	0	2	1	2	7763.14	0.0132
2	1	1	1	2	2	0	2	2	3	7763.256	0.0291
2	1	1	1	0	2	0	2	2	1	7763.317	-0.0176
2	1	1	4	4	2	0	2	5	5	7763.585	0.0086
2	0	2	3	3	1	1	1	3	2	13645.35	-0.0121

2	0	2	5	5	1	1	1	4	4	13646.02	0.0297
2	0	2	1	0	1	1	1	2	1	13646.23	-0.0145
2	0	2	5	4	1	1	1	4	5	13645.9	0.0269
2	0	2	1	2	1	1	1	2	2	13646.27	0.0028
2	0	2	5	4	1	1	1	2	3	13645.54	-0.0197

Table 23. Azaborine line list for H_5B^{11}-$N^{14}DC_4$. Frequencies are given in MHz.

J'	Ka'	Kc'	J"	K_a"	Kc"	obs
1	0	1	0	0	0	7728.933
1	1	1	0	0	0	8312.632
2	0	2	1	0	1	13557.518

B.2.4. Supplemental information for Chapter III, section 3.5

Protein expression, purification and crystallization. The T4 lysozyme mutant L99A was constructed in the cysteine-free pseudo wide-type form as reported previously.[47] Protein was expressed in the *E. coli* RR1 strain. In brief, the bacteria were grown in 4.0 liters of LB media with ampicillin (100 mg/liter) at 37°C within an agitating fermentor (250 rpm) with filtered air supply. When the optical density of the broth reached 0.6 at 600mm, the temperature and agitating speed were lowered to 28°C and 150 rpm, and isopropyl-β-D-1-thiogalactopyranoside (IPTG) was added in a final concentration of 1.0 mM to induce the protein expression.

After 5 hours induction, the 4.0 liters of culture was moved to a 4L beaker. 20 ml of 0.5M EDTA, pH 8.0, was added and the culture was stirred at room temperature for 1h. The solution becomes very viscous and 20 ml of 1M $MgCl_2$ was added, followed by 20 mg of DNaseI. The solution was stirred till the viscosity lowered to normal. The solution was then spun and the supernatant collected. The supernatant was dialyzed against nano-pure water until the conductivity was less than 4.0 milli-Siemens and the

pH was adjusted to 7.0±0.5. The solution was then loaded onto a CM Sepharose CL-6B (Pharmacia) column, pre-equilibrated with equilibration buffer of 50 mM Tris, 1 mM EDTA, pH 7.3, by gravity feed, and washed by 100ml of equilibration buffer. The column was then eluted by an 800 ml linear gradient between 50 mM NaCl and 300 mM NaCl within the equilibration buffer, and the fractions were collected. The fractions containing T4 lysozyme mutant L99A were pooled and dialyzed against 50 mM sodium phosphate, 0.02% NaN_3, pH 5.8 buffer, and loaded onto a column of 3 ml SP Sephadex C-50 (Pharmacia), and washed with 20 ml of the same buffer. The protein was then directly eluted by and stored in the harvesting buffer (100 mM sodium phosphate, 550 mM NaCl, 0.02% NaN_3, pH 6.5). The protein concentration was adjusted to 40 mg/ml for crystallization.

The crystals were obtained by vapor-diffusion hanging-drop method. The protein solution (5 μl) was mixed with equal volume of reservoir solution (2.0-2.2 M sodium/potassium phosphate, pH 6.9, 50 mM 2-mercaptoethanol, 50 mM 2-hydroxyethyl disulfide), and equilibrated against 1 ml of the reservoir solution. Crystals normally grew to their maximum size in 2 weeks.

Complex preparation. The protein complexes with**1**, **15** (see Chapter II, Table 2), benzene, and ethylbenzene were prepared by vapor diffusion method. To remove trace amount of oxygen in the crystals, the soaking buffer around the crystals was exchanged with the pre-deoxygenated reservoir buffer 3 times within a thin glass tube in the glove chamber with N_2 protection. The ligand (~15 mg) was then added and sealed in the glass tube. The sample was allowed to equilibrate at 4°C for 3 days. For the

benzene and ethylbenzene complexes, a similar protocol was followed except there was no need for N_2 protection.

Data collection, structure determination and refinement. Prior to X-ray data collection the crystals were flash-frozen in liquid nitrogen with protection of N-paratone (Hampton Research). To avoid loss or potential oxidation of the ligand, the time from removal of the crystal from the sealed tube to mounting and freezing did not exceed 5 min. Data for T4 lysozyme complexed with **15** were collected on beamline ID-23-B at the Advanced Photon Source, Argonne, IL, and for the complex with **1**, benzene, and ethylbenzene were collected from beamline 5.0.2 at the Advanced Light Source, Berkeley, CA. Both datasets were to 1.25 Å resolution. For each dataset, the low- and high-resolution data were collected with sweeps of 1 sec and 10 sec exposure time per degree, respectively. Data were processed and merged with HKL2000,[48] and the structures were isomorphous with wildtype lysozyme. The ligand-free T4 lysozyme L99A structure (PDB code: 3DMV) was used as the starting model for refinement with all solvent molecules removed. The refinements were done using the CCP4 package[49] and graphics modeling with COOT.[50] Coordinates for the ligands were introduced into the cavity at the final stage of the refinement, with placement based on the F_o-F_c maps.

Table 24. X-ray data collection and structure refinement statistics for **15** and ethylbenzene

Ligand	**15**	Ethylbenzene
Data collection		
Beam line	ID-23-B, APS	5.0.2, ALS
Wavelength (Å)	1.0332	0.9791
Space group	$P3_221$	$P3_221$

Cell constants (Å)	$a = b = 59.9$, $c = 95.47$	$a = b = 59.83$, $c = 95.60$
Resolution (Å)	52-1.25 (1.27-1.25)	52-1.25 (1.27-1.25)
Completeness (%)	99.1 (88.1)	99.9 (100.0)
I/s(I)	34.9 (8.8)	44.1 (9.9)
R_{merge} (%)	5.3 (15.8)	5.2 (22.1)
Refinement		
Resolution (Å)	52.0-1.25	52.0-1.25
R	0.163	0.162
R_{free}	0.182	0.182

Numbers in parentheses give the values for the outermost shell of data.

Table 25. X-ray data collection and structure refinement statistics for **1** and benzene

Ligand	**1**	Benzene
Data collection		
Beam line	5.0.2, ALS	5.0.2, ALS
Wavelength (Å)	0.9791	0.9791
Space group	$P3_221$	$P3_221$
Cell constants (Å)	$a = b = 59.90$, $c = 95.44$	$a = b = 60.00$, $c = 95.65$
Resolution (Å)	52-1.25 (1.27-1.25)	52-1.25 (1.27-1.25)
Completeness (%)	99.0 (100.0)	100.0 (100.0)
I/s(I)	33.6 (9.1)	34.3 (10.7)
R_{merge} (%)	7.1 (26.9)	6.7 (26.7)
Refinement		
Resolution (Å)	52.0-1.25	52.0-1.25

R	0.170	0.170
R_{free}	0.190	0.194

Numbers in parentheses give the values for the outermost shell of data.

APPENDIX C

SYNTHESIS AND CHARACTERIZATION OF TOLAN ANALOGS AND DIYNE SCAFFOLDS

C.1. Introduction

The interest in conjugated organic molecules has grown significantly over the last several decades. The incorporation of boron in conjugated materials has been shown to impart unique properties relative to their carbonaceous analogs.[1,2] The fundamental consequences of replacing CC units with BN units in tolan derivatives provides a glimpse at the potential of 1,2-azaborine heterocycles in materials applications.

C.2. Experimental

C.2.1. General

All oxygen- and moisture-sensitive manipulations were carried out under an inert atmosphere using either standard Schlenk techniques or a glove box.

THF, Et_2O, CH_2Cl_2, and pentane were purified by passing through a neutral alumina column under argon. Cyclohexene was dried over CaH_2 and distilled under N_2 prior to use.

Trisacetonitrile(tricarbonyl)chromium(0) was purchased from Acros or Aldrich and used as received. All other chemicals and solvents were purchased (Aldrich or

Strem) and used as received.

Silica gel (230-400 mesh) was heated under vacuum in a 200 °C sand bath for 12 hours. Flash chromatography was performed with this silica gel under an inert atmosphere.

^{11}B NMR spectra were recorded on a Varian Unity/Inova 600 spectrometer at ambient temperature. ^{1}H NMR spectra were recorded on a Varian Unity/Inova 300 or Varian Unity/Inova 600 spectrometer. ^{13}C NMR spectra were recorded on a Varian Unity/Inova 300 or Varian Unity/Inova 500 spectrometer. COSY and HETCOR NMR spectroscopy was performed on a Varian Unity/Inova 300 spectrometer. ^{11}B NMR spectra were externally referenced to $BF_3 \bullet Et_2O$ (δ 0).

IR spectra were recorded on a Nicolet Magna 550 FT-IR instrument with OMNIC software. UV-Vis spectra were recorded on an Agilent 8453 spectrometer with ChemStation software. Fluorescence spectra were recorded on a Horiba Jobin-Yvon Fluoromax 4 fluorometer.

High-resolution mass spectroscopy data were obtained at the Mass Spectroscopy Facilities and Services Core of the Environmental Health Sciences Center at Oregon State University. Financial support for this facility has been furnished in part by the National Institute of Environmental Health Sciences, NIH (P30 ES00210).

C.2.2. Supplemental information for Chapter IV, section 4.3

Synthesis of Compound 4. 1,2-Azaborine **3** (0.500 g, 2.20 mmol) and Et_2O (20 mL) were combined in a flask and cooled to –10 °C, whereupon phenylethylnylmagnesium bromide (0.7 M in THF; 3.45 mL, 2.42 mmol) was added

dropwise with stirring. The flask was allowed to warm to rt, whereupon approximately one-half of the solvent was removed under reduced pressure. Solids were filtered, and the remaining solvents were removed under reduced pressure. Column chromatography (Et_2O/pentane) yielded **4** as a white, crystalline solid (0.490 g, 76%).

^{1}H NMR (300 MHz, CH_2Cl_2): δ 7.60 (dd, $^3J_{HH}$ = 11.2, 5.6 Hz, 1H), 7.51 (m, 2H), 7.35 (m, 4H), 6.90 (d, $^3J_{HH}$ = 11.1 Hz, 1H), 6.40 (app t, $^3J_{HH}$ = 6.4 Hz, 1H), 0.95 (s, 9H), 0.63 (s, 6H). ^{13}C NMR (75 MHz, CD_2Cl_2): δ 144.0, 139.3, 134 (br), 132.6, 131.9, 128.9, 128.8, 124.7, 112.8, 27.0, 19.6, –1.9. ^{11}B NMR (192.5 MHz, CD_2Cl_2): δ 29.3. FTIR (thin film) 3065, 3031, 2956, 2929, 2884, 2858, 2175, 1602, 1504, 1490, 1470, 1452, 1391, 1363, 1274, 1253, 1194, 1126, 1070, 1017, 987, 938, 913, 843, 822, 786, 710, 690, 626 cm^{-1}. HRMS (EI) calcd for $C_{18}H_{24}BNSi$ (M^+) 293.17711, found 293.17778.

Compound 5. A vial was charged with a solution of **4** (0.500 g, 1.70 mmol in 30 mL THF) and $(MeCN)_3Cr(CO)_3$ (0.663 g, 2.56 mmol) and stirred at rt for 1 h. Solvents were removed and column chromatography was performed (CH_2Cl_2/pentane) which provided **5** as a red, crystalline solid (0.667 g, 91%).

^{1}H NMR (300 MHz, CH_2Cl_2): δ 7.52 (m, 2H), 7.37 (m, 3H), 6.03 (dd, $^3J_{HH}$ = 7.9, 5.2 Hz, 2H), 5.23 (app t, $^3J_{HH}$ = 5.8 Hz, 1H), 4.74 (d, $^3J_{HH}$ = 9.7 Hz, 1H), 1.00 (s, 9H), 0.73 (s, 3H), 0.46 (s, 3H). ^{13}C NMR (75 MHz, CD_2Cl_2): δ 230.6, 132.1, 129.5, 129.0, 123.6, 108.4, 103.8, 88 (br), 83.4, 27.1, 20.2, –1.1, –3.8. ^{11}B NMR (96.3 MHz, CD_2Cl_2): δ 14.3. FTIR (CH_2Cl_2) 1971, 1902, 1879 cm^{-1}. HRMS (EI) calcd for $C_{21}H_{24}BNSiCrO_3$ (M^+) 429.10237, found 429.10066.

Compound 6. A vial was charged with a solution of **5** (0.667 g, 1.55 mmol in 10

mL THF) and cooled to –20 °C. A solution of HF-pyridine (0.5 M in THF; 3.1 mL, 1.55 mmol) was added dropwise. The reaction was allowed to warm to rt and stirred for 10 min. Solvents were removed and column chromatography was performed (CH_2Cl_2/pentane) which provided **6** as an orange-red solid (0.416 g, 85%).

^{1}H NMR (300 MHz, CH_2Cl_2): δ 7.52 (m, 2H), 7.34 (m, 3H), 6.15 (app t, $^3J_{HH}$ = 5.3 Hz, 2H), 5.91 (dd, $^3J_{HH}$ = 8.6, 6.2 Hz, 1H), 5.34 (br, 1H), 5.26 (dd, $^3J_{HH}$ = 7.2, 5.0 Hz, 1H), 4.76 (d, $^3J_{HH}$ = 5.5 Hz). ^{13}C NMR (75 MHz, CD_2Cl_2): δ 230.0, 132.6, 129.7, 129.0, 122.9, 107.9, 98.6, 86 (br), 82.1. ^{11}B NMR (192.5 MHz, CD_2Cl_2): δ 11.7. FTIR (CH_2Cl_2) 3361, 2185, 1976, 1906, 1880 cm^{-1}. HRMS (EI) calcd for $C_{15}H_{10}BNCrO_3$ (M^+) 315.01589, found 315.01578.

Synthesis of BN tolan 1. Complex **6** (0.383 g, 1.22 mmol) and MeCN (10 mL) were combined in a vial and stirred at rt for 12 h. Approximately two-thirds of the solvent was removed under reduced pressure. Column chromatography (CH_2Cl_2/pentane) provided BN tolan **1** as a white, crystalline solid (0.198 g, 91%).

^{1}H NMR (300 MHz, CH_2Cl_2): δ 8.44 (br, 1H), 7.76 (dd, $^3J_{HH}$ = 10.8, 6.7 Hz, 1H), 7.59 (m, 2H), 7.40 (m, 3H), 7.00 (d, $^3J_{HH}$ = 11.1 Hz, 1H), 6.44 (app t, $^3J_{HH}$ = 6.5 Hz, 1H). ^{13}C NMR (125.8 MHz, CD_2Cl_2): δ 145.1, 134.9, 132.4, 132 (br), 129.0, 124.1, 111.9, 104.8, 84 (br). ^{11}B NMR (192.5 MHz, CD_2Cl_2): δ 25.8. FTIR (thin film) 3380, 3140, 3075, 3049, 3027, 2178, 1606, 1538, 1487, 1460, 1440, 1421, 1349, 1265, 1235, 1213, 1191, 1126, 1108, 1080, 995, 842, 793, 760, 733, 692, 681 cm^{-1}. HRMS (EI) calcd for $C_{12}H_{10}BN$ (M^+) 179.09063, found 179.09122.

Compound 8. Ethylmagnesium bromide (1M in THF; 1.96 mL, 1.96 mmol) and

ethynylmagnesium bromide (0.5M in THF; 3.91 mL, 1.96 mmol) were combined in a vial and stirred at rt for 30 minutes during which time significant gas evolution was observed. The reaction was stirred an additional 12 h, then added to a solution of **3** (0.890 g, 3.91 mmol in 10 mL THF) with stirring at rt. The reaction was stirred an additional 48 h, at which point the solvent was removed. Column chromatography (CH_2Cl_2/pentane) yielded **8** as a light-yellow solid (0.732 g, 91%).

^{1}H NMR (300 MHz, CH_2Cl_2): δ 7.58 (dd, $^3J_{HH}$ = 11.0, 6.1 Hz, 1H), 7.28 (d, $^3J_{HH}$ = 6.3 Hz, 1H), 6.82 (d, $^3J_{HH}$ = 11.2 Hz, 1H), 6.38 (app t, $^3J_{HH}$ = 6.3, 6.1 Hz, 1H). ^{13}C NMR (75 MHz, CD_2Cl_2): δ 143.7, 139.3, 122 (br), 112.5, 27.0, 19.6, –1.8. ^{11}B NMR (192.5 MHz, CD_2Cl_2): δ 28.7. FTIR (thin film) 3007, 2927, 2882, 2857, 1875, 1600, 1503, 1467, 1450, 1389, 1364, 1270, 1257, 1216, 1173, 1153, 1097, 989, 938, 842, 822, 810, 739, 705, 694, 634 cm^{-1}. HRMS (EI) calcd for $C_{22}H_{38}B_2N_2Si_2$ (M^+) 408.27597, found 408.27775.

Compound 10. To a stirred solution of **8** (0.732 g, 1.79 mmol in 18 mL THF) was added $(MeCN)_3Cr(CO)_3$ (0.976 g, 3.76 mmol). The reaction was stirred at rt for 1 h, then solvents were removed and column chromatography (CH_2Cl_2/pentane) was performed to give a mixture of **9** and **10**. The mixture was taken up in THF (15 mL) and $(MeCN)_3Cr(CO)_3$ (0.300 g, 1.16 mmol) was added. The reaction was stirred at rt for 1 h. Solvents were removed and the crude material was subjected to column chromatograpy (CH_2Cl_2/pentane) which provided **10** as an orange-red, crystalline solid (0.365 g, 30%).

^{1}H NMR (300 MHz, CH_2Cl_2): δ 5.9-6.0 (m, 2H), 5.19 (app t, $^3J_{HH}$ = 6.1 Hz, 1H), 4.61 (d, $^3J_{HH}$ = 6.2 Hz, 1H). ^{13}C NMR (75 MHz, CD_2Cl_2): δ 230.3, 108.0, 103.5, 83.3, 27.2, –0.8, –3.9. ^{11}B NMR (192.5 MHz, CD_2Cl_2): δ 13.6. FTIR (CH_2Cl_2) 1971, 1899 (br)

cm^{-1}.

Compound 11. A solution of complex **10** (0.228 g, 0.335 mmol in 15 mL) was cooled to –20 °C, whereupon HF-pyridine (0.5 M in THF; 1.34 mL, 0.67 mmol) was added dropwise. The reaction was kept at –20 °C for 30 min., then allowed to warm to rt. Solvents were removed to provide a crude mixture which was used directly in the preparation of **2**.

Synthesis of BN tolan 2. The crude material containing complex **11** was combined in a vial with MeCN (5 mL) and stirred at rt for 10 min. Solvents were removed, whereupon column chromatograpy (Et_2O/pentane) gave **2** as a white, crystalline solid (0.028 g, 46.5% from **10**).

^{1}H NMR (300 MHz, CH_2Cl_2): δ 8.43 (br, 1H), 7.71 (dd, $^3J_{HH}$ = 10.8, 6.6 Hz, 1H), 7.36 (app t, $^3J_{HH}$ = 7.2 Hz, 1H), 6.89 (d, $^3J_{HH}$ = 11.1 Hz, 1H), 6.40 (app t, $^3J_{HH}$ = 6.5 Hz). ^{13}C NMR (125.8 MHz, CD_2Cl_2): δ 145.1, 134.8, 131 (br), 111.8. ^{11}B NMR (192.5 MHz, CD_2Cl_2): δ 25.4. FTIR (CH_2Cl_2) 3370, 3091, 3053, 3031, 2978, 1611, 1532, 1464, 1420, 1352, 1223, 1202, 1151, 1082, 998, 852, 740, 677 cm^{-1}. HRMS (EI) calcd for $C_{10}H_{10}B_2N_2$ (M^+) 180.10301, found 180.10330.

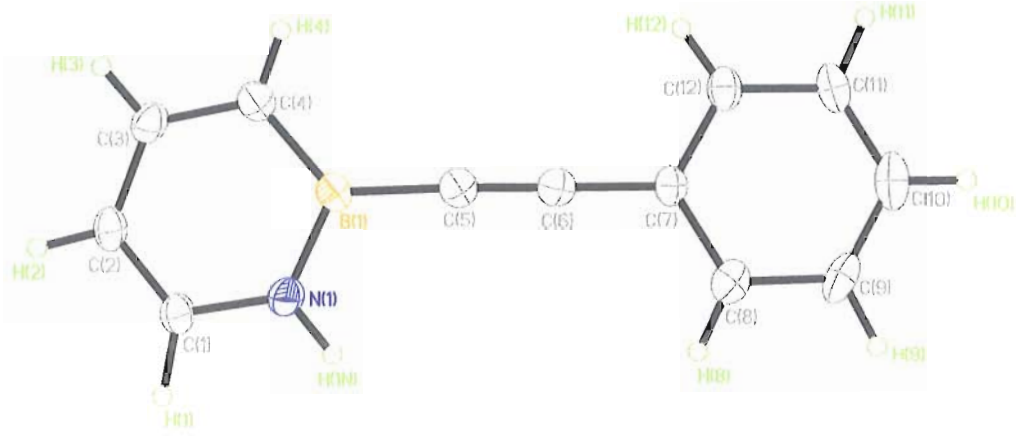

Figure 1. ORTEP illustration of **1**, with thermal ellipsoids drawn at the 35% level.

X-ray Crystal Structure Determination. Crystals of **1** suitable for X-ray diffraction were obtained by evaporation of a solution of **1** in Et_2O.

Diffraction intensity data were collected with a Bruker Smart Apex CCD diffractometer at 173(2) K using MoKα - radiation (0.71073 Å). The structure was solved using direct methods, completed by subsequent difference Fourier syntheses, and refined by full matrix least-squares procedures on F^2. All non-H atoms were refined with anisotropic thermal parameters. H atoms were found on the residual density map and refined with isotropic thermal parameters. The Flack parameter is 0.00(8). All software and sources scattering factors are contained in the SHELXTL (6.10) program package (G.Sheldrick, Bruker XRD, Madison, WI). Crystallographic data and some details of data collection and crystal structure refinement for $C_{12}H_{10}BN$ are given in the following tables.

Table 1. Crystal data and structure refinement for liu72.

Identification code	liu72
Empirical formula	$C_{12}\ H_{10}\ B\ N$

Formula weight	179.02	
Temperature	173(2) K	
Wavelength	0.71073 ≈	
Crystal system	Orthorhombic	
Space group	Fdd2	
Unit cell dimensions	a = 23.388(11) Å	α= 90°.
	b = 31.934(15) Å	β= 90°.
	c = 5.423(3) Å	γ = 90°.
Volume	4051(3) $Å^3$	
Z	16	
Density (calculated)	1.174 Mg/m^3	
Absorption coefficient	0.067 mm^{-1}	
F(000)	1504	
Crystal size	0.21 x 0.12 x 0.02 mm^3	
Theta range for data collection	2.16 to 25.00°.	
Index ranges	-27<=h<=27, -37<=k<=37, -6<=l<=6	
Reflections collected	8757	
Independent reflections	1791 [R(int) = 0.0942]	
Completeness to theta = 25.00∞	100.0 %	
Absorption correction	Semi-empirical from equivalents	
Max. and min. transmission	0.9987 and 0.9860	
Refinement method	Full-matrix least-squares on F^2	
Data / restraints / parameters	1791 / 1 / 167	
Goodness-of-fit on F^2	1.034	
Final R indices [I>2sigma(I)]	R1 = 0.0571, wR2 = 0.1043	
R indices (all data)	R1 = 0.0946, wR2 = 0.1198	
Absolute structure parameter	0(6)	
Largest diff. peak and hole	0.143 and -0.161 e.≈$^{-3}$	

Table 2. Atomic coordinates (x 10^4) and equivalent isotropic displacement parameters ($Å^2$x 10^3) for liu72. U(eq) is defined as one third of the trace of the orthogonalized U^{ij} tensor.

	x	y	z	U(eq)
N(1)	601(1)	1001(1)	4888(6)	41(1)
B(1)	122(2)	917(1)	3334(8)	33(1)
C(1)	1013(2)	1296(1)	4348(8)	42(1)

C(2)	974(2)	1525(1)	2256(7)	40(1)
C(3)	514(2)	1462(1)	595(8)	42(1)
C(4)	95(2)	1173(1)	1045(7)	41(1)
C(5)	-319(1)	596(1)	4301(7)	37(1)
C(6)	-665(1)	352(1)	5158(7)	36(1)
C(7)	-1077(1)	65(1)	6161(6)	33(1)
C(8)	-965(2)	-154(1)	8367(7)	40(1)
C(9)	-1367(2)	-438(1)	9266(8)	49(1)
C(10)	-1877(2)	-502(1)	8034(9)	55(1)
C(11)	-1999(2)	-280(1)	5913(9)	49(1)
C(12)	-1601(2)	0(1)	4952(7)	41(1)

Table 3. Bond lengths [Å] and angles [°] for liu72.

N(1)-C(1)	1.380(4)
N(1)-B(1)	1.427(5)
N(1)-H(1N)	0.92(5)
B(1)-C(4)	1.488(5)
B(1)-C(5)	1.545(5)
C(1)-C(2)	1.352(5)
C(1)-H(1)	1.04(4)
C(2)-C(3)	1.417(5)
C(2)-H(2)	0.95(3)
C(3)-C(4)	1.368(5)
C(3)-H(3)	0.91(3)
C(4)-H(4)	0.93(3)
C(5)-C(6)	1.216(4)
C(6)-C(7)	1.436(5)
C(7)-C(12)	1.406(5)
C(7)-C(8)	1.410(5)
C(8)-C(9)	1.395(5)
C(8)-H(8)	0.95(5)
C(9)-C(10)	1.383(6)
C(9)-H(9)	0.96(4)
C(10)-C(11)	1.381(6)
C(10)-H(10)	0.96(4)
C(11)-C(12)	1.391(5)
C(11)-H(11)	0.99(4)
C(12)-H(12)	0.94(3)
C(1)-N(1)-B(1)	123.5(3)
C(1)-N(1)-H(1N)	120(3)
B(1)-N(1)-H(1N)	116(3)
N(1)-B(1)-C(4)	114.9(3)
N(1)-B(1)-C(5)	116.6(3)
C(4)-B(1)-C(5)	128.3(3)
C(2)-C(1)-N(1)	120.0(4)
C(2)-C(1)-H(1)	130(2)
N(1)-C(1)-H(1)	110(2)
C(1)-C(2)-C(3)	120.5(3)
C(1)-C(2)-H(2)	115(2)
C(3)-C(2)-H(2)	125(2)

C(4)-C(3)-C(2)	121.7(4)
C(4)-C(3)-H(3)	118.8(19)
C(2)-C(3)-H(3)	119.4(19)
C(3)-C(4)-B(1)	119.4(4)
C(3)-C(4)-H(4)	121(2)
B(1)-C(4)-H(4)	120(2)
C(6)-C(5)-B(1)	177.2(4)
C(5)-C(6)-C(7)	179.7(4)
C(12)-C(7)-C(8)	119.0(3)
C(12)-C(7)-C(6)	120.1(3)
C(8)-C(7)-C(6)	120.9(3)
C(9)-C(8)-C(7)	119.6(4)
C(9)-C(8)-H(8)	117(3)
C(7)-C(8)-H(8)	123(3)
C(10)-C(9)-C(8)	120.6(4)
C(10)-C(9)-H(9)	123(2)
C(8)-C(9)-H(9)	116(2)
C(11)-C(10)-C(9)	120.2(4)
C(11)-C(10)-H(10)	119(3)
C(9)-C(10)-H(10)	120(3)
C(10)-C(11)-C(12)	120.3(4)
C(10)-C(11)-H(11)	124(2)
C(12)-C(11)-H(11)	115(2)
C(11)-C(12)-C(7)	120.2(4)
C(11)-C(12)-H(12)	124(2)
C(7)-C(12)-H(12)	116(2)

Symmetry transformations used to generate equivalent atoms:

Table 4. Anisotropic displacement parameters ($Å^2 x\ 10^3$)for liu72. The anisotropic displacement factor exponent takes the form: $-2\pi^2[\ h^2a^{*2}U^{11} + ... + 2\ h\ k\ a^*\ b^*\ U^{12}\ ]$

	U^{11}	U^{22}	U^{33}	U^{23}	U^{13}	U^{12}
N(1)	49(2)	30(2)	43(2)	8(2)	-6(2)	-7(2)
B(1)	32(2)	19(2)	47(2)	-2(2)	-1(2)	4(2)
C(1)	47(3)	34(2)	46(3)	4(2)	-2(2)	-13(2)
C(2)	42(2)	26(2)	52(2)	2(2)	6(2)	-5(2)
C(3)	46(2)	35(2)	45(3)	11(2)	3(2)	4(2)
C(4)	37(2)	36(2)	48(3)	1(2)	-3(2)	0(2)
C(5)	36(2)	27(2)	48(2)	0(2)	-1(2)	6(2)
C(6)	41(2)	25(2)	43(2)	-2(2)	-2(2)	6(2)
C(7)	39(2)	19(2)	41(2)	-6(2)	4(2)	1(1)
C(8)	55(3)	21(2)	44(2)	-6(2)	5(2)	7(2)
C(9)	77(3)	28(2)	42(3)	4(2)	19(2)	3(2)
C(10)	57(3)	35(2)	73(3)	-6(2)	27(3)	-7(2)
C(11)	43(2)	36(2)	66(3)	-7(2)	8(2)	-11(2)
C(12)	46(2)	28(2)	49(3)	-5(2)	7(2)	-3(2)

Table 5. Hydrogen coordinates ($x\ 10^4$) and isotropic displacement parameters ($Å^2 x\ 10^3$) for liu72.

	x	y	z	U(eq)
H(1N)	625(18)	847(13)	6320(90)	95(17)
H(1)	1305(18)	1315(12)	5800(80)	86(14)

H(2)	1276(13)	1720(9)	2020(60)	38(9)
H(3)	510(12)	1603(9)	-870(60)	27(9)
H(4)	-198(13)	1130(9)	-80(70)	37(10)
H(8)	-627(19)	-114(13)	9310(90)	86(16)
H(9)	-1282(15)	-564(11)	10830(80)	53(11)
H(10)	-2172(17)	-674(12)	8760(80)	74(14)
H(11)	-2353(14)	-314(10)	4930(80)	51(11)
H(12)	-1658(13)	156(9)	3510(70)	39(10)

Table 6. Torsion angles [°] for liu72.

C(1)-N(1)-B(1)-C(4)	0.2(5)
C(1)-N(1)-B(1)-C(5)	-176.1(3)
B(1)-N(1)-C(1)-C(2)	0.1(5)
N(1)-C(1)-C(2)-C(3)	-0.4(5)
C(1)-C(2)-C(3)-C(4)	0.3(6)
C(2)-C(3)-C(4)-B(1)	0.0(5)
N(1)-B(1)-C(4)-C(3)	-0.2(5)
C(5)-B(1)-C(4)-C(3)	175.6(4)
N(1)-B(1)-C(5)-C(6)	47(7)
C(4)-B(1)-C(5)-C(6)	-129(7)
B(1)-C(5)-C(6)-C(7)	120(100)
C(5)-C(6)-C(7)-C(12)	6(92)
C(5)-C(6)-C(7)-C(8)	-173(100)
C(12)-C(7)-C(8)-C(9)	1.9(4)
C(6)-C(7)-C(8)-C(9)	-178.5(3)
C(7)-C(8)-C(9)-C(10)	-1.0(5)
C(8)-C(9)-C(10)-C(11)	-1.0(6)
C(9)-C(10)-C(11)-C(12)	2.1(6)
C(10)-C(11)-C(12)-C(7)	-1.2(5)
C(8)-C(7)-C(12)-C(11)	-0.8(5)
C(6)-C(7)-C(12)-C(11)	179.6(3)

Symmetry transformations used to generate equivalent atoms:

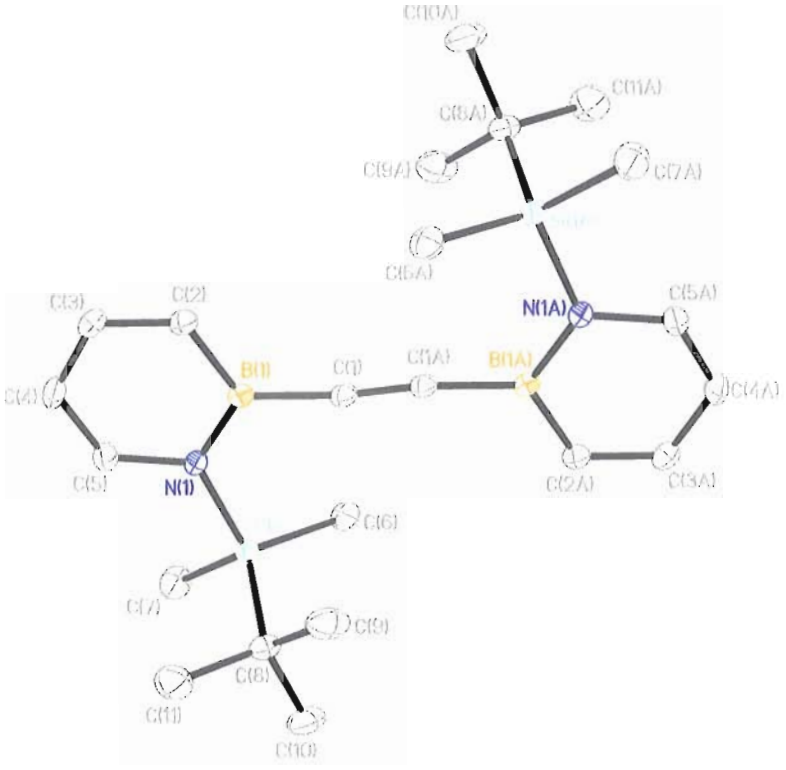

Figure 2. ORTEP illustration of **8**, with thermal ellipsoids drawn at the 35% probability level. Hydrogen atoms have been omitted for clarity.

X-ray Crystal Structure Determination. Crystals of **8** suitable for X-ray diffraction were obtained by evaporation of a solution of **8** in Et_2O.

Diffraction intensity data were collected with a Bruker Smart Apex CCD diffractometer at 173(2) K using MoKα - radiation (0.71073 Å). The structure was solved using direct methods, completed by subsequent difference Fourier syntheses, and refined by full matrix least-squares procedures on F^2. All non-H atoms were refined with anisotropic thermal parameters. H atoms were found on the residual density map and refined with isotropic thermal parameters. The Flack parameter is 0.00(8). All software and sources scattering factors are contained in the SHELXTL (6.10) program package (G.Sheldrick, Bruker XRD, Madison, WI). Crystallographic data and some details of data collection and crystal

structure refinement for $C_{22}H_{38}B_2N_2Si_2$ are given in the following tables.

Table 7. Crystal data and structure refinement for **8** (liu49).

Identification code	liu49	
Empirical formula	$C_{22}\ H_{38}\ B_2\ N_2\ Si_2$	
Formula weight	408.34	
Temperature	173(2) K	
Wavelength	0.71073 Å	
Crystal system	Monoclinic	
Space group	P2(1)/n	
Unit cell dimensions	a = 11.3135(12) Å	α= 90°.
	b = 8.3715(9) Å	β= 101.892(2)°.
	c = 13.7353(14) Å	γ = 90°.
Volume	1273.0(2) $Å^3$	
Z	2	
Density (calculated)	1.065 Mg/m^3	
Absorption coefficient	0.149 mm^{-1}	
F(000)	444	
Crystal size	0.19 x 0.12 x 0.05 mm^3	
Theta range for data collection	2.13 to 27.00°.	
Index ranges	-14<=h<=14, -10<=k<=10, -17<=l<=17	
Reflections collected	13631	
Independent reflections	2780 [R(int) = 0.0429]	
Completeness to theta = 27.00°	99.9 %	
Absorption correction	Semi-empirical from equivalents	
Max. and min. transmission	0.9926 and 0.9722	
Refinement method	Full-matrix least-squares on F^2	
Data / restraints / parameters	2780 / 0 / 203	
Goodness-of-fit on F^2	1.074	
Final R indices [I>2sigma(I)]	R1 = 0.0520, wR2 = 0.1194	
R indices (all data)	R1 = 0.0712, wR2 = 0.1301	
Largest diff. peak and hole	0.340 and -0.165 $e.Å^{-3}$	

Table 8. Atomic coordinates (x 10^4) and equivalent isotropic displacement parameters ($Å^2$x 10^3) for liu49. U(eq) is defined as one third of the trace of the orthogonalized U^{ij} tensor.

	x	y	z	U(eq)
Si(1)	7763(1)	2417(1)	5157(1)	27(1)
N(1)	6997(1)	2347(2)	6184(1)	26(1)
B(1)	5893(2)	1485(3)	6194(2)	26(1)
C(1)	5284(2)	437(2)	5312(1)	28(1)
C(2)	5356(2)	1622(3)	7109(1)	32(1)
C(3)	5916(2)	2529(3)	7882(2)	39(1)
C(4)	6994(2)	3330(3)	7833(2)	47(1)
C(5)	7489(2)	3234(3)	7019(2)	40(1)
C(6)	7796(3)	419(3)	4574(2)	39(1)
C(7)	9363(2)	2986(4)	5673(2)	47(1)
C(8)	7014(2)	3968(3)	4241(2)	35(1)
C(9)	5686(3)	3583(4)	3828(2)	56(1)
C(10)	7683(3)	4052(4)	3377(2)	54(1)
C(11)	7109(3)	5618(3)	4743(2)	55(1)

Table 9. Bond lengths [Å] and angles [°] for liu49.

Si(1)-N(1)	1.8010(16)
Si(1)-C(6)	1.858(2)
Si(1)-C(7)	1.865(3)
Si(1)-C(8)	1.884(2)
N(1)-C(5)	1.384(3)
N(1)-B(1)	1.445(3)
B(1)-C(2)	1.508(3)
B(1)-C(1)	1.539(3)
C(1)-C(1)#1	1.206(4)
C(2)-C(3)	1.352(3)
C(2)-H(2)	0.97(2)
C(3)-C(4)	1.405(3)
C(3)-H(3)	0.93(2)
C(4)-C(5)	1.352(3)
C(4)-H(4)	0.93(3)
C(5)-H(5)	0.98(2)
C(6)-H(6A)	0.92(4)
C(6)-H(6B)	0.92(3)
C(6)-H(6C)	0.95(3)
C(7)-H(7A)	0.99(3)
C(7)-H(7B)	0.90(3)
C(7)-H(7C)	0.94(4)
C(8)-C(9)	1.527(3)
C(8)-C(10)	1.536(3)
C(8)-C(11)	1.537(3)
C(9)-H(9A)	0.98(3)
C(9)-H(9B)	0.99(3)
C(9)-H(9C)	0.92(3)
C(10)-H(10A)	1.04(3)
C(10)-H(10B)	0.98(3)
C(10)-H(10C)	0.98(3)
C(11)-H(11A)	0.96(3)

C(11)-H(11B)	0.98(3)
C(11)-H(11C)	0.95(3)
N(1)-Si(1)-C(6)	111.34(10)
N(1)-Si(1)-C(7)	107.24(10)
C(6)-Si(1)-C(7)	106.84(14)
N(1)-Si(1)-C(8)	108.84(9)
C(6)-Si(1)-C(8)	112.24(11)
C(7)-Si(1)-C(8)	110.21(12)
C(5)-N(1)-B(1)	117.42(16)
C(5)-N(1)-Si(1)	117.09(13)
B(1)-N(1)-Si(1)	125.46(13)
N(1)-B(1)-C(2)	117.90(18)
N(1)-B(1)-C(1)	121.65(16)
C(2)-B(1)-C(1)	120.45(17)
C(1)#1-C(1)-B(1)	172.5(2)
C(3)-C(2)-B(1)	119.53(19)
C(3)-C(2)-H(2)	120.1(13)
B(1)-C(2)-H(2)	120.3(13)
C(2)-C(3)-C(4)	120.1(2)
C(2)-C(3)-H(3)	122.2(15)
C(4)-C(3)-H(3)	117.6(15)
C(5)-C(4)-C(3)	121.5(2)
C(5)-C(4)-H(4)	117.8(17)
C(3)-C(4)-H(4)	120.7(17)
C(4)-C(5)-N(1)	123.6(2)
C(4)-C(5)-H(5)	120.4(13)
N(1)-C(5)-H(5)	116.0(13)
Si(1)-C(6)-H(6A)	112(2)
Si(1)-C(6)-H(6B)	113(2)
H(6A)-C(6)-H(6B)	112(3)
Si(1)-C(6)-H(6C)	107.5(16)
H(6A)-C(6)-H(6C)	100(3)
H(6B)-C(6)-H(6C)	112(2)
Si(1)-C(7)-H(7A)	109.5(16)
Si(1)-C(7)-H(7B)	115.7(19)
H(7A)-C(7)-H(7B)	106(2)
Si(1)-C(7)-H(7C)	109(2)
H(7A)-C(7)-H(7C)	106(3)
H(7B)-C(7)-H(7C)	109(3)
C(9)-C(8)-C(10)	109.1(2)
C(9)-C(8)-C(11)	109.2(2)
C(10)-C(8)-C(11)	107.8(2)
C(9)-C(8)-Si(1)	112.04(16)
C(10)-C(8)-Si(1)	108.81(17)
C(11)-C(8)-Si(1)	109.85(17)
C(8)-C(9)-H(9A)	112.7(17)
C(8)-C(9)-H(9B)	110.9(17)
H(9A)-C(9)-H(9B)	109(2)
C(8)-C(9)-H(9C)	111.4(18)
H(9A)-C(9)-H(9C)	107(2)
H(9B)-C(9)-H(9C)	105(2)
C(8)-C(10)-H(10A)	108.7(17)

C(8)-C(10)-H(10B)	110.7(17)
H(10A)-C(10)-H(10B)	106(2)
C(8)-C(10)-H(10C)	115.0(17)
H(10A)-C(10)-H(10C)	104(2)
H(10B)-C(10)-H(10C)	112(2)
C(8)-C(11)-H(11A)	111.4(19)
C(8)-C(11)-H(11B)	110(2)
H(11A)-C(11)-H(11B)	107(3)
C(8)-C(11)-H(11C)	108.1(19)
H(11A)-C(11)-H(11C)	106(3)
H(11B)-C(11)-H(11C)	114(3)

Symmetry transformations used to generate equivalent atoms:
#1 -x+1,-y,-z+1

Table 10. Anisotropic displacement parameters ($Å^2 x\ 10^3$)for liu49. The anisotropic displacement factor exponent takes the form: $-2p^2[\ h^2a^{*2}U^{11} + ... + 2\ h\ k\ a^*\ b^*\ U^{12}\ ]$

	U^{11}	U^{22}	U^{33}	U^{23}	U^{13}	U^{12}
Si(1)	27(1)	33(1)	24(1)	-1(1)	9(1)	-4(1)
N(1)	30(1)	29(1)	20(1)	-2(1)	6(1)	-5(1)
B(1)	29(1)	26(1)	21(1)	3(1)	4(1)	-2(1)
C(1)	28(1)	34(1)	24(1)	1(1)	9(1)	-5(1)
C(2)	34(1)	37(1)	27(1)	1(1)	10(1)	-5(1)
C(3)	52(1)	45(1)	24(1)	-5(1)	16(1)	-6(1)
C(4)	61(2)	54(2)	28(1)	-17(1)	14(1)	-22(1)
C(5)	45(1)	44(1)	31(1)	-10(1)	11(1)	-19(1)
C(6)	45(1)	40(1)	38(1)	-5(1)	20(1)	2(1)
C(7)	32(1)	67(2)	43(1)	-6(1)	10(1)	-8(1)
C(8)	37(1)	39(1)	30(1)	6(1)	12(1)	-1(1)
C(9)	44(2)	65(2)	54(2)	27(2)	-2(1)	-3(1)
C(10)	69(2)	60(2)	39(1)	12(1)	25(1)	-4(2)
C(11)	71(2)	40(2)	57(2)	5(1)	17(2)	7(1)

Table 11. Hydrogen coordinates (x 10^4) and isotropic displacement parameters ($Å^2 x\ 10^3$) for liu49.

	x	y	z	U(eq)
H(2)	4600(20)	1080(30)	7138(16)	40(6)
H(3)	5590(20)	2700(30)	8440(18)	41(6)
H(4)	7400(20)	3930(30)	8370(20)	68(8)
H(5)	8260(20)	3770(30)	7007(16)	35(6)
H(6A)	8170(30)	-330(50)	5020(30)	110(13)
H(6B)	7050(30)	90(40)	4240(20)	82(10)
H(6C)	8350(20)	470(30)	4140(20)	58(8)
H(7A)	9710(20)	2250(30)	6220(20)	62(8)
H(7B)	9480(30)	3990(40)	5920(20)	66(9)
H(7C)	9820(30)	2850(40)	5180(30)	89(11)
H(9A)	5200(30)	3560(40)	4350(20)	69(9)
H(9B)	5330(30)	4360(30)	3310(20)	66(8)
H(9C)	5600(30)	2600(30)	3510(20)	55(8)
H(10A)	7290(30)	4940(40)	2890(20)	77(9)
H(10B)	7590(30)	3050(40)	3000(20)	68(9)
H(10C)	8530(30)	4380(30)	3560(20)	67(9)
H(11A)	6710(30)	6420(40)	4300(20)	80(10)

H(11B)	7960(30)	5930(40)	4940(20)	85(11)
H(11C)	6690(30)	5570(40)	5270(20)	77(10)

Table 12. Torsion angles [°] for liu49.

C(6)-Si(1)-N(1)-C(5)	139.95(18)
C(7)-Si(1)-N(1)-C(5)	23.4(2)
C(8)-Si(1)-N(1)-C(5)	-95.81(18)
C(6)-Si(1)-N(1)-B(1)	-42.3(2)
C(7)-Si(1)-N(1)-B(1)	-158.80(18)
C(8)-Si(1)-N(1)-B(1)	81.98(17)
C(5)-N(1)-B(1)-C(2)	0.3(3)
Si(1)-N(1)-B(1)-C(2)	-177.52(14)
C(5)-N(1)-B(1)-C(1)	-178.83(19)
Si(1)-N(1)-B(1)-C(1)	3.4(3)
N(1)-B(1)-C(1)-C(1)#1	174(2)
C(2)-B(1)-C(1)-C(1)#1	-5(2)
N(1)-B(1)-C(2)-C(3)	-0.1(3)
C(1)-B(1)-C(2)-C(3)	179.0(2)
B(1)-C(2)-C(3)-C(4)	-0.3(3)
C(2)-C(3)-C(4)-C(5)	0.7(4)
C(3)-C(4)-C(5)-N(1)	-0.6(4)
B(1)-N(1)-C(5)-C(4)	0.1(3)
Si(1)-N(1)-C(5)-C(4)	178.1(2)
N(1)-Si(1)-C(8)-C(9)	-60.5(2)
C(6)-Si(1)-C(8)-C(9)	63.2(2)
C(7)-Si(1)-C(8)-C(9)	-177.8(2)
N(1)-Si(1)-C(8)-C(10)	178.84(17)
C(6)-Si(1)-C(8)-C(10)	-57.5(2)
C(7)-Si(1)-C(8)-C(10)	61.5(2)
N(1)-Si(1)-C(8)-C(11)	61.1(2)
C(6)-Si(1)-C(8)-C(11)	-175.23(18)
C(7)-Si(1)-C(8)-C(11)	-56.3(2)

Symmetry transformations used to generate equivalent atoms:
#1 -x+1,-y,-z+1

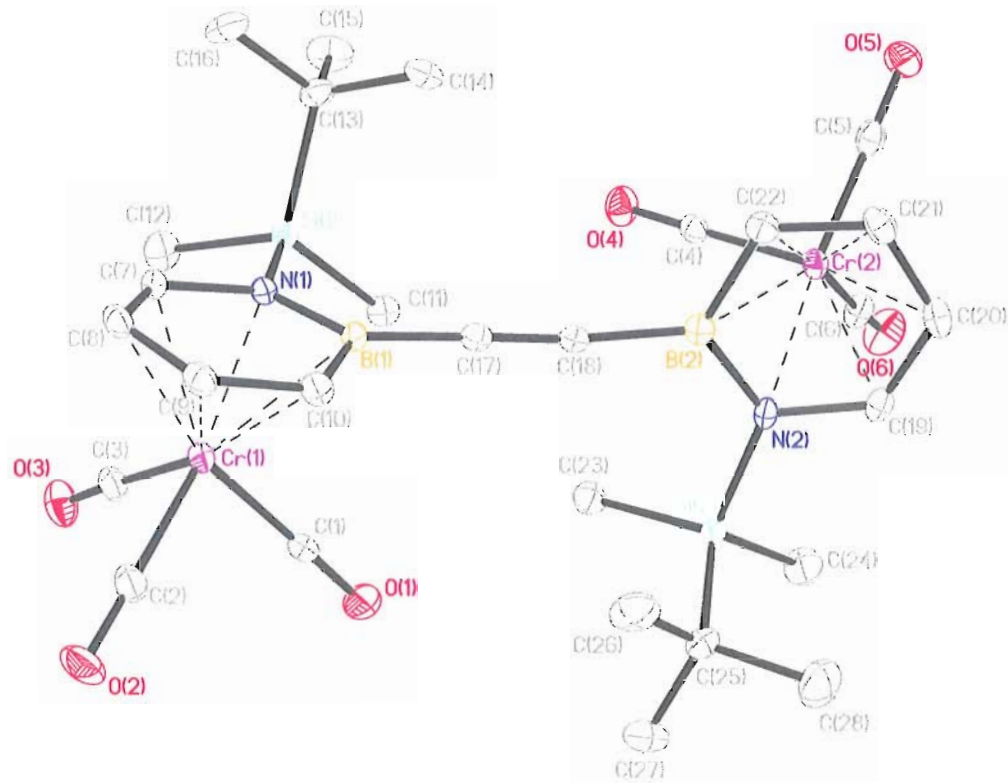

Figure 3. ORTEP illustration of **10**, with thermal ellipsoids drawn at the 35% probability level. Hydrogen atoms have been omitted for clarity.

X-ray Crystal Structure Determination. Crystals of **10** suitable for X-ray diffraction were obtained by evaporation of a solution of **10** in Et_2O.

Diffraction intensity data were collected with a Bruker Smart Apex CCD diffractometer at 173(2) K using MoKα - radiation (0.71073 Å). The structure was solved using direct methods, completed by subsequent difference Fourier syntheses, and refined by full matrix least-squares procedures on F^2. All non-H atoms were refined with anisotropic thermal parameters. H atoms were found on the residual density map and refined with isotropic thermal parameters. The Flack parameter is 0.00(8). All software and sources scattering factors are contained in the SHELXTL (6.10) program package (G.Sheldrick, Bruker XRD, Madison, WI). Crystallographic data and some details of data collection and crystal

structure refinement for $C_{28}H_{38}B_2N_2O_6Si_2$ are given in the following tables.

Table 13. Crystal data and structure refinement for **10** (liu50).

Identification code	liu50	
Empirical formula	$C_{28}\ H_{38}\ B_2\ Cr_2\ N_2\ O_6\ Si_2$	
Formula weight	680.40	
Temperature	173(2) K	
Wavelength	0.71073 Å	
Crystal system	Orthorhombic	
Space group	Pbca	
Unit cell dimensions	a = 12.8679(12) Å	α= 90°.
	b = 20.821(2) Å	β= 90°.
	c = 25.082(2) Å	γ = 90°.
Volume	6719.9(11) $Å^3$	
Z	8	
Density (calculated)	1.345 Mg/m^3	
Absorption coefficient	0.759 mm^{-1}	
F(000)	2832	
Crystal size	0.12 x 0.04 x 0.02 mm^3	
Theta range for data collection	1.62 to 25.00°.	
Index ranges	-15<=h<=15, -24<=k<=24, -29<=l<=29	
Reflections collected	52442	
Independent reflections	5928 [R(int) = 0.1524]	
Completeness to theta = 25.00°	100.0 %	
Absorption correction	Semi-empirical from equivalents	
Max. and min. transmission	0.9850 and 0.9145	
Refinement method	Full-matrix least-squares on F^2	
Data / restraints / parameters	5928 / 0 / 379	
Goodness-of-fit on F^2	1.031	
Final R indices [I>2sigma(I)]	R1 = 0.0610, wR2 = 0.1073	
R indices (all data)	R1 = 0.1086, wR2 = 0.1262	
Largest diff. peak and hole	0.412 and -0.367 $e.Å^{-3}$	

Table 14. Atomic coordinates (x 10^4) and equivalent isotropic displacement parameters ($Å^2$x 10^3) for liu50. U(eq) is defined as one third of the trace of the orthogonalized U^{ij} tensor.

	x	y	z	U(eq)
Cr(1)	6961(1)	1763(1)	6635(1)	23(1)
Cr(2)	7037(1)	419(1)	3540(1)	23(1)
Si(1)	8380(1)	331(1)	6166(1)	24(1)
Si(2)	7451(1)	2074(1)	3982(1)	26(1)
O(1)	7840(3)	2564(2)	5746(1)	49(1)
O(2)	6167(3)	2944(2)	7181(1)	48(1)
O(3)	8953(3)	2022(2)	7214(1)	45(1)
O(4)	8613(3)	-12(2)	4340(1)	40(1)
O(5)	7081(3)	-902(2)	3071(1)	44(1)
O(6)	8790(3)	692(2)	2788(1)	52(1)
N(1)	7186(3)	765(2)	6348(1)	20(1)
N(2)	6620(3)	1372(2)	3864(1)	21(1)
B(1)	6447(4)	1050(2)	5962(2)	21(1)
B(2)	6272(4)	914(3)	4277(2)	22(1)
C(1)	7495(4)	2256(2)	6080(2)	30(1)
C(2)	6474(4)	2492(3)	6967(2)	32(1)
C(3)	8195(4)	1906(2)	6991(2)	30(1)
C(4)	7995(4)	159(2)	4033(2)	25(1)
C(5)	7051(4)	-388(3)	3249(2)	31(1)
C(6)	8108(4)	610(2)	3081(2)	32(1)
C(7)	6951(4)	781(2)	6894(2)	24(1)
C(8)	6058(4)	1060(2)	7095(2)	26(1)
C(9)	5366(4)	1390(2)	6755(2)	26(1)
C(10)	5538(4)	1402(2)	6209(2)	26(1)
C(11)	8959(4)	726(2)	5578(2)	28(1)
C(12)	9298(4)	396(3)	6740(2)	40(1)
C(13)	8010(4)	-529(2)	6053(2)	30(1)
C(14)	7231(4)	-597(2)	5589(2)	38(1)
C(15)	8994(4)	-911(3)	5909(2)	47(2)
C(16)	7518(4)	-818(2)	6555(2)	43(1)
C(17)	6568(3)	1008(2)	5357(2)	23(1)
C(18)	6510(3)	995(2)	4875(2)	21(1)
C(19)	6253(4)	1303(2)	3343(2)	27(1)
C(20)	5583(4)	814(2)	3194(2)	30(1)
C(21)	5316(4)	320(2)	3554(2)	31(1)
C(22)	5645(3)	351(2)	4082(2)	26(1)
C(23)	8432(4)	1878(2)	4498(2)	33(1)
C(24)	8145(4)	2265(3)	3354(2)	45(2)
C(25)	6561(4)	2748(2)	4174(2)	36(1)
C(26)	5838(4)	2571(3)	4637(2)	50(2)
C(27)	7243(5)	3321(3)	4344(2)	60(2)
C(28)	5895(5)	2951(3)	3693(2)	65(2)

Table 15. Bond lengths [Å] and angles [°] for liu50.

Cr(1)-C(2)	1.841(5)
Cr(1)-C(3)	1.846(5)
Cr(1)-C(1)	1.859(5)
Cr(1)-C(7)	2.145(4)
Cr(1)-C(8)	2.196(5)
Cr(1)-C(9)	2.215(5)
Cr(1)-N(1)	2.217(4)
Cr(1)-C(10)	2.249(5)
Cr(1)-B(1)	2.341(5)
Cr(2)-C(4)	1.828(5)
Cr(2)-C(5)	1.831(5)
Cr(2)-C(6)	1.840(5)
Cr(2)-C(19)	2.156(5)
Cr(2)-N(2)	2.211(4)
Cr(2)-C(20)	2.221(5)
Cr(2)-C(21)	2.225(5)
Cr(2)-C(22)	2.253(4)
Cr(2)-B(2)	2.334(5)
Si(1)-N(1)	1.840(4)
Si(1)-C(11)	1.846(5)
Si(1)-C(12)	1.866(5)
Si(1)-C(13)	1.875(5)
Si(2)-N(2)	1.834(4)
Si(2)-C(23)	1.853(5)
Si(2)-C(24)	1.854(5)
Si(2)-C(25)	1.875(5)
O(1)-C(1)	1.146(5)
O(2)-C(2)	1.153(5)
O(3)-C(3)	1.151(5)
O(4)-C(4)	1.163(5)
O(5)-C(5)	1.161(5)
O(6)-C(6)	1.156(6)
N(1)-C(7)	1.402(5)
N(1)-B(1)	1.481(6)
N(2)-C(19)	1.397(5)
N(2)-B(2)	1.477(6)
B(1)-C(10)	1.513(7)
B(1)-C(17)	1.529(7)
B(2)-C(22)	1.506(7)
B(2)-C(18)	1.540(7)
C(7)-C(8)	1.382(6)
C(7)-H(7A)	1.0000
C(8)-C(9)	1.411(6)
C(8)-H(8A)	1.0000
C(9)-C(10)	1.387(6)
C(9)-H(9A)	1.0000
C(10)-H(10A)	1.0000
C(11)-H(11A)	0.9800
C(11)-H(11B)	0.9800
C(11)-H(11C)	0.9800
C(12)-H(12A)	0.9800
C(12)-H(12B)	0.9800

C(12)-H(12C)	0.9800
C(13)-C(16)	1.533(6)
C(13)-C(15)	1.537(7)
C(13)-C(14)	1.542(7)
C(14)-H(14A)	0.9800
C(14)-H(14B)	0.9800
C(14)-H(14C)	0.9800
C(15)-H(15A)	0.9800
C(15)-H(15B)	0.9800
C(15)-H(15C)	0.9800
C(16)-H(16A)	0.9800
C(16)-H(16B)	0.9800
C(16)-H(16C)	0.9800
C(17)-C(18)	1.211(6)
C(19)-C(20)	1.387(6)
C(19)-H(19A)	1.0000
C(20)-C(21)	1.411(7)
C(20)-H(20A)	1.0000
C(21)-C(22)	1.392(6)
C(21)-H(21A)	1.0000
C(22)-H(22A)	1.0000
C(23)-H(23A)	0.9800
C(23)-H(23B)	0.9800
C(23)-H(23C)	0.9800
C(24)-H(24A)	0.9800
C(24)-H(24B)	0.9800
C(24)-H(24C)	0.9800
C(25)-C(26)	1.533(7)
C(25)-C(28)	1.539(7)
C(25)-C(27)	1.539(7)
C(26)-H(26A)	0.9800
C(26)-H(26B)	0.9800
C(26)-H(26C)	0.9800
C(27)-H(27A)	0.9800
C(27)-H(27B)	0.9800
C(27)-H(27C)	0.9800
C(28)-H(28A)	0.9800
C(28)-H(28B)	0.9800
C(28)-H(28C)	0.9800

C(2)-Cr(1)-C(3)	86.6(2)
C(2)-Cr(1)-C(1)	90.5(2)
C(3)-Cr(1)-C(1)	87.4(2)
C(2)-Cr(1)-C(7)	130.25(19)
C(3)-Cr(1)-C(7)	90.7(2)
C(1)-Cr(1)-C(7)	139.02(19)
C(2)-Cr(1)-C(8)	97.5(2)
C(3)-Cr(1)-C(8)	107.95(19)
C(1)-Cr(1)-C(8)	162.96(19)
C(7)-Cr(1)-C(8)	37.12(17)
C(2)-Cr(1)-C(9)	84.9(2)
C(3)-Cr(1)-C(9)	141.96(19)
C(1)-Cr(1)-C(9)	129.6(2)

C(7)-Cr(1)-C(9)	67.61(18)
C(8)-Cr(1)-C(9)	37.31(16)
C(2)-Cr(1)-N(1)	164.44(18)
C(3)-Cr(1)-N(1)	101.27(18)
C(1)-Cr(1)-N(1)	103.12(17)
C(7)-Cr(1)-N(1)	37.44(14)
C(8)-Cr(1)-N(1)	67.36(15)
C(9)-Cr(1)-N(1)	80.61(15)
C(2)-Cr(1)-C(10)	102.3(2)
C(3)-Cr(1)-C(10)	169.7(2)
C(1)-Cr(1)-C(10)	97.51(19)
C(7)-Cr(1)-C(10)	79.66(18)
C(8)-Cr(1)-C(10)	66.16(17)
C(9)-Cr(1)-C(10)	36.19(16)
N(1)-Cr(1)-C(10)	68.88(15)
C(2)-Cr(1)-B(1)	138.8(2)
C(3)-Cr(1)-B(1)	133.9(2)
C(1)-Cr(1)-B(1)	85.19(19)
C(7)-Cr(1)-B(1)	67.20(17)
C(8)-Cr(1)-B(1)	78.85(17)
C(9)-Cr(1)-B(1)	67.31(18)
N(1)-Cr(1)-B(1)	37.79(15)
C(10)-Cr(1)-B(1)	38.42(17)
C(4)-Cr(2)-C(5)	89.5(2)
C(4)-Cr(2)-C(6)	88.9(2)
C(5)-Cr(2)-C(6)	86.7(2)
C(4)-Cr(2)-C(19)	136.30(19)
C(5)-Cr(2)-C(19)	134.1(2)
C(6)-Cr(2)-C(19)	91.3(2)
C(4)-Cr(2)-N(2)	100.40(17)
C(5)-Cr(2)-N(2)	166.47(19)
C(6)-Cr(2)-N(2)	102.57(18)
C(19)-Cr(2)-N(2)	37.29(14)
C(4)-Cr(2)-C(20)	160.51(19)
C(5)-Cr(2)-C(20)	101.1(2)
C(6)-Cr(2)-C(20)	107.8(2)
C(19)-Cr(2)-C(20)	36.90(17)
N(2)-Cr(2)-C(20)	66.88(15)
C(4)-Cr(2)-C(21)	129.37(19)
C(5)-Cr(2)-C(21)	86.0(2)
C(6)-Cr(2)-C(21)	140.9(2)
C(19)-Cr(2)-C(21)	67.46(18)
N(2)-Cr(2)-C(21)	80.55(16)
C(20)-Cr(2)-C(21)	37.00(17)
C(4)-Cr(2)-C(22)	96.32(18)
C(5)-Cr(2)-C(22)	100.94(19)
C(6)-Cr(2)-C(22)	170.7(2)
C(19)-Cr(2)-C(22)	79.66(18)
N(2)-Cr(2)-C(22)	69.03(15)
C(20)-Cr(2)-C(22)	65.78(17)
C(21)-Cr(2)-C(22)	36.23(16)
C(4)-Cr(2)-B(2)	83.09(19)
C(5)-Cr(2)-B(2)	136.4(2)

C(6)-Cr(2)-B(2)	135.7(2)
C(19)-Cr(2)-B(2)	66.87(18)
N(2)-Cr(2)-B(2)	37.81(15)
C(20)-Cr(2)-B(2)	77.96(18)
C(21)-Cr(2)-B(2)	66.98(18)
C(22)-Cr(2)-B(2)	38.29(17)
N(1)-Si(1)-C(11)	108.45(19)
N(1)-Si(1)-C(12)	107.5(2)
C(11)-Si(1)-C(12)	109.2(2)
N(1)-Si(1)-C(13)	107.2(2)
C(11)-Si(1)-C(13)	114.0(2)
C(12)-Si(1)-C(13)	110.3(2)
N(2)-Si(2)-C(23)	109.5(2)
N(2)-Si(2)-C(24)	108.4(2)
C(23)-Si(2)-C(24)	108.2(2)
N(2)-Si(2)-C(25)	106.4(2)
C(23)-Si(2)-C(25)	113.7(2)
C(24)-Si(2)-C(25)	110.6(2)
C(7)-N(1)-B(1)	119.3(4)
C(7)-N(1)-Si(1)	115.7(3)
B(1)-N(1)-Si(1)	124.8(3)
C(7)-N(1)-Cr(1)	68.5(2)
B(1)-N(1)-Cr(1)	75.7(2)
Si(1)-N(1)-Cr(1)	130.55(19)
C(19)-N(2)-B(2)	119.1(4)
C(19)-N(2)-Si(2)	115.4(3)
B(2)-N(2)-Si(2)	125.3(3)
C(19)-N(2)-Cr(2)	69.2(2)
B(2)-N(2)-Cr(2)	75.6(2)
Si(2)-N(2)-Cr(2)	129.25(19)
N(1)-B(1)-C(10)	115.0(4)
N(1)-B(1)-C(17)	124.1(4)
C(10)-B(1)-C(17)	120.8(4)
N(1)-B(1)-Cr(1)	66.5(2)
C(10)-B(1)-Cr(1)	67.5(3)
C(17)-B(1)-Cr(1)	136.3(3)
N(2)-B(2)-C(22)	115.9(4)
N(2)-B(2)-C(18)	123.5(4)
C(22)-B(2)-C(18)	120.6(4)
N(2)-B(2)-Cr(2)	66.6(2)
C(22)-B(2)-Cr(2)	67.9(3)
C(18)-B(2)-Cr(2)	137.4(3)
O(1)-C(1)-Cr(1)	178.6(5)
O(2)-C(2)-Cr(1)	179.1(5)
O(3)-C(3)-Cr(1)	177.1(4)
O(4)-C(4)-Cr(2)	178.9(4)
O(5)-C(5)-Cr(2)	178.4(5)
O(6)-C(6)-Cr(2)	176.0(5)
C(8)-C(7)-N(1)	123.0(4)
C(8)-C(7)-Cr(1)	73.5(3)
N(1)-C(7)-Cr(1)	74.1(2)
C(8)-C(7)-H(7A)	118.2
N(1)-C(7)-H(7A)	118.2

Cr(1)-C(7)-H(7A)	118.2
C(7)-C(8)-C(9)	120.6(4)
C(7)-C(8)-Cr(1)	69.4(3)
C(9)-C(8)-Cr(1)	72.1(3)
C(7)-C(8)-H(8A)	118.9
C(9)-C(8)-H(8A)	118.9
Cr(1)-C(8)-H(8A)	118.9
C(10)-C(9)-C(8)	120.3(4)
C(10)-C(9)-Cr(1)	73.2(3)
C(8)-C(9)-Cr(1)	70.6(3)
C(10)-C(9)-H(9A)	119.4
C(8)-C(9)-H(9A)	119.4
Cr(1)-C(9)-H(9A)	119.4
C(9)-C(10)-B(1)	121.2(4)
C(9)-C(10)-Cr(1)	70.6(3)
B(1)-C(10)-Cr(1)	74.1(3)
C(9)-C(10)-H(10A)	119.0
B(1)-C(10)-H(10A)	119.0
Cr(1)-C(10)-H(10A)	119.0
Si(1)-C(11)-H(11A)	109.5
Si(1)-C(11)-H(11B)	109.5
H(11A)-C(11)-H(11B)	109.5
Si(1)-C(11)-H(11C)	109.5
H(11A)-C(11)-H(11C)	109.5
H(11B)-C(11)-H(11C)	109.5
Si(1)-C(12)-H(12A)	109.5
Si(1)-C(12)-H(12B)	109.5
H(12A)-C(12)-H(12B)	109.5
Si(1)-C(12)-H(12C)	109.5
H(12A)-C(12)-H(12C)	109.5
H(12B)-C(12)-H(12C)	109.5
C(16)-C(13)-C(15)	109.2(4)
C(16)-C(13)-C(14)	108.4(4)
C(15)-C(13)-C(14)	108.1(4)
C(16)-C(13)-Si(1)	110.8(3)
C(15)-C(13)-Si(1)	108.7(3)
C(14)-C(13)-Si(1)	111.5(3)
C(13)-C(14)-H(14A)	109.5
C(13)-C(14)-H(14B)	109.5
H(14A)-C(14)-H(14B)	109.5
C(13)-C(14)-H(14C)	109.5
H(14A)-C(14)-H(14C)	109.5
H(14B)-C(14)-H(14C)	109.5
C(13)-C(15)-H(15A)	109.5
C(13)-C(15)-H(15B)	109.5
H(15A)-C(15)-H(15B)	109.5
C(13)-C(15)-H(15C)	109.5
H(15A)-C(15)-H(15C)	109.5
H(15B)-C(15)-H(15C)	109.5
C(13)-C(16)-H(16A)	109.5
C(13)-C(16)-H(16B)	109.5
H(16A)-C(16)-H(16B)	109.5
C(13)-C(16)-H(16C)	109.5

H(16A)-C(16)-H(16C)	109.5
H(16B)-C(16)-H(16C)	109.5
C(18)-C(17)-B(1)	170.5(5)
C(17)-C(18)-B(2)	170.5(5)
C(20)-C(19)-N(2)	122.6(4)
C(20)-C(19)-Cr(2)	74.1(3)
N(2)-C(19)-Cr(2)	73.5(2)
C(20)-C(19)-H(19A)	118.4
N(2)-C(19)-H(19A)	118.4
Cr(2)-C(19)-H(19A)	118.4
C(19)-C(20)-C(21)	120.9(4)
C(19)-C(20)-Cr(2)	69.0(3)
C(21)-C(20)-Cr(2)	71.6(3)
C(19)-C(20)-H(20A)	118.5
C(21)-C(20)-H(20A)	118.5
Cr(2)-C(20)-H(20A)	118.5
C(22)-C(21)-C(20)	120.2(4)
C(22)-C(21)-Cr(2)	73.0(3)
C(20)-C(21)-Cr(2)	71.4(3)
C(22)-C(21)-H(21A)	119.6
C(20)-C(21)-H(21A)	119.6
Cr(2)-C(21)-H(21A)	119.6
C(21)-C(22)-B(2)	120.5(4)
C(21)-C(22)-Cr(2)	70.8(3)
B(2)-C(22)-Cr(2)	73.8(3)
C(21)-C(22)-H(22A)	119.4
B(2)-C(22)-H(22A)	119.4
Cr(2)-C(22)-H(22A)	119.4
Si(2)-C(23)-H(23A)	109.5
Si(2)-C(23)-H(23B)	109.5
H(23A)-C(23)-H(23B)	109.5
Si(2)-C(23)-H(23C)	109.5
H(23A)-C(23)-H(23C)	109.5
H(23B)-C(23)-H(23C)	109.5
Si(2)-C(24)-H(24A)	109.5
Si(2)-C(24)-H(24B)	109.5
H(24A)-C(24)-H(24B)	109.5
Si(2)-C(24)-H(24C)	109.5
H(24A)-C(24)-H(24C)	109.5
H(24B)-C(24)-H(24C)	109.5
C(26)-C(25)-C(28)	108.7(5)
C(26)-C(25)-C(27)	108.9(4)
C(28)-C(25)-C(27)	108.8(5)
C(26)-C(25)-Si(2)	112.6(3)
C(28)-C(25)-Si(2)	110.1(4)
C(27)-C(25)-Si(2)	107.6(4)
C(25)-C(26)-H(26A)	109.5
C(25)-C(26)-H(26B)	109.5
H(26A)-C(26)-H(26B)	109.5
C(25)-C(26)-H(26C)	109.5
H(26A)-C(26)-H(26C)	109.5
H(26B)-C(26)-H(26C)	109.5
C(25)-C(27)-H(27A)	109.5

C(25)-C(27)-H(27B)	109.5
H(27A)-C(27)-H(27B)	109.5
C(25)-C(27)-H(27C)	109.5
H(27A)-C(27)-H(27C)	109.5
H(27B)-C(27)-H(27C)	109.5
C(25)-C(28)-H(28A)	109.5
C(25)-C(28)-H(28B)	109.5
H(28A)-C(28)-H(28B)	109.5
C(25)-C(28)-H(28C)	109.5
H(28A)-C(28)-H(28C)	109.5
H(28B)-C(28)-H(28C)	109.5

Symmetry transformations used to generate equivalent atoms:

Table 16. Anisotropic displacement parameters ($Å^2 x\ 10^3$)for liu50. The anisotropic displacement factor exponent takes the form: $-2p^2[\ h^2a^{*2}U^{11} + ... + 2\ h\ k\ a^*\ b^*\ U^{12}\ ]$

	U^{11}	U^{22}	U^{33}	U^{23}	U^{13}	U^{12}
Cr(1)	28(1)	23(1)	18(1)	-2(1)	1(1)	1(1)
Cr(2)	25(1)	26(1)	17(1)	-2(1)	1(1)	1(1)
Si(1)	27(1)	23(1)	23(1)	2(1)	1(1)	6(1)
Si(2)	30(1)	23(1)	23(1)	4(1)	-2(1)	-4(1)
O(1)	80(3)	34(2)	34(2)	7(2)	9(2)	-10(2)
O(2)	67(3)	33(2)	45(2)	-17(2)	14(2)	3(2)
O(3)	40(3)	62(3)	33(2)	-10(2)	-5(2)	-9(2)
O(4)	37(2)	47(2)	37(2)	-2(2)	-7(2)	11(2)
O(5)	66(3)	32(2)	33(2)	-12(2)	5(2)	3(2)
O(6)	41(3)	72(3)	43(2)	12(2)	21(2)	7(2)
N(1)	23(2)	20(2)	17(2)	-1(2)	1(2)	-1(2)
N(2)	21(2)	26(2)	16(2)	1(2)	-3(2)	3(2)
B(1)	24(3)	21(3)	18(3)	0(2)	-4(2)	-3(2)
B(2)	20(3)	25(3)	22(3)	-2(2)	2(2)	3(2)
C(1)	44(3)	20(3)	27(3)	-5(2)	-1(3)	1(2)
C(2)	36(3)	34(3)	25(3)	-5(2)	1(2)	-5(3)
C(3)	34(3)	33(3)	23(3)	-6(2)	3(2)	-5(2)
C(4)	27(3)	26(3)	23(3)	-5(2)	5(2)	-2(2)
C(5)	34(3)	40(3)	20(3)	2(2)	4(2)	3(3)
C(6)	34(3)	38(3)	26(3)	4(2)	2(3)	9(3)
C(7)	31(3)	23(3)	17(2)	0(2)	-3(2)	-2(2)
C(8)	29(3)	27(3)	21(2)	-6(2)	5(2)	-4(2)
C(9)	26(3)	26(3)	27(3)	-6(2)	5(2)	0(2)
C(10)	25(3)	27(3)	26(3)	-2(2)	-2(2)	3(2)
C(11)	22(3)	29(3)	34(3)	1(2)	0(2)	2(2)
C(12)	33(3)	46(4)	41(3)	0(3)	-7(3)	15(3)
C(13)	35(3)	23(3)	33(3)	4(2)	6(3)	5(2)
C(14)	47(4)	24(3)	42(3)	-7(2)	-1(3)	-5(2)
C(15)	40(4)	34(3)	68(4)	-5(3)	8(3)	15(3)
C(16)	52(4)	25(3)	53(4)	12(3)	9(3)	3(3)
C(17)	20(3)	20(3)	27(3)	0(2)	-2(2)	2(2)
C(18)	20(3)	19(3)	25(3)	-2(2)	1(2)	-1(2)
C(19)	30(3)	31(3)	20(2)	4(2)	0(2)	2(2)
C(20)	24(3)	43(3)	24(3)	-6(2)	-3(2)	-1(2)
C(21)	22(3)	38(3)	34(3)	-7(2)	-4(2)	-4(2)

C(22)	20(3)	28(3)	28(3)	2(2)	1(2)	-5(2)
C(23)	28(3)	35(3)	36(3)	0(2)	-3(2)	-9(2)
C(24)	49(4)	46(4)	41(3)	9(3)	6(3)	-16(3)
C(25)	46(4)	29(3)	33(3)	3(2)	-7(3)	8(3)
C(26)	56(4)	37(4)	57(4)	0(3)	12(3)	20(3)
C(27)	95(6)	27(3)	59(4)	-3(3)	-3(4)	-2(3)
C(28)	77(5)	62(5)	55(4)	0(3)	-18(4)	32(4)

Table 17. Hydrogen coordinates (x 10^4) and isotropic displacement parameters ($Å^2$x 10^3) for liu50.

	x	y	z	U(eq)
H(7A)	7498	640	7151	29
H(8A)	5992	1119	7489	31
H(9A)	4824	1676	6913	32
H(10A)	5128	1707	5984	31
H(11A)	9132	1172	5666	42
H(11B)	8461	719	5282	42
H(11C)	9592	496	5473	42
H(12A)	9485	847	6795	60
H(12B)	9926	146	6664	60
H(12C)	8964	228	7062	60
H(14A)	7055	-1051	5540	57
H(14B)	7545	-430	5261	57
H(14C)	6600	-354	5671	57
H(15A)	8810	-1362	5849	71
H(15B)	9494	-882	6203	71
H(15C)	9303	-733	5585	71
H(16A)	7331	-1267	6488	65
H(16B)	6893	-575	6649	65
H(16C)	8017	-798	6850	65
H(19A)	6557	1582	3058	33
H(20A)	5445	746	2805	36
H(21A)	4987	-82	3417	38
H(22A)	5562	-34	4316	31
H(23A)	8869	1523	4373	49
H(23B)	8079	1751	4828	49
H(23C)	8866	2255	4566	49
H(24A)	8606	1908	3260	68
H(24B)	8558	2656	3403	68
H(24C)	7639	2332	3067	68
H(26A)	5390	2938	4722	75
H(26B)	6254	2458	4950	75
H(26C)	5406	2203	4534	75
H(27A)	6797	3682	4447	91
H(27B)	7688	3449	4045	91
H(27C)	7677	3195	4647	91
H(28A)	5433	3303	3797	97
H(28B)	5478	2585	3572	97
H(28C)	6349	3094	3403	97

Table 18. Torsion angles [°] for liu50.

C(11)-Si(1)-N(1)-C(7)	-147.3(3)
C(12)-Si(1)-N(1)-C(7)	-29.4(4)
C(13)-Si(1)-N(1)-C(7)	89.2(3)
C(11)-Si(1)-N(1)-B(1)	37.0(4)
C(12)-Si(1)-N(1)-B(1)	154.9(4)
C(13)-Si(1)-N(1)-B(1)	-86.5(4)
C(11)-Si(1)-N(1)-Cr(1)	-64.5(3)
C(12)-Si(1)-N(1)-Cr(1)	53.5(3)
C(13)-Si(1)-N(1)-Cr(1)	172.1(2)
C(2)-Cr(1)-N(1)-C(7)	-43.3(7)
C(3)-Cr(1)-N(1)-C(7)	76.1(3)
C(1)-Cr(1)-N(1)-C(7)	166.1(3)
C(8)-Cr(1)-N(1)-C(7)	-28.8(3)
C(9)-Cr(1)-N(1)-C(7)	-65.2(3)
C(10)-Cr(1)-N(1)-C(7)	-100.8(3)
B(1)-Cr(1)-N(1)-C(7)	-130.1(4)
C(2)-Cr(1)-N(1)-B(1)	86.8(7)
C(3)-Cr(1)-N(1)-B(1)	-153.8(3)
C(1)-Cr(1)-N(1)-B(1)	-63.8(3)
C(7)-Cr(1)-N(1)-B(1)	130.1(4)
C(8)-Cr(1)-N(1)-B(1)	101.3(3)
C(9)-Cr(1)-N(1)-B(1)	64.9(3)
C(10)-Cr(1)-N(1)-B(1)	29.3(3)
C(2)-Cr(1)-N(1)-Si(1)	-149.3(6)
C(3)-Cr(1)-N(1)-Si(1)	-29.9(3)
C(1)-Cr(1)-N(1)-Si(1)	60.0(3)
C(7)-Cr(1)-N(1)-Si(1)	-106.1(3)
C(8)-Cr(1)-N(1)-Si(1)	-134.8(3)
C(9)-Cr(1)-N(1)-Si(1)	-171.3(3)
C(10)-Cr(1)-N(1)-Si(1)	153.1(3)
B(1)-Cr(1)-N(1)-Si(1)	123.9(4)
C(23)-Si(2)-N(2)-C(19)	-147.4(3)
C(24)-Si(2)-N(2)-C(19)	-29.6(4)
C(25)-Si(2)-N(2)-C(19)	89.3(3)
C(23)-Si(2)-N(2)-B(2)	36.5(4)
C(24)-Si(2)-N(2)-B(2)	154.3(4)
C(25)-Si(2)-N(2)-B(2)	-86.7(4)
C(23)-Si(2)-N(2)-Cr(2)	-64.2(3)
C(24)-Si(2)-N(2)-Cr(2)	53.6(3)
C(25)-Si(2)-N(2)-Cr(2)	172.5(2)
C(4)-Cr(2)-N(2)-C(19)	166.5(3)
C(5)-Cr(2)-N(2)-C(19)	-57.0(8)
C(6)-Cr(2)-N(2)-C(19)	75.2(3)
C(20)-Cr(2)-N(2)-C(19)	-29.0(3)
C(21)-Cr(2)-N(2)-C(19)	-65.0(3)
C(22)-Cr(2)-N(2)-C(19)	-100.7(3)
B(2)-Cr(2)-N(2)-C(19)	-129.4(4)
C(4)-Cr(2)-N(2)-B(2)	-64.2(3)
C(5)-Cr(2)-N(2)-B(2)	72.4(8)
C(6)-Cr(2)-N(2)-B(2)	-155.4(3)
C(19)-Cr(2)-N(2)-B(2)	129.4(4)
C(20)-Cr(2)-N(2)-B(2)	100.4(3)

C(21)-Cr(2)-N(2)-B(2)	64.4(3)
C(22)-Cr(2)-N(2)-B(2)	28.7(3)
C(4)-Cr(2)-N(2)-Si(2)	60.0(3)
C(5)-Cr(2)-N(2)-Si(2)	-163.5(6)
C(6)-Cr(2)-N(2)-Si(2)	-31.2(3)
C(19)-Cr(2)-N(2)-Si(2)	-106.5(3)
C(20)-Cr(2)-N(2)-Si(2)	-135.5(3)
C(21)-Cr(2)-N(2)-Si(2)	-171.5(3)
C(22)-Cr(2)-N(2)-Si(2)	152.8(3)
B(2)-Cr(2)-N(2)-Si(2)	124.1(4)
C(7)-N(1)-B(1)-C(10)	6.3(6)
Si(1)-N(1)-B(1)-C(10)	-178.2(3)
Cr(1)-N(1)-B(1)-C(10)	-48.4(4)
C(7)-N(1)-B(1)-C(17)	-174.2(4)
Si(1)-N(1)-B(1)-C(17)	1.4(6)
Cr(1)-N(1)-B(1)-C(17)	131.1(5)
C(7)-N(1)-B(1)-Cr(1)	54.7(3)
Si(1)-N(1)-B(1)-Cr(1)	-129.8(3)
C(2)-Cr(1)-B(1)-N(1)	-156.0(3)
C(3)-Cr(1)-B(1)-N(1)	37.0(4)
C(1)-Cr(1)-B(1)-N(1)	118.7(3)
C(7)-Cr(1)-B(1)-N(1)	-30.3(2)
C(8)-Cr(1)-B(1)-N(1)	-67.3(3)
C(9)-Cr(1)-B(1)-N(1)	-104.5(3)
C(10)-Cr(1)-B(1)-N(1)	-132.8(4)
C(2)-Cr(1)-B(1)-C(10)	-23.2(4)
C(3)-Cr(1)-B(1)-C(10)	169.8(3)
C(1)-Cr(1)-B(1)-C(10)	-108.5(3)
C(7)-Cr(1)-B(1)-C(10)	102.5(3)
C(8)-Cr(1)-B(1)-C(10)	65.5(3)
C(9)-Cr(1)-B(1)-C(10)	28.3(3)
N(1)-Cr(1)-B(1)-C(10)	132.8(4)
C(2)-Cr(1)-B(1)-C(17)	88.5(6)
C(3)-Cr(1)-B(1)-C(17)	-78.6(6)
C(1)-Cr(1)-B(1)-C(17)	3.2(5)
C(7)-Cr(1)-B(1)-C(17)	-145.8(6)
C(8)-Cr(1)-B(1)-C(17)	177.2(5)
C(9)-Cr(1)-B(1)-C(17)	140.0(5)
N(1)-Cr(1)-B(1)-C(17)	-115.5(6)
C(10)-Cr(1)-B(1)-C(17)	111.7(6)
C(19)-N(2)-B(2)-C(22)	7.6(6)
Si(2)-N(2)-B(2)-C(22)	-176.4(3)
Cr(2)-N(2)-B(2)-C(22)	-48.2(4)
C(19)-N(2)-B(2)-C(18)	-171.8(4)
Si(2)-N(2)-B(2)-C(18)	4.2(6)
Cr(2)-N(2)-B(2)-C(18)	132.4(5)
C(19)-N(2)-B(2)-Cr(2)	55.8(3)
Si(2)-N(2)-B(2)-Cr(2)	-128.2(3)
C(4)-Cr(2)-B(2)-N(2)	116.9(3)
C(5)-Cr(2)-B(2)-N(2)	-161.1(3)
C(6)-Cr(2)-B(2)-N(2)	35.6(4)
C(19)-Cr(2)-B(2)-N(2)	-30.6(2)
C(20)-Cr(2)-B(2)-N(2)	-67.7(3)

C(21)-Cr(2)-B(2)-N(2)	-104.9(3)
C(22)-Cr(2)-B(2)-N(2)	-133.7(4)
C(4)-Cr(2)-B(2)-C(22)	-109.4(3)
C(5)-Cr(2)-B(2)-C(22)	-27.4(4)
C(6)-Cr(2)-B(2)-C(22)	169.3(3)
C(19)-Cr(2)-B(2)-C(22)	103.1(3)
N(2)-Cr(2)-B(2)-C(22)	133.7(4)
C(20)-Cr(2)-B(2)-C(22)	66.0(3)
C(21)-Cr(2)-B(2)-C(22)	28.8(3)
C(4)-Cr(2)-B(2)-C(18)	2.3(5)
C(5)-Cr(2)-B(2)-C(18)	84.2(6)
C(6)-Cr(2)-B(2)-C(18)	-79.0(6)
C(19)-Cr(2)-B(2)-C(18)	-145.3(6)
N(2)-Cr(2)-B(2)-C(18)	-114.6(6)
C(20)-Cr(2)-B(2)-C(18)	177.7(5)
C(21)-Cr(2)-B(2)-C(18)	140.5(6)
C(22)-Cr(2)-B(2)-C(18)	111.7(6)
C(2)-Cr(1)-C(1)-O(1)	74(20)
C(3)-Cr(1)-C(1)-O(1)	-12(20)
C(7)-Cr(1)-C(1)-O(1)	-101(20)
C(8)-Cr(1)-C(1)-O(1)	-167(19)
C(9)-Cr(1)-C(1)-O(1)	158(20)
N(1)-Cr(1)-C(1)-O(1)	-113(20)
C(10)-Cr(1)-C(1)-O(1)	177(100)
B(1)-Cr(1)-C(1)-O(1)	-147(20)
C(3)-Cr(1)-C(2)-O(2)	-79(33)
C(1)-Cr(1)-C(2)-O(2)	-167(100)
C(7)-Cr(1)-C(2)-O(2)	9(34)
C(8)-Cr(1)-C(2)-O(2)	28(33)
C(9)-Cr(1)-C(2)-O(2)	63(33)
N(1)-Cr(1)-C(2)-O(2)	42(34)
C(10)-Cr(1)-C(2)-O(2)	95(33)
B(1)-Cr(1)-C(2)-O(2)	110(33)
C(2)-Cr(1)-C(3)-O(3)	-25(8)
C(1)-Cr(1)-C(3)-O(3)	66(8)
C(7)-Cr(1)-C(3)-O(3)	-155(8)
C(8)-Cr(1)-C(3)-O(3)	-122(8)
C(9)-Cr(1)-C(3)-O(3)	-102(8)
N(1)-Cr(1)-C(3)-O(3)	169(8)
C(10)-Cr(1)-C(3)-O(3)	-175(100)
B(1)-Cr(1)-C(3)-O(3)	146(8)
C(5)-Cr(2)-C(4)-O(4)	38(25)
C(6)-Cr(2)-C(4)-O(4)	-48(25)
C(19)-Cr(2)-C(4)-O(4)	-139(25)
N(2)-Cr(2)-C(4)-O(4)	-151(25)
C(20)-Cr(2)-C(4)-O(4)	162(100)
C(21)-Cr(2)-C(4)-O(4)	123(25)
C(22)-Cr(2)-C(4)-O(4)	139(25)
B(2)-Cr(2)-C(4)-O(4)	175(100)
C(4)-Cr(2)-C(5)-O(5)	-19(17)
C(6)-Cr(2)-C(5)-O(5)	70(17)
C(19)-Cr(2)-C(5)-O(5)	159(17)
N(2)-Cr(2)-C(5)-O(5)	-156(17)

C(20)-Cr(2)-C(5)-O(5)	178(100)
C(21)-Cr(2)-C(5)-O(5)	-148(17)
C(22)-Cr(2)-C(5)-O(5)	-115(17)
B(2)-Cr(2)-C(5)-O(5)	-98(17)
C(4)-Cr(2)-C(6)-O(6)	73(7)
C(5)-Cr(2)-C(6)-O(6)	-17(7)
C(19)-Cr(2)-C(6)-O(6)	-151(7)
N(2)-Cr(2)-C(6)-O(6)	173(6)
C(20)-Cr(2)-C(6)-O(6)	-118(6)
C(21)-Cr(2)-C(6)-O(6)	-97(6)
C(22)-Cr(2)-C(6)-O(6)	-163(6)
B(2)-Cr(2)-C(6)-O(6)	152(6)
B(1)-N(1)-C(7)-C(8)	-0.8(6)
Si(1)-N(1)-C(7)-C(8)	-176.8(4)
Cr(1)-N(1)-C(7)-C(8)	57.4(4)
B(1)-N(1)-C(7)-Cr(1)	-58.2(4)
Si(1)-N(1)-C(7)-Cr(1)	125.9(2)
C(2)-Cr(1)-C(7)-C(8)	33.5(4)
C(3)-Cr(1)-C(7)-C(8)	119.7(3)
C(1)-Cr(1)-C(7)-C(8)	-153.5(3)
C(9)-Cr(1)-C(7)-C(8)	-28.2(3)
N(1)-Cr(1)-C(7)-C(8)	-132.6(4)
C(10)-Cr(1)-C(7)-C(8)	-63.9(3)
B(1)-Cr(1)-C(7)-C(8)	-102.0(3)
C(2)-Cr(1)-C(7)-N(1)	166.1(3)
C(3)-Cr(1)-C(7)-N(1)	-107.8(3)
C(1)-Cr(1)-C(7)-N(1)	-20.9(4)
C(8)-Cr(1)-C(7)-N(1)	132.6(4)
C(9)-Cr(1)-C(7)-N(1)	104.3(3)
C(10)-Cr(1)-C(7)-N(1)	68.6(2)
B(1)-Cr(1)-C(7)-N(1)	30.6(2)
N(1)-C(7)-C(8)-C(9)	-4.8(7)
Cr(1)-C(7)-C(8)-C(9)	52.9(4)
N(1)-C(7)-C(8)-Cr(1)	-57.7(4)
C(2)-Cr(1)-C(8)-C(7)	-154.9(3)
C(3)-Cr(1)-C(8)-C(7)	-66.0(3)
C(1)-Cr(1)-C(8)-C(7)	87.6(7)
C(9)-Cr(1)-C(8)-C(7)	133.8(4)
N(1)-Cr(1)-C(8)-C(7)	29.0(2)
C(10)-Cr(1)-C(8)-C(7)	105.0(3)
B(1)-Cr(1)-C(8)-C(7)	66.8(3)
C(2)-Cr(1)-C(8)-C(9)	71.3(3)
C(3)-Cr(1)-C(8)-C(9)	160.2(3)
C(1)-Cr(1)-C(8)-C(9)	-46.2(8)
C(7)-Cr(1)-C(8)-C(9)	-133.8(4)
N(1)-Cr(1)-C(8)-C(9)	-104.8(3)
C(10)-Cr(1)-C(8)-C(9)	-28.8(3)
B(1)-Cr(1)-C(8)-C(9)	-67.0(3)
C(7)-C(8)-C(9)-C(10)	4.3(7)
Cr(1)-C(8)-C(9)-C(10)	56.0(4)
C(7)-C(8)-C(9)-Cr(1)	-51.7(4)
C(2)-Cr(1)-C(9)-C(10)	118.9(3)
C(3)-Cr(1)-C(9)-C(10)	-163.2(3)

C(1)-Cr(1)-C(9)-C(10)	32.4(4)
C(7)-Cr(1)-C(9)-C(10)	-103.5(3)
C(8)-Cr(1)-C(9)-C(10)	-131.6(4)
N(1)-Cr(1)-C(9)-C(10)	-66.9(3)
B(1)-Cr(1)-C(9)-C(10)	-29.9(3)
C(2)-Cr(1)-C(9)-C(8)	-109.5(3)
C(3)-Cr(1)-C(9)-C(8)	-31.6(4)
C(1)-Cr(1)-C(9)-C(8)	164.1(3)
C(7)-Cr(1)-C(9)-C(8)	28.1(3)
N(1)-Cr(1)-C(9)-C(8)	64.7(3)
C(10)-Cr(1)-C(9)-C(8)	131.6(4)
B(1)-Cr(1)-C(9)-C(8)	101.7(3)
C(8)-C(9)-C(10)-B(1)	1.6(7)
Cr(1)-C(9)-C(10)-B(1)	56.4(4)
C(8)-C(9)-C(10)-Cr(1)	-54.7(4)
N(1)-B(1)-C(10)-C(9)	-6.8(7)
C(17)-B(1)-C(10)-C(9)	173.7(4)
Cr(1)-B(1)-C(10)-C(9)	-54.7(4)
N(1)-B(1)-C(10)-Cr(1)	48.0(3)
C(17)-B(1)-C(10)-Cr(1)	-131.6(4)
C(2)-Cr(1)-C(10)-C(9)	-63.2(3)
C(3)-Cr(1)-C(10)-C(9)	86.4(11)
C(1)-Cr(1)-C(10)-C(9)	-155.4(3)
C(7)-Cr(1)-C(10)-C(9)	66.0(3)
C(8)-Cr(1)-C(10)-C(9)	29.7(3)
N(1)-Cr(1)-C(10)-C(9)	103.4(3)
B(1)-Cr(1)-C(10)-C(9)	132.2(4)
C(2)-Cr(1)-C(10)-B(1)	164.6(3)
C(3)-Cr(1)-C(10)-B(1)	-45.8(11)
C(1)-Cr(1)-C(10)-B(1)	72.4(3)
C(7)-Cr(1)-C(10)-B(1)	-66.2(3)
C(8)-Cr(1)-C(10)-B(1)	-102.5(3)
C(9)-Cr(1)-C(10)-B(1)	-132.2(4)
N(1)-Cr(1)-C(10)-B(1)	-28.8(2)
N(1)-Si(1)-C(13)-C(16)	-59.0(4)
C(11)-Si(1)-C(13)-C(16)	-179.0(3)
C(12)-Si(1)-C(13)-C(16)	57.8(4)
N(1)-Si(1)-C(13)-C(15)	-179.0(3)
C(11)-Si(1)-C(13)-C(15)	61.0(4)
C(12)-Si(1)-C(13)-C(15)	-62.2(4)
N(1)-Si(1)-C(13)-C(14)	61.9(4)
C(11)-Si(1)-C(13)-C(14)	-58.1(4)
C(12)-Si(1)-C(13)-C(14)	178.7(3)
N(1)-B(1)-C(17)-C(18)	160(3)
C(10)-B(1)-C(17)-C(18)	-20(3)
Cr(1)-B(1)-C(17)-C(18)	-109(3)
B(1)-C(17)-C(18)-B(2)	-44(5)
N(2)-B(2)-C(18)-C(17)	153(3)
C(22)-B(2)-C(18)-C(17)	-26(3)
Cr(2)-B(2)-C(18)-C(17)	-116(3)
B(2)-N(2)-C(19)-C(20)	-1.0(7)
Si(2)-N(2)-C(19)-C(20)	-177.3(4)
Cr(2)-N(2)-C(19)-C(20)	58.0(4)

B(2)-N(2)-C(19)-Cr(2)	-59.0(4)
Si(2)-N(2)-C(19)-Cr(2)	124.7(2)
C(4)-Cr(2)-C(19)-C(20)	-151.5(3)
C(5)-Cr(2)-C(19)-C(20)	32.1(4)
C(6)-Cr(2)-C(19)-C(20)	118.7(3)
N(2)-Cr(2)-C(19)-C(20)	-132.0(4)
C(21)-Cr(2)-C(19)-C(20)	-27.5(3)
C(22)-Cr(2)-C(19)-C(20)	-63.2(3)
B(2)-Cr(2)-C(19)-C(20)	-101.0(3)
C(4)-Cr(2)-C(19)-N(2)	-19.5(4)
C(5)-Cr(2)-C(19)-N(2)	164.1(3)
C(6)-Cr(2)-C(19)-N(2)	-109.3(3)
C(20)-Cr(2)-C(19)-N(2)	132.0(4)
C(21)-Cr(2)-C(19)-N(2)	104.6(3)
C(22)-Cr(2)-C(19)-N(2)	68.9(3)
B(2)-Cr(2)-C(19)-N(2)	31.0(2)
N(2)-C(19)-C(20)-C(21)	-6.3(7)
Cr(2)-C(19)-C(20)-C(21)	51.5(4)
N(2)-C(19)-C(20)-Cr(2)	-57.8(4)
C(4)-Cr(2)-C(20)-C(19)	81.1(7)
C(5)-Cr(2)-C(20)-C(19)	-157.1(3)
C(6)-Cr(2)-C(20)-C(19)	-67.1(3)
N(2)-Cr(2)-C(20)-C(19)	29.3(3)
C(21)-Cr(2)-C(20)-C(19)	135.0(4)
C(22)-Cr(2)-C(20)-C(19)	105.7(3)
B(2)-Cr(2)-C(20)-C(19)	67.4(3)
C(4)-Cr(2)-C(20)-C(21)	-53.8(7)
C(5)-Cr(2)-C(20)-C(21)	67.9(3)
C(6)-Cr(2)-C(20)-C(21)	158.0(3)
C(19)-Cr(2)-C(20)-C(21)	-135.0(4)
N(2)-Cr(2)-C(20)-C(21)	-105.7(3)
C(22)-Cr(2)-C(20)-C(21)	-29.2(3)
B(2)-Cr(2)-C(20)-C(21)	-67.6(3)
C(19)-C(20)-C(21)-C(22)	6.1(7)
Cr(2)-C(20)-C(21)-C(22)	56.4(4)
C(19)-C(20)-C(21)-Cr(2)	-50.3(4)
C(4)-Cr(2)-C(21)-C(22)	28.5(4)
C(5)-Cr(2)-C(21)-C(22)	114.6(3)
C(6)-Cr(2)-C(21)-C(22)	-165.6(3)
C(19)-Cr(2)-C(21)-C(22)	-103.7(3)
N(2)-Cr(2)-C(21)-C(22)	-67.3(3)
C(20)-Cr(2)-C(21)-C(22)	-131.1(4)
B(2)-Cr(2)-C(21)-C(22)	-30.3(3)
C(4)-Cr(2)-C(21)-C(20)	159.6(3)
C(5)-Cr(2)-C(21)-C(20)	-114.3(3)
C(6)-Cr(2)-C(21)-C(20)	-34.5(5)
C(19)-Cr(2)-C(21)-C(20)	27.4(3)
N(2)-Cr(2)-C(21)-C(20)	63.9(3)
C(22)-Cr(2)-C(21)-C(20)	131.1(4)
B(2)-Cr(2)-C(21)-C(20)	100.8(3)
C(20)-C(21)-C(22)-B(2)	1.1(7)
Cr(2)-C(21)-C(22)-B(2)	56.7(4)
C(20)-C(21)-C(22)-Cr(2)	-55.6(4)

N(2)-B(2)-C(22)-C(21)	-7.8(7)
C(18)-B(2)-C(22)-C(21)	171.7(4)
Cr(2)-B(2)-C(22)-C(21)	-55.3(4)
N(2)-B(2)-C(22)-Cr(2)	47.6(4)
C(18)-B(2)-C(22)-Cr(2)	-133.0(4)
C(4)-Cr(2)-C(22)-C(21)	-158.2(3)
C(5)-Cr(2)-C(22)-C(21)	-67.5(3)
C(6)-Cr(2)-C(22)-C(21)	77.5(13)
C(19)-Cr(2)-C(22)-C(21)	65.8(3)
N(2)-Cr(2)-C(22)-C(21)	103.0(3)
C(20)-Cr(2)-C(22)-C(21)	29.8(3)
B(2)-Cr(2)-C(22)-C(21)	131.4(4)
C(4)-Cr(2)-C(22)-B(2)	70.4(3)
C(5)-Cr(2)-C(22)-B(2)	161.1(3)
C(6)-Cr(2)-C(22)-B(2)	-53.9(13)
C(19)-Cr(2)-C(22)-B(2)	-65.6(3)
N(2)-Cr(2)-C(22)-B(2)	-28.3(3)
C(20)-Cr(2)-C(22)-B(2)	-101.6(3)
C(21)-Cr(2)-C(22)-B(2)	-131.4(4)
N(2)-Si(2)-C(25)-C(26)	53.0(4)
C(23)-Si(2)-C(25)-C(26)	-67.6(4)
C(24)-Si(2)-C(25)-C(26)	170.5(4)
N(2)-Si(2)-C(25)-C(28)	-68.5(4)
C(23)-Si(2)-C(25)-C(28)	170.9(4)
C(24)-Si(2)-C(25)-C(28)	48.9(5)
N(2)-Si(2)-C(25)-C(27)	173.0(3)
C(23)-Si(2)-C(25)-C(27)	52.4(4)
C(24)-Si(2)-C(25)-C(27)	-69.5(4)

Symmetry transformations used to generate equivalent atoms:

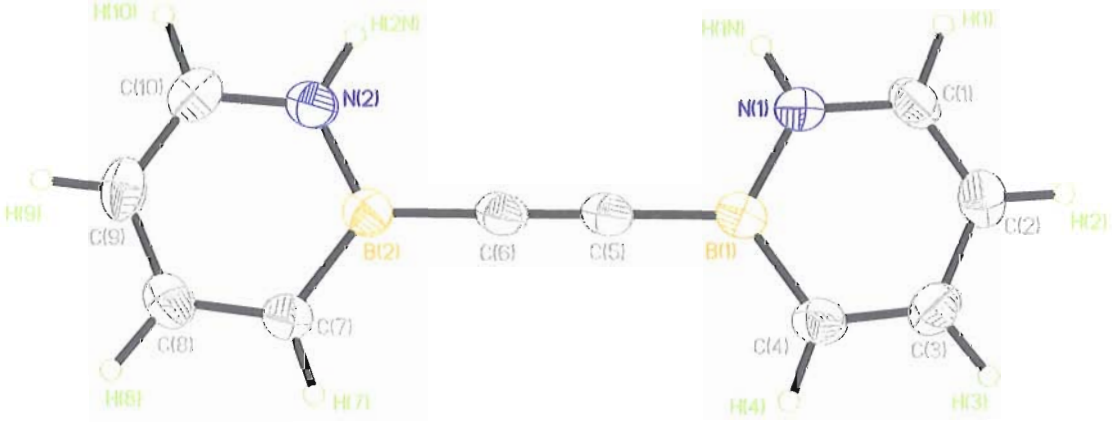

Figure 4. ORTEP illustration of **2**, with thermal ellipsoids drawn at the 35% probability level.

X-ray Crystal Structure Determination. Crystals of **2** suitable for X-ray diffraction were obtained by evaporation of a solution of **2** in Et_2O.

Diffraction intensity data were collected with a Bruker Smart Apex CCD diffractometer at 173(2) K using MoKα - radiation (0.71073 Å). The structure was solved using direct methods, completed by subsequent difference Fourier syntheses, and refined by full matrix least-squares procedures on F^2. All non-H atoms were refined with anisotropic thermal parameters. H atoms were found on the residual density map and refined with isotropic thermal parameters. The Flack parameter is 0.00(8). All software and sources scattering factors are contained in the SHELXTL (6.10) program package (G.Sheldrick, Bruker XRD, Madison, WI). Crystallographic data and some details of data collection and crystal structure refinement for $C_{10}H_{10}B_2N_2$ are given in the following tables.

Table 19. Crystal data and structure refinement for **2** (liu60).

Identification code	liu60	
Empirical formula	$C_{10}\,H_{10}\,B_2\,N_2$	
Formula weight	179.82	
Temperature	173(2) K	
Wavelength	0.71073 Å	
Crystal system	Orthorhombic	
Space group	Pbcn	
Unit cell dimensions	a = 19.076(6) Å	α= 90°.
	b = 9.301(3) Å	β= 90°.
	c = 10.997(3) Å	γ = 90°.
Volume	1951.1(10) $Å^3$	
Z	8	
Density (calculated)	1.224 Mg/m^3	
Absorption coefficient	0.071 mm^{-1}	

F(000)	752
Crystal size	0.34 x 0.16 x 0.12 mm^3
Theta range for data collection	2.14 to 27.00°.
Index ranges	-24<=h<=24, -11<=k<=11, -13<=l<=12
Reflections collected	9364
Independent reflections	2125 [R(int) = 0.0438]
Completeness to theta = 27.00°	99.6 %
Absorption correction	Semi-empirical from equivalents
Max. and min. transmission	0.9915 and 0.9762
Refinement method	Full-matrix least-squares on F^2
Data / restraints / parameters	2125 / 0 / 167
Goodness-of-fit on F^2	1.034
Final R indices [I>2sigma(I)]	R1 = 0.0463, wR2 = 0.1012
R indices (all data)	R1 = 0.0743, wR2 = 0.1157
Largest diff. peak and hole	0.170 and -0.151 $e.Å^{-3}$

Table 20. Atomic coordinates (x 10^4) and equivalent isotropic displacement parameters ($Å^2$x 10^3) for liu60. U(eq) is defined as one third of the trace of the orthogonalized U^{ij} tensor.

	x	y	z	U(eq)
N(1)	3774(1)	901(2)	1950(1)	35(1)
N(2)	5752(1)	-3060(2)	3802(1)	36(1)
B(1)	3698(1)	407(2)	3169(2)	31(1)
B(2)	5190(1)	-2612(2)	4578(2)	31(1)
C(1)	3358(1)	1931(2)	1452(2)	40(1)
C(2)	2829(1)	2524(2)	2098(2)	41(1)
C(3)	2697(1)	2082(2)	3305(2)	41(1)
C(4)	3096(1)	1060(2)	3855(2)	37(1)
C(5)	4221(1)	-706(2)	3669(1)	34(1)
C(6)	4645(1)	-1550(2)	4070(1)	34(1)
C(7)	5196(1)	-3249(2)	5831(2)	35(1)
C(8)	5707(1)	-4201(2)	6136(2)	39(1)
C(9)	6235(1)	-4587(2)	5302(2)	41(1)
C(10)	6253(1)	-4018(2)	4164(2)	40(1)

Table 21. Bond lengths [Å] and angles [°] for liu60.

N(1)-C(1)	1.359(2)
N(1)-B(1)	1.425(2)
N(2)-C(10)	1.367(2)
N(2)-B(2)	1.431(2)
B(1)-C(4)	1.502(3)
B(1)-C(5)	1.539(3)

B(2)-C(7)	1.500(2)
B(2)-C(6)	1.539(2)
C(1)-C(2)	1.352(3)
C(2)-C(3)	1.413(3)
C(3)-C(4)	1.360(2)
C(5)-C(6)	1.210(2)
C(7)-C(8)	1.359(2)
C(8)-C(9)	1.410(3)
C(9)-C(10)	1.359(3)
C(1)-N(1)-B(1)	123.22(16)
C(10)-N(2)-B(2)	122.66(15)
N(1)-B(1)-C(4)	114.79(15)
N(1)-B(1)-C(5)	119.16(15)
C(4)-B(1)-C(5)	126.04(15)
N(2)-B(2)-C(7)	115.34(16)
N(2)-B(2)-C(6)	118.39(15)
C(7)-B(2)-C(6)	126.27(16)
C(2)-C(1)-N(1)	120.72(17)
C(1)-C(2)-C(3)	120.60(17)
C(4)-C(3)-C(2)	121.37(17)
C(3)-C(4)-B(1)	119.24(16)
C(6)-C(5)-B(1)	178.17(18)
C(5)-C(6)-B(2)	179.45(18)
C(8)-C(7)-B(2)	119.27(17)
C(7)-C(8)-C(9)	121.25(17)
C(10)-C(9)-C(8)	121.18(17)
C(9)-C(10)-N(2)	120.30(17)

Symmetry transformations used to generate equivalent atoms:

Table 22. Anisotropic displacement parameters ($Å^2 x\ 10^3$)for liu60. The anisotropic displacement factor exponent takes the form: $-2\pi^2[\ h^2a^{*2}U^{11} + ... + 2\ h\ k\ a^*\ b^*\ U^{12}\ ]$

	U^{11}	U^{22}	U^{33}	U^{23}	U^{13}	U^{12}
N(1)	38(1)	39(1)	28(1)	0(1)	4(1)	3(1)
N(2)	41(1)	37(1)	30(1)	0(1)	2(1)	-1(1)
B(1)	34(1)	31(1)	28(1)	0(1)	0(1)	-5(1)
B(2)	36(1)	29(1)	30(1)	-2(1)	-2(1)	-2(1)
C(1)	45(1)	46(1)	29(1)	7(1)	-4(1)	1(1)
C(2)	38(1)	40(1)	45(1)	8(1)	-6(1)	3(1)
C(3)	34(1)	42(1)	47(1)	1(1)	7(1)	4(1)
C(4)	40(1)	39(1)	32(1)	3(1)	6(1)	-2(1)
C(5)	40(1)	36(1)	26(1)	-1(1)	4(1)	-1(1)
C(6)	43(1)	35(1)	24(1)	-2(1)	2(1)	0(1)
C(7)	39(1)	36(1)	29(1)	-1(1)	1(1)	1(1)
C(8)	46(1)	38(1)	34(1)	3(1)	-8(1)	-1(1)
C(9)	35(1)	36(1)	53(1)	-2(1)	-12(1)	5(1)
C(10)	34(1)	38(1)	46(1)	-7(1)	2(1)	0(1)

Table 23. Hydrogen coordinates (x 10^4) and isotropic displacement parameters ($Å^2 x\ 10^3$) for liu60.

	x	y	z	U(eq)

H(1N)	4117(10)	596(19)	1497(17)	42(5)
H(2N)	5797(10)	-2700(20)	2985(19)	56(6)
H(1)	3465(9)	2187(19)	586(18)	53(5)
H(2)	2539(10)	3290(20)	1738(17)	54(5)
H(3)	2307(10)	2560(19)	3723(17)	46(5)
H(4)	2994(10)	819(18)	4694(17)	48(5)
H(7)	4856(10)	-3024(19)	6422(18)	50(5)
H(8)	5720(10)	-4656(19)	6964(17)	51(5)
H(9)	6606(9)	-5242(19)	5534(15)	42(5)
H(10)	6624(9)	-4290(18)	3529(17)	49(5)

Table 24. Torsion angles [°] for liu60.

C(1)-N(1)-B(1)-C(4)	2.9(2)
C(1)-N(1)-B(1)-C(5)	-176.74(15)
C(10)-N(2)-B(2)-C(7)	1.0(2)
C(10)-N(2)-B(2)-C(6)	-178.84(15)
B(1)-N(1)-C(1)-C(2)	-1.6(3)
N(1)-C(1)-C(2)-C(3)	-0.2(3)
C(1)-C(2)-C(3)-C(4)	0.5(3)
C(2)-C(3)-C(4)-B(1)	1.0(3)
N(1)-B(1)-C(4)-C(3)	-2.6(2)
C(5)-B(1)-C(4)-C(3)	177.05(16)
N(1)-B(1)-C(5)-C(6)	83(5)
C(4)-B(1)-C(5)-C(6)	-96(5)
B(1)-C(5)-C(6)-B(2)	-18(22)
N(2)-B(2)-C(6)-C(5)	-64(19)
C(7)-B(2)-C(6)-C(5)	116(19)
N(2)-B(2)-C(7)-C(8)	-1.3(2)
C(6)-B(2)-C(7)-C(8)	178.56(15)
B(2)-C(7)-C(8)-C(9)	0.7(3)
C(7)-C(8)-C(9)-C(10)	0.2(3)
C(8)-C(9)-C(10)-N(2)	-0.5(3)
B(2)-N(2)-C(10)-C(9)	-0.1(3)

Symmetry transformations used to generate equivalent atoms:

Additional photophysical data for 1 and 2.

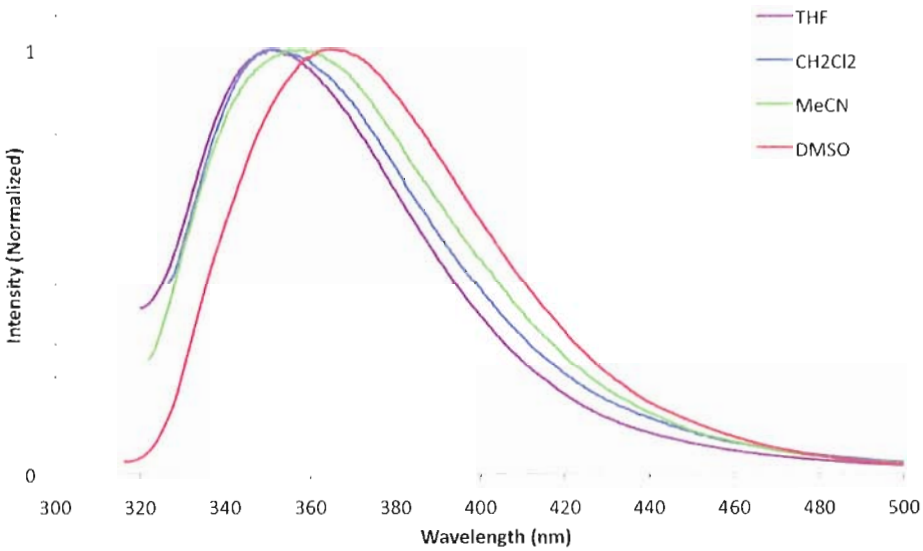

Figure 5. Normalized emission spectra of **1** in various solvents.

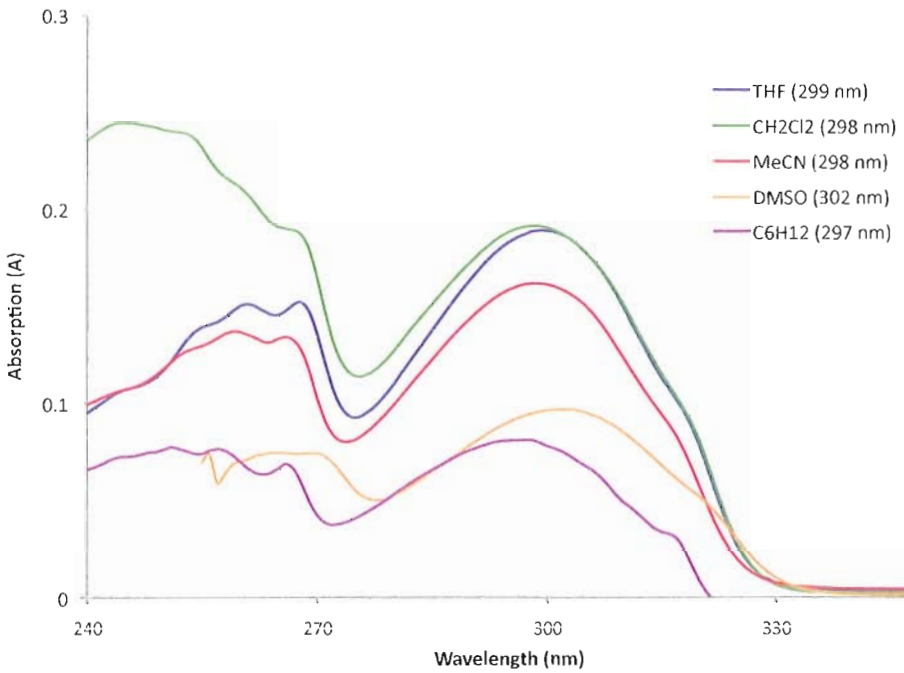

Figure 6. Absorption spectra of **1** in various solvents (10^{-5} M in each solvent). The trace for DMSO (orange) is cut off at 255 nm for clarity.

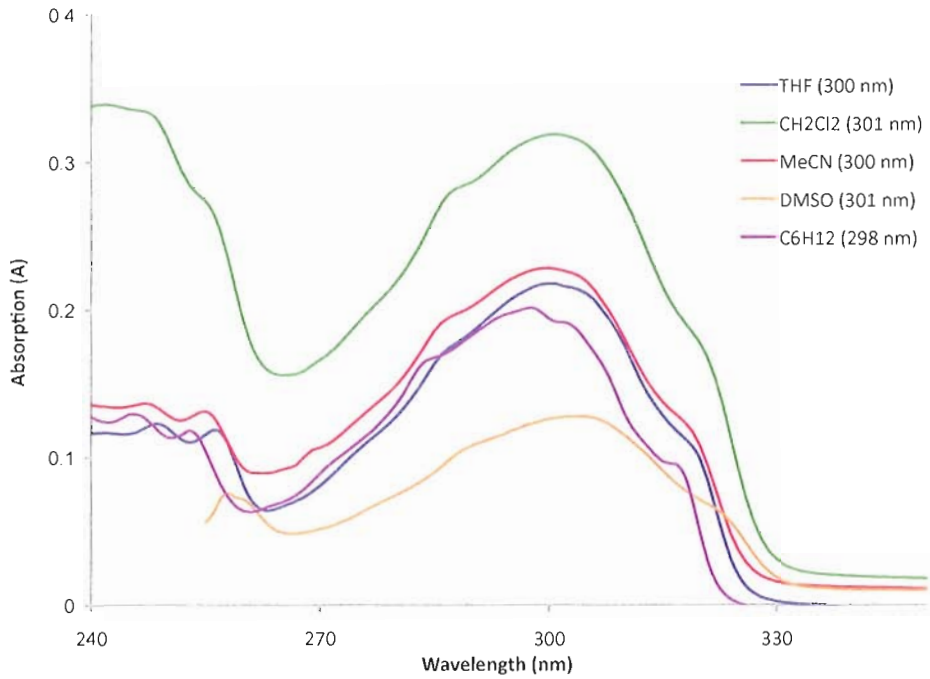

Figure 7. Absorption spectra of **2** in various solvents (10^{-5} M in each solvent). The trace for DMSO (orange) is cut off at 255 nm for clarity.

C.2.3. Supplemental information for Chapter IV, section 4.4

Synthesis of compound 13. A solution of 1,2-azaborine **3** (2.0 g, 8.79 mmol in 60 mL CH_2Cl_2) was cooled to –20 °C, to which a solution of Br_2 (0.48 mL, 9.31 mmol in 60 mL CH_2Cl_2) was added dropwise. The reaction was allowed to warm to rt and was stirred for 30 min. Solvent was removed under reduced pressure and 30 mL pentane was added. Solids were filtered through an Acrodisc, and the remaining solvent was removed under reduced pressure. Vacuum distillation (62-65 °C, 120 mT) provided brominated **13** as a clear, colorless liquid (1.63 g, 61%).

^{1}H NMR (300 MHz, CH_2Cl_2): δ 7.87 (d, $^3J_{HH}$ = 7.0 Hz, 1H), 7.27 (d, $^3J_{HH}$ = 6.7 Hz, 1H), 6.22 (app t, $^3J_{HH}$ = 6.7 Hz, 1H), 0.94 (s, 9H), 0.54 (s, 6H). ^{13}C NMR (75.4 MHz, CD_2Cl_2): δ 147.0, 139.0, 111.8, 26.9, 19.7, –1.3. ^{11}B NMR (192.5 MHz, CD_2Cl_2): δ 37.4.

FTIR (thin film) 3098, 2931, 2860, 2280, 1685, 1601, 1495, 1471, 1441, 1393, 1364, 1336, 1264, 1210, 1192, 1126, 1090, 999, 938, 823, 764, 714, 657, 577, 499, 443 cm^{-1}. HRMS (EI) calcd for $C_{10}H_{18}BNSiCl^{81}Br(M^+)$ 307.01530, found 307.01500.

Compound 14. A solution of phenylethynylmagnesium bromide (1M in THF; 2.88 mL, 2.88 mmol) was added to a solution of **13** (0.800 g, 2.61 mmol in 10 mL THF) at rt, and was stirred for 16 h. Solvents were removed and column chromatography was performed (Et_2O/pentane), which gave compound **14** as a white, crystalline solid (0.738 g, 76%).

^1H NMR (300 MHz, CH_2Cl_2): δ 7.95 (d, $^3J_{HH}$ = 7.3 Hz, 1H), 7.60 (m, 2H), 7.37 (m, 4H), 6.31 (app t, $^3J_{HH}$ = 7.0 Hz, 1H), 1.00 (s, 9H), 0.67 (s, 6H). ^{13}C NMR (125.8 MHz, CD_2Cl_2): δ 145.3, 138.8, 132.2, 132.0, 129.3, 129.0, 124.3, 112.5, 110.8, 97 (br), 27.0, 19.7, –1.8. ^{11}B NMR (192.5 MHz, CD_2Cl_2): δ 28.5. FTIR (thin film) 2953, 2927, 2881, 2856, 2182, 1595, 1490, 1470, 1441, 1341, 1354, 1273, 1254, 1181, 1132, 1000, 845, 757, 678 cm^{-1}. HRMS (EI) calcd for $C_{18}H_{23}BNSi^{81}Br(M^+)$ 371.08762, found 371.08818.

Compound 15. Method A in Chapter 4, Scheme 4: A flask was charged with CuI (0.005 g, 0.027 mmol), $Pd(Cl)_2(PPh_3)_2$ (0.009 g, 0.0134 mmol), phenylacetylene (0.069 g, 0.672 mmol), 1,2-azaborine **14** (0.050 g, 0.134 mmol), NEt_3 (0.1 mL), and THF (3 mL). The reaction was stirred at rt for 24 h, whereupon solvents were removed under reduced pressure and the crude mixture was redissolved in CD_2Cl_2. ^1H NMR analysis indicated diyne **15** was formed in a 1:3 ratio relative to unreacted bromide **14**.

Method B in Chapter 4, Scheme 4: A vial was charged with CuI (0.008 g, 0.04

mmol), $Pd(Cl)_2(PhCN)_2$ (0.015 g, 0.04 mmol), $P(^tBu)_3$ (0.016 g, 0.08 mmol), phenylacetylene (0.178 g, 1.74 mmol), 1,2-azaborine **14** (0.500 g, 1.34 mmol), NEt_3 (0.5 mL), and THF (10 mL). The reaction was stirred at rt for 24 h, whereupon solvents were removed under reduced pressure and the crude mixture was redissolved in CH_2Cl_2. The solution was passed through a dry plug of silica and flushed with CH_2Cl_2. The solvent was removed under reduced pressure and column chromatography was performed (Et_2O/pentane), which provided **15** as a viscous, brown oil (0.450 g, 85%).

^1H NMR (300 MHz, CH_2Cl_2): δ 7.83 (d, $^3J_{HH}$ = 6.7 Hz, 1H), 7.3-7.6 (m, 11H), 6.46 (app t, $^3J_{HH}$ = 7.1 Hz, 1H), 1.00 (s, 9H), 0.67 (s, 6H). ^{13}C NMR (125.8 MHz, CD_2Cl_2): δ 146.8, 139.9, 132.0, 131.9, 129.1, 129.0, 128.8, 128.0, 125.3, 124.5, 112.6, 110.4, 106.5, 93.9, 26.9, 19.6, –1.8. ^{11}B NMR (192.5 MHz, CD_2Cl_2): δ 30.0. FTIR (thin film) 3061, 2955, 2928, 2897, 2858, 2179, 1597, 1585, 1513, 1489, 1470, 1442, 1342, 1251, 1185, 1148, 1078, 1043, 844, 812, 756, 690 cm^{-1}.

Compound 16. A vial was charged with diyne **15** (0.238 g, 0.605 mmol), $(MeCN)_3Cr(CO)_3$ (0.282 g, 1.09 mmol), and THF (5 mL), and was stirred at rt for 16 h. Solvents were removed and column chromatography (Et_2O/pentane) was performed, which gave complex **16** as a red, crystalline solid (0.138 g, 43%).

^1H NMR (300 MHz, CH_2Cl_2): δ 7.3-7.6 (m, 10H), 6.30 (d, $^3J_{HH}$ = 6.5 Hz, 1H), 6.05 (d, $^3J_{HH}$ = 4.4 Hz, 1H), 5.27 (app t, $^3J_{HH}$ = 6.2 Hz, 1H), 1.02 (s, 9H), 0.78 (s, 3H), 0.46 (s, 3H). ^{11}B NMR (96.3 MHz, CD_2Cl_2): δ 14.9.

Compound 12. A solution of complex **16** (0.212 g, 0.40 mmol in 4 mL THF) was cooled to –20 °C, to which was added a solution of HF-pyridine (0.5 M in THF; 0.88 mL,

0.44 mmol). The reaction was allowed to warm to rt and was stirred for 1 h. Solvents were removed and the crude mixture was redissolved in MeCN (5 mL). The solution was stirred at rt for 12 h, whereupon approximately one-half of the solvent was removed under reduced pressure. The remaining solution was passed through a dry plug of silica gel and flushed with Et_2O. Solvents were removed and column chromatography was performed (Et_2O/pentane), which provided diyne **12** as a light brown oil, which crystallized when stored at –20 °C (0.021 g, 19% from complex **16**).

^{1}H NMR (300 MHz, CH_2Cl_2): δ 8.58 (br, 1H), 7.89 (d, $^3J_{HH}$ = 7.1 Hz, 1H), 7.3-7.6 (m, 11H), 6.47 (app t, $^3J_{HH}$ = 7.0 Hz, 1H). ^{13}C NMR (125.8 MHz, CD_2Cl_2): δ 147.6, 135.2, 132.6, 131.9, 129.3, 129.0, 128.9, 128.2, 111.8. ^{11}B NMR (192.5 MHz, CD_2Cl_2): δ 26.9. FTIR (thin film) 3366, 3079, 3018, 2927, 2179, 1599, 1535, 1489, 1442, 1301, 1228, 1028, 912, 753, 685 cm^{-1}. HRMS (EI) calcd for $C_{20}H_{14}BN$ (M^+) 279.12193, found 279.12247.

Compound 20. A solution of ethylmagnesium bromide (1.0 M in THF; 0.98 mL, 0.98 mmol) was added to a solution of 4-(dibutylamino)phenylacetylene (0.225 g, 0.98 mmol in 5 mL THF) at rt. Gas evolution was observed, which ceased after approximately 30 min. The reaction was stirred an additional 2 h, and this solution was then added dropwise to a stirring solution of **13** (0.300 g, 0.98 mmol in 5 mL THF) at rt. Solvent was removed and column chromatography was performed (CH_2Cl_2/Et_2O/pentane), which gave alkyne **20** as a yellow oil (0.318 g, 65%).

^{1}H NMR (300 MHz, CH_2Cl_2): δ 7.86 (d, $^3J_{HH}$ = 7.3 Hz, 1H), 7.39 (d, $^3J_{HH}$ = 4.0 Hz, 2H), 7.31 (app t, $^3J_{HH}$ = 9.1 Hz, 1H), 6.60 (d, $^3J_{HH}$ = 5.0 Hz, 2H), 6.22 (app t, $^3J_{HH}$ =

6.7 Hz, 1H), 3.30 (t, $^3J_{HH}$ = 7.6 Hz, 4H), 1.60 (m, 4H), 1.39 (m, 4H), 0.98 (m, 15H), 0.64 (s, 6H). ^{13}C NMR (125.8 MHz, CD_2Cl_2): δ 149.0, 144.8, 138.6, 133.8, 133.5, 113.1, 111.8, 109.5, 94 (br), 85.5, 74.9, 51.2, 29.9, 27.0, 20.9, 19.7, 14.4, –1.7. ^{11}B NMR (192.5 MHz, CD_2Cl_2): δ 28.0. FTIR (thin film) 3308, 3093, 2956, 2930, 2859, 2166, 1606, 1518, 1490, 1469, 1343, 1288, 1260, 1222, 1172, 1130, 1109, 1040, 1001, 926, 844, 812, 788, 763, 680 cm^{-1}.

Compound 21. A vial was charged with CuI (0.013 g, 0.07 mmol), $Pd(Cl)_2(PhCN)_2$ (0.027 g, 0.07 mmol), $P(^tBu)_3$ (0.028 g, 0.014 mmol), 4-cyanophenylacetylene (0.194 g, 1.53 mmol), 1,2-azaborine **20** (0.695 g, 1.39 mmol), NEt_3 (0.5 mL), and THF (5 mL). The reaction was stirred at rt for 48 h, whereupon solvents were removed under reduced pressure and the crude mixture was redissolved in CH_2Cl_2. The solution was passed through a dry plug of silica and flushed with CH_2Cl_2. The solvent was removed under reduced pressure and column chromatography (Et_2O/pentane) was performed, which provided **21** as a an orange-red, crystalline solid (0.454 g, 60%).

^{1}H NMR (300 MHz, CH_2Cl_2): δ 7.82 (d, $^3J_{HH}$ = 7.1 Hz, 1H), 7.59 (s, 4H), 7.41 (d, $^3J_{HH}$ = 6.5 Hz, 1H), 7.33 (d, $^3J_{HH}$ = 7.0 Hz, 2H), 6.60 (d, $^3J_{HH}$ = 7.0 Hz, 2H), 6.40 (app t, $^3J_{HH}$ = 6.7 Hz, 1H), 3.30 (t, $^3J_{HH}$ = 7.6 Hz, 4H), 1.60 (m, 4H), 1.39 (m, 4H), 0.98 (m, 15H), 0.66 (s, 6H). ^{13}C NMR (125.8 MHz, CD_2Cl_2): δ 149.0, 147.3, 140.9, 133.4, 132.6, 132.3, 130.5, 119.4, 112.9, 112.0, 111.7, 110.9, 109.5, 99.4, 94 (br), 92.3, 51.2, 29.9, 27.0,, 20.9, 19.6, 14.3, –1.8. ^{11}B NMR (192.5 MHz, CD_2Cl_2): δ 29.7. FTIR (thin film) 3068, 3042, 2956, 2930, 2859, 2225, 2204, 2171, 1605, 1587, 1517, 1495, 1469, 1444, 1343, 1288, 1251, 1288, 1251, 1222, 1175, 1145, 1110, 1079, 1042, 1004, 927, 881, 842, 812, 789,

730, 691 cm^{-1}.

Compound 17. A solution of TBAF (0.1 M in THF; 0.5 mL, 0.05 mmol) was added to a stirred solution of diyne **21** (0.025 g, 0.046 mmol in 3 mL THF) at rt. The reaction was stirred for 20 min., whereupon the solution was passed through a dry silica plug and flushed with THF. The solvent was removed, and column chromatography was performed (Et_2O/pentane), which provided **17** as a yellow solid (0.008 g, 40%).

^1H NMR (300 MHz, CH_2Cl_2): δ 8.50 (br, 1H), 7.88 (d, $^3J_{HH}$ = 7.0 Hz, 1H), 7.62 (s, 4H), 7.36 (m, 3H), 6.58 (d, $^3J_{HH}$ = 7.0 Hz, 2H), 6.40 (app t, $^3J_{HH}$ = 7.0 Hz, 1H), 3.30 (t, $^3J_{HH}$ = 7.6 Hz, 4H), 1.60 (m, 4H), 1.39 (m, 4H), 0.98 (t, $^3J_{HH}$ = 7.3 Hz, 6H). ^{11}B NMR (96.3 MHz, CD_2Cl_2): δ 27.3.

Compound 23. A solution of ethylmagnesium bromide (1.0 M in THF; 0.98 mL, 0.98 mmol) was added to a solution of 4-cyanophenylacetylene (0.125 g, 0.98 mmol in 5 mL THF) at rt. Gas evolution was observed, which ceased after approximately 30 min. The reaction was stirred an additional 1 h, and this solution was then added dropwise to a stirring solution of **13** (0.300 g, 0.98 mmol in 10 mL THF) at rt. Solvent was removed and column chromatography was performed (CH_2Cl_2/Et_2O/pentane), which gave alkyne **23** as a yellow solid (0.268 g, 69%).

^1H NMR (300 MHz, CH_2Cl_2): δ 7.92 (d, $^3J_{HH}$ = 7.3 Hz, 1H), 7.62 (s, 4H), 7.37 (d, $^3J_{HH}$ = 6.2 Hz, 1H), 6.33 (app t, $^3J_{HH}$ = 7.3 Hz, 1H), 0.96 (s, 9H), 0.62 (s, 6H). ^{13}C NMR (125.8 MHz, CD_2Cl_2): δ 145.6, 138.9, 133.2, 132.7, 132.5, 128.8, 119.0, 113, 112.5, 108.5, 81.8, 26.8, 19.6, –1.9. ^{11}B NMR (192.5 MHz, CD_2Cl_2): δ 27.6. FTIR (thin film) 3237, 2954, 2932, 2886, 2859, 2224, 2188, 1598, 1490, 1471, 1445, 1404, 1344, 1266,

1257, 1173, 1133, 1102, 1036, 1003, 936, 826, 812, 767, 716, 680, 644 cm^{-1}.

Compound 25. A vial was charged with CuI (0.009 g, 0.049 mmol), $Pd(Cl)_2(PhCN)_2$ (0.019 g, 0.049 mmol), $P(^tBu)_3$ (0.020 g, 0.100 mmol), 4-(dibutylamino)phenylacetylene (0.146 g, 0.64 mmol), 1,2-azaborine **13** (0.150 g, 0.49 mmol), NEt_3 (0.5 mL), and THF (5 mL). The reaction was stirred at rt for 16 h, whereupon solvents were removed. Pentane (8 mL) was added, and solids were filtered through an Acrodisc. Compound **25** was not purified further.

^1H NMR (300 MHz, CH_2Cl_2): δ 7.65 (app t, $^3J_{HH}$ = 7.0 Hz, 1H), 7.1 (m, 3H), 6.58 (d, $^3J_{HH}$ = 7.0 Hz, 2H), 6.37 (app t, $^3J_{HH}$ = 6.7 Hz, 1H), 3.25 (t, $^3J_{HH}$ = 7.6 Hz, 4H), 1.5 (m, 8H), 0.98 (m, 15H), 0.58 (s, 6H). ^{11}B NMR (96.3 MHz, CD_2Cl_2): δ 38.2.

Compound 24. A solution of ethylmagnesium bromide (1.0 M in THF; 0.63 mL, 0.63 mmol) was added to a stirred solution of 4-cyanophenylacetylene (0.081 g, 0.63 mmol). The solution was stirred for 1 h at rt and was then added to a solution of **25** (assumed 0.49 mmol from previous step) in THF (6 mL). The reaction was stirred at 2 h, whereupon solvents were removed and column chromatography (Et_2O/pentane) was performed, which gave **24** as an orange-red solid (0.117 g, 44%).

^1H NMR (300 MHz, CH_2Cl_2): δ 7.78 (d, $^3J_{HH}$ = 7.0 Hz, 1H), 7.62 (s, 4H), 7.38 (d, $^3J_{HH}$ = 6.7 Hz, 1H), 7.23 (d, $^3J_{HH}$ = 7.0 Hz, 2H), 6.55 (d, $^3J_{HH}$ = 7.0 Hz, 2H), 6.49 (app t, $^3J_{HH}$ = 6.7 Hz, 1H), 3.25 (t, $^3J_{HH}$ = 7.6 Hz, 4H), 1.57 (m, 4H), 1.39 (m, 4H), 0.98 (m, 15H), 0.62 (s, 6H). ^{13}C NMR (75.4 MHz, CD_2Cl_2): δ 148.2, 145.6, 138.8, 133.0, 132.7, 132.5, 119.1, 113.1, 112.1, 111.7, 110.4, 108.2, 95.8, 90.0, 51.1, 29.9, 26.8, 20.8, 19.6, 14.3, –1.9. ^{11}B NMR (96.3 MHz, CD_2Cl_2): δ 30.9. FTIR (thin film) 2956, 2930, 2859, 2227,

2178, 1605, 1586, 1520, 1507, 1469, 1443, 1343, 1251, 1221, 1146, 1078, 1043, 1004, 927, 842, 812, 789, 746, 692, 556, 529 cm^{-1}. HRMS (EI) calcd for $C_{35}H_{44}BN_3Si(M^+)$ 545.33976, found 545.33853.

Compound 24 from 23. Method A: A vial was charged with CuI (0.010 g, 0.050 mmol), $Pd(Cl)_2(PhCN)_2$ (0.020 g, 0.050 mmol), $P(^tBu)_3$ (0.022 g, 0.108 mmol), 4-(dibutylamino)phenylacetylene (0.150 g, 0.655 mmol), 1,2-azaborine **13** (0.150 g, 0.49 mmol), NEt_3 (0.5 mL), and THF (5 mL). The reaction was stirred at rt for 48 h, and then heated to 60 °C for 24 h. Solvents were then removed, whereupon ^1H NMR analysis indicated **24** was formed in a 40:60 ratio with unreacted **23**. Compounds **23** and **24** were inseparable by column chromatography.

Method B: A solution of 4-(dibutylamino)phenylacetylene (0.127 g, 0.55 mmol in 3 mL) was cooled to –78 °C, to which was added a solution of n-BuLi (1.6 M in hexanes; 0.35 mL, 0.55 mmol). The lithiate solution was then added to a solution of $ZnCl_2$ (1.0 M in Et_2O; 0.55 mL, 0.55 mmol) at –78 °C, which was allowed to warm to rt. The zincate solution was added to a flask containing **23** (0.200 g, 0.50 mmol), $Pd(PPh_3)_4$ (0.058 g, 0.050 mmol), and THF (1 mL) at rt. The reaction was heated to 80 °C for 48 h, whereupon solvents were removed, after which column chromatography (Et_2O/pentane) provided **24** (0.060 g, 22%).

Compound 18. A vial was charged with diyne 24 (0.064 g, 0.117 mmol), (MeCN)3Cr(CO)3 (0.152 g, 0.587 mmol), and THF (12 mL), and was stirred at rt for 16 h. The reaction was cooled to –20 °C, whereupon a solution of HF-pyridine (0.5 M in THF; 0.235 mL, 0.117 mmol) was added dropwise. The vial was allowed to warm to rt and was

stirred for 1 h. Solvents were then removed and the crude material was redissolved in MeCN (3 mL) and stirred at rt for 3 h. Approximately one-half of the solvent was removed and column chromatography performed, which gave diyne 18 as a light yellow solid (0.003 g, 6% from **24**).

^{1}H NMR (300 MHz, CH_2Cl_2): δ 8.55 (br, 1H), 7.81 (d, $^3J_{HH}$ = 5.8 Hz, 1H), 7.65 (s, 4H), 7.35 (app t, $^3J_{HH}$ = 7.9 Hz, 1H), 7.28 (d, $^3J_{HH}$ = 7.0 Hz, 2H), 6.56 (d, $^3J_{HH}$ = 7.0 Hz, 2H), 6.46 (app t, $^3J_{HH}$ = 7.0 Hz, 1H), 3.27 (t, $^3J_{HH}$ = 7.6 Hz, 4H), 1.60 (m, 4H), 1.39 (m, 4H), 0.98 (t, $^3J_{HH}$ = 7.3 Hz, 6H). ^{11}B NMR (192.5 MHz, CD_2Cl_2): δ 26.8. HRMS (EI) calcd for $C_{29}H_{30}BN_3(M^+)$ 431.25328, found 431.25011.

Compound 28. A solution of ethylmagnesium bromide (1.0 M in THF; 0.44 mL, 0.44 mmol) was added to a solution of 4-(dibutylamino)phenylacetylene (0.100 g, 0.44 mmol in 2 mL THF) at rt. Gas evolution was observed, which ceased after approximately 30 min. The reaction was stirred an additional 2 h, and this solution was then added dropwise to a stirring solution of **3** (0.100 g, 0.44 mmol in 3 mL THF) at rt. Solvent was removed and column chromatography was performed (Et_2O/pentane), which gave alkyne **28** as a yellow oil (0.145 g, 78%).

^{1}H NMR (300 MHz, CH_2Cl_2): δ 7.58 (dd, $^3J_{HH}$ = 10.9, 6.3 Hz, 1H), 7.31 (m, 3H), 6.84 (d, $^3J_{HH}$ = 11.0 Hz, 1H), 6.55 (d, $^3J_{HH}$ = 8.9 Hz, 2H), 6.32 (app t, $^3J_{HH}$ = 6.4 Hz, 1H), 3.25 (t, $^3J_{HH}$ = 7.6 Hz, 4H), 1.57 (m, 4H), 1.39 (m, 4H), 0.98 (m, 15H), 0.62 (s, 6H). ^{13}C NMR (75 MHz, CD_2Cl_2): δ 148.7, 143.5, 139.2, 133.2, 112.2, 111.7, 110.0, 109.5, 51.2, 29.9, 27.0, 20.9, 19.6, 14.3, –1.8. ^{11}B NMR (192.5 MHz, CD_2Cl_2): δ 29.0. FTIR (thin film) 2956, 2930, 2859, 2164, 1603, 1517, 1505, 1452, 1390, 1368, 1284, 1259, 1185,

1124, 1071, 987, 843, 822, 812, 785, 742, 689 cm^{-1}.

Compound 29. A solution of ethylmagnesium bromide (1.0 M in THF; 0.44 mL, 0.44 mmol) was added to a solution of 4-cyanophenylacetylene (0.056 g, 0.44 mmol in 2 mL THF) at rt. Gas evolution was observed, which ceased after approximately 30 min. The reaction was stirred an additional 1 h, and this solution was then added dropwise to a stirring solution of **3** (0.100 g, 0.44 mmol in 3 mL THF) at rt. Solvent was removed and column chromatography was performed (Et_2O/pentane), which gave alkyne **29** as a yellow solid (0.090 g, 64%).

^1H NMR (500 MHz, CH_2Cl_2): δ 7.65 (d, $^3J_{HH}$ = 7.6 Hz, 2H), 7.58 (m, 3H), 7.40 (d, $^3J_{HH}$ = 6.4 Hz, 1H), 6.92 (d, $^3J_{HH}$ = 10.9 Hz, 1H), 6.44 (app t, $^3J_{HH}$ = 6.4 Hz, 1H), 0.96 (s, 9H), 0.62 (s, 6H). ^{13}C NMR (125.8 MHz, CD_2Cl_2): δ 144.4, 139.5, 132.7, 132.3, 129.4, 119.0, 113.3, 112.0, 105.7, 26.8, 19.6, –2.0. ^{11}B NMR (192.5 MHz, CD_2Cl_2): δ 28.6. FTIR (thin film) 2955, 2929, 2884, 2858, 2228, 1602, 1505, 1464, 1470, 1451, 1392, 1354, 1273, 1253, 1197, 1125, 1072, 1018, 988, 840, 787, 747, 696 cm^{-1}.

Compound 30. A vial was charged with alkyne **28** (0.050 g, 0.119 mmol), $(MeCN)_3Cr(CO)_3$ (0.037 g, 0.143 mmol), and THF (1.5 mL), and was stirred at rt for 1 h. Solvents were then removed and column chromatography performed (Et_2O/pentane), giving complex **30** as a red, crystalline solid (0.044 g, 66%).

^1H NMR (500 MHz, CH_2Cl_2): δ 7.32 (d, $^3J_{HH}$ = 9.0 Hz, 2H), 6.58 (d, $^3J_{HH}$ = 9.0 Hz, 2H), 6.01 (m, 2H), 5.20 (app t, $^3J_{HH}$ = 6.1 Hz, 1H), 4.71 (d, $^3J_{HH}$ = 9.3 Hz, 1H), 3.29 (t, $^3J_{HH}$ = 7.6 Hz, 4H), 1.57 (m, 4H), 1.39 (m, 4H), 0.98 (m, 15H), 0.74 (s, 3H), 0.44 (s, 3H). ^{13}C NMR (75 MHz, CD_2Cl_2): δ 231.0, 149.1, 133.5, 111.7, 110.3, 108.8, 108.6, 103.9,

88.3, 83.2, 51.2, 29.9, 27.3, 20.9, 20.2, 14.3, –0.9, –3.7. ^{11}B NMR (192.5 MHz, CD_2Cl_2): δ 14.7. FTIR (thin film) 2957, 2932, 2861, 2167, 1967, 1897, 1874, 1605, 1520, 1371, 1287, 1111, 1052, 989, 813, 668 cm^{-1}.

Compound 31. A vial was charged with alkyne **29** (0.025 g, 0.080 mmol), $(MeCN)_3Cr(CO)_3$ (0.025 g, 0.095 mmol), and THF (2 mL), and was stirred at rt for 1 h. Solvents were then removed and column chromatography performed (Et_2O/pentane), giving complex **31** as a red, crystalline solid (0.028 g, 77%).

^{1}H NMR (300 MHz, CH_2Cl_2): δ 7.62 (m, 4H), 6.03 (m, 2H), 5.24 (app t, $^3J_{HH}$ = 5.9 Hz, 1H), 4.72 (d, $^3J_{HH}$ = 9.4 Hz, 1H), 0.96 (m, 9H), 0.61 (s, 3H), 0.45 (s, 3H). ^{13}C NMR (125.8 MHz, CD_2Cl_2): δ 230.4, 132.9, 132.7, 132.5, 128.3, 108.2, 103.8, 83.5, 27.0, 20.2, –1.1, –3.8. ^{11}B NMR (192.5 MHz, CD_2Cl_2): δ 13.6. FTIR (thin film) 2931, 2860, 2228, 1969, 1890, 1602, 1500, 1465, 1407, 1374, 1272, 1113, 989, 841, 807, 792, 664 cm^{-1}.

Compound 32. A solution of HF-pyridine (0.5 M in THF; 0.174 mL, 0.087 mmol) was added dropwise to a solution of complex **30** (0.044 g, 0.079 mmol in 1 mL THF) at –20 °C. The reaction was allowed to warm to rt and was stirred for 1 h, whereupon the solvent was removed and column chromatography (Et_2O/pentane) was performed, providing complex **32** as an orange-red solid (0.020 g, 57%).

^{1}H NMR (500 MHz, CH_2Cl_2): δ 7.34 (d, $^3J_{HH}$ = 9.0 Hz, 2H), 6.55 (d, $^3J_{HH}$ = 9.0 Hz, 2H), 6.15 (app t, $^3J_{HH}$ = 5.3 Hz, 1H), 5.91 (dd, $^3J_{HH}$ = 9.7, 5.8 Hz, 1H), 5.3 (br, 1H), 5.20 (app t, $^3J_{HH}$ = 5.9 Hz, 1H), 4.74 (d, $^3J_{HH}$ = 9.4 Hz, 1H), 3.29 (t, $^3J_{HH}$ = 7.6 Hz, 4H), 1.57 (m, 4H), 1.39 (m, 4H), 0.96 (t, $^3J_{HH}$ = 7.3 Hz, 6H). FTIR (thin film) 3359, 2958, 2932, 2872, 2168, 1970, 1898, 1604, 1520, 1471, 1441, 1369, 1288, 1223, 1102, 1046,

937, 815, 664, 625 cm^{-1}.

Compound 33. A solution of HF-pyridine (0.5 M in THF; 0.121 mL, 0.061 mmol) was added dropwise to a solution of complex **31** (0.025 g, 0.055 mmol in 1 mL THF) at –20 °C. The reaction was allowed to warm to rt and was stirred for 1 h, whereupon the solvent was removed and column chromatography (Et_2O/pentane) was performed, providing complex **33** as an orange-red solid (0.010 g, 53%).

^1H NMR (300 MHz, CH_2Cl_2): δ 7.64 (m, 4H), 6.19 (br app t, 1H), 5.91 (dd, $^3J_{HH}$ = 9.1, 6.1 Hz, 1H), 5.4 (br, 1H), 5.29 (app t, $^3J_{HH}$ = 5.6 Hz, 1H), 4.77 (d, $^3J_{HH}$ = 9.7 Hz, 1H). FTIR (thin film) 3356, 2230, 2073, 1969, 1889, 1472, 1266, 1178, 1105, 839, 739, 663, 628 cm^{-1}.

Compound 26. Complex **32** (0.020 g, 0.045 mmol) was dissolved in MeCN (5 mL) and stirred for 3 h at rt. Approximately one-half of the solvent was removed and column chromatography was performed (Et_2O/pentane) to give **26** as a light yellow solid (0.011 g, 79%).

^1H NMR (300 MHz, CH_2Cl_2): δ 8.31 (br, 1H), 7.76 (dd, $^3J_{HH}$ = 11.4, 6.7 Hz, 1H), 7.32 (m, 4H), 6.87 (d, $^3J_{HH}$ = 11.5 Hz, 1H), 6.55 (d, $^3J_{HH}$ = 9.1 Hz, 1H), 6.34 (app t, $^3J_{HH}$ = 6.7 Hz, 1H), 3.29 (t, $^3J_{HH}$ = 7.6 Hz, 4H), 1.59 (m, 4H), 1.39 (m, 4H), 0.96 (t, $^3J_{HH}$ = 7.3 Hz, 6H). ^{13}C NMR (125.8 MHz, CD_2Cl_2): δ 148.8, 144.6, 134.7, 133.7, 132 (br), 111.7, 111.2, 109.2, 106.6, 51.2, 29.9, 20.8, 14.3. ^{11}B NMR (192.5 MHz, CD_2Cl_2): δ 25.9. FTIR (thin film) 3376, 3074, 3028, 2957, 2931, 2871, 2165, 1606, 1533, 1518, 1460, 1420, 1402, 1369, 1350, 1286, 1222, 1187, 1123, 1105, 1075, 991, 926, 814, 733, 680 cm^{-1}.

Compound 27. Complex **33** (0.010 g, 0.0294 mmol) was dissolved in MeCN (5

mL) and stirred for 3 h at rt. Approximately one-half of the solvent was removed and column chromatography performed, which gave **27** as a light yellow solid (0.003 g, 50%).

^{1}H NMR (300 MHz, CH_2Cl_2): δ 8.49 (br, 1H), 7.76 (dd, $^{3}J_{HH}$ = 11.4, 6.7 Hz, 1H), 7.65 (s, 4H), 7.40 (app t, $^{3}J_{HH}$ = 7.6 Hz, 1H), 6.94 (d, $^{3}J_{HH}$ = 11.1 Hz, 1H), 6.47 (app t, $^{3}J_{HH}$ = 6.4 Hz, 1H). ^{13}C NMR (125.8 MHz, CD_2Cl_2): δ 145.4, 134.9, 133.0, 132.9, 132.7, 128.9, 119.0, 112.4, 112.3. ^{11}B NMR (192.5 MHz, CD_2Cl_2): δ 25.5. FTIR (thin film) 3366, 3030, 2229, 2072, 1942, 1602, 1539, 1460, 1419, 1350, 1263, 1105, 1077, 838, 735, 651 cm^{-1}.

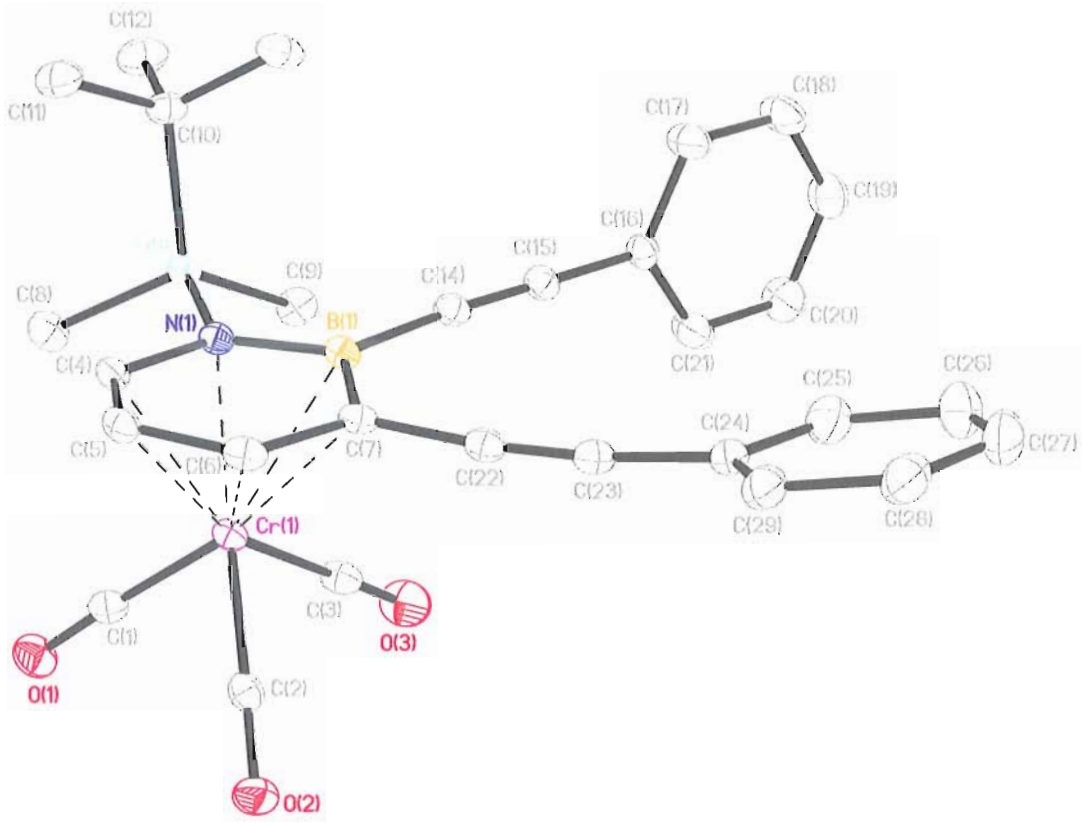

Figure 8. ORTEP illustration of **16**, with thermal ellipsoids drawn at the 35% probability level. Hydrogen atoms have been omitted for clarity.

X-ray Crystal Structure Determination. Crystals of **16** suitable for X-ray diffraction were obtained by evaporation of a solution of **16** in Et_2O.

Diffraction intensity data were collected with a Bruker Smart Apex CCD diffractometer at 173(2) K using MoKα - radiation (0.71073 Å). The structure was solved using direct methods, completed by subsequent difference Fourier syntheses, and refined by full matrix least-squares procedures on F^2. All non-H atoms were refined with anisotropic thermal parameters. H atoms were found on the residual density map and refined with isotropic thermal parameters. The Flack parameter is 0.00(8). All software and sources scattering factors are contained in the SHELXTL (6.10) program package (G.Sheldrick, Bruker XRD, Madison, WI). Crystallographic data and some details of data collection and crystal structure refinement for $C_{29}H_{28}BCrNO_3Si$ are given in the following tables.

Table 25. Crystal data and structure refinement for **18** (liu67).

Identification code	liu67	
Empirical formula	$C_{29}H_{28}BCrNO_3Si$	
Formula weight	529.42	
Temperature	173(2) K	
Wavelength	0.71073 Å	
Crystal system	Monoclinic	
Space group	P2(1)/n	
Unit cell dimensions	a = 11.7332(19) Å	α= 90°.
	b = 11.0286(17) Å	β= 104.091(3)°.
	c = 21.993(4) Å	γ= 90°.
Volume	2760.3(8) $Å^3$	
Z	4	
Density (calculated)	1.274 Mg/m^3	
Absorption coefficient	0.488 mm^{-1}	
F(000)	1104	
Crystal size	0.31 x 0.31 x 0.11 mm^3	

Theta range for data collection	1.91 to 27.00°.
Index ranges	-11<=h<=14, -13<=k<=13, -28<=l<=28
Reflections collected	15944
Independent reflections	5863 [R(int) = 0.0279]
Completeness to theta = 27.00°	97.4 %
Absorption correction	Semi-empirical from equivalents
Max. and min. transmission	0.9483 and 0.8635
Refinement method	Full-matrix least-squares on F^2
Data / restraints / parameters	5863 / 0 / 437
Goodness-of-fit on F^2	1.040
Final R indices [I>2sigma(I)]	R1 = 0.0391, wR2 = 0.0937
R indices (all data)	R1 = 0.0508, wR2 = 0.1014
Largest diff. peak and hole	0.442 and -0.230 e.Å^{-3}

Table 26. Atomic coordinates (x 10^4) and equivalent isotropic displacement parameters (Å^{2}x 10^3) for liu67. U(eq) is defined as one third of the trace of the orthogonalized U^{ij} tensor.

	x	y	z	U(eq)
Cr(1)	903(1)	2297(1)	2107(1)	22(1)
Si(1)	-1024(1)	4271(1)	2780(1)	24(1)
O(1)	-422(1)	119(1)	2382(1)	40(1)
O(2)	2129(1)	428(1)	1507(1)	37(1)
O(3)	-839(2)	2651(2)	863(1)	52(1)
N(1)	393(1)	3836(1)	2632(1)	23(1)
B(1)	903(2)	4407(2)	2148(1)	25(1)
C(1)	53(2)	989(2)	2280(1)	29(1)
C(2)	1670(2)	1156(2)	1740(1)	26(1)
C(3)	-171(2)	2521(2)	1338(1)	33(1)
C(4)	1053(2)	2976(2)	3041(1)	25(1)
C(5)	2179(2)	2633(2)	3015(1)	26(1)
C(6)	2677(2)	3055(2)	2534(1)	26(1)
C(7)	2090(2)	3919(2)	2095(1)	24(1)
C(8)	-1615(2)	2940(2)	3120(1)	38(1)
C(9)	-2082(2)	4661(2)	2032(1)	34(1)
C(10)	-696(2)	5555(2)	3367(1)	31(1)
C(11)	141(2)	5122(3)	3978(1)	42(1)
C(12)	-1863(2)	5959(3)	3505(1)	45(1)
C(13)	-144(2)	6641(2)	3116(1)	42(1)
C(14)	280(2)	5414(2)	1711(1)	27(1)
C(15)	-112(2)	6194(2)	1336(1)	29(1)
C(16)	-615(2)	7121(2)	890(1)	29(1)
C(17)	-432(2)	8339(2)	1043(1)	45(1)
C(18)	-912(3)	9224(2)	613(1)	53(1)
C(19)	-1581(2)	8916(2)	29(1)	50(1)
C(20)	-1774(3)	7718(3)	-129(1)	56(1)

C(21)	-1294(2)	6819(2)	297(1)	46(1)
C(22)	2634(2)	4360(2)	1621(1)	26(1)
C(23)	3108(2)	4818(2)	1255(1)	29(1)
C(24)	3707(2)	5472(2)	860(1)	30(1)
C(25)	3105(2)	6327(2)	431(1)	44(1)
C(26)	3710(3)	7018(3)	89(1)	58(1)
C(27)	4897(3)	6858(3)	160(1)	58(1)
C(28)	5501(2)	6010(2)	574(1)	48(1)
C(29)	4908(2)	5320(2)	926(1)	36(1)

Table 27. Bond lengths [Å] and angles [°] for liu67.

Cr(1)-C(2)	1.843(2)
Cr(1)-C(1)	1.845(2)
Cr(1)-C(3)	1.863(2)
Cr(1)-C(4)	2.1541(19)
Cr(1)-N(1)	2.2157(15)
Cr(1)-C(5)	2.2167(19)
Cr(1)-C(6)	2.2280(19)
Cr(1)-C(7)	2.2713(19)
Cr(1)-B(1)	2.329(2)
Si(1)-N(1)	1.8336(16)
Si(1)-C(9)	1.853(2)
Si(1)-C(8)	1.857(2)
Si(1)-C(10)	1.892(2)
O(1)-C(1)	1.158(2)
O(2)-C(2)	1.154(2)
O(3)-C(3)	1.152(2)
N(1)-C(4)	1.404(2)
N(1)-B(1)	1.482(3)
B(1)-C(7)	1.524(3)
B(1)-C(14)	1.533(3)
C(4)-C(5)	1.389(3)
C(4)-H(4)	0.95(2)
C(5)-C(6)	1.407(3)
C(5)-H(5)	0.92(2)
C(6)-C(7)	1.411(3)
C(6)-H(6)	0.906(19)
C(7)-C(22)	1.433(3)
C(8)-H(8A)	0.97(3)
C(8)-H(8B)	0.92(3)
C(8)-H(8C)	0.92(3)
C(9)-H(9A)	0.94(3)
C(9)-H(9B)	0.93(3)
C(9)-H(9C)	0.96(3)
C(10)-C(13)	1.528(3)
C(10)-C(11)	1.536(3)
C(10)-C(12)	1.539(3)
C(11)-H(11A)	0.97(3)
C(11)-H(11B)	0.97(3)
C(11)-H(11C)	0.97(2)
C(12)-H(12A)	1.01(3)
C(12)-H(12B)	0.95(3)
C(12)-H(12C)	0.99(3)
C(13)-H(13A)	0.95(3)
C(13)-H(13B)	0.96(2)
C(13)-H(13C)	0.97(2)
C(14)-C(15)	1.202(3)
C(15)-C(16)	1.440(3)
C(16)-C(17)	1.388(3)
C(16)-C(21)	1.393(3)
C(17)-C(18)	1.379(3)
C(17)-H(17)	0.95(2)
C(18)-C(19)	1.375(4)

C(18)-H(18)	0.93(3)
C(19)-C(20)	1.371(4)
C(19)-H(19)	0.97(3)
C(20)-C(21)	1.387(4)
C(20)-H(20)	0.89(3)
C(21)-H(21)	0.88(3)
C(22)-C(23)	1.197(3)
C(23)-C(24)	1.436(3)
C(24)-C(29)	1.392(3)
C(24)-C(25)	1.398(3)
C(25)-C(26)	1.383(4)
C(25)-H(25)	0.89(2)
C(26)-C(27)	1.374(4)
C(26)-H(26)	0.87(3)
C(27)-C(28)	1.375(4)
C(27)-H(27)	0.91(3)
C(28)-C(29)	1.387(3)
C(28)-H(28)	0.99(3)
C(29)-H(29)	0.87(2)

C(2)-Cr(1)-C(1)	84.45(9)
C(2)-Cr(1)-C(3)	89.28(8)
C(1)-Cr(1)-C(3)	90.65(9)
C(2)-Cr(1)-C(4)	136.04(8)
C(1)-Cr(1)-C(4)	89.82(8)
C(3)-Cr(1)-C(4)	134.43(8)
C(2)-Cr(1)-N(1)	166.81(7)
C(1)-Cr(1)-N(1)	105.24(7)
C(3)-Cr(1)-N(1)	99.37(7)
C(4)-Cr(1)-N(1)	37.45(6)
C(2)-Cr(1)-C(5)	102.37(8)
C(1)-Cr(1)-C(5)	102.98(8)
C(3)-Cr(1)-C(5)	162.75(8)
C(4)-Cr(1)-C(5)	37.02(7)
N(1)-Cr(1)-C(5)	67.10(6)
C(2)-Cr(1)-C(6)	86.30(8)
C(1)-Cr(1)-C(6)	134.64(8)
C(3)-Cr(1)-C(6)	133.56(9)
C(4)-Cr(1)-C(6)	67.42(7)
N(1)-Cr(1)-C(6)	80.52(7)
C(5)-Cr(1)-C(6)	36.90(7)
C(2)-Cr(1)-C(7)	99.60(8)
C(1)-Cr(1)-C(7)	169.00(7)
C(3)-Cr(1)-C(7)	99.59(8)
C(4)-Cr(1)-C(7)	80.15(7)
N(1)-Cr(1)-C(7)	69.28(6)
C(5)-Cr(1)-C(7)	66.22(7)
C(6)-Cr(1)-C(7)	36.53(7)
C(2)-Cr(1)-B(1)	134.73(8)
C(1)-Cr(1)-B(1)	140.14(8)
C(3)-Cr(1)-B(1)	84.07(8)
C(4)-Cr(1)-B(1)	67.42(7)
N(1)-Cr(1)-B(1)	37.94(6)

C(5)-Cr(1)-B(1)	78.70(7)
C(6)-Cr(1)-B(1)	67.49(7)
C(7)-Cr(1)-B(1)	38.66(7)
N(1)-Si(1)-C(9)	110.10(9)
N(1)-Si(1)-C(8)	108.00(10)
C(9)-Si(1)-C(8)	107.79(12)
N(1)-Si(1)-C(10)	105.95(8)
C(9)-Si(1)-C(10)	114.34(11)
C(8)-Si(1)-C(10)	110.51(11)
C(4)-N(1)-B(1)	119.48(15)
C(4)-N(1)-Si(1)	116.40(12)
B(1)-N(1)-Si(1)	123.92(13)
C(4)-N(1)-Cr(1)	68.89(10)
B(1)-N(1)-Cr(1)	75.19(10)
Si(1)-N(1)-Cr(1)	131.62(8)
N(1)-B(1)-C(7)	116.15(17)
N(1)-B(1)-C(14)	122.96(17)
C(7)-B(1)-C(14)	120.87(17)
N(1)-B(1)-Cr(1)	66.87(10)
C(7)-B(1)-Cr(1)	68.61(11)
C(14)-B(1)-Cr(1)	134.72(14)
O(1)-C(1)-Cr(1)	175.43(17)
O(2)-C(2)-Cr(1)	178.59(17)
O(3)-C(3)-Cr(1)	179.5(2)
C(5)-C(4)-N(1)	122.60(17)
C(5)-C(4)-Cr(1)	73.94(11)
N(1)-C(4)-Cr(1)	73.66(10)
C(5)-C(4)-H(4)	120.7(12)
N(1)-C(4)-H(4)	116.7(12)
Cr(1)-C(4)-H(4)	125.4(12)
C(4)-C(5)-C(6)	120.98(18)
C(4)-C(5)-Cr(1)	69.04(11)
C(6)-C(5)-Cr(1)	71.99(11)
C(4)-C(5)-H(5)	117.5(13)
C(6)-C(5)-H(5)	121.3(13)
Cr(1)-C(5)-H(5)	127.4(13)
C(5)-C(6)-C(7)	121.01(17)
C(5)-C(6)-Cr(1)	71.12(11)
C(7)-C(6)-Cr(1)	73.41(11)
C(5)-C(6)-H(6)	116.7(12)
C(7)-C(6)-H(6)	122.2(12)
Cr(1)-C(6)-H(6)	125.4(11)
C(6)-C(7)-C(22)	119.80(17)
C(6)-C(7)-B(1)	119.30(17)
C(22)-C(7)-B(1)	120.86(17)
C(6)-C(7)-Cr(1)	70.06(11)
C(22)-C(7)-Cr(1)	131.14(13)
B(1)-C(7)-Cr(1)	72.73(11)
Si(1)-C(8)-H(8A)	104.5(17)
Si(1)-C(8)-H(8B)	111.2(18)
H(8A)-C(8)-H(8B)	104(2)
Si(1)-C(8)-H(8C)	111.0(16)
H(8A)-C(8)-H(8C)	114(2)

H(8B)-C(8)-H(8C)	112(2)
Si(1)-C(9)-H(9A)	108.4(15)
Si(1)-C(9)-H(9B)	109.8(15)
H(9A)-C(9)-H(9B)	107(2)
Si(1)-C(9)-H(9C)	114.8(16)
H(9A)-C(9)-H(9C)	110(2)
H(9B)-C(9)-H(9C)	106(2)
C(13)-C(10)-C(11)	108.86(19)
C(13)-C(10)-C(12)	108.7(2)
C(11)-C(10)-C(12)	109.05(19)
C(13)-C(10)-Si(1)	111.95(14)
C(11)-C(10)-Si(1)	110.19(16)
C(12)-C(10)-Si(1)	108.01(15)
C(10)-C(11)-H(11A)	111.4(14)
C(10)-C(11)-H(11B)	113.2(14)
H(11A)-C(11)-H(11B)	109(2)
C(10)-C(11)-H(11C)	109.3(14)
H(11A)-C(11)-H(11C)	108(2)
H(11B)-C(11)-H(11C)	106.1(19)
C(10)-C(12)-H(12A)	113.3(15)
C(10)-C(12)-H(12B)	107.1(16)
H(12A)-C(12)-H(12B)	105(2)
C(10)-C(12)-H(12C)	110.0(15)
H(12A)-C(12)-H(12C)	112(2)
H(12B)-C(12)-H(12C)	109(2)
C(10)-C(13)-H(13A)	111.6(15)
C(10)-C(13)-H(13B)	109.7(14)
H(13A)-C(13)-H(13B)	107(2)
C(10)-C(13)-H(13C)	110.2(14)
H(13A)-C(13)-H(13C)	108(2)
H(13B)-C(13)-H(13C)	110(2)
C(15)-C(14)-B(1)	172.9(2)
C(14)-C(15)-C(16)	178.3(2)
C(17)-C(16)-C(21)	118.5(2)
C(17)-C(16)-C(15)	120.63(18)
C(21)-C(16)-C(15)	120.9(2)
C(18)-C(17)-C(16)	120.4(2)
C(18)-C(17)-H(17)	119.8(15)
C(16)-C(17)-H(17)	119.8(15)
C(19)-C(18)-C(17)	120.7(2)
C(19)-C(18)-H(18)	121.2(18)
C(17)-C(18)-H(18)	118.1(18)
C(20)-C(19)-C(18)	119.8(2)
C(20)-C(19)-H(19)	119.4(16)
C(18)-C(19)-H(19)	120.8(16)
C(19)-C(20)-C(21)	120.2(2)
C(19)-C(20)-H(20)	122.8(17)
C(21)-C(20)-H(20)	117.0(18)
C(20)-C(21)-C(16)	120.5(2)
C(20)-C(21)-H(21)	119.9(17)
C(16)-C(21)-H(21)	119.7(17)
C(23)-C(22)-C(7)	174.3(2)
C(22)-C(23)-C(24)	174.1(2)

C(29)-C(24)-C(25)	118.9(2)
C(29)-C(24)-C(23)	120.59(19)
C(25)-C(24)-C(23)	120.4(2)
C(26)-C(25)-C(24)	119.8(3)
C(26)-C(25)-H(25)	120.2(15)
C(24)-C(25)-H(25)	119.9(15)
C(27)-C(26)-C(25)	120.5(3)
C(27)-C(26)-H(26)	121(2)
C(25)-C(26)-H(26)	118(2)
C(26)-C(27)-C(28)	120.5(2)
C(26)-C(27)-H(27)	123(2)
C(28)-C(27)-H(27)	116(2)
C(27)-C(28)-C(29)	119.7(3)
C(27)-C(28)-H(28)	122.5(16)
C(29)-C(28)-H(28)	117.8(16)
C(28)-C(29)-C(24)	120.6(2)
C(28)-C(29)-H(29)	121.7(15)
C(24)-C(29)-H(29)	117.7(15)

Symmetry transformations used to generate equivalent atoms:

Table 28. Anisotropic displacement parameters ($Å^2 x\ 10^3$)for liu67. The anisotropic displacement factor exponent takes the form: $-2p^2[\ h^2a^{*2}U^{11} + ... + 2\ h\ k\ a^*\ b^*\ U^{12}\ ]$

	U^{11}	U^{22}	U^{33}	U^{23}	U^{13}	U^{12}
Cr(1)	21(1)	19(1)	26(1)	-1(1)	4(1)	1(1)
Si(1)	22(1)	23(1)	29(1)	-2(1)	7(1)	0(1)
O(1)	39(1)	32(1)	52(1)	1(1)	14(1)	-9(1)
O(2)	42(1)	31(1)	38(1)	-2(1)	12(1)	10(1)
O(3)	51(1)	51(1)	41(1)	-2(1)	-13(1)	8(1)
N(1)	24(1)	20(1)	26(1)	0(1)	6(1)	3(1)
B(1)	26(1)	21(1)	26(1)	-3(1)	4(1)	-2(1)
C(1)	25(1)	29(1)	32(1)	-4(1)	6(1)	2(1)
C(2)	25(1)	24(1)	28(1)	4(1)	4(1)	0(1)
C(3)	33(1)	24(1)	38(1)	-4(1)	3(1)	4(1)
C(4)	29(1)	21(1)	26(1)	2(1)	5(1)	1(1)
C(5)	26(1)	21(1)	28(1)	1(1)	0(1)	2(1)
C(6)	20(1)	24(1)	33(1)	-6(1)	3(1)	1(1)
C(7)	24(1)	20(1)	28(1)	-4(1)	5(1)	-2(1)
C(8)	34(1)	33(1)	48(1)	1(1)	14(1)	-6(1)
C(9)	25(1)	42(1)	36(1)	-1(1)	6(1)	5(1)
C(10)	29(1)	30(1)	34(1)	-7(1)	10(1)	0(1)
C(11)	44(1)	43(2)	36(1)	-9(1)	3(1)	-2(1)
C(12)	40(1)	50(2)	51(1)	-17(1)	20(1)	2(1)
C(13)	47(2)	28(1)	54(1)	-10(1)	16(1)	-5(1)
C(14)	26(1)	24(1)	31(1)	-2(1)	9(1)	1(1)
C(15)	28(1)	26(1)	32(1)	0(1)	7(1)	0(1)
C(16)	31(1)	26(1)	30(1)	3(1)	8(1)	3(1)
C(17)	60(2)	30(1)	35(1)	-1(1)	-6(1)	5(1)
C(18)	76(2)	26(1)	48(1)	5(1)	-1(1)	8(1)
C(19)	64(2)	41(2)	40(1)	14(1)	3(1)	11(1)
C(20)	75(2)	50(2)	33(1)	4(1)	-9(1)	-2(1)
C(21)	62(2)	31(1)	38(1)	-1(1)	-1(1)	-4(1)

C(22)	25(1)	22(1)	30(1)	-5(1)	4(1)	-1(1)
C(23)	29(1)	26(1)	31(1)	-6(1)	7(1)	0(1)
C(24)	38(1)	27(1)	26(1)	-5(1)	10(1)	-4(1)
C(25)	52(2)	46(2)	35(1)	3(1)	12(1)	2(1)
C(26)	90(2)	47(2)	39(1)	13(1)	21(1)	1(2)
C(27)	88(2)	53(2)	42(1)	-2(1)	33(1)	-27(2)
C(28)	54(2)	55(2)	42(1)	-13(1)	23(1)	-18(1)
C(29)	42(1)	35(1)	31(1)	-5(1)	12(1)	-7(1)

Table 29. Hydrogen coordinates (x 10^4) and isotropic displacement parameters ($Å^2$x 10^3) for liu67.

	x	y	z	U(eq)
H(4)	691(18)	2629(17)	3343(9)	25(5)
H(5)	2558(18)	2062(19)	3301(9)	28(5)
H(6)	3369(17)	2718(16)	2510(8)	17(5)
H(8A)	-2430(30)	3150(30)	3099(13)	72(9)
H(8B)	-1670(20)	2270(30)	2863(14)	68(9)
H(8C)	-1180(20)	2780(20)	3520(13)	57(8)
H(9A)	-2840(20)	4610(20)	2094(11)	52(7)
H(9B)	-2030(20)	4100(20)	1727(12)	51(7)
H(9C)	-1960(20)	5440(30)	1866(12)	62(8)
H(11A)	-200(20)	4460(20)	4168(11)	51(7)
H(11B)	900(20)	4870(20)	3925(10)	46(7)
H(11C)	290(20)	5780(20)	4276(11)	46(7)
H(12A)	-2480(20)	6180(20)	3118(13)	64(8)
H(12B)	-2170(20)	5280(20)	3675(12)	57(8)
H(12C)	-1720(20)	6620(20)	3817(12)	56(7)
H(13A)	-30(20)	7300(20)	3402(12)	55(8)
H(13B)	-660(20)	6920(20)	2730(11)	43(6)
H(13C)	610(20)	6420(20)	3042(11)	47(7)
H(17)	30(20)	8560(20)	1442(12)	54(7)
H(18)	-770(30)	10030(30)	729(13)	74(9)
H(19)	-1930(20)	9530(20)	-271(12)	60(8)
H(20)	-2190(30)	7480(20)	-507(14)	67(9)
H(21)	-1420(20)	6050(20)	193(12)	53(8)
H(25)	2340(20)	6460(20)	397(10)	40(7)
H(26)	3320(30)	7570(30)	-162(15)	75(10)
H(27)	5330(30)	7310(30)	-43(16)	88(11)
H(28)	6360(20)	5870(20)	638(12)	62(8)
H(29)	5266(19)	4770(20)	1188(10)	36(6)

Table 30. Torsion angles [°] for liu67.

C(9)-Si(1)-N(1)-C(4)	-148.69(15)
C(8)-Si(1)-N(1)-C(4)	-31.24(16)
C(10)-Si(1)-N(1)-C(4)	87.18(15)
C(9)-Si(1)-N(1)-B(1)	36.45(18)
C(8)-Si(1)-N(1)-B(1)	153.90(16)
C(10)-Si(1)-N(1)-B(1)	-87.68(16)
C(9)-Si(1)-N(1)-Cr(1)	-64.24(14)
C(8)-Si(1)-N(1)-Cr(1)	53.21(14)
C(10)-Si(1)-N(1)-Cr(1)	171.64(10)
C(2)-Cr(1)-N(1)-C(4)	-67.5(3)
C(1)-Cr(1)-N(1)-C(4)	68.84(12)
C(3)-Cr(1)-N(1)-C(4)	162.09(12)
C(5)-Cr(1)-N(1)-C(4)	-29.08(11)
C(6)-Cr(1)-N(1)-C(4)	-65.02(11)
C(7)-Cr(1)-N(1)-C(4)	-101.13(11)
B(1)-Cr(1)-N(1)-C(4)	-130.36(15)
C(2)-Cr(1)-N(1)-B(1)	62.9(3)
C(1)-Cr(1)-N(1)-B(1)	-160.80(11)
C(3)-Cr(1)-N(1)-B(1)	-67.54(12)
C(4)-Cr(1)-N(1)-B(1)	130.36(15)
C(5)-Cr(1)-N(1)-B(1)	101.28(11)
C(6)-Cr(1)-N(1)-B(1)	65.35(11)
C(7)-Cr(1)-N(1)-B(1)	29.24(10)
C(2)-Cr(1)-N(1)-Si(1)	-174.6(3)
C(1)-Cr(1)-N(1)-Si(1)	-38.30(12)
C(3)-Cr(1)-N(1)-Si(1)	54.95(12)
C(4)-Cr(1)-N(1)-Si(1)	-107.14(15)
C(5)-Cr(1)-N(1)-Si(1)	-136.22(12)
C(6)-Cr(1)-N(1)-Si(1)	-172.16(12)
C(7)-Cr(1)-N(1)-Si(1)	151.73(12)
B(1)-Cr(1)-N(1)-Si(1)	122.50(15)
C(4)-N(1)-B(1)-C(7)	5.4(3)
Si(1)-N(1)-B(1)-C(7)	-179.89(12)
Cr(1)-N(1)-B(1)-C(7)	-49.34(15)
C(4)-N(1)-B(1)-C(14)	-175.85(17)
Si(1)-N(1)-B(1)-C(14)	-1.1(3)
Cr(1)-N(1)-B(1)-C(14)	129.41(18)
C(4)-N(1)-B(1)-Cr(1)	54.74(14)
Si(1)-N(1)-B(1)-Cr(1)	-130.55(12)
C(2)-Cr(1)-B(1)-N(1)	-163.39(10)
C(1)-Cr(1)-B(1)-N(1)	29.67(16)
C(3)-Cr(1)-B(1)-N(1)	113.54(11)
C(4)-Cr(1)-B(1)-N(1)	-30.12(10)
C(5)-Cr(1)-B(1)-N(1)	-67.11(10)
C(6)-Cr(1)-B(1)-N(1)	-103.98(11)
C(7)-Cr(1)-B(1)-N(1)	-133.01(15)
C(2)-Cr(1)-B(1)-C(7)	-30.38(15)
C(1)-Cr(1)-B(1)-C(7)	162.68(12)
C(3)-Cr(1)-B(1)-C(7)	-113.45(12)
C(4)-Cr(1)-B(1)-C(7)	102.89(11)
N(1)-Cr(1)-B(1)-C(7)	133.01(15)
C(5)-Cr(1)-B(1)-C(7)	65.90(11)

C(6)-Cr(1)-B(1)-C(7)	29.02(10)
C(2)-Cr(1)-B(1)-C(14)	82.4(2)
C(1)-Cr(1)-B(1)-C(14)	-84.5(2)
C(3)-Cr(1)-B(1)-C(14)	-0.64(19)
C(4)-Cr(1)-B(1)-C(14)	-144.3(2)
N(1)-Cr(1)-B(1)-C(14)	-114.2(2)
C(5)-Cr(1)-B(1)-C(14)	178.7(2)
C(6)-Cr(1)-B(1)-C(14)	141.8(2)
C(7)-Cr(1)-B(1)-C(14)	112.8(2)
C(2)-Cr(1)-C(1)-O(1)	18(2)
C(3)-Cr(1)-C(1)-O(1)	107(2)
C(4)-Cr(1)-C(1)-O(1)	-119(2)
N(1)-Cr(1)-C(1)-O(1)	-153(2)
C(5)-Cr(1)-C(1)-O(1)	-84(2)
C(6)-Cr(1)-C(1)-O(1)	-62(2)
C(7)-Cr(1)-C(1)-O(1)	-95(2)
B(1)-Cr(1)-C(1)-O(1)	-172(2)
C(1)-Cr(1)-C(2)-O(2)	27(7)
C(3)-Cr(1)-C(2)-O(2)	-64(7)
C(4)-Cr(1)-C(2)-O(2)	111(7)
N(1)-Cr(1)-C(2)-O(2)	165(7)
C(5)-Cr(1)-C(2)-O(2)	129(7)
C(6)-Cr(1)-C(2)-O(2)	163(7)
C(7)-Cr(1)-C(2)-O(2)	-163(7)
B(1)-Cr(1)-C(2)-O(2)	-145(7)
C(2)-Cr(1)-C(3)-O(3)	79(26)
C(1)-Cr(1)-C(3)-O(3)	-5(26)
C(4)-Cr(1)-C(3)-O(3)	-96(26)
N(1)-Cr(1)-C(3)-O(3)	-111(26)
C(5)-Cr(1)-C(3)-O(3)	-148(100)
C(6)-Cr(1)-C(3)-O(3)	163(100)
C(7)-Cr(1)-C(3)-O(3)	179(100)
B(1)-Cr(1)-C(3)-O(3)	-146(26)
B(1)-N(1)-C(4)-C(5)	0.2(3)
Si(1)-N(1)-C(4)-C(5)	-174.88(15)
Cr(1)-N(1)-C(4)-C(5)	58.02(17)
B(1)-N(1)-C(4)-Cr(1)	-57.80(15)
Si(1)-N(1)-C(4)-Cr(1)	127.10(10)
C(2)-Cr(1)-C(4)-C(5)	30.36(17)
C(1)-Cr(1)-C(4)-C(5)	112.16(13)
C(3)-Cr(1)-C(4)-C(5)	-157.10(13)
N(1)-Cr(1)-C(4)-C(5)	-131.96(17)
C(6)-Cr(1)-C(4)-C(5)	-27.50(12)
C(7)-Cr(1)-C(4)-C(5)	-63.29(12)
B(1)-Cr(1)-C(4)-C(5)	-101.47(13)
C(2)-Cr(1)-C(4)-N(1)	162.32(11)
C(1)-Cr(1)-C(4)-N(1)	-115.88(11)
C(3)-Cr(1)-C(4)-N(1)	-25.14(16)
C(5)-Cr(1)-C(4)-N(1)	131.96(17)
C(6)-Cr(1)-C(4)-N(1)	104.46(12)
C(7)-Cr(1)-C(4)-N(1)	68.67(10)
B(1)-Cr(1)-C(4)-N(1)	30.49(10)
N(1)-C(4)-C(5)-C(6)	-5.9(3)

Cr(1)-C(4)-C(5)-C(6)	51.96(17)
N(1)-C(4)-C(5)-Cr(1)	-57.89(16)
C(2)-Cr(1)-C(5)-C(4)	-158.95(12)
C(1)-Cr(1)-C(5)-C(4)	-71.88(13)
C(3)-Cr(1)-C(5)-C(4)	69.5(3)
N(1)-Cr(1)-C(5)-C(4)	29.39(11)
C(6)-Cr(1)-C(5)-C(4)	134.76(18)
C(7)-Cr(1)-C(5)-C(4)	105.89(13)
B(1)-Cr(1)-C(5)-C(4)	67.34(12)
C(2)-Cr(1)-C(5)-C(6)	66.29(13)
C(1)-Cr(1)-C(5)-C(6)	153.36(12)
C(3)-Cr(1)-C(5)-C(6)	-65.2(3)
C(4)-Cr(1)-C(5)-C(6)	-134.76(18)
N(1)-Cr(1)-C(5)-C(6)	-105.37(12)
C(7)-Cr(1)-C(5)-C(6)	-28.87(11)
B(1)-Cr(1)-C(5)-C(6)	-67.42(12)
C(4)-C(5)-C(6)-C(7)	5.4(3)
Cr(1)-C(5)-C(6)-C(7)	56.11(16)
C(4)-C(5)-C(6)-Cr(1)	-50.66(17)
C(2)-Cr(1)-C(6)-C(5)	-116.34(12)
C(1)-Cr(1)-C(6)-C(5)	-37.88(16)
C(3)-Cr(1)-C(6)-C(5)	158.19(13)
C(4)-Cr(1)-C(6)-C(5)	27.58(11)
N(1)-Cr(1)-C(6)-C(5)	64.23(11)
C(7)-Cr(1)-C(6)-C(5)	132.07(17)
B(1)-Cr(1)-C(6)-C(5)	101.45(13)
C(2)-Cr(1)-C(6)-C(7)	111.60(12)
C(1)-Cr(1)-C(6)-C(7)	-169.94(11)
C(3)-Cr(1)-C(6)-C(7)	26.12(16)
C(4)-Cr(1)-C(6)-C(7)	-104.48(12)
N(1)-Cr(1)-C(6)-C(7)	-67.84(11)
C(5)-Cr(1)-C(6)-C(7)	-132.07(17)
B(1)-Cr(1)-C(6)-C(7)	-30.61(11)
C(5)-C(6)-C(7)-C(22)	178.18(17)
Cr(1)-C(6)-C(7)-C(22)	-126.78(17)
C(5)-C(6)-C(7)-B(1)	0.5(3)
Cr(1)-C(6)-C(7)-B(1)	55.55(16)
C(5)-C(6)-C(7)-Cr(1)	-55.04(16)
N(1)-B(1)-C(7)-C(6)	-5.8(3)
C(14)-B(1)-C(7)-C(6)	175.47(17)
Cr(1)-B(1)-C(7)-C(6)	-54.27(15)
N(1)-B(1)-C(7)-C(22)	176.60(16)
C(14)-B(1)-C(7)-C(22)	-2.2(3)
Cr(1)-B(1)-C(7)-C(22)	128.08(17)
N(1)-B(1)-C(7)-Cr(1)	48.52(15)
C(14)-B(1)-C(7)-Cr(1)	-130.26(18)
C(2)-Cr(1)-C(7)-C(6)	-70.23(12)
C(1)-Cr(1)-C(7)-C(6)	40.6(4)
C(3)-Cr(1)-C(7)-C(6)	-161.12(12)
C(4)-Cr(1)-C(7)-C(6)	65.14(11)
N(1)-Cr(1)-C(7)-C(6)	102.41(11)
C(5)-Cr(1)-C(7)-C(6)	29.15(11)
B(1)-Cr(1)-C(7)-C(6)	131.15(16)

C(2)-Cr(1)-C(7)-C(22)	42.42(18)
C(1)-Cr(1)-C(7)-C(22)	153.3(4)
C(3)-Cr(1)-C(7)-C(22)	-48.47(19)
C(4)-Cr(1)-C(7)-C(22)	177.79(19)
N(1)-Cr(1)-C(7)-C(22)	-144.94(19)
C(5)-Cr(1)-C(7)-C(22)	141.80(19)
C(6)-Cr(1)-C(7)-C(22)	112.6(2)
B(1)-Cr(1)-C(7)-C(22)	-116.2(2)
C(2)-Cr(1)-C(7)-B(1)	158.63(11)
C(1)-Cr(1)-C(7)-B(1)	-90.5(4)
C(3)-Cr(1)-C(7)-B(1)	67.73(12)
C(4)-Cr(1)-C(7)-B(1)	-66.00(11)
N(1)-Cr(1)-C(7)-B(1)	-28.73(10)
C(5)-Cr(1)-C(7)-B(1)	-102.00(11)
C(6)-Cr(1)-C(7)-B(1)	-131.15(16)
N(1)-Si(1)-C(10)-C(13)	60.10(17)
C(9)-Si(1)-C(10)-C(13)	-61.34(19)
C(8)-Si(1)-C(10)-C(13)	176.84(17)
N(1)-Si(1)-C(10)-C(11)	-61.20(17)
C(9)-Si(1)-C(10)-C(11)	177.36(16)
C(8)-Si(1)-C(10)-C(11)	55.54(18)
N(1)-Si(1)-C(10)-C(12)	179.76(16)
C(9)-Si(1)-C(10)-C(12)	58.33(19)
C(8)-Si(1)-C(10)-C(12)	-63.49(19)
N(1)-B(1)-C(14)-C(15)	-174.5(16)
C(7)-B(1)-C(14)-C(15)	4.2(18)
Cr(1)-B(1)-C(14)-C(15)	-85.5(17)
B(1)-C(14)-C(15)-C(16)	158(6)
C(14)-C(15)-C(16)-C(17)	105(7)
C(14)-C(15)-C(16)-C(21)	-75(7)
C(21)-C(16)-C(17)-C(18)	-0.2(4)
C(15)-C(16)-C(17)-C(18)	179.7(2)
C(16)-C(17)-C(18)-C(19)	0.3(4)
C(17)-C(18)-C(19)-C(20)	-0.1(5)
C(18)-C(19)-C(20)-C(21)	-0.1(5)
C(19)-C(20)-C(21)-C(16)	0.2(5)
C(17)-C(16)-C(21)-C(20)	-0.1(4)
C(15)-C(16)-C(21)-C(20)	-179.9(2)
C(6)-C(7)-C(22)-C(23)	-104(2)
B(1)-C(7)-C(22)-C(23)	73(2)
Cr(1)-C(7)-C(22)-C(23)	167(2)
C(7)-C(22)-C(23)-C(24)	5(4)
C(22)-C(23)-C(24)-C(29)	89(2)
C(22)-C(23)-C(24)-C(25)	-87(2)
C(29)-C(24)-C(25)-C(26)	-1.0(3)
C(23)-C(24)-C(25)-C(26)	175.0(2)
C(24)-C(25)-C(26)-C(27)	0.8(4)
C(25)-C(26)-C(27)-C(28)	0.1(4)
C(26)-C(27)-C(28)-C(29)	-0.8(4)
C(27)-C(28)-C(29)-C(24)	0.6(3)
C(25)-C(24)-C(29)-C(28)	0.3(3)
C(23)-C(24)-C(29)-C(28)	-175.68(19)

Symmetry transformations used to generate equivalent atoms:

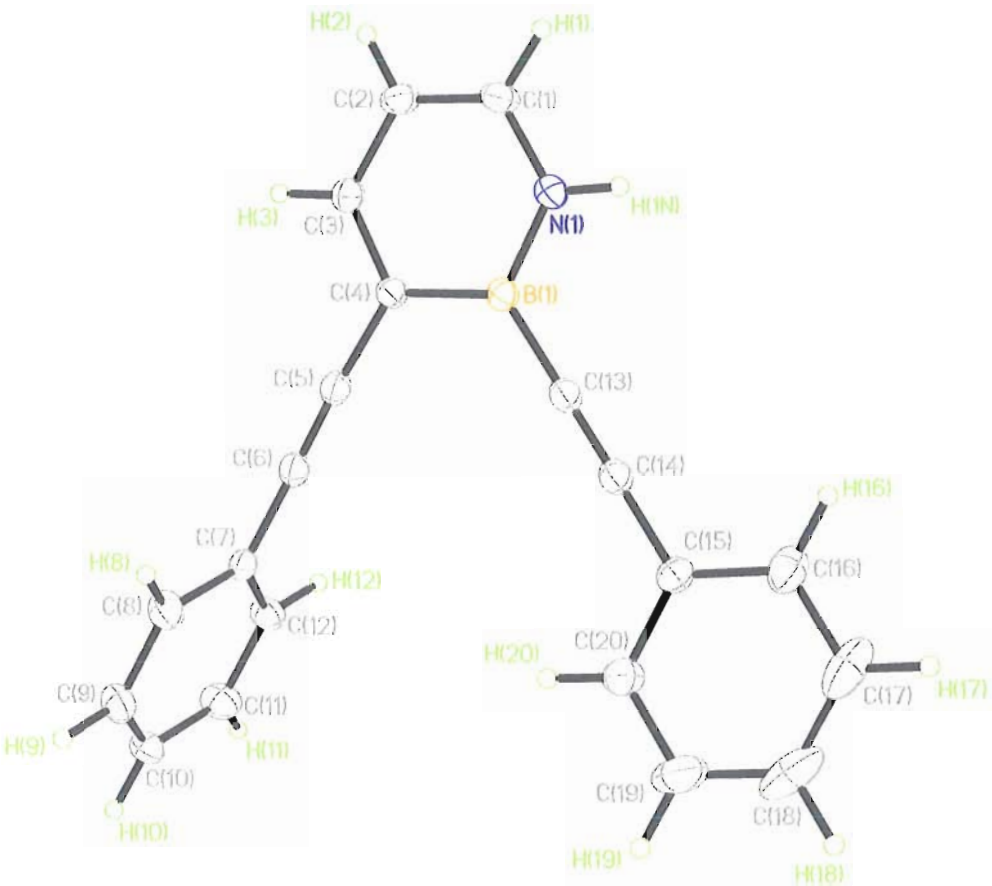

Figure 9. ORTEP illustration of **12**, with thermal ellipsoids drawn at the 35% probability level.

X-ray Crystal Structure Determination. Crystals of **12** suitable for X-ray diffraction were obtained by evaporation of a solution of **12** in Et_2O.

Diffraction intensity data were collected with a Bruker Smart Apex CCD diffractometer at 173(2) K using MoKα - radiation (0.71073 Å). The structure was solved using direct methods, completed by subsequent difference Fourier syntheses, and refined by full matrix least-squares procedures on F^2. All non-H atoms were refined with anisotropic thermal parameters. H atoms were found on the residual density map and refined with isotropic thermal parameters. The Flack parameter is 0.00(8). All software and sources scattering factors are contained in the SHELXTL (6.10) program package (G.Sheldrick,

Bruker XRD, Madison, WI). Crystallographic data and some details of data collection and crystal structure refinement for $C_{20}H_{14}BN$ are given in the following tables.

Table 31. Crystal data and structure refinement for **12** (liu70a).

Identification code	liu70a	
Empirical formula	$C_{20}H_{14}BN$	
Formula weight	279.13	
Temperature	173(2) K	
Wavelength	0.71073 Å	
Crystal system	Monoclinic	
Space group	P2(1)/c	
Unit cell dimensions	a = 9.9028(13) Å	α= 90°.
	b = 17.214(2) Å	β= 108.420(2)°.
	c = 9.5769(13) Å	γ = 90°.
Volume	1548.9(4) $Å^3$	
Z	4	
Density (calculated)	1.197 Mg/m^3	
Absorption coefficient	0.068 mm^{-1}	
F(000)	584	
Crystal size	0.23 x 0.12 x 0.08 mm^3	
Theta range for data collection	2.17 to 27.00°.	
Index ranges	-12<=h<=12, -21<=k<=21, -12<=l<=12	
Reflections collected	17029	
Independent reflections	3382 [R(int) = 0.0245]	
Completeness to theta = 27.00°	100.0 %	
Absorption correction	Semi-empirical from equivalents	
Max. and min. transmission	0.9945 and 0.9844	
Refinement method	Full-matrix least-squares on F^2	
Data / restraints / parameters	3382 / 0 / 256	
Goodness-of-fit on F^2	1.035	
Final R indices [I>2sigma(I)]	R1 = 0.0465, wR2 = 0.1059	
R indices (all data)	R1 = 0.0595, wR2 = 0.1147	
Largest diff. peak and hole	0.219 and -0.223 $e.Å^{-3}$	

Table 32. Atomic coordinates (x 10^4) and equivalent isotropic displacement parameters ($Å^2$x 10^3) for liu70a. U(eq) is defined as one third of the trace of the orthogonalized U^{ij} tensor.

	x	y	z	U(eq)
N(1)	3364(1)	2267(1)	6575(1)	34(1)
N(1A)	4784(1)	1005(1)	8182(2)	36(1)
B(1)	2833(2)	1981(1)	7687(2)	29(1)
B(1A)	3634(1)	1293(1)	8560(1)	29(1)
C(1)	4507(2)	1948(1)	6276(2)	38(1)
C(2)	5207(2)	1330(1)	7045(2)	39(1)
C(3)	4784(1)	1005(1)	8182(2)	36(1)
C(3A)	3364(1)	2267(1)	6575(1)	34(1)
C(4)	3634(1)	1293(1)	8560(1)	29(1)
C(4A)	2833(2)	1981(1)	7687(2)	29(1)
C(5)	3214(1)	939(1)	9741(1)	33(1)
C(6)	2794(1)	675(1)	10690(1)	33(1)
C(7)	2268(1)	338(1)	11793(1)	30(1)
C(8)	1375(2)	-310(1)	11461(2)	40(1)
C(9)	847(2)	-629(1)	12506(2)	43(1)
C(10)	1205(2)	-316(1)	13895(2)	42(1)
C(11)	2095(2)	320(1)	14244(2)	47(1)
C(12)	2622(2)	647(1)	13201(2)	39(1)
C(13)	1544(2)	2365(1)	7912(1)	33(1)
C(14)	499(2)	2661(1)	8061(1)	34(1)
C(15)	-797(1)	2990(1)	8168(2)	35(1)
C(16)	-1373(2)	3651(1)	7364(2)	53(1)
C(17)	-2668(2)	3934(1)	7403(2)	71(1)
C(18)	-3369(2)	3575(1)	8267(3)	76(1)
C(19)	-2771(2)	2937(1)	9099(3)	74(1)
C(20)	-1494(2)	2643(1)	9056(2)	50(1)

Table 33. Bond lengths [Å] and angles [°] for liu70a.

N(1)-C(1)	1.3676(18)
N(1)-B(1)	1.4172(18)
N(1)-H(1N)	0.898(18)
N(1A)-B(1A)	1.3906(18)
N(1A)-C(2)	1.4006(19)
N(1A)-H(3)	0.983(16)
B(1)-C(13)	1.5118(19)
B(1)-B(1A)	1.5198(19)
B(1A)-C(5)	1.4564(18)
C(1)-C(2)	1.353(2)
C(1)-H(1)	0.994(16)
C(2)-H(2)	0.966(16)
C(5)-C(6)	1.2015(18)
C(6)-C(7)	1.4406(18)
C(7)-C(12)	1.3875(19)
C(7)-C(8)	1.3946(19)
C(8)-C(9)	1.381(2)
C(8)-H(8)	0.962(18)
C(9)-C(10)	1.374(2)
C(9)-H(9)	0.973(19)

C(10)-C(11)	1.378(2)
C(10)-H(10)	0.974(17)
C(11)-C(12)	1.385(2)
C(11)-H(11)	0.984(18)
C(12)-H(12)	0.990(17)
C(13)-C(14)	1.2016(19)
C(14)-C(15)	1.4354(19)
C(15)-C(20)	1.388(2)
C(15)-C(16)	1.392(2)
C(16)-C(17)	1.384(3)
C(16)-H(16)	1.01(2)
C(17)-C(18)	1.383(3)
C(17)-H(17)	0.96(2)
C(18)-C(19)	1.376(3)
C(18)-H(18)	0.96(2)
C(19)-C(20)	1.375(2)
C(19)-H(19)	1.00(2)
C(20)-H(20)	0.96(2)

C(1)-N(1)-B(1)	123.07(12)
C(1)-N(1)-H(1N)	117.2(11)
B(1)-N(1)-H(1N)	119.8(11)
B(1A)-N(1A)-C(2)	122.04(13)
B(1A)-N(1A)-H(3)	119.0(9)
C(2)-N(1A)-H(3)	119.0(9)
N(1)-B(1)-C(13)	119.06(12)
N(1)-B(1)-B(1A)	115.54(12)
C(13)-B(1)-B(1A)	125.40(12)
N(1A)-B(1A)-C(5)	120.74(12)
N(1A)-B(1A)-B(1)	117.55(12)
C(5)-B(1A)-B(1)	121.70(11)
C(2)-C(1)-N(1)	121.16(13)
C(2)-C(1)-H(1)	122.9(9)
N(1)-C(1)-H(1)	115.9(9)
C(1)-C(2)-N(1A)	120.63(13)
C(1)-C(2)-H(2)	120.2(9)
N(1A)-C(2)-H(2)	119.2(9)
C(6)-C(5)-B(1A)	175.99(14)
C(5)-C(6)-C(7)	177.98(15)
C(12)-C(7)-C(8)	118.45(12)
C(12)-C(7)-C(6)	121.21(12)
C(8)-C(7)-C(6)	120.34(12)
C(9)-C(8)-C(7)	120.69(14)
C(9)-C(8)-H(8)	120.7(11)
C(7)-C(8)-H(8)	118.6(11)
C(10)-C(9)-C(8)	120.28(14)
C(10)-C(9)-H(9)	119.4(10)
C(8)-C(9)-H(9)	120.3(10)
C(9)-C(10)-C(11)	119.72(14)
C(9)-C(10)-H(10)	119.9(10)
C(11)-C(10)-H(10)	120.4(10)
C(10)-C(11)-C(12)	120.41(14)
C(10)-C(11)-H(11)	120.8(11)

C(12)-C(11)-H(11)	118.8(11)
C(11)-C(12)-C(7)	120.45(14)
C(11)-C(12)-H(12)	121.6(9)
C(7)-C(12)-H(12)	117.9(9)
C(14)-C(13)-B(1)	178.40(15)
C(13)-C(14)-C(15)	176.73(15)
C(20)-C(15)-C(16)	119.59(15)
C(20)-C(15)-C(14)	120.22(13)
C(16)-C(15)-C(14)	120.18(14)
C(17)-C(16)-C(15)	119.63(19)
C(17)-C(16)-H(16)	119.9(12)
C(15)-C(16)-H(16)	120.4(13)
C(18)-C(17)-C(16)	120.3(2)
C(18)-C(17)-H(17)	120.0(13)
C(16)-C(17)-H(17)	119.8(14)
C(19)-C(18)-C(17)	119.85(18)
C(19)-C(18)-H(18)	119.7(14)
C(17)-C(18)-H(18)	120.4(14)
C(20)-C(19)-C(18)	120.5(2)
C(20)-C(19)-H(19)	118.9(14)
C(18)-C(19)-H(19)	120.6(14)
C(19)-C(20)-C(15)	120.08(19)
C(19)-C(20)-H(20)	121.5(11)
C(15)-C(20)-H(20)	118.4(11)

Symmetry transformations used to generate equivalent atoms:

Table 34. Anisotropic displacement parameters ($Å^2 x\ 10^3$)for liu70a. The anisotropic displacement factor exponent takes the form: $-2p^2[\ h^2a^{*2}U^{11} + ... + 2\ h\ k\ a^*\ b^*\ U^{12}\ ]$

	U^{11}	U^{22}	U^{33}	U^{23}	U^{13}	U^{12}
N(1)	36(1)	34(1)	34(1)	7(1)	14(1)	4(1)
N(1A)	36(1)	35(1)	36(1)	6(1)	13(1)	7(1)
B(1)	31(1)	27(1)	28(1)	-1(1)	10(1)	-2(1)
B(1A)	33(1)	28(1)	28(1)	-1(1)	11(1)	-1(1)
C(1)	37(1)	46(1)	35(1)	5(1)	19(1)	0(1)
C(2)	34(1)	48(1)	41(1)	2(1)	18(1)	6(1)
C(3)	36(1)	35(1)	36(1)	6(1)	13(1)	7(1)
C(3A)	36(1)	34(1)	34(1)	7(1)	14(1)	4(1)
C(4)	33(1)	28(1)	28(1)	-1(1)	11(1)	-1(1)
C(4A)	31(1)	27(1)	28(1)	-1(1)	10(1)	-2(1)
C(5)	36(1)	29(1)	33(1)	1(1)	11(1)	5(1)
C(6)	37(1)	29(1)	34(1)	3(1)	12(1)	6(1)
C(7)	31(1)	28(1)	32(1)	5(1)	11(1)	6(1)
C(8)	50(1)	36(1)	35(1)	-4(1)	13(1)	-5(1)
C(9)	45(1)	34(1)	53(1)	3(1)	17(1)	-6(1)
C(10)	45(1)	43(1)	45(1)	11(1)	23(1)	4(1)
C(11)	56(1)	54(1)	35(1)	-4(1)	20(1)	-7(1)
C(12)	44(1)	37(1)	39(1)	-3(1)	16(1)	-7(1)
C(13)	39(1)	29(1)	32(1)	4(1)	14(1)	-1(1)
C(14)	40(1)	30(1)	32(1)	3(1)	14(1)	-1(1)
C(15)	36(1)	35(1)	33(1)	-5(1)	11(1)	1(1)
C(16)	68(1)	53(1)	36(1)	4(1)	16(1)	24(1)

C(17)	69(1)	78(1)	50(1)	-12(1)	-2(1)	39(1)
C(18)	35(1)	87(2)	101(2)	-44(1)	12(1)	9(1)
C(19)	56(1)	62(1)	122(2)	-23(1)	56(1)	-11(1)
C(20)	52(1)	41(1)	69(1)	-3(1)	35(1)	-3(1)

Table 35. Hydrogen coordinates (x 10^4) and isotropic displacement parameters ($Å^2$x 10^3) for liu70a.

	x	y	z	U(eq)
H(1)	4783(16)	2198(9)	5471(17)	46(4)
H(1N)	2939(17)	2675(10)	6025(19)	50(5)
H(2)	6020(17)	1116(9)	6830(17)	44(4)
H(3)	5326(17)	565(9)	8740(17)	42(4)
H(8)	1124(19)	-524(10)	10480(20)	60(5)
H(9)	223(19)	-1079(11)	12266(19)	60(5)
H(10)	842(17)	-549(10)	14631(19)	52(5)
H(11)	2377(19)	545(10)	15240(20)	61(5)
H(12)	3252(18)	1108(10)	13426(18)	52(5)
H(16)	-870(20)	3915(12)	6730(20)	87(7)
H(17)	-3080(20)	4382(13)	6830(20)	87(7)
H(18)	-4250(30)	3783(13)	8330(20)	93(7)
H(19)	-3260(20)	2679(14)	9740(30)	95(7)
H(20)	-1071(19)	2190(12)	9620(20)	67(6)

Table 36. Torsion angles [°] for liu70a.

C(1)-N(1)-B(1)-C(13)	-178.80(13)
C(1)-N(1)-B(1)-B(1A)	0.93(19)
C(2)-N(1A)-B(1A)-C(5)	179.51(13)
C(2)-N(1A)-B(1A)-B(1)	0.2(2)
N(1)-B(1)-B(1A)-N(1A)	-0.90(18)
C(13)-B(1)-B(1A)-N(1A)	178.81(13)
N(1)-B(1)-B(1A)-C(5)	179.79(12)
C(13)-B(1)-B(1A)-C(5)	-0.5(2)
B(1)-N(1)-C(1)-C(2)	-0.2(2)
N(1)-C(1)-C(2)-N(1A)	-0.6(2)
B(1A)-N(1A)-C(2)-C(1)	0.6(2)
N(1A)-B(1A)-C(5)-C(6)	-172(2)
B(1)-B(1A)-C(5)-C(6)	7(2)
B(1A)-C(5)-C(6)-C(7)	94(4)
C(5)-C(6)-C(7)-C(12)	176(100)
C(5)-C(6)-C(7)-C(8)	-4(4)
C(12)-C(7)-C(8)-C(9)	0.6(2)
C(6)-C(7)-C(8)-C(9)	-178.94(13)
C(7)-C(8)-C(9)-C(10)	-0.5(2)
C(8)-C(9)-C(10)-C(11)	-0.1(2)
C(9)-C(10)-C(11)-C(12)	0.5(2)
C(10)-C(11)-C(12)-C(7)	-0.4(2)
C(8)-C(7)-C(12)-C(11)	-0.2(2)
C(6)-C(7)-C(12)-C(11)	179.36(13)
N(1)-B(1)-C(13)-C(14)	75(5)
B(1A)-B(1)-C(13)-C(14)	-105(5)
B(1)-C(13)-C(14)-C(15)	4(7)

C(13)-C(14)-C(15)-C(20)	92(3)
C(13)-C(14)-C(15)-C(16)	-87(3)
C(20)-C(15)-C(16)-C(17)	-3.1(2)
C(14)-C(15)-C(16)-C(17)	175.95(15)
C(15)-C(16)-C(17)-C(18)	1.7(3)
C(16)-C(17)-C(18)-C(19)	0.5(3)
C(17)-C(18)-C(19)-C(20)	-1.3(3)
C(18)-C(19)-C(20)-C(15)	-0.1(3)
C(16)-C(15)-C(20)-C(19)	2.3(3)
C(14)-C(15)-C(20)-C(19)	-176.73(16)

Symmetry transformations used to generate equivalent atoms:

APPENDIX D

SYNTHESIS AND CHARACTERIZATION OF NITROLIPIDS

D.1. Introduction

The interest in conjugated organic molecules has grown significantly over the last several decades. The incorporation of boron in conjugated materials has been shown to impart unique properties relative to their carbonaceous analogs.[1,2] The fundamental consequences of replacing CC units with BN units in tolan derivatives provides a glimpse at the potential of 1,2-azaborine heterocycles in materials applications.

D.2. Experimental

D.2.1. General

THF was distilled over Na/benzophenone. CH_2Cl_2 was distilled over CaH_2. Commercially available reagents were used as received. Thin layer chromatography was performed on Sigma-Aldrich TLC plates (general purpose, silica gel on polyester with UV indicator). Column chromatography was performed on Sorbent Technologies silica gel (60 Å). ^{1}H and ^{13}C NMR data were collected on a Varian spectrometer at 300 MHz and 75 MHz, respectively. IR spectroscopy data were collected on a Nicolet Magna FT-IR 550 spectrometer. High-resolution mass spectrometry data were collected by Jeff

Morre at Oregon State University, Environmental Health Sciences Center on a JEOL MSRoute Spectrometer in chemical ionization positive ionization mode.

1-Nitrononane (9). Silver nitrite (24 g, 0.156 mol) was added to a flask protected from light with aluminum foil, suspended in Et_2O, and purged with N_2. 1-bromononane (21 g, 0.101 mol) was then added and the solution stirred at rt for 7 d. Solids were then removed by passing the solution through a plug of celite. The solvent was removed under vacuum and **9** purified by vacuum distillation (88 °C, 0.1 Torr) in 60% yield (10.5 g) as a faintly yellow liquid.

^{1}H NMR (300 MHz, $CDCl_3$) δ 4.35 (t, J = 8 Hz, 2H), 1.96 (m, 2H), 1.25 (br m, 12H), 0.82 (t, J = 7.5 Hz, 3H); ^{13}C NMR (75 MHz, $CDCl_3$) δ 77.8, 31.9, 29.3, 29.2, 28.9, 27.5, 26.3, 22.7, 14.1; IR (KBr) ν 2927, 2857, 1555, 1466, 1436, 1382, 1136, 874, 723, 613 cm^{-1}.

Compound 10. Oleic acid (20.0 g, 0.071 mol) dissolved in dry CH_2Cl_2 (200 mL) in an oven-dried flask was cooled to –78 °C with stirring under O_2. O_3 was then bubbled into the solution until a faint blue color was observed (45 min.), after which the solution was purged with N_2 for 20 min. and brought to rt. Dimethylsulfide (7.3 mL, 0.10 mol) was added via syringe and the solution stirred for 3 h. Excess Me_2S and solvent were then removed under reduced pressure and the mixture dissolved in EtOAc (100 mL). The solution was then washed three times with satd. NaCl soln., dried with $MgSO_4$, and solvent removed under vacuum. **10** was then purified by column chromatography (1:1 hexanes: ethyl acetate) in 90% yield as a colorless liquid.

^{1}H NMR (300 MHz, $CDCl_3$) δ 11.4 (br s, 1H), 9.68 (t, J = 1.8 Hz, 1H), 2.41 (t, J = 7.5 Hz, 2H), 2.35 (t, J = 7.5 Hz, 2H), 1.6 (br m, 4H), 1.25 (br m, 6H).

Compound 11. A flask was charged with **10** (2.5 g, 15 mmol), N,N'-dicyclohexylcarbodiimide (DCC) (3.5 g, 17 mmol), and CH_2Cl_2 (50 mL), and cooled to 0 °C under N_2. N,N-dimethyl-4-aminopyridine (DMAP) (50 mg) was then added and the solution stirred for 30 minutes, after which allyl alcohol was added and the solution stirred for 2 h. The reaction was then warmed to rt and stirred overnight. The solution was passed through a plug of silica/celite, and solvents were removed under reduced pressure. Allyl ester **11** was purified by vacuum distillation (110 °C, 0.1 Torr) in 65% yield (2.0 g, colorless liquid)

^{1}H NMR (300 MHz, $CDCl_3$) δ 9.74 (t, J = 1.8 Hz, 1H), 5.88 (m, 1H), 5.22 (m, 2H), 4.55 (d, J = 9.6 Hz, 2H), 2.40 (t, J = 7.5 Hz, 2H), 2.30 (t, J = 7.5 Hz, 2H), 1.60 (br m, 4H), 1.32 (br m, 6H); ^{13}C NMR (75 MHz, $CDCl_3$) δ 202.3, 172.9, 132.1, 117.7, 64.5, 43.5, 33.8, 28.7, 28.6, 28.5, 24.5, 21.6; IR (KBr) ν 2934, 2858, 2720, 1736, 1649, 1458, 1418, 1378, 1174, 1105, 991, 933 cm^{-1}.

Compound 12. Nitroalkane **9** (1.0 eq.) and aldehyde **11** (1.2 eq.) were added to a flask along with EtOAc (2 M in aldehyde). 1,8-Diazabicyclo[5.4.0]undec-7-ene (0.1 eq.) was then added under N_2 at rt and the solution stirred 24 h. The solution was then partitioned with Et_2O and 1 M HCl, the aqueous layer extracted three times with Et_2O, and the combined organic layer washed with brine and dried over $MgSO_4$. The drying agent was then filtered and solvents removed under vacuum. Product **12** (colorless oil)

was purified by column chromatography (5% EtOAc in hexanes) as a mixture of diastereomers (75-85% yield):

^{1}H NMR (300 MHz, $CDCl_3$) δ 5.88 (m, 1H), 5.22 (m, 2H), 4.60 (d, J = 9.6 Hz, 2H), 4.45 (m, 1H), 3.95 (m, 1H), 2.40 (t, J = 7.5 Hz, 2H), 2.10 (br m, 2H), 1.80 (br m, 2H), 1.65 (br m, 2H), 1.4 (br m, 20H), 0.92 (t, J = 7.5 Hz, 3H); ^{13}C NMR (75 MHz, $CDCl_3$) δ 173.7, 132.5, 118.3, 93.1, 92.6, 72.5, 72.2, 65.2, 34.4, 33.7, 33.3, 32.0, 30.7, 29.4, 29.3, 29.2, 29.1, 28.2, 26.2, 25.9, 25.7, 25.4, 25.0, 22.8, 14.3; IR (KBr) ν 3481, 2928, 2857, 1736, 1649, 1552, 1458, 1379, 1175, 1108, 989, 931, 733 cm^{-1}.

Compound 13. Hydroxy-nitro intermediate **12** (2.0 g) was added to a flask containing acetic anhydride (as solvent, approximately 0.1 M in starting material) and *p*-toluenesulfonic acid (1-5mol%), whereupon the solution was stirred under N_2, overnight, at rt. The solution was partitioned with Et_2O and H_2O, the aqueous layer extracted three times with Et_2O, and the combined organic layer washed once with brine. The organic layer was dried over $MgSO_4$, and solvents removed under vacuum (azeotropic removal of acetic anhydride/acetic acid was achieved by addition of 3 x 20 mL toluene), after which the desired product **13** (mixture of diastereomers) was purified by column chromatography (5% EtOAc in hexanes) as a colorless liquid in 99% yield:

^{1}H NMR (300 MHz, $CDCl_3$) δ 5.88 (m, 1H), 5.22 (m, 2H), 5.15 (m, 1H), 4.58 (m, 1H), 4.56 (d, J = 9.6 Hz, 2H), 2.25 (t, J = 7.5 Hz, 2H), 2.02 (s, 0.5H), 1.98 (s, 0.5H), 1.90 (br m, 2H), 1.6 (br m, 4H), 1.4 (br m, 20H), 0.82 (t, J = 7.5 Hz, 3H); ^{13}C NMR (75 MHz, $CDCl_3$) δ 173.1, 170.0, 169.6, 132.2, 117.8, 89.9, 89.4, 72.6, 72.5, 64.7, 33.9, 31.6, 30.6, 29.6, 29.4, 29.0, 28.9, 28.87, 28.8, 28.72, 28.68, 25.7, 25.4, 25.1, 24.6, 24.3,

22.4, 20.6, 20.5, 13.9; IR (KBr) ν 3086, 2929, 2857, 1743, 1649, 1555, 1465, 1375, 1226, 1175, 1108, 989, 928, 855, 724 cm^{-1}.

Compound 14. Acetylated intermediate **13** (1.5 g) was combined with Na_2CO_3 (0.5 eq.) and benzene (60 mL) in a flask connected to a Dean-Stark trap and reflux condenser. The solution was heated to 90 °C for 24 h ensuring azeotropic removal of H_2O, at which time the solution was cooled to rt and partitioned with satd. NH_4Cl and Et_2O. The aqueous layer was extracted 3 x Et_2O, and the combined organic layer washed with H_2O and brine. The organic layer was dried over $MgSO_4$, the solvent removed under vacuum, and the desired product **14** purified by column chromatography (5% EtOAc in hexanes) as a faintly yellow liquid in 74% yield:

^1H NMR (300 MHz, $CDCl_3$) δ 7.05 (t, J = 7.8 Hz, 1H), 5.88 (m, 1H), 5.22 (m, 2H), 4.56 (d, J = 9.6 Hz, 2H), 2.55 (t, J = 7.5 Hz, 2H), 2.31 (t, J = 7.5 Hz, 2H), 2.20 (q, J = 7.5 Hz, 2H), 1.6 (br m, 2H), 1.45 (br m, 4H), 1.3 (br m, 16H), 0.82 (t, J = 7.5 Hz, 3H); ^{13}C NMR (75 MHz, $CDCl_3$) δ 173.2, 151.8, 136.1, 132.2, 117.9, 64.8, 34.0, 31.7, 29.1, 29.0, 28.9, 28.8, 28.3, 27.8, 26.2, 24.7, 22.5, 14.0; IR (KBr) ν 2928, 2857, 1739, 1667, 1521, 1459, 1336, 1171, 989, 928, 732 cm^{-1}.

Compound 2. An oven-dried flask was charged with THF (15 mL), 98% formic acid (0.05 mL, 1.3 mmol), and allyl ester **14** (0.052 mmol). The solution was purged with N_2 and $Pd(PPh_3)_4$ (5 mol%, dry) added. The solution was purged for 10 min. with N_2 and then immediately immersed in an oil bath at 80 °C. The solution was refluxed under N_2 for 24 h, then cooled to rt and solvents removed under vacuum. The desired

product was purified by column chromatography (1% AcOH, 12% EtOAc in hexanes) in 95% yield:

^{1}H NMR (300 MHz, $CDCl_3$) δ 7.05 (t, J = 7.8 Hz, 1H), 2.59 (t, J = 7.5 Hz, 2H), 2.38 (t, J = 7.5 Hz, 2H), 2.22 (q, J = 7.2 Hz, 2H), 1.6 (br m, 2H), 1.45 (br m, 4H), 1.3 (br m, 16H), 0.82 (t, J = 7.5 Hz, 3H); ^{13}C NMR (75 MHz, $CDCl_3$) δ 180.4, 151.9, 136.2, 33.9, 31.7, 29.2, 29.1, 29.0, 28.9, 28.8, 28.4, 27.9, 27.8, 26.3, 24.5, 22.6, 14.0; IR (KBr) ν 3500-2500, 2927, 2856, 1709, 1666, 1519, 1462, 1413, 1336, 1114, 913, 854, 733 cm^{-1}; HRMS for $C_{18}H_{34}NO_4$, calcd. 328.24878; found 328.24826

Compound 16. Ph_2Se_2 (0.106 g, 0.68 mmol) was dissolved in absolute ethanol (10 mL), to which was slowly added $NaBH_4$ (0.026 g, 0.68 mmol). The solution was stirred under N_2 at rt until it turned colorless. Nitroolefin **7** (0.223 g, 0.68 mmol) was then added and solution stirred at rt for 1 h, at which point the mixture was cooled to –78 °C. Acetic acid (0.04 mL, 0.68 mmol) was then added and the solution kept at –78 °C for 1 h, whereupon the flask was warmed to rt. Water (10 mL) was then added, ethanol removed under reduced pressure, and the aqueous solution extracted three times with EtOAc. The collected organic layer was dried over Na_2SO_4 and solvent removed under reduced pressure. The crude intermediate was then dissolved in CH_2Cl_2 (5 mL) and THF (5 mL), the solution cooled to 0 °C, and 30% H_2O_2 (0.07 mL, 0.68 mmol) added slowly. Stirring at 0 °C continued for 10 min. after which the flask was warmed to rt, H_2O (10 mL) was added, and CH_2Cl_2 and THF were removed under vacuum. The remaining solution was then extracted three times with Et_2O and the combined organic layer washed with satd. $NaHCO_3$. The organic layer was then dried over Na_2SO_4 and

solvent removed under reduced pressure. A mixture of isomers was obtained in 76% yield (0.169g) as a pale yellow waxy solid. ^{1}H NMR of the crude product showed (*Z*) isomer 85%. Compound **12** was further purified by column chromatography (1% MeOH in $CHCl_3$):

^{1}H NMR (300 MHz, $CDCl_3$) δ 5.65 (t, J = 7.5 Hz, 1H), 2.49 (t, J = 6.9 Hz, 2H), 2.33 (m, 4H), 1.62 (br m, 2H), 1.45 (br m, 4H), 1.3 (br m, 16H), 0.87 (t, J = 6.6 Hz, 3H); ^{13}C NMR (75 MHz, $CDCl_3$) δ 180.0, 151.4, 131.5, 34.0, 32.7, 31.8, 29.1, 28.9, 28.86, 28.8, 28.7, 28.2, 27.2, 24.5, 22.6, 14.1; IR (KBr) ν 3500-2500, 2928, 2857, 1709, 1551, 1522, 1465, 1340, 1285, 939, 859, 724 cm^{-1}.

ω-Dodecalactone (20). A flask was charged with cyclododecanone (2.0 g, 0.011 mol), *m*-chloroperoxybenzoic acid (4.2 g, 0.021 mol), and dry $CHCl_3$ (25 mL), and heated at reflux for 48 h. Absence of peroxide was then confirmed by KI/starch test and the solution cooled to 0 °C. Precipitated *m*-chlorobenzoic acid was removed by filtration and solvent reduced under vacuum. The crude product was taken up in Et_2O and washed with K_2CO_3 followed by brine. Lactone **20** was purified by column chromatography (5% EtOAc in hexanes) as a colorless oil (2.03 g, 93%)

^{1}H NMR (300 MHz, $CDCl_3$) δ 4.15 (t, J = 5.4 Hz, 2H), 2.38 (m, 2H), 1.65 (br m, 4H), 1.36 (br m, 14H).

Compound 21. Lactone **20** (2.03 g, 0.010 mol) was dissolved in EtOH (50 mL) to which was then added KOH (1.5 eq. in **20**). The solution was refluxed for 3 h, after which H_2O (50 mL) was added and the solution cooled to rt. 5N H_2SO_4 was then added slowly until pH = 4, after which the resulting precipitate was collected by filtration, washed 3 x H_2O, and dried under vacuum to give crude product **21** as a white solid which was used without further purification (1.77 g, 80%).

Compound 22. Acid intermediate **21** (1.0 g, 4.6 mmol) was combined with H_2O (7 mL) and $NaHCO_3$ (0.39 g, 4.6 mmol) in a flask and stirred until complete dissolution of starting material. A prepared solution of CH_2Cl_2 (7 mL), Aliquat 336 (1.84 g, 4.6 mmol), and allyl bromide (0.6 g, 4.6 mmol) was then added to the aqueous solution and stirred at rt for 72 h. The mixture was then extracted three times with CH_2Cl_2, dried over $MgSO_4$, and solvents removed under reduced pressure. The desired product was purified by column chromatography (5% EtOAc in hexanes) giving **22** as a white solid (0.92 g, 78%):

^{1}H NMR (300 MHz, $CDCl_3$) δ 5.85 (m, 1H), 5.22 (m, 2H), 4.58 (d, J = 9.6 Hz, 2H), 3.62 (t, J = 6.3 Hz, 2H), 2.3 (t, J = 7.2 Hz, 2H), 1.6 (br m, 4H), 1.3 (br m, 14H); ^{13}C NMR (75 MHz, $CDCl_3$) δ 173.8, 132.5, 118.3, 65.1, 63.0, 34.4, 33.0, 29.7, 29.6, 29.4, 29.3, 26.0, 25.1; IR (KBr) ν 3357, 2927, 2852, 1737, 1649, 1463, 1176, 1108, 1062, 991, 925 cm^{-1}.

Compound 23. DMSO (0.6 mL, 8.5 mmol) in CH_2Cl_2 (4 mL) was added dropwise to a flask containing oxalyl chloride (0.34 mL, 4.3 mmol) in CH_2Cl_2 (24 mL) at –60 °C under argon. The reaction was stirred for 5 min., after which alcohol **15** (0.58 g, 2.3 mmol) dissolved in CH_2Cl_2 (10 mL) was added. The solution was warmed to –50 °C and stirred for an additional 20 min., then cooled to –70 °C and Et_3N (3 mL, dry) added slowly. After 20 min., H_2O (10 mL) was added and the solution allowed to warm to rt. The organic layer was separated, the aqueous layer extracted three times with CH_2Cl_2, and the combined organic layer washed 2 x brine and dried over $MgSO_4$. Solvents were removed under reduced pressure and the desired aldehyde **23** purified by column chromatography (5% EtOAc in hexanes) in 95% yield (0.55 g):

^{1}H NMR (300 MHz, $CDCl_3$) δ 9.76 (t, J = 1.8 Hz, 1H), 5.88 (m, 1H), 5.22 (m, 2H), 4.55 (d, J = 9.6 Hz, 2H), 2.42 (t, J = 7.5 Hz, 2H), 2.33 (t, J = 7.5 Hz, 2H), 1.60 (br m, 4H), 1.32 (br m, 12H); ^{13}C NMR (75 MHz, $CDCl_3$) δ 202.9, 173.5, 132.3, 118.0, 64.9, 43.9, 34.2, 29.3, 29.2, 29.1, 24.9, 22.0; IR (KBr) ν 2934, 2858, 2720, 1736, 1649, 1458, 1418, 1378, 1174, 1105, 991, 933 cm^{-1}.

Compound 24. The condensation of 1-nitrohexane with aldehyde **23** by methods identical to those in the preparation of nitroaldol product **12** gave **24** in 95% yield:

^{1}H NMR (300 MHz, $CDCl_3$) δ 5.88 (m, 1H), 5.22 (m, 2H), 4.60 (d, J = 9.6 Hz, 2H), 4.45 (m, 1H), 3.95 (m, 1H), 2.40 (t, J = 7.5 Hz, 2H), 2.10 (br m, 2H), 1.80 (br m, 2H), 1.65 (br m, 2H), 1.4 (br m, 20H), 0.92 (t, J = 7.5 Hz, 3H); ^{13}C NMR (75 MHz, $CDCl_3$) δ 173.4, 132.0, 117.7, 93.0, 92.3, 72.1, 71.9, 64.7, 34.0, 33.1, 33.0, 30.9, 30.8,

30.0, 29.2, 29.1, 29.06, 29.0, 28.8, 28.1, 25.4, 25.3, 25.1, 25.0, 24.7, 22.1, 13.6; IR (KBr) ν 3481, 2927, 2856, 1736, 1649, 1549, 1458, 1379, 1175, 1111, 989, 931, 842, 733 cm^{-1}.

Compound 25. Compound **25** was acetylated in an identical manner to the formation of **13**, giving intermediate **25** in 99% yield

^1H NMR (300 MHz, $CDCl_3$) δ 5.88 (m, 1H), 5.22 (m, 2H), 5.15 (m, 1H), 4.58 (m, 1H), 4.56 (d, J = 9.6 Hz, 2H), 2.25 (t, J = 7.5 Hz, 2H), 2.02 (s, 0.5H), 1.98 (s, 0.5H), 1.90 (br m, 2H), 1.6 (br m, 4H), 1.4 (br m, 20H), 0.82 (t, J = 7.5 Hz, 3H); ^{13}C NMR (75 MHz, $CDCl_3$) δ 173.3, 170.1, 169.7, 132.3, 117.9, 90.0, 89.5, 72.8, 72.7, 64.8, 34.1, 31.0, 30.9, 30.7, 29.7, 29.6, 29.3, 29.2, 29.1, 29.0, 28.8, 25.4, 25.2, 25.1, 24.8, 24.4, 22.1, 20.7, 20.6, 13.7; IR (KBr) ν 3086, 2929, 2857, 1744, 1649, 1554, 1462, 1373, 1228, 1173, 1111, 1023, 990, 931, 842, 732 cm^{-1}.

BIBLIOGRAPHY

Chapter I

(1) Faraday, M. *Phil. Trans. Royal Soc. London* **1825**, *115*, 440-466.

(2) Stock, A.; Pohland, E. *Ber. Dtsch. Chem. Ges.* **1926**, *59*, 2210-2215.

(3) Ulrich, G.; Ziessel, R.; Harriman, A. *Angew. Chem. Int. Ed.* **2008**, *47*, 1184-1201.

(4) Loudet, A.; Burgess, K. *Chem. Rev.* **2007**, *107*, 4891-4932.

(5) Bosdet, M. J. D.; Piers, W. E. *Can. J. Chem.* **2008**, *86*, 8-29.

(6) Dewar, M. J. S.; Marr, P. A. *J. Am. Chem. Soc.* **1962**, *84*, 3782.

(7) White, D. G. *J. Am. Chem. Soc.* **1963**, *85*, 3634-3636.

(8) Davies, K. M.; Dewar, M. J. S.; Rona, P. *J. Am. Chem. Soc.* **1967**, *89*, 6294-6297.

(9) Ferles, M.; Polivka, Z. *Collect. Czech. Chem. Commun.* **1968**, *33*, 2121-2129.

(10) Polivka, Z.; Kubelka, V.; Holubova, N.; Ferles, M. *Collection Czechoslov. Chem. Commun.* **1970**, *35*, 1131-1146.

(11) Le Toumelin, J. –B.; Baboulène, M. *New J. Chem.* **1999**, 111-116.

(12) Wille, H.; Goubeau, J. *Chem. Ber.* **1972**, *105*, 2156-2168.

(13) Wille, H.; Goubeau, J. *Chem. Ber.* **1974**, *107*, 110-116.

(14) Gronowitz, S.; Ander, I. *Chem. Scr.* **1980**, *15*, 23-26.

(15) Gronowitz, S.; Ander, I. *Chem. Scr.* **1980**, *15*, 135-144.

(16) Gronowitz, S.; Ander, I. *Chem. Scr.* **1980**, *15*, 145-151.

(17) Gronowitz, S.; Ander, I.; Zanirato, P. *Chem. Scr.* **1983**, *22*, 55-59.

(18) Ansorge, A.; Brauer, D. J.; Bürger, H.; Dörrenbach, F.; Hagen, T.; Pawelke, G.; Weuter, W. *J. Organomet. Chem.* **1990**, *396*, 253-267.

(19) Brauer, D. J.; Bürger, H.; Dittmar, T.; Pawelke, G. *Chem. Ber.* **1996**, *129*, 1541-1545.

(20) Jego, J. M.; Carboni, B.; Vaultier, M. *J. Organomet. Chem.* **1992**, *435*, 1-8.

(21) Bogdanov, V. S. ; Kiselev, V. G. ; Naumov, A. D. ; Vasil'ev, L. S. ; Dmitrikov, V. P. ; Dorokhov, V. A. ; Mikhailov, B. M. *Zhur. Obshchei Khim.* **1972**, *42*, 1547-1553.

(22) Vasil'ev, L. S. ; Dmitrilov, V. P. ; Bogdanov, V. S. ; Mikhailov, B. M. *Zhur. Obshchei Khim.* **1972**, *42*, 1318-1326.

(23) Chavant, P. Y.; Lhermitte, F.; Vaultier, M. *Synlett.* **1993**, *7*, 519-521.

(24) Münster, J.; Paetzold, P.; Schröder, E.; Schwan, H.; von Bennigsen-Mackiewicz, T. *Z. Anorg. Allg. Chem.* **2004**, *630*, 2641-2651.

(25) Ashe, A. J., III; Fang, X. *Org. Lett.* **2000**, *2*, 2089-2091.

(26) Ashe, A. J., III; Fang, X.; Fang, X.; Kampf, J. W. *Organometallics* **2001**, *20*, 5413-5418.

(27) Paetzold, P. *Adv. Inorg. Chem.* **1987**, *31*, 123-170.

(28) Schmidt, R. E.; Massa, W. *Z. Naturforsch.* **1984**, *39B*, 213-216.

(29) Pan, J.; Kampf, J. W.; Ashe, A. J., III *Organometallics* **2004**, *23*, 5626-5629.

(30) Pan, J.; Kampf, J. W.; Ashe, A. J., III *Organometallics* **2006**, *25*, 197-202.

(31) Pan, J.; Kampf, J. W.; Ashe, A. J., III *Organometallics* **2008**, *27*, 1345-1347.

(32) Pan, J.; Kampf, J. W.; Ashe, A. J., III *J. Organomet. Chem.* **2009**, *694*, 1036-1040.

(33) Pan, J.; Kampf, J. W.; Ashe, A. J., III *Org. Lett.* **2007**, *9*, 679-681.

(34) Abbey, E. R.; Zakharov, L. N.; Liu, S. –Y. *J. Am. Chem. Soc.* **2008**, *130*, 7250-7252.

(35) Campbell, P. G.; Zakharov, L. N.; Grant, D. J.; Dixon, D. A.; Liu, S. –Y. *J. Am. Chem. Soc.* **2010**, *132*, 3289-3291.

(36) Scheideman, M.; Wang, G.; Vedejs, E. *J. Am. Chem. Soc.* **2008**, *130*, 8669-8676.

(37) Hoffmann, R. *J. Chem. Phys.* **1964**, *40*, 2474-2480.

(38) Kaufman, J. J.; Hamann, J. R. *Adv. Chem. Ser.* **1964**, *42*, 270-280.

(39) Dewar, M. J. S. *Adv. Chem. Ser.* **1964**, *42*, 227-250.

(40) Carbó, R.; De Giambiagi, M. S.; Giambiagi, M. *Theo. Chim. Acta* **1969**, *14*, 147-162.

(41) Michl, J. *Collect. Czech. Chem. Commun.* **1971**, *36*, 1248-1278.

(42) Massey, S. T.; Zoellner, R. W. *Int. J. Quant. Chem.* **1991**, *39*, 787-804.

(43) Kranz, M.; Clark, T. *J. Org. Chem.* **1992**, *57*, 5492-5500.

(44) Del Bene, J. E.; Yáñez, M.; Alkorta, I.; Elguero, J. *J. Chem. Theory Comput.* **2009**, *5*, 2239-2247.

(45) Matus, M. H.; Liu, S. –Y.; Dixon, D. A. *J. Phys. Chem. A* **2010**, *114*, 2644-2654.

(46) Silva, P. J.; Ramos, M. J. *J. Org. Chem.* **2009**, *74*, 6120-6129.

(47) Sagara, T.; Ganz, E. *J. Phys. Chem. C* **2008**, *112*, 3515-3518.

(48) Wong, M.; Van Kuiken, B. E.; Buda, C.; Dunietz, B. D. *J. Phys. Chem. C* **2009**, *113*, 12571-12579.

(49) Fazen, P. J.; Burke, L. A. *Inorg. Chem.* **2006**, *45*, 2494-2500.

(50) Gilbert, T. M. *Tet. Lett.* **1998**, *39*, 9147-9150.

(51) Gilbert, T. M. *Organometallics* **2000**, *19*, 1160-1165.

(52) Gilbert, T. M. *Organometallics* **1998**, *17*, 5513-5520.

(53) Gilbert, T. M. *Organometallics* **2003**, *22*, 3748-3752.

(54) Bissett, K. M.; Gilbert, T. M. *Organometallics* **2004**, *23*, 5048-5053.

(55) Gilbert, T. M. *Organometallics* **2005**, *24*, 6445-6449.

(56) Dewar, M. J. S.; Dietz, R. *J. Chem. Soc.* **1959**, 2728-2730.

(57) Dewar, M. J. S.; Dietz, R.; Kubba, V. P.; Lepley, A. R. *J. Am. Chem. Soc.* **1961**, *83*, 1754-1756.

(58) Dewar, M. J. S.; Dietz, R. *Tetrahedron* **1961**, *15*, 26-34.

(59) Dewar, M. J. S.; Dietz, R. *J. Org. Chem.* **1961**, *26*, 3253-3256.

(60) Dewar, M. J. S.; Hashmall, J.; Kubba, V. P. *J. Org. Chem.* **1964**, *29*, 1755-1757.

(61) Dewar, M. J. S.; Gleicher, G. J.; Robinson, B. P. *J. Am. Chem. Soc.* **1964**, *86*, 5698-5699.

(62) Dewar, M. J. S.; Jones, R. *J. Am. Chem. Soc.* **1968**, *90*, 2137-2144.

(63) Davis, F. A.; Dewar, M. J. S.; Jones, R.; Worley, S. D. *J. Am. Chem. Soc.* **1969**, *91*, 2094-2097.

(64) Davis, F. A.; Dewar, M. J. S.; Jones, R. *J. Am. Chem. Soc.* **1968**, *90*, 706-708.

(65) Dewar, M. J. S.; Worley, S. D. *J. Chem. Phys.* **1969**, *50*, 654-667.

(66) Dewar, M. J. S.; Jones, R. *Tet. Lett.* **1968**, *22*, 2707-2708.

(67) Paetzold, P. I.; Stohr, G.; Maisch, H.; Lenz, H. *Chem. Ber.* **1968**, *101*, 2881-2888.

(68) Meller, E. G.; Luthin, W. *Z. Anorg. Allg. Chem.* **1988**, *560*, 18-26.

(69) Paetzold, P.; Stanescu, C.; Stubenrauch, J. R.; Bienmüller, M.; Englert, U. *Z. Anorg. Allg. Chem.* **2004**, *630*, 2632-2640.

(70) Boese, R.; Finke, N.; Henkelmann, J.; Meier, G.; Paetzold, P.; Reisenauer, H. P.; Schmid, G. *Chem. Ber.* **1985**, *118*, 1644-1654.

(71) Pan, J.; Kampf, J. W.; Ashe, A. J., III *Organometallics* **2009**, *28*, 506-511.

(72) Fang, X.; Yang, H.; Kampf, J. W.; Banaszak Holl, M. M.; Ashe, A. J., III *Organometallics* **2006**, *25*, 513-518.

(73) Ishida, N.; Narumi, M.; Murakami, M. *Org. Lett.* **2008**, *10*, 1279-1281.

(74) McCormick, C. L.; Butler, G. B. *J. Org. Chem.* **1976**, *41*, 2803-2808.

(75) Catlin, J. C.; Snyder, H. R. *J. Org. Chem.* **1969**, *34*, 1660-1663.

(76) Catlin, J. C.; Snyder, H. R. *J. Org. Chem.* **1969**, *34*, 1664-1668.

(77) Köster, R.; Iwasaki, K.; Hattori, S.; Morita, Y. *Just. Lieb. Ann. Chem.* **1969**, *720*, 23-31.

(78) Scheideman, M.; Shapland, P.; Vedejs, E. *J. Am. Chem. Soc.* **2003**, *125*, 10502-10503.

(79) Midland, M. M.; Kazubski, A. *J. Org. Chem.* **1992**, *57*, 2953-2956.

(80) Dang, H. –S.; Diart, V.; Roberts, B. P. *J. Chem. Soc., Perkin Trans. 1* **1994**, *8*, 1033-1041.

(81) Dang, H. –S.; Diart, V.; Roberts, B. P.; Tocher, D. A. *J. Chem. Soc., Perkin Trans. 2* **1994**, *5*, 1039-1045.

(82) Sobieralski, T. J.; Hancock, K. G. *J. Am. Chem. Soc.* **1982**, *104*, 7533-7541.

(83) Sobieralski, T. J.; Hancock, K. G. *J. Am. Chem. Soc.* **1982**, *104*, 7542-7548.

(84) Kafka, S.; Trska, P.; Kytner, J.; Taufmann, P.; Ferles, M. *Collect. Czech. Chem. Commun.* **1987**, *52*, 2047-2056.

(85) Michl, J.; Jones, R. *Collect. Czech. Chem. Commun.* **1971**, *36*, 1233-1247.

(86) Hammond, H. A. *Theo. Chim. Acta* **1970**, *18*, 239-249.

(87) Kar, T.; Elmore, D. E.; Scheiner, S. *J. Mol. Struct. (Theochem)* **1997**, *392*, 65-74.

(88) Maouche, B.; Gayoso, J.; Ouamerali, O. *Rev. Roumaine Chim.* **1984**, *29*, 613-620.

(89) De Giambiagi, M. S.; Giambiagi, M.; Schrott, A. G. *J. Chim. Phys. Phys. Chim. Bio.* **1976**, *73*, 909-911.

(90) Paetzold, P.; Richter, A.; Thijssen, T.; Würtenberg, S. *Chem. Ber.* **1979**, *112*, 3811-3827.

(91) Paetzold, P.; Schröder, E.; Schmid, G.; Boese, R. *Chem. Ber.* **1985**, *118*, 3205-3216.

(92) Gilbert, T. M. *Organometallics* **2003**, *22*, 2298-2304.

(93) Ashe, A. J., III; Yang, H.; Fang, X.; Kampf, J. W. *Organometallics* **2002**, *21*, 4578-4580.

(94) Pan, J.; Wang, J.; Banaszak Holl, M. M.; Kampf, J. W.; Ashe, A. J., III *Organometallics* **2006**, *25*, 3463-3467.

(95) Orian, L. *Rev. Roumaine Chim.* **2007**, *52*, 551-558.

(96) Wrackmeyer, B.; Ordung, I.; Schwarze, B. *J. Organomet. Chem.* **1997**, *532*, 71-77.

(97) Wrackmeyer, B.; Schwarze, B. *J. Organomet. Chem.* **1997**, *534*, 181-186.

(98) Wrackmeyer, B.; Schwarze, B.; Milius, W. *J. Organomet. Chem.* **1997**, *545-546*, 297-308.

(99) Matteson, D. S.; Biernbaum, M. S.; Bechtold, R. A.; Campbell, J. D.; Wilcsek, R. J. *J. Org. Chem.* **1978**, *43*, 950-954.

(100) Dewar, M. J. S.; Kubba, V. P.; Pettit, R. *J. Chem. Soc.* **1958**, 3073-3076.

(101) Dewar, M. J. S.; Kubba, V. P. *Tetrahedron* **1959**, *7*, 213-222.

(102) Dewar, M. J. S.; Kubba, V. P. *J. Org. Chem.* **1960**, *25*, 1722-1724.

(103) Dewar, M. J. S.; Kubba, V. P. *J. Am. Chem. Soc.* **1961**, *83*, 1757-1760.

(104) Dewar, M. J. S.; Miatlis, P. M. *J. Am. Chem. Soc.* **1961**, *83*, 187-193.

(105) Dewar, M. J. S.; Maitlis, P. M. *Tetrahedron* **1961**, *15*, 35-45.

(106) Köster, R.; Hattori, S.; Morita, Y. *Angew. Chem., Int. Ed.* **1965**, *4*, 695.

(107) Harris, K. D. M.; Kariuki, B. M.; Lambropoulos, C.; Philp, D.; Robinson, J. M. A. *Tetrahedron* **1997**, *53*, 8599-8612.

(108) Robinson, J. M. A.; Kariuki, B. M.; Philp, D.; Harris, K. D. M. *Tet. Lett.* **1997**, *38*, 6281-6284.

(109) Dewar, M. J. S.; Kaneko, C.; Bhattacharyee, M. K. *J. Am. Chem. Soc.* **1962**, *84*, 4884-4887.

(110) Bosdet, M. J. D.; Jaska, C. A.; Piers, W. E.; Sorensen, T. S.; Parvez, M. *Org. Lett.* **2007**, *9*, 1395-1398.

(111) Jaska, C. A.; Piers, W. E.; McDonald, R.; Parvez, M. *J. Org. Chem.* **2007**, *72*, 5234-5243.

(112) Grisdale, P. J.; Williams, J. L. R. *J. Org. Chem.* **1969**, *34*, 1675-1677.

(113) Grisdale, P. J.; Glogowski, M. E.; Williams, J. L. R. *J. Org. Chem.* **1971**, *36*, 3821-3824.

(114) Glogowski, M. E.; Grisdale, P. J.; Williams, J. L. R.; Regan, T. H. *J. Organomet. Chem.* **1973**, *54*, 51-60.

(115) Glogowski, M. E.; Williams, J. L. R. *J. Organomet. Chem.* **1980**, *195*, 123-135.

(116) Hannant, M. H.; Wright, J. A.; Lancaster, S. J.; Hughes, D. L.; Horton, P. N.; Bochmann, M. *Dalton Trans.* **2006**, 2415-2426.

(117) Mulller, K. D.; Niedenzu, K. *Inorg. Chim. Acta* **1977**, *25*, L53-L54.

(118) Chissick, S. S.; Dewar, M. J. S.; Maitlis, P. M. *Tet. Lett.* **1960**, *23*, 8-10.

(119) Leardini, R.; Zanirato, P. *J. Chem. Soc., Chem. Comm.* **1983**, *7*, 396-397.

(120) Zanirato, P. *J. Organomet. Chem.* **1985**, *293*, 285-293.

(121) Barton, J. W.; Lapham, D. J. *Tet. Lett.* **1979**, *37*, 3571-3572.

(122) Wrackmeyer, B.; Schwarze, B.; Milius, W.; Boese, R.; Parchment, O. G.; Webb, G. A. *J. Organomet. Chem.* **1998**, *552*, 247-254.

(123) Dewar, M. J. S.; Poesche, W. H. *J. Am. Chem. Soc.* **1963**, *85*, 2253-2256.

(124) Culling, G. C.; Dewar, M. J. S.; Marr, P. A. *J. Am. Chem. Soc.* **1964**, *86*, 1125-1127.

(125) Dewar, M. J. S.; Poesche, W. H. *J. Org. Chem.* **1964**, *29*, 1757-1762.

(126) Ashton, P. R.; Harris, K. D. M.; Kariuki, B. M.; Philp, D.; Robinson, J. M. A.; Spencer, N. *J. Chem. Soc., Perkin Trans. 2* **2001**, 2166-2173.

(127) Dewar, M. J. S.; Poesche, W. H. *J. Chem. Soc.* **1963**, 2201-2203.

(128) Bosdet, M. J. D.; Piers, W. E.; Sorensen, T. S.; Parvez, M. *Angew. Chem. Int. Ed.* **2007**, *46*, 4940-4943.

(129) Enders, M.; Ludwig, G.; Pritzkow, H. *Organometallics* **2002**, *21*, 3856-3859.

(130) Mayer, E. P.; Nöth, H. *Chem. Ber.* **1993**, *126*, 1551-1557.

(131) Doerksen, R. J.; Thakkar, A. J. *J. Phys. Chem. A* **1998**, *102*, 4679-4686.

(132) Asakura, M.; Oki, M.; Toyota, S. *Organometallics* **2000**, *19*, 206-208.

(133) Maitlin, P. M. *J. Chem. Soc.* **1961**, 425-429.

(134) Bel'skii, V. K.; Nesterova, S. V.; Reikhsfel'd *Zh. Struct. Khim.* **1987**, *28*, 186-187.

(135) Kranz, M.; Hampel, F.; Clark, T. *J. Chem. Soc., Chem. Comm.* **1992**, 1247-1248.

(136) Agou, T.; Kobayashi, J.; Kawashima, T. *Org. Lett.* **2006**, *8*, 2241-2244.

(137) Agou, T.; Kobayashi, J.; Kawashima, T. *Chem. Comm.* **2007**, 3204-3206.

(138) Agou, T.; Sekine, M.; Kobayashi, J.; Kawashima, T. *Chem. Comm.* **2009**, 1894-1896.

(139) Agou, T.; Sekine, M.; Kobayashi, J.; Kawashima, T. *Chem. Eur. J.* **2009**, *15*, 5056-5062.

(140) Agou, T.; Kojima, T.; Kobayashi, J.; Kawashima, T. *Org. Lett.* **2009**, *11*, 3534-3537.

(141) Massey, S. T.; Zoellner, R. W. *Inorg. Chem.* **1991**, *30*, 1063-1066.

(142) Schreyer, P.; Paetzold, R.; Boese, R. *Chem. Ber.* **1988**, *121*, 195-205.

(143) Köster, R.; Iwasaki, K. *Adv. Chem. Ser.* **1964**, *42*, 148-165.

(144) Turner, H. S.; Warne, R. J.; Lawrenson, I. J. *Chem. Comm.* **1965**, 20-21.

(145) Bartlett, R. K.; Turner, H. S.; Warne, R. J.; Young, M. A.; Lawrenson, I. J. *J. Chem. Soc. A, Inorg. Phys. Theo.* **1966**, 479-500.

(146) Blackborow, J. R.; Lockhart, J. C. *J. Chem. Soc., Dalton Trans.* **1973**, 1303-1308.

(147) Allaoud, S.; El Mouhtadi, M.; Frange, B. *Nouveau J. Chim.* **1985**, *9*, 499-504.

(148) Cueilleron, J.; Frange, B. *Bull. Soc. Chim. France* **1972**, 107-110.

(149) Frange, B. *Bull. Soc. Chim. France* **1972**, 2165-2168.

(150) Devallez, B.; Frange, B. *J. Chim. Phys.* **1977**, *74*, 1010-1014.

(151) Alloud, S.; Karim, A.; Mortreux, A.; Petit, F.; Frange, B. *J. Organomet. Chem.* **1989**, *379*, 89-95.

(152) Allaoud, S.; Conté, S.; Fenet, B.; Frange, B.; Robert, F.; Sécheresse, F.; Karim, A. *J. Organomet. Chem.* **1994**, *469*, 59-68.

(153) Abouhamza, B.; Ali, M. A.; Alloud, S.; Blacque, O.; Frange, B.; Karim, A. *Acta Cryst. C* **2001**, *C57*, 796-798.

(154) Nöth, H.; Fritz, P. *Z. Anorg. Allg. Chem.* **1963**, *324*, 129-145.

(155) Goetze, R.; Nöth, H. *J. Organomet. Chem.* **1978**, *145*, 151-166.

(156) Carmalt, C. J.; Clegg, W.; Cowley, A. H.; Lawlor, F. J.; Marder, T. B.; Norman, N. C.; Rice, C. R.; Sandoval, O. J.; Scott, A. J. *Polyhedron* **1997**, *16*, 2325-2328.

(157) Brubaker, G. L.; Shore, S. G. *Inorg. Chem.* **1969**, *8*, 2804-2806.

(158) Alibadi, M. A. M.; Batsanov, A. S.; Bramham, G.; Charmant, J. P. H.; Haddow, M. F.; MacKay, L.; Mansell, S. M.; McGrady, J. E.; Norman, N. C.; Roffey, A.; Russell, C. A. *Dalton Trans.* **2009**, 5348-5354.

(159) Dai, C.; Johnson, S. M.; Lawlor, F. J.; Lightfoot, P.; Marder, T. B.; Norman, N. C.; Orpen, G. A.; Pickett, N. L.; Quayle, M. J.; Rice, C. R. *Polyhedron* **1998**, *17*, 4139-4143.

(160) Siebert, W.; Full, R. *Angew. Chem. Int. Ed.* **1976**, *15*, 45-46.

(161) Siebert, W.; Full, R.; Schmidt, H. *J. Organomet. Chem.* **1980**, *191*, 15-25.

(162) Schmidt, H.; Siebert, W. *J. Organomet. Chem.* **1978**, *155*, 157-163.

(163) Asgarouladi, B.; Full, R.; Schaper, K. –J.; Siebert, W. *Chem. Ber.* **1974**, *107*, 34-47.

(164) Thiele, B.; Paetzold, P.; Englert, U. *Chem. Ber.* **1992**, *125*, 2681-2686.

(165) Emslie, D. J. H.; Piers, W. E.; Parvez, M. *Angew. Chem. Int. Ed.* **2003**, *42*, 1252-1255.

(166) Jaska, C. A.; Emslie, D. J. H.; Bosdet, M. J. D.; Piers, W. E.; Sorensen, T. S.; Parvez, M. *J. Am. Chem. Soc.* **2006**, *128*, 10885-10896.

(167) Forster, T. D.; Krahulic, K. E.; Tuononen, H. M.; McDonald, R.; Parvez, M.; Roesler, R. *Angew. Chem. Int. Ed.* **2006**, *45*, 6356-6359.

(168) Krahulic, K. E.; Tuononen, H. M.; Parvez, M.; Roesler, R. *J. Am. Chem. Soc.* **2009**, *131*, 5858-5865.

(169) Prasang, C.; Donnadieu, B.; Bertrand, G. *J. Am. Chem. Soc.* **2005**, *127*, 10182-10183.

(170) Miller, N. E.; Muetterties, E. L. *Inorg. Chem.* **1964**, *3*, 1196-1197.

(171) Miller, N. E.; Murphy, M. D.; Reznicek, D. L. *Inorg. Chem.* **1966**, *5*, 1832-1834.

(172) Miller, N. E. *Inorg. Chem.* **1977**, *16*, 2664-2667.

(173) Miller, N. E. *J. Organomet. Chem.* **1977**, *137*, 131-143.

(174) Miller, N. E. *J. Organomet. Chem.* **1984**, *269*, 131-143.

(175) Magera, M. J.; Miller, N. E. *J. Organomet. Chem.* **1988**, *339*, 231-239.

(176) Miller, N. E.; Reznicek, D. L. *J. Organomet. Chem.* **1988**, *349*, 11-22.

(177) Miller, N. E. *Inorg. Chem.* **1988**, *27*, 2196-2200.

(178) Miller, N. E. *Inorg. Chem.* **1991**, *30*, 2228-2231.

(179) Webb, K. M.; Miller, N. E. *J. Organomet. Chem.* **1993**, *460*, 1-6.

(180) Hseu, T. H.; Larsen, L. A. *Inorg. Chem.* **1975**, *14*, 330-334.

(181) Gragg, B. R.; Ryschkewitsch, G. E. *Inorg. Chem.* **1976**, *15*, 1209-1212.

(182) Hesse, G.; Witte, H. *Angew. Chem. Int. Ed.* **1963**, *2*, 617.

(183) Bresadola, S.; Carraro, G.; Pecile, C.; Turco, A. *Tet. Lett.* **1964**, 3185-3188.

(184) Hesse, G.; Witte, H. *Justus Liebigs Ann. Chem.* **1965**, *687*, 1-9.

(185) Hesse, G.; Witte, H.; Bittner, G. *Justus Liebigs Ann. Chem.* **1965**, *687*, 9-14.

(186) Tanaka, J.; Carter, J. C. *Tet. Lett.* **1965**, 329-332.

(187) Bresdola, S.; Rossetto, F.; Puosi, G. *Tet. Lett.* **1965**, 4775-4778.

(188) Hesse, G.; Witte, H.; Haussleiter, H. *Angew. Chem. Int. Ed.* **1966**, *5*, 723.

(189) Casanova, J., Jr.; Kiefer, H. R. *J. Org. Chem.* **1969**, *34*, 2579-2583.

(190) Tamm, M.; Lügger, T.; Hahn, F. E. *Organometallics* **1996**, *15*, 1251-1256.

(191) Padilla-Martínez, I. I.; Rosalez-Hoz, M. d. J.; Contreras, R.; Kerschl, S.; Wrackmeyer, B. *Chem. Ber.* **1994**, *127*, 343-346.

(192) Padilla-Martínez, I. I.; Martínez-Martínez, F. J.; López-Sandoval, A.; Girón-Castillo, K. I.; Brito, M. A.; Contreras, R. *Eur. J. Inorg. Chem.* **1998**, 1547-1553.

(193) Okada, K.; Suzuki, R.; Oda, M. *J. Chem. Soc., Chem. Comm.* **1995**, 2069-2070.

(194) Wacker, A.; Pritzkow, H.; Siebert, W. *Eur. J. Inorg. Chem.* **1999**, 789-793.

(195) Arrowsmith, M.; Heath, A.; Hill, M. S.; Hitchcock, P. B.; Köhn-Kociok, G. *Organometallics* **2009**, *28*, 4550-4559.

(196) Ishikura, M.; Mano, T.; Oda, I.; Terashima, M. *Heterocycles* **1984**, *22*, 2471-2474.

(197) Hodgkins, T. G. *Inorg. Chem.* **1993**, *32*, 6115-6116.

(198) Hodgkins, T. G.; Powell, D. R. *Inorg. Chem.* **1996**, *35*, 2140-2148.

(199) Garcia, F.; Hopkins, A. D.; Kowenicki, R. A.; McPartlin, M.; Silvia, J. S.; Rawson, J. M.; Rogers, M. C.; Wright, D. S. *Chem. Comm.* **2007**, 568-588.

(200) Murafuji, T.; Mouri, R.; Sugihara, Y. *Tetrahedron* **1996**, *52*, 13933-13938.

(201) Luckert, S.; Eversheim, E.; Müller, M.; Redenz-Stormanns, B.; Englert, U.; Paetzold, P. *Chem. Ber.* **1995**, *128*, 1029-1035.

(202) Paetzold, P.; Kiesgen, J.; Luckert, S.; Spaniol, T.; Englert, U. *Z. Anorg. Allg. Chem.* **2002**, *628*, 1631-1635.

Chapter II

(1) Dewar, M. J. S. *Adv. Chem. Ser.* **1964**, *42*, 227-250.

(2) Fang, X.; Yang, H.; Kampf, J. W.; Banaszak Holl, M. M.; Ashe, A. J., III *Organometallics* **2006**, *25*, 513-518.

(3) Bosdet, M. J. D.; Jaska, C. A.; Piers, W. E.; Sorensen, T. S.; Parvez, M. *Org. Lett.* **2007**, *9*, 1395-1398.

(4) Bosdet, M. J. D.; Piers, W. E.; Sorensen, T. S.; Parvez, M. *Angew. Chem. Int. Ed.* **2007**, *46*, 4940-4943.

(5) Dewar, M. J. S.; Marr, P. A. *J. Am. Chem. Soc.* **1962**, *84*, 3782.

(6) White, D. G. *J. Am. Chem. Soc.* **1963**, *85*, 3634-3636.

(7) Ashe, A. J., III; Fang, X.; Fang, X.; Kampf, J. W. *Organometallics* **2001**, *20*, 5413-5418.

(8) Ashe, A. J., III; Fang, X. *Org. Lett.* **2000**, *2*, 2089-2091.

(9) Pan, J.; Kampf, J. W.; Ashe, A. J., III *Organometallics* **2004**, *23*, 5626-5629.

(10) Pan, J.; Kampf, J. W.; Ashe, A. J., III *Organometallics* **2006**, *25*, 197-202.

(11) Pan, J.; Kampf, J. W.; Ashe, A. J., III *Organometallics* **2009**, *28*, 506-511.

(12) Pan, J.; Kampf, J. W.; Ashe, A. J., III *J. Organomet. Chem.* **2009**, *694*, 1036-1040.

(13) Marwitz, A. J. V.; Abbey, E. R.; Jenkins, J. T.; Zakharov, L. N.; Liu, S. –Y. *Org. Lett.* **2007**, *9*, 4905-4908.

(14) Zúñiga, C.; Garduño, L.; Cruz, M. d. C.; Salazar, M.; Pérez-Pastén, R.; Chamorro, G.; Labarrios, F.; Tamariz, J. *Drug. Dev. Res.* **2005**, *64*, 28-40.

(15) Sundermeier, M.; Zapf, A.; Beller, M. *Eur. J. Inorg. Chem.* **2003**, 3513–3526.

(16) Fehlhammer, W. P.; Fritz, M. *Chem. Rev.* **1993**, *93*, 1243–1280.

(17) Ellis, G. P.; Romney-Alexander, T. M. *Chem. Rev.* **1987**, *87*, 779–794.

(18) Marwitz, A. J. V.; McClintock, S. P.; Zakharov, L. N.; Liu, S. –Y. *Chem. Comm.* **2010**, *46*, 779-781.

(19) Tishkov, A. A.; Mayr, H. *Angew. Chem., Int. Ed.* **2005**, *44*, 142–145.

(20) Chen, Z.; Wannere, C. S.; Corminboeuf, C.; Puchta, R.; Schleyer, P. R. *Chem. Rev.* **2005**, *105*, 3842–3888.

(21) Wu, T. K.; Dailey, B. P. *J. Chem. Phys.* **1964**, *41*, 2796.

(22) Herberich, G. E.; Schmidt, B.; Englert, U. *Organometallics* **1995**, *14*, 471-480.

(23) Hoic, D. A.; DiMare, M.; Fu, G. C. *J. Am. Chem. Soc.* **1997**, *119*, 7155-7156.

(24) Manzer, L. E.; Seidel, W. C. *J. Am. Chem. Soc.* **1975**, *97*, 1956-1957.

(25) Manzer, L. E.; Anton, M. F. *Inorg. Chem.* **1977**, *16*, 1229-1231.

(26) Marynick, D. S.; Throckmorton, L.; Bacquet, R. *J. Am. Chem. Soc.* **1982**, *104*, 1-5.

(27) Hahn, F. E.; Tamm, M.; Lügger, T. *Angew. Chem.* **1994**, *106*, 1419-1421.

(28) Hahn, F. E.; Plumed, C. G.; Münder, M.; Lügger, T. *Chem. Eur. J.* **2004**, *10*, 6285-6293.

(29) Paek, J. H.; Song, K. H.; Jung, I.; Kang, S. O.; Ko, J. *Inorg. Chem.* **2007**, *46*, 2787-2796.

(30) Beck, G.; Lappert, M. F.; Hitchcock, P. B. *J. Organomet. Chem.* **1994**, *468*, 143-148.

(31) Fehlhammer, W. P.; Schoder, F.; Weinberger, B.; Stolzenberg, H.; Beck, W. *Z. Anorg. Allg. Chem.* **2009**, *635*, 1367-1373.

(32) Goetz, C.; Stolzenberg, H.; Fehlhammer, W. P. *J. Chem. Soc., Chem. Comm.* **1982**, 184-185.

(33) King, R. B. *Inorg. Chem.* **1967**, *6*, 25-29.

(34) Dale, J. *Tetrahedron* **1993**, *49*, 8707-8725.

(35) Abbey, E. R.; Zakharov, L. N.; Liu, S. –Y. *J. Am. Chem. Soc.* **2008**, *130*, 7250-7252.

(36) Qiao, S.; Hoic, D. A.; Fu, G. C. *J. Am. Chem. Soc.* **1996**, *118*, 6329-6330.

(37) Schödel, H.; Näther, C.; Bock, H. *Acta. Cryst. C* **1995**, *C51*, 1841-1844.

(38) Mantina, M.; Chamberlin, A. C.; Valero, R.; Cramer, C. J.; Truhlar, D. G. *J. Phys. Chem. A* **2009**, *113*, 5806-5812.

(39) Allen, F. H.; Kennard, O.; Watson, D. G.; Brammer, L.; Orpen. A. G.; Taylor, R. *J. Chem. Soc. Perkin Trans. II* **1987**, S1-S19.

(40) Balaban, A. T.; Paraschiv, M. *Rev. Roumaine Chim.* **1982**, 27, 513-521.

(41) Dewar, M. J. S.; Maitlis, P. M. *Tetrahedron* **1961**, *15*, 35-45.

(42) Gillespie, R. J.; Bytheway, I.; Robinson, E. A. *Inorg. Chem.* **1998**, *37*, 2811-2825.

(43) Cordero, B.; Gómez, V.; Platero-Prats, A. E.; Revés, M.; Echeverría, J.; Cremades, E.; Barragán, F.; Alvarez, S. *Dalton Trans.* **2008**, 2832-2838.

(44) Anand, B.; Nöth, H.; Schwenk-Kircher, H.; Troll, A. *Eur. J. Inorg. Chem.* **2008**, 3186-3199.

(45) Dewar, M. J. S.; Dietz, R. *J. Chem. Soc.* **1959**, 2728-2730.

(46) Paetzold, P.; Stanescu, C.; Stubenrauch, J. R.; Bienmüller, M.; Englert, U. *Z. Anorg. Allg. Chem.* **2004**, *630*, 2632-2640.

(47) Harris, K. D. M.; Kariuki, B. M.; Lambropoulos, C.; Philp, D.; Robinson, J. M. A. *Tetrahedron* **1997**, *53*, 8599-8612.

(48) Mavridis, A. *Acta Cryst. B* **1977**, *B33*, 3612-3615.

(49) Keefe, C. D.; Brand, E. *J. Mol. Struct.* **2004**, *691*, 181-189.

(50) Tanjaroon, C.; Daly, A.; Marwitz, A. J. V.; Liu, S. –Y.; Kukolich, S. J. Chem. Phys. 2009, 131, 224312/1-224312/9

(51) Pan, J.; Kampf, J. W.; Ashe, A. J., III *Org. Lett.* **2007**, *9*, 679-681.

(52) Lamm, A. N.; Liu, S. –Y. *Mol. BioSyst.* **2009**, *5*, 1303-1305.

Chapter III

(1) Faraday, M. *Philos. Trans. R. Soc. London* **1825**, *115*, 440-466.

(2) Schleyer, P. v. R. *Chem. Rev.* **2005**, *105*, 3433-3435.

(3) Astruc, D. In *Modern Arene Chemistry*; Astruc, D., Ed.; Wiley-VCH: Weinheim, **2002**, pp. 1-19.

(4) Stock, A.; Pohland, E. *Ber. Dtsch. Chem. Ges.* **1926**, *59*, 2210-2215.

(5) Schleyer, P. v. R.; Jiao, H.; Hommes, N. J. R. v. E.; Malkin, V. G.; Malkina, O. L. *J. Am. Chem. Soc.* **1997**, *119*, 12669-12670.

(6) Chiavarino, B.; Crestoni, M. E.; Di Marzio, A.; Fornarini, S.; Rosi, M. *J. Am. Chem. Soc.* **1999**, *121*, 11204-11210.

(7) Islas, R.; Chamorro, E.; Robles, J.; Heine, T.; Santos, J. C. *Struct. Chem.* **2007**, *18*, 833-839.

(8) Mokhtari, M.; Park, H. S.; Roesky, H. W.; Johnson, S. E.; Bolse, W.; Conrad, J.; Plass, W. *Chem. Eur. J.* **1996**, *2*, 1269-1274.

(9) Fazen, P. J.; Remsen, E. E.; Beck, J. S.; Carroll, P. J.; McGhie, A. R.; Sneddon, L. G. *Chem. Mater.* **1995**, *7*, 1942-1956.

(10) Stephens, F. H.; Pons, V.; Baker, R. T. *Dalton Trans.* **2007**, 2613-2626.

(11) Dewar, M. J. S. *Adv. Chem. Ser.* **1964**, *42*, 227-250.

(12) Bosdet, M. J. D.; Piers, W. E.; Sorensen, T. S.; Parvez, M. *Angew. Chem. Int. Ed.* **2007**, *46*, 4940-4943.

(13) Paetzold, P.; Stanescu, C.; Stubenrauch, J. R.; Bienmüller, M.; Englert, U. *Z. Anorg. Allg. Chem.* **2004**, *630*, 2632-2640.

(14) Dewar, M. J. S.; Marr, P. A. *J. Am. Chem. Soc.* **1962**, *84*, 3782.

(15) White, D. G. *J. Am. Chem. Soc.* **1963**, *85*, 3634-3636.

(16) Ashe, A. J., III; Fang, X. *Org. Lett.* **2000**, *2*, 2089-2091.

(17) Ashe, A. J., III; Fang, X.; Fang, X.; Kampf, J. W. *Organometallics* **2001**, *20*, 5413-5418.

(18) Marwitz, A. J. V.; Abbey, E. R.; Jenkins, J. T.; Zakharov, L. N.; Liu, S. – Y. *Org. Lett.* **2007**, *9*, 4905-4908.

(19) Davies, K. M.; Dewar, M. J. S.; Rona, P. *J. Am. Chem. Soc.* **1967**, *89*, 6294-6297.

(20) Greene, T. W.; Wuts, P. G. M. In *Protective Groups in Organic Synthesis*; Wuts, P. G. M., Ed.; John Wiley & Sons: Hoboken, NJ, **1999**, pp. 579-580.

(21) Pan, J.; Kampf, J. W.; Ashe, A. J., III *Organometallics* **2004**, *23*, 5626-5629.

(22) Jung, M. E.; Lyster, M. A. *J. Org. Chem.* **1977**, *42*, 3761-3764.

(23) Ikemoto, N.; Schreiber, S. L. *J. Am. Chem. Soc.* **1992**, *114*, 2524-2536.

(24) Bull, S. D.; Davies, S. G.; Fenton, G.; Mulvaney, A. W.; Prasad, R. S.; Smith, A. D. *Chem. Comm.* **2000**, 337-338.

(25) Marwitz, A. J. V.; Matus, M. H.; Zakharov, L. N.; Dixon, D. A.; Liu, S. –Y. *Angew. Chem. Int. Ed.* **2009**, *48*, 973-977.

(26) Pan, J.; Kampf, J. W.; Ashe, A. J., III *Org. Lett.* **2007**, *9*, 679-681.

(27) Abbey, E. R.; Zakharov, L. N.; Liu, S. –Y. *J. Am. Chem. Soc.* **2008**, *130*, 7250-7252.

(28) Chen, Z.; Wannere, C. S.; Corminboeuf, C.; Puchta, R.; Schleyer, P. v. R. *Chem. Rev.* **2005**, *105*, 3842-3888.

(29) Cyranski, M. K. *Chem. Rev.* **2005**, *105*, 3773-3811.

(30) Feller, D.; Dixon, D. A. J. Phys. Chem. A 2000, 104, 3048-3056.

(31) Matus, M. H.; Anderson, K.; Camaioni, D. M.; Autrey, S. T.; Dixon, D. A. *J. Phys. Chem. A* **2007**, *111*, 4411-4421.

(32) Hoic, D. A.; Davis, W. M.; Fu, G. C. *J. Am. Chem. Soc.* **1995**, *117*, 8480-8481.

(33) Wang, Y.; Angermund, K.; Goddard, R.; Kruger, C. *J. Am. Chem. Soc.* **1987**, *109*, 587-589.

(34) Michl, J. *Collect. Czech. Chem. Commun.* **1971**, *36*, 1248-1278.

(35) Massey, S. T.; Zoellner, R. W. *Int. J. Quant. Chem.* **1991**, *39*, 787-804.

(36) Vormann, K.; Dreizler, H.; Doose, J.; Guarnieri, A. *Z. Naturforsch., A* **1991**, *46*, 770-776.

(37) Legon, A. C.; Warner, H. E. *J. Chem. Soc., Chem. Comm.* **1991**, 1397-1399.

(38) Thorne, L. R.; Suenram, R. D.; Lovas, F. J. *J. Chem. Phys.* **1983**, *78*, 167-171.

(39) Daly, A. M.; Tanjaroon, C.; Marwitz, A. J. V.; Liu, S. –Y.; Kukolich, S. G. *J. Am. Chem. Soc.* **2010**, *132*, 5501-5506.

(40) Hunter, P. *EMBO Rep.* **2009**, *10*, 125-128.

(41) Bennett, A.; Rowe, R. I.; Soch, N.; Eckhert, C. D. *J. Nutr.* **1999**, *129*, 2236-2238.

(42) Probst, T. U. *Fresenius J. Anal. Chem.* **1999**, *364*, 391-403.

(43) Rock, F. L.; Mao, W.; Yaremchuk, A.; Tukalo, M.; Crépin, T.; Zhou, H.; Zhang, Y. –K.; Hernandez, V.; Akama, T.; Baker, S. J.; Plattner, J. J.; Shapiro, L.; Martinis, S. A.; Benkovic, S. J.; Cusack, S.; Alley, M. R. K. *Science* **2007**, *316*, 1759-1761.

(44) Barth, R. F.; Coderre, J. A.; Vicente, M. G. H.; Blue, T. E. *Clin. Cancer Res.* **2005**, *11*, 3987-4002.

(45) Morton, A.; Baase, W. A.; Matthews, B. W. *Biochemistry* **1995**, *34*, 8564-8575.

(46) Liu, L.; Marwitz, A. J. V.; Matthews, B. W.; Liu, S. –Y. *Angew. Chem. Int. Ed.* **2009**, *48*, 6817-6819.

Chapter IV

(1) Grimsdale, A. C.; Chan, K. L.; Martin, R. E.; Jokisz, P. G.; Holmes, A. B. *Chem. Rev.* **2009**, *109*, 897-1091.

(2) Kippelen, B.; Brédas, J. –L. *Energy Environ. Sci.* **2009**, *2*, 251-261.

(3) Marder, S. R.; Perry, J. W. *Adv. Mater.* **1993**, *5*, 804-815.

(4) Entwistle, C. D.; Marder, T. B. *Angew. Chem. Int. Ed.* **2002**, *41*, 2927-2931.

(5) Matsumi, N.; Naka, K.; Chujo, Y. *J. Am. Chem. Soc.* **1998**, *120*, 5112-5113.

(6) Hoic, D. A.; Davis, W. M.; Fu, G. C. *J. Am. Chem. Soc.* **1995**, *117*, 8480-8481.

(7) Qiao, S.; Hoic, D. A.; Fu, G. C. *Organometallics* **1997**, *16*, 1501-1502.

(8) Lee, B. Y.; Wang, S.; Putzer, M.; Bartholemew, G. P.; Bu, X.; Bazan, G. C. *J. Am. Chem. Soc.* **2000**, *122*, 3969-3970.

(9) Mercier, L. G.; Piers, W. E.; Parvez, M. *Angew. Chem. Int. Ed.* **2009**, *48*, 6108-6111.

(10) Bosdet, M. J. D.; Jaska, C. A.; Piers, W. E.; Sorensen, T. S.; Parvez, M. *Org. Lett.* **2007**, *9*, 1395-1398.

(11) Bosdet, M. J. D.; Piers, W. E.; Sorensen, T. S.; Parvez, M. *Angew. Chem. Int. Ed.* **2007**, *46*, 4940-4943.

(12) Ashe, A. J., III; Fang, X. *Org. Lett.* **2000**, *2*, 2089-2091.

(13) Ashe, A. J., III; Fang, X.; Fang, X.; Kampf, J. W. *Organometallics* **2001**, *20*, 5413-5418.

(14) Marwitz, A. J. V.; Abbey, E. R.; Jenkins, J. T.; Zakharov, L. N.; Liu, S. – Y. *Org. Lett.* **2007**, *9*, 4905-4908.

(15) Marwitz, A. J. V.; Matus, M. H.; Zakharov, L. N.; Dixon, D. A.; Liu, S. – Y. *Angew. Chem. Int. Ed.* **2009**, *48*, 973-977.

(16) Ferrante, C.; Kensy, U.; Dick, B. *J. Phys. Chem.* **1993**, *97*, 13457-13463.

(17) Müller, M.; Kübel, C.; Morgenroth, F.; Iyer, V. S.; Müllen, K. *Carbon* **1998**, *36*, 827-831.

(18) Sebastiani, D.; Parker, M. A. *Symmetry* **2009**, *1*, 226-239.

(19) Voronkov, M. G.; Yarosh, O. G. *Izvest. Akad. Nauk SSSR, Seriya Khim.* **1988**, 851-852.

(20) Daly, A. M.; Tanjaroon, C.; Marwitz, A. J. V.; Liu, S. –Y.; Kukolich, S. G. *J. Am. Chem. Soc.* **2010**, *132*, 5501-5506.

(21) Braga, D.; Grepioni, F.; Tedesco, E. *Organometallics* **1998**, *17*, 2669-2672.

(22) Steiner, T. *Angew. Chem. Int. Ed.* **2002**, *41*, 48-76.

(23) Pan, J.; Kampf, J. W.; Ashe, A. J., III *Organometallics* **2004**, *23*, 5626-5629.

(24) Spitler, E. L.; Johnson, C. A., III, Haley, M. M. *Chem. Rev.* **2006**, *106*, 5344-5386.

(25) Magyar, R. J.; Tretiak, S.; Gao, Y.; Wang, H. –L.; Shreve, A. P. *Chem. Phys. Lett.* **2005**, *401*, 149-156.

(26) Stone, M. T.; Heemstra, J. M.; Moore, J. S. *Acc. Chem. Res.* **2006**, *39*, 11-20.

(27) Castro, C. E.; Gaughan, E. J.; Owsley, D. C. *J. Org. Chem.* **1966**, *31*, 4071-4078.

(28) Samori, S.; Tojo, S.; Fujitsuka, M.; Ryhding, T.; Fix, A. G.; Armstrong, B. M.; Haley, M. M.; Majima, T. *J. Org. Chem.* **2009**, *74*, 3776-3782.

(29) Lewis, K. D.; Matzger, A. J. *J. Am. Chem. Soc.* **2005**, *127*, 9968-9969.

(30) Pan, J.; Kampf, J. W.; Ashe, A. J., III *Org. Lett.* **2007**, *9*, 679-681.

(31) Chinchilla, R.; Nájera, C. *Chem. Rev.* **2007**, *107*, 874-922.

(32) Hundertmark, T.; Littke, A. F.; Buchwald, S. L.; Fu, G. C. *Org. Lett.* **2000**, *2*, 1729-1731.

(33) Spitler, E. L.; Monson, J. M.; Haley, M. M. *J. Org. Chem.* **2008**, *73*, 2211-2223.

(34) Kivala, M.; Boudon, C.; Gisselbrecht, J. –P.; Seiler, P.; Gross, M.; Diederich, F. *Angew. Chem. Int. Ed.* **2007**, *46*, 6357-6360.

(35) Michinobu, T.; Boudon, C.; Gisselbrecht, J. –P.; Seiler, P.; Frank, B.; Moonen, N. N. P.; Gross, M.; Diederich, F. *Chem. Eur. J.* **2006**, *12*, 1889-1905.

(36) Spitler, E. L.; Haley, M. M. *Org. Biomol. Chem.* **2008**, *6*, 1569-1576.

(37) Zucchero, A. J.; McGrier, P. L.; Bunz, U. H. F. *Acc. Chem. Res.* **2010**, *43*, 397-408.

(38) Sonoda, M.; Inaba, A.; Itahashi, K.; Tobe, Y. *Org. Lett.* **2001**, *3*, 2419-2421.

Chapter V

(1) *Nitric Oxide: Biology and Pathobiology*, Ignarro, L. J., Ed.; Academic Press: New York, **2000.**

(2) Beckman, J. S.; Beckman, T. W.; Chen, J.; Marshall, P. A.; Freeman, B. *A. Proc. Natl. Acad. Sci. USA* **1990**, *87*, 1620-1624.

(3) Gow, A.; Duran, D.; Thom, S. R.; Ischiropoulos, H. *Arch. Biochem. Biophys.* **1996**, *333*, 42-48.

(4) Freeman, B. A.; Baker, P. R. S.; Schopfer, F. J.; Woodcock, S. R.; Napolitano, A.; d'Ischia, M. *J. Biol. Chem.* **2008**, *283*, 15515-15519.

(5) Rudolph, T. K.; Freeman, B. A. *Science Signaling* **2009**, *2*, 1-13.

(6) Schopfer, F. J.; Cole, M. P.; Groeger, A. L.; Chen, C. –S.; Khoo, N. K. H.; Woodcock, S. R.; Golin-Bisello, F.; Motanya, U. N.; Li, Y.; Zhang, J.; Garcia-Barrio, M. T.; Rudolph, T. K.; Rudolph, V.; Bonacci, G.; Baker, P. R. S.; Xu, H. E.; Batthyany, C. I.; Chen, Y. E.; Hallis, T. M.; Freeman, B. A. *J. Biol. Chem.* **2010**, *285*, 12321-12333.

(7) Baker, L. M. S.; Golin-Bisello, F.; Schopfer, F. J.; Fink, M.; Woodcock, S. R.; Branchaud, B. P.; Radi, R.; Freeman, B. A. *J. Biol. Chem.* **2007**, *282*, 31085-31093.

(8) Batthyany, C.; Schopfer, F. J.; Baker, P. R. S.; Duran, R.; Baker, L. M. S.; Huang, Y.; Cervenansky, C.; Branchaud, B. P.; Freeman, B. A. *J. Biol. Chem.* **2006**, *281*, 20450-20463.

(9) d'Ischia, M.; Rega, N.; Barone, V. *Tetrahedron* **1999**, *55*, 9297-9308.

(10) Napolitano, A.; Camera, E.; Picardo, M.; d'Ischia, M. J. Org. Chem. **2000**, *65*, 4853-4860.

(11) Napolitano, A.; Crescenzi, O.; Camera, E.; Giudicianni, I.; Picardo, M.; d'Ischia, M. *Tetrahedron* **2004**, *58*, 5061-5067.

(12) O'Donnell, V. B.; Eiserich, J. P.; Bloodsworth, A.; Chumley, P. H.; Kirk, M.; Barnes, S.; Darley-Usmar, V. M.; Freeman, B. A. In *Methods Enzymol.*; Academic Press: New York, **1999**; Vol. 301, pp. 454-470.

(13) Rosini, G. In *Comprehensive Organic Synthesis*; Trost, B. M.; Fleming, I.; Heathcock, C. H., Eds.; Pergamon Press: New York, **1991**; Vol. 2, pp. 321-340.

(14) Gorczynski, M. J.; Huang, J.; King, S. B. *Org. Lett.* **2006**, 8, 2305-2308.

(15) Tranchepain, I.; Le Berre, F.; Dureault, A.; Le Merrer, Y.; Depezay, J. C. *Tetrahedron* **1989**, *45*, 2057-2065.

(16) Kornblum, N.; Ungnade, H. E. *Org. Synth. Coll. Vol. IV*, 724-727.

(17) Ono, N.; Maruyama, K. *Bull. Chem. Soc. Jpn.* **1988**, *61*, 4470-4472.

(18) Hey, H.; Arpe, H. –J. *Angew. Chem. Int. Ed. Engl.* **1973**, *12*, 928-929.

(19) Woodcock. S. R.; Marwitz, A. J. V.; Bruno, P.; Branchaud, B. P. *Org. Lett.* **2006**, *8*, 3931-3933.

(20) Baker, P. R. S.; Lin, Y.; Schopfer, F. J.; Woodcock, S. R.; Groeger, A. L.; Batthyany, C.; Sweeney, S.; Long, M. H.; Iles, K. E.; Baker, L. M. S.; Branchaud, B. P.; Chen, Y. E.; Freeman, B. A. *J. Biol. Chem.* **2005**, *280*, 42464-42475.

(21) Vogel, A. I. In *Vogel's Textbook of Practical Organic Chemistry, 5th Edition*, rev. by Furniss, B. S.; Hannaford, A. J.; Smith, P. W. G.; Tatchell, A. R., Addison Wesley Longman: London, **1998**, p. 733.

(22) Mirviss, S. B. *J. Org. Chem.* **1989**, *54*, 1948-1951.

Appendix A

(1) Ashe, A. J., III; Fang, X. *Org. Lett.* **2000**, *2*, 2089-2091.

(2) Spartan '08, Wavefunction Inc., Irvine CA.

(3) Gaussian 03, Revision D.02, Frisch, M. J.; Trucks, G. W.; Schlegel, H. B.; Scuseria, G. E.; Robb, M. A.; Cheeseman, J. R.; Montgomery, J. A., Jr.; Vreven, T.; Kudin, K. N.; Burant, J. C.; Millam, J. M.; Iyengar, S. S.; Tomasi, J.; Barone, V.; Mennucci, B.; Cossi, M.; Scalmani, G.; Rega, N.; Petersson, G. A.; Nakatsuji, H.; Hada, M.; Ehara, M.; Toyota, K.; Fukuda, R.; Hasegawa, J.; Ishida, M.; Nakajima, T.; Honda, Y.; Kitao, O.; Nakai, H.; Klene, M.; Li, X.; Knox, J. E.; Hratchian, H. P.; Cross, J. B.; Bakken, V.; Adamo, C.; Jaramillo, J.; Gomperts, R.; Stratmann, R. E.; Yazyev, O.; Austin, A. J.; Cammi, R.; Pomelli, C.; Ochterski, J. W.; Ayala, P. Y.; Morokuma, K.; Voth, G. A.; Salvador, P.; Dannenberg, J. J.; Zakrzewski, V. G.; Dapprich, S.; Daniels, A. D.; Strain, M. C.; Farkas, O.; Malick, D. K.; Rabuck, A. D.; Raghavachari, K.; Foresman, J. B.; Ortiz, J. V.; Cui, Q.; Baboul, A. G.; Clifford, S.; Cioslowski, J.; Stefanov, B. B.; Liu, G.; Liashenko, A.; Piskorz, P.; Komaromi, I.; Martin, R. L.; Fox, D. J.; Keith, T.; Al-Laham, M. A.; Peng, C. Y.; Nanayakkara, A.; Challacombe, M.; Gill, P. M. W.; Johnson, B.; Chen, W.; Wong, M. W.; Gonzalez, C.; Pople, J. A., Gaussian, Inc., Wallingford CT, **2004**.

(4) Marwitz, A. J. V.; Matus, M. H.; Zakharov, L. N.; Dixon, D. A.; Liu, S. -Y. *Angew. Chem. Int. Ed.* **2009**, *48*, 973-977.

(5) Dunne, K. S.; Lee, S. E.; Gouverneur, V. *J. Organomet. Chem.* **2006**, *691*, 5246-5259.

Appendix B

(1) Davies, K. M.; Dewar, M. J. S.; Rona, P. *J. Am. Chem. Soc.* **1967**, *89*, 6294-6297.

(2) Ashe, A. J., III; Fang, X. *Org. Lett.* **2000**, *2*, 2089-2091.

(3) Marwitz, A. J. V.; Abbey, E. R.; Jenkins, J. T.; Zakharov, L. N.; Liu, S. – Y. *Org. Lett.* **2007**, *9*, 4905-4908.

(4) Feller, D.; Peterson, K. A. *J. Chem. Phys.* **1998**, *108*, 154-176.

(5) Feller, D.; Dixon, D. A. *J. Phys. Chem. A* **2000**, *104*, 3048-3056.

(6) Feller, D.; Dixon, D. A. *J. Chem. Phys.* **2001**, *115*, 3484-3496.

(7) Ruscic, B.; Wagner, A. F.; Harding, L. B.; Asher, R. L.; Feller, D.; Dixon, D. A.; Peterson, K. A.; Song, Y.; Qian, X.; Ng, C. –Y.; Liu, J.; Chen, W.; Schwenke, D. W. *J. Phys. Chem. A* **2002**, *106*, 2727-2747.

(8) Matus, M. H.; Anderson, K.; Camaioni, D. M.; Autrey, S. T.; Dixon, D. A. *J. Phys. Chem A* **2007**, *111*, 4411-4421.

(9) Pollack, L.; Windus, T. L.; de Jong, W. A.; Dixon, D. A. *J. Phys. Chem. A* **2005**, *109*, 6934-6938.

(10) Bartlett, R. J.; Musial, M. *Rev. Mod. Phys.* **2007**, *79*, 291-352.

(11) Dunning, T. H. *J. Chem. Phys.* **1989**, *90*, 1007-1023.

(12) Kendall, R. A.; Dunning, T. H.; Harrison, R. J. *J. Chem. Phys.* **1992**, *96*, 6796-6806.

(13) Peterson, K. A.; Woon, D. E.; T. H. Dunning, T. H., Jr. *J. Chem. Phys.* **1994**, *100*, 7410-7415.

(14) Peterson, K. A.; Dunning, T. H., Jr. *J. Chem. Phys.* **2002**, *117*, 10548-10560.

(15) Woon, D. E.; Dunning, T. H., Jr. *J. Chem. Phys.* **1993**, *98*, 1358-1371.

(16) Douglas, M.; Kroll, N. M. *Ann. Phys.* **1974**, *82*, 89-155.

(17) Hess, B. A. *Phys. Rev. A* **1985**, *32*, 756-763.

(18) Hess, B. A. *Phys. Rev. A* **1986**, *33*, 3742-3748.

(19) de Jong, W. A.; Harrison, R. J.; Dixon, D. A. *J. Chem. Phys.* **2001**, *114*, 48-53.

(20) Moore, C. E. *Atomic Energy Levels*; Washington, D.C., Vol. U.S. National Bureau of Standards Circular **1949**, *467*, NBS.

(21) Head-Gordon, M.; Pople, J. A.; Frisch, M. J. *Chem. Phys. Lett.* **1988**, *153*, 503-506.

(22) Shimanouchi, T. In *Tables of Molecular Vibrational Frequencies Consolidated Volume I*, NSRDS-NBS **1972**, *39*, National Bureau of Standards, Washington, D.C.

(23) Jacox, M. E. *J. Phys. Chem. Ref. Data* **1994**, *Monograph No. 3*.

(24) Curtiss, L. A.; Redfern, P. C.; Raghavachari, K.; Rassolov, V.; Pople, J. A. *J. Chem. Phys.* **1997**, *110*, 4703-4709.

(25) Chase, M. W., Jr. *NIST-JANAF J. Phys. Chem. Ref. Data* **1998**, *Monograph No. 9.*

(26) Karton, A.; Martin, J. M. L. *J. Phys. Chem., A* **2007**, *111*, 5936-5944.

(27) Curtiss, L. A.; Raghavachari, K.; Redfern, P. C.; Pople, J. A. *J. Chem. Phys.* **1997**, *106*, 1063-1079.

(28) Becke, A. D. *J. Chem. Phys.* **1993**, *98*, 5648-5652.

(29) Lee, C.; Yang, W.; Parry, R. G. *Phys. Rev. B* **1988**, *37*, 785-789.

(30) Godbout, N.; Salahub, D. R.; Andzelm, J.; Wimmer, E. *Can. J. Chem.* **1992**, *70*, 560-571.

(31) Schäfer, A.; Horn, H.; Ahlrichs, R. *J. Chem. Phys.* **1992**, *97*, 2571-2577.

(32) Wolinski, K.; Hinton, J. F.; Pulay, P. *J. Am. Chem. Soc.* **1990**, *112*, 8251-8260.

(33) Chen, Z.; Wannere, C. S.; Corminboeuf, C.; Puchta, R.; Schleyer, P. v. R. *Chem. Rev.* **2005**, *105*, 3842-3888.

(34) Stratmann, R. E.; Scuseria, G. E.; Frisch, M. J. *J. Chem. Phys.* **1998**, *109*, 8218-8224.

(35) Bauernschmitt, R.; Ahlrichs, R. *Chem. Phys. Lett.* **1996**, *256*, 454-464.

(36) Casida, M. E.; Jamorski, C.; Casida, K. C.; Salahub, D. R. *J. Chem. Phys.* **1998**, *108*, 4439-4449.

(37) Korona, T.; Werner, H. –J. *J. Chem. Phys.* **2003**, *118*, 3006-3019.

(38) Gaussian 03, Revision C.01, Frisch, M. J.; Trucks, G. W.; Schlegel, H. B.; Scuseria, G. E.; Robb, M. A.; Cheeseman, J. R.; Montgomery, J. A., Jr.; Vreven, T.; Kudin, K. N.; Burant, J. C.; Millam, J. M.; Iyengar, S. S.; Tomasi, J.; Barone, V.; Mennucci, B.; Cossi, M.; Scalmani, G.; Rega, N.; Petersson, G. A.; Nakatsuji, H.; Hada, M.; Ehara, M.; Toyota, K.; Fukuda, R.; Hasegawa, J.; Ishida, M.; Nakajima, T.; Honda, Y.; Kitao, O.; Nakai, H.; Klene, M.; Li, X.; Knox, J. E.; Hratchian, H. P.; Cross, J. B.; Bakken, V.; Adamo, C.; Jaramillo, J.; Gomperts, R.; Stratmann, R. E.; Yazyev, O.; Austin, A. J.; Cammi, R.; Pomelli, C.; Ochterski, J. W.; Ayala, P. Y.; Morokuma, K.; Voth, G. A.; Salvador, P.; Dannenberg, J. J.;

Zakrzewski, V. G.; Dapprich, S.; Daniels, A. D.; Strain, M. C.; Farkas, O.; Malick, D. K.; Rabuck, A. D.; Raghavachari, K.; Foresman, J. B.; Ortiz, J. V.; Cui, Q.; Baboul, A. G.; Clifford, S.; Cioslowski, J.; Stefanov, B. B.; Liu, G.; Liashenko, A.; Piskorz, P.; Komaromi, I.; Martin, R. L.; Fox, D. J.; Keith, T.; Al-Laham, M. A.; Peng, C. Y.; Nanayakkara, A.; Challacombe, M.; Gill, P. M. W.; Johnson, B.; Chen, W.; Wong, M. W.; Gonzalez, C.; Pople, J. A., Gaussian, Inc., Wallingford CT, (2004).

(39) Werner, H. –J.; Knowles, P. J.; Amos, R. D.; Bernhardsson, A.; Berning, A.; Celani, P.; Cooper, D. L.; Deegan, M. J. O.; Dobbyn, A. J.; Eckert, F.; Hampel, C.; Hetzer, G.; Korona, T.; Lindh, R.; Lloyd, A. W.; McNicholas, S. J.; Manby, F. R.; Meyer, W.; Mura, M. E.; Nicklass, A.; Palmieri, P.; Pitzer, R.; Rauhut, G.; Schütz, M.; Schumann, U.; Stoll, H.; Stone, A. J.; Tarroni, R.; Thorsteinsson, T., MOLPRO, 2002.6.

(40) Apra, E.; Bylaska, E. J.; Jong, W. D.; Hackler, M. T.; Hirata, S.; Pollack, L.; Smith, D.; Straatsma, T. P.; Windus, T. L.; Harrison, R. J.; Nieplocha, J.; Tipparaju, V.; Kumar, M.; Brown, E.; Cisneros, G.; Dupuis, M.; Fann, G. I.; Fruchtl, H.; Garza, J.; Hirao, K.; Kendall, R.; Nichols, J. A.; Tsemekhman; K.; Valiev, M.; Wolinski, K.; Anchell, J.; Bernholdt, D.; Borowski, P.; Clark, T.; Clerc, D.; Dachsel, H.; Deegan, M.; Dyall, K.; Elwood, D.; Glendening, E.; Gutowski, M.; Hess, A.; Jaffe, J.; Johnson, B.; Ju, J.; Kobayashi, R.; Kutteh, R.; Lin, Z.; Littlefield, R.; Long, X.; Meng, B.; Nakajima, T.; Niu, S.; Rosing, M.; Sandrone, G.; Stave, M.; Taylor, H.; Thomas, G.; Lenthe, J. V.; Wong, A.; Zhang, Z. NWChem., PNNL, 2003.

(41) Kendall, R. A.; Apra, E.; Bernholdt, D. E.; Bylaska, E. J.; Dupuis, M.; Fann, G. I.; Harrison, R. J.; Ju, J.; Nichols, J. A.; Nieplocha, J.; Straatsma, T. P.; Windus, T. L.; Wong, A. T. *Computer Phys. Comm.* **2000**, *128*, 260-283.

(42) Spartan '04, Wavefunction Inc., Irvine CA.

(43) Cyrański, M. K. *Chem Rev.* **2005**, *105*, 3773-3811.

(44) Pedley, J. B. In *Thermochemical Data and Structures of Organic Compounds, Volume I*, TRC Data Series, Thermodynamics Research Center, College Station TX, **1994**.

(45) Dixon, D. A.; Gutowski, M. *J. Phys. Chem. A* **2005**, *109*, 5129-5135.

(46) Grant, D.; Dixon, D. A. *J. Phys. Chem. A* **2006**, *110*, 12955-12962.

(47) Errisson, A. E.; Baase, W. A.; Matthews, B. W. *J. Mol. Biol.* **1993**, *229*, 747-769.

(48) Otwinowski, Z.; Minor, W. *Methods Enzymol.* **1997**, *276*, 307-326.

(49) CCP4: Collaborative Computational Project Nr4. *Acta Cryst.* **1994**, *D50*, 760-763.

(50) Emsley, P.; Cowtan, K. *Acta Cryst.* **2004**, *D60*, 2126-2132.

Appendix C

(1) Bosdet, M. J. D.; Jaska, C. A.; Piers, W. E.; Sorensen, T. S.; Parvez, M. *Org. Lett.* **2007**, *9*, 1395-1398.

(2) Bosdet, M. J. D.; Piers, W. E.; Sorensen, T. S.; Parvez, M. *Angew. Chem. Int. Ed.* **2007**, *46*, 4940-4943.